

**Integrating single-cell multi-omics and experimental therapeutics to identify and validate novel secondary therapies against relapsed/refractory cancers**

by

Sayak Chakravarti

A dissertation submitted to the Graduate Faculty of  
Auburn University  
in partial fulfillment of the  
requirements for the Degree of  
Doctor of Philosophy

Auburn, Alabama

May 8<sup>th</sup>, 2023

Keywords: Drug- resistance, Combination therapy, Single-cell RNA sequencing, Next-generation sequencing, Prostate Cancer, Hematological malignancies

Copyright 2023 by Sayak Chakravarti

Approved by

Dr. Amit K. Mitra, Chair, Assistant Professor, Department of Drug Discovery and Development  
Dr. Timothy M. Moore, Co-chair, Interim Dean, Harrison School of Pharmacy  
Dr. Robert D. Arnold, Professor, Department of Drug Discovery and Development  
Dr. Murali Dhanasekaran, Professor, Department of Drug Discovery and Development  
Dr. Bruce F. Smith, Professor, Department of Pathobiology

## **Abstract**

Drug resistance has remained the Achilles' heel in cancer chemotherapy which serves as the principal limiting factor in achieving favorable treatment outcomes in cancer patients. Drug resistance that exists even before drug exposure (intrinsic resistance) or resistance that develops with the course of treatment (acquired) is responsible for therapy failure and clinical progression (relapse or recurrence) in 90% of the cases. Intra-patient and inter-patient tumoral heterogeneity also play a significant role in therapy resistance and failure as they govern the treatment response. Recent evidence indicates that the underlying sub-cellular molecular characteristics of the tumor govern the heterogeneity in drug response. The treatment-refractory subpopulations of tumor cells or cancer stem-like cells (CSCs) are believed to drive drug resistance and disease relapse in various cancers. Due to their quiescent nature, which allows them to escape conventional therapeutics, standard agents fail to improve long-term clinical outcomes significantly. Thus, the development of drug resistance and disease relapse in cancer is primarily attributed to the treatment-refractory subpopulations of tumor cells or cancer stem-like cells (CSCs) with potential self-renewal and differentiation capacities. Moreover, a significant limitation of cancer drug discovery is the low predictive value of the pre-clinical studies as they mostly ignore the cellular heterogeneity and complexity, which resulted in extensive inter-individual variation in response, drug resistance, and dose-limiting toxicities. So, deciphering key features within patients' underlying tumor heterogeneity and personalized sensitivity to chemotherapy is essential to predict the efficacy of anti-cancer drugs and prevent delays in selecting more effective alternative strategies.

## Acknowledgments

*I would like to dedicate the thesis to my parents, maternal uncle, late grandparents, and my pet clowder!*

*My parents have been my pillar of strength throughout this endeavor. Words can hardly describe my thanks and appreciation for them. My parents have been my source of inspiration, support, and guidance. They have taught me to be determined, to believe in myself, and to always persevere. Without them, I would not have achieved this.*

*I would like to express my sincere gratitude to my Ph.D. advisor Dr. Amit K. Mitra, for his unwavering support and guidance throughout this journey. I would like to thank my committee members Dr. Moore, Dr. Arnold, Dr. Smith, and Dr. Murali, for their valuable insights and encouragement. I am thankful to Dr. Panagiotis Mistriotis for agreeing to serve as the external reader. I sincerely thank Dr. Allison Church Bird for her technical support.*

*I am extremely thankful to my lab mate Dr. Suman Mazumder and my collaborator/mentor, Dr. Taraswi Mitra Ghosh, for their continuous support and mentorship.*

*I would also like to thank each and every person in my department, including the head of the department Dr. Gary Piazza, and Graduate Student Services Administrator Jennifer Johnston for their support and help.*

*Last but not least, I would like to express my deepest love for my pet cats, my biggest stress busters.*

“Man can’t discover new oceans unless he has the courage to lose sight of the shore.”

## Table of Contents

Abstract.....	2
Acknowledgments.....	3
List of Tables.....	5-7
List of Figures.....	8-14
List of Abbreviations.....	15-20
Chapter 1: Review of Literature on Drug Resistance in Cancer	
Chapter 1.1 Cancer.....	22-26
Chapter 1.2 Drug Resistance in Cancer.....	27-30
Chapter 1.3 Types of Cancer.....	30-35
Chapter 1.4 Multiple Myeloma & Drug Resistance.....	36-46
Chapter 1.5 Mantle Cell Lymphoma & Drug Resistance.....	47-61
Chapter 1.6 Prostate Cancer & Drug Resistance.....	62-80
Chapter 1.7 Gap in Knowledge & secDrug Algorithm.....	81-83
Chapter 2: Validation of secondary therapies in Multiple Myeloma.....	85-128
Chapter 3: Validation of secondary therapies in Prostate Cancer.....	130-214
Chapter 4: Validation of secondary therapies in Mantle Cell Lymphoma.....	215-243
Chapter 5: Validation of in-litro predicted secondary therapies in B-cell Malignancies.....	244-306
Summary.....	307
References.....	308-330

## **List of Tables in Chapter 1**

Table 1 Recurrence Statistics of Different Cancer.....	27-28
Table 2 Clinically relevant mutations observed in RRMM patients.....	42
Table 3 List of immunophenotypic markers used to identify and classify MCL.....	49
Table 4 Stages of prostate cancer and their characteristics.....	68
Table 5 Current treatment modalities for different stages of prostate cancer.....	69
Table 6 FDA-approved drugs for different stages of prostate cancer.....	69-70
Table 7 Molecular mechanism of resistance towards Taxane drugs.....	76

## **List of Tables in Chapter 2**

Table 1A Immunophenotyping panel for CyTOF analysis; Cell surface targets.....	92
Table 1B Immunophenotyping panel for CyTOF analysis; Intra-cellular targets.....	93
Table 2 secDrug algorithm predicted top combination treatment against B-cell cancer....	97-98
Table 3 DE genes between 17-AAG sensitive and resistant HMCLs.....	124-125

### List of Tables in Chapter 3

Table 1 Drugs and Reagents.....	134
Table 2 Top secDrugs derived from our pharmacogenomics data-driven analysis against PCa.....	144-145

## List of Figures in Chapter 1

Figure 1 Estimated new cancer cases and cancer-related deaths incidence in the US in 2022.....	22
Figure 2 Estimated new cancer cases and cancer-related deaths incidence globally in 2020.....	23
Figure 3 Classification of Hematological Malignancies.....	31
Figure 4 Hematopoiesis .....	33
Figure 5 Anatomy of prostate .....	62
Figure 6 Prostate Cancer incidence rate and mortality rate in the US .....	63
Figure 7A Prostate Cancer Risk from Birth Over Time .....	63
Figure 7B Age-wise prevalence of Prostate Cancer among US males.....	64
Figure 7C Age-adjusted incidence rates of Prostate Cancer among US men.....	64
Figure 7D Age-adjusted incidence rates of Prostate Cancer among US males by Race.....	65
Figure 8 Molecular Mechanism of Prostate Cancer Development.....	71
Figure 9 Dynamic transition model of prostate cancer clinical states.....	73
Figure 10 Course of clinical progression to AR <sup>null</sup> mCRPC.....	77
Figure 11 Schematic diagram of identification, validation, and characterization of secDrug predicted novel secondary anti-cancer agents.....	83

## List of Figures in Chapter 2

Figure 1 secDrugs decrease in vitro cell viability in multiple myeloma .....	99
Figure 2 scRNAseq data of the myeloma cell line pair U266-P/VR.....	100
Figure 3 secDrug 17AAG (Hsp90 inhibitor) synergizes with PIs, FK866 and IMiD.....	103-108
Figure 4 CyTOF analysis results in patient primary multiple myeloma cells.....	110-111
Figure 5 WB analysis of 17-AAG treatment-induced changes in key protein level.....	112-113
Figure 6 17-AAG induces apoptosis via a mitochondrial-mediated pathway in MM.....	114
Figure 7 17-AAG induced cell death was comparable with Hsp90 knockdown.....	115-116
Figure 8 N-Ras mutant HMCL showed high sensitivity to 17-AAG treatment.....	117
Figure 9 Differential gene expression analysis of 17-AAG single-agent treatment.....	119
Figure 10 Differential gene expression analysis of 17-AAG + PI treatment.....	121-123

### List of Figures in Chapter 3

Figure 1 Single-cell transcriptomics identifies signatures of epithelial to mesenchymal transition (EMT) and stemness in metastatic prostate cancer cells.....	146-149
Figure 2 Comparison of the single-cell gene expression markers between taxane-sensitive and the clonally derived acquired taxane-resistant mCRPC cell line.....	150-151
Figure 3 Pharmacogenomics data-driven algorithm predicted secDrug TAK715 is effective against TX-resistant and stem-cell-like sub-clones in lethal PCa.....	153-155
Figure 4 Top predicted secondary drugs effectively reduce cellular viability .....	156-161
Figure 5 In vitro cytotoxicity assay of secDrug combination treated cells.....	162-173
Figure 6 Top predicted secDrugTAK-715 inhibits multiple Kinases.....	174
Figure 7 Caspase 3/7 activity assay on Docetaxel and TAK-715 treated cells.....	175
Figure 8 AnnexinV-FITC/ PI assay on Docetaxel and TAK-715 treated cells.....	176
Figure 9 Assessment of cellular morphology of Docetaxel and TAK-715 treated cells.....	177
Figure 10 Assessment of nuclear morphology of Docetaxel and TAK-715 treated cells.....	178
Figure 11 Novel microfluidics-based assay to study the effect of TAK-715 on EMT.....	179-180
Figure 12 Wound healing assay on Docetaxel and TAK-715 treated cells.....	181-182
Figure 13 Colony formation assay on Docetaxel and TAK-715 treated cells.....	183
Figure 14 DEG analysis on Docetaxel and TAK-715 treated cells.....	184-185
Figure 15 Ingenuity Pathway Analysis of top DE genes.....	187-188
Figure 16 Causal network analysis on top DE genes obtained from RNAseq data.....	189-190
Figure 17 In silico analysis of HES1 expression and its impact in prostate cancer followed by in vitro validation.....	191-194
Figure 18 Measurement of TAK-715 induced cellular ROS generation (DCFDA assay).....	195
Figure 19 Measurement of TAK-715 induced Cellular superoxide anions (DHE assay).....	196

Figure 20 Measurement of TAK-715 induced change in MMP (JC-1 assay).....	197
Figure 21 Identification of TAK-715 induced change in cell cycle by flow-cytometry.....	198
Figure 22 Identification of TAK-715 induced DNA damage by comet assay.....	199
Figure 23 Identification of TAK-715-induced reduction in side-population load in taxane resistant mCRPC cell lines by DyeCycle Violet assay.....	200
Figure 24 Investigation of the effect of TAK-715 on stem-cell population in PCa.....	201-202
Figure 25 TAK715 erodes sub-clones responsible for drug resistance and stemness.....	203
Figure 26 Investigation of TAK-715 induced change in the oxygen consumption rate by Seahorse Extracellular Flux Technology.....	206
Figure 27 Validation of TAK-715 treatment-induced gene signatures using Patient datasets.....	207
Figure 28 Validation of TAK-715 treatment-induced gene signatures using Patient datasets with biochemical recurrence.....	208
Figure 29 Proposed mechanism of action of TAK-715 in ARlow mCRPC cells.....	213

## List of Figures in Chapter 4

Figure 1 Single Cell transcriptomics (scRNAseq)-based secDrug screening.....	219
Figure 2 Cytotoxicity assay: Single agent PI, BTKi, YM155 & S63845 in MCL cells...	220-222
Figure 3 Cytotoxicity assay: YM155, S63845 + PI, BTKi in MCL cells.....	224-227
Figure 4 Drug target validation of S63845 & YM155 using western blot.....	228
Figure 5 Cytotoxicity assay of YM155 & S63845 combination in MCL cells.....	228
Figure 6 Apoptosis assays: YM155, S63845 +PI, BTKi in MCL cells.....	229-231
Figure 7 Effect of YM155 on cell adhesion of MCL cells to BMSC.....	232
Figure 8 Effect of YM155 on cancer stem cells in MCL by ALDH activity assay.....	233-234
Figure 9 RNAseq data to identify the mechanism of action of YM155 in MCL cells.....	235-236
Figure 10 IPA analysis on YM155 induced top DE gene.....	237
Figure 11 Effect of YM155 treatment on genes associated with OS & PFS.....	238
Figure 12 KEGG pathway enrichment analysis: mechanistic insights of YM155 action.....	239-240

## List of Figures in Chapter 5.1

Figure 1 Cytotoxicity assay: Single agent PI, BTKi, CLF in MCL cells.....	255-256
Figure 2A Cytotoxicity assay: CLF in combination with PI in MCL cells.....	258
Figure 2B Cytotoxicity assay of CLF in combination with BTKi in MCL cells.....	258
Figure 2C Combination index value of CLF+PI combination treatment.....	259
Figure 2D Combination index value of CLF+BTKi combination treatment.....	259
Figure 3 CLF+PI & CLF+BTKi enhance apoptosis in drug-resistant MCL cells.....	260-262
Figure 4 CLF activates mitochondrial-mediated pathway of apoptosis in MCL cells.....	263-265
Figure 5 CLF reduces side-population load in drug-resistant MCL cells .....	266-267
Figure 6 CLF reduces Aldefluor activity.....	268-269
Figure 7 Effect of CLF on TME-induced drug resistance in MCL cells.....	270
Figure 8 Effect of CLF treatment on OCR by SeaHorse ECF technology.....	271
Figure 9 RNAseq data to identify the mechanism of action of CLF in MCL cell.....	273-276
Figure 10 Effect of CLF on genes and pathways involved in poor clinical outcome.....	277-279
Figure 11 Effect of CLF treatment on cell cycle.....	279
Figure 12 scRNA-seq data on pre-vs post- CLF treated resistant MCL cells.....	280-281
Figure 13 CLF reduces MYC and CCND1 expression in MCL-Initiating cells involved in relapse and chemo-resistance.....	282
Figure 14 Validation of CLF treatment-related gene signatures using patient cohort Datasets.....	283-286

## List of Figures in Chapter 5.2

Figure 1 Cytotoxicity assay: Single agent CLF in MM cell lines and primary cells.....	297
Figure 2 Cytotoxicity assay: CLF in combination with PI, IMiD in MCL cells.....	298-301
Figure 3 Identification of CLF-induced key proteomic changes by CyTOF & WB analysis.....	302-304

### List of Abbreviations

ABC	ATP-binding cassette
ABCB1	ATP-binding cassette sub-family B member 1
ABCG2	ATP binding cassette subfamily G member 2
ADCC	Antibody-dependent cellular cytotoxicity
ADT	Androgen deprivation therapy
AIPC	Androgen independent prostate cancer
ALDH	Aldehyde dehydrogenase
AR	Androgen receptor
ARE	Androgen response element
ARF	alternative reading frame
ARID3A	AT-Rich Interaction Domain 3A
ARSi	Androgen receptor signaling inhibitor
ATM	Ataxia-Telangiectasia Mutated
ATR	Ataxia-Telangiectasia Mutated
Bcl-2	B-cell lymphoma 2
B-CLL	B-Cell Chronic Lymphocytic Leukemia
BCR	B Cell Receptor
bFGF	Basic Fibroblast Growth Factor
BLNK	B Cell Linker
BMSC	Bone-marrow stromal cells
BRCA 1/ 2	BReast CAncer gene 1/ 2
BTK	Bruton's tyrosine kinase
BTKi	Bruton's tyrosine kinase inhibitor
CARD11	Caspase Recruitment Domain Family Member 11
CAR-T	Chimeric antigen receptor therapy
CCND1	Cyclin D1
CDC	Complement-dependent cytotoxicity
CDK	Cyclin-dependent kinases
CDKN2A	cyclin dependent kinase inhibitor 2A

cfDNA	cell-free DNA
CHEK1/ 2	Checkpoint kinase 1/ 2
CHOP	C/EBP homologous protein
CLP	Common lymphoid progenitor
CRBN	Cereblon
CREB	cAMP Response Element-Binding Protein
CRISPR	Clustered regularly interspaced short palindromic repeats
CSC	Cancer Stem Cell
CTC	Circulating tumor cells
CTL	Cytotoxic T lymphocyte
CXCL12	C-X-C Motif Chemokine Ligand 12
CXCR4	C-X-C Motif Chemokine Receptor 4)
CytoF	Cytometry by Time of Flight
DAG	Diacylglycerol
DHT	Dihydrotestosterone
DOR	Duration of Response
DSB	Double strand break
ECM	Extra-cellular matrix
EGF	Epidermal Growth Factor
EGFR	Epidermal Growth Factor Receptor
EGR1	Early Growth Response 1
eIF2 $\alpha$	Eukaryotic Translation Initiation Factor 2A
EMT	Epithelial-mesenchymal transition
ER	Endoplasmic reticulum
ERK	Extracellular signal-regulated kinases
EZH2	Enhancer Of Zeste 2 Polycomb Repressive Complex 2 Subunit
FDA	U.S. Food and Drug Administration
FGFR3	Fibroblast Growth Factor Receptor 3
FISH	FLUORESCENCE IN SITU HYBRIDIZATION
FOXO3a	Forkhead box O3

GDSC	Genomics of Drug Sensitivity in Cancer
HIF-1	Hypoxia-Inducible Factor-1
HMCL	Human myeloma cell line
HRPC	Hormone refractory prostate cancer
HSC	Hematopoietic stem cell niche
HSP 70/ 90	Heat shock proteins 70/ 90
IC50	Half maximal inhibitory concentration
IDH 1/ 2	Isocitrate Dehydrogenase 1/ 2
IgD	Immunoglobulin D
IGH	Immunoglobulin Heavy Locus
IKZF-1	IKAROS family zinc finger 1
IKZF-3	IKAROS family zinc finger 3
IL-2	Interleukin 2
IL-6	Interleukin 6
IL-7	Interleukin-7
IMiD	Immunomodulatory drug
IMWG	International Myeloma Working Group
IP3	Inositol trisphosphate
IPA	Ingenuity pathway analysis
IRE1 $\alpha$	Inositol-requiring enzyme 1 $\alpha$
IRF4	Interferon Regulatory Factor 4
ITAM	Immunoreceptor Tyrosine Based Activation Motif
I $\kappa$ B	IkappaB
JNK	c-Jun N-terminal kinases
KDM6B	Lysine demethylase 6B
KLF4	Krüppel-like factor 4
LDH	Lactate Dehydrogenase
LHRH	Luteinizing hormone-releasing hormone
LMPP	Lympho-myeloid primed progenitor cell
M3P	Multiple Myeloma Mutation

mAb	Monoclonal antibody
MAPK	Mitogen-activated Protein Kinases
MCL	Mantle Cell Lymphoma
Mcl-1	Myeloid cell leukemia 1
mCRPC	Metastatic castration-resistant prostate cancer
mCSPC	Metastatic Castration-Sensitive Prostate Cancer
MDM2	Mouse double minute 2 homolog
MDR	Multi drug resistance
MET	Mesenchymal–epithelial transition
MGUS	Monoclonal gammopathy of undetermined significance
MM	Multiple myeloma
MMP	Mitochondrial membrane potential
MMSET	Multiple myeloma SET domain
MSH2	MutS homolog 2
MT1B	Metallothionein 1B
MTA	Microtubule targeting agent
MYD88	Myeloid differentiation primary response 88
NAMPT	Nicotinamide phosphoribosyl transferase
NEPC	Neuroendocrine prostate cancer
NFAT	Nuclear factor of activated T-cells
NF- $\kappa$ B	Nuclear factor- $\kappa$ B
NGS	Next generation sequencing
NHL	Non-Hodgkin lymphoma
NK cells	Natural killer cell
nmMCL	Non nodal Mantle Cell Lymphoma
ORR	Over-all Response Rate
OS	Over-all survival
PAX5	Paired Box 5
PCa	Prostate Cancer
PDGF	Platelet-derived growth factor

PERK	protein kinase R (PKR)-like endoplasmic reticulum kinase
PFS	Progression free survival
P-gp	P-glycoprotein
PI	Proteasome Inhibitor
PI3K	Phosphoinositide 3-kinase
PIP2	Phosphatidylinositol 4,5-bisphosphate
PIP3	Phosphatidylinositol (3,4,5)-trisphosphate
PKC $\beta$	Protein kinase C beta
PLCG2	Phospholipase Cgamma2
PRDM1	PR/SET Domain 1
PSA	Prostate Specific Antigen
PSMB5	Proteasome 20S Subunit Beta 5
PTEN	Phosphatase and tensin homolog
PTPN11	Protein Tyrosine Phosphatase Non-Receptor Type 11
PVDF	Polyvinylidene fluoride
R/R MCL	Relapsed-Refractory Mantle Cell Lymphoma
RAG 1/ 2	Recombination-activating gene 1/ 2
Rb	Retinoblastoma
ROS	Reactive oxygen species
RRMM	Relapsed-Refractory Multiple Myeloma
SAPK	Stress-activated protein kinases
SCF complex	Skp, Cullin, F-box containing complex
scRNA-seq	Single-cell RNA sequencing
SEER	Surveillance, Epidemiology, and End Results Program
SH2/ 3	Src Homology 2/ 3
SLAMF7	Signaling lymphocytic activation molecule Family Member 7
SOD	Superoxide dismutase type 1
SOX11	Sex-determining region Y protein Box Transcription Factor 11
SP	Side Population
SP140	Speckled Protein 140

STAT3	Signal Transducer and Activator of Transcription 3
SYK	Spleen Associated Tyrosine Kinase
TME	Tumor microenvironment
TNF- $\alpha$	Tumour Necrosis Factor alpha
TNM	Tumor, Node, Metastasis
TRAF 2/ 3	TNF receptor-associated factor 2/ 3
TRAIL	TNF-related apoptosis-inducing ligand
t-SNE	t-distributed stochastic neighbor embedding
TTP	Time to progression
UPR	Unfolded protein response
UTR	Untranslated region
VEGF	Vascular endothelial growth factors
VLA-4	Very late antigen 4
XPO1	Exportin 1
ZNGHX4	zinc finger homeobox 4

# **CHAPTER 1**

## ***Review of Literature: Drug Resistance in Cancer***

## 1.1 Cancer

Cancer is a group of diseases characterized by the uncontrolled proliferation of abnormal cells in the body that arises due to the malignant transformation of normal cells and may remain localized in a particular tissue or organ or can spread to the other part of the body (metastasis).<sup>1,2</sup>

### 1.1.1 Statistics

Cancer is the second leading cause of death in the US after cardiac disease, with estimated 1,918,030 new cancer cases (~ 439 people per 100,000 people) and 609,360 deaths (~ 146 people per 100,000 people) reported in 2022.<sup>3-5</sup>

**Figure 1A: Estimated new cancer cases in the US, in 2022**

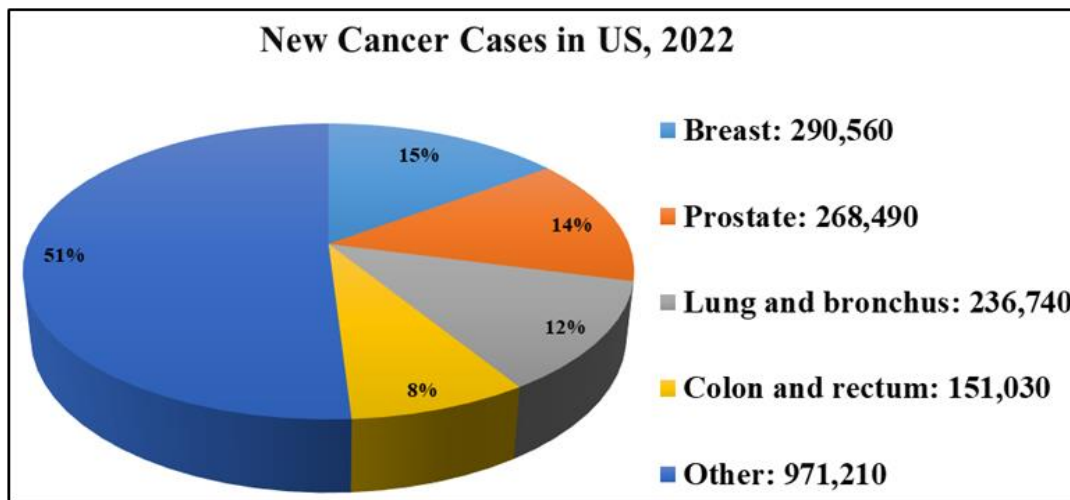
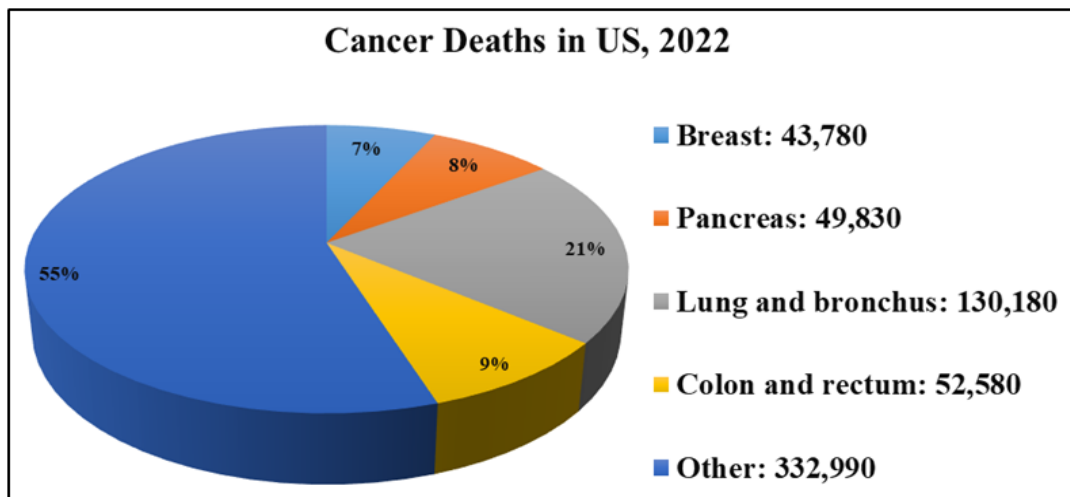


**Figure 1B: Estimated cancer-related deaths incidence in the US, in 2022**



Globally, cancer is the second most common cause of death after cardiovascular disease, with an estimated reported 19.3 million new cases and 10 million cancer deaths in 2020.<sup>6-8</sup>

**Figure 2A: Estimated new cancer cases globally in 2020**

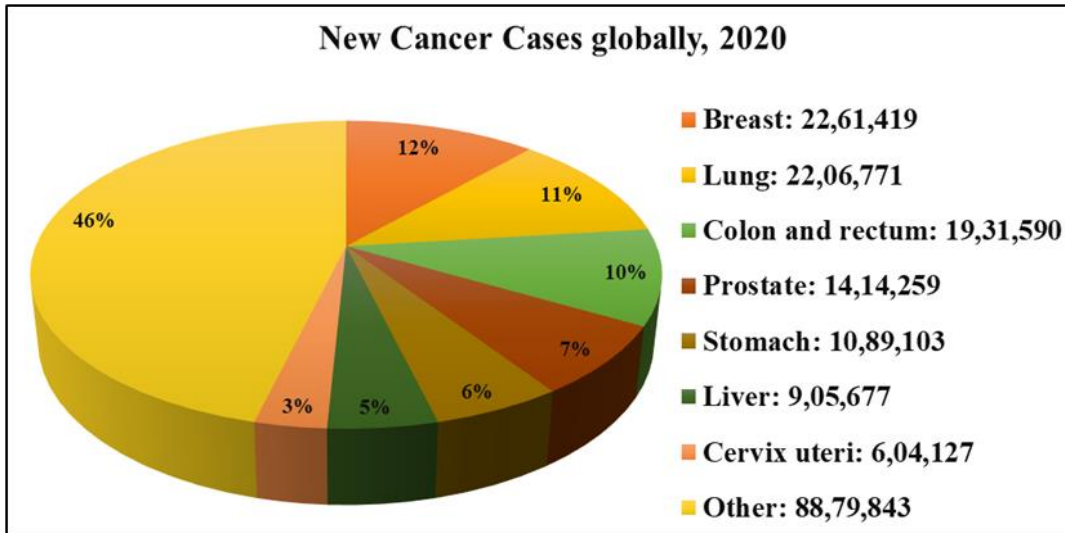
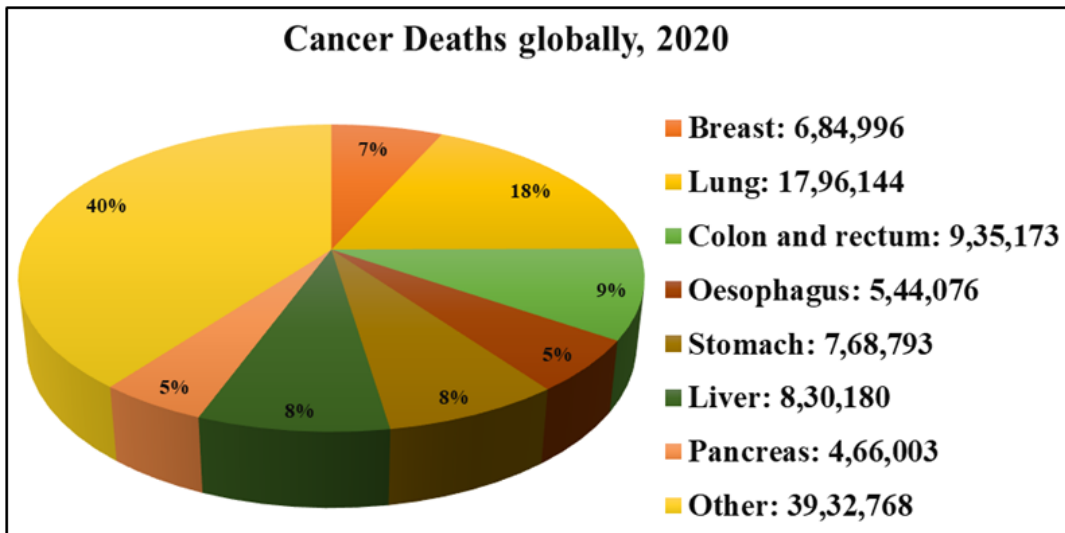


**Figure 2B: Estimated cancer-related deaths incidence globally in 2020**



## 1.1.2 Molecular Mechanism of Cancer Development

- i. Sustaining Proliferative Signaling:** Cells require growth factor signals through the surface receptor (e.g., Epidermal growth factor (EGF)/ Epidermal growth factor receptor (EGFR) they express, which then activate the intracellular signaling cascades and promote cell growth and division.<sup>1,9,10</sup> In normal cells, this process happens in a coordinated manner through a feedback mechanism.<sup>10</sup> But cancer cells acquire the ability to grow and divide even without external growth signals, leading to the uncontrolled proliferation of the cells and the formation of mass or tumor.<sup>10-12</sup> It happens due to the mutation in the receptor genes that leads to the constitutive activation of the signaling pathways that promote cell proliferation, such as Akt, MAPK/ERK, and mTOR.<sup>9,13,14</sup>
- ii. Evading Growth Suppressors:** The cell cycle that leads the cell division is a tightly regulated event controlled through several signaling pathways and checkpoints that prevent the division of cells with damaged DNA and induce senescence or apoptosis.<sup>11,15,16</sup> Cyclin and Cyclin-dependent kinases (CDKs) are the regulatory proteins that control the checkpoint for the next phase of the cell cycle. Anti-growth factors such as TP53, phosphatase and tensin homolog (PTEN), and Retinoblastoma protein (Rb) are the proteins that inhibit cell growth to ensure cell division doesn't continue unchecked.<sup>17-19</sup> However, in cancer cells, this regulatory mechanism gets disrupted as the expressions of these anti-growth factors get suppressed due to loss-of-function mutation or deletion of the gene, and cancer cells stop responding to the growth-inhibitory signals from the growth suppressors.<sup>1,20,21</sup>
- iii. Activating Invasion and Metastasis:** Cancer cells spread to the tissues and organs beyond their site of origin and form new tumors (secondary and tertiary sites). This process, known as metastasis, involves invasion, intravasation, and extravasation.<sup>1,22-24</sup> Invasion is where the cancer cells detach from the original site, extend to the adjacent tissues, and penetrate that space by breaching the extracellular matrix (ECM).<sup>23-25</sup> In this step, the tumor cell undergoes epithelial to mesenchymal transition (EMT) by down-regulating epithelial proteins such as E-cadherin, an upregulation of mesenchymal proteins such as N-cadherin and vimentin, which causes loss of polarity and enable them to migrate freely.<sup>22,24,26,27</sup> This is followed by intravasation, where the cancer cells migrate through the blood vessels to the new site. The cancer cells integrate with the new site's tissues in the metastasis phase.<sup>23,28</sup> This step involves

the Mesenchymal to Epithelial transition (MET), where the cells revert to epithelial cells and form tumors.<sup>29,30</sup>

**iv. Enabling replicative mortality:** Normal cells have limited replicative potential, which means they can grow and divide only a limited number of times, after which they undergo programmed cell death or apoptosis.<sup>1,31</sup> On the other hand, cancer cells acquire genetic mutations that enable them to replicate for an indefinite number of times and evade apoptotic signals.<sup>1,32</sup> The probable mechanism involves maintaining the telomere's length by increasing the telomerase's expression through up-regulation of oncoproteins and de-differentiated to the stem-like phenotype in response to the signaling pathway such as Hippo and Wnt/ $\beta$ -Catenin which are found to be frequently over-expressed in cancer cells.<sup>1,31,33-35</sup>

**v. Inducing angiogenesis:** Angiogenesis refers to the formation of new blood vessels from pre-existing blood vessels.<sup>35,36</sup> Hypoxic core of the tumor mass leads to the stabilized expression of hypoxia-inducible factor-1 (HIF-1), which is a transcription factor and induces the expression of cytokines such as vascular endothelial growth factor (VEGF), fibroblast growth factor (bFGF), or platelet-derived growth factor (PDGF) which are found to be over-expressed in cancer cells.<sup>37,38</sup> They stimulate endothelial cells to promote angiogenesis which plays an essential role in tumor growth.<sup>39</sup> In normal cells, angiogenesis is a tightly regulated process.<sup>40</sup> On the other hand, tumor cells remain dormant or benign if they don't receive an adequate supply of blood and nutrients. Activation of the angiogenic switch, which is the imbalance between stimulatory and inhibitory factors, promotes new blood and lymphatic vessel formation. This vascular network allows the adequate supply of nutrients and oxygen as well as the removal of metabolic waste, which leads to the sustained growth of the tumor cells.<sup>40,41</sup>

**vi. Resisting cell death:** Normal cells have limited replicative potential, after which they undergo programmed cell death known as apoptosis which causes nuclear condensation, cellular shrinkage, and ultimately, the formation of apoptotic bodies.<sup>1,42</sup> Apoptosis is mediated by two factors: regulators present on the cell surface and receive death stimuli (in case of the extrinsic pathway of apoptosis), and effectors such as Caspase-3, caspase-6, and caspase-7 that execute the action of apoptosis.<sup>42,43</sup> In the intrinsic pathway of apoptosis, the balance between pro-apoptotic (Bax, Bad, Bik, Bim, Bid, etc.) and anti-apoptotic (Bcl-2, Bcl-xL, Mcl-1) Bcl-2 family of proteins is critical to determine the cells' fate.<sup>44,45</sup> In normal cells, following

cytotoxic or genotoxic stress (such as DNA damage), the apoptotic pathway gets activated, which leads to cell death.<sup>46</sup> But in cancer cells, the hypoxic stress, genomic instability, and oncogenic stress fail to trigger the apoptotic pathway due to defects in the DNA damage sensing mechanism or alteration in the proteins involved in apoptosis.<sup>47,48</sup> Cancer cells are characterized by over-expression of the anti-apoptotic proteins and down-regulation of pro-apoptotic proteins that prevent the induction of apoptotic events.<sup>44,45,49</sup> Apart from that, reduced expression of p53 due to loss-of-function mutation and deletion, which functions as an apoptosis gatekeeper by regulating the cellular response to DNA damage and other genomic aberrations, also leads to the inhibition of apoptosis.<sup>50,51</sup>

### **1.1.3 Treatment<sup>52-54</sup>**

- 1. Surgery**
- 2. Radiation therapy**
- 3. Chemotherapy:** Alkylating agents, Antimetabolites, Anti-tumor antibiotics, Topoisomerase inhibitors, Mitotic inhibitors, Plant alkaloids, Corticosteroids
- 4. Immunotherapy:** CAR-T therapy, monoclonal antibodies (mAbs), immune checkpoint inhibitors, immunomodulatory drugs
- 5. Hormone therapy:** Aromatase inhibitors, androgen deprivation therapy, androgen blockers, antiestrogens, LHRH agonists
- 6. Targeted drug therapy:** Proteasome inhibitors, Bruton Tyrosine Kinase Inhibitors
- 7. Bone marrow transplant**

## 1.2 Drug Resistance in Cancer

### 1.2.1 Drug resistance in cancer is responsible for recurrence or relapse

Despite significant advancements and clinical success achieved by the classical chemotherapeutic drugs and novel targeted drugs, resistance against them remains the major impediment in cancer therapies.<sup>55-57</sup> Drug resistance in cancer patients poses a significant clinical challenge to the clinical success of the treatment regimen, where it accounts for almost 90% of the cases of morbidities due to treatment failure and clinical progression.<sup>56,58</sup>

**Table 1. Recurrence Statistics of Different Cancers**

Cancer Type	Recurrence Rate
Bladder <sup>59</sup>	50% after cystectomy
Breast <sup>60,61</sup>	30% overall 5% to 9% with letrozole or placebo during a median of 10.6 years
Colorectal <sup>62</sup>	17% after curative surgical resection with microscopically clear margins
Glioblastoma <sup>63</sup>	Nearly 100%
Head and neck, stage IV <sup>64</sup>	After intensified, split-course, hyper-fractionated multiagent chemoradiotherapy: 17%, locoregional 22% distant
Hodgkin lymphoma <sup>65,66</sup>	10% to 13% after primary treatment 20% to 50% after second-line treatment
Lymphoma, DLBCL <sup>67</sup>	30% to 40%
Lymphoma, PTCL <sup>68</sup>	75%
Melanoma <sup>69</sup>	15% to 41%, depending on the stage 87%, metastatic disease
NSCLC <sup>70,71</sup>	26% after curative surgery 27% after chemoradiotherapy for locally advanced disease
Osteosarcoma <sup>72</sup>	11%-12% local recurrence 5%-45% metastasis
Ovarian <sup>73</sup>	85%
Pancreas <sup>74,75</sup>	36% within 1 year after curative surgery 38% local recurrence after adjuvant chemotherapy 46% distant metastasis after adjuvant chemotherapy
Prostate <sup>76</sup>	After prostatectomy at 10 years:

	<p>24% low-risk disease</p> <p>40% intermediate-risk disease</p> <p>48% of high-risk disease</p>
Soft tissue sarcoma <sup>77</sup>	<p>50% after adjuvant chemotherapy</p> <p>Nearly 100% of advanced disease</p>

Cancer drug resistance is a multi-faceted phenomenon that renders the cancer cells insensitive to pharmaceutical perturbations that ultimately cause therapy failure and cancer relapse.<sup>55</sup> Cancer cells can evade the cytotoxic effects of the drug by its intrinsic and/or acquired ability and regrow the tumor, which is referred to as a relapse.<sup>78</sup> The significant drivers behind this phenomenon are alteration of the drug target and the downstream signaling pathway (for e.g., point mutation, chromosomal translocation), the enhanced expression level of drug efflux molecules such as transmembrane transporters (ABC transporter superfamily), reduction in intracellular drug accumulation, over-activation of the DNA damage repair pathway, inhibition of the apoptotic pathway, Intra-tumoral heterogeneity such as genetic, temporal, metabolic and spatial (distribution of cancer cells, stromal cells, and immune cells), the chemoprotective effect of tumor microenvironment.<sup>55,56,79</sup>

### 1.2.2 Types of cancer drug resistance

There are two different mechanisms cancer cells become resistant to chemotherapy: Innate resistance and Emerging/ acquired resistance.<sup>57,80</sup>

**i. Innate resistance:** Innate resistance is the resistance that is already present in the patient even before the first exposure to the drug and reduces its clinical efficacy.<sup>56,57</sup> This type of resistance may develop due to the presence of a small subpopulation of cells that are insensitive to the standard-of-care treatment due to the presence of the genetic mutation.<sup>78,81</sup>

**ii. Acquired resistance:** Acquired or Emerging resistance is the type of resistance that develops after the initial exposure to the drug or over the course of the treatment, which gradually reduces its clinical efficacy.<sup>78,80,82</sup> Activation of alternative pathways such as the genetic mutation that alters the drug target or its activation level, activation of the secondary proto-oncogenes, driver mutation expression, interaction with the tumor microenvironment such as bone marrow stromal cells, immune cells (NK cells, macrophages), the dominance of resistant sub-clones is the major reasons behind the emergence of this type of resistance.<sup>78,81-84</sup>

### 1.2.3 Driving factors behind drug resistance in cancer

**a. Intra-tumoral heterogeneity:** Intra-tumoral heterogeneity refers to the presence of distinct subpopulations of cancer cells with different molecular and histopathological profiles within a single tumor specimen.<sup>85,86</sup> This plays a significant role in therapeutic resistance and treatment failure, leading to relapse and disease progression with poor progression-free and overall survival.<sup>86,87</sup> The mosaic nature contributes to the spatial variation in drug sensitivity due to the different expression levels of target molecules through clonal evolution, and intra-tumor heterogeneity due to the presence of treatment-refractory subpopulations or cancer stem-like cells leads towards drug resistance and disease relapse.<sup>88-90</sup> Single-cell RNA sequencing is an effective approach to capturing this cellular landscape.<sup>90</sup>

**b. Tumor microenvironment (TME):** The tumor microenvironment is the complex and dynamic ecosystem that is present around the tumor cells within the body.<sup>91,92</sup> In addition to the tumor cells, the component of TME includes extra-cellular matrix/ ECM (collagen, fibronectin, hyaluronan, laminin), stromal cells (fibroblasts, endothelial cells), immune cells (microglia, macrophages, dendritic cells, NK cells, lymphocytes).<sup>93,94</sup> Cross-talk between TME and the malignant cells promotes tumor growth, invasion, and metastasis with poor clinical outcomes.<sup>91,92</sup> TME interacts with the tumor cells through a complex network that includes i) ECM-mediated cell-cell interaction, ii) interaction through soluble mediators such as cytokines, chemokines, growth factors, matrix modulating enzymes, iii) interactions through vesicles such as circulating tumor cells (CTCs), exosomes, cell-free DNA (cfDNA).<sup>91,94-96</sup> Together, all these factors create a safe environment for the malignant cells to evade the therapy-induced apoptosis and provide further oncogenic cues that ultimately lead to the de novo drug resistance development.

**c. Cancer stem cells:** Cancer stem cells are a small subpopulation of self-renewing cancer cells that function as tumor-initiating cells and drive chemo-resistance, therapy failure, and disease progression.<sup>79,97,98</sup> They have high tumorigenic potentials and are characterized by the over-expression of ATP-binding cassette (ABC) transporters, a family of membrane proteins that serve as the drug-efflux pump to nullify the effect of the drugs.<sup>97-99</sup>

**d. Multidrug resistance (MDR):** Activation of efflux drug transporters such as Classical MDR (P-glycoprotein) and non-Pgp MDR (MRP), which prevents the accumulation of the drug inside the cells by pumping it out.<sup>79</sup>

## **1.3 Types of cancer**

**Cancers are of two types:**

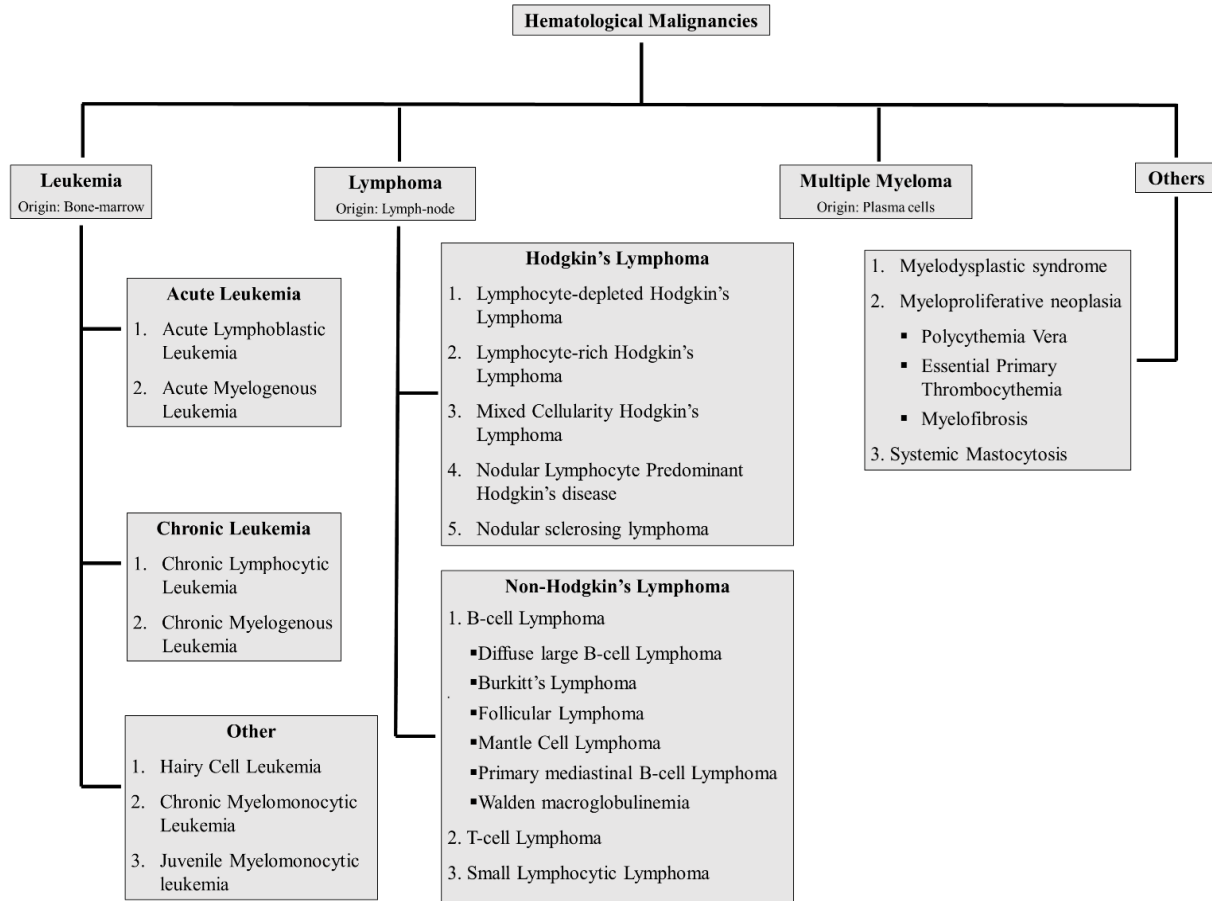
- i. Solid tumor or organ tumor**
- ii. Liquid tumor or blood cancer, or hematological malignancies**

### **1.3.1 Hematological Malignancies**

Hematological malignancy is the neoplastic disease of hematopoietic tissue, such as bone marrow and lymphoid tissue or blood-forming cells (T cells, B cells, and natural killer cells).<sup>100</sup> It accounts for almost 10% of all new cancer cases in the US and nearly 6% globally in 2021, with a total estimated case of >1.2 million and death cases of >700,000 (7% of all cancer deaths).<sup>101,102</sup>

There are four main types of hematological malignancies: Leukemia, Lymphoma, Multiple myeloma, and others that include Myelodysplastic syndromes.<sup>103,104</sup>

**Figure 3. Classification of Hematological Malignancies<sup>105</sup>**

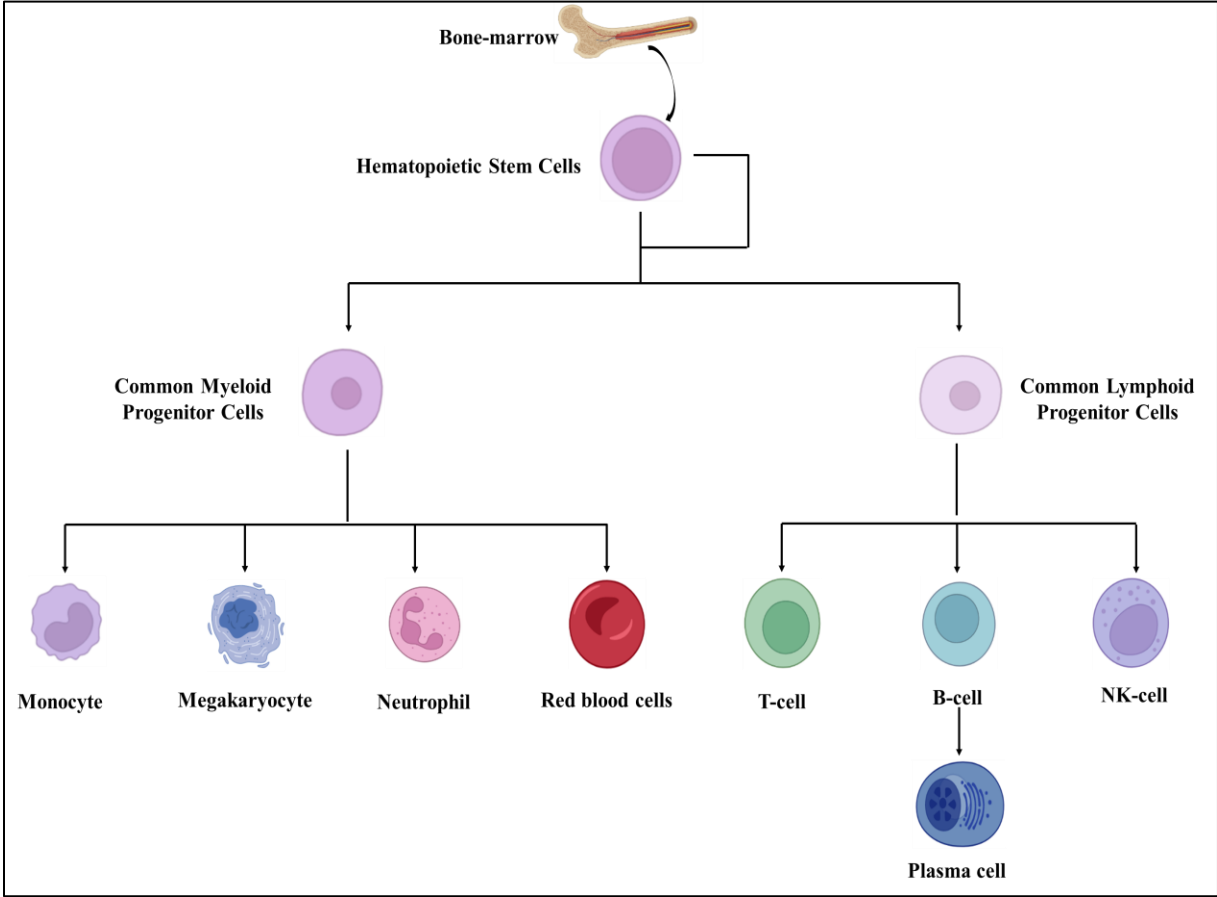


### **1.3.1.1 Hematopoiesis**

Hematopoiesis is the process of the formation of a wide variety of blood cells. Hematopoiesis during the early stages of embryogenesis occurs in the yolk sac and subsequently in the liver.<sup>106</sup> During the 3<sup>rd</sup> to 7<sup>th</sup> month of gestation, it primarily occurs in the spleen and, just before birth, shifts to the marrow cavity.<sup>107,108</sup> In adults, hematopoiesis occurs in the bone marrow, which is the soft, spongy, gelatinous tissue found in the hollow spaces in the medullary cavities (centers) of the bone.<sup>106,108</sup>

This process begins with the pluripotent hematopoietic stem cells (HSCs) in the specialized bone marrow regions called niches. As they divide, they give rise to multipotent HSCs that can become any type of blood cell as regulated by growth factors and other mediators.<sup>106,108,109</sup> HSCs are capable of self-renewal through asymmetric cell division, where some of the daughter cells remain as HSCs to maintain the pool, and the other daughters become progenitor cells.<sup>110</sup> Progenitor cells are the multipotent cells that follow either Lymphoid or Myeloid lineage commitment and differentiate into more specialized or mature blood cells.<sup>106,110</sup> Common lymphoid progenitor cells give rise to lymphocytes (T cell, B cell, NK cells), and common myeloid cells generate monocytes, macrophages, neutrophils, basophils, eosinophils, erythrocytes, and megakaryocytes to platelets.<sup>106</sup>

**Figure 4. Hematopoiesis**



### **1.3.1.2 B-cell malignancies**

B-cell malignancies are a group of cancers and the fifth most common cancers, which include B-cell lymphoma, B-cell leukemia, and plasma cell dyscrasias (Multiple Myeloma).<sup>111</sup> They arise from different stages of B-cell development and differentiation. They are characterized by intra-and inter-patient heterogeneity that dictates the clinical progression of the disease and the treatment outcome.<sup>111</sup> Despite the high number of approved therapies, primary and acquired therapeutic resistance poses significant challenges in managing B-cell malignancies.<sup>111–113</sup> Especially when they progress to the resistant or refractory disease state, they exhibit dismal clinical prognosis and poor survival rates with limited or no therapeutic options.<sup>111,112</sup>

Thus, it demands a continuous expansion of the therapeutic arsenal for the clinical management of B-cell malignancies.

### **1.3.1.3 B-cell development and differentiation**

The B-cell development and maturation process mainly involves the generation of the B-cell receptor (BCR) with a diverse repertoire to fight against a wide array of antigens which is the cornerstone of adaptive immunity.<sup>114–116</sup> This is achieved through V(D)J recombination event, which gives rise to a fully functional antibody that contains two light chains and two heavy chains through the random assembly. Each light chain contains variable (V), joining (J), and constant NAÏVE gene segments, and each heavy chain consists of variable (V), diversity (D), joining (J), and constant NAÏVE gene segments.<sup>114,117</sup> It starts in multipotent progenitor cells, which migrate to the bone marrow and receive the signals (CXCL12) from the bone marrow stromal cells (BMSC) that binds to the chemokine receptor 4 (CXCR4) expressed on its surface.<sup>116</sup> MPP then transformed into (lymphocyte primed multilineage progenitors (LMPP) by expressing FLT-3, which interacts with the FLT-3 ligand present on the BMSC that, in turn, induces the synthesis of IL-7 receptor (IL-7R).<sup>118</sup> LMPP then become Common lymphoid progenitor cells (CLP) committed to the development of cells of B-cell lineage by receiving the signals such as Cytokines (IL-7) that leads to the over-expression of Mcl-1 and c-Myc.<sup>119</sup> In CD34<sup>+</sup> CLP, this cytokine signaling induces the terminal deoxynucleotidyl transferase (TdT) and recombinase activating genes 1 and 2 (RAG-1 & RAG-2) to join the immunoglobulin heavy chain (IgH) to the D-J gene segment (D-JH) and becomes Pre-Pro B-cells. They express CD45 which is a B-cell lineage-specific marker.<sup>114,116,119</sup> This receptor complex also contains the signal

transduction component of BCR: Ig- $\alpha$  (CD79a) and Ig- $\beta$  (CD79b), and the pre-BCR mediated signaling cascade is essential for the development of the B-cell.<sup>120</sup> Upon antigen engagement, Ig  $\alpha$ - Ig  $\beta$  sends the downstream signal through the phosphorylation of the Immunoreceptor Tyrosine Activation Motifs (ITAMs) that reduce the expression of RAG 1/ 2 and form large pre-B cells that are rapidly proliferating in nature.<sup>121</sup> In non-dividing small Pre-B cells, light chain (Ig $\kappa$ / Ig $\lambda$ ) rearrangements (joining of V-J with L chain) occur following re-expression of the RAG 1/ 2, which is also accompanied by the expression of  $\mu$  chain.<sup>114,120</sup> Following this, the light chain and heavy chain combine to express complete IgM BCR on immature B-cell membranes.<sup>114</sup> When these immature naïve B-cells leave the bone marrow, they start expressing IgD on their surface, which helps them to avoid binding with the self-antigen. They are now called mature naïve B-cells, capable of evoking immunogenic response against exposure to the foreign pathogen.<sup>114,122</sup>

This thesis will discuss two types of B-cell malignancies:

- 1) **Multiple Myeloma:** Malignancy of the post-germinal center B-cells or plasma cells.<sup>123</sup>
- 2) **Mantle Cell Lymphoma:** Malignancy of the Pre-germinal B cells.<sup>124</sup>

## **1.4 Multiple Myeloma**

### **1.4.1 What is Multiple Myeloma?**

Multiple Myeloma (MM) is an incurable, age-dependent, post-germinal center-derived B cells or plasma cells neoplasm characterized by abnormal monoclonal proliferation and accumulation of malignant clones within the bone marrow, crowding out the normal, healthy plasma cells.<sup>125,126</sup>

The terminally differentiated clonal plasma cells or B cells usually protect our body against foreign pathogens by producing antibodies. But, when they become malignant, the clonally expanded plasma cells secrete an excess amount of a specific isotype of monoclonal protein (M-protein or para-protein or M-spike) such as heavy chain (IgG/IgA/IgD) or light chain (kappa/lambda) immunoglobulin which is non-functional and may result in poor immunity, renal failure, hypercalcemia, over-thickening of the blood, bone lesions, thrombocytopenia, and anemia.<sup>127</sup>

### **1.4.2 Statistics**

This is the second most prevalent hematological malignancy (10%), with 34,470 estimated new cases (1.8% of all new cases) & 12,640 estimated deaths (2.1% of all cancer deaths) in the USA in 2022. The typical survival without treatment is seven months, while with current therapies, it is 4-5 years, with a 5-year survival rate of 57.9%. The lifetime risk of getting myeloma is 1 in 132 (0.76%).<sup>128,129</sup>

### **1.4.3 Symptoms and Diagnosis**

Common symptoms of Multiple myeloma are termed CRAB, which stands for C = Calcium (elevated) – hypercalcemia, R = Renal failure, A = Anemia, and B = Bone lesions.<sup>127</sup>

### **1.4.4 Diagnostic tests for Multiple Myeloma**

- a) Complete blood count test
- b) Blood chemistry tests: Creatinine, Albumin, Calcium levels, lactic dehydrogenase (LDH), immunoglobulins level (IgA, IgD, IgE, IgG, and IgM)

- c) Electrophoresis to detect abnormal monoclonal antibody/ M-spike/ paraprotein and light chain of antibody/ Bence Jones protein in serum and urine, respectively.
- d) Bone marrow biopsy: Immunohistochemistry, Flow cytometry, Cytogenetics, Fluorescent in situ hybridization (FISH)

### 1.4.5 Current Treatment Strategies

- a. Radiation Therapy:** Targeting cancer cells with high-energy X-rays or proton beam is a treatment option for the localized disease state.
- b. Immunotherapy:** Immunotherapy stimulates the body's own system to recognize and attack the malignant cells, which otherwise evade the immune attack by producing certain proteins.<sup>130</sup> Example of such a drug is Teclistamab (Tecvayli) which is a Bispecific T cell engager (BiTE); one part of this is attached to the T-cells, whereas the other part binds the BCMA protein on myeloma cells which then stimulates the T-cells to attack the myeloma cells.<sup>131</sup>

Monoclonal antibodies (mAbs) such as Daratumumab (Darzalex) are another type of immunotherapy where they bind with the CD38, a transmembrane glycoprotein highly expressed in myeloma cells, and induce apoptosis via antibody-dependent cellular cytotoxicity (ADCC), complement-dependent cytotoxicity (CDC).<sup>132</sup>

Elotuzumab (Empliciti) is another mAb that attaches to Signaling lymphocytic activation molecule F7 (SLAMF7), a cell surface glycoprotein expressed in myeloma cells and activates NK cells mediated myeloma cell killing and antibody-dependent cellular cytotoxicity (ADCC).<sup>133</sup>

- c. Chemotherapy:** Cyclophosphamide (Cytoxan), Etoposide (VP-16), Doxorubicin (Adriamycin), Liposomal doxorubicin (Doxil), Melphalan, Bendamustine (Treanda).
- d. Steroids:** Corticosteroids, such as dexamethasone and prednisone, reduce inflammation by inhibiting pro-inflammatory cytokines (IL-6) and nuclear factor kappa B (NF-κB). They also modulate the immune cells to fight against cancer cells.

### **1.4.6 Relapsed Refractory MM (RRMM)**

According to the International Myeloma Working Group (IMWG) guidelines, Relapsed and Refractory Multiple Myeloma is defined as the disease state that shows clinical signs (increase in M-protein level, one or more CRAB symptoms) of recurrence after initial response and becomes unresponsive or shows clinical progression while on treatment or within 60 days of most recent treatment where patient showed at least minimal response.<sup>134,135</sup>

### **1.4.7 Mutational landscape of RRMM**

MM is a highly heterogeneous disease at the cytogenetic and molecular levels. There is multi-step genetic (somatic mutations, quantitative and qualitative chromosomal aberrations), epigenetic and micro-environmental transformation involved behind the development and progression from normal plasma cells to monoclonal gammopathy of undetermined significance (MGUS), Smoldering MM, symptomatic MM and aggressive extra-medullary disease including plasma cell leukemia.<sup>136,137</sup> There are at least 12 different molecular sub-types of multiple myeloma with unique clinical and pathological features and varying degrees of response toward the treatment.<sup>138,139</sup> Lack of identifiable universal driver mutation, intra-patient & inter-patient heterogeneity at the clonal and sub-clonal level associated with disease progression increase its complexity. Due to the heterogeneous nature of this disease, standard therapeutic strategy yields variable response and treatment outcome that is observed across patient populations. Rather than using a ‘one size fits all’ approach, pharmacogenomics-guided precision medicine holds great potential to increase therapeutic efficacy and reduce side effects by pairing the right patients with the right medications based on their genetic architecture. Somatic mutations, which affect the cellular function of many genes involved in many critical molecular pathways, have been shown to be a driving factor behind the development of Multiple myeloma and significantly influence the treatment outcome and survival of the patients.<sup>140,141</sup> Molecular profiling of the individual MM patients by the high throughput omics technology like next generation sequencing enable the clinicians to identify somatic mutations associated with clinical and prognostic features like drug response, drug resistance, drug toxicity, overall survival, and progression-free survival. This is particularly useful in identifying the actionable mutations in individual patients and designing the treatment strategy accordingly to correct the abnormal gene functions to improve the therapeutic efficacy and quality of life.

### 1.4.8 Mutation profile of RRMM

Various studies have reported that mutational profile has a strong influence on the treatment outcome of multiple myeloma (Table 2).<sup>142</sup>

The frequency of mutation in genes involved in the RAS/RAF pathway is very high, especially in newly diagnosed MM. Patients harboring RAS mutations have higher  $\beta 2$  micro-globulin levels and are characterized by enhanced activation of the MAPK pathway, shorter survival, and aggressive phenotype, as compared to the wild type of RAS patients but phase III Myeloma XI trial didn't find any correlation between RAS mutation and adverse outcome.<sup>143,144</sup>

Mutation in codons 12, 13, and 61 of KRAS and NRAS has been reported. The low abundance of RAS mutation in MGUS as compared to MM indicates that RAS mutation is an essential factor behind the transformation from MGUS to MM.<sup>143</sup>

N-RAS is highly mutated in RRMM. In single-agent Bortezomib-treated patients but not in high-dose dexamethasone-treated patients, N-RAS mutation is associated with reduced drug sensitivity, shorter TTP, higher chances of relapse, lower response rate, and progression-free survival. K-RAS mutated patients have shown poor survival. KRAS<sup>G12D</sup> mutation is associated with ERK activation.<sup>143-145</sup>

MEK inhibitor Trametinib has shown moderate response overall with few cases of remissions) and has shown to be effective in overcoming paradoxical activation of the MAPK pathway. The Arkansas group, in a retrospective study, has demonstrated that in patients harboring both RAS and RAF mutation, combination therapy of B-RAF inhibitor and MEK inhibitor could enhance the partial response rate.<sup>146</sup>

BRAF<sup>V600E</sup> mutation constitutively activates the MEK-ERK pathway. Studies have reported that BRAF mutation in MM is characterized by aggressiveness, extramedullary disease, shorter Progression-free survival (PFS), and Overall survival (OS).<sup>146</sup> Dabrafenib and Vemurafenib have shown anti-tumor activity in B-RAF mutated cells where they block the kinase activity of BRAF. Inactivating BRAF mutations such as BRAF<sup>D594N</sup> may activate MEK-ERK signaling by heterodimerization with C-RAF. In mutated BRAF<sup>V600E</sup> cells, NRAS mutations (NRAS<sup>G12A</sup>) have been shown to confer resistance to vemurafenib, which is a major concern for using B-RAF inhibitors as monotherapy since MM patients may harbor sub-clonal RAS mutation in BRAF

mutated tumor.<sup>143,144,146</sup> A recent case study has depicted this scenario where a proteasome inhibitor was used to overcome Vemurafenib resistance.<sup>147</sup> Thus, combination therapy is ideal for patients with mutational heterogeneity at the sub-clonal level.

Del(17p) mutated cells have shown enhanced sensitivity towards Panobinostat and BCL2/ BCL-xL inhibitor Navitoclax, but BCL2 inhibitor Venetoclax has fewer effects on them.<sup>148</sup> This observation is useful in determining the treatment regimen for the relapsed del(17p) patients. Venetoclax has shown to be effective in combination with bortezomib and dexamethasone, where it achieved a significantly improved overall response rate in all groups. Venetoclax treatment increases progression-free survival and overall response rate in patients with high BCL2 expression in t (11;14) mutated patients. Combination therapy with Venetoclax and dexamethasone has yielded positive results in t (11;14) and del17p.<sup>145,149</sup>

Although FGFR3 and MMSET over-expression is observed in t (4;14) mutated cells, the cells didn't show significant sensitivity towards FGFR inhibitors.<sup>145,149</sup> Instead, Histone demethylase inhibitor GSK-4j showed potential therapeutic efficacy by inhibiting the demethylation on lysine 27 trimethylation on histone H3 (H3K27me3) by JMJD3/ KDM6B.<sup>150,151</sup> t (4;14) cells also showed sensitivity towards Pomalidomide, Linsitinib, dual PI3K-mTOR inhibitors but not towards Navitoclax.<sup>151</sup> An activating p.Arg248Cys mutation and an activating read-through stop lost mutation \*809Cys46 have been identified in MM patients. K650E, G384D, and Y377C are the activating mutations in FGFR3 that confers resistance against anti-FGFR3 antibody PRO-011 in MM cell lines. A recent study has shown that dexamethasone could sensitize NRAS-mutant cell lines to FGFR3 inhibition by FGFR3 inhibitor, BIBF 1000.<sup>150,152</sup> FGFR-specific tyrosine kinase inhibitor SU5402 has demonstrated sensitivity in FGFR3 activating mutation carrying cells and resistance in cells with no FGFR3 expression.<sup>150</sup>

Mutations in Epigenetic modifier IDH do not affect PFS but significantly reduce OS.<sup>142,145</sup>

p. Arg132His is an activating mutation found in 1 MM patients and provides a druggable site, which is vital in MM therapy. AG-120 and AG-221 are the drugs under clinical trial for treating patients with IDH-1 and IDH-2 activating mutations.<sup>149</sup>

TP53 gene is recurrently mutated in MM and is significantly associated with shorter relapse-free survival and high-risk patient cohort. A patient harboring 7181C>T (S2394L) ATM mutation

has shown poor response toward melphalan and died after six months of diagnosis. IVS-1G/C-mutation is a splice site mutation associated with poor treatment outcomes.<sup>142,145,153</sup>

CCND1 is significantly mutated in the t (11;14) subgroup, where it is associated with lowered OS and poor prognostic value. Up-regulated expression of CCND1 due to juxtaposition with IGH enhancer can be inhibited by CDK4/6 inhibitor Palbociclib is an attractive therapeutic approach in MM.<sup>145,154</sup>

Mutation in CRBN is linked with Immunomodulatory Drug (IMiD) resistance like p.Asn316Lys carrying patients are unresponsive to IMiD therapy. CUL4B mutation is also associated with IMiD resistance. DDB1 mutation (Ala971Asp) affects its binding with CUL4A, thus impairing its function, which leads to IMiD and steroid resistance.<sup>153</sup>

Mutation in PTPN11/SHP-2 at Gly503Arg, a gene associated with drug resistance in cancer, leads to the activation of the MAPK pathway. A potent and selective inhibitor GS-493 is in a preclinical trial.<sup>153</sup>

A tumor suppressor gene SP140 has been found to be frequently mutated in Multiple myeloma, which has a significant effect on the MM prognosis. Inactivating mutations (2 frameshifts, one nonsense, one splice site, and one missense) in this top driver gene have been reported to be associated with an increased risk of relapse. The role of two truncating mutations, p.Arg576\* and p.Glu75\*, and one missense mutation, p.Glu856Ly are yet to be known. PRDM1 is another highly mutated gene found in myeloma patients. Mutation in this gene has been associated with favorable outcomes.<sup>140,145,154</sup>

#### **1.4.9 Multiple Myeloma Mutation Panel (M3P) panel**

Targeted sequencing of untreated and multi-drug refractory patients (treated with IMiD, Proteasome Inhibitors) using M3P, which consists of genes known to be frequently mutated in MM, genes which are associated with therapy and its outcomes revealed that MEK-ERK pathway, NF-kB pathway, and Cyclin D pathway are the most frequently mutated pathway in MM. Mutations in genes involved in CCND1 and DNA repair pathways like TP53, ATM, ATR, and ZNFHX4 have a negative impact on survival, but IRF4 and EGR1 mutations favor OS.<sup>155,156</sup>

The top 10 recurrently detected non-synonymous mutations were KRASQ61H, NRASQ61R, NRASQ61K, BRAFV600E, KRASG12D/G12V, NRASG13D, NRASG13R/Q61H and

KRASG12A. In addition, the study has found a total of 10 patients carrying eight individual types of BRAFnon-V600E mutations within the kinase domain (CR3), including previously reported inactivating mutations G466V (n=1), G469E (1), D594A (1), D594G (2) and D594N (2), as well as activating mutations G469R (1), K601E (1); and one mutation with unknown function N581I.<sup>155,156</sup>

**Table 2. Clinically relevant mutations observed in RRMM patients<sup>155–157</sup>**

<b>Gene</b>	<b>Mutation</b>	<b>Clinical Significance</b>
K-RAS	KRASQ61H, KRASG12A, KRASG12D/G12V	high-risk MM, including del17p, has less frequency and relatively more in relapsed MM.
N-RAS	NRASQ61R, NRASQ61K NRASG13D, NRASG13R/Q61H	high-risk MM, including del17p, has less frequency and relatively more in relapsed MM
B-RAF	V600E Gly466Val	Activating mutation, druggable site Paradoxically activate MAPK pathway via C-RAF
TP-53	Lys132Asn Met237Ile	Associated with impaired event-free survival & overall survival (OS) in non-del cohorts
DIS3	Arg418Gly Arg780Thr	Exclusively present in t (4;14) & t (11;14) patients Causes significant aberration in exoribonucleolytic activity
FAM46C	Ile276Thr	
IRF4	Lys89Asn Lys123Arg Gly43Ser	Len refractory Responsive to the dose-adapted treatment of Len & Dexamethasone Affecting the CRBN pathway; Associated with IMiD resistance
CRBN	Asn316Lys Ile393Metfs*10 Asn316Lys	Len refractory Impaired CRBN-IMiD binding IMiD resistance
IKZF3	Gly191Arg	Len resistant
XPB1	Glu99Lys	Bz refractory
NR3C1	Lys772Asn	Steroid Drug resistance
CUL4B	Asp426Gly	Affecting the CRBN pathway; Associated with IMiD resistance
DDB1	Ala971Asp	Affecting the CRBN pathway; Associated with IMiD resistance
FGFR3	Arg248Cys *809Cys	Activating mutation Activating read-through stops lost mutation
IDH1	Arg132His	Activating mutation; druggable target
RASA2		Activates MAPK pathway
PTPN11	Gly503Arg	Acquired resistance to targeted therapy

### **1.4.10 RRMM treatment**

FDA-approved therapy for RRMM includes proteasome inhibitors (PI) such as Velcade (Bortezomib), Kyprolis (Carfilzomib), and Ninlaro (Ixazomib); Immunomodulatory drugs such as thalidomide, lenalidomide, and pomalidomide.<sup>158</sup>

### **1.4.11 Proteasome Inhibitor (PI)**

Proteasome inhibitors are the class of drug that inhibits the activity of the enzyme complexes called proteasomes, thereby preventing ubiquitin-proteasome pathway-mediated degradation of the protein.<sup>159,160</sup> The proteasomal system, present in both normal and cancer cells, is a proteolytic pathway for intracellular protein degradation to control cellular protein turnover.<sup>161,162</sup> It plays a pivotal role in maintaining cellular homeostasis by breaking down damaged and unwanted proteins as well as undamaged proteins marked with a poly-ubiquitin chain to small peptides, which is critical for proper cellular functioning.<sup>161,162</sup> Aberrant proteasome-dependent proteolysis of essential pro-apoptotic and cell-cycle regulatory proteins such as p53, p21, and p27, as well as activation of the oncogenic signaling pathway nuclear factor kappa-B (NF- $\kappa$ B) by proteasome-mediated degradation of its inhibitor I $\kappa$ B, has been observed in many cancers.<sup>161,162</sup> Proteasome inhibitor induces unfolded protein response (UPR) by blocking the degradation of the misfolded proteins and activating the ER stress.<sup>159,160</sup> Prolonged ER stress leads to programmed cell death by activating PERK/eIF2 $\alpha$ /CHOP signaling, IRE1 $\alpha$  signaling, and caspase pathway.<sup>159</sup>

#### **1.4.11.1 FDA-Approved Proteasome Inhibitor (PI) for RRMM management**

**Bortezomib:** Bortezomib/ Velcade is a first-in-class proteasome inhibitor. It is a dipeptide boronic acid derivative approved initially for the treatment of multiple myeloma. It has been approved by the FDA for the treatment of R/R MCL based on the data obtained from results of the landmark PINNACLE trial where single agent Bortezomib treatment provided an extended period of durable and complete drug response as measured by a median duration of response (DOR), Median time to progression (TTP) and Median time to next therapy (TTNT) which were 9.2 months, 12.4 months, 14.3 months respectively in responding patients. It was also associated with remarkable survival in patients with relapsed or refractory MCL as measured by overall survival (OS), which was 35.4 months.<sup>163</sup>

### **Mechanism of Action of Bortezomib**

Bortezomib specifically inhibits the ATP-independent chymotryptic activity of the 26S proteasome through reversible binding to the  $\beta$ 5-subunit (PSMB5) of the 20S multi-catalytic protease core.<sup>159</sup> Bortezomib has thus been shown to interfere with tumor metastasis and angiogenesis by accelerating unfolded protein response (UPR) - ubiquitin-dependent proteolysis of critical regulatory proteins involved in key physiological and pathophysiological cellular processes in cancer cells.<sup>161</sup> That leads to the disruption of cellular homeostasis, which ultimately activates the apoptosis pathway.<sup>161</sup> Bortezomib also inhibits proteasome-mediated degradation of key pro-apoptotic proteins, which eventually leads to the cell cycle arrest during the G<sub>2</sub>-M phase and interferes with the NF- $\kappa$ B-enabled regulation of cell adhesion-mediated drug resistance by preventing uncontrolled degradation of I $\kappa$ B- an inhibitor of NF- $\kappa$ B.<sup>159,160</sup>

### **Molecular mechanism of resistance towards Proteasome Inhibitor (PI)**

**a. PSMB5 point mutation:** Amino acid substitution in the S1 binding pocket that recognizes the peptide bond of the substrate in the  $\beta$ 5-subunit encoding gene PSMB5 has been frequently observed in the Bortezomib-resistant cell lines. Substitution of Ala49 with Thr or Val, A50V, C52F, M45V, M45I, C63F, and T21A that are in or near the S1 binding pocket affect Bortezomib binding by constricting the S1 pocket or reducing favorable hydrophobic interactions.<sup>164</sup>

**b. Over-expression of PSMB5:** PSMB5 expression level found to be upregulated in many Bortezomib-resistant cancer cell lines, which is an adaptive compensatory mechanism to retain sufficient chymotrypsin-like proteasomal activity in PSMB5 mutant cells to maintain cellular homeostasis and it's down-regulation restores the Bortezomib sensitivity.<sup>165</sup>

### **1.4.12 Immunomodulatory Drugs (IMiD)**

Immunomodulators are the class of drugs that modify the activity of the immune system in a favorable manner (by increasing immune stimulators such as lymphocytes, macrophages, neutrophils, natural killer/ NK cells, and cytotoxic T lymphocytes/ CTL. and decreasing immune suppressors) to intensify the immune response to threats such as malignant cells and infections.<sup>166</sup>

#### **1.4.12.1 FDA-Approved Immunomodulatory Drugs (IMiD) for RRMM management**

**Lenalidomide:** Lenalidomide/ Revlimid is an orally bioavailable immunomodulatory drug which has been approved by the FDA in 2006 for the treatment of multiple myeloma-based clinical trials where it showed significant clinical benefits in terms of prolonging median time to progression. It is a thalidomide derivative with a potent immunomodulatory effect.<sup>167</sup>

##### **Mechanism of Action of Lenalidomide**

Lenalidomide primarily acts by modulating the substrate specificity of CRL4<sup>CRBN</sup> E3 ubiquitin ligase, composed of damaged DNA-binding protein 1 (DDB1), cullin 4a (CUL4A), and regulator of cullins 1 (ROC1).<sup>168</sup> Lenalidomide binds to CRBN, the substrate adaptor of this cullin-ring ligase complex, and induces the recruitment of the substrates, followed by subsequent ubiquitination-mediated degradation.<sup>168,169</sup> In multiple myeloma (MM), CRBN induces the proteasomal degradation of two essential transcription factors for B-cell differentiation, IKAROS Family Zinc Finger 1 & 3 (IKZF1 & IKZF3).<sup>169</sup> In MM cells, IKZF1 transcriptionally regulates interferon regulatory factor 4 (IRF4), which plays an important role in MYC-mediated oncogenic programs. A proteomic study showed degradation of IKZF1 leads to the down-regulation of IRF-4.<sup>169</sup> On the other hand, IKZF3 transcriptionally represses the expression of proinflammatory cytokine Interleukin-2 (IL-2).<sup>168,170</sup> Degradation of IKZF3 transcriptionally up-regulates the expression of IL-2 as well as IFN- $\gamma$  that in turn, stimulate the proliferation of natural killer (NK) cells and CD3 T cell-mediated activation of CD4<sup>+</sup> T cells (Th1 subset).<sup>169</sup> All these events lead to enhanced NK-cell mediated cellular cytotoxicity and antibody-dependent cellular cytotoxicity (ADCC), which kill the MM cells.<sup>168,169</sup>

##### **Molecular mechanism of resistance towards Immunomodulatory Drugs**

**a. Down-regulation of target protein Cereblon (CRBN):** CRBN is the direct target of the IMiD drugs. CRBN serves as the substrate adapter for the CRL4<sup>CRBN</sup> E3 ubiquitin ligase complex that consists of damaged DNA-binding protein 1 (DDB1), cullin 4a (CUL4A), and regulator of cullins 1 (ROC1); IMiD drug interacts with the CRBN and induces the proteasomal degradation of 2 zinc finger transcription factors Ikaros (IKZF1) and Aiolos (IKZF3). Studies have shown significant down-regulation in the expression of CRBN both at the mRNA and protein level transcriptional, post-transcriptional factors such miRNA, post-translational modifications such as proteasomal degradation by SCF<sup>Fbxo7</sup> ubiquitin ligase due to down-

regulation of CSN9 signalosome complex, can be observed in acquired IMiD resistant MM cells and patients' population. Patients with low CRBN expression levels show poor responses to IMiD therapy with poor survival benefits.<sup>171,172</sup>

**b. Mutation in the genes involved in CRBN–IKZF1–IRF4 axis:** Mutation-mediated alteration in the activities or the functional inactivation of the member of the CRBN–IKZF1–IRF4 axis genes such as IKZF1, IRF4, are observed in both innate and acquired IMiD-resistant MM patients. A152T mutation in IKZF1 alters the Lenalidomide sensitivity. In contrast, the treatment-induced mutation in CRBN (truncating mutation such as pIle393Metfs\*10, p.Pro241Argfs\*10, p.Gln327\* [#12], and splicing acceptor c.551-2T>C; a mutation that alters the IMiD binding domain such as F381C, P411H), the mutation in CUL4B, are observed in acquired IMiD resistant MM patients. IRF4 harbors a truncating mutation that renders it resistant towards Lenalidomide-mediated downregulation.<sup>171–173</sup>

**c. Mutation in other important genes:** Targeted sequencing on the IMiD refractory MM patients revealed activating mutations in the genes involved in RAS oncogenic pathways such as KRAS, NRAS, and BRAF. Deletion mutation (del17P) in the TP53 gene and RASA2 and PTPN11 genes are also observed. Mutations in the latter two genes activate the MAPK pathway that induces IMiD resistance.<sup>173,174</sup>

**d. Increase in cell adhesion:** Lenalidomide induces the activation of Wnt/ $\beta$ -catenin signaling, which promotes the nuclear translocation of  $\beta$ -catenin that causes transcriptional up-regulation of its target gene, CD44. CD44 enhances the interaction between MM cells and the stromal cells that confers cell-adhesion-mediated resistance.<sup>175</sup>

**e. Up-regulation of IL-6/ STAT3 pathway:** Transcriptome study of the Lenalidomide resistant MM cells showed up-regulation of IL-6 and STAT3 expression as compared to Lenalidomide sensitive MM cells. Lenalidomide-induced enhanced autocrine signal from IL-6 leads to the constitutive expression of the STAT3 gene, which initiates a cascade of oncogenic events such as dysregulation of IKZF1/ IKZF3, IRF4, which inhibits their IMiD mediated down-regulation; up-regulation of MYC, activation of MAPK and PI3K pathway.<sup>171</sup>

## 1.5 Mantle Cell Lymphoma

### 1.5.1 What is Mantle Cell Lymphoma?

Mantle cell lymphoma is typically an aggressive, rare form of B-cell non-Hodgkin lymphoma (NHL) that arises due to the malignant transformation of a B lymphocyte in the outer edge of a lymph node follicle (the mantle zone).<sup>176</sup>

Mantle cell lymphoma (MCL) accounts for  $\approx 7\%$  of all non-Hodgkin lymphomas (NHL).<sup>177</sup>

Age is a risk factor for Mantle Cell Lymphoma as it is more frequent in older people, with the median age at diagnosis being  $>60$ .

### 1.5.2 Signs & Symptoms<sup>176</sup>

- i. Loss of appetite and weight
- ii. Fever
- iii. Night sweats and unexplained itching
- iv. Nausea and/or vomiting
  - v. Swollen lymph nodes in the neck, armpits, or groin
  - vi. Heartburn, abdominal pain/ abdominal swelling (distension), or bloating
  - vii. A sense of fullness or discomfort from enlarged tonsils, liver (hepatomegaly), or spleen (splenomegaly)
- viii. Pressure or pain in the lower back, often going down one or both legs
- ix. Fatigue related to anemia (low red blood cell count that leads to low Oxygen transport)
- x. Malignant lymphocytes crowd out the bone marrow, leading to a) **Anemia** or abnormally low levels of the oxygen-transporting red blood cells that leads to fatigue, b) **Thrombocytopenia** or low count of platelets that plays an essential role in blood clotting (coagulation) and c) **Neutropenia** or low neutrophil count – a type of white blood cell helps the body to fight infection.

### 1.5.3 Cellular Origin of Mantle Cell Lymphoma

Lymph nodes, a part of the lymphatic system, are small, bean-shaped structures and a critical component of the adaptive immune system. Lymph nodes are the secondary lymphoid organ of the human body located in the neck, armpit, chest, abdomen (belly), and groin.<sup>178,179</sup> They serve

as the primary reservoir for the B & T lymphocytes, which exposes them to the antigens filtered from the interstitial fluid. The lymph node consists of three cellular compartments: the cortex, where mostly B cells reside; the paracortex, which mainly contains T cells; Medulla, which houses plasma cells. Dendritic cells and macrophages predominantly.<sup>178-180</sup> In the cortex of unstimulated lymph node, naïve B-cells and the loose meshwork of dendritic cells form primary follicles. Antigen exposure makes B-cells activated, which leads to their rapid proliferation and forms a germinal center along with the tightly packed network of dendritic cells and macrophages. There is another outside layer or ring of resting B-cells with dendritic cells forming the mantle zone around the germinal center. The germinal center, together with the mantle zone, forms the secondary follicle, which serves as the site for antigen-dependent B-cell maturation and moves to the medulla to proliferate as antibody-secreting plasma cells.<sup>178,179</sup>

Mantle cell lymphoma (MCL) arises from the malignant transformation of a subset of naive pre-germinal center B cells localized in the mantle zone of the lymph node follicle.<sup>178,179</sup>

#### **1.5.4 Diagnosis**<sup>176,181,182</sup>

**i. Bone marrow and lymph node biopsy:** Sample tissues are collected from lymph node(s) and/or bone marrow to check the reason behind the swollenness and to check the possible spread or metastasis of the lymphoma cells to the bone marrow, respectively. The samples are observed under a microscope to detect the presence of abnormal or cancerous cells and to detect specific types/ subtypes of NHL.

**ii. Cytogenetic analysis:** Cytogenetic analysis by Fluorescence in situ hybridization (FISH) is an indispensable tool in the diagnosis and risk stratification of MCL. This method helps to detect the gene fusions involving the IGH gene at 14q32 and CCND1 at 11q13 with the help of a fluorescently labeled probe that finds and then binds to its matching sequence within the set of chromosomes.

**iii. Immunophenotyping:** Flow cytometric analysis is another important tool for precise disease diagnosis, classification & staging, risk stratification, and oncogenic progression. These phenotypic markers distinguish the cell lineages and the differentiation steps, which are crucial for the identification of separate disease entities. For e.g., MCL has a characteristic expression of CD5 but lacks CD23 expression, which contrasts with B-CLL.<sup>181,182</sup>

**Table 3.** List of immunophenotypic markers used to identify and classify MCL<sup>182,183</sup>

Marker	Expression Pattern
CD19	+
CD20	+
CD22	+
CD23	-
CD25	-
FMC7	+ (-)
CD79b	+
CD5	+
slg	+
CD10	-
CD11C	-
CD103	-
CD43	+
CD30	-
CD45	+
CD138	-
Bcl-1	+
Bcl-2	+
Bcl-6	-
Heavy chain (IgG, IgA, IgM)	+
Light chain Ig (kappa or lambda)	+ (moderate expression)

**iv. Blood Test:**

- a. Comprehensive blood count (CBC)
- b. Differential blood count
- c. **Lactate Dehydrogenase (LDH) Test:** High LDH activity indicates upregulated glycolytic stress due to hypoxia, higher tumorigenic activity, and correlated with poor prognosis and unfavorable outcome.
- d. Uric acid level test
- e. Comprehensive metabolic panel (CMP)
- f.  **$\beta$ 2 Microglobulin:** This is secreted by B-cells in the blood, and its high level indicates oncogenesis.

**v. Positron emission tomography (PET) scan:** This is an imaging test where a special dye containing radioactive tracer is administered through vein/ oral ingestion, which creates the image of the tissue/ organ of interest. This helps the physicians to check for the disease.

**vi. Computed tomography (CT) scan:** This is another imaging-based test where a series of X-rays is taken, and then computer technology processes them to build the 3D images of the soft tissues and bones.

## **vii. Colonoscopy**

### **1.5.5 Molecular pathways involved in the pathogenesis of MCL**

**a. Mutation:** Reciprocal chromosomal translocation–t (11;14) (q13; q32) is the most observed genetic event in the pathogenesis of MCL, as it is found in ~90% of all cases. This is the primary/ initial oncogenic process that happens in the bone marrow in an early B cell at the pre-B stage of differentiation during the V(D)J recombination process by the recombination activating gene (RAG) enzymes. It is considered to be the hallmark of MCL pathogenesis which involves the juxtaposition of the proto-oncogene Cyclin D1 (CCND1) locus to the immunoglobulin heavy chain (IGH) regulatory locus. This genetic lesion causes constitutive expression of Cyclin D1, which is not observed in normal B lymphocytes. Cyclin D1 is a positive regulator of the cell cycle and belongs to a family of proteins that play a pivotal role in regulating cell cycle progression and cell proliferation. Its over-expression causes malignant transformation of the naive pre-germinal center B-lymphocytes by dysregulating the cell cycle at the G<sub>1</sub>/S phase through binding and activating the G1 Cyclin-dependent kinases, CDK4 & CDK6. Cyclin D1, upon translocation to the nucleus, forms a holoenzyme complex with CDK4/6 and activates the E2F transcription factor by releasing it through the phosphorylation-mediated inactivation of the Retinoblastoma (Rb) protein. Overexpression of Cyclin D1 also leads to the ubiquitination-mediated degradation of the p27 by ubiquitin ligase F-box protein Skp2 and promotes Cyclin E/CDK2 mediated entry to the S-phase of the cell cycle.<sup>179,184,185</sup>

In some cases (4-10% of all MCL cases), genetic changes other than t (11;14) are responsible for the over-expression of Cyclin D1 that includes secondary chromosomal rearrangements at the 3' untranslated regions (3'UTR) region of the Cyclin D1a isoform of the Cyclin D1 transcripts. Cyclin D1 has five exons and gives rise to two different isoforms, Cyclin D1a and Cyclin D1b, by alternative splicing. Genomic deletions at the 3' of the gene or point mutations at the 3' UTR of the Cyclin D1a transcript led to the expression of truncated Cyclin D1 transcripts. These shorter transcripts lack the full-length functional 3' UTR and are devoid of the mRNA destabilizing AU-rich elements, which extend its half-life, unlike the full-length

Cyclin D1a that has full-length 3' UTR. It also lacks the binding sites for the translation inhibitory microRNAs like miR15/16. Together, these additional genetic events result in higher and prolonged Cyclin D1 protein expression that increases its tumorigenic potential, which resulted in poor survival outcomes for the patients.<sup>184,185</sup>

Whole genome profiling of the MCL samples also showed amplification of the translocated (11;14) allele might also contribute to the over-expression of Cyclin D1.<sup>184</sup>

**b. Cyclin D1<sup>-</sup> MCL:** Some rare sub-set of MCL patients (<5% of all MCL cases) do not exhibit the over-expression of Cyclin D1 or the t (11;14) translocation, although they have a similar phenotype, gene expression profile, secondary genetic events, and clinical outcome. FISH and NGS analysis of this Cyclin D1<sup>-</sup> MCL show over-expression of Cyclin D2 & Cyclin D3 driven by the chromosomal rearrangements – t (2;12) (p12; p13) translocation that causes fusion between  $\kappa$  light Ig chain gene locus and the Cyclin D2/D3 gene loci.<sup>184,186,187</sup>

**c. Deletions of INK4A/ARF (CDKN2A) Locus and TP53 mutation:** Another common genetic alteration observed in ~20% of MCL cases is the homozygous deletion of the CDKN2A locus (9p21) that encodes two tumor suppressor gene p16<sup>INK4A</sup> and p14<sup>ARF</sup>. These tumor suppressor genes act as negative regulators of the cell cycle and inhibit the uncontrolled proliferation of the cells; its deletion leads to poor treatment outcomes and shorter overall survival in the patients. p16<sup>INK4A</sup> inhibits the cell cycle stimulatory effect of both CDK4/6, which otherwise form a complex with the member of the Cyclin family of proteins (Cyclin D1/D2/D3) to inactivate Retinoblastoma (Rb) protein by phosphorylation to release E2F, a transcriptional activator and promote G1 to S phase cell cycle progression. p14<sup>ARF</sup> is an E3 ubiquitin ligase that stabilizes p53- one of the most important tumor suppressors that inhibits tumor formation and promotes apoptosis by preventing its MDM2-mediated degradation. p14<sup>ARF</sup> does so by interacting with the C-terminal domain of the proto-oncogene MDM2 through its N-terminal domain, which in turn promotes the degradation of Mdm2.<sup>186,187</sup>

In some cases, it has been reported that despite having the wild type of CDKN2A, the amplification and the over-expression of BMI 1 by amplification at 10p11.23, a polycomb transcriptional repressor inhibits its normal function. Other secondary genetic events such as RB1 deletion and amplification of the CDK4 also lead to cell cycle dysregulation and contribute to the oncogenic progression.<sup>186,187</sup>

**d. SOX11 expression:** Sex-determining region Y-box 11/ SOX11, a neuronal transcription factor, has been reported to be over-expressed in the conventional MCL (cMCL) due to hypomethylation of the distant enhancer region of SOX11 leads to the alteration of the 3 - dimensional chromatin configuration that brings it near the promoter region of the gene. It is an important prognostic factor in MCL pathogenesis as SOX11 expression is absent in Normal B lymphocytes throughout its different differentiation phases, and the non-nodal MCL (nnMCL), as well as other lymphoid neoplasms, lack the SOX11 expression. Studies suggested that SOX11 blocks terminal B-cell differentiation locks it in a more primitive form and promotes MCL tumor growth and aggressiveness by directly regulating the expression level of its target gene PAX5- a critical transcriptional factor that determines and regulates the B-cell development by activating the specific sets of genes responsible for B-cell lineage identity and inhibits the genes that drive the plasma cell differentiation. Moreover, SOX11 also blocks the entry of MCL cells to the germinal center by inhibiting the expression of its other target, BCL-6, and promotes angiogenesis through Platelet-derived Growth Factor A (PDGFA). It is also reported that SOX11 modulates the tumor microenvironment and promotes cell migration and adhesion to confer stromal cell-mediated drug resistance in MCL cells by up-regulating the expression of C-X-C chemokine receptor type 4 (CXCR-4) and C-X-C chemokine receptor type 12 (CXCR-12) which in turn induces the FAK (Focal Adhesion Kinase) expression.<sup>188,189</sup>

**e. DNA damage response pathway alterations:** The deletion of the 11q22-23 region in the chromosome is one of the most frequent genetic alterations observed on MCL. Ataxia-telangiectasia mutated (ATM) gene, located in this locus, encodes a serine/threonine kinase which is a member of the Phosphoinositide 3-kinase family of proteins and plays a pivotal role in the activation of p53 in response to the DNA damage, e.g., DNA Double Stranded Break (DSB). Naïve B cells in the mantle zone of the lymphoid follicle express ATM, but the immature B-cells in the bone marrow and the follicular germinal center cells lack ATM expression as physiological DSB occurs in the pre-B cell stage for the initial Immunoglobulin gene rearrangements (VDJ recombination) or during the VH somatic hypermutations (SHM) and immunoglobulin class switching that occurs in antigen-activated follicular germinal center B cells that contributes to the generation high-affinity antibody maturation. ATM cytogenetic alterations, including truncating or missense mutation accompanied by the loss of the other

allele, are observed in almost 40-75% of all MCL cases and mainly affect the PI3K domain or lead to the formation of unstable truncated ATM protein. Inactive ATM in the Naïve B cells of the mantle zone facilitates the onset of genomic instability and promotes oncogenesis. ATM inactivation is believed to be an early event in the pathogenic progression of MCL, which allows the accumulation of chromosomal aberrations due to compromised DNA damage response pathways. Serine/ Threonine Kinases Checkpoint Kinase 1 (CHEK 1) and Checkpoint Kinase 2 (CHEK 2) are the two downstream targets that act as an S-phase checkpoint to arrest cell cycle by integrating DNA damage response signal from ATM & ATR. Germline mutation of CHEK 2 and down-regulation of CHEK 1 have been reported in some MCL cases with high chromosomal imbalance. Overall, the mutations in the DNA damage response pathway and mitotic checkpoints don't have a significant impact on the pathogenesis of MCL, but they serve as the driving factor to give rise to the complex tetraploid karyotype with a high genomic imbalance that promotes MCL lymphomagenesis.<sup>179,184-187</sup>

Point mutation and 17p13 deletion-mediated p53 inactivation are also observed in ~30% of MCL. These chromosomal aberrations in p53 deregulate CDK inhibitor p21, inhibit p53-mediate cell cycle arrest, DNA damage response induced apoptosis, senescence in both cMCL and nnMCL and are reported to be associated with aggressive disease state and poor overall survival.<sup>186</sup>

### 1.5.6 Current Treatment Strategies<sup>176,190</sup>

**a. Chemotherapy and immunotherapy:** Rituximab-based combination treatment regimen is the first line of the treatment strategy. Rituximab is the monoclonal antibody that recognizes and targets CD20, which is a pre-B and mature B-lymphocytes specific marker including malignant B-cell in MCL and induces apoptosis by blocking the signaling pathways p38 mitogen-activated protein kinase (MAPK), Nuclear factor kappa B (NF-κB), extracellular signal-regulated kinase 1/2 (ERK 1/2), AKT antiapoptotic survival pathways, Complement dependent cellular cytotoxicity (CDC) and Antibody-dependent cellular cytotoxicity (ADCC).<sup>191</sup> The following combination treatment regimens are commonly used: **R-CHOP** (rituximab plus cyclophosphamide, doxorubicin, vincristine, and prednisone), **BR** (bendamustine and rituximab), **(R-BAC)** rituximab, bendamustine and cytarabine, **R-DHAP** (Rituximab (Rituxan®), Dexamethasone (Decadron®), **High-dose Ara-C** (Cytarabine), CisPlatin),

**Hyper-CVAD** (cyclophosphamide, vincristine sulfate, doxorubicin (Adriamycin), dexamethasone), **VcR-CAP** (bortezomib (Velcade), rituximab (Rituxan), cyclophosphamide, doxorubicin (Adriamycin), prednisone), **R-FCM** ([Rituxan, fludarabine (Fludara®), cyclophosphamide and mitoxantrone], **R-CVP** (Rituxan, cyclophosphamide, vincristine, and prednisone), **R-CBP** [Rituxan, cyclophosphamide, bortezomib (Velcade®) and prednisone].

**b. Steroids:** Prednisolone, Dexamethasone, and Methylprednisolone are the most common steroids that boost the efficiency of chemotherapy and help in reducing the side effects.

**c. Radiotherapy:** Radiotherapy is the treatment option for the 1<sup>st</sup> and 2<sup>nd</sup> stage Mantle Cell Lymphoma patients.

**d. Stem cell transplant:** Allogenic stem cell transplantation is where patients receive healthy blood-forming stem cells from a donor to replace their own bone marrow, either crowded with malignant cells or has been destroyed by chemotherapy in order to suppress the disease or restore the immune system. This is the treatment option for the relapsed disease state to restore the drug sensitivity or prolong the drug response and is also beneficial for some high-risk fit-chemo-sensitive patients who are able to undergo intensive chemo-therapy treatment regimen for e.g., BEAM (carmustine, etoposide, cytarabine, and melphalan) & LEAM (lomustine, etoposide, cytarabine, and melphalan). For older patients, allogenic transplantation is coupled with reduced-intensity chemotherapy. This may help in sustained remission. Another treatment option is autologous stem cell transplantation, where patients' own stem cells are infused to attack the cancer cells to achieve enhanced response to induction therapy and prolong remission.

### 1.5.7 Mantle Cell Lymphoma (R/R MCL)

However, despite these recent advancements in the treatment landscape, MCL remains incurable with limited therapeutic options owing to drug resistance, extensive inter-individual variation in drug response, and toxicity profile that limits their efficacy in clinical settings with progression-free survival (PFS) of ~1-2 years and median overall survival (OS) of < 3 years. Patients who show a high response rate to the initial treatment eventually become refractory or unresponsive to the standard of care treatment. **Relapsed Mantle Cell Lymphoma** is the disease state where it responded initially to the treatment but returned after a brief period of remission. **Refractory**

**Mantle Cell Lymphoma** is the disease state when it does not respond to the initial treatment or responds only for a short period of time, and the cancer cells continue to grow.<sup>192,193</sup>

Currently available chemotherapeutic treatment options for R/R MCL include the three Bruton's Tyrosine Kinase Inhibitors (BTKi): Ibrutinib, Acalabrutinib, Zanubrutinib; Proteasome Inhibitors: Bortezomib; Immunomodulatory drug: Lenalidomide.<sup>192,194</sup>

Despite the recent advances in the treatment landscape, R/R MCL remains incurable with a high recurrence rate and poor long-term prognosis. It has limited therapeutic options owing to drug resistance, extensive inter-individual variation in response, and toxicity profile that limits efficacy in clinical settings with median progression-free survival (PFS) of <15 months and Overall Survival (OS) of 1-2 years.<sup>192,195</sup>

The available therapies for the R/R MCL (e.g., Bruton Tyrosine Kinase inhibitor Ibrutinib) are not curative and confer modest progression-free survival (PFS) of 13–14.6 months as compared to 4-9 months in non-BTKi treated patients. Despite the impressive initial clinical advantage, Ibrutinib treatment is not durable, and eventually, most of the patients show signs of clinical progression within 18-24 months with poor prognosis and shorter periods of remission. Once patients develop resistance, the median overall survival is only 6-10 months. Only one-third of patients respond to their next line of treatment; those who do respond experience only brief remissions and have poor outcomes, irrespective of stem cell transplantation.<sup>179,185,192,195</sup>

## **1.5.8 Bruton's Tyrosine Kinase Inhibitors (BTKi)**

**1.5.8.1 Bruton's Tyrosine Kinase:** Bruton tyrosine kinase (BTK) gene encodes for a cytoplasmic non-receptor tyrosine kinase, a member of Tec (Tyrosine kinase expressed in hepatocellular carcinoma) family of non-receptor tyrosine kinases. BTK is an enzyme containing 659 amino acid residues, primarily expressed in both normal and malignant B-lymphocytes, myeloid cells, and platelets, and has five structural domains: i) N-terminal pleckstrin homology domain (PH) that binds to the protein and recruit to the cell membrane; ii) proline-rich TEC homology domain (TH) containing zinc finger motifs regulating its activity and stability, iii) & iv) Src homology domains 2 (SH2) and 3 (SH3) that modulate the protein-protein interaction, v) the catalytic kinase C-terminal domain. It plays a central role in the B-cell receptor (BCR) mediated cell signaling by catalyzing the incorporation of a phosphate group (phosphorylation)

from ATP to the tyrosine residues of other proteins, activating an array of signaling cascade including phosphoinositide 3-kinase (PI3K)-AKT pathway, PLC, PKC, and nuclear factor- $\kappa$ B (NF- $\kappa$ B). These BCR signaling-mediated downstream signaling cascades that get triggered by the antigen engagement to BCR, followed by its subsequent activation, play a pivotal role in the maintenance and normal functioning of B-cells. Aberrance in this signaling pathway, especially in secondary lymphatic organs, is reportedly responsible for the development and progression of B-cell malignancies.<sup>194,196</sup>

**1.5.8.2 Bruton's Tyrosine Kinase in B-cell receptor signaling:** BCR is a multimeric protein structure consisting of surface transmembrane immunoglobulin (IgM) with a very short cytoplasmic domain and coupled with the disulfide-linked transmembrane signal transduction unit: Ig $\alpha$  (CD79A) and Ig $\beta$  (CD79B) heterodimer (Ig- $\alpha$ /Ig- $\beta$ (CD79a/CD79b) that have immunoreceptor tyrosine-based activation motifs (ITAMs) in their cytoplasmic tails.<sup>196,197</sup>

BCR signaling is an antigen-dependent signaling pathway where antigen engagement of BCR induces receptor aggregation followed by ITAM phosphorylation by Src-family protein tyrosine kinases LYN, FYN, BLK, and LCK and creates docking sites for a spleen tyrosine kinase (SYK). SYK, upon binding with ITAM, gets activated, which in turn activates the B cell linker scaffold protein (BLNK). LYN and SYK also phosphorylate tyrosine residues in the cytoplasmic tail of B-cell co-receptor CD19 and/or the adaptor protein B-cell PI3K adaptor (BCAP), which promote the recruitment and activation of PI3K and guanine nucleotide exchange factor VAV. VAV, through activation of Rac1- a member of the Rho family of GTPases promotes the enzymatic activity of PI3K (PI3K $\delta$ ), which in turn phosphorylates PIP2 to PIP3- a critical intracellular second messenger which activates the subsequent downstream signaling cascade. PIP3, by interacting transiently with the PH-domain of BTK, recruits it to the plasma membrane, which is otherwise essentially present in the cytosol in the unphosphorylated and catalytically inactive state. SYK or SRC family kinases phosphorylate BTK at Y551 upon its recruitment to the plasma membrane, which promotes its catalytic activity and subsequent phosphorylation at Y223 of the SH3 domain to become physiologically active and stable. Activated BTK can interact with adapter protein BLNK/SLP65 through its SH2 domain, and the complex binds to the downstream target phospholipase C  $\gamma$ 2 (PLC $\gamma$ 2) followed by its activation by phosphorylation at Y753 & Y759, producing intracellular second messenger Inositol triphosphate (IP3) and DAG

(Diacylglycerol) through hydrolysis. IP3 binds to its receptor in the endoplasmic reticulum (ER), which causes the release of Ca<sup>2+</sup> from ER store and this sustained influx of Ca<sup>2+</sup> activates the nuclear factor of activated T-cells (NFAT) by Calmodulin and Calcineurin through its dephosphorylation mediated translocation to the nucleus. DAG, on the other hand, activates AKT/ PKC $\beta$  that in turn activates down-stream transcriptional activation and pro-survival signaling pathway such as nuclear factor  $\kappa$ B (NF- $\kappa$ B) signaling pathway, mitogen-activated protein kinase pathways [ERK 1/ ERK 2, p38MAPK, JNK/SAPK pathway. Other important downstream targets of BTK include transcription factors such as STAT3, forkhead transcription factors (FOXOs), BAP-135/TFII-I, and ARID3A. Thus, BTK plays an essential role in B-cell development, differentiation, and proliferation through regulation and coordination among cell cycle regulators and pro- and apoptotic proteins.<sup>196-199</sup>

### **1.5.8.3 FDA Approved BTKi for R/R MCL management**

**i. Ibrutinib:** Ibrutinib/ Imbruvica (previously PCI-32765) is a potent, irreversible, covalent oral inhibitor of BTK that binds to Cys-481 near the ATP-binding domain of the BTK molecule/ allosteric inhibitory segment of BTK (TK/SH1 domain) leading to irreversible inhibition of enzymatic activity and BCR-mediated survival signals in human B cells. It inhibits BTK's full activation by inhibiting its autophosphorylation at Tyr-223.<sup>199</sup>

US Food and Drug Administration (FDA) approved Ibrutinib in November 2013 for the treatment of adult patients with Mantle cell lymphoma who have received at least one prior therapy based on Phase II PCYC-1104 single-arm clinical trial in 111 previously treated patients with relapsed or refractory MCL that showed improved overall response rate (ORR) and duration of response (DOR). The median age of the patients was 68 years, and 86% of them had an intermediate or high risk of MCL. Ibrutinib was able to achieve an ORR of 69% (complete response rate = 21%; partial response rate = 48%) and a median duration response of 17.5 months with a median progression-free survival (PFS) of 13.9 months.<sup>199,200</sup>

## **Mechanism of Action of Ibrutinib:**

### **Ibrutinib exhibits its cytotoxic effect by disrupting key B-cell processes**

**a. Inhibits proliferation and survival:** BTK signaling plays a pivotal role in MCL cell survival and proliferation. Studies have shown BTK inhibition by Ibrutinib induces dose and time-dependent cytotoxicity in MCL and CLL cell lines in vitro. Ibrutinib inhibits the expression of the Bcl-2 family of proteins such as Bcl-2, Bcl-xL, and Mcl-1 and induces the activation of the caspase-3-dependent apoptotic pathway.<sup>201,202</sup>

**b. Inhibits cellular adhesion and modulates chemotaxis and trafficking:** Interaction between malignant B cells and the tumor microenvironment plays a major role in the pathogenesis and the disease progression in MCL. Interplays among cytokines, chemokines, and the adhesion molecules drive the B-cell migration and homing to the tissue microenvironment, where they adhere to the stromal cells. This interaction provides adhesion-mediated drug resistance and confers survival benefits to the malignant B-cells. Ibrutinib abrogates these growth and survival advantages inhibiting chemokine receptors such as CXCL12, and CXCL13 as well as disrupting BCR signaling; integrin-mediated (VLA-4 on B cells to VCAM-1 on stromal cells) homing and adhesion to the tissue microenvironment (lymph node and bone-marrow).<sup>199,202</sup>

**ii. Acabrutinib:** Acabrutinib/ CALQUENCE is the second-generation orally bioavailable small molecule BTK inhibitor which was approved in 2017 by the FDA for the treatment of patients with relapsed/refractory (R/R) MCL based on the ACE-LY-004 trial where single-agent Acabrutinib treatment showed a high rate of durable responses and a favorable safety profile.<sup>203–205</sup>

**Mechanism of action of Acabrutinib:** Both Acabrutinib and its active metabolite, ACP-5862, bind covalently with the Cys481 residue in the BTK active site with higher specificity than Ibrutinib, which inhibits its enzymatic activity and subsequent downstream signaling proteins such as BCR activation markers CD86 and CD69.<sup>203–205</sup>

**iii. Zanubrutinib:** Zanubrutinib/ BRUKINSA is another second-generation, orally bioavailable small molecule BTK inhibitor that got FDA approval for treating R/R MCL in 2019 based on

its efficacy in the BGB-3111-206 clinical trial. Its mechanism of action is similar to Acalabrutinib.<sup>206</sup>

#### **1.5.8.4 Molecular mechanism of resistance towards BTK inhibitors**

##### **a. Innate resistance (Refractory disease state)**

**i. Activation of PI3K-AKT pathway:** Constitutive activation of the PI3K/AKT pathway and overexpression of the phosphorylated Akt (pS473) are observed in the primary resistance against BTKi in MCL cells. Activated Akt phosphorylates tumor suppressor FOXO3a, which leads to its cytoplasmic sequestration and subsequent degradation. As a result, FOXO3a-mediated transcriptional activation of the pro-apoptotic genes PTEN and bim gets inhibited.<sup>207,208</sup>

**ii. Activation of alternative NF- $\kappa$ B pathway:** Ibrutinib-resistant MCL cells show activation of alternative NF- $\kappa$ B pathway (MAP3K14-NF $\kappa$ B) as compared to the classical NF- $\kappa$ B pathway (BCR-BTK- NF- $\kappa$ B) that is observed in Ibrutinib sensitive cells. Mutations in the negative regulator of this pathway, such as loss of function mutation in tumor necrosis factor receptor-associated factor 2 (TRAF2) and deletions in TRAF3, are observed in BTK-resistant patients. This causes stabilization of MAP3K14 that causes constitutive activation of alternative NF- $\kappa$ B pathway.<sup>207-210</sup>

**iii. Over-expression of Cyclin D1:** Mutation in the CCND1 like E36K, Y44D, or C47S causes less protein degradation. This enhanced CCND1 protein level leads to cell cycle progression by promoting the degradation of Rb and causes Ibrutinib resistance.<sup>208</sup>

##### **b. Acquired resistance (Relapsed disease state)**

**i. Mutation:** Mutation in the BTK inhibitor interacting residue of BTK (C481S) reduces the binding affinity of BTKi for BTK and attenuates its covalent binding making the bond reversible. Thus, BTKi becomes less potent in inhibiting the mutant BTK and the phosphorylation-mediated activation of downstream PLCG2, AKT, and ERK signaling pathways, which results in diminished clinical activity. Other BTK mutations such as T474I, T474S, and T316A further abrogate the selectivity and binding affinity to BTKi and inhibits its interaction with other proteins that drive the resistance.<sup>207,211</sup>

Mutation in the PLCG2 gene, such as R665W, L845F, and S707Y, is another common phenomenon in the development of Ibrutinib resistance. These mutations lead to the independent activation of BCR signaling by LYN and SYK kinase bypassing the BTK, which causes enhanced  $\text{Ca}^{2+}$  influx that activates different oncogenic signaling pathways.<sup>208</sup>

Deletion of the short arm of chromosome 8 (8p) leads to haploinsufficiency of TNF-related apoptosis-inducing ligand receptor (TRAIL-R), which causes downregulation of TRAIL-R1 and TRAIL-R2 genes which inhibits their binding to TRAIL and TRAIL-induced apoptosis. This mutation, along with other driver mutations such as MLL2, SF3B1, RPS15, and EP300, play a pivotal role in conferring survival advantage in response to BTKi.<sup>208,210,211</sup>

Another chromosomal aberration that plays an essential role in the development of acquired resistance against Ibrutinib is the gain of the short arm of chromosome 2 (2p+) which results in overexpression of Exportin-1 (XPO1). Exportin 1 exports several cell cycles regulatory proteins such as p53, FOXO, and retinoblastoma (pRb) from the nucleus to the cytoplasm, where they get degraded and thereby nullifying their tumor suppressor effects.

Also, constitutive activation of BCR signaling due to the mutation in BCR signaling pathway molecules CARD11, CD79A/B, TNFAIP3, and MYD88 promotes Ibrutinib resistance.<sup>212</sup>

**ii. Aberrant signaling pathway:** Interaction of mantle cell lymphoma cells with the tumor microenvironment activates the PI3K–Akt–mTOR pathway and Integrin  $\beta$ 1 signaling that drives Ibrutinib resistance. Apart from that, overexpression of Bcl-2 has also been reported in Ibrutinib-resistant cells.<sup>207,211</sup>

### **1.5.9 Cancer Stem cells (CSCs) and their role in drug resistance in MCL**

Cancer stem cells (CSCs) are the rare subpopulation of cancer cells present within tumors with self-renewal, differentiation capabilities, and tumorigenic potential. CSCs are believed to be the most crucial driving factor behind tumor initiation, disease progression, therapy resistance, and post-therapy relapse. In MCL, these putative stem-like cells include side populations (SP),  $\text{CD45}^+\text{CD19}^-$  cells or MCL-initiating cells (MCL-ICs), and relatively quiescent-highly clonogenic aldehyde dehydrogenase positive /  $\text{ALDH}^+$  cells.<sup>213–215</sup>

Side populations (SP) are the distinct subset of cancer stem cells that has the intrinsic capacity of pumping out DNA-binding dye Hoechst 33342 due to their expression of adenosine triphosphate (ATP)-binding cassette (ABC) membrane transporter ABCG2, ABCB1, which are absent in the non-SP cells. These cells display higher self-renewal and proliferation capacity with reduced expression of differentiation markers and elevated tumorigenic potential as compared to the non-SP cells.<sup>216</sup> All these are the hallmarks of tumor-initiating cells that are responsible for drug resistance and relapse. It is believed that this SP population contains a minor subpopulation of cells that lacks CD19 expression, which is a 95 KD transmembrane glycoprotein belonging to the immunoglobulin (Ig) superfamily and a prototypic B cell surface marker. These CD45<sup>+</sup>CD19<sup>-</sup> MCL cells display very high tumorigenic activity and self-renewal capacity as compared to the CD45<sup>+</sup>CD19<sup>+</sup> MCL cells. This relatively quiescent, highly heterogeneous population sub-population of cells is referred to as Mantle-Cell Lymphoma Initiating cells (MCL-ICs) and has significantly increased aldehyde dehydrogenase (ALDH1 and ALDH2) enzymatic activity.<sup>213,214,216,217</sup> MCL-ICs also exhibit elevated reactive oxygen species scavenging capacity through the higher expression of antioxidant enzymes like Metallothionein 1B (MT1B) and Superoxide dismutase 2 (SOD2), which protects them from ROS-mediated apoptosis. They have higher expression of a marker of a chemo-resistance gene such as ATP transporters ABCC3, ABCC6, and cell surface adhesion receptor CD44.<sup>213,214</sup> MCL-ICs are also characterized by the over-expression of the oncogenic signaling pathways genes such as Wnt-β catenin and enriched expression for stemness markers like Nanog, Oct4, KLF4.<sup>213–215,217–219</sup>

Previous studies have shown that intra-tumoral heterogeneity due to the presence of treatment-refractory subpopulations or cancer stem-like cells (CSCs) drives drug resistance and disease relapse in various cancers.<sup>215</sup>

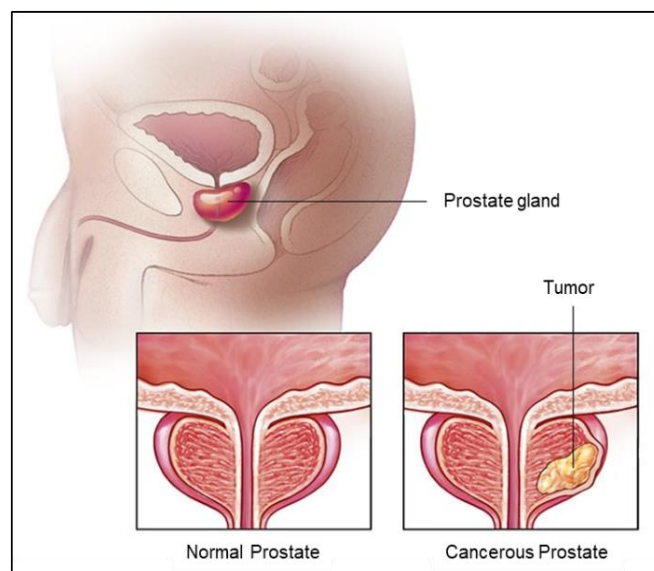
Most importantly, no study so far has attempted to develop drugs explicitly targeting these sub-clones. Standard of care drugs Ibrutinib is ineffective in targeting MCL-CSCs.<sup>208</sup>

## 1.6 Prostate Cancer

### 1.6.1 What is Prostate Cancer?

The prostate is a small walnut-shaped gland, found only in males, located below the bladder at the base of the penis, in front of the rectum, that produces the seminal fluid that helps in the nourishment and transportation of sperm. Uncontrolled proliferation of the prostate gland cells is termed Prostate cancer.<sup>220</sup>

**Figure 5: Anatomy of Prostate**



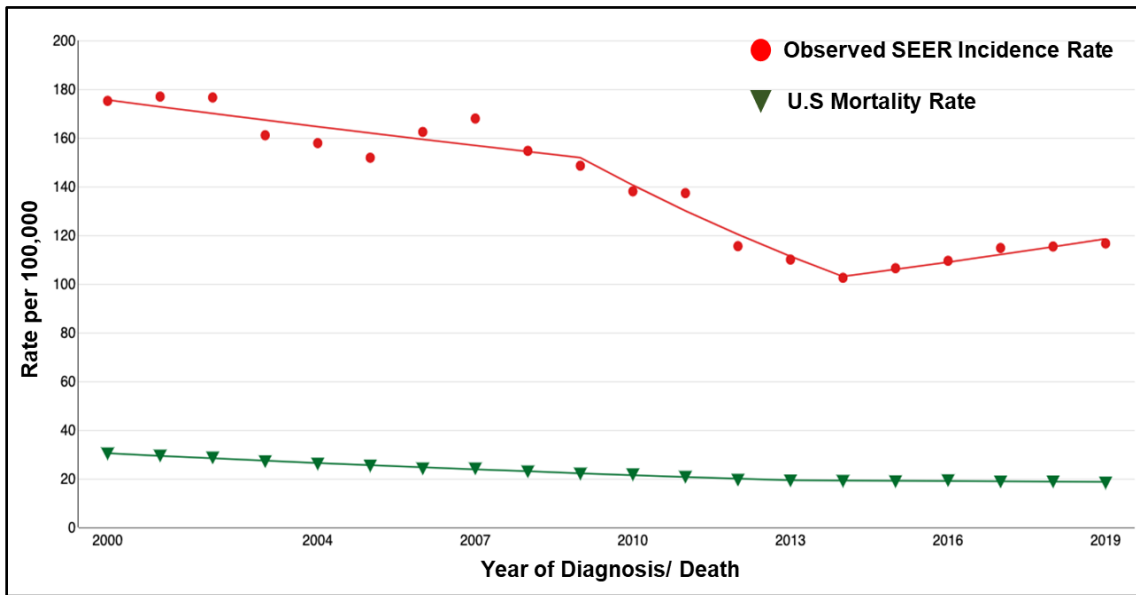
### 1.6.2 Statistics

Prostate cancer is the 2<sup>nd</sup> most common cancer after skin cancer and the second leading cause of death after lung cancer in US men.<sup>221</sup>

In the US, the estimated number of new cases of prostate cancer in 2022 is 268,490 (14% of all new cancer cases), and the estimated number of deaths is 34,500 (5.7% of all cancer deaths). About one man in 8 is at risk of getting diagnosed with prostate cancer during his lifetime. It is one of the most common cancers in American men, with a 6% increase in occurrence rate and a 7% increase in mortality rate in 2019 as compared to 2018. About 1 in 41 men will die of prostate cancer, and every 17 minutes, another man in the U.S. dies from the same.<sup>222</sup>

**Figure 6. Prostate Cancer incidence rate and mortality rate in the U.S.**

Source: SEER\*Explorer



### 1.6.3 Risk factors<sup>221–223</sup>

Scientific studies suggested a few factors responsible for the development of prostate cancer.

- **Age:** Age is one of the most critical risk factors for prostate cancer. The chances of getting diagnosed with prostate cancer increase significantly after age 50 (≈60% of all cases) but are rare in the case of men younger than 40.

**Figure 7A: Prostate Cancer Risk from Birth Over Time; Source: SEER\*Explorer**

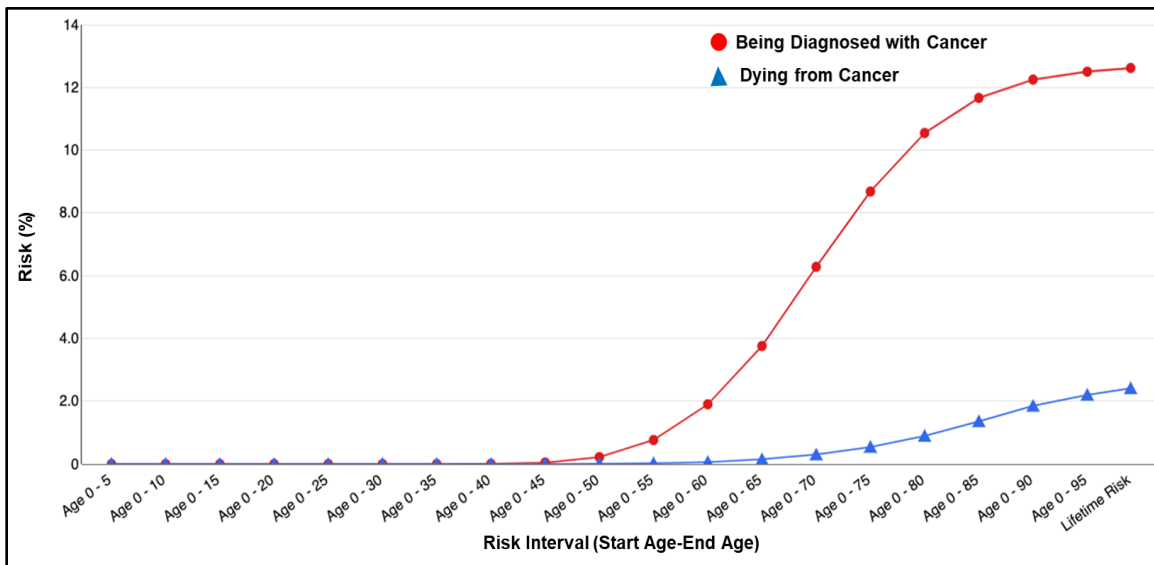


**Figure 7B. Age-wise prevalence of Prostate Cancer among the US males; Source: SEER\*Explorer**

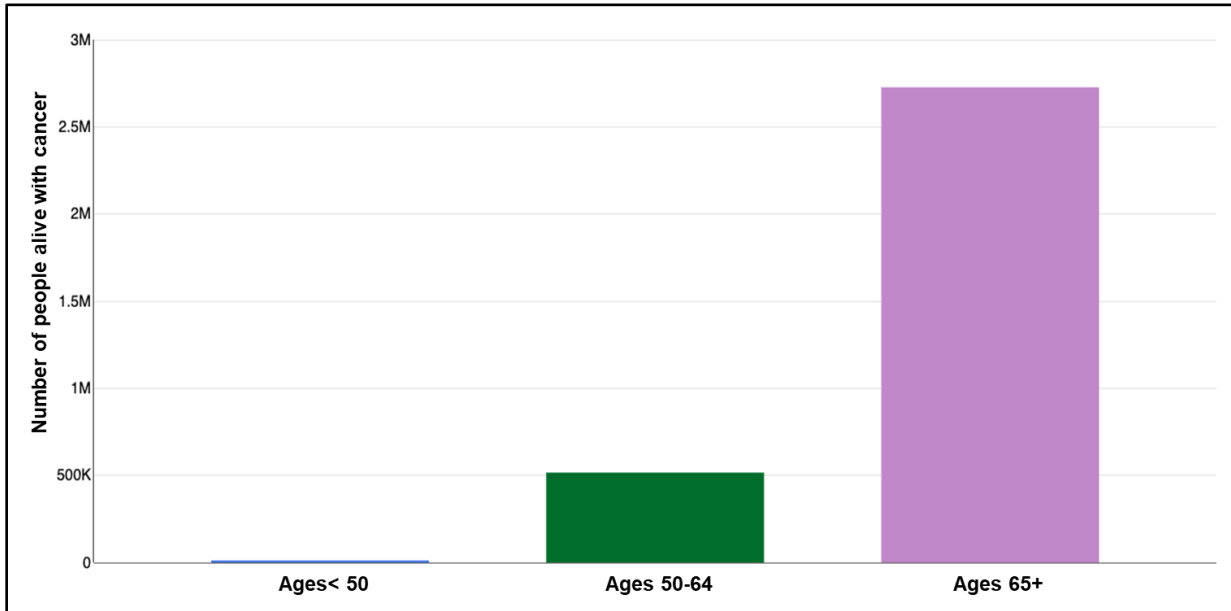
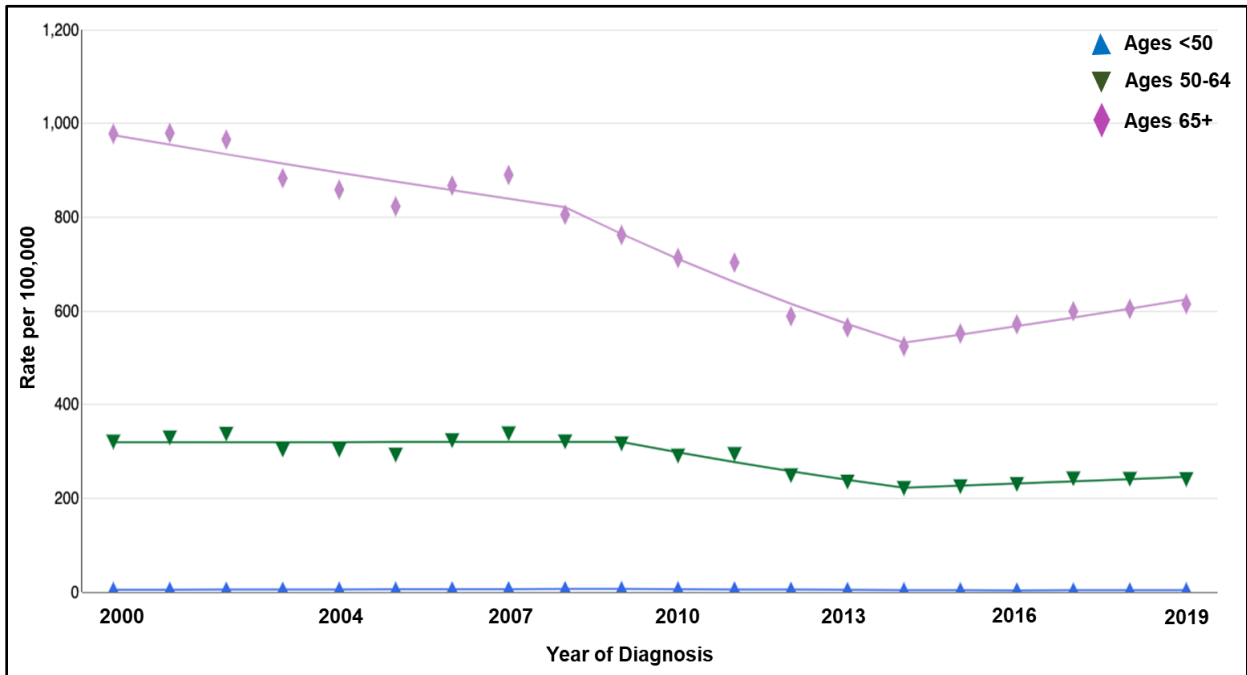
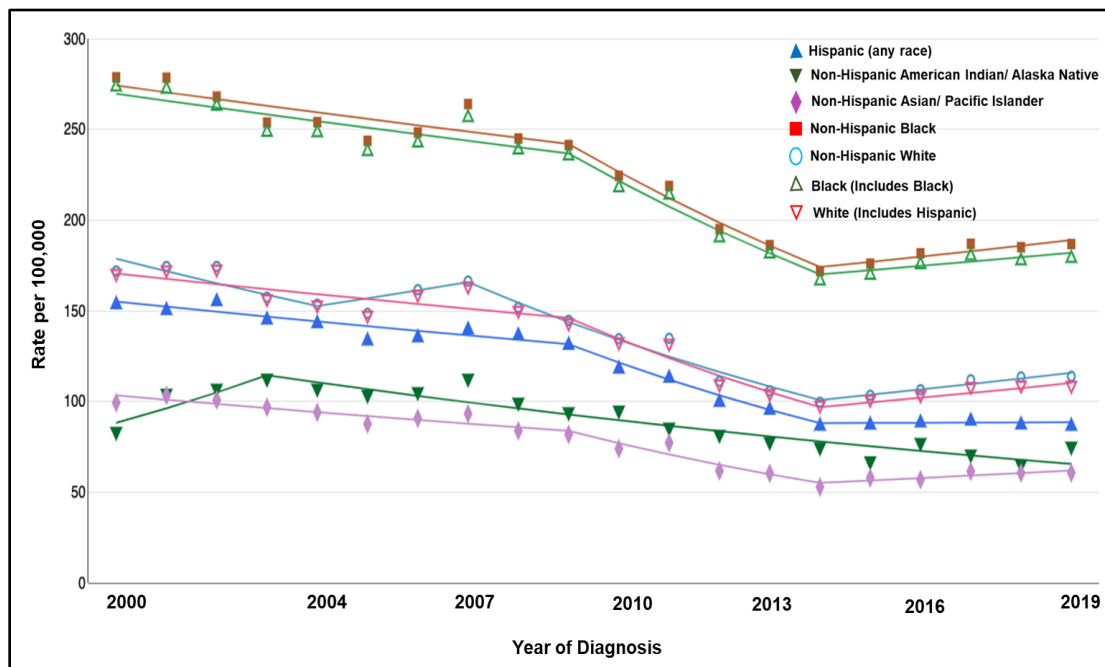


**Figure 7C. Age-adjusted incidence rates of Prostate Cancer among US men. Source: SEER\*Explorer**



- Race/ Ethnicity:** African American men are at higher risk of developing and dying from prostate cancer than white men and men of other races (1.7 times higher chances of getting diagnosed and 2.1 times higher chances of death). Also, they are more prone to develop aggressive or advanced disease states). Prostate cancer has less occurrence in Asian American and Hispanic/Latino men than in non-Hispanic whites. Genetic predisposition, diet & obesity, socio-economic status, and access to health care may contribute to this differential racial distribution.

**Figure 7D. Age-adjusted incidence rates of Prostate Cancer among US males by Race/ Ethnicity. Source: SEER\*Explorer**



- Family history:** Genetics and heredity are essential risks factor for the onset of prostate cancer, and familial prostate cancer makes up  $\approx 20\%$  of all cases. Having a first-degree relative (father or brother) with prostate cancer increases the risk of prostate cancer by almost two folds than the average risk. The higher the number of blood relatives affected by prostate cancer, the higher the risk.<sup>223–225</sup>

Inherited or germline mutations in the DNA repair gene of BRCA1 or BRCA2 genes, which are commonly associated with increased risk of breast and ovarian cancer in women in some

families, can also enhance the risk of prostate cancer in men (especially mutations in BRCA2).<sup>224</sup>

- **Genetic factors:** i) Inherited mutation in BRCA1, BRCA2, CHEK2, ATM, PALB2, RAD51D, DNA mismatch repair genes (MSH2, MSH6, MLH1, PMS2), RNASEL, HOXB13 genes ii) acquired mutation in androgen (testosterone) producing gene which increases its level is linked to the development of prostate cancer.<sup>223</sup>

#### 1.6.4 Types of Prostate Cancer

Prostate cancer has two types:

**i. Adenocarcinoma of the prostate:** This is the most common type of prostate cancer that arises in the glandular epithelial cells that make the lining of the prostate gland and the associated tubes.<sup>220,226</sup>

There are two sub-types of prostate adenocarcinoma

**a. Acinar adenocarcinoma:** This is the carcinoma of the acinar cells that make the lining of the prostate's fluid-secreting glands.<sup>226</sup>

**b. Ductal adenocarcinoma of the prostate:** This is a rare and aggressive subtype of prostate adenocarcinoma that develops in the cells lining the tubes (ducts) of the prostate gland.<sup>226</sup>

**ii. Other types of prostate cancer** include Transitional cell carcinoma/ urothelial cancer, Neuroendocrine prostate cancer that includes small cell prostate cancer, Squamous cell carcinoma, etc.<sup>226</sup>

#### 1.6.7 Symptoms<sup>227</sup>

- Trouble and frequent urination (especially at night).
- Decreased force of the urine flow or the need to strain to empty the bladder.
- Pain or burning during urination, discomfort when sitting caused by an enlarged prostate.
- Blood in the urine and in the semen
- Sudden weight loss and bone pain
- Erectile dysfunction

### 1.6.8 Screening Test

**i. Prostate-specific antigen (PSA) test:** Prostate-specific antigen (PSA) is a protein that is produced naturally by the cells in the prostate gland (both normal cells and cancer cells). PSA generally presents in small amounts in the bloodstream, but blood PSA level increases (which is measured in units called nanograms per milliliter (ng/mL) if there is any abnormality in the prostate gland, such as prostate cancer. A high PSA level (> 4 ng/ ml) enhances the chances of prostate cancer.<sup>228,229</sup>

**ii. Digital rectal exam (DRE):** The doctor examines the prostate which is adjacent to the rectum, by inserting a gloved, lubricated finger into the rectum to check if there are any abnormalities in the texture, shape, or size of the gland.<sup>228</sup>

### 1.6.9 Diagnostic Test

**i. Prostate Biopsy:** A biopsy is a procedure where small samples of the prostate are removed, followed by examination under the microscope. A core needle biopsy is the main method used to diagnose prostate cancer where a urologist inserts a thin, hollow needle is inserted into the prostate through either a transrectal or trans-perineal route followed by removal of small cylinders (core) of prostate tissue for further examination to identify the presence of abnormal/cancerous cells.<sup>220,228,230</sup>

**ii. Transrectal ultrasound (TRUS):** This procedure involves transrectal ultrasound by insertion of a small probe into the rectum, which is the size and shape of a cigar that creates a picture of the prostate gland.<sup>230</sup>

**iii. Magnetic resonance imaging (MRI):** Magnetic resonance imaging creates detailed images of soft tissues in the body using radio waves and strong magnets. MRI coupled with ultrasound creates 3D images that help the doctor to locate and target areas of the prostate that are most likely to be cancerous. This method is particularly useful in biopsy procedures and in determining the spread of cancer, i.e., metastasis.<sup>230</sup>

### 1.6.10 Prostate Cancer Grades

Based on the Prostate-specific antigen (PSA) test and the grade group, Prostate cancer is divided into four stages.

**Table 4. Stages of prostate cancer and their characteristics**<sup>231,232</sup>

Stage	Substage	PSA level	Grade Group	Gleason Score	Localization
Stage I		<10	1	6 or less	Found only in the prostate
Stage II	IIA	Between 10 - 20	1	6 or less	Confined only in prostate tissue, found in more than one-half of one side or on both sides of the prostate
	IIB	< 20	2	7	Found in one or both sides of the prostate
	IIC	< 20	3 or 4	7 or 8	Found in one or both sides of the prostate
Stage III	IIIA	At least 20	1,2,3 or 4	< 6 to 8	Found in one or both sides of the prostate
	IIIB	Any level	1,2,3 or 4	< 6 to 8	Has spread from the prostate to the seminal vesicles or to nearby tissue or organs, such as the rectum, bladder, or pelvic wall
	IIIC	Any level	5	9 or 10	Found in one or both sides of the prostate and may have spread to the seminal vesicles or to nearby tissue or organs, such as the rectum, bladder, or pelvic wall
Stage IV	IVA	Any level	1,2,3,4 or 5	< 6 to 10	Found in one or both sides of the prostate and may have spread to the seminal vesicles or to nearby tissue or organs, such as the rectum, bladder, pelvic wall, nearby lymph nodes
	IVB	Any level	1,2,3,4 or 5	< 6 to 10	has spread to other parts of the body, such as the bones or distant lymph nodes.

### 1.6.11 Treatment options

Current treatment approaches include surgical removal, radiation therapy, hormone therapy, cryosurgery, chemotherapy, immunotherapy, CAR-T therapy, and monoclonal antibody. Different treatment modalities are available based on the stage of cancer.<sup>233–235</sup>

**Table 5: Current treatment modalities for different stages of prostate cancer**<sup>233–235</sup>

Stage	Standard Treatment Options	Under Clinical Trial
Stage I	Radical prostatectomy, External-beam radiation therapy (EBRT) with or without adjuvant hormonal therapy, Interstitial implantation of radioisotopes.	High-intensity focused ultrasound therapy, Photodynamic therapy
Stage II	Radical prostatectomy, External-beam radiation therapy (EBRT) with or without adjuvant hormonal therapy, Interstitial implantation of radioisotopes	Ultrasound-guided percutaneous cryosurgery, Proton-beam radiation therapy, Photodynamic therapy, neoadjuvant hormonal therapy followed by radical prostatectomy
Stage III	External-beam radiation therapy (EBRT) with or without adjuvant hormonal therapy, Hormonal manipulations (with or without radiation therapy), Radical prostatectomy with or without EBRT	
Stage IV	Hormonal manipulations with or without chemotherapy, Bisphosphonates, External-beam radiation therapy, Palliative radiation therapy (EBRT) with or without adjuvant hormonal therapy, Palliative radiation therapy, Palliative surgery with transurethral resection of the prostate (TURP)	

Different classes of drugs are approved for the treatment of different stages of prostate cancer.

**Table 6. FDA-approved drugs for different stages of prostate cancer**<sup>235,236</sup>

Class	Drugs	Comments
Cancer vaccine	Sipuleucel-T	Used to treat advanced prostate cancer that's no longer responding to hormone therapy but is causing few or no symptoms
Immune Checkpoint inhibitor	PD-1 inhibitor	
Chemotherapy	Docetaxel, Cabazitaxel Mitoxantrone Estramustine	Used when cancer spreads outside the prostate gland and hormone therapy isn't working
<b>Hormone therapy:</b> Treatment to lower testicular androgen levels	Orchiectomy (surgical castration)	Removal of the testicles, where most of the androgens (testosterone and DHT) are made
	<i>LHRH agonists:</i> Leuprolide, Goserelin,	Lower the amount of testosterone made by the testicles
	<i>LHRH antagonists:</i> Degarelix	Used to treat advanced prostate cancer
<b>Hormone therapy:</b>	Abiraterone	Blocks an enzyme (protein) called CYP17, which helps stop these cells from making androgens. It can be used in men with

Treatment to lower androgen levels from the adrenal glands		advanced prostate cancer that is either: High risk or Castration-resistant
	Ketoconazole	Used to treat men just diagnosed with advanced prostate cancer
<b>Hormone Therapy:</b> Drugs that stop androgens from working	<i>Anti-androgens:</i> Flutamide Bicalutamide Nilutamide	If orchiectomy or an LHRH agonist or antagonist is no longer working by itself,
<b>Hormone Therapy:</b> Newer anti-androgen	Enzalutamide Darolutamide Apalutamide	Men with cancer that has not spread but is no longer responding to other forms of hormone therapy (known as non-metastatic castrate-resistant prostate cancer (CRPC))
	Abiraterone- acetate	It's approved for men with advanced prostate cancer who have tried other hormone therapies.

### 1.6.12 Molecular pathogenesis of Prostate Cancer and the role of Androgen Signaling Pathway in its development

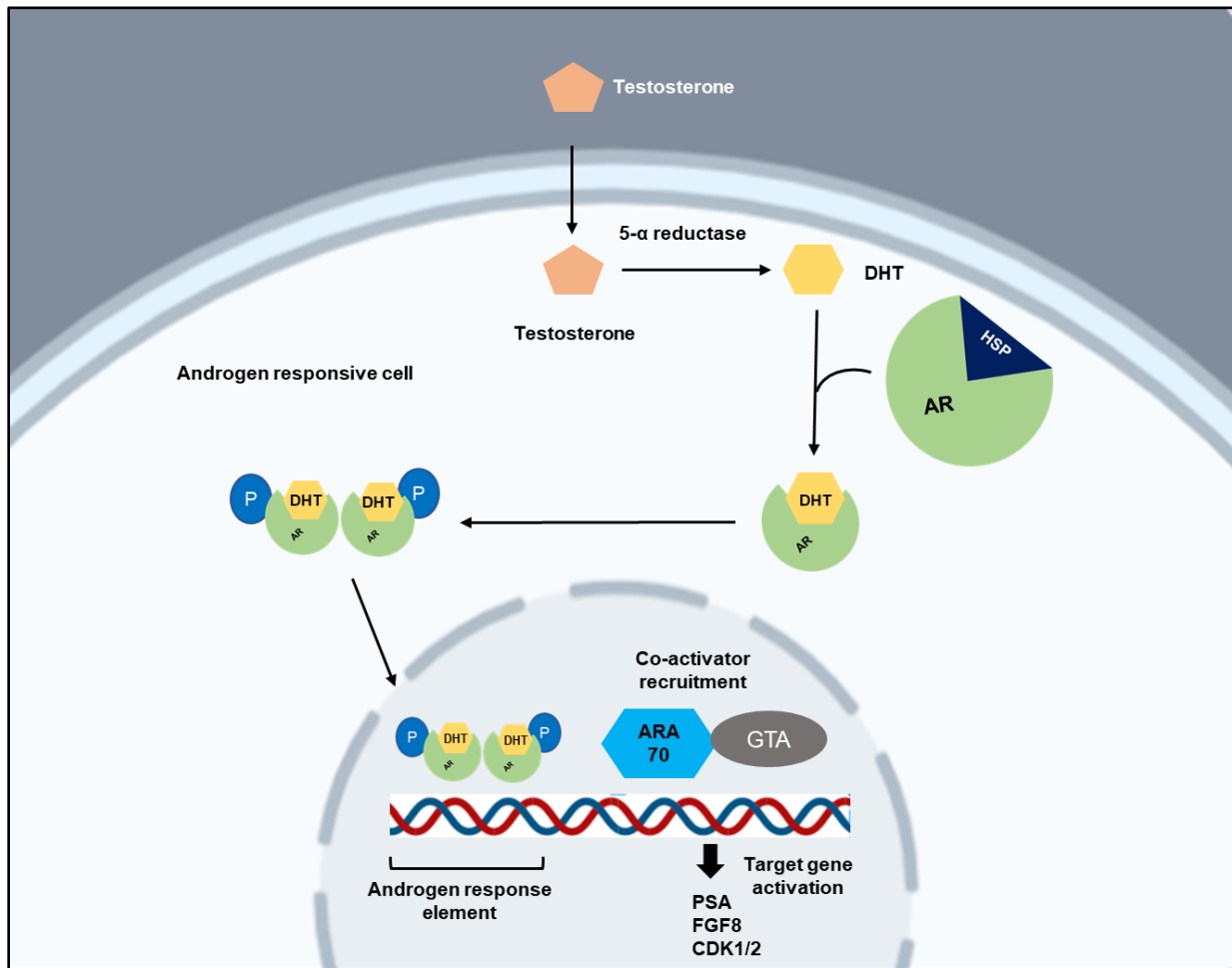
The androgen signaling pathway is the key regulator in the pathogenesis of prostate cancer. Androgen receptor (AR) is a type of nuclear receptor and a member of the steroid receptor superfamily NR3C4 (nuclear receptor subfamily 3, group C, member 4). It is a phosphoprotein that is composed of four functionally distinct domains: an amino-terminal domain (NTD), a carboxy-terminal ligand-binding domain (LBD), a DNA-binding domain (DBD), and a flexible hinge region that joins the LBD and the DBD. DBD contains a Zinc finger motif that allows its interaction with DNA.<sup>237,238</sup>

Androgen (Testosterone and Dihydrotestosterone/DHT) is the steroid hormone that promotes the growth of cancer cells. Within the prostate cancer cells, Testosterone gets converted into Dihydrotestosterone (DHT) by an enzyme called 5 $\alpha$ -reductase.<sup>239,240</sup>

In the ligand unoccupied state, AR remains localized in the cytoplasm in its inactive form as a complex with three heat-shock proteins (HSP90, HSP70, and HSP56), which prevents its degradation. Upon phosphorylation, the ligand binding domain becomes available for ligand (androgen hormone) binding. When DHT binds to the AR, it becomes activated by phosphorylation and gets released from the complex, followed by its nuclear translocation. This event also causes its conformational change and subsequent dimerization, which facilitates its binding to the androgen response element (ARE) present in the promoter region of its target

genes. AR then recruits transcriptional co-activators such as members of the p160 family (SRC-1/2, TRAM1), pCAF, and Cyclic adenosine monophosphate Response Element Binding Protein (CREB-binding protein) to drive the transcription of specific genes like PSA, FGF8, CDK1/2, TMPRSS2 that promote cancer cell proliferation.<sup>237-241</sup>

**Figure 8. Molecular Mechanism of Prostate Cancer Development**



### 1.6.13 Stages of Prostate Cancer Progression

**i. Localized Prostate Cancer:** It is the indolent disease state where the tumor remains localized within the prostate gland. This is the early stage of prostate cancer (T1 or T2), where it shows very slow growth or no growth at all with a very low risk of spreading. Active surveillance, i.e., regular tests to check on cancer and watchful waiting, are the two ways of monitoring. The treatment options for localized prostate cancer include radical prostatectomy, external beam radiotherapy, and high dose-rate brachytherapy, which are nearly curative with a 5-year survival rate of nearly 100%.<sup>241-243</sup>

Locally advanced prostate cancer is the disease state where the prostate cancer cells have broken through the capsule or covering that surrounds the prostate and start to spread into nearby tissue or organs such as bladders and seminal vesicles. According to the classification of Malignant Tumors TNM/ tumor (T), nodes (N), and metastases (M) staging, this disease is categorized either under T3, where the prostate cancer cells have started or completed the rupture of the capsules or T4 where the malignant cells already migrated to the nearby organs.<sup>242</sup>

**ii. Metastatic Hormone-Sensitive Prostate Cancer (mHSPC)/ Metastatic Castration-sensitive prostate cancer (mCSPC):** This disease state is defined clinically as where the patients show radiographical evidence of cancer spreading to the other parts of the body, yet the patients are still either hormone naïve or responsive to the hormone ablation therapy. The frontline therapy for mHSPC is either surgical castration (bilateral orchidectomies) or medical castration, such as Androgen Deprivation Therapy using Luteinizing hormone-releasing hormone (LHRH) agonists. In some cases, ADT is coupled with Androgen pathway-directed therapy (Abiraterone acetate, Apalutamide, enzalutamide or Chemotherapy (Taxanes: Docetaxel or Cabazitaxel) or Radiotherapy.<sup>241,244</sup>

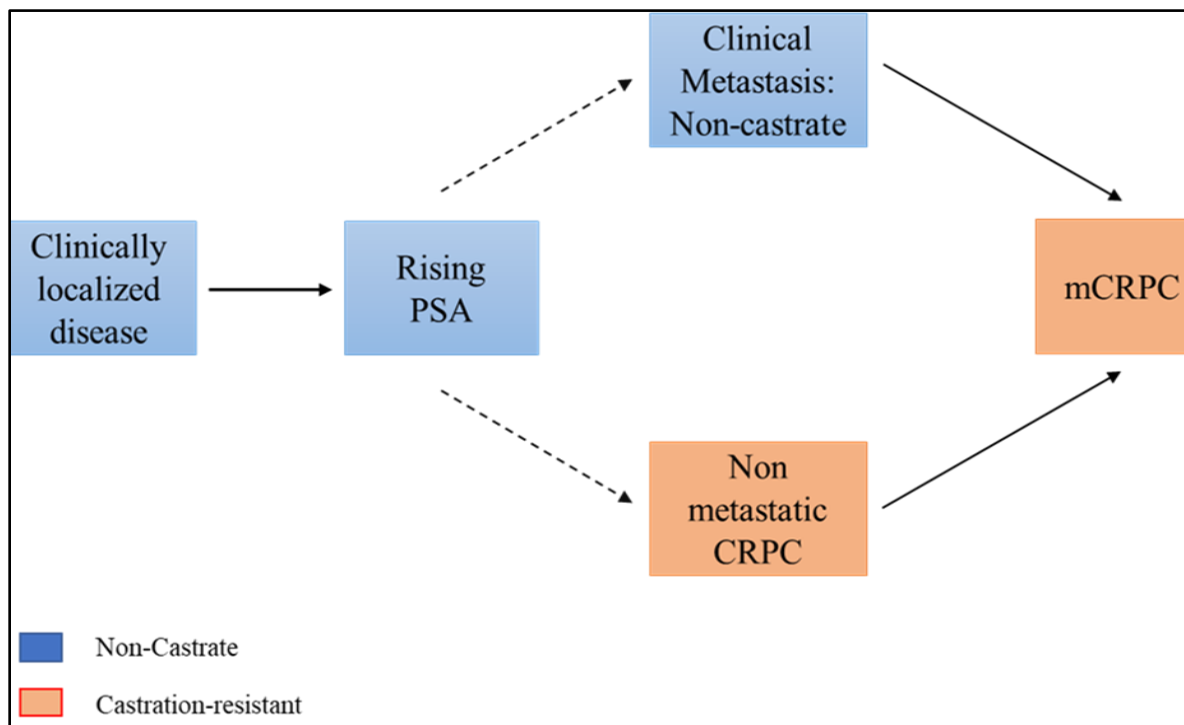
However, most of the patients with mHSPC experience a transition into the metastatic castrate-resistant (mCRPC) state. In most cases, relapse occurs in response to the initial localized treatment, but de novo metastatic condition is also observed in small populations.<sup>241,244</sup>

**iii. Castration-Resistant Prostate Cancer (CRPC)/ Androgen-independent (AIPC)/ Hormone-refractory prostate cancer (HRPC):** Due to the initial reliance of prostate cancer cells on androgens for growth and evading apoptosis, the standard treatment option for early-

stage PCa is androgen-deprivation therapy (ADT/medical castration) through surgical or pharmacological approaches. Most of the early-stage PCa patients who have been treated with ADT show good initial responses. However, the vast majority of these men eventually become unresponsive towards hormone therapy within the five years of ADT, with more > than 80% of cases showing metastases and despite low levels of androgen, patients show signs of progression of pre-existing disease condition, i.e., sustained rise in prostate serum antigen (PSA) level with/ without metastases even with castration or low testosterone levels (serum testosterone < 50 ng/dL or 1.7 nmol/L). This aggressive form of prostate cancer is termed Castration-resistant prostate cancer (CRPC).<sup>241,245,246</sup>

CRPC state can be categorized as either **non-metastatic (nmCRPC)** or **metastatic (mCRPC)**.<sup>241,246</sup>

**Figure 9. Dynamic transition model of prostate cancer clinical states**



**a. Non-Metastatic Castrate-Resistant Prostate Cancer (nmCRPC):** This is the type of CRPC that is characterized by the absence of radiographic evidence of metastases with a minimum PSA level of  $\geq 1$  ng/mL that shows a continuous trend of rising, i.e., at least 2 ng/mL higher

than the nadir PSA which indicates the lowest PSA level after ADT. Treatment options include second-generation anti-androgen like Enzalutamide, Apalutamide, and Darolutamide.<sup>246,247</sup>

Studies showed that, within five years of diagnosis, >50% of the men with nmCRPC eventually progress into metastatic disease state (mCRPC), which is a more aggressive and lethal disease state.<sup>241</sup>

**b. Metastatic Castrate-Resistant Prostate Cancer (mCRPC):** mCRPC is the advanced form of prostate cancer where cancer becomes unresponsive to the hormone ablation therapy, which spreads to the other parts of the body such as bones, lymph nodes, bladder, rectum, liver, lungs, and brain. This is the lethal disease state with poor prognosis, a median survival of < 3 years, and a 5-year survival rate of <30 %. Most of the patients progress to mCRPC within two years from the initiation of ADT.<sup>248-250</sup>

The earlier treatment options for mCRPC were mitoxantrone and Estramustine, which have failed to improve overall survival. Taxane-based chemotherapy (Docetaxel & Cabazitaxel) is the current first line of treatment for the mCRPC. TAX327 & SWOG 9916 trial showed that Docetaxel improves median OS by 2-2.9 months, whereas TROPIC trial data revealed that Cabazitaxel is effective in improving OS and prolonging treatment-free survival as a second line to therapy after Docetaxel.<sup>248,251</sup>

Apart from the Taxanes, immunotherapy (sipuleucel-T), second-generation anti-androgens/ARSi (Enzalutamide, abiraterone), and Radium, 223 dichloride are the other treatment options for mCRPC.<sup>252</sup>

#### **1.6.14 Taxane for the treatment of mCRPC**

Taxane drugs, such as Docetaxel and Cabazitaxel, are FDA-approved drugs for the treatment of metastatic castration-resistant prostate cancer. These microtubule targeting agents (MTA), which bind to the microtubules and disrupt their normal functions, are the frontline treatment for mCRPC.

Taxane exerts its action by binding with the microtubule, a cellular organelle that plays an essential role in cell division (mitosis) as well as trafficking vital proteins. It is composed of  $\alpha$ - and  $\beta$ -tubulin. 4 In prostate cancer, the important androgen receptor (AR) protein is trafficked via microtubules from the cell surface into the nucleus, where it binds DNA and leads to cancer

cell growth. The binding of Taxane with the tubulin leads to the prevention of the microtubule assembly as well as microtubular polymerization and stabilization of these tracks, which prevents the AR from moving into the nucleus. As prostate cancer cells rapidly proliferate, the effect on microtubule causes cell-cycle arrest in metaphase and, ultimately, apoptosis.<sup>253,254</sup>

#### **1.6.14.1 FDA-Approved Taxanes for mCRPC treatment**

**i. Docetaxel:** Docetaxel/ Taxotere is the intravenously administered taxoid antineoplastic drug that got FDA approval in 2004 as the frontline chemotherapy for the treatment of mCRPC based on the TAX327 & SWOG 9916, which showed that Docetaxel is effective in improving the median OS by 2-2.9 months.<sup>251</sup>

However, Docetaxel has a very high adverse effect (AE) profile. The common side effects of Docetaxel include neutropenia and anemia.

**ii. Cabazitaxel:** Cabazitaxel/ Jevtana is the intravenously administered, second-generation taxane that has a similar mechanism of action to Docetaxel but has less affinity towards drug efflux pump such as P-glycoprotein (P-gp), which makes it more effective in multi-drug resistance scenario and have better toxicity profile than Docetaxel.<sup>255</sup>

In 2014, FDA approved Cabazitaxel as a second line of therapy after Docetaxel in the treatment of mCRPC based on TROPIC trial data that revealed Cabazitaxel is effective in improving OS and prolonging treatment-free survival.<sup>255,256</sup>

#### **1.6.14.2 Mechanism of Action of Taxane Drugs**

**a. Inhibition of microtubular depolymerization:** It binds to the polymerized  $\beta$ -tubulin at a site within the lumen of the microtubule and promotes and stabilizes microtubule assembly in the absence of GTP. This leads to the disruption of microtubule dynamics and subsequent cell cycle arrest, followed by activation of the apoptotic pathway within the cells.<sup>256,257</sup>

**b. Inhibition of AR nuclear translocation:** Docetaxel can inhibit androgen receptor (AR) transcriptional activity by constraining AR expression, blocking AR nuclear translocation, and facilitating FOXO1-mediated repression of AR transcriptional activity.<sup>257</sup>

**c. Attenuation of the effect of Bcl-2 & Bcl-xL gene expression:** Docetaxel-mediated microtubule stabilization induces Bcl-2 phosphorylation, which leads to the loss of Bcl-2

antiapoptotic function by decreasing its binding to the proapoptotic Bax protein followed by apoptosis. In PC-3 cell lines, it decreases mRNA expression of Bcl-xL.<sup>258</sup>

#### 1.6.14.3 Table 7 Molecular mechanism of resistance towards Taxane drugs<sup>259,260</sup>

Tubulin alterations	Overexpression of $\beta$ III sub-unit of tubulin, which has less affinity towards taxane binding
B-tubulin mutation	T26A, A595G, and F270I mutation in the M40 isotype of $\beta$ I-tubulin which impairs the taxane-mediated polymerization
Kinesin	Involved in taxane resistance by interacting with microtubule filaments.
AR/AR-variants	Androgen receptor variants AR-v7 & AR-v567 promote Taxane resistance
TMPRSS2-ERG rearrangement	ERG fusion protein leads to the induction of Taxane-resistance by altering microtubule dynamics
Cancer stem cells	Enriched expression of CD133, CD44, NOTCH & Hedgehog signalling promote Taxane resistance
Multi-drug resistance	Over-expression of drug-efflux transporter MDR-1
PI3K/AKT signaling	Dysregulation of PI3K/AKT pathway and up-regulation of phosphorylated AKT due to inactivation of PTEN.

#### 1.6.15 Androgen Receptor Signaling Inhibitor (ARSi) for the treatment of mCRPC

Drugs belonging to this class directly target the AR-signaling axis by competitively inhibiting the ligand binding to the receptor or by inhibiting the synthesis of androgen and blocking the downstream activation and subsequent expression of AR-target genes.<sup>261,262</sup>

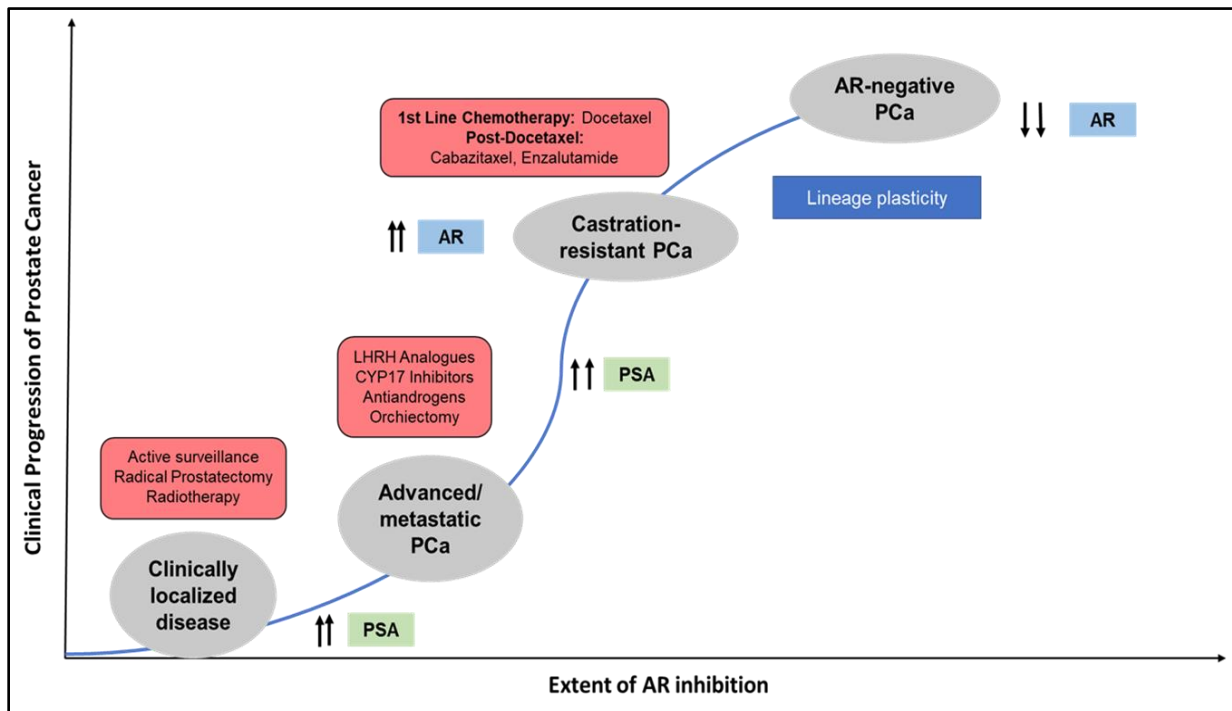
**i. Enzalutamide:** Enzalutamide/ Xtandi is the orally bioavailable second-generation ARSi that got FDA approval as the treatment option from mCRPC patients previously treated with Docetaxel based on the AFFIRM clinical trial where it improved median OS by almost five months.<sup>263,264</sup>

Enzalutamide acts as an antagonist of androgen signaling, where it competitively blocks the binding of androgen to the androgen receptor in the cytosol and blocks its nuclear translocation by preventing intramolecular N–C interaction and subsequent transcription of the target genes.<sup>263</sup>

### 1.6.16 AR<sup>null</sup> mCRPC / AR-negative mCRPC and emergence of neuro-endocrine phenotype: Neuro-Endocrine Prostate Cancer (NEPC)

Taxanes (TX) and the Androgen Receptor Signaling inhibitor (ARSi) are the front line of therapy to treat mCRPC. Despite a good initial response, most patients eventually encounter drug resistance. Under the treatment pressure of ARSi, ultimately, a subset of mCRPC patients progress into a more advanced disease state- an aggressive variant of prostate cancer (AVPCa) where the prostate cancer cells undergo de-differentiation that involves lineage plasticity, extensive transcriptional reprogramming (SOX2, SOX11), loss of p53 & phosphatase and tensin homolog (PTEN), chromatin structure rewiring and ultimately acquire androgen receptor (AR)–independent phenotype. This AR<sup>null</sup> / AR<sup>low</sup>/ AR-negative mCRPC is a rapidly progressing, hormone therapy unresponsive disease state that has a poor prognosis, mean survival of 1-3 years, and higher tumor burden. Shows signs of metastasis to the visceral organ such as liver, lung, etc., lytic bone lesions in the backdrop of slowly rising PSA-level with limited or no therapeutic options. <sup>265–269</sup>

**Figure 10. The course of clinical progression to AR<sup>null</sup> mCRPC**



In normal prostate tissue, the neuroendocrine (NE) type of epithelial cells is present in very less numbers (<1% of the total epithelial cells) as compared to the other two types of prostate epithelial cells: basal cells and luminal cells, but its number gets increased significantly in prostate adenocarcinoma. AR-negative mCRPC is characterized by the neuro-endocrine differentiation of the CRPC adenocarcinoma cells, which are evolved either by divergent clonal evolution or trans-differentiation that leads to the loss of luminal and epithelial markers. Neuromodulators such as bombesin, serotonin; cytokines (IL-1 $\beta$ , IL-6, IL-8); gene rearrangements of ETS transcription factor family member ETG and ARSi mediated AR blockade induced downregulation of TMPRSS2-ERG protein expression; amplification of Aurora kinase A (AURKA) and N-myc (MYCN); molecular signaling pathways for e.g., Wnt- $\beta$  catenin, PI3K–Akt–mTOR pathway; aberrant expression of EZH2 and downregulation of REST (regulator of neuronal gene expression) promote this NE differentiation.<sup>266,270,271</sup>

Neuroendocrine differentiation is a phenotypic change that occurs in prostate cancer cells in which they undergo trans-differentiation and acquire the structural and functional features of cells of neuronal, endocrine origin, or a mixture of both. These neuroendocrine (NE) like cells are post-mitotic cells characterized by the absence of AR and PSA; they express markers like prostatic acid phosphatase, synaptophysin (Syn), E-cadherin(E-cad), K18 and K8 cytokeratins (CK), CD56; secrete peptide hormones such as neuron-specific enolase (NSE), chromogranin A (CgA) and growth factors that facilitate the growth of the surrounding malignant cells in a paracrine manner. De novo origin of Neuroendocrine Prostate Cancer (NEPC) is very rare and found it in only <2% of the cases. This histological subtype of pure or mixed small-epithelial glandular cells has aggressive clinical manifestations such as disease progression, treatment resistance, poor overall survival of <2 years due to its dormant phenotype, and high-level expression of anti-apoptotic genes such as Bcl-2, Survivin, etc. Poor therapeutic response due to treatment-emergent NEPC (t-NEPC) is primarily observed in CRPC patients (>25% of the total CRPC cases), where the emergence of NE-like cells is directly correlated with the treatment resistance towards ADT, chemotherapy (Docetaxel, Cabazitaxel), radiotherapy. Previous studies also showed that tumors of almost 40% of the patients that are resistant towards ARSi (enzalutamide and abiraterone) display this NE phenotype.<sup>265-273</sup>

Pathological classification based on spatial and morphological features classified Neuroendocrine differentiation into five types.<sup>274,275</sup>

**i. Small cell carcinoma/ Pure NED:** In this type of NED, the tumor is made up of entirely NE cells. This is the universal NED which is extremely rare (occurrence rate of < 2%) with poor clinical outcome (OS <1 year) and characterized by small-cell carcinoma of the prostate gland (SCCP). These tumor cells show a high mitotic index (ki67 index >80%) and nucleus-to-cytoplasm ratio.<sup>266,270,272,276</sup>

**ii. Prostate adenocarcinoma with focal NED:** Focal NED or the mixed tumors that have the phenotype of both prostate adenocarcinoma and small-cell carcinoma and display features of focal NE, like cells are present either as scattered or in clusters of densely packed cells in primary and/or secondary sites. Here, only a subpopulation of tumor cells undergoes NED. This is rather more common (5-10% of cases) than Pure NED with better clinical outcomes.<sup>266,270,276</sup>

**iii. Adenocarcinoma with Paneth cell NED: This distinct sub-type of** Neuroendocrine differentiation leads to the acquirement of Paneth cell-like change of the prostatic epithelium where its resemblance to the Paneth cells of the small intestine is prominent. It is characterized by the abundant presence of large eosinophilic granules in the cytoplasm of tumor cells and the lack of prominent nucleoli.<sup>276</sup>

**iv. Large cell NE carcinoma (LCNEC):** This is a rare, aggressive, high-grade sub-type of NED (median overall survival <9 months) characterized by the presence of large tumor cells (larger than the SCCP) with a high mitotic rate (Ki67 proliferative index>50%) and abundant cytoplasm, vesicular clumpy chromatin, and prominent nucleoli with signs of necrosis. LCNEC expressed CD56, CD57, chromogranin A, and synaptophysin and is believed to be developed following long-term hormonal therapy.<sup>265,266,276</sup>

**v. Mixed (small or large cell) NE carcinoma—acinar adenocarcinoma:** This is a biphasic carcinoma that exhibits features of both NE (small cell or large cell) carcinoma and conventional acinar or ductal adenocarcinoma. Immunohistochemistry analysis shows cells are positive for NE markers such as synaptophysin, CD56, and chromogranin. It has a characteristic mixed PSA expression that shows a positive expression pattern from the acinar adenocarcinoma cells but variable PSA expression from the NE cells.<sup>266,276</sup>

AR-targeted therapy fails to achieve clinical benefits in NEPC patients. Due to its biological similarities with Small Cell Lung Cancer (SCLC), the treatment regimen that mainly contains platinum-based chemotherapy Cisplatin/ Carboplatin is the front-line treatment option for NEPC.<sup>267</sup>

## Gap in knowledge

Most advanced state cancer (relapsed/ refractory) are difficult to cure, highly heterogeneous with high recurrence rates, and have a poor long-term prognosis.<sup>277,278</sup> There are only limited therapeutic options available owing to drug resistance, extensive inter-individual variation in response, and toxicity profile that limits efficacy in clinical settings. Also, the response toward standard-of-care drugs is not durable, and patients who show good initial response often tend to progress to a more aggressive or terminal disease state. Once the standard-of-care therapy stops working, very few or no therapeutic options are available. Previous studies have shown that intra-tumoral heterogeneity due to the presence of treatment-refractory subpopulations or cancer stem-like cells (CSCs) drives drug resistance and disease relapse in various cancers. Most importantly, no study so far has attempted to develop drugs explicitly targeting these stem-like sub-clones. Standard-of-care drugs are mostly ineffective in targeting CSCs.<sup>85,215</sup>

*Therefore, there is an unmet need to discover novel drugs against R/R cancer that also specifically target cancer stem-like cells to manage these treatment-resistant malignancies.*

Our **goal** is to identify rational combination therapy with the explicit aim of improving overall survival and progression-free survival to improve the quality of life of cancer patients.

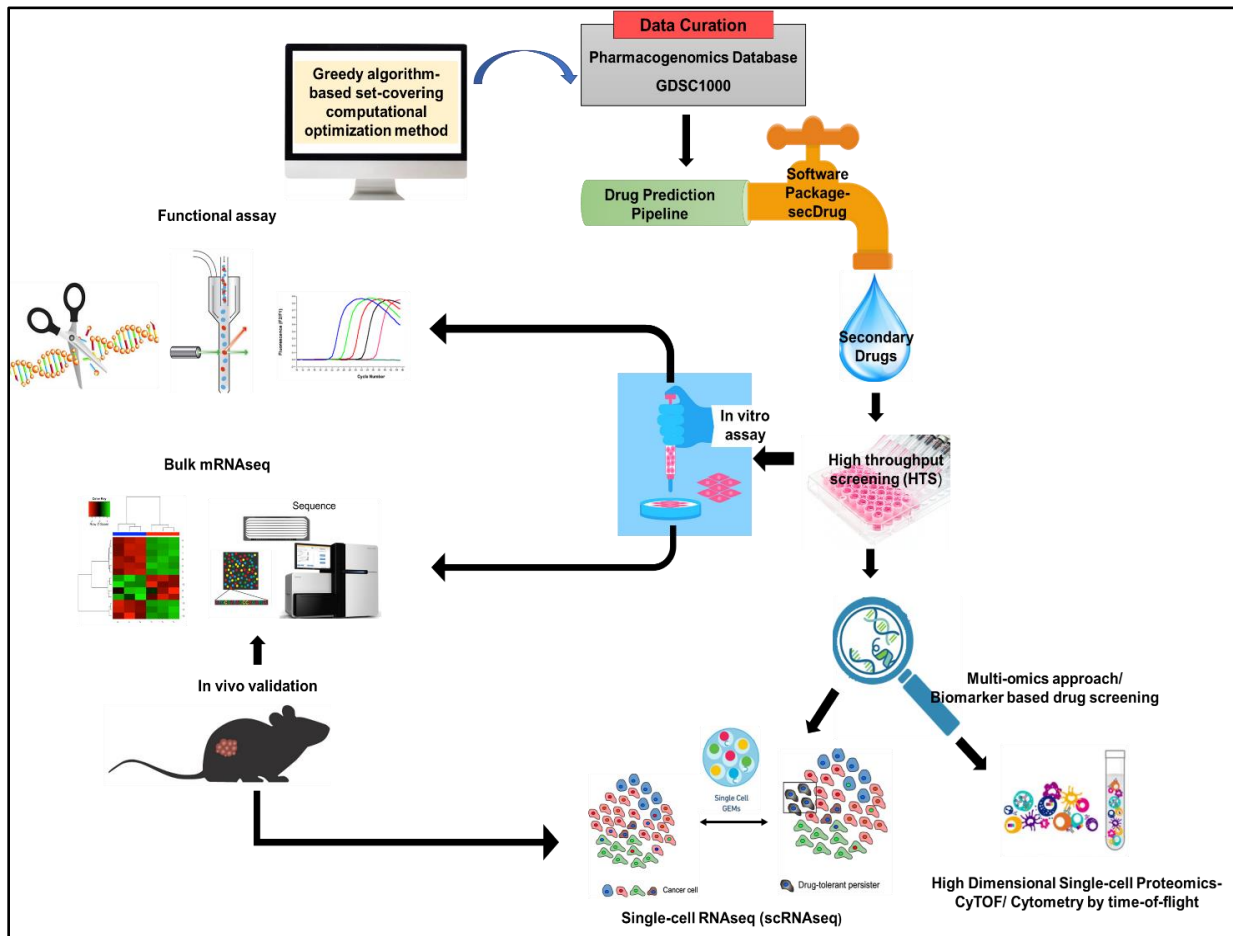
## 1.7 secDrug algorithm

Assessing the survival endpoints in clinical applications requires the treatment of a large number of patients with these drugs that need to be measured in months to years. Therefore, developing prediction algorithms of response can be a long process. One alternative is to use collections of human cancer cell lines from patient tumors that represent a broad spectrum of the biological and genetic heterogeneity of cancer, commonly known as *in vitro* modeling of drug response. We have compiled a panel of >70 human myeloma cell lines (HMCLs) representing innate and acquired PI resistance representing the broad spectrum of biological and genetic heterogeneity of myeloma patients.

Our goal was to create a multi-pronged approach/pipeline to discover, validate and characterize novel drugs as potential secondary choices for circumventing resistance to primary drugs in myeloma and generate better treatment outcomes.

1. We have created a computational pipeline by utilizing a greedy algorithm-based set-covering computational optimization method followed by a regularization technique to seek all secondary drugs that could kill a maximum number of cell lines of the test disease (B-cell malignancies/ Sex hormone-dependent malignancies) resistant to the test drug (Proteasome inhibitor/ Immunomodulatory drugs/ Bruton Tyrosine Kinase inhibitor/ Taxanes/ Androgen receptor Signaling Inhibitor) in a sequential manner ordered by the number of cell lines killed. A greedy algorithm constructs a solution to an optimization problem piece by piece through a sequence of choices to find the overall, or globally, optimal solution.
2. Toward this goal, we used the vast array of human cancer cell lines in the Genomics of Drug Sensitivity in Cancer (GDSC version GDSC1000) database. The Genomics of Drug Sensitivity in Cancer (GDSC1000) resource is the largest public collection of information on drug sensitivity in human cancer cells (contains drug-sensitivity data on 265 drugs covering a wide range of targets and processes involved in cancer biology on more than 1000 human tumor cell lines, representing a wide spectrum of human cancers, along with a wide array of genetic information including gene expression analysis data)

**Figure 11: Schematic diagram of identification, validation, and characterization of secDrug predicted novel secondary anti-cancer agents.**



## **Hypothesis**

We hypothesize that a combination of our predicted secDrugs with standard-of-care drugs will be useful in curbing oncogenic progressions in relapsed/ refractory cancer, abrogate drug resistance, and specifically target the sub-clones representing cancer stemness.

## **CHAPTER 2**

### **Validation of secondary therapies against Multiple Myeloma**

## **Abstract**

Multiple myeloma (MM) is the second-most common hematological malignancy in the US. MM is an incurable, age-dependent plasma cell neoplasm with a 5-year survival rate of less than 50%. Extensive inter-individual variation in response to standard-of-care drugs like proteasome inhibitors (PIs) and immunomodulatory drugs (IMiDs), drug resistance, and dose-limiting toxicities are critical problems for the treatment of MM. Clinical success in anti-myeloma treatment, therefore, warrants continuous development of novel combination therapy strategies with the explicit goal of improving the therapeutic efficacy by concomitantly targeting multiple signaling pathways.

We have created a computational pipeline that uses pharmacogenomics data-driven optimization-regularization/greedy algorithm to predict novel drugs (“secDrugs”) against drug-resistant myeloma. Next, we used single-cell RNA sequencing (scRNA-seq) as a screening tool to predict top combination candidates based on the enrichment of target genes. For in vitro validation of secDrugs, we used a panel of human myeloma cell lines representing drug-sensitive, innate/refractory, and acquired/relapsed PI- and IMiD resistance. Next, we performed single-cell proteomics (CyTOF or Cytometry time of flight) in patient-derived bone marrow cells (ex vivo), genome-wide transcriptome analysis (bulk RNA sequencing), and functional assays like CRISPR-based gene editing to explore molecular pathways underlying secDrug efficacy and drug synergy. Finally, we developed a universally applicable R-software package for predicting novel secondary therapies in chemotherapy-resistant cancers that outputs a list of the top drug combination candidates with rank and confidence scores.

Thus, using 17AAG (HSP90 inhibitor) + FK866 (NAMPT inhibitor) as proof of the principle of secDrugs, we established a novel pipeline to introduce several new therapeutic options that have the potential to revolutionize clinical decision-making by minimizing the number of drugs required for discovering successful combination chemotherapy regimens against drug-resistant myeloma.

## Introduction

Multiple myeloma (MM) is the second-most common hematopoietic malignancy in the United States.<sup>279</sup> MM is an age-dependent plasma cell neoplasm characterized by clonal expansion of malignant antibody-producing post-germinal-center B cell-derived plasma cells within the bone marrow with significant complexity and heterogeneity at the molecular level.<sup>279–281</sup> Proteasome inhibitors (PIs) are standard-of-care chemotherapeutic agents for myeloma that impede tumor metastasis and angiogenesis by accelerating unfolded protein response (UPR) or the ubiquitin-dependent proteolysis of critical regulatory proteins involved in key physiological and pathophysiological cellular processes in cancer cells and by interfering with the NF- $\kappa$ B-enabled regulation of cell adhesion-mediated drug resistance. Bortezomib (Bz/Velcade) was the first PI to be approved by U.S. Food and Drug Administration (FDA) for clinical application in 2003 for the treatment of relapsed and refractory myeloma.<sup>279,282,283</sup> Other examples include second-generation PIs Carfilzomib (Cz/Kyprolis) and the oral medication Ixazomib (Ix/Ninlaro/MLN9708).<sup>282–284</sup> PIs are effective anti-MM drugs when used alone or in combination with other anti-cancer agents like immunomodulatory drugs (IMiDs), alkylating agents, topoisomerase inhibitors, corticosteroids, and histone deacetylase inhibitors (HDACi).<sup>279,281</sup> However, despite these and other recent improvements in therapies, myeloma still remains a difficult-to-cure disease with dose-limiting toxicities and drug resistance and a median survival rate of only around seven years.<sup>285,286</sup> Not all patients respond equally well to treatment, and those who do often develop resistance over the course of treatment. Drug resistance may therefore be categorized into (1) innate resistance already presents in drug-naïve patients who never respond to treatment, or (2) emerging/acquired resistance where a patient's tumor ultimately undergoes relapse or “acquires” the ability to resist therapy in the course of treatment despite good response to initial treatment.<sup>280,286</sup> Therefore, there is an urgent need to search for novel secondary therapeutic options where new agents may be combined with standard-of-care drugs to achieve synergistic effects for treating drug resistance in myeloma.

Deciphering key features within patients underlying tumor heterogeneity and personalized sensitivity to chemotherapy is essential to predict the efficacy of anti-cancer drugs and to prevent delay in the selection of more effective alternative strategies.<sup>279,280,285–288</sup> However, assessing the survival endpoints in clinical applications requires the treatment of a large number of patients with these drugs that need to be measured in months to years. Therefore, developing prediction

algorithms of response can be a long process. One alternative is to use collections of human cancer cell lines from patient tumors that represent a broad spectrum of the biological and genetic heterogeneity of cancer, commonly known as in vitro modeling of drug response. We have compiled a panel of >70 human myeloma cell lines (HMCLs) representing the broad spectrum of biological and genetic heterogeneity of myeloma patients.<sup>287</sup>

In this study, we have developed a computational method called secDrug for discovering novel synergistic secondary drug combinations that may effectively reverse resistance as combination regimens and allow for reduced dosing and toxicity of FDA-approved myeloma drugs. Next, we introduced single-cell transcriptomics as a novel screening tool for prioritizing secDrug combinations based on the sub clonal expression of the drug targets and observed that the 17AAG + FK866 combination is potentially highly efficacious.

Further, to validate our prediction results, we used our HMCL panel as in vitro model system representing inter-individual heterogeneity in drug response/resistance to show that the top predicted secondary secDrugs are indeed effective against PI- and IMiD resistance as single agents or as a combination. Further, using 17-AAG (an HSP90 inhibitor) as the test secDrug, we added functional assays, next-generation RNA sequencing, CRISPR-based gene editing, and high-dimensional mass cytometry (CyTOF/cytometry time of flight) in primary bone marrow cells (PMCs; ex vivo model system) from myeloma patients to create a multi-pronged approach/pipeline to discover, validate and characterize novel drugs as potential secondary choices for circumventing resistance to primary drugs in myeloma and to generate better treatment outcomes. This also allowed the identification of differentially expressed (DE) genes and novel pathways associated with successful drug combinations.

## **Materials and Methods**

### **In silico prediction of secondary drugs**

Design and development of the secDrug pipeline are non-trivial and mathematically involved (details provided in Supplementary Methods section). Briefly, we utilized we used the vast array of human cancer cell lines in the Genomics of Drug Sensitivity in Cancer (GDSC version GDSC1000) database and created a pharmacogenomics data-driven greedy algorithm-based set-covering computational optimization method followed by a regularization technique to seek all secondary drugs that could kill the maximum number of cell lines of the test disease (B-cell cancers) resistant to the test drug (PI) in a sequential manner ordered by the number of cell lines killed. A greedy algorithm constructs a solution to an optimization problem piece by piece through a sequence of choices to find the overall, or globally, optimal solution. The GDSC1000 database is the largest public collection of information on sensitivity to >250 drugs covering a wide range of targets and processes involved in cancer biology in >1000 human cancer cell lines

### **Drugs, reagents, antibodies, and kits**

Ixazomib (Ixa) was procured from Takeda (Takeda Pharmaceuticals Inc., Deerfield, IL, USA). All other drugs were purchased from Selleck Chemicals (Houston, TX, USA). Drugs were dissolved in dimethyl sulfoxide (DMSO) and stored at  $-20^{\circ}\text{C}$ . Recombinant Human IL-6 was obtained from PeproTech, Inc. (Cranbury, NJ, US)

Cleaved caspase-3/8/9, HSP90, c-Myc, p65, and IRF4 antibodies were purchased from Cell Signaling Technology (Danvers, MA, US). Monoclonal Anti- $\beta$ -Actin-Peroxidase antibody produced in mouse was purchased from Sigma-Aldrich (St Louis, MO, USA). Goat anti-Mouse/Rabbit IgG (H + L) secondary antibody (HRP conjugated) was obtained from ThermoFisher Scientific (Waltham, MA, USA). DHE (Dihydroethidium) assay kit and JC-1 Mitochondrial Membrane Potential (MMP) assay kits were purchased from Abcam (Waltham, MA, USA). Caspase-Glo 3/7 Assay System and CellTiter-Glo 2.0 Assay were purchased from Promega (Madison, WI, USA).

### **Human myeloma cell lines (HMCLs)**

HMCLs generated through the immortalization of primary myeloma cells were used as in vitro model systems to screen top secDrugs against sensitive, innate resistant, and acquired (Parental/P

vs. clonally-derived resistant/R pairs generated using dose escalation over a period of time) myeloma.<sup>287</sup> We have also generated in vitro drug response profiles for the four PIs: Bz, Cz, Oprozomib (Opz), and Ixa as single agents in all the HMCLs included in the panel. PI-sensitivity in these cell lines was highly correlated, which suggests that any of these four PIs could be used as surrogates. Therefore, we used Ixazomib as the representative PI in this study. Further, we have used machine learning-based computational approaches to derive a gene expression signature predictive of baseline PI-response in myeloma.<sup>287</sup> The creation of the ANBL6 N-Ras (ANBL6/Ras) codon 61 activating mutant cell line has been described earlier.<sup>289,290</sup> The IMiD-resistant cell line, MM1S LenR, was obtained as a gift from Dr. Keith Stewart, Mayo Clinic, AZ. All cell lines were authenticated at source and tested randomly at regular intervals at the AU Center for Pharmacogenomics and Single-Cell Omics (AUPharmGx) using Gene-Print 24 System from Promega (Madison, WI, USA). All cell lines are mycoplasma negative. HMCLs were maintained in HMCL media supplemented with IL-6.

### **Human primary myeloma cells (PMCs)**

Bone marrow-derived CD138<sup>+</sup> patient PMCs were obtained through Mayo Clinic, MN following written informed consent and used as ex vivo model systems. Prior IRB approval was obtained from the Mayo Clinic review board. Participants were identified by number, not by name.

### **Establishment of RPMI8226 Hsp90 CRISPR-knockout cell line**

Chemically-modified synthetic single-guide RNA (sgRNA) was designed to target the Hsp90AA1 gene and synthesized by Synthego Corporation (Menlo Park, CA, USA). The sgRNAs were required to meet strict off-target requirements of at least two mismatches within an early exon and target a common exon present in the majority of annotated transcripts. The sgRNAs were complexed together with the spCas9 to form a ribonucleoprotein (RNP). The RNPs were then delivered to RPMI8226 cells via an optimized electroporation setting. The transfected cells were then recovered for two days before the edits created were evaluated. Positive control sgRNA (RELA) was transfected at the same time. The edited site was PCR-amplified, and Sanger sequencing was performed on the amplicon's Sequencing data was then analyzed using Synthego's Inference of CRISPR Edits (ICE) software tool to determine the percentage of knock-out (KO) sequences of the genetic target.<sup>291</sup> ICE identifies the editing

frequency and the specific indels present in the pool. Additionally, ICE calculates the frequency of the desired KO, reported as the KO score. Finally, once minimum KO editing efficiency was confirmed, RPMI8226/Hsp90KO cells were expanded, and QC tested.

### **In vitro chemosensitivity assays and drug synergy analysis**

Cells were treated with increasing concentrations of secDrugs and PIs (represented by Ixazomib) or IMiDs (represented by Lenalidomide) as single agents or in combination for 48 h, and cytotoxicity assays were performed using CellTiter-Glo® Luminescent cell viability assay (Promega Madison, WI). Luminescence was recorded in a Neo2 Microplate Reader (Biotek), and half-maximal inhibitory concentration (IC<sub>50</sub>) values were determined using GraphPad Prism software by calculating the nonlinear regression using sigmoidal dose-response equation (variable slope). Drug synergy was calculated using Calcsyn software based on Chou–Talalay’s combination index (CI) method and the isobologram algorithm (Biosoft, US) [21].

### **Apoptosis assays**

Caspase-3/7 activity assay was performed on the HMCLs using Caspase-Glo 3/7 luminescent assay kit according to the manufacturer’s instructions (Promega Madison, WI) using Synergy 2 Microplate Reader (BioTek; Winooski, VT, US). Cell death by apoptosis was also measured by immunoblotting analysis.

### **Determination of superoxide levels**

Cells were incubated with 5 µM DHE (in RPMI) for 15 min in the dark at 37 °C. Cells were then washed once with cell-based assay buffer, and red fluorescence was recorded by Synergy Neo2 multi-plate reader.

### **Measurement of mitochondrial membrane potential (MMP)**

Cells were incubated with 5 µM JC-1 dye for 15 min in the dark at 37 °C and washed twice in PBS, and then analyzed for red and green fluorescence by Synergy 2 Microplate Reader (BioTek; Winooski, VT, US).

### **Mass cytometry (CyTOF)**

Thirty-seven antibody targets directed against cell surface and intracellular markers were utilized as Immunophenotyping Panel for CyTOF analysis. The Antibody markers and respective metal

conjugates are described in Table 1. Panels were designed using the web-based panel designer software: Maxpar Panel Designer ([www.fluidigm.com](http://www.fluidigm.com)) for optimal signals, minimum background due to oxidation, isotopic purity, and sufficient sensitivity for each targeted marker. Pre-labeled antibodies were purchased from Fluidigm Corporation (South San Francisco, CA, USA). Purified antibodies from BioLegend (San Diego, CA, USA) and Santa Cruz Biotechnology, Inc. (Dallas, TX, USA) were labeled using an X8 polymer MaxPAR antibody conjugation kit (Fluidigm) according to the manufacturer's instructions. CyTOF analysis was performed on PMCs treated with DMSO (vehicle/control), 0.2  $\mu$ M 17AAG, 1  $\mu$ M 17AAG, and 5  $\mu$ M 17AAG.

**Table 1:** Immunophenotyping panel for CyTOF analysis

**A. Cell surface targets**

SN.	Targets	Metal Tag	Source/Manufacturer	Catalog No.
1.	CD45	89Y	Fluidigm	3089003B
2.	CD38	114Nd	Fluidigm	3144014B
3.	CD138	168Er	Fluidigm	3168009B
4.	CD3	141Pr	Fluidigm	3141019B
5.	CD56	149Sm	Fluidigm	3149021B
6.	CD19	169Tm	Fluidigm	3169011B
7.	CD81	145Nd	Fluidigm	3145007B
8.	CD20	147Sm	Fluidigm	3147001B
9.	CD34	148Nd	Fluidigm	3148001B
10.	CD274	159Tb	Fluidigm	3159029B
11.	CD27	167Er	Fluidigm	3167006B
12.	CD229	174Yb	Fluidigm	3174017B
13.	CD16	209Bi	Fluidigm	3209002B
14.	CD86	150Nd	Fluidigm	3150020B
15.	CD117*	173Yb	BioLegend	313223
16.	CD28*	154Sm	BioLegend	302937
17.	CD147*	161Dy	BioLegend	306206
18.	CD71*	170Er	BioLegend	334102

## B. Intracellular targets

SN.	Targets	Metal Tag	Source/Manufacturer	Catalog No.
1.	IkB $\alpha$	164Dy	Fluidigm	3164004A
2.	pERK 1/2 [T202/Y204]	171Yb	Fluidigm	3171010A
3.	pStat3 [Y705]	158Gd	Fluidigm	3158005A
4.	IRF4	155Gd	Fluidigm	3155014B
5.	IKZF1	143Nd	Fluidigm	3143024B
6.	Ki-67	172Yb	Fluidigm	3172024B
7.	pS6 [S235/S236]	175Lu	Fluidigm	3175009A
8.	MCL 1	163Dy	Fluidigm	3163006A
9.	Caspase 3/Cleaved	142Nd	Fluidigm	3142004A
10.	pAkt [S473]	152Sm	Fluidigm	3152005A
11.	p38 [T180/Y182]	156Gd	Fluidigm	3156002A
12.	pRb [S807/811]	166Er	Fluidigm	3166011A
13.	pCREB [S133]	165Ho	Fluidigm	3165009A
14.	IKZF3	162Dy	Fluidigm	3162032B
15.	c-Myc	176Yb	Fluidigm	3176012B
16.	Ig kappa/light chain	160Gd	Fluidigm	3160005B
17.	Ig lambda/light chain	151Eu	Fluidigm	3151004B
18.	BCL-2*	153Eu	BioLegend	658702
19.	Cyclin D1*	146Nd	Santa Cruz Biotechnology	SC-8396

## CyTOF data analysis

Cytobank software version 7.3.0 (Santa Clara, CA, USA) was used for the cleanup of cell debris and removal of doublets and dead cells. Cleaned .fcs files were further gated and analyzed by Cytobank. Plasma cells were identified as CD19<sup>-</sup>, CD16<sup>-</sup>, CD3<sup>-</sup>, CD38<sup>+</sup>, and kappa OR lambda<sup>+</sup> (based on each patient's kappa or lambda restriction from clinical flow data). If the plasma cells had diminished surface CD38 expression as a result of previous daratumumab exposure, CD229 was used as a positive selection marker. T-distributed stochastic neighbor embedding (t-SNE), viSNE, and FlowSom plots were generated to visualize the subpopulation architecture based on markers of interest. Relative marker intensities and cluster abundances per sample were visualized by a heatmap.

## Single-cell RNA sequencing (scRNA-seq)

Automated single-cell capture, and cDNA synthesis were performed at ~1500 tumor cells/sample using the 10X Genomics Chromium platform from 10X Genomics (Pleasanton, CA, USA) that uses droplet-sequencing-based chemistry. Single-cell RNA sequencing was

performed on Illumina HiSeq 2500 NGS platform (Paired-end.  $2 \times 125$  bp, 100 cycles. v3 chemistry) from Illumina (San Diego, CA, USA) at >50 million reads per sample.

### **scRNA-seq data analysis**

scRNAseq datasets were obtained as matrices in the Hierarchical Data Format (HDF5 or H5). A combination of Seurat and Partek Flow software packages was used to pre-process the data and perform single-cell transcriptomics analysis. Highly variable genes for clustering analysis were selected based on a graph-based clustering approach. The visualization of cell populations was performed by t-SNE.

### **Next-generation RNA sequencing (NGS)**

HMCLs were plated at a density of  $4 \times 10^5$  cells per mL, and 0.5  $\mu$ M of 17-AAG was added as a single agent or in combination with 15 nM of Ixazomib. Baseline (untreated) and post-treatment (treated) cells were collected 24 h post-treatment. High-quality RNA was extracted using QIA shredder and RNeasy kit (Qiagen). RNA concentration and integrity were assessed using a Nanodrop-8000 spectrophotometer (Thermo-Fisher Scientific; Waltham, MA, USA) and Agilent 2100 Bioanalyzer (Agilent Technologies; Santa Clara, CA, USA) and stored at  $-80$  °C. An RNA integrity number threshold of eight was applied, and RNA-seq libraries were constructed using Illumina TruSeq RNA Sample Preparation kit v2 from Illumina (San Diego, CA, USA)

NGS Libraries were size-selected, and RNA sequencing (RNAseq) was performed on Illumina's NovaSeq platform using a 150 bp paired-end protocol with a depth of >20 million reads per sample.

### **RNAseq data analysis**

Gene expression data were pre-processed, log<sub>2</sub>-transformed, and analyzed using a combination of command-line-based analysis pipeline (DEseq2 and edgeR) and Partek Flow software to identify differential gene expression profiling (GEP) signatures. Genes with mean counts < 10 were removed, and CPM (counts per million) data was used to perform differential expression testing to identify GEP signatures. Due to the small sample sizes, we used GSA to perform differential gene expression analysis between groups that applies limma, an empirical Bayesian method, to detect the DE genes (DEGs). Genes with mean fold-change > |1| and  $p < 0.05$  were

considered as the threshold for reporting significant differential gene expression. Heatmaps were generated using unsupervised hierarchical clustering (HC) analysis based on the top DEGs.

### **Pathway analysis**

Ingenuity pathway analysis (IPA) software (QIAGEN, Hilden, Germany) was used to identify the molecular pathways and upstream regulators predicted to be activated or inhibited in response to 17-AAG treatment (single-agent and combination with PIs) based on the list of significantly differentially regulated genes.

### **Western Blotting**

HMCLs treated with 17-AAG alone, Ixa alone, or 17-AAG + Ixa combination were harvested, washed, and lysed using radioimmunoprecipitation assay (RIPA) lysis buffer containing 50 mM Tris-HCl, pH 7.5, 150 mM NaCl, 1% NP40, 5 mM EDTA, 1 mM DTT, phosphatase, and protease inhibitors cocktail (Sigma) and incubated on ice for 15 min. Samples were then centrifuged at 14,000 rpm at 4 °C for 30 min. The supernatant was then aspirated and quantified using Pierce™ BCA Protein Assay Kit (Thermo-Fisher Scientific; Waltham, MA, USA). Samples were solubilized in sodium dodecyl sulfate-polyacrylamide gel electrophoresis sample buffer, and equal amounts of protein were loaded per lane of 10% sodium dodecyl sulfate-polyacrylamide gels and transferred onto PVDF membranes (Millipore; Billerica, MA, USA). Membranes were blocked in TBS with SuperBlock™ blocking buffer (Thermo-Fisher Scientific; Waltham, MA, USA) incubated with primary antibodies and secondary antibodies in TBS with 0.2% Tween 20 and 2.5% bovine serum albumin. Immunoreactivity was detected by chemiluminescent HRP substrate (Bio-Rad Laboratories; Hercules, CA, USA), and the exposed image was captured using a ChemiDoc™ MP Imaging System (Bio-Rad). Densitometry analysis was performed using Image J software from the National Institutes of Health (NIH; Bethesda, MD, USA).

### **Statistical analysis**

All statistical analyses were performed using R (the project for statistical computing and graphics) and GraphPad Prism 9.0 software. All tests were two-sided, and  $p < 0.05$  was considered statistically significant.

## Results

### Identification of secondary drugs using the secDrug algorithm

A novel modified greedy algorithm-based set-covering computational optimization-regularization pipeline was used to identify all secondary drugs that could kill the maximum number of cell lines in the GDSC1000 database belonging to the test disease (B-cell cancers, including myeloma) and which are resistant to the PI/PI drug Bortezomib (Bz/Velcade; the primary anti-myeloma drug). A total of 1091 cell lines were present in the GDSC1000 database.<sup>292,293</sup> The following filtering criteria were applied to select computable B-cell lines: target cell—B-cell; cancer type—blood; tissue—blood; histology—lymphoid\_neoplasm/haematopoietic\_neoplasm; site—haematopoietic\_and\_lymphoid\_tissue; no missing data). A total of 94 cell lines satisfied the above filtering criteria and were selected for further analysis. IC<sub>50</sub> values were processed, imputed, and categorized as S (PI-sensitive), R (PI-resistant), and N (“Neutral”/Intermediate PI IC<sub>50</sub> values) prior to analysis. We applied our computation algorithm to the GDSC1000 dataset and predicted the top secDrugs that can be best combined with PIs to achieve response in N and R lines. The predicted top secondary drug combinations in PI-resistant + PI-neutral B-cell cancers with a PI backbone are shown in **Table 2**. These include HSP90 inhibitor (17-AAG), Nicotinamide phosphoribosyl transferase or Nampt inhibitor (FK866), PIKfyve inhibitor (YM201636), Raf inhibitor (PLX-4720), Bcl2 inhibitor (Navitoclax), SB505124 (transforming growth factor- $\beta$  type I receptor, ALK4, ALK7 inhibitor), S6K1-specific inhibitor (PF-4708671), and the neddylation inhibitor (MLN4924). Furthermore, when only the top PI-resistant cell lines (R; highest 33% PI IC<sub>50</sub>) were considered, the following drugs were predicted to be highly effective: 17 AAG, PLX4720, YM201636, and the AKT inhibitor KIN001.102.

**Table 2:** Detailed list of top combination treatment regimens with a proteasome inhibitor (PI) backbone predicted using the secDrug optimization-regularization computational algorithm. Percent coverage (cell lines predicted to be killed by the treatment) of the B-Cell cancer lines included in the prediction model is also provided.

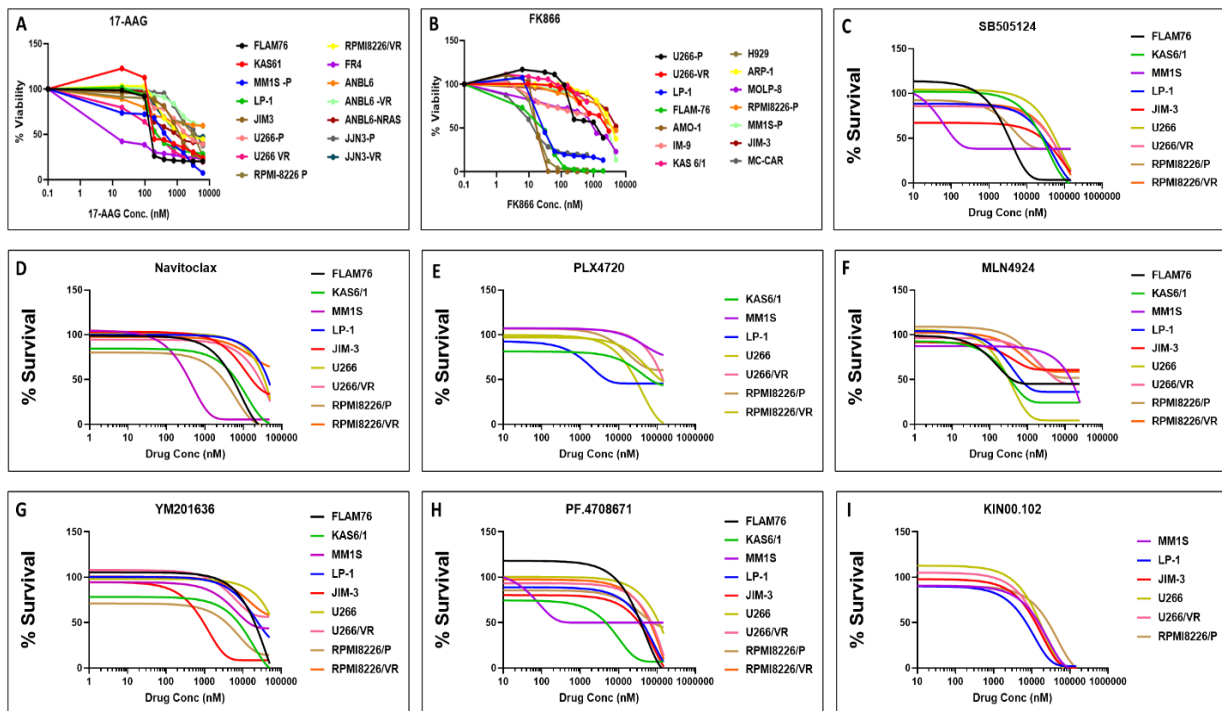
Sl. No.	No-Drug	PI only	PI + 2 secDrugs	PI + 3 secDrugs
1	0	33.0%	PI + FK866 + 17.AAG 72.2%	PI + FK866 + 17.AAG + SB216763 82.5%
2	0	33.0%	PI + XAV939 + 17.AAG 71.1%	PI + XAV939 + 17.AAG + VNLG.124 83.5%
3	0	33.0%	PI + PF.4708671 + Bleomycin 76.3%	PI + PF.4708671 + Bleomycin + FK866 87.6%
4	0	33.0%	PI + Bleomycin + SB505124 75.3%	PI + Bleomycin + SB505124 + Navitoclax 86.6%
5	0	33.0%	PI + PLX4720 + Navitoclax 75.3%	PI + PLX4720 + Navitoclax + Roscovitine 84.5%
6	0	33.0%	PI + Afatinib + Navitoclax 72.2%	PI + Afatinib + Navitoclax + MLN4924 82.5%
7	0	33.0%	PI + PD.173074 + MLN4924 71.1%	PI + PD.173074 + MLN4924 + KIN001.055 82.5%
8	0	33.0%	PI + SN.38 + SB505124 73.2%	PI + SN.38 + SB505124 + ATRA 85.6%
9	0	33.0%	PI + Bicalutamide + Navitoclax 72.2%	PI + Bicalutamide + Navitoclax + EHT1864 82.5%
10	0	33.0%	PI + MLN4924 + PIK.93 74.2%	PI + MLN4924 + PIK.93 + SB505124 84.5%
11	0	33.0%	PI + UNC0638 + 17.AAG 72.2%	PI + UNC0638 + 17.AAG + EHT1864 82.5%
12	0	33.0%	PI + YM201636 + Temozolomide 72.2%	PI + YM201636 + Temozolomide + AZD8055 82.5%
13	0	33.0%	PI + Methotrexate + JW.7.24.1 73.2%	PI + Methotrexate + JW.7.24.1 + AMG.706 84.5%
14	0	33.0%	PI + KU.55933 + GSK269962A 72.2%	PI + KU.55933 + GSK269962A + KIN001.055 83.5%
15	0	33.0%	PI + NU.7441 + JQ1 72.2%	PI + NU.7441 + JQ1 + EHT1864 82.5%

16			PI + AZD6482 + UNC0638	PI + AZD6482 + UNC0638 + MLN4924
	0	33.0%	74.2%	84.5%
17			PI + CCT018159 + CP466722	PI + CCT018159 + CP466722 + JQ1
	0	33.0%	72.2%	82.5%
18			PI + JQ1 + Doxorubicin	PI + JQ1 + Doxorubicin + 17.AAG
	0	33.0%	74.2%	84.5%
19			PI + UNC0638 + AS605240	PI + UNC0638 + AS605240 + Roscovitine
	0	33.0%	74.2%	83.5%
20			PI + YK4.279 + TL.2.105	PI + YK4.279 + TL.2.105 + Temsirolimus
	0	33.0%	73.2%	82.5%
21			PI + AICAR + SN.38	PI + AICAR + SN.38 + SB505124
	0	33.0%	71.1%	83.5%
22			PI + Docetaxel + Bleomycin	PI + Docetaxel + Bleomycin + Roscovitine
	0	33.0%	72.2%	83.5%
23			PI + PD.0332991 + Gefitinib	PI + PD.0332991 + Gefitinib + Bicalutamide.1
	0	33.0%	71.1%	80.4%
24			PI + AG.014699 + Trametinib	PI + AG.014699 + Trametinib + Roscovitine
	0	33.0%	71.1%	81.4%
25			PI + GSK269962A + Navitoclax	PI + GSK269962A + Navitoclax + Cetuximab
	0	33.0%	71.1%	81.4%
26			PI + piperlongumine + CP466722	PI + piperlongumine + CP466722 + MLN4924
	0	33.0%	72.2%	80.4%
27			PI + Trametinib + CP466722	PI + Trametinib + CP466722 + SB505124
	0	33.0%	72.2%	82.5%
28			PI + KIN001.055 + Temozolomide	PI + KIN001.055 + Temozolomide + Temsirolimus
	0	33.0%	73.2%	82.5%

## Top secDrugs induce loss of viability in HMCLs as single-agent treatment

First, we used our panel of HMCLs as in vitro validation screens to evaluate the top predicted secDrugs, including 17-AAG, PF.4708671, SB505124, Navitoclax, PLX4720, MLN4924, YM201636, FK866, KIN001.002. As shown in Figure 1, the predicted secDrugs showed high single-agent in vitro cytotoxicity in our myeloma cell line panel, including innate and acquired PI-resistant and IMiD-resistant myeloma cell lines compared to untreated control at increasing concentrations of secondary drugs.

**Figure 1. secDrugs decrease in vitro cell viability in multiple myeloma.**



Single-agent dose-response plots for secDrugs in HMCLs.

**A** 17AAG; **B** FK866; **C** SB505124; **D** Navitoclax; **E** PLX4720; **F** MLN4924; **G** YM201636; **H** PF.4708671; **I** KIN001.002.

## Single-cell transcriptomics (scRNA-seq)-based drug screening predicted 17-AAG + FK866 as potentially effective against myeloma

Next, we used single-cell RNA sequencing (scRNA-seq) as a novel biomarker-based drug screen to identify single-cell sub-clones (represented by t-SNE clusters) that harbor secDrug target genes in the untreated/baseline HMCLs representing sensitive or myeloma tumors. Our scRNA-

seq data in (representative t-SNE clusters shown in Figure 2) demonstrated that the majority of the single-cell clusters in drug-sensitive and drug-resistant myeloma have high expression of 17-AAG target genes HSP90AA1, HSP90AB1, and the FK866 target gene NAMPT indicating that 17-AAG and FK866 combination may be effective against these subpopulation clusters. The 17-AAG target gene list was derived from the Harvard Medical School (HMS)'s NIH Library of integrated network-based cellular signatures perturbagen database, a publicly available database devoted to understanding how human cells respond to perturbation by drugs, the environment, and mutation.<sup>292,294</sup>

**Figure 2A. Results from the single-cell RNAseq) analysis on the myeloma cell line pair U266-P/VR.**

Comparison of the t-SNE/Graph-based clusters between U266P vs. U266VR cell lines (U266P—parental/sensitive, U266VR—acquired-resistant).

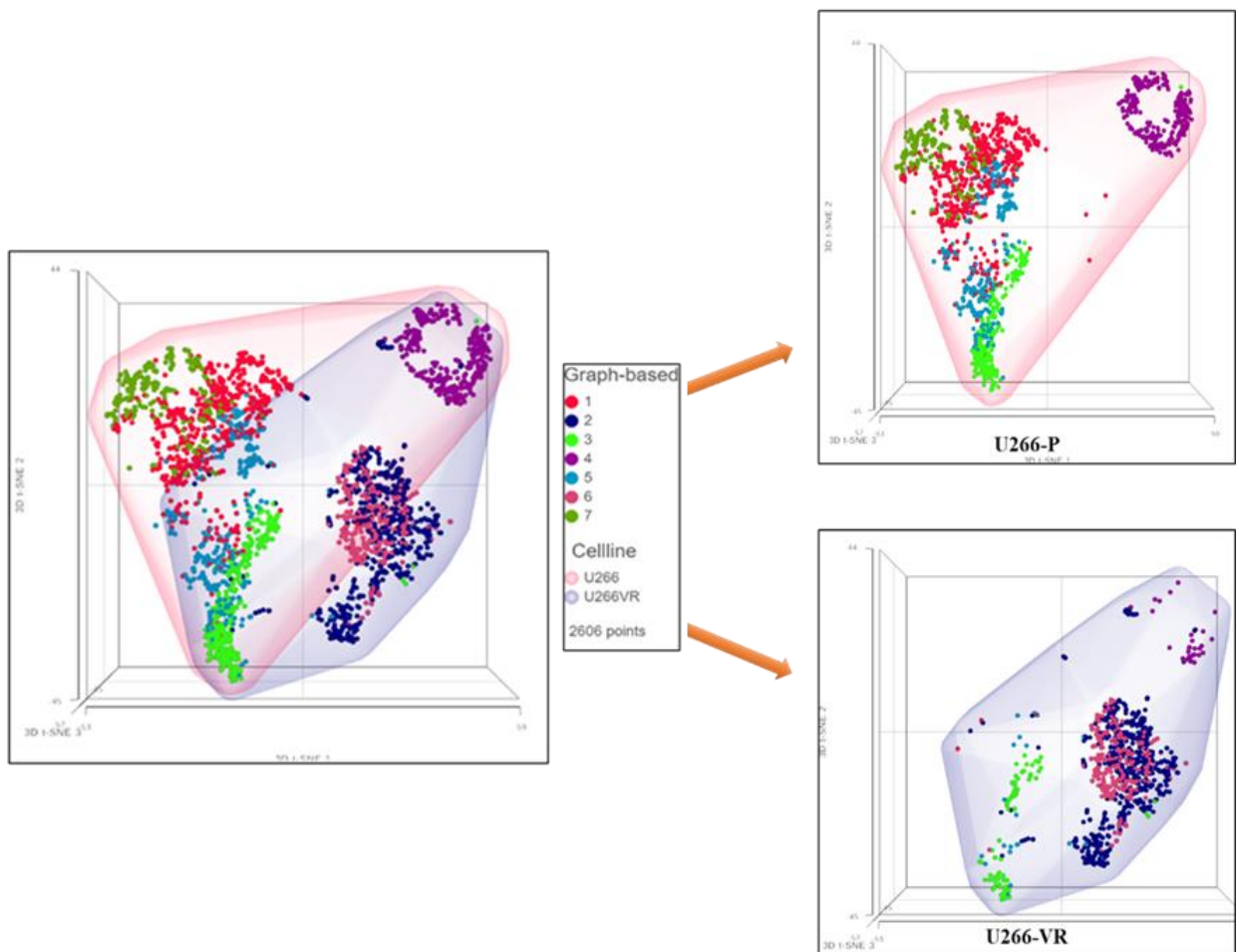
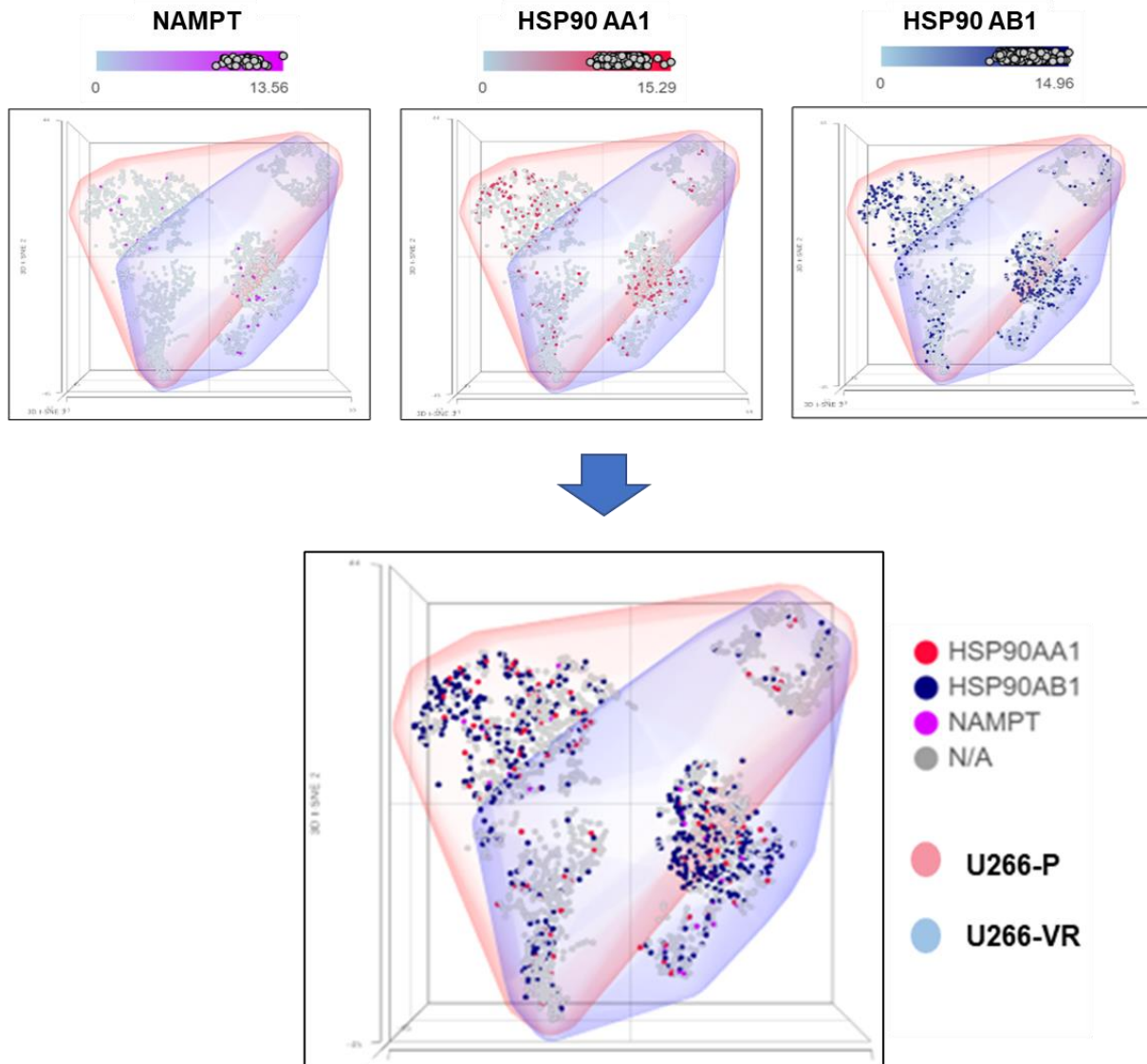


**Figure 2B. Results from the single-cell RNAseq) analysis on the myeloma cell line pair U266-P/VR.**

Single cells with an enriched expression of the target genes of 17AAG (HSP90AA1, HSP90AB1) and FK866 (NAMPT).



**17-AAG shows synergy with PIs, IMiDs, and FK866**

We used a sub-panel of HMCLs representing PI-sensitive (FLAM76, KAS6/1, MM1S), innate resistance (JIM-3, LP-1; representing refractory disease), and acquired PI/IMiD resistant clonal pairs (U266P/VR, RPMI8226P/VR, JJN-3P/VR, and MM1SP/LenR; representing relapse MM) to evaluate the effect of the predicted secDrug-based combination regimen, 17-AAG + FK866

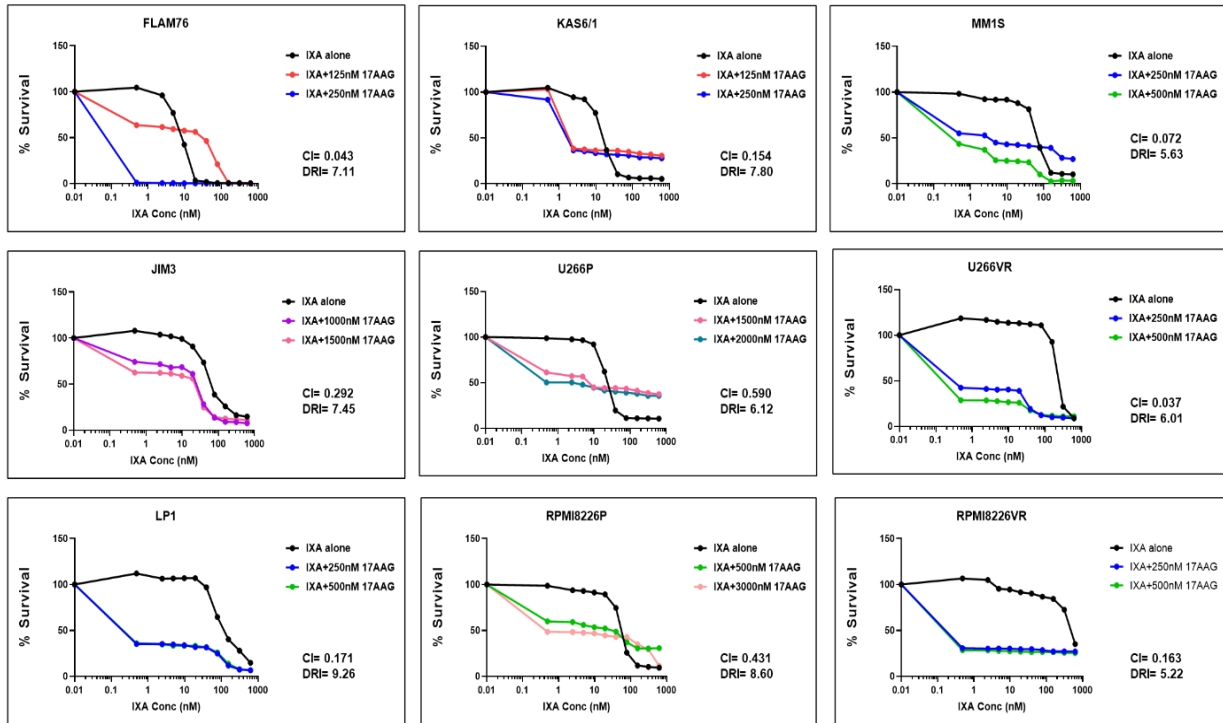
either as a combination of these two secDrugs or using PIs or IMiDs as the backbone. Cell survival curves representing 17-AAG + Ixazomib, 17-AAG + FK866, and 17-AAG + Lenalidomide combination are shown in Figure 3A–C. We found that 17-AAG not only showed synergy with PIs and IMiDs, but the combination of 17-AAG and FK866 also showed significant synergy, as depicted by the dose-response curves and CI values representing the combination treatments. CI values were consistently less than 1, which indicates synergy.<sup>295</sup> In addition, FK866 also showed synergy with Ixazomib (Ixa + FK866 survival curves are shown in Figure 3D). Cell survival curves representing other top secDrugs + Ixazomib combination in innate sensitive, innate resistant, and acquired resistant HMCLs are shown in Figure 3E–I. Figure S1: Predicted top secDrugs synergize with Ixazomib (secDrug+ IXA) in myeloma cell lines representing innate sensitive, Innate resistance, Parental/sensitive, and clonally-derived acquired PI resistance. D) FK866; E) PLX4720; F) YM201636; G) Navitoclax; H) MLN4924; I) PF.4708671.

Cell viability was assessed by CellTiter-Glo assay (48h). CI – Combination index calculated using Chou-Talalay's CI theorem). (CI>1 – antagonism; CI=1 – additive; CI<1 – synergism) (VR-Velcade/bortezomib/PI-resistant cell lines).

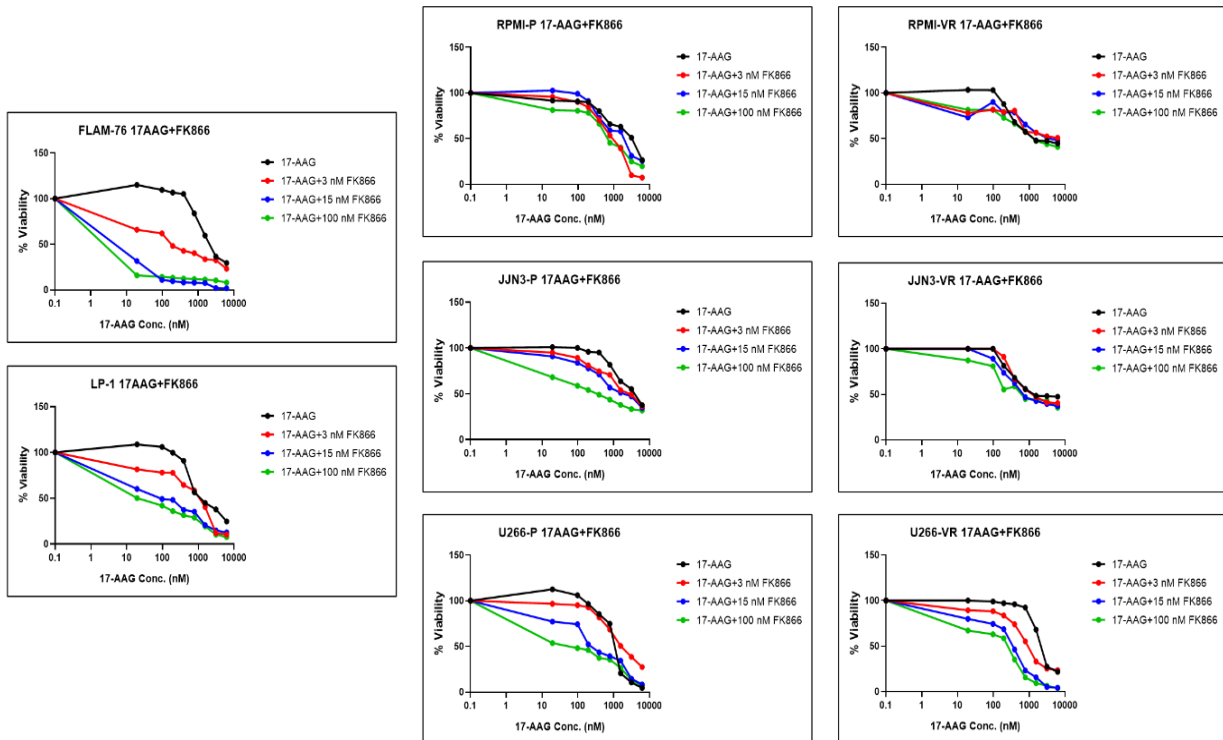
These secDrugs also showed strikingly high synergy with Ixazomib, as depicted by the CI values. Further, based on dose reduction index (DRI) values, the IC<sub>50</sub> of Ixazomib in myeloma cell lines was predicted to be significantly reduced in the presence of these secDrugs.

Figure 3J shows the relative decrease of the predicted effective IC<sub>50</sub> (nM concentration) of Ixazomib when used in combination with 17-AAG. The DRI values, calculated using the CI theorem, demonstrated that 17-AAG improved the therapeutic index of PI and IMiD administration to the cells and decreased the amount of PI/IMiD required to achieve effective responses<sup>295</sup>. This points towards the possibility of reducing the dose and, thereby, the toxicity of PIs when administered as a 17AAG + PI combination. Drug-induced apoptosis was confirmed in HMCLs using Caspase 3/7 activity assays (data not shown).

**Figure 3A. The secDrug 17AAG synergizes with PIs (17AAG + IXA)**



**Figure 3B. The secDrug 17AAG synergizes with FK866 (17AAG + FK866)**



**Figure 3C. The secDrug 17AAG synergizes with IMiDs (17AAG + Lenalidomide)**

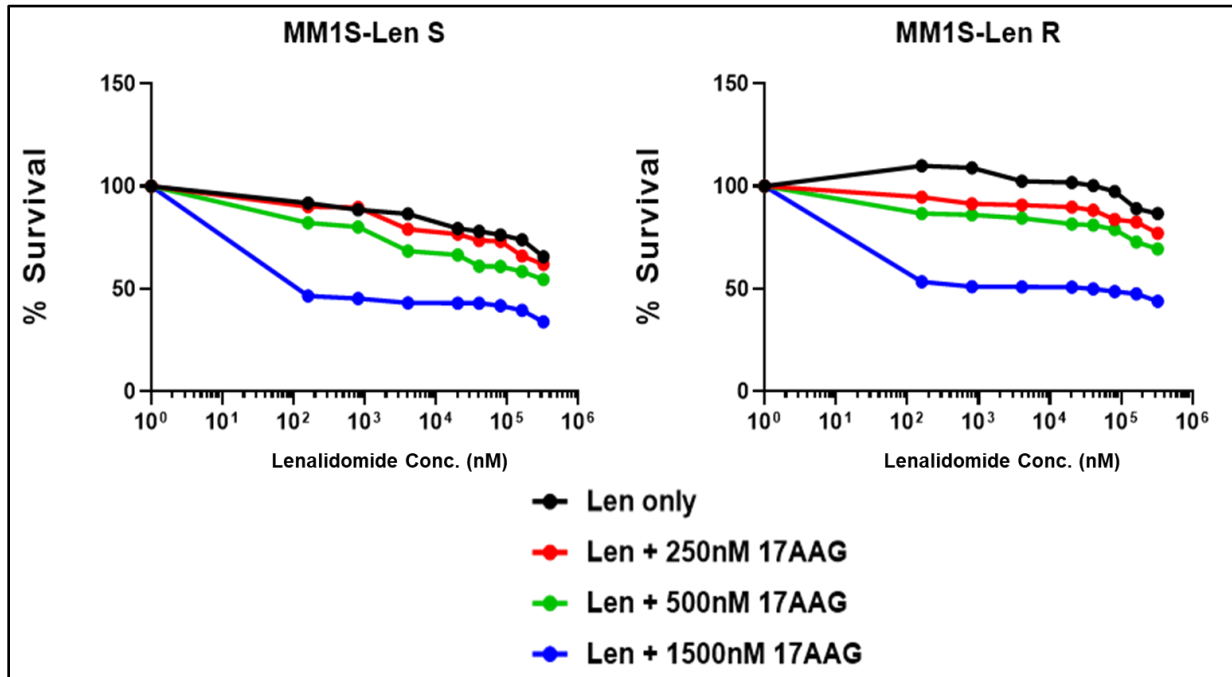


**Figure 3D: Predicted top secDrug FK866 synergize with Ixazomib (secDrug+ IXA) in myeloma cell lines representing innate sensitive, Innate resistant, Parental/sensitive, and clonally-derived acquired PI resistance**

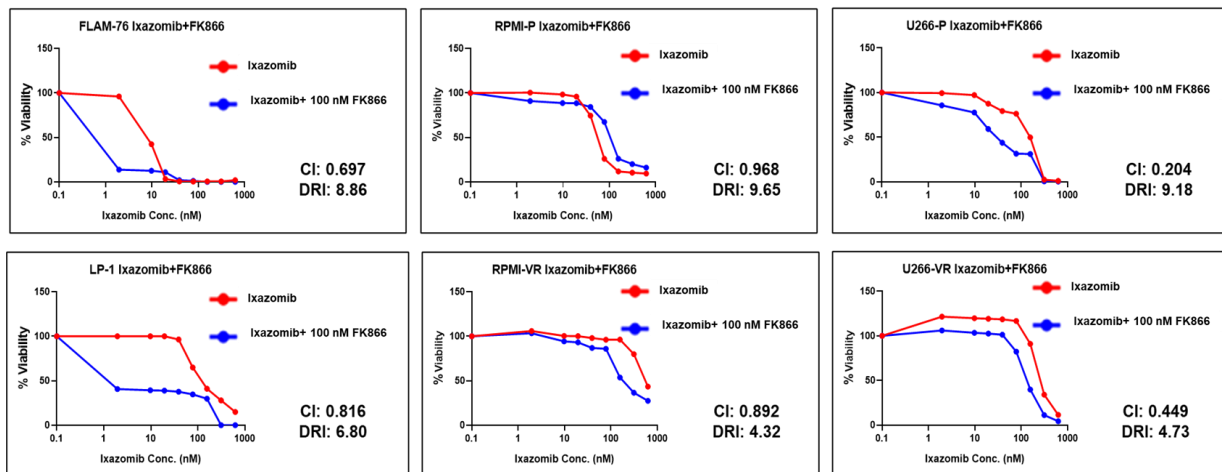


**Figure 3E: Predicted top secDrug PLX4720 synergize with Ixazomib in MM cell lines representing innate sensitivity/ resistance, Parental/sensitive, and clonally-derived acquired PI resistance**

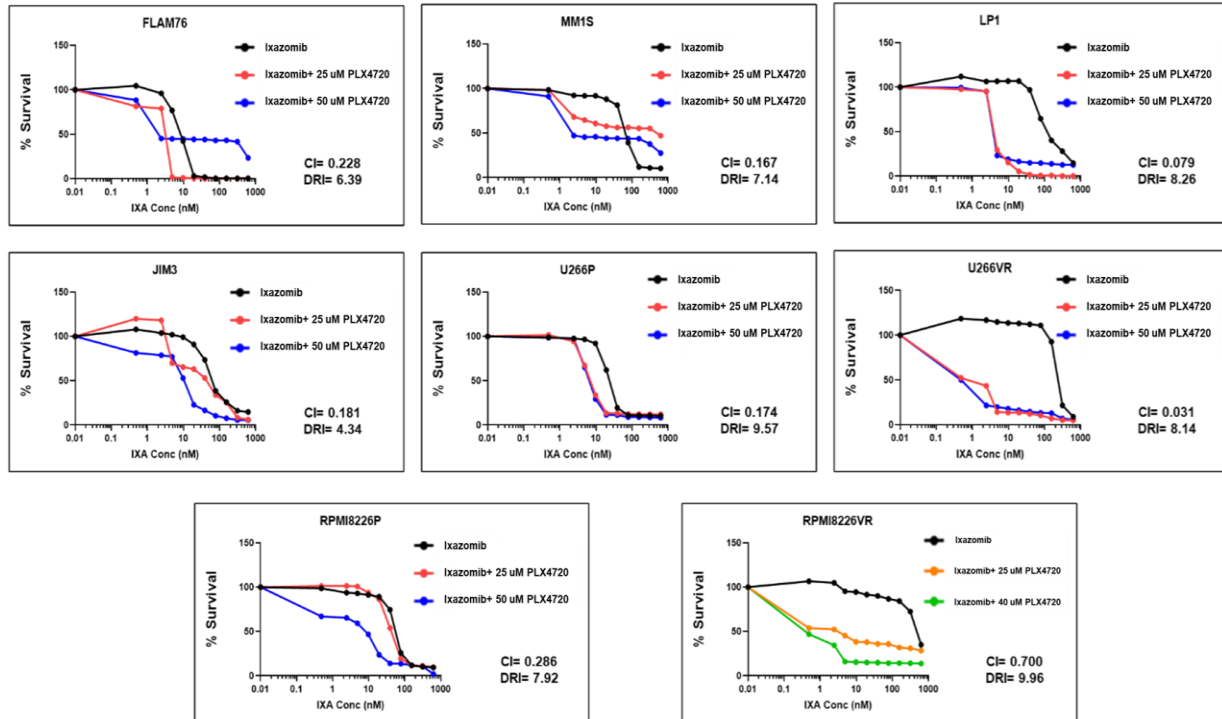


**Figure 3F: Predicted top secDrug YM201636 synergize with Ixazomib in MM cell lines representing innate sensitivity/ resistance, Parental/sensitive, and clonally-derived acquired PI resistance**

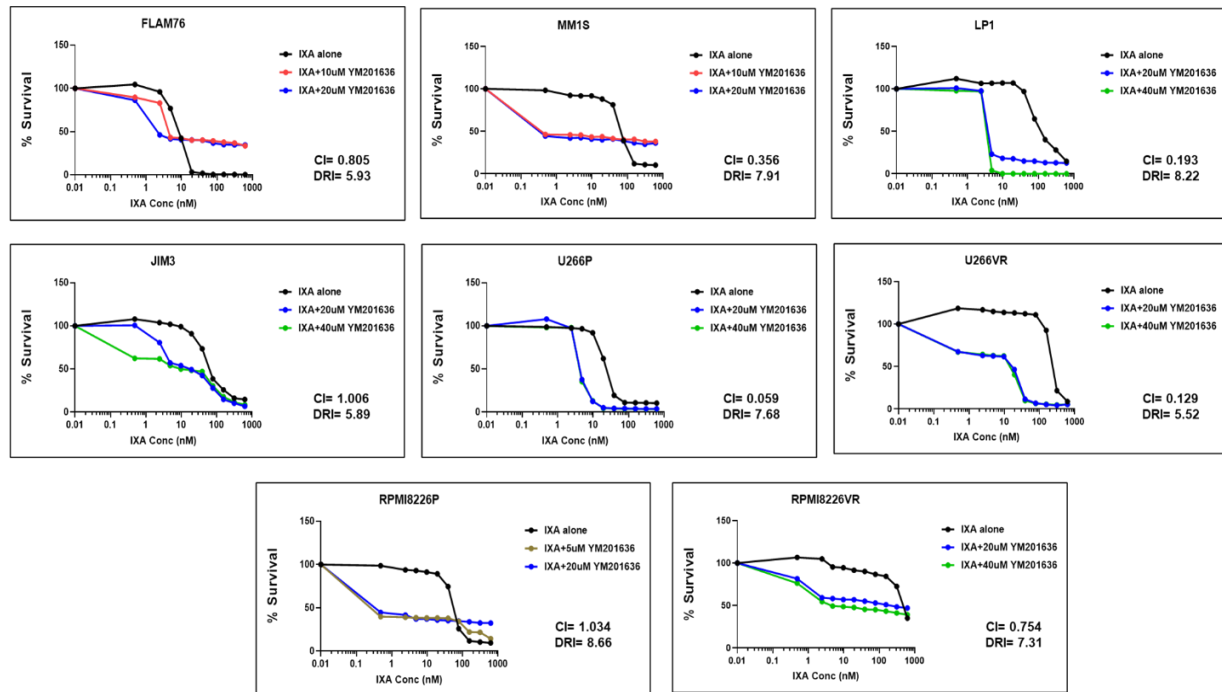


**Figure 3G: Predicted top secDrug YM201636 synergize with Ixazomib in MM cell lines representing innate sensitivity/ resistance, Parental/sensitive, and clonally-derived acquired PI resistance**

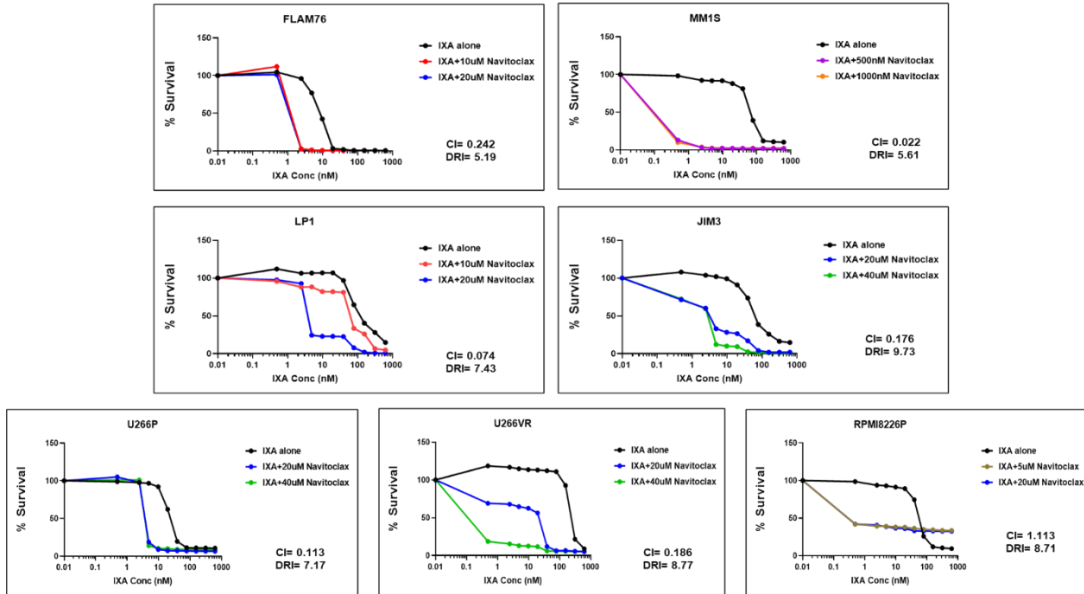


**Figure 3H: Predicted top secDrug MLN4924 synergizes with Ixazomib in MM cell lines representing innate sensitivity/ resistance, Parental/sensitive, and clonally-derived acquired PI resistance**

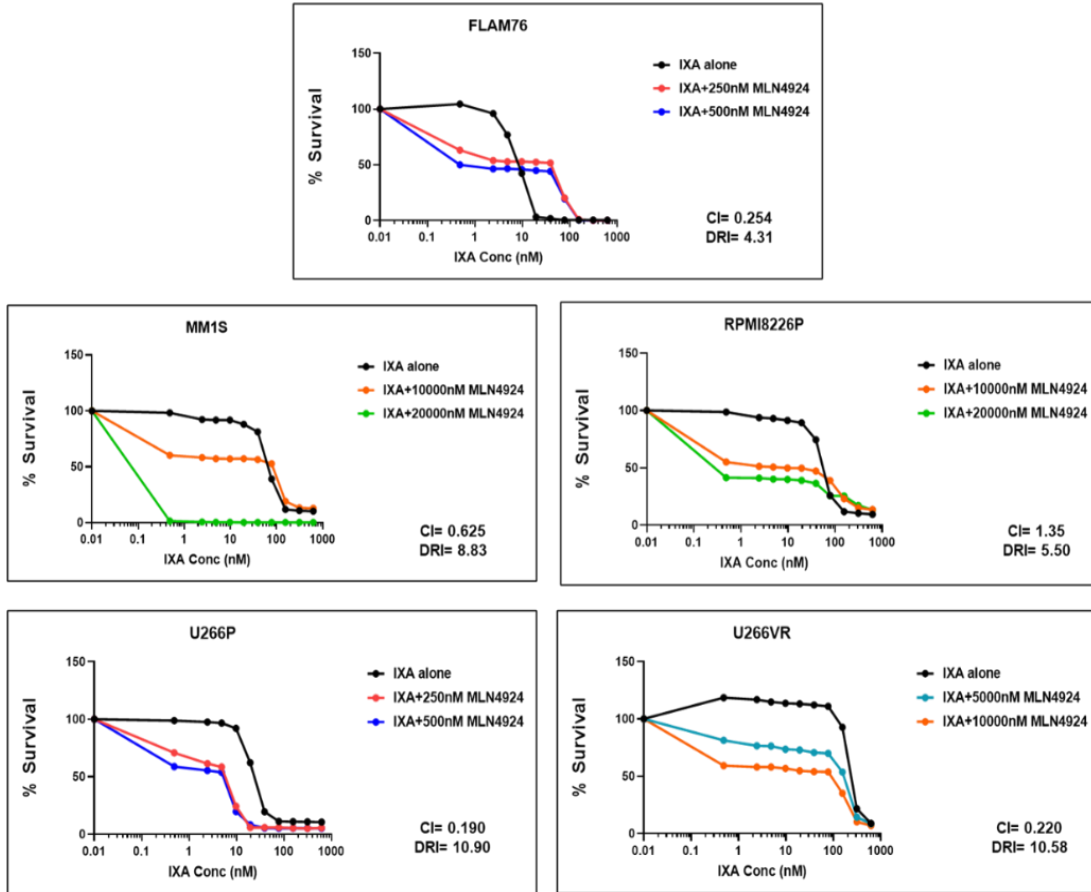


**Figure 3H: Predicted top secDrug MLN4924 synergize with Ixazomib in MM cell lines representing innate sensitivity/ resistance, Parental/sensitive, and clonally-derived acquired PI resistance**

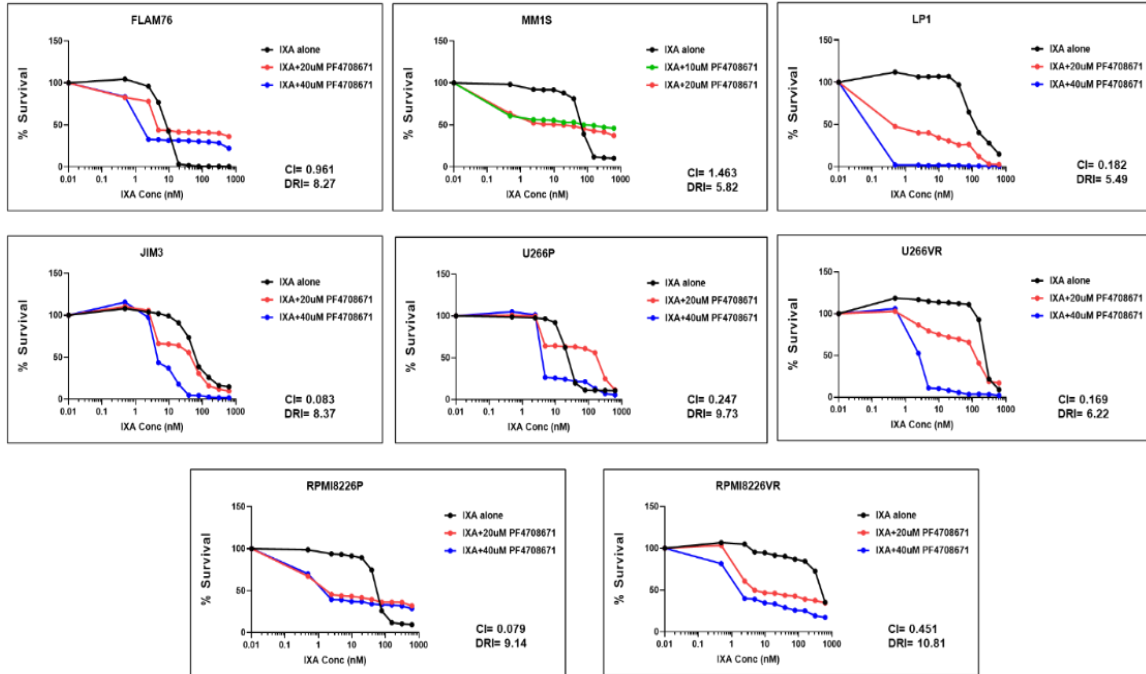
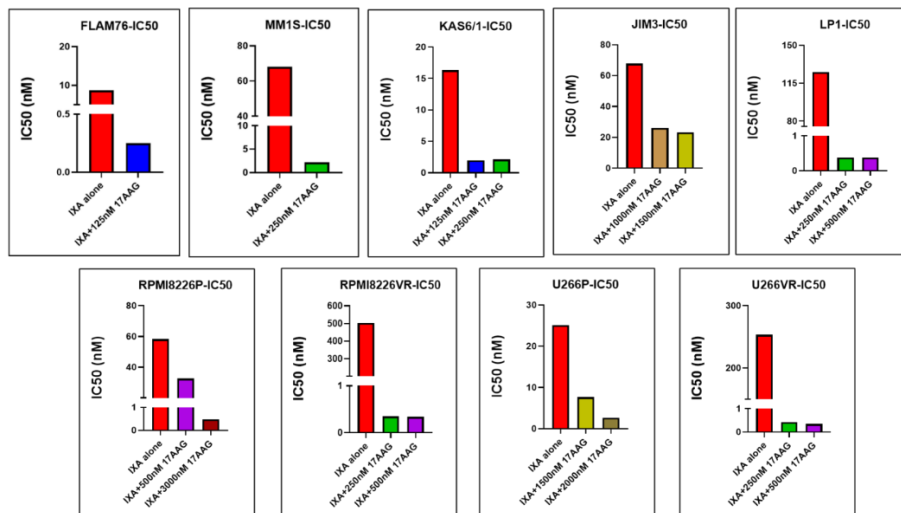


**Figure 3J: Predicted decrease in IC50 (nM concentration) in 17-AAG+PI combination. Dose reduction index (DRI) values demonstrated that 17-AAG improved the therapeutic index of PI and IMiD administration to the cells and decreased the amount of PI/IMiD required to achieve a response.**



In vitro, dose-response plots for secDrug combination treatment in HMCLs representing innate sensitivity, innate resistance, Parental/sensitive, and clonally derived PI/IMiD acquired resistance. Cell viability was assessed by CellTiter-Glo assay (48 h). CI (combination index) and DRI (dose reduction index) values were calculated using Chou–Talalay’s CI theorem. (CI > 1—

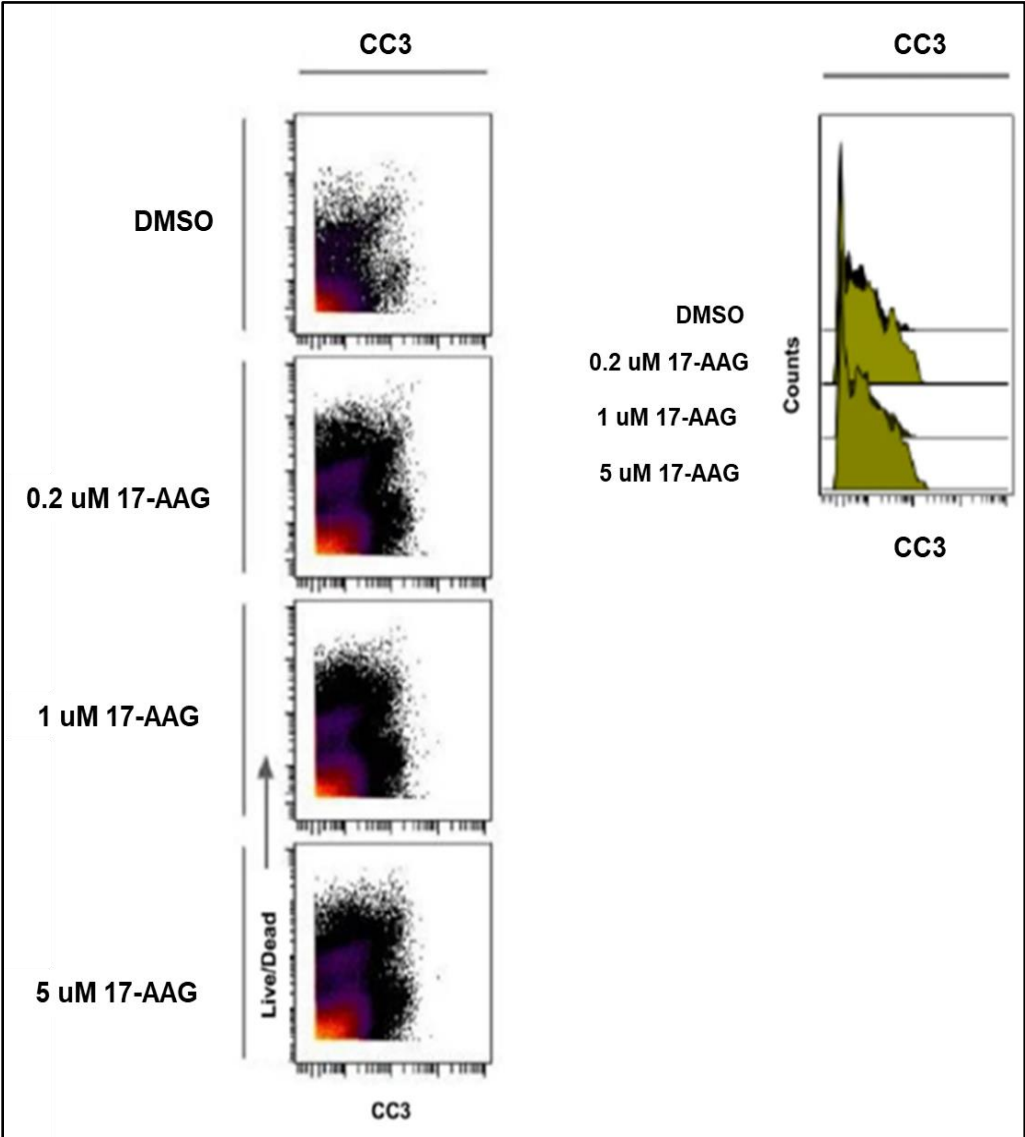
antagonism;  $CI = 1$ —additive;  $CI < 1$ —synergism) (VR-Velcade/bortezomib/PI-resistant cell lines, LenR- Lenalidomide/IMiD-resistant cell line).

### **CyTOF analysis revealed 17-AAG-induced cell death of PMCs and key changes in myeloma-specific proteomic markers**

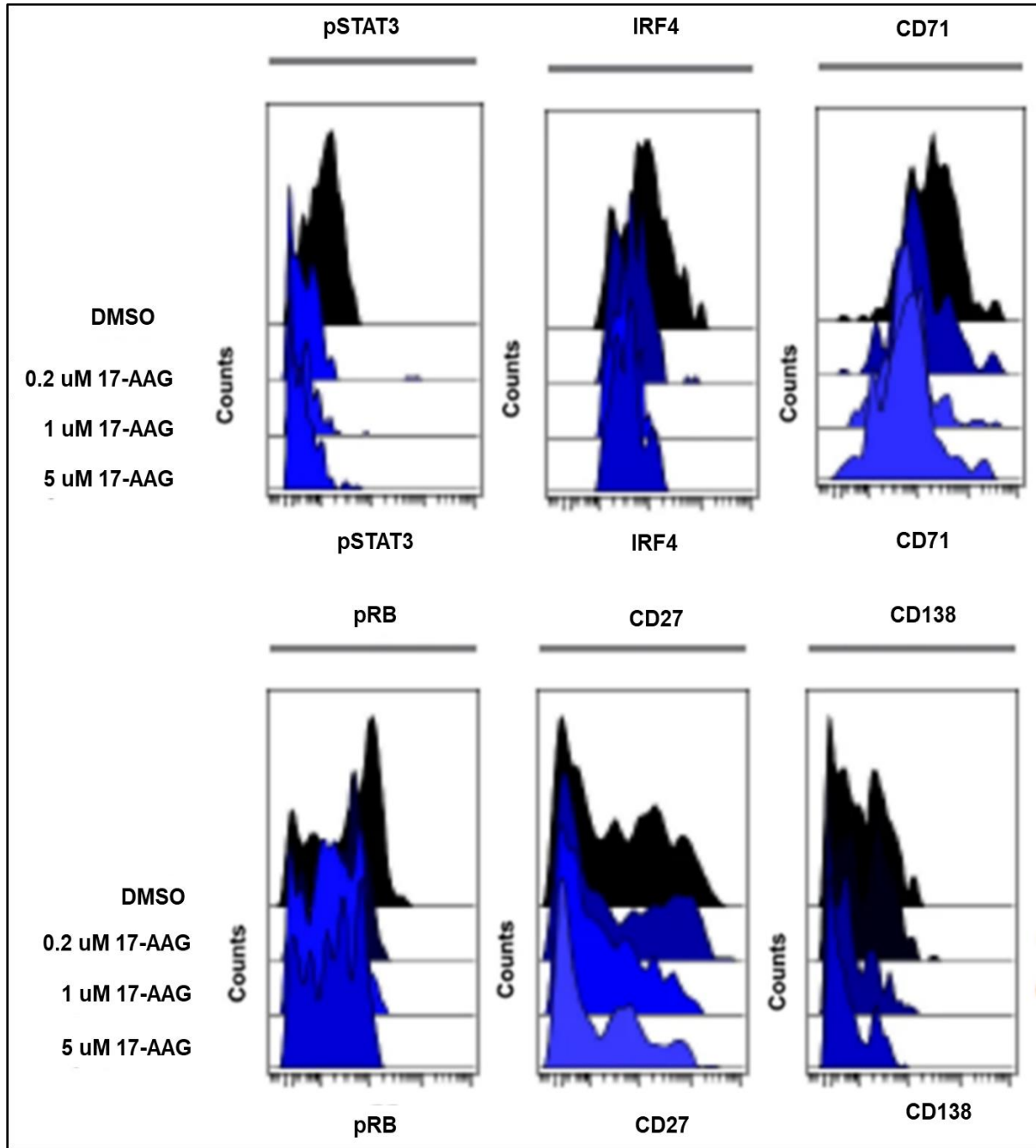
High-dimensional mass cytometry or CyTOF analysis is a deep immunophenotyping method that combines flow cytometry and elemental mass spectrometry.<sup>296</sup> We performed CyTOF analysis on PMCs obtained from myeloma patients ( $n = 6$ ) to assess 17-AAG-induced cell death through apoptosis as well as to evaluate changes in phenotypic and functional markers in MM cells at the single-cell/sub-clonal proteomics levels. As shown in Figure 4A, CyTOF analysis following exposure to 17-AAG treatment revealed a distinct cluster of cells defined by elevated cleaved caspase levels in the primary samples, indicating treatment-induced cell death by apoptosis in the cells exposed to 17-AAG.

Figure 4. Representative figures showing CyTOF analysis results in patient primary multiple myeloma cells.

Figure 4A



**Figure 4B**



CytoTOF analysis was performed on Live cells (n=6). (A) 17-AAG induces elevated cleaved caspase 3 levels. Samples were treated with 17-AAG (2, 5, and 10  $\mu$ M) or DMSO and Gated on LIVE cells. (i) The FlowSOM meta-cluster results were condensed into cc3 positive and negative cell subsets based on cc3 expression UMAPs and plotted over CLF dose. (ii) cc3 induction is also shown in the violin plots. (B) Downregulation of genes associated with myeloma cell

survival. Representative violin plots of CyTOF analysis in patient primary myeloma cells showing expression of myeloma markers following 17-AAG treatment, including IRF4, pSTAT3, IZKF3, CD138, CD71, pRB, and CD27.

### Immunoblotting

Treatment-induced protein expression of the phenotypic/functional markers of myeloma (p65/NFκB, IRF4, and cMyc) and markers of apoptosis (including Cleaved Caspase-3, Cleaved Caspase-9, etc.) was confirmed using immunoblotting analysis in HMCLs. Figure 5A shows representative pre- vs. post- 17-AAG treatment immunoblotting results on these myeloma cell survival and apoptotic pathways. Densitometry analysis results are provided in Figure 5A. Our results show a substantial decrease in IRF4, p65, and cMyc following 17-AAG treatment and a concurrent increase in Cleaved Caspase-3, Cleaved Caspase-9 protein expression, which was also confirmed at the mRNA level using pre- vs. post-17AAG-treatment differential gene expression (RNAseq) analysis, along with several other myeloma protein/survival markers like STAT1, RELB, NFKB1A, NFKB2, and IKZF3.

**Figure 5. Immunoblotting analysis results show 17-AAG treatment-induced changes in protein markers.**

**Figure 5A**

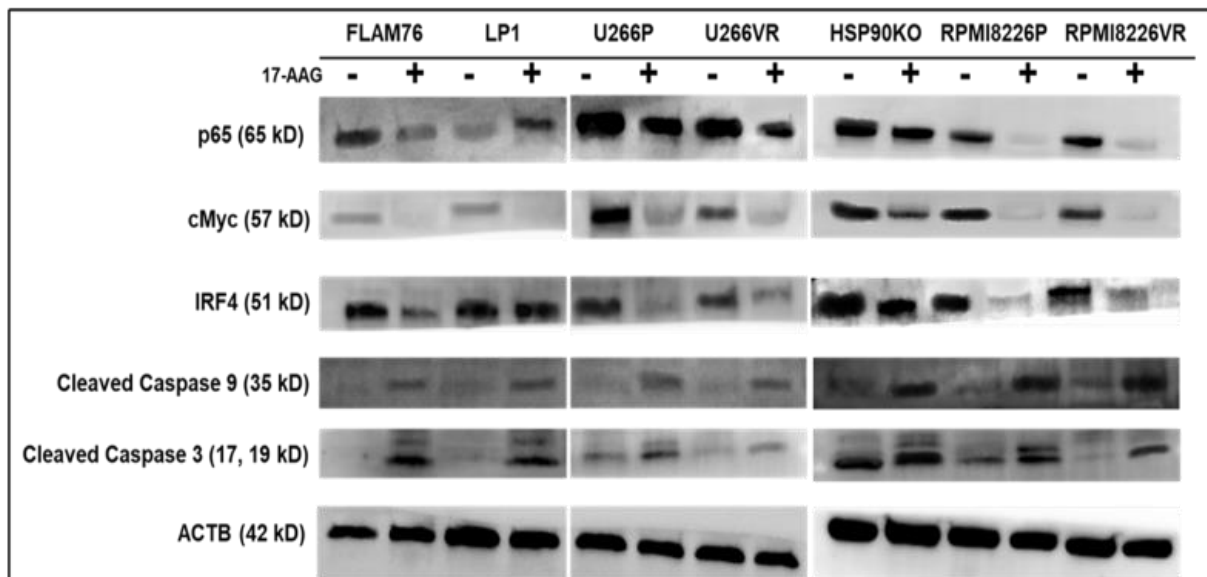
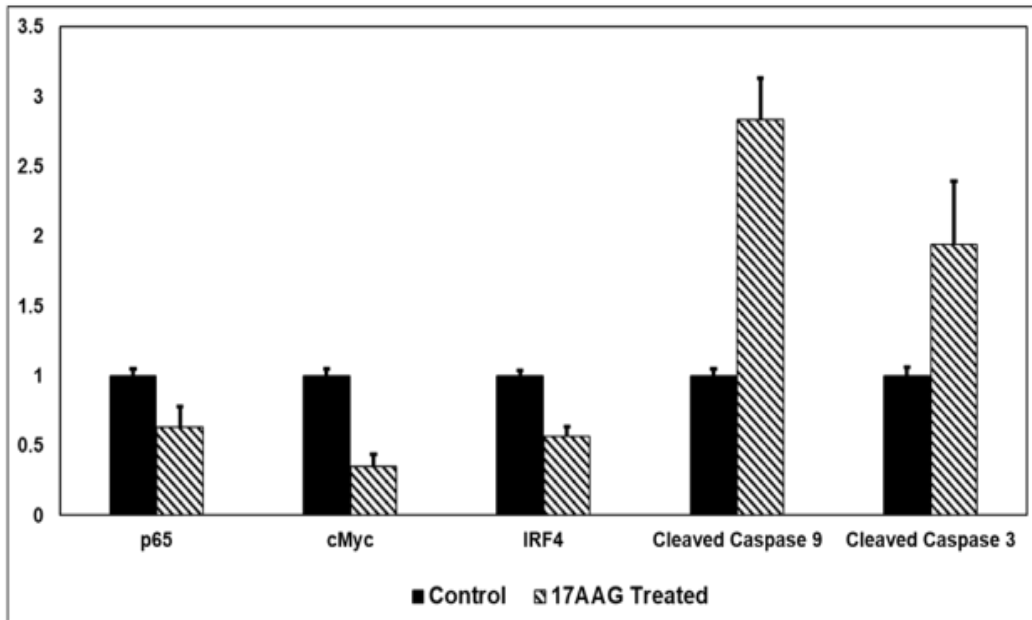


**Figure 5B**



(A) Representative western blots confirm the differential expression of proteins involved in myeloma cell survival and apoptotic pathways in innate sensitive (FLAM76), Innate resistant (LP1), and Clonally-derived acquired resistant HMCLs (U266P/VR, RPMI8226P/VR). (B) Densitometry analysis. Beta-actin was used for the normalization of the Western blots.

### **17-AAG induces apoptosis via a mitochondrial-mediated pathway in myeloma**

To investigate if 17-AAG imparts its cytotoxic effects in myeloma by generating reactive oxygen species (ROS), particularly super-oxides and hydrogen peroxide ( $H_2O_2$ ), cellular superoxide anions were measured by using the fluorescent dye DHE. MMP was assessed using JC-1. JC-1 is a cationic carbocyanine dye that accumulates in mitochondria. The dye exists as a monomer (green fluorescence) at low concentrations and changes color from green to red in energized mitochondria.

We observed the induction of cellular superoxide anions (Figure 6A) and intracellular ROS production (Figure 6B) that causes mitochondrial membrane depolarization following 17-AAG treatment in myeloma cells representing sensitive and resistant disease.

Figure 6. 17-AAG induces super-oxide levels, intracellular ROS generation, and mitochondrial membrane potential (MMP) in myeloma cell lines.

Figure 6A

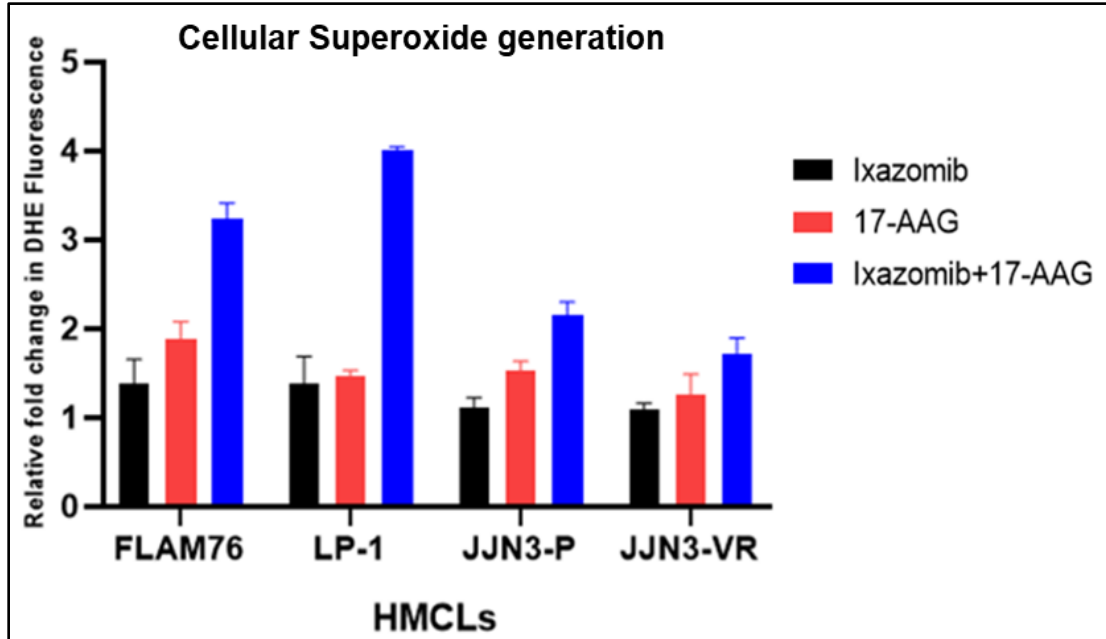
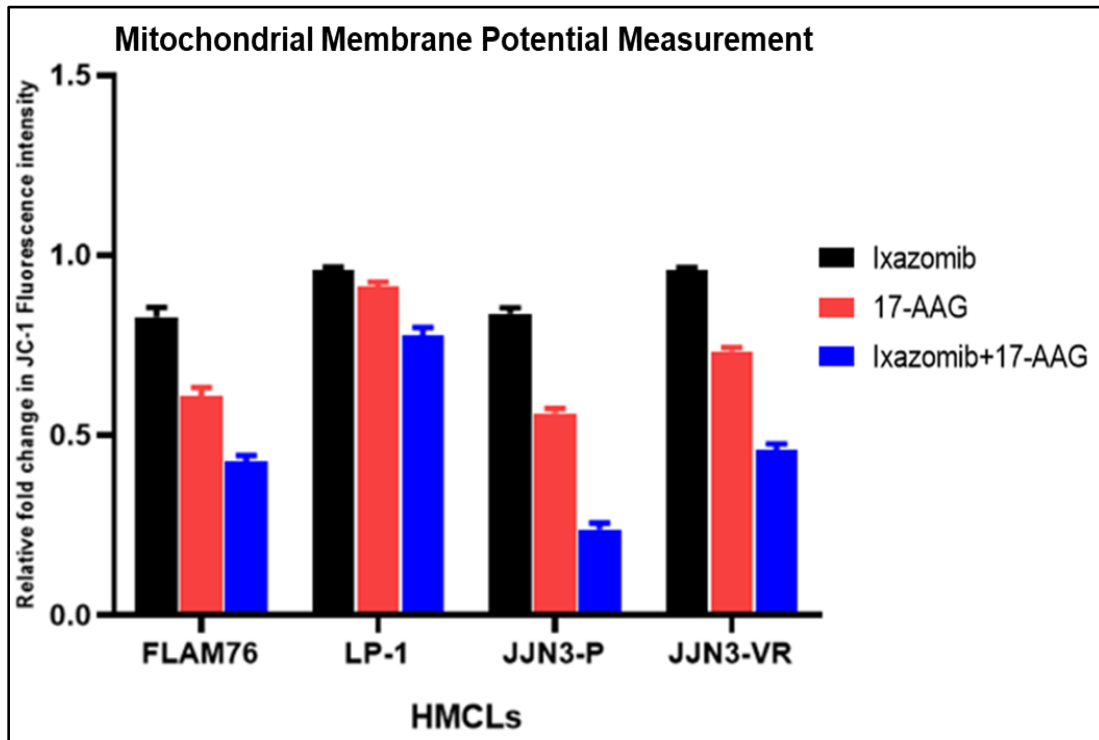


Figure 6B



(A) Super-oxide. Cellular superoxide anions were measured by using the fluorescent dye DHE (Abcam), and red fluorescence was detected by the Synergy Neo2 multi-plate reader. (B) Mitochondrial membrane potential (MMP) was assessed using JC-1 (Abcam), a cationic carbocyanine dye that accumulates in mitochondria. The dye exists as a monomer (green fluorescence) at low mitochondrial membrane potential and changes color from green to red in energized mitochondria. Cells were incubated with 5  $\mu$ M JC-1 dye for 15 min in the dark at 37 °C, washed twice in PBS, and then analyzed for red and green fluorescence by Synergy Neo2 multi-plate reader.

### 17-AAG-induced cell death was comparable with Hsp90 knockdown

Next, we compared the effect of Ixa and Ixa+17-AAG combination therapy between wild-type and CRISPR-mediated HSP90AA1 gene knockdown cell lines. Dose-response curves in Figure 7 show that the in vitro cytotoxicity in RPMI8226 cell lines was comparable following HSP90 inhibition, either through 17-AAG treatment or CRISPR-mediated HSP90 knockdown. This points toward an on-target effect of 17-AAG therapy leading to the anti-MM efficacy.

**Figure 7: Comparison of Ixazomib dose-response curves and Ixa-IC<sub>50</sub> values following HSP90 inhibition, either through 17-AAG treatment or CRISPR-mediated HSP90 knockdown.**

**Figure 7A**

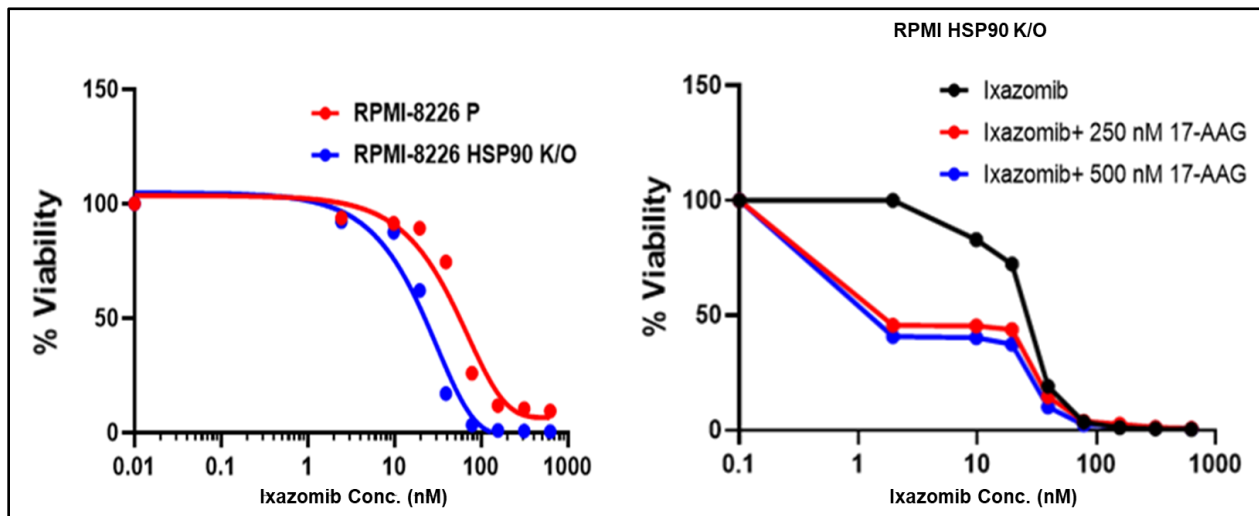


Figure 7B

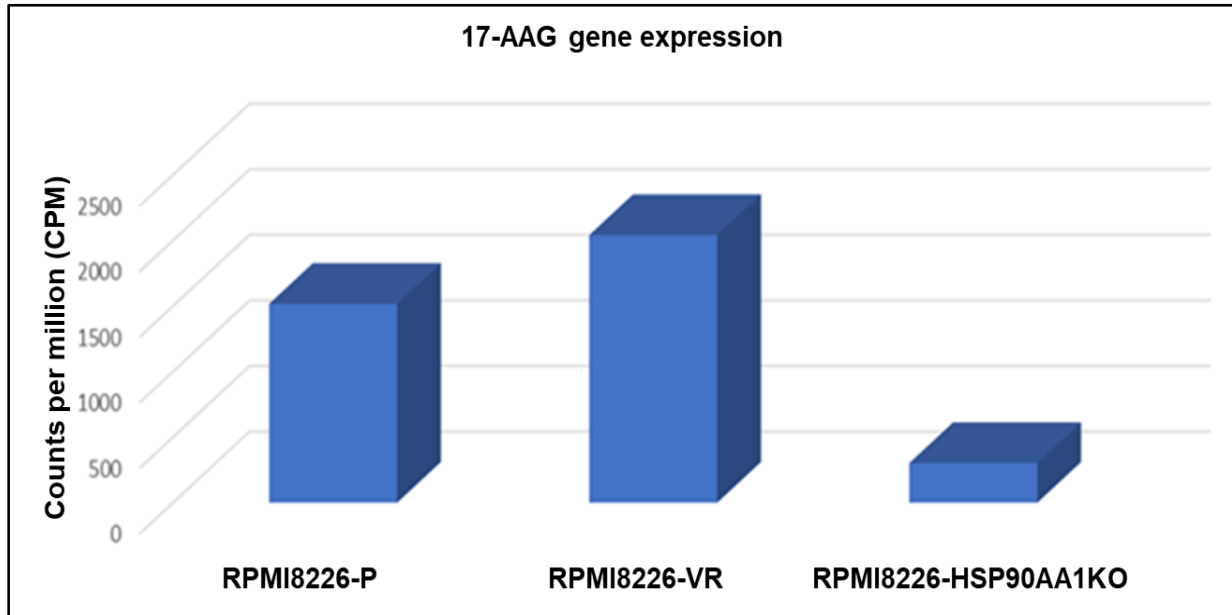
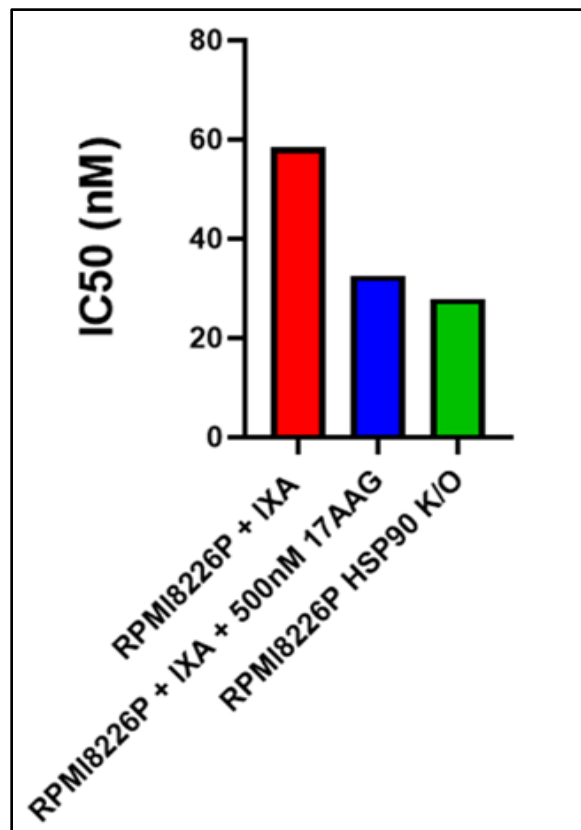


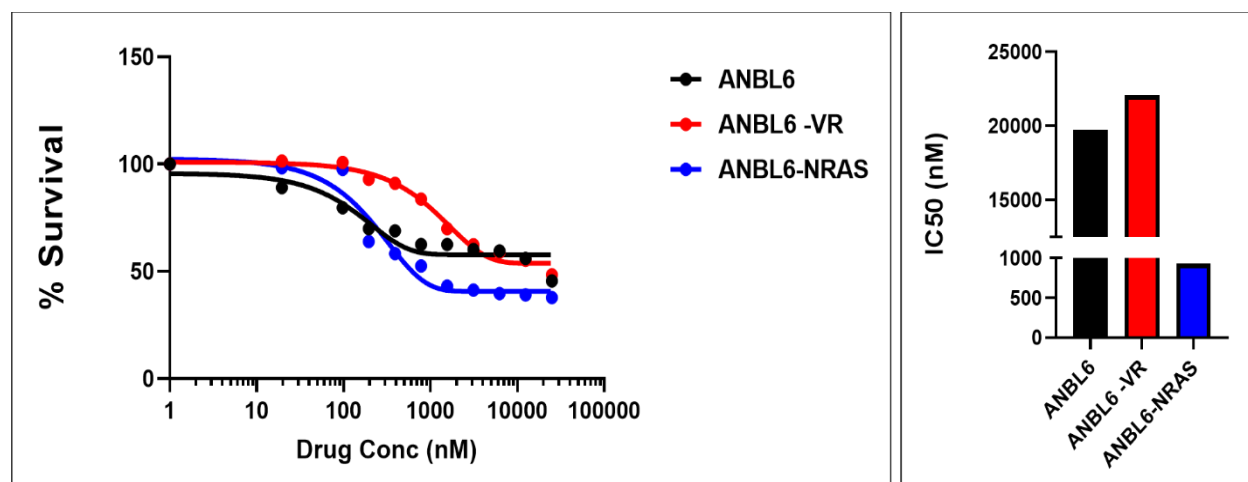
Figure 7C



### N-Ras mutant HMCL showed high sensitivity to 17-AAG treatment

Finally, the myeloma cell lines ANBL6P, ANBL6VR, and ANBL6 N-Ras mutant were treated with single-agent 17-AAG, Ixa, and 17-AAG + Ixa combination. We have described earlier that these activating mutations of the Ras oncogenes in ANBL6 (ANBL6 N-Ras) may lead to growth factor independence and suppression of apoptosis [18]. Notably, our ANBL6 N-Ras mutant cell line showed 20 times greater 17-AAG sensitivity (lower IC<sub>50</sub>) compared to the ANBL6P or VR cell lines. (Figure 8)

**Figure 8. Comparison of dose-response curves of PI-sensitive, PI-resistant, and N-Ras mutant HMCLs following 17-AAG treatment.**



### Gene-expression profiling analysis results

First, we compared the baseline (untreated) bulk mRNA sequencing analysis profiles of the HMCLs representing extraordinary responses (top-most sensitive vs. top-most resistant) to 17-AAG. At  $p < 0.05$ , next-generation mRNA sequencing analysis showed 421 genes were DE between the 17-AAG-sensitive and the 17-AAG-resistant groups (fold-difference $\neq$ 1). Among these, 360 genes had a fold change difference of  $>2$  or  $<-2$  between sensitive and resistant groups. Table 3 shows the top 50 genes (top 25 upregulated + top 25 downregulated) that were most DE as signatures of 17-AAG sensitivity in myeloma. IPA analysis revealed B Cell Receptor Signaling ( $p = 1.90E-03$ ), RhoGDI Signaling ( $p = 1.22E-03$ ), and IL-10 Signaling ( $p = 1.43E-03$ ) as the top canonical pathways associated with 17-AAG sensitivity in myeloma based on the genes that were DE.

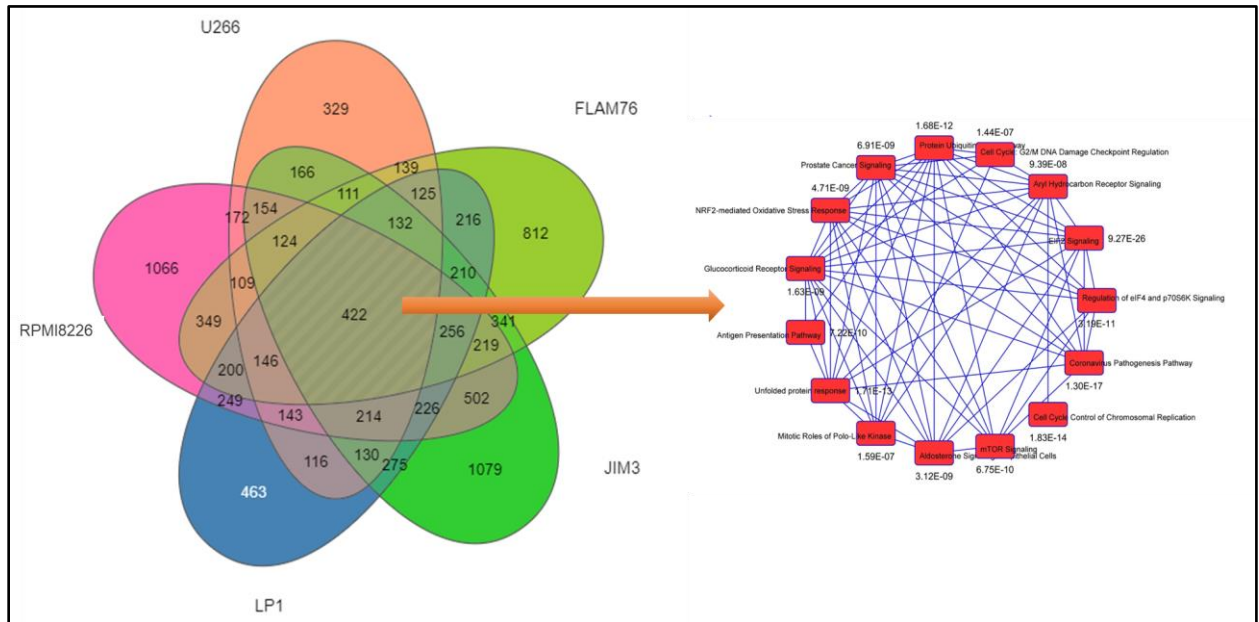
Differential gene expression analysis of kinetic (treatment-induced) changes between baseline (untreated) vs. single-agent 17-AAG (0.5  $\mu$ M) treatment (24 h) in HMCLs representing sensitive + intermediate + resistant myeloma showed a total of 1449 genes were DE in response to 17-AAG with p-value less than 0.05 ( $|\text{fold-change}| > 1$ ). Among these, 865 genes had a  $|\text{fold-change}| > 2$ . Figure 9A shows a heat map of the top 36 DEGs ( $|\text{fold-change}| > 1$ ; false-discovery rate (FDR)  $< 0.05$ ). When single-agent 17-AAG-induced kinetic changes were considered separately for each HMCL (RPMI8226, FLAM76, JIM3, U266, and LP1), 422 genes were found common between all the Treated vs. Untreated signatures at  $|\text{fold-change}| > 2$  ( $p < 0.05$ ), as shown in the Venn diagram (Figure 9B). IPA analysis (Figure 9C) based on the DEG signatures of 17-AAG single-agent treatment revealed cell cycle control of chromosomal replication (z-score  $-4.243$ ; p-value  $3.30E-12$ ), EIF2 signaling ( $2.496$ ;  $p = 1.12E-04$ ), aryl hydrocarbon receptor signaling (z-score  $-3.464$ ; p-value  $1.96E-03$ ), and protein ubiquitination pathway (PUP;  $p = 7.90E-08$ ) as top canonical pathways. Downregulation of CEBPB (z-score  $-6.670$ ; p-value of overlap  $5.28E-19$ ), ERBB2 (z-score  $-5.358$ ; p-value  $2.57E-08$ ), CSF2 (z-score  $-4.750$ ; p-value  $1.24E-05$ ) and CCND1 (z-score  $-3.707$ ; p-value  $2.40E-07$ ) and upregulation of the microRNAs let-7 (z-score  $5.501$ ; p-value  $2.01E-09$ ) were predicted as the top upstream regulator based on significantly DEGs (Figure 9D). Interestingly, IPA analysis also showed that gene signatures of 17-AAG treatment were positively correlated with that of bortezomib (z-score  $2.048$ ; p-value  $1.68E-05$ ) and lenalidomide (z-score  $2.774$ ; p-value  $2.80E-02$ ), indicating a possible basis for 17-AAG + PI and 17-AAG + IMiD synergy.

**Figure 9. Differential gene expression analysis of 17-AAG single-agent treatment**

**Figure 9A**



**Figure 9B**



(A) Heatmaps generated using unsupervised hierarchical clustering (HC) analysis showing top differentially expressed genes (bulk RNAseq data) that showed significant de-regulation 24 h following Single-agent 17-AAG exposure. IPA analysis results show (B) Venn diagram and IPA analysis results represent differentially expressed genes from the comparison of single-agent 17-AAG-induced kinetic changes (Treated vs. Untreated signatures) when each cell line (RPMI8226, FLAM76, JIM3, U266, and LP1) were considered separately ( $|\text{fold-change}| > 2$ ;  $p < 0.05$ ). (C) canonical pathways and (D) graphical summary. Columns represent cell lines, and rows represent genes. Prior to Hierarchical clustering, gene expression values were z-score normalized.

A total of 3974 genes changed significantly between untreated vs. 17-AAG + Ixa combination-treated samples ( $p < 0.05$ ;  $\text{fold-difference} \neq 1$ ). Among these, 853 genes showed  $|\text{fold-change}| > 2$  with an  $\text{FDR} < 0.05$ . Figure 10A depicts a heatmap of the top 50 genes associated with 17-AAG + Ixa combination treatment. IPA analysis based on DEGs significantly associated with 17AAG + Ixa treatment revealed PUP ( $p = 3.89\text{E}-23$ ) as the top canonical pathway (Figure 10B). Upstream regulator prediction analysis revealed inhibition of the transcriptional regulators CEBPB (z-score  $-8.871$ ; p-value of overlap  $1.38\text{e}-22$ ), MYC (z-score  $-6.732$ ; p-value of overlap  $3.83\text{e}-18$ ), as well as VEGF (z-score  $-6.805$ ; p-value  $9.76\text{e}-07$ ), HGF (z-score  $-7.139$ ; p-value  $2.08\text{e}-10$ ), and CSF2 (z-score  $-6.770$ ; p-value  $4.16\text{e}-07$ ) following 17-AAG + PI combination treatment (Figure 10C).

The Venn diagram in Figure 10D shows 50 genes that were common between the three comparisons (17-AAG vs. Control, 17-AAG + Ixa vs. Control, and Ixa vs. control). Further, Figure 10D also shows IPA-predicted canonical pathways that these 50 common genes ( $p < 0.05$ ) represent.

Finally, IPA predicted upregulation of the microRNA let-7 (z-score  $7.180$ ; p-value  $5.02\text{e}-12$ ) as the top upstream regulator based on significant DEGs (Figure 10E)

**Figure 10: Differential gene expression analysis of 17-AAG + PI combination treatment**

**Figure 10A**

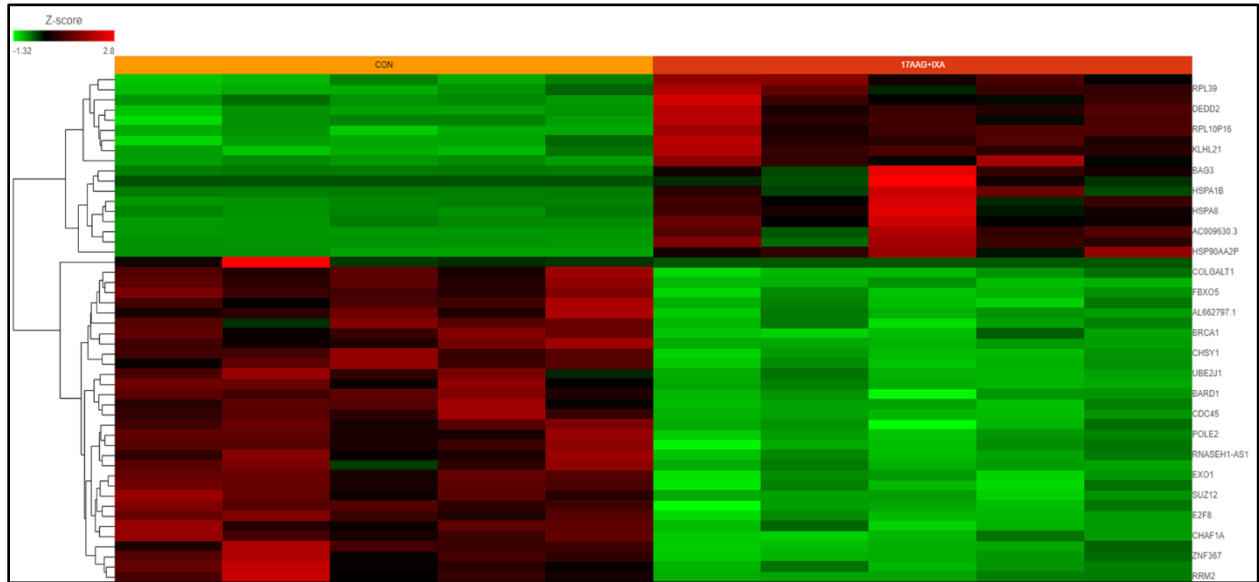


**Figure 10B**

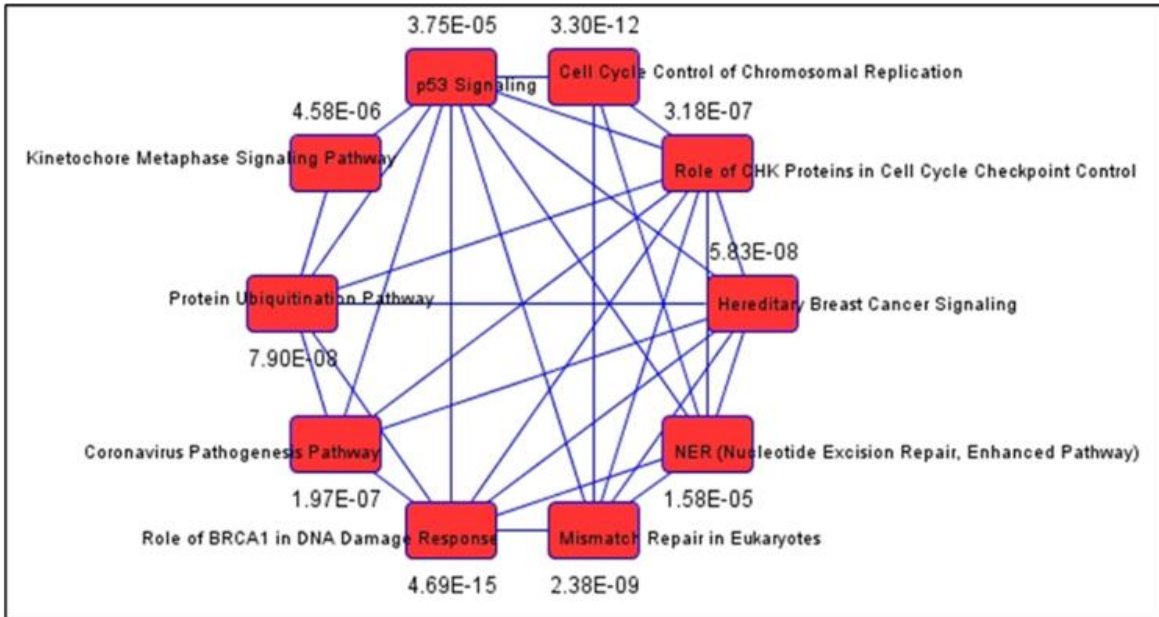


**Figure 10C**

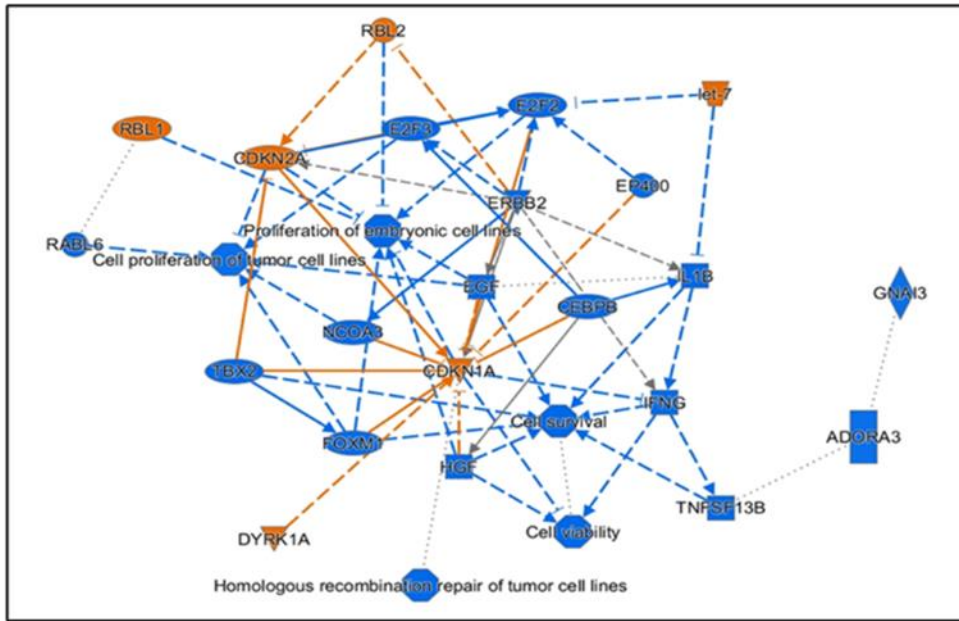


**Figure 10D**

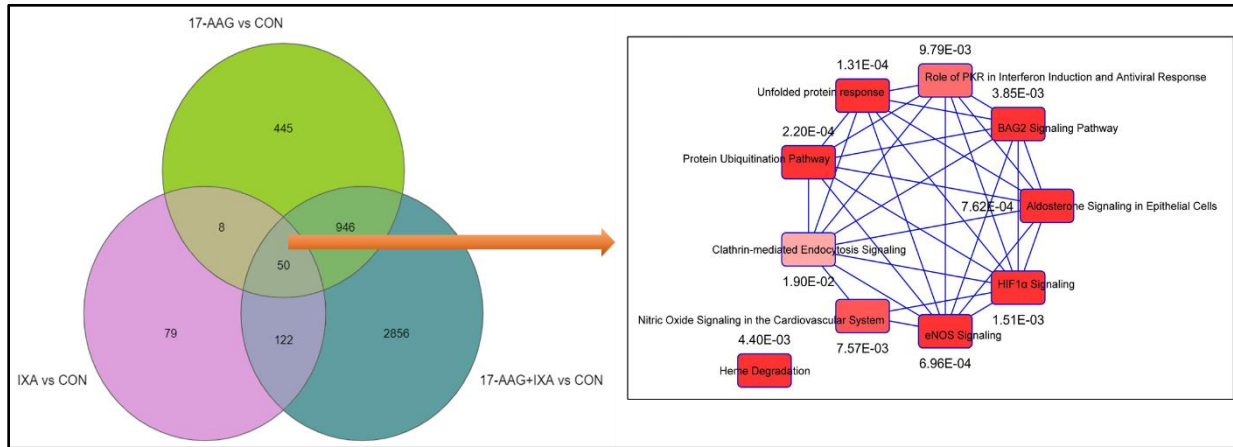
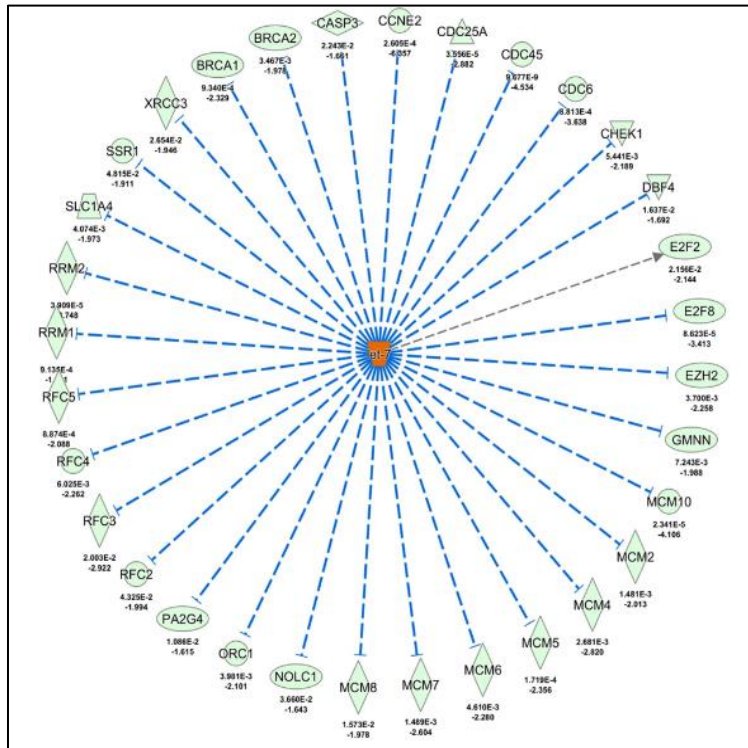


**Figure 10E**



(A) Heatmaps generated using unsupervised hierarchical clustering (HC) analysis showing top differentially expressed genes (bulk RNAseq data) that showed significant de-regulation, 24 h following 17-AAG + Ixazomib combination treatment. IPA analysis results show (B) the top 10 canonical pathways and (C) a graphical summary. Columns represent cell lines, and rows represent genes. Prior to Hierarchical clustering, gene expression values were  $z$ -score normalized. (D) Venn Diagram showing genes that were significant ( $p < 0.05$ ) in either 17-AAG vs. CON, IXA vs. CON and/or 17-AAG+IXA vs. CON. The image shows the top IPA-predicted canonical pathways represented by the 50 genes common to all the subsets. (E) IPA predicted upregulation of the microRNA let-7 as the top upstream regulator based on significantly differentially expressed genes following 17AAG+Ixa combination treatment.

**Table 3:** Top 50 (25 upregulated + 25 downregulated) differentially expressed genes between 17-AAG sensitive and resistant HMCLs

Genes	Fold change (17AAG_Res vs. 17AAG_Sen)	P-value (17AAG_Res vs. 17AAG_Sen)
PTPRCAP	-183.73	2.56E-03
NAP1L3	-102.49	9.77E-03
LTBR	-97.47	1.46E-03
PITX1	-88.67	1.81E-04
GABRB2	-69.98	2.17E-02
RTKN2	-67.63	4.26E-04
PCLO	-63.18	3.40E-02
DYNC2H1	-62.76	4.20E-02
CAPN5	-62.71	1.65E-02
ARHGEF6	-57.08	4.20E-03
PLEKHA5	-54.43	1.46E-03
LGALS3BP	-54.04	2.14E-02
KIAA1549	-51.40	4.35E-04
CDC42BPA	-40.97	1.11E-02
IGKC	-38.91	3.60E-02
GBP2	-36.97	1.68E-02
TRIM2	-36.45	2.29E-03
HSPA12A	-33.95	8.10E-03
EPB41L4A	-31.70	4.25E-02
COL18A1	-29.29	4.75E-02
WBP5	-26.12	2.41E-02
CES3	-24.97	1.21E-02
NRSN2	-24.29	1.76E-02
DOK2	-19.94	5.93E-03
SOX4	-19.76	1.16E-02
HOMER3	15.61	1.38E-02
ASAP2	19.43	5.38E-03
PPDPF	19.67	2.41E-02
NLRP11	19.78	2.01E-02
ABCG2	21.88	1.12E-02
CDKN1C	22.68	3.89E-02
CLEC7A	25.90	1.62E-02
BIRC3	27.52	2.20E-02
HERC5	31.88	2.02E-02
AC005301.5	33.82	5.65E-03
CD74	40.50	4.40E-02
CD28	42.10	1.31E-03

RP11-844P9.2	48.85	1.69E-03
BLK	50.65	2.05E-02
ARL4C	55.17	3.78E-03
IFIT3	55.20	2.31E-02
SYNM	59.18	2.55E-02
HLA-DRA	61.95	2.26E-02
RGS1	76.85	3.87E-02
LAPTM4B	125.55	3.13E-02
FAM64A	156.03	1.54E-05
KCNK1	250.60	9.67E-03
RND3	324.32	3.78E-03
SCML1	788.94	3.19E-04
IGLC3	818.72	4.82E-03

### Creation of secDrug software package

Finally, we developed an R software package based on our secDrug pipeline for predicting novel secondary therapies in chemotherapy-resistant cancers. secDrug takes a query of any cancer type and any test/primary/standard-of-care drug and outputs a list of the top secondary drug combinations with a confidence score and biological pathway visualization. Thus, secDrug has potential application in clinical decision-making for discovering resistance-reversing cancer chemotherapy regimens. R codes for the package are available at <https://github.com/Ujjal-Mukherjee/secDrug/tree/main/CombinationDrugMyeloma>, and the datasets are available at the [GitHub](#) repository.

### Discussion

Drug resistance is a major obstacle in achieving a complete and sustained therapeutic effect in cancer chemotherapy.<sup>280,283,297,298</sup> Chemo-resistance may also lead to over-dosing and unwanted exposure to ineffective anti-tumor agents, thereby increasing the risk of adverse side effects and the cost of drug development.<sup>299,300</sup>

In this study, we demonstrate the creation of a novel pipeline for drug development/drug repurposing that integrates in-silico computational prediction, single-cell multi-omics (single-cell transcriptomics/scRNAseq and single-cell proteomics/CyTOF analysis) with in vitro and ex vivo validation, including the use of whole-genome transcriptomics (RNAseq) and genome editing technologies to identify and functionally validate secondary treatment regimens to

circumvent drug resistance in myeloma. Notably, we applied the pipeline to predict several drugs as potential candidates for anti-MM secDrugs for combining with PIs. These (“top secDrugs”) include, HSP90 inhibitor/17-AAG, Nicotinamide phosphoribosyl transferase or Nampt-inhibitor/FK866, Survivin-inhibitor/YM155, PIKfyve-inhibitor/YM201636, Raf-inhibitor/PLX-4720, Bcl2-inhibitor/Navitoclax, AKT inhibitor/KIN00102, transforming growth factor- $\beta$  type I receptor, ALK4, ALK7-inhibitor/SB505124, HDAC-inhibitors (Panobinostat, SAHA), S6K1-specific inhibitor/PF-4708671, and the neddylation-inhibitor/MLN4924.

Further, we performed extensive in vitro, ex vivo, and functional validation in research models of refractory and resistant myeloma to validate 17-AAG + FK866, 17AAG + PI, and 17-AAG + IMID as combination treatment candidates that also served as a proof-of-principle for our secDrug pipeline. Overall, our validation results corroborated with our in-silico prediction of secondary drugs based on secDrug analysis.

17-AAG/Tanespimycin has previously been shown to work against myeloma, in vitro, in vivo (animal studies) as well in clinical studies.<sup>301–303</sup> However, to our knowledge, this is the first study that evaluates explicitly the use of 17-AAG combination therapy in relapsed and refractory myeloma models. Further, in our study, the ANBL6 Ras mutant cell line showed 20 times lower 17-AAG cytotoxicity compared to the ANBL6P/VR cell lines. An earlier study in metastatic malignant melanoma has shown that a patient harboring NRAS-activating mutation exhibited disease stabilization for 49 months following the administration of pharmacologically active doses of 17-AAG.<sup>304</sup> Mutations of NRAS have earlier been shown to be significantly associated with lower single-agent PI-sensitivity and shorter time to progression in bortezomib-treated myeloma patients.<sup>305</sup> Thus, our study points towards a unique niche (N-Ras mutant myeloma) where 17-AAG could be highly effective as a single agent as well as in combination with PIs and FK866, in addition to relapse and refractory myelomas. Moreover, we evaluated the molecular pathways involved in response to the top secondary drugs, which provided additional insights into the mechanism of action of 17-AAG as a secDrug.

Myeloma tumor cells have elevated intracellular NAD<sup>+</sup> levels that support the high rate of energy metabolism for uncontrolled proliferation, tumor cell growth, and survival.<sup>306,307</sup> FK866 is a chemical inhibitor of Nampt (Nicotinamide phosphoribosyl transferase), a key enzyme in NAD<sup>+</sup> metabolism<sup>307</sup>. Consequently, FK866 has been shown to reduce myeloma tumor growth

in PI-sensitive and PI-resistant myeloma through the activation of autophagy and cell death in myeloma cells.<sup>308</sup> In this study, we showed that FK866 not only overcomes PI-resistance when used as a single-agent or as an Ixa combination, combining 17-AAG + FK866 is highly synergistic against our validation models of relapsed/refractory myeloma.

Our study introduces several novel secDrugs as potential synergistic partners of PIs that have never been studied as potent single-agent or combination therapy options in myeloma model systems, including KIN001-102 (A6730; Akt1/2 kinase inhibitor) and SB505124 (inhibitor of transforming growth factor- $\beta$  type I receptor or ALK4, ALK7 that activates the SMAD2/3 pathway). These may serve as novel candidates for further studies on the pre-clinical and clinical validation in xenograft or mouse models of myeloma.

Although some of the other predicted secDrugs have earlier been shown to be effective against myeloma, very few studies have explored their efficacy as drug combinations with PIs/IMiDs in models of refractory/resistant myeloma. For example, PF-4708671 is a P70S6K1 isoform-specific inhibitor that has recently been shown to induce statistically significant apoptosis in HMCLs and PMCs in combination with several standard-of-care therapies.<sup>309</sup> NEDD8-activating enzyme/neddylation-inhibitor/MLN4924 has once earlier been shown effective against a subset of cell lines represented by cell surface expression of TNFR1.<sup>310</sup> PLX4720 (a small-molecule, ATP-competitive inhibitor of Mutant BRAF kinase) was earlier shown to have a partial single-agent response in patients harboring sub clonal BRAF mutations.<sup>311</sup> Our in-silico predictions and single-agent cytotoxicity data thus build a strong case to test these drugs as secDrug combination regimens in a broader panel of HMCLs representing refractory and clonally derived acquired resistant cell lines. Among the other secDrugs, Navitoclax is a high-affinity small-molecule BH3 mimetic that inhibits Bcl2 and BCL-xL. Navitoclax has been shown to inhibit cell proliferation in myeloma leading to the induction of apoptosis.<sup>312,313</sup> YM201636 is an inhibitor of PIKfyve, a mammalian protein involved in the regulation of crucial cellular functions, including nuclear signaling and autophagy. Few recent studies demonstrated the therapeutic efficacy of PIKfyve inhibitors in myeloma cell lines.

Overall, we present here a unique pipeline that introduces not only novel secDrugs but also provides additional niches for secondary drugs that are already under preclinical or clinical investigation in relapsed/refractory myeloma.<sup>314,315</sup>

Our findings provide a strong case for combining the top predicted secDrugs with PIs and IMiDs to overcome resistance and thereby improve patient outcomes. This potentially introduces many more drugs as new and more effective therapeutic options for the management of resistant myeloma with a high probability of clinical success that promises to improve the quality of treatment, maximize drug efficacy, minimize toxicities and adverse drug reactions from overdosing and decrease the rate of mortality in myeloma patients. A logical extension of this pipeline would be the development of model systems where a combination of more than two secDrugs can be effectively tested.

The integration of in silico modeling-based pipeline with single-cell technologies (scRNAseq and CyTOF analysis) introduces an innovative, evidence-based application in clinical decision-making that will minimize the number of test drugs required for discovering successful combination chemotherapy regimens against drug-resistant cancers.

## **CHAPTER 3**

### **Validation of secondary therapies against Prostate Cancer**

## Abstract

Prostate cancer/PCa is the second leading cause of cancer deaths in US men. Most early-stage patients are treated with androgen deprivation therapy/ADT. However, despite a good initial response, patients eventually acquire ADT resistance and develop metastatic castration resistant PCa/mCRPC, a progressive disease state with poor median survival (<3 years). Metastatic castration-resistant prostate cancer (mCRPC) is the most advanced and lethal stage of prostate cancer. A subset of advanced CRPC patients eventually develops an aggressive variant of prostate cancer (AVPCa), a rapidly progressive disease state with a lack of AR expression (AR-negative mCRPC) and limited or no therapeutic options. Therefore, there is an unmet need to identify novel agents for the management of AVPCa. We have developed a novel *in silico* algorithm, secDrug, that used computational optimization-regularization technique to identify the p38MAPK inhibitor, TAK715, as a top secondary drug that can confer a significant clinical advantage over TX monotherapy by enhancing the magnitude of therapeutic efficacy and reducing the required TX dose. Notably, in CRPC, the MAPK pathway is involved in sustaining AR-independent cell proliferation. Using the HMS LINCS database, we identified CSNK1D, MAPK14, MAP4K4, and CSNK1A1 (an activator of  $\beta$ -Catenin) as the target genes of TAK715. Through using single-cell transcriptomic analysis, we showed that cell subpopulations expressing the PCa stemness marker CD44, drug-resistant markers (CXCL8, CDK1), or epithelial-to-mesenchymal transition markers (Vimentin, TGFB1) were also a very high expression of TAK715 target genes (CSNK1D, MAPK14, MAP4K4) indicating TAK715 is potentially effective against treatment-refractory and stem-cell-like subclones. Next, we confirmed the efficacy of TAK715 alone and in combination with TXs in human PCa cell lines using *in vitro* cytotoxicity assays. TAK715 displayed high single-agent efficacy and strong synergism with TX (combination index/CI<0.7 indicating synergy). Synergy was particularly profound in the DUTXR (acquired TX-resistance) and PC3M (high metastatic property) cell lines. Notably, the TX+TAK715 combination lowered the effective TX dose required to achieve the desired therapeutic response by >10-folds (Dose Reduction Index/DRI 10.62 $\pm$ 11.42). Further, cell-based phenotypic assays, including caspase 3/7 assay, Annexin-V/PI assay, cell cycle analysis, *in-vitro* live-cell imaging, scratch assay, and clonogenic assay strongly suggested that TX+TAK715 combination have higher effectiveness compared to TX alone, and exhibits strong synergism, particularly in androgen-independent aggressive mCRPC, possibly involving

stem-cell-based TX resistant single-cell subclones. Using a novel microfluidic chip-based Confined Cell migration assay, we also showed that the drug combination reduces both confined and unconfined migration, indicating potential inhibition of the metastatic potential of PCa. Gene expression profiling (mRNA sequencing) followed by Ingenuity pathway analysis (IPA) revealed upregulation of mitochondrial dysfunction and oxidative phosphorylation (OXPHOS) as the top dysregulated pathways following single-agent and combination treatment, which were confirmed by immunoblotting. In vitro ROS generation assay and Mitochondrial membrane potential measurement following combination treatment confirmed elevated intra-cellular ROS level ( $\approx 7$  folds, indicating oxidative stress) and membrane depolarization (indicating mitochondrial dysfunction), respectively, in mCRPC lines. Furthermore, our IPA causal network analysis predicted significant upregulation of microRNA-132 and downregulation of the RICTOR pathway, miR-21, in response to combination treatment. Using in silico analysis on multiple GEO PCa datasets, we found low expression level of miR-132 was associated with poor clinical prognosis, the transition from androgen-dependent (AD) to independent (AI) stage, and metastasis. miRNA 21 was significantly up regulated in the GEO PCa datasets. miRNA 21 is an AR-regulated miRNA that plays a key role in nullifying the effect of castration, driving progression to the androgen-independent stage, TX resistance, and cellular invasiveness through down-regulation of tumor suppressor PTEN.

Together, we conclude that the TAK715+Taxane combination may be useful in curbing oncogenic progressions in AVPCa through simultaneous inhibition of multiple oncogenic factors/pathways. Our multi-pronged approach towards screening and pre-clinical validation for drug re-purposing represents a new paradigm in the management of aggressive treatment-refractory subtypes of PCa.

## Introduction

Prostate cancer (PCa) is the second leading cause of non-cutaneous cancer-related deaths in the US (www.cancer.org).<sup>316</sup> The androgen signaling pathway plays a crucial role in PCa development.<sup>237,239,262</sup> Therefore, the standard treatment options for PCa are radical prostatectomy (RP) or radiation therapy with androgen-deprivation therapy (ADT).<sup>234</sup> Most early-stage PCa patients (castration sensitive or CSPC) treated with ADT show good initial response with a high 5-year survival rate.<sup>317</sup> However, a vast majority of these men eventually become unresponsive towards hormone therapy, and despite low levels of androgen, the disease progresses with continuously rising Prostate Serum Antigen (PSA), eventually developing more aggressive forms called Castration-resistant prostate cancer (CRPC).<sup>237,241,245,250</sup> Metastatic castration-resistant prostate cancer (mCRPC) is the clinically most advanced and lethal disease state with signs of metastasis to distant organs like the brain, bone, lung, lymph node, and median survival of less than 3 years (5-year median survival rate of 31%).<sup>245</sup> Although next-generation AR-targeting chemotherapeutic treatments like abiraterone plus prednisone (AA/P) or enzalutamide (ENZ), and combination with taxanes (Docetaxel/DTX or Cabazitaxel/CBZ), increase survival rate slightly, eventual development of resistance (acquired resistance) is nearly universal where progression-free survival approaches ~0% in 3 years, often with severe side effects.<sup>318</sup> Chemotherapy options become limited once patients fail DTX therapy. Further, neuroendocrine PCa or NEPC (also known as small cell carcinoma) is an intrinsically resistant, poorly differentiated aggressive variant of PCa that lacks AR expression<sup>266</sup>

In addition, several groups, including ours, have shown that the presence of cancer stem-like cells (CSCs) like side populations (SPs) and CD133<sup>+</sup> cells with self-renewal and differentiation (acquisition of mesenchymal phenotype or epithelial to mesenchymal trans-differentiation/EMT) capacities significantly contribute to tumor aggressiveness and the development of drug resistance.<sup>28,97,98,216</sup>

Drug development for these clinically most-aggressive and lethal variants of PCa (AVPC) thus poses a significant challenge with very few therapeutic successes.

Our laboratory has designed a pharmacogenomics data-driven computational pipeline (secDrug) that identifies novel secondary drugs (“secDrugs”) for the treatment of drug-resistant advanced-state cancers.<sup>319</sup>

In this study, we applied the secDrug algorithm to PCa models and identified several novel secondary drug candidates for the treatment of AVPC. Next, using single-cell RNA sequencing (scRNA-seq), we demonstrated the presence of PCa subclones representing aggressive, TX-resistant, and cancer stem-like cells. Further, our scRNA-seq data predicted that the secDrug, TAK-715 (a p38 $\alpha$  MAPK/ MAPK14 inhibitor), is potentially effective against PCa subclones with enrichment of treatment-resistant and stem-like genes. We hypothesize that our predicted and pre-screened secDrugs would be helpful in curbing oncogenic progressions as single-agent or in combination with taxanes in AVPC through simultaneous inhibition of multiple oncogenic factors/pathways. Using in vitro model systems of treatment-refractory and treatment-emergent AVPC (representing mCRPC, NEPC, and EMT), we demonstrated that the TAK-715 not only showed efficacy as a single-agent but also enhanced the efficacy of the taxane drugs DTX and CBZ. Further, we performed a sophisticated microfluidic chip-based confined cell migration assay that recapitulates diverse micro-environmental cues encountered by cancer cells during locomotion (e.g., the dimensionality of pores and 3D longitudinal, channel-like tracks) to investigate the effect of TAK-715-based regimens on cancer cell invasion, motility, and metastasis. Finally, we demonstrated the impact of TAK-715 in eroding ‘stem-like’ subpopulations (including SPs, quiescent/dormant cells, and ALDH1<sup>+</sup> cells).

Next, we performed pre- vs. posttreatment bulk and single-cell tumor RNAseq to identify differentially expressed genes (DEGs) and potential molecular pathways associated with the TAK-715 mechanism of action in AVPC at the tumor and sub clonal levels. Finally, using comparative analysis of whole-genome transcriptomics data between clinically sensitive and resistant PCa patients, we demonstrated that TAK-715 has the potential to be clinically effective based on the reverse matching of GEP signatures and top dysregulated pathways.

Hence, using an innovative approach that integrates single-cell -omics technologies, microfluidics, and tumor mRNA sequencing with In vitro studies and patient data-based validation, we conclude that TAK-715 has the potential to improve the clinical outcome in AVPC chemotherapy by enhancing the therapeutic efficacy and abrogating the possibilities of development of bulk and sub clonal drug resistance. Such an evidence-based approach promises to minimize the chances of trial failures and improve the probability of clinical success.

## Materials and Methods

### Drugs and Reagents

Drugs, reagents, antibodies, and kits are listed in **Table 1**

Reagents	Manufacturer	Location
Fetal bovine serum (FBS)	Hyclone (Thermo-Fisher Scientific Inc.)	Rockford, IL, USA
Trypsin (0.25% w/v)	Hyclone (Thermo-Fisher Scientific Inc.)	Rockford, IL, USA
Penicillin-Streptomycin (10,000 U/mL)	Gibco™ (Thermo-Fisher Scientific Inc.)	Waltham, MA, USA
Docetaxel	Selleck Chemicals LLC	Houston, TX, USA
Cabazitaxel	Selleck Chemicals LLC	Houston, TX, USA
TAK-715	Selleck Chemicals LLC	Houston, TX, USA
FITC Annexin V Apoptosis Detection Kit	BD Biosciences	San Jose, CA, USA
FxCycle™ PI/RNase Staining Solution kit	Thermo-Fisher Scientific Inc	Waltham, MA, USA
RIPA lysis buffer	Thermo-Fisher Scientific Inc	Waltham, MA, USA
Protease Inhibitor Cocktail	Thermo-Fisher Scientific Inc	Waltham, MA, USA
Phosphatase Inhibitor	Thermo-Fisher Scientific Inc	Waltham, MA, USA
Pierce™ ECL Western Blotting Substrate	Thermo-Fisher Scientific Inc	Waltham, MA, USA
HES-1 specific primer Hs00172878_m1	Thermo-Fisher Scientific Inc	Waltham, MA, USA
TaqMan Gene Expression Assays	Thermo-Fisher Scientific Inc	Waltham, MA, USA
Vybrant™ DyeCycle™ Violet Stain	Thermo-Fisher Scientific Inc	Waltham, MA, USA
CM-H2DCFDA (General Oxidative Stress Indicator)	Thermo-Fisher Scientific Inc	Waltham, MA, USA
NucBlue™ Live ReadyProbes™ Reagent (Hoechst 33342)	Thermo-Fisher Scientific Inc	Waltham, MA, USA
RNeasy Plus Mini Kit	QIAGEN	Hilden, Germany
QuantiTect Reverse Transcription Kit	QIAGEN	Hilden, Germany
Quick Start Bovine Serum Albumin Standard	Bio-Rad	Hercules, CA, USA
Tris Buffer Saline (TBS)	Bio-Rad	Hercules, CA, USA
10% Tween 20	Bio-Rad	Hercules, CA, USA
Polyvinylidene fluoride membrane (PVDF)	EMD Millipore	Billerica, MA, USA
Bovine Serum Albumin (BSA)	VWR	Radnor, PA, USA
3-(4,5-dimethylthiazol-2-yl)-2,5-diphenyltetrazolium bromide (MTT)	Sigma-Aldrich Inc	St. Louis, MO, USA
Dimethyl sulfoxide (DMSO)	Sigma-Aldrich Inc	St. Louis, MO, USA
2',7'-Dichlorofluorescein diacetate (DCFDA)	Sigma-Aldrich Inc	St. Louis, MO, USA
Bradford Reagent	Sigma-Aldrich Inc	St. Louis, MO, USA
JC-1 - Mitochondrial Membrane Potential Assay Kit	Abcam	Waltham, MA, USA
HES1 (11988S)	Cell Signaling Technology	Danvers, MA, USA
CD44 (3570T)	Cell Signaling Technology	Danvers, MA, USA
Cleave-caspase 9 (9505T)	Cell Signaling Technology	Danvers, MA, USA
Cleave-caspase 3 (9661T)	Cell Signaling Technology	Danvers, MA, USA
Anti-rabbit IgG, HRP-linked Antibody (7074S)	Cell Signaling Technology	Danvers, MA, USA
β-actin (A3854)	Sigma-Aldrich Inc	St. Louis, MO, USA

## Identification of secondary drugs (secDrugs)

We used a pharmacogenomics data-driven approach to identify potential agents that can be repurposed as novel secondary drugs to treat cancers resistant to standard-of-care (primary) drugs when used in combination with the primary drug. As the data source, we used the GDSC1000 (Genomics of Drug Sensitivity in Cancer) database, a large-scale pharmacogenomics database of dose-response results ( $IC_{50}$  or AUC) on 265 compounds in >1000 cell lines representing a wide spectrum of human cancers<sup>320</sup>. These 265 drugs cover a wide range of targets and processes involved in cancer biology, which include drugs that are either approved and used in the clinic, or are undergoing clinical development, or in clinical trials, or are tool compounds in early-phase development. For the purpose of this study, we used inclusion criteria to filter cell lines with Genito-urinal cancer subtypes. A total of 136 cell lines were selected from the GDSC1000 database breast (n=52), cervix (n=14), endometrium (n=11), ovary (n=45), prostate (n=8), testis (n=3), vulva (n=3).

First, we assumed that  $IC_{50}$  values of DTX in these lines (including PCa cell lines) were  $S_{bi}: i \in \{1, \dots, n\}$ , where there are  $n$  cell lines. Also, we assumed that there are  $K$  other drugs, and the  $IC_{50}$  values of the  $n$  cell lines for the  $K$  drugs are given by:

$$R_{ki}: k \in \{1, \dots, K\}, i \in \{1, \dots, n\}.$$

Next, we classified the cell lines as sensitive or resistant to DTX using a quantile of the empirical distribution of  $R_{ki}$ , and a threshold criterion to achieve the classification. Finally, we identified secondary drugs or secDrugs that could kill the maximum number of DTX-resistant cell lines based on individual  $IC_{50}$  values. In the case of ties between the top secDrugs, we chose the drug with the lower mean  $IC_{50}$  values.

## Human Prostate Cancer Cell Lines

AR<sup>lo</sup> mCRPC/NEPC (PC3, PC3M, DU145) Osteotropic subline C42b. murine prostate gland carcinoma cell RM-1 was obtained from the American Type Culture Collection (ATCC) (Manassas, VA, USA). The taxane-resistant cell lines PC3-TXR and DUTXR were generated using dose-escalation of taxanes over time, as described earlier. The cell lines were authenticated at the source and tested randomly at regular intervals for tissue specimen provenance and cell lineage at the AU Center for Pharmacogenomics and Single-Cell Omics (AUPharmGx) using Gene-Print 24 System (Promega). All cell lines are mycoplasma negative. PC-3, PC-3M cells

were maintained in 10% (v/v) (FBS) supplemented in F-12K, DU145 in Eagle's Minimum Essential Medium (EMEM). PC3-TXR and DUTXR were maintained in RPMI-1640 media with 1% Penicillin-Streptomycin at 37°C, 21% O<sub>2</sub>, and 5% CO<sub>2</sub> in a humidified cell culture chamber (Heracell™ VIOS 160i CO<sub>2</sub>; Thermo-Fisher Scientific™).

## **Patient Samples**

**Cancer Genome Atlas (TCGA) database:** Gene expression on PCa patients was extracted from The Cancer Genome Atlas (TCGA) Data Portal Genomic Data Commons (GDCs) server (cancergenome.nih.gov). The interactive web-portals UALCAN and Gene Expression Profiling Interactive Analysis (GEPIA) were used for in-depth analysis of TCGA gene expression data files and to compare transcriptome data on target candidate pathway genes with tumor metastasis and patient survival from the prostate expression data matrix<sup>321,322</sup>.

## ***In vitro* cytotoxicity assays and drug synergy analysis**

*In vitro* chemo-sensitivity assays were performed on human PCa cell lines using mitochondrial enzyme activity or MTT (3-(4,5-dimethylthiazol-2-yl)-2,5-diphenyltetrazolium bromide reagent) assay. Briefly, cells were plated in a 96-well culture plate at  $2 \times 10^3$  cells/well and incubated for 24 h at 37°C with 5% CO<sub>2</sub>. Cells were treated with increasing concentrations of DTX (0- 2250nM), CBZ (0-2250nM), Enzalutamide (0-5062.5nM), Bicalutamide (0-5062.5nM) and TAK-715 (0- 625nM) as a single agent, or the combination of DTX+TAK-715, and CBZ+TAK-715. Following 48-hour incubation, the tetrazolium dye MTT was added according to the manufacturer's instructions, and absorbance was measured at 550 nm using Synergy Neo2 Microplate Reader (BioTek, USA). Percent change relative to untreated controls was calculated at each drug concentration, and the effect of drug exposure was determined by constructing cytotoxicity (growth) curves. Half-maximal inhibitory drug concentration (IC<sub>50</sub>) values were estimated by nonlinear regression using a sigmoidal dose-response equation (variable slope). Drug synergy was calculated by comparing single-agent and combination drug-response data based on Chou-Talalay's combination index (CI) method and the isobologram algorithm (CompuSyn software; Biosoft, US)<sup>323</sup>. CI values between 0.9-0.3 and 0.3-0.1 signify synergism and strong synergism, respectively, between the drugs treated in combination.

## **Caspase-3/7 activity assay**

Cell death by apoptosis was measured using Caspase-Glo 3/7 luminescent assay system kit according to the manufacturer's instructions (Promega Madison, WI). Briefly,  $2 \times 10^3$  cells/well were seeded into 96-well plates (triplicates) and treated at the estimated single-agent vs. combination  $IC_{50}$  values calculated by MTT assay. Following 48 hours of incubation, Caspase-Glo 3/7 reagent was added and incubated for 2 hours, and luminescence was measured using a Synergy Neo2 Microplate Reader (BioTek, USA). The apoptosis level in each treatment group was normalized to the control group (no drug treatment with baseline caspase 3/7 assay luminescence) for each cell line.

### **Annexin V and propidium iodide (PI) staining**

Annexin V and PI staining was used to assess apoptosis and necrosis by flow cytometry. Briefly, cells were seeded in 6 well plates at indicated concentrations and exposed to DTX and TAK-715 as a single agent and as combinations. After 48h, cells were labeled with binding buffer containing annexin V-FITC (25  $\mu$ g/ml) and PI (25  $\mu$ g/ml) as well as 10 mM HEPES, 140 mM NaCl, 5 mM KCl, 1 mM  $MgCl_2$ , and 1.8 mM  $CaCl_2$  (pH = 7.4), incubated for 10 min., followed by three washes in binding buffer. Both detached and attached cells were combined, and staining was quantified using a Becton Dickinson FACS Calibur flow cytometer (BD Biosciences, San Jose, CA) at 10,000 events per measurement.

### **Assessment of cellular and nuclear morphology**

**Cellular morphology**, PCa cells were seeded  $0.025 \times 10^6$  cells/ml in 6-well plates and exposed to TAK-715, either as a single agent or in combination with DTX for 48 h. Three areas with approximately equal cell densities were identified in each well, and images were captured with an EVOS FL digital cell imaging system (Thermo-Fisher Scientific, Inc.) using a 10X objective.

For **nuclear morphology**, PCa cells were plated on top of the glass coverslip ( $1.5 \times 10^5$  cells/ml), incubated overnight, and treated with either vehicle or TAK-715 alone or as a combination with DTX. After 48h, the cells were labeled with NucBlue Live reagent and incubated for 20 minutes. Images were captured using a Nikon Eclipse Ti2 microscope and recorded in bright field and phase contrast modes at 20X and 40X magnifications. Images were analyzed using Image J software (National Institutes of Health, Bethesda, MD, USA).

### **Z' LYTE Assay<sup>324</sup>**

The assay was outsourced to Thermo-Fisher Scientific to identify the targets of TAK-715. Briefly, 100 nL of 100X Test Compound (for each test concentration) in 100% DMSO was taken in a black 384-well plate. 2.4 µL of Kinase buffer was added to each well. 5 µL of 2X Peptide/Kinase Mixture (for each of the target kinases) was added to the corresponding wells. 2.5 µL of 4X ATP Solution was added in each well, followed by a 30-second plate shake. The plate was incubated for 60 minutes for Kinase Reaction at room temperature. 5 µL of Development Reagent Solution was added, followed by a 30-second plate shake. The plate was again incubated for 60 minutes for Development Reaction at room temperature. The fluorescence reading was captured in a plate reader, and the data was analyzed.

### **Assessment of cell cycle**

Control (no drug) and post-treated cells were prepared for cell cycle analysis by staining with PI (50 µg/ml) in sample buffer [PBS + 1% (w/v) glucose], containing RNase A (100 units/ml) for 30 min at room temperature and analyzed by flow cytometry using a Becton Dickinson FACS Calibur flow cytometer (BD Biosciences, San Jose, CA). Cell cycle data were analyzed using CytExpert (Beckman Coulter Inc, Indianapolis, IN). Data are presented as the mean ± SEM of three separate experiments (n = 3/study).

### **Determination of intracellular ROS levels (DCFDA assay) and superoxide levels (DHE assay)**

Cells were plated at a seeding density of 2000 cells/well and incubated overnight at 37°C. After 24h, 100 µl of 10 µM DCFDA solution was added to each well and incubated in the dark for 45 minutes at 37°C. DCFDA solution was then discarded and treated with either vehicle (0.5% DMSO) or TAK-715 single agent and in combination with DTX. Samples were collected at different time points (2, 4, 8, and 24h). Fluorescent intensity was measured on Synergy Neo2 Hybrid Multi-Mode Microplate Reader, BioTek (Winooski, VT, USA) at excitation - 485nm and emission - 535 nm in endpoint mode.

Prostate cancer cells were pre-incubated with 5 µM DHE for 15 min in the dark at 37 °C. Cells were then cells treated with TAK-715-based regimens for 24h. After that, cells were washed

once with a cell-based assay buffer, and red fluorescence was recorded by Synergy Neo2 multi-plate reader.

### **Assessment of Mitochondrial Membrane Potential**

Cell lines were treated with DTX, TAK-715, and DTX+TAK-715. Further, 100  $\mu$ L/well of working JC-1 solution was added to the plate and incubated at 37°C for 10 minutes in the dark. Read plate endpoint in the presence of compounds and media on a fluorescent plate reader Synergy Neo2 Hybrid Multi-Mode Microplate Reader, BioTek (Winooski, VT, USA) at 535 nm.

### **Assessment of Side Population**

A total of  $1 \times 10^6$  /ml cells were cultured in 6 well plates and treated with TAK-715 alone or in combination with DTX. After 24h, cells were stained with 5  $\mu$ M Vybrant DyeCycle Violet and 1  $\mu$ g of 7-AAD for 30 min at 37°C. Following dye incubation, cells were immediately analyzed (10,000 events per measurement) using a Becton Dickinson FACS Calibur flow cytometer (BD Biosciences, San Jose, CA).

### **Colony formation assay**

PCa cells were seeded in a 6-well plate at  $0.025 \times 10^6$  cells/ml, incubated overnight, and treated with DTX and TAK-715 as a single agent or in combination. The cells were then harvested and plated in a 24-well plate at a concentration of 1000 cells/well and incubated for 1- 2 weeks. The colonies were fixed with 100% methanol and stained with Crystal Violet. Images were taken for control, treated cells, and the colonies using an EVOS FL digital cell imaging system (Thermo-Fisher Scientific, Inc.). Images were recorded in bright field and phase contrast modes at 20X and 40X magnifications and analyzed using Image J software.

### **Cell migration/Scratch Assay**

Cells were plated in 6-well plates at  $1 \times 10^5$  cells/well and incubated for 48 h to a 95% confluency. The monolayer was scratched with an SPLScar Scratcher 6 well Tip at a width of 0.50 mm at the center of the well. TAK-715 as single-agent or DTX+TAK-715 combination doses were applied to the cells in the respective wells. F-12K culture medium supplemented with 10% FBS containing the vehicle (0.05 % DMSO) was added to the cells in the control wells. Micrographs of the wound areas were obtained at 0, 24, and 48 hours using an EVOS FL digital cell imaging

system (Thermo-Fisher Scientific, Inc.). Images were recorded in brightfield and phase contrast modes at 20X and 40X magnifications. The area of the initial wound (at 0 h) and the “gap area” were measured at 48 hours with Image J software.

### **Comet Assay**

Comet assay was performed following the manufacturer’s protocol (R&D Systems). Briefly, PCa cells were treated with DTX+TAK-715 combination for 48 hours. After that, the cells were collected and washed with PBS. Then, the cells were mixed with low-melting agarose and immobilized on the Comet slide. Next, the cells were treated with a lysis solution to break open the cell membrane, and DNA was denatured under alkaline conditions. Cells were then stained with propidium iodide, and Images were captured by Gel Doc EZ Gel Documentation System, followed by analysis through ImageJ software.

### **Microfluidic ( $\mu$ )-channel Cell Migration Assay**

The fabrication of a Polydimethylsiloxane (PDMS)-based  $\mu$ -channel assay using standard multilayer photolithography and replica molding has been demonstrated earlier (Figure 11C). In this study, PCa cells were seeded in 6 well plates exposed to TAK-715 as a single agent and TAK-715+DTX combinations at indicated concentrations. Next,  $1-1.5 \times 10^5$  cells were introduced into the cell seeding inlet line of the microfluidic channel via pressure-driven flow and were allowed to adhere for 30 min at 37°C, 5% CO<sub>2</sub>. Next, the cell suspension was removed and substituted with a serum-free medium. Medium supplemented with 10% FBS was added into the chemoattractant inlet line to trigger cell entry into the channels. The devices were placed on an automated Nikon Ti2 Inverted Microscope equipped with a Tokai Stage-Top incubator unit, which maintained cells at 37 °C and 5% CO<sub>2</sub>. Cell entry into the channels was recorded via time-lapse microscopy. Images were recorded every 20 min for 10 h with a 10x /0.45 NA Ph1 objective.

### **Pre- and post-treatment tumor mRNA sequencing (RNA-seq):**

The effects of DTX and TAK-715 as a single agent and in combination exposure on gene expression in PCa cell lines were assessed using next-generation RNA sequencing of bulk tumor cells. Pre- and post- drug-exposure TAK-715 single-agent, TX+TAK-715 combination) tumor cells were harvested, and high-quality RNA was extracted using QIAshredder and RNeasy kit

(Qiagen) according to the manufacturer's protocol. RNA concentration and integrity were assessed using a Nanodrop-8000 spectrophotometer (Thermo-Fisher Scientific, USA), Qubit 2.0 Fluorometer (Invitrogen, Carlsbad, CA, USA), and Agilent 2100 Bioanalyzer (Applied Biosystems, Carlsbad, CA, USA) and stored at  $-80^{\circ}\text{C}$ . An RNA integrity number (RIN) threshold  $>8$  was applied, and RNA-seq libraries were constructed using Illumina TruSeq RNA Sample Preparation kit v2. Libraries were then size-selected to generate inserts of  $\sim 200$  bp, and RNA sequencing was performed on Illumina's NovaSeq platform using a 150bp paired-end protocol with a depth of  $> 20$  million reads per sample. Average quality scores were thoroughly above Q30 for all libraries in both R1 and R2.

### **RNAseq data analysis**

RNA-seq data from the cell lines and patient RNAseq data (described above) was pre-processed and normalized, and differential expression (DE) analysis was performed using command-line-based analysis pipeline (DEseq2 and edgeR) and Partek Flow software (Partek, Inc, USA). Quality control (QC) check on the RNA-seq raw reads was performed using the FastQC tool, followed by read-trimming to remove base positions that have a low median (or bottom quartile) score. STAR Aligner tool mapped processed RNA-seq reads to the hg38 human genome build. Next, we used GSA that applies limma, an empirical Bayesian method, to perform differential gene expression analysis between groups and detect the DE genes. Genes with mean fold-change  $>|1|$  and  $p < 0.05$  were considered as the threshold for reporting significant differential gene expression. Heatmaps were generated using unsupervised hierarchical clustering (HC) analysis based on the differentially expressed genes (DEGs).

### **Pre- and post-treatment Single-cell RNA sequencing (scRNA-seq)**

Automated single-cell capture, and cDNA synthesis were performed on the untreated and TAK-715-treated acquired taxane-resistant mCRPC DUTXR using the 10X Genomics Chromium platform. Single-cell RNAseq-based gene expression analysis will be performed on Illumina HiSeq 2500 NGS platform (Paired-end.  $2 \times 125$ bp, 100 cycles. v3 chemistry) at  $\sim 10$  million reads per sample.

### **scRNA-seq data analysis**

Single-cell RNAseq datasets were obtained as matrices in the Hierarchical Data Format (HDF5 or H5). We used CellRanger, Seurat, and Partek Flow software packages will be used to pre-process the scRNA-seq data and perform single-cell transcriptomics. Highly variable genes were selected for clustering analysis based on a graph-based clustering approach. The visualization of cell populations was performed by T-distributed stochastic neighbor embedding (t-SNE) and UMAP (Uniform Manifold Approximation and Projection) for biomarker-based identification of subclones representing TX-resistant cells, potential TAK-715 target subclones, and cancer stem cell signatures, as well as TAK-715 treatment-induced erosion of these subclones.

### **Ingenuity pathway analysis (IPA)**

Ingenuity pathway analysis (IPA; Qiagen) analysis was performed using top DEGs to reveal molecular pathways/mechanisms, upstream regulator molecules, downstream effects, biological processes, and predicted causal networks governing TAK-715 function and successful drug combinations in AVPC.

### **Quantitative Reverse Transcriptase Polymerase chain reaction (qRT-PCR)**

Cell lines were plated and treated with TAK-715 alone and in combination with DTX or with vehicle (0.5% DMSO) for 24 hours. Total RNA isolation and quantification were performed as described above. cDNA was then prepared using a QuantiTect Reverse Transcription kit (Qiagen). Following reverse transcription, TaqMan gene expression assay was performed using HES-1 specific TaqMan primers (Hs00172878\_m1) and TaqMan Fast Advanced Master Mix in CFX96 Touch Real-Time PCR Detection System (Bio-Rad, Hercules, CA).

### **Isolation of the CD44<sup>+</sup> population**

DUTXR cells were collected and washed with PBS, followed by permeabilization using cold methanol. Cells were then washed 2X with PBS and resuspended in 500 ul of antibody dilution buffer containing CD44PE-conjugated antibody, followed by 1-hour incubation at room temperature in the dark. After that, the cells were washed with PBS 1X and sorted using MoFlo XPD Flow Cytometer. The sorted cells were immediately put in culture using DMEM/F12 (1:1) basal media containing human epidermal growth factor, basic fibroblast growth factor, and recombinant human leukemia inhibitory factor.

### **Measurement of Oxygen Consumption Rate (OCR)**

We measured the OCR using the Agilent Seahorse Extracellular Flux (XF) Technology. Briefly, DUTXR cells were plated in an XFp plate and treated with vehicle control (0.5% DMSO), Docetaxel, and TAK-715 for 24 hrs. On the next day, using the Agilent Seahorse XF Cell Mito Stress Test kit, the mitochondrial function was measured by the XFp seahorse analyzer. First, oligomycin and Fluoro-carbonyl cyanide phenylhydrazone (FCCP) were injected sequentially, followed by a third injection of a mixture of Rotenone and Antimycin A. Oligomycin inhibits ATP synthase and reduces OCR, followed by FCCP that raises OCR to the maximal rate by collapsing the inner membrane gradient and increasing the electron transport chain activity. Lastly, rotenone and antimycin A, which are complex I and antimycin complex III inhibitors, respectively inhibit the electron transport chain and reduce the OCR to a minimal value.

Data were normalized to the protein concentration at the end of each experiment. Data was calculated, and graphs were plotted using Agilent Seahorse Wave Desktop software and report generator, MS Excel, and GraphPad Prism.

### **Statistical analysis**

All statistical analysis was performed using R (the project for statistical computing and graphics) version 4.1.0 and GraphPad Prism v9.0. All tests were two-sided, and  $p < 0.05$  to be considered statistically significant. We used a non-parametric Wilcoxon rank-sum test for differential expression analysis between two groups of cells.

## **Results**

### **Identification of secondary drugs against aggressive PCa using the secDrug algorithm**

A total of 1091 cell lines were present in the Genomics of Drug Sensitivity in Cancer (GDSC1000) database. The following filtering criteria were applied to select computable B-cell lines: Target Cell - B-Cell; Cancer Type blood; Tissue - blood; Histology - lymphoid\_neoplasm or haematopoietic\_neoplasm; Site - haematopoietic\_and\_lymphoid\_tissue; No missing data). A total of 94 cell lines satisfied the above filtering criteria and were selected for further analysis. IC<sub>50</sub> values were processed, imputed, and categorized as S (PI-sensitive), R (PI-resistant), and N ('Neutral'/Intermediate PI IC<sub>50</sub> values) prior to analysis (*further details in the Methods section*). We applied secDrug to cell lines denoted as N and R (PI-resistant and PI-neutral) in this

GDSC1000 dataset and predicted the top drugs that can be best combined with a PI backbone to achieve a response. The predicted top secondary drug combinations in PI-resistant+ PI-neutral B-cell cancers are shown in **Table 1**. These include HSP90 inhibitor (17-AAG), Nicotinamide Phosphoribosyl Transferase or Nampt inhibitor (FK866), Survivin inhibitor (YM155), PIKfyve inhibitor (YM201636), Raf inhibitor (PLX-4720), Bcl2 inhibitor (Navitoclax), SB505124 (transforming growth factor- $\beta$  type I receptor, ALK4, ALK7 inhibitor), S6K1-specific inhibitor (PF-4708671), and the neddylation inhibitor (MLN4924). Furthermore, when the top PI-resistant cell lines (R; highest 33% PI IC<sub>50</sub>), the following drugs were predicted to be highly effective in combination with PIs: 17. AAG, PLX4720, YM201636, and the AKT inhibitor KIN001.102.

The top agents predicted by our *in silico/secDrug* approach as potential novel secondary drugs for aggressive variants of TX-resistant PCa include FK866 (a specific inhibitor of NAMPT), YM155 (surviving inhibitor), TAK715- a potent p38 MAPK inhibitor, XAV939 -an inhibitor of Wnt/ $\beta$ -catenin pathway, and RDEA119 – a non-ATP competitive inhibitor of MEK1/2.

**Table 1: Top drugs ('secDrugs') derived from our pharmacogenomics data-driven analysis**

	<b>Drug Name</b>	<b>Target</b>	<b>Target Pathway</b>
1	Afatinib	ERBB2, EGFR	EGFR signaling
2	AKT inhibitor VIII	AKT1, AKT2, AKT3	PI3K/AKT pathway
3	AMG-706 (Motesanib)	VEGFR, RET, KIT, PDGFR	RTK signaling
4	AZD6482	PI3K $\beta$	PI3K/MTOR signaling
5	Cetuximab	EGFR	EGFR signaling
6	CP724714	ERBB2	RTK signaling
7	FH535	PPAR $\gamma$ , PPAR $\delta$	Wnt/ $\beta$ -catenin signaling
8	FK866	NAMPT	NAD <sup>+</sup> salvage pathway
9	GSK2126458 (Omipalisib)	PI3K (class 1), MTORC1, MTORC2	PI3K/MTOR signaling
10	GW441756	NTRK1	RTK signaling
11	KIN001-260	IKKB	NF- $\kappa$ B pathway
12	LY317615	PKCB	Other, kinases
13	MK-2206	AKT1, AKT2	PI3K/MTOR signaling
14	Navitoclax	BCL2, BCL-XL, BCL-W	Apoptosis regulation
15	NSC-87877	SHP-1 (PTPN6), SHP-2 (PTPN11)	Other
16	PD-0325901	MEK1, MEK2	ERK MAPK signaling
17	PD-173074	FGFR1, FGFR2, FGFR3	RTK signaling
18	PI-103	PI3K $\alpha$ , DAPK3, CLK4, PIM3, HIPK2	Other, kinases
19	RDEA119	MEK1, MEK2	ERK MAPK signaling

20	SNX-2112	HSP90	Protein stability and degradation
21	TAK-715	p38 $\alpha$ , p38 $\beta$	JNK and p38 signaling
22	TL-2-105	C-RAF	ERK MAPK signaling
23	WZ3105	SRC, ROCK2, NTRK2, FLT3, IRAK1	Other
24	XAV939	TNKS1, TNKS2	WNT signaling
25	YM155	BIRC5	Apoptosis regulation

### scRNA-seq showed AR<sup>low</sup> PCa cells with signatures of Epithelial-mesenchymal transition (EMT) and cancer ‘stemness’ and reveals

Figure 1A displays t-SNE clusters generated from baseline (untreated) scRNA-seq data in mCSPC and mCRPC cell lines. Each dot represents a single cell. Further, the AR status of each cell is represented in Figure 1B. Epithelial-mesenchymal transitions have been mechanistically linked with the generation and maintenance of stem-like cell populations during tumorigenesis. PCa cells that have undergone EMT are phenotypically and genomically similar to stem cells. For example, Vimentin is a well-characterized filament protein that is highly expressed in mesenchymal cells. Thus, enhanced levels of Vimentin and downregulation of E-cadherin served as markers for identifying cells that have undergone EMT. Figures 1C-E demonstrate that the AR<sup>low</sup> cells (primarily belonging to the mCRPC subtype) show higher expression of several mesenchymal gene signatures involved in Epithelial-mesenchymal transition with NEPC phenotype, including Vimentin (Figure 1C); N-cadherin (CDH2), Fibronectin (FN1), S100A4, Snail (SNAI1), Slug (SNAI2) (Figure 1D); and other major EMT markers CDH11, TWIST1, ZEB1 (Figure 1E). Further, Figures 1F-G show upregulation of cancer stemness-related markers Urokinase-type plasminogen activator (PLAU), Urokinase-type plasminogen activator receptor (PLAUR), and CD44, primarily in mCRPC cells.

Interestingly, signatures of cancer stemness and EMT trans-differentiation were also observed in a subgroup of AR<sup>low</sup> single cells within the mCSPC cell lines, 22Rv1, LnCaP.

Next, we compared the single-cell gene expression markers between taxane-sensitive (DU145) and the clonally derived acquired taxane-resistant mCRPC cell line DUTXR (Figure 2A). We observed upregulation of gene signatures association with mesenchymal transition (VIM and TGFB1) and downregulation of the epithelial marker epithelial cadherin/E-cadherin (CDH1) in the DUTXR cell line compared to DU145 (Figure 2B-D). Further, the taxane-resistant DUTXR also showed enrichment of biomarkers that play significant roles in cancer progression,

development, and maintenance of cancer stemness (CD44; Figure 2E-F) and drug resistance (CDK1, CXCL8; Figure 2G-H), indicating probable involvement in mCRPC development and progression.

**Figure 1A**

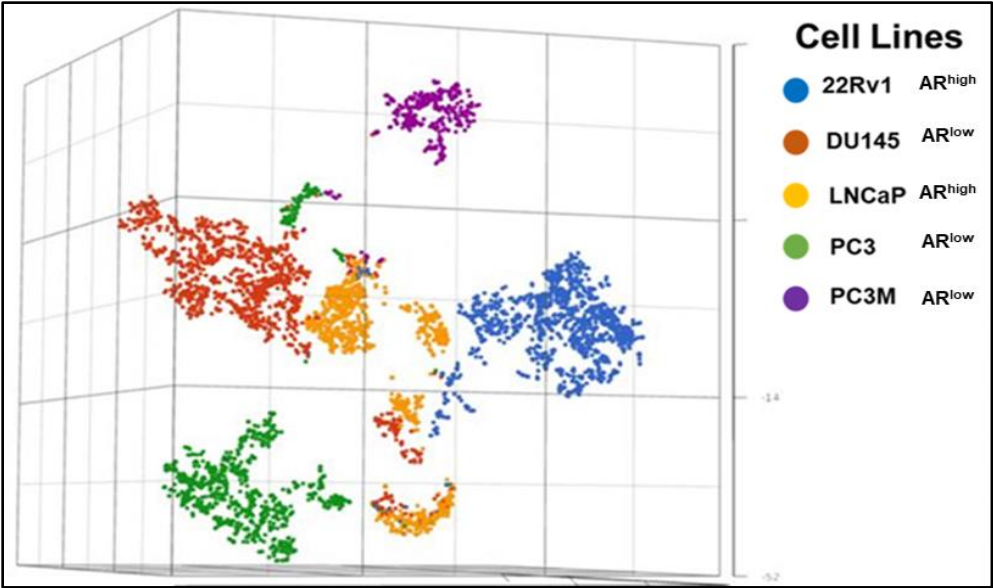


**Figure 1B**

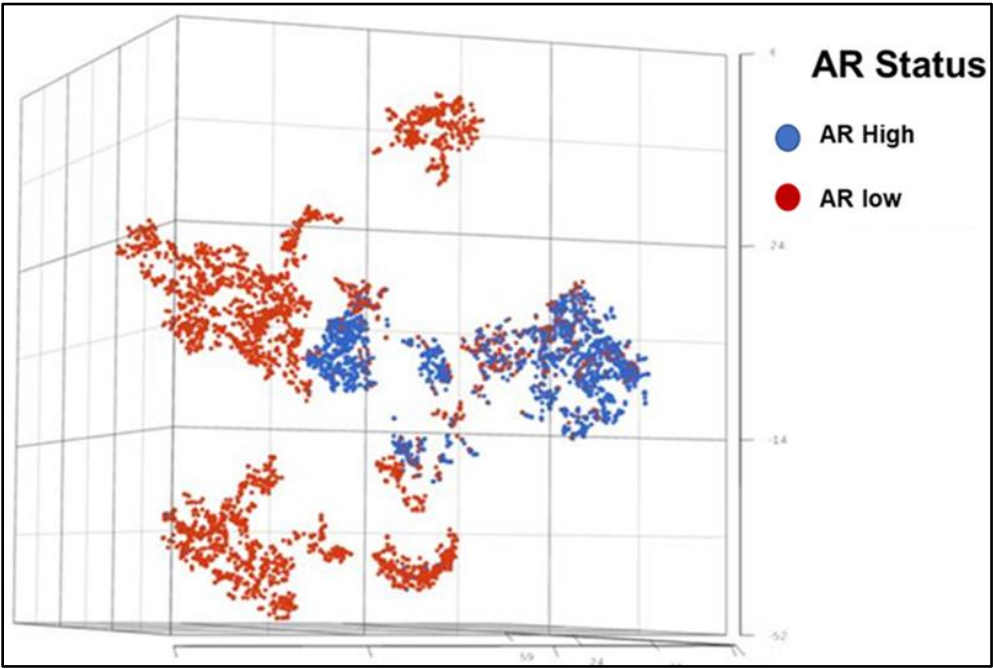


Figure 1C

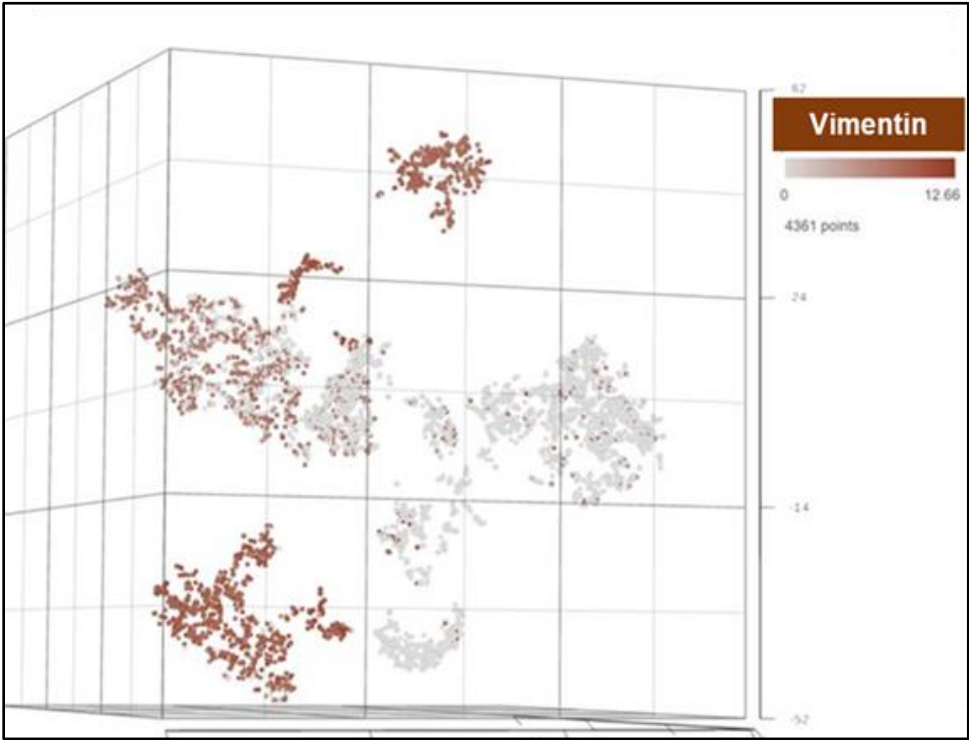
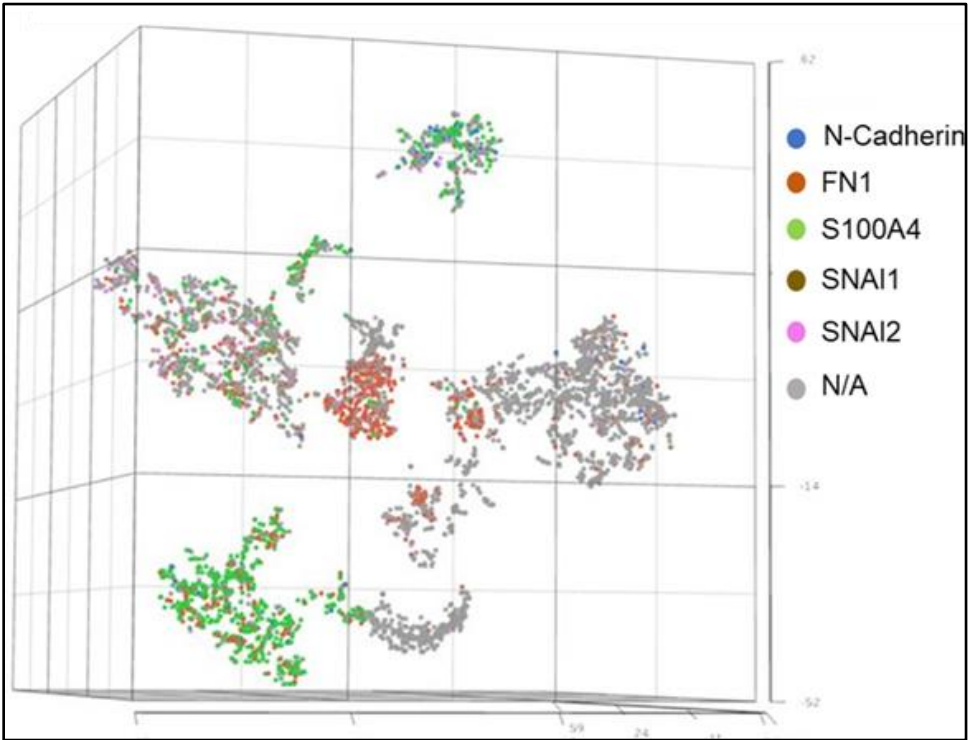
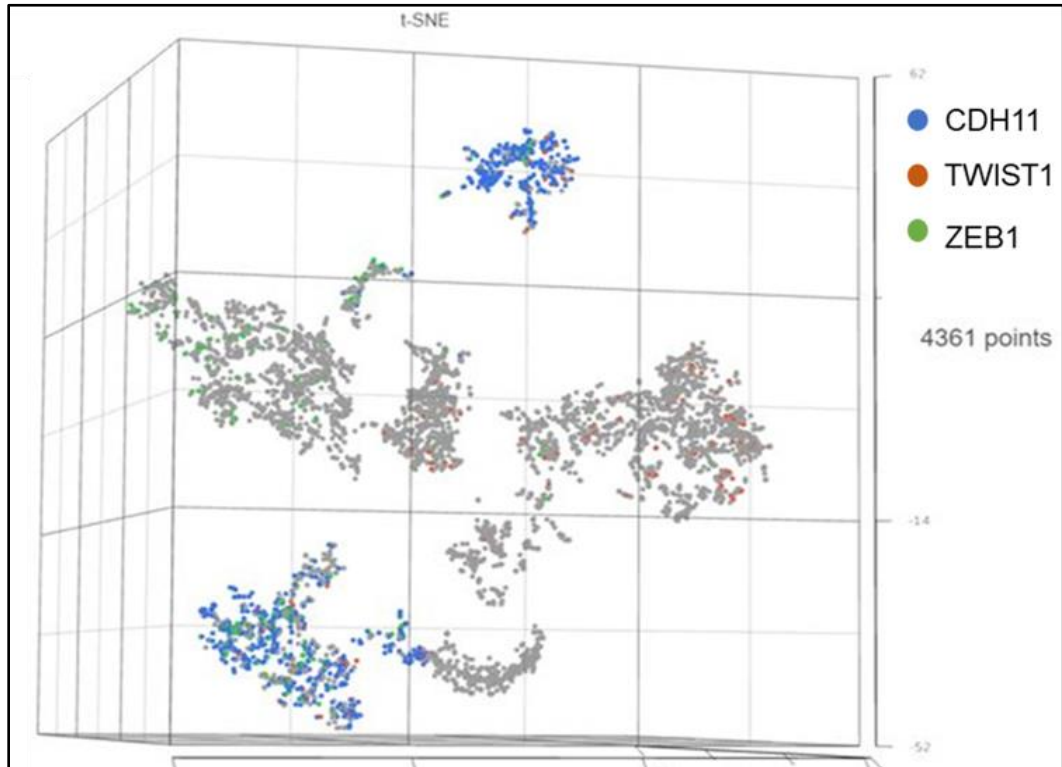


Figure 1D



**Figure 1E**



**Figure 1F**

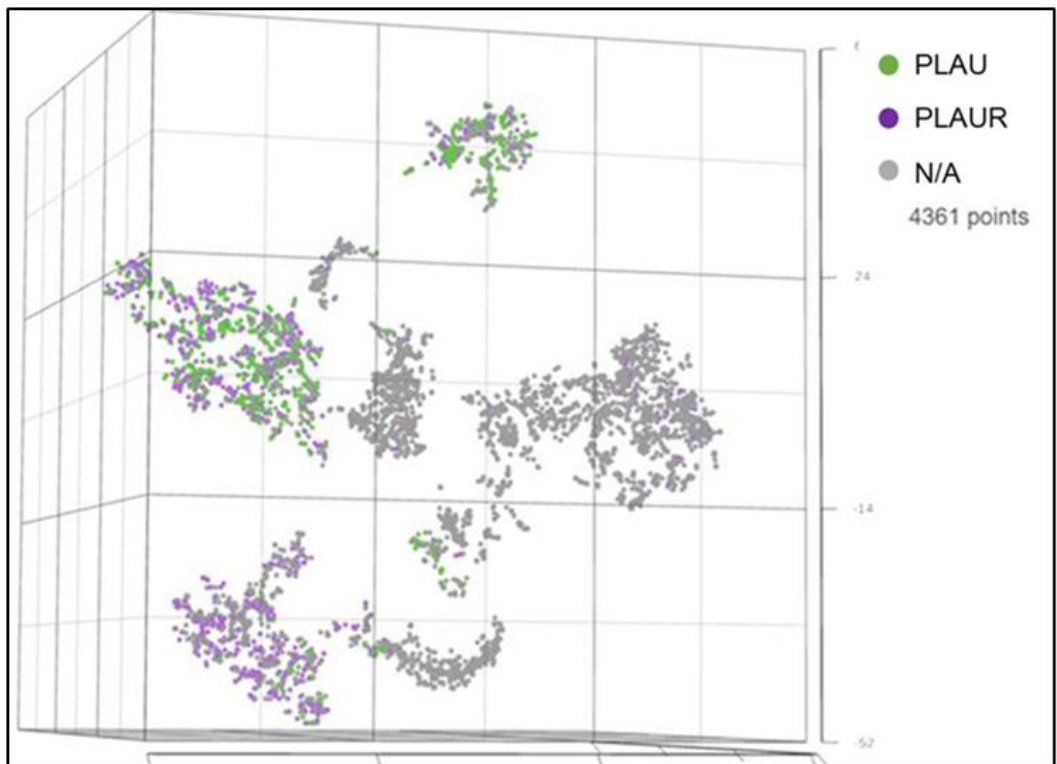


**Figure 1G**

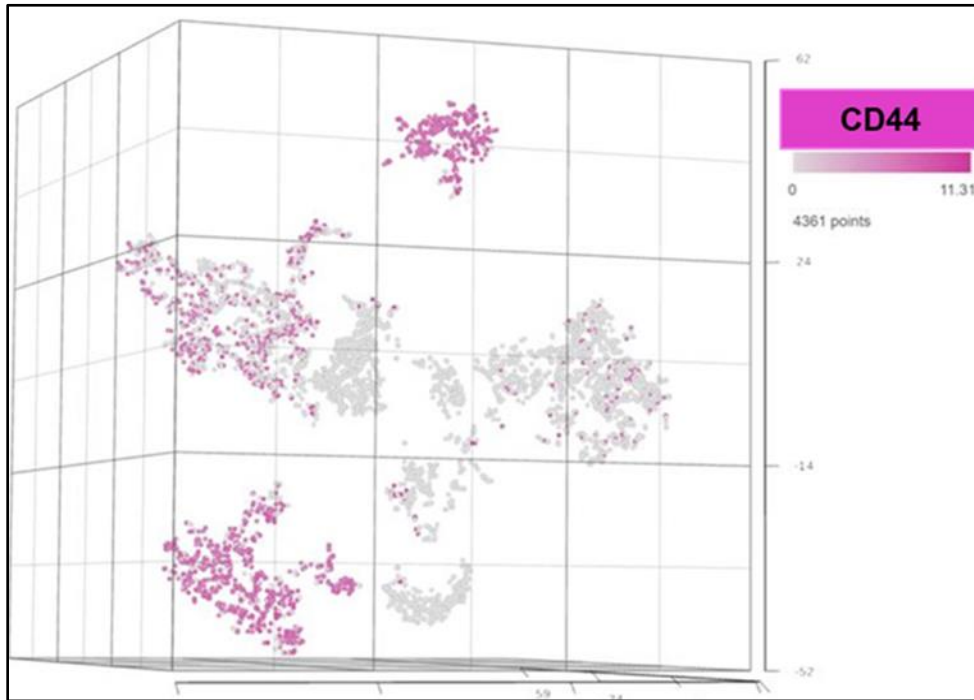


**Figure 1. Single-cell transcriptomics identifies signatures of epithelial to mesenchymal transition (EMT) and stemness in metastatic prostate cancer cells.**

Single-cell RNA sequencing using the Droplet sequencing method (10X Genomics) was performed on the PCa cell lines 22Rv1, LnCAP, DU145, PC3, and PC3M. t-distributed stochastic neighbor embedding (t-SNE) plots showing the comparison between the single-cell clusters representing **A)** All cell lines; **B)** AR Status

Expression of mesenchymal markers involved in EMT trans-differentiation, including the **C)** Vimentin (VIM); **D)** N-Cadherin (CDH1), Fibronectin (FN1), S100A4, Snail (SNAI1), Slug (SNAI2); other major EMT markers **E)** CDH11, TWIST1, ZEB1.

Expression of genes potentially involved in Cancer stemness **F)** Urokinase-type plasminogen activator (PLAU), and Urokinase-type plasminogen activator receptor (PLAUR); **G)** CD44 Each dot represents a single cell. Contaminated (doublet) cells were not included.

**Figure 2: Taxane-resistant DUTXR shows enrichment of biomarkers that play significant roles in cancer progression, development, and cancer stemness as compared to DU145**

**Figure 2A**

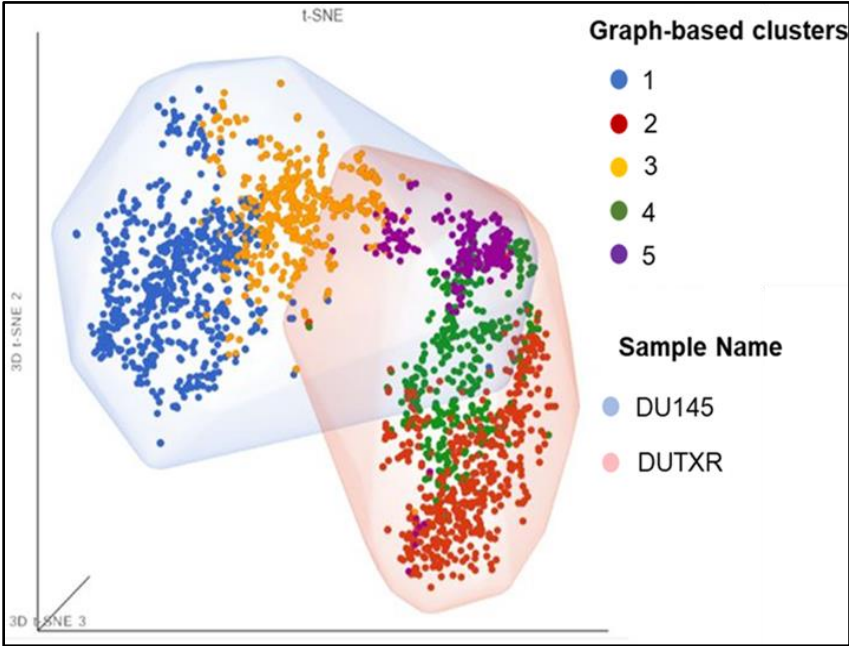


**Figure 2B**

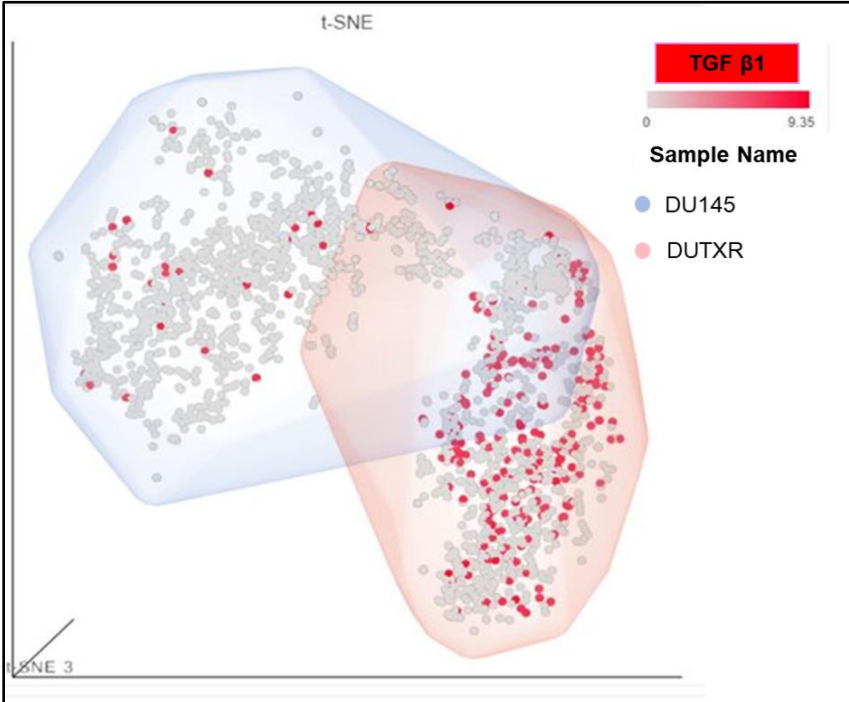


Figure 2C

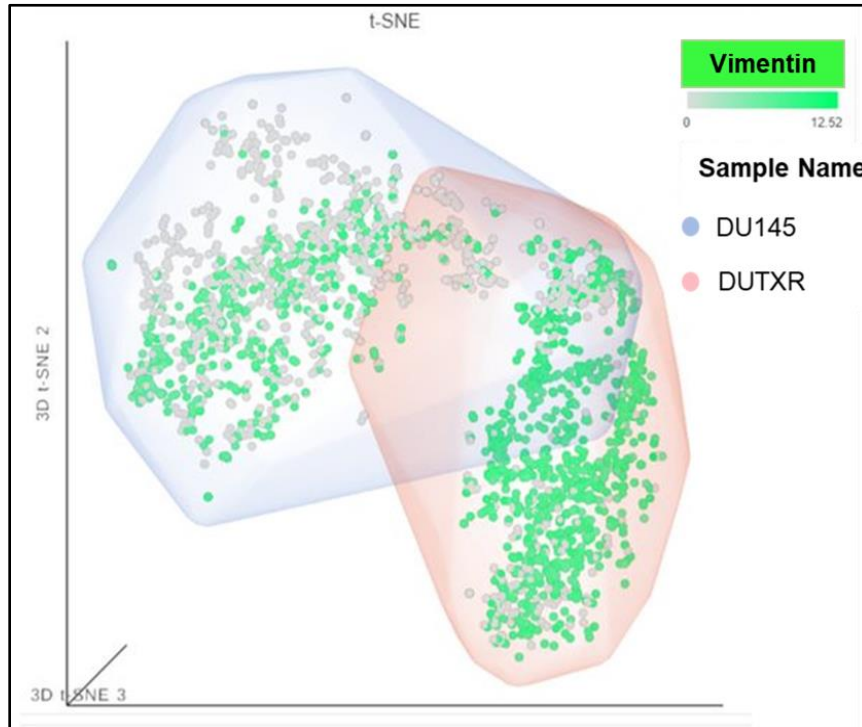
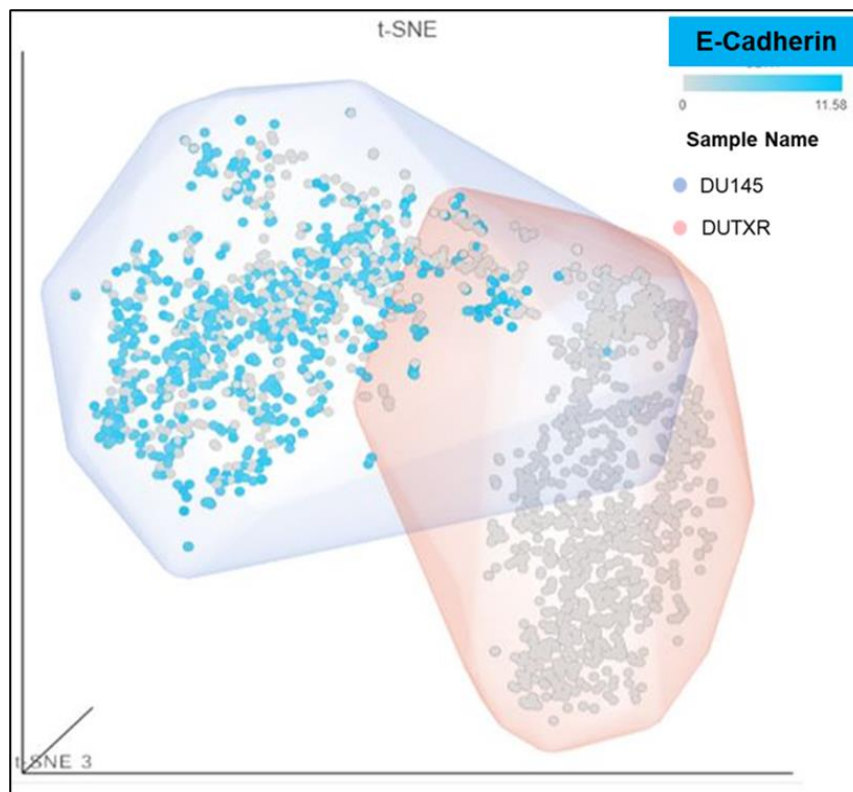


Figure 2D



**Figure 2. Comparison of the single-cell gene expression markers between taxane-sensitive (DU145) and the clonally derived acquired taxane-resistant mCRPC cell line DUTXR.** 1000 single cells were captured, and RNAseq of each of them was performed. Each dot represents a single cell. 4 t-SNE clusters were identified and represented by 4 different colors.

**A)** All 4 t-SNE clusters, **B-D)** showing the expression of Vimentin (Vim), TGF-B1, E-cadherin (CDH1)

TGF-B1 and Vimentin, which are the marker of aggressiveness and metastasis have more enriched expression at the sub-clonal level in DUTXR as compared to DU145. DUTXR has a low abundance of E-Cadherin which is a negative regulator of metastasis as compared to DU145.

### **Pharmacogenomics data-driven algorithm predicted secDrug TAK715 is effective against TX-resistant and stem-cell-like sub-clones in lethal PCa**

**Figure 3. Taxane-resistant DUTXR shows enrichment of biomarkers that play significant roles in cancer progression, development, and cancer stemness**

To begin with, we used single-cell RNA sequencing (scRNA-seq) as a biomarker-based drug screen to identify chemo-resistant, drug-tolerant single-cell sub-clones in mCRPC cell lines that harbor secDrug target genes. Our pharmacogenomics data-driven in silico prediction algorithm (described in the Methods section) identified several potential agents that can be re-purposed as novel secondary drugs (“secDrugs”; Table XX) to treat DTX-resistant Prostate cancer when used as single-agent or in combination with the primary drug (Taxanes). These include FK866 (NAMPT inhibitor), TAK715 (p38 MAPK inhibitor), YM155 (Survivin inhibitor), MK-2206 (Akt1/Akt2/Akt3 inhibitor), LY317615 (PKC $\beta$  inhibitor), XAV939 (Wnt/ $\beta$ -catenin pathway inhibitor), RDEA119 (MEK1/2 inhibitor), and WZ3146 (mutant-selective irreversible inhibitor of EGFR (L858R)/EGFR (E746\_A750)).

Our scRNA-seq data on the untreated acquired taxane-resistant cell line DUTXR showed that the majority of t-distributed stochastic neighbor embedding (t-SNE) clusters (Figure 3A) representing single-cell subpopulations (subclones) have high expression of genes that play a major role in cancer progression, development, and maintenance of cancer stemness (CD44; Figure 3B), and drug resistance (CXCL8, Figure 3C), CDK1 (Figure 3D) indicating probable

involvement in mCRPC development and progression. TAK715 target genes were derived from the Harvard Medical School (HMS)'s NIH Library of Integrated Network-based Cellular Signatures (LINCS) perturbagen database, a publicly available database devoted to understanding human cells respond to perturbation by drugs, the environment, and mutation. Interestingly, these subclusters also showed high expression potential TAK715 target genes MAPK14, MAP4K4, and CSNK1D (Figure 3E), indicating that TAK715 may be effective against these taxane-resistant and stem-cell-like subpopulation clusters.

**Figure 3A**

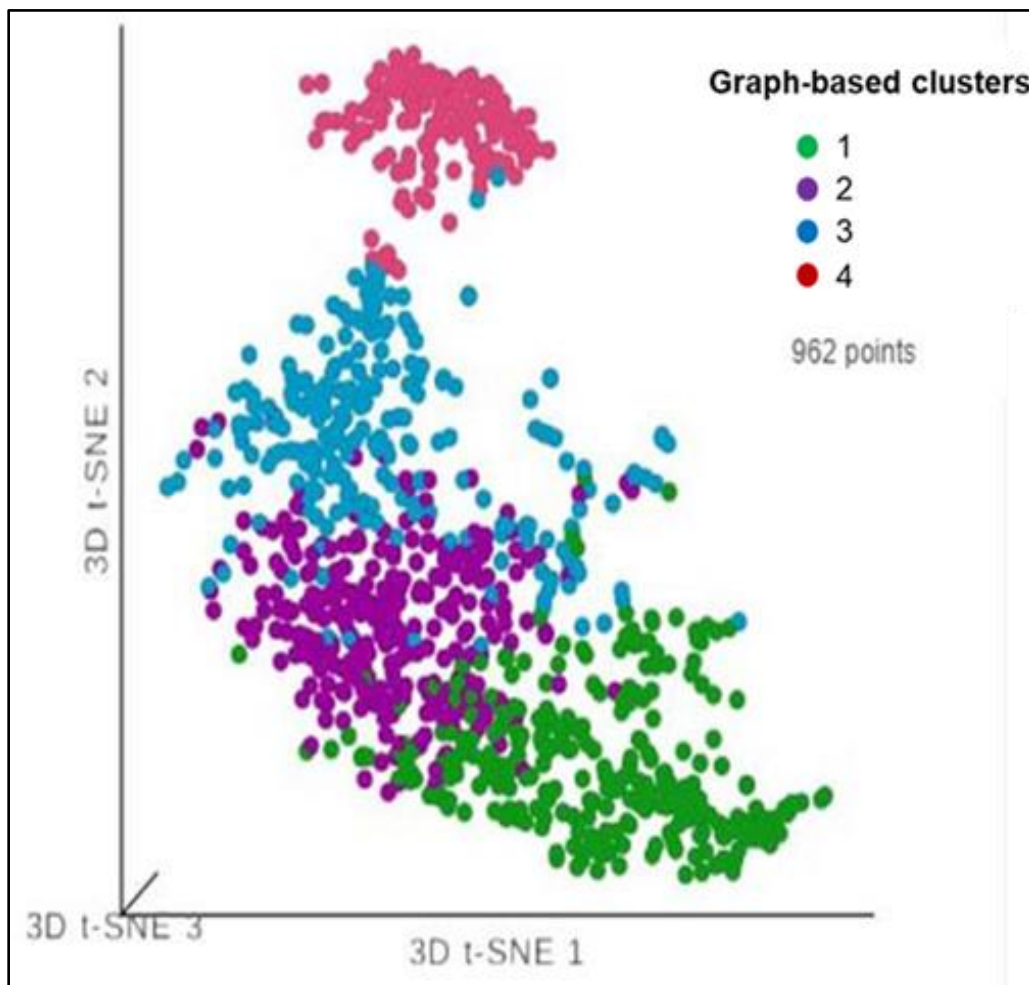


**Figure 3B**

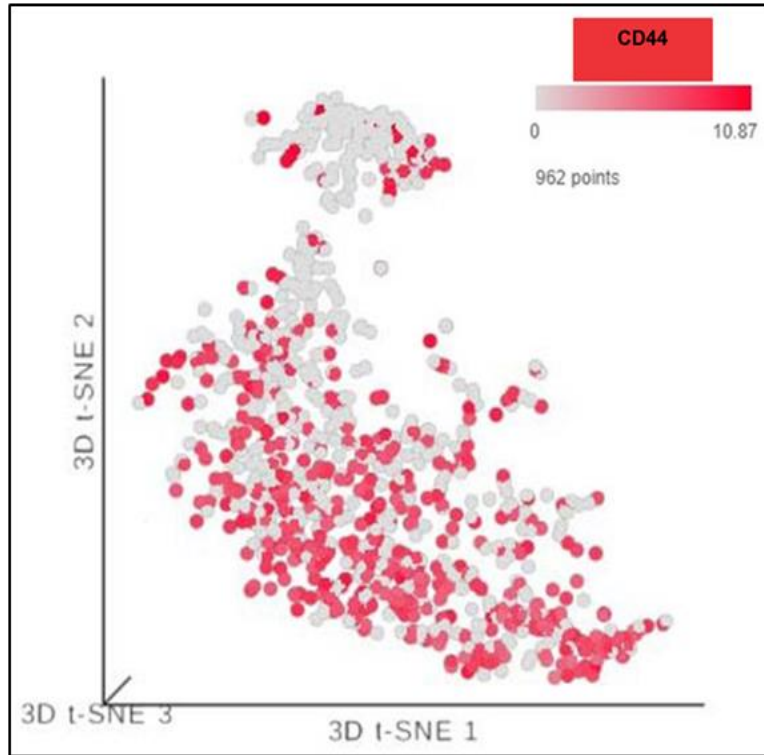


**Figure 3C**

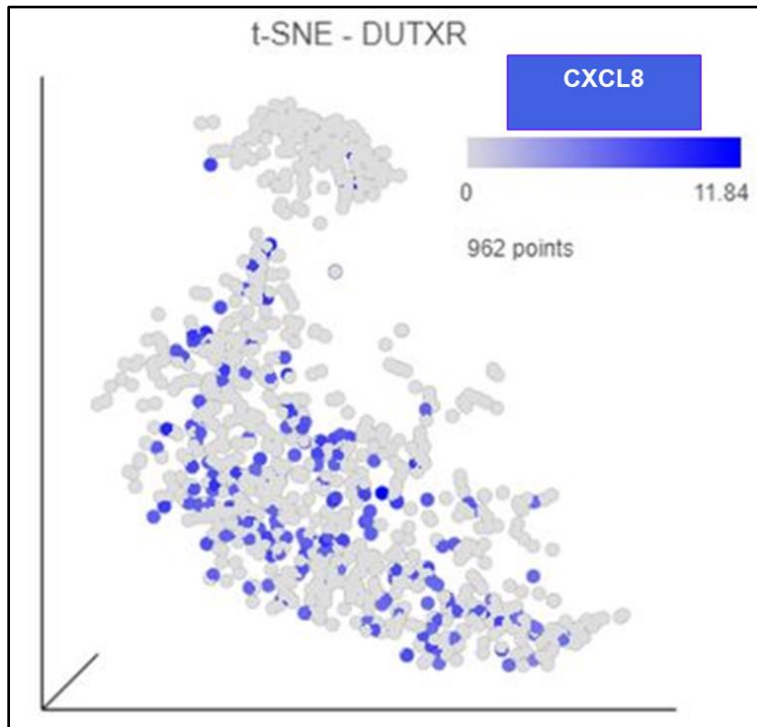


Figure 3D

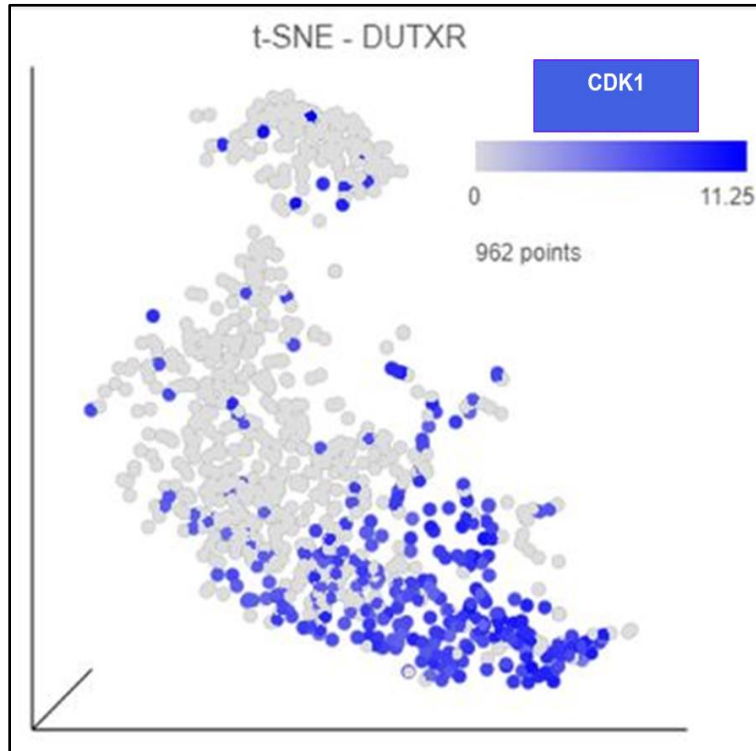
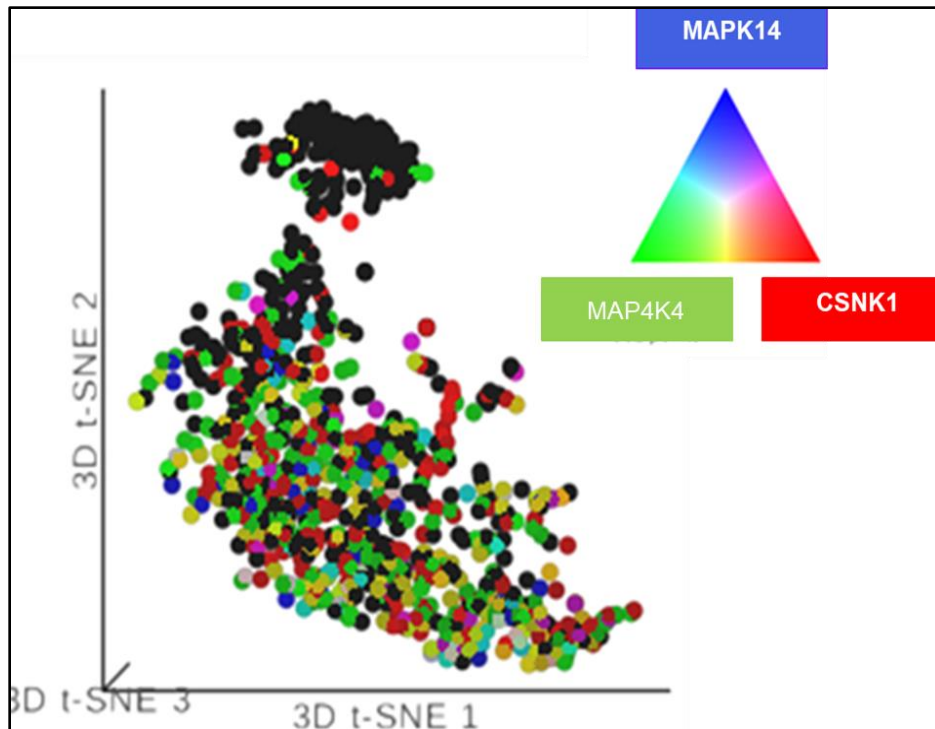


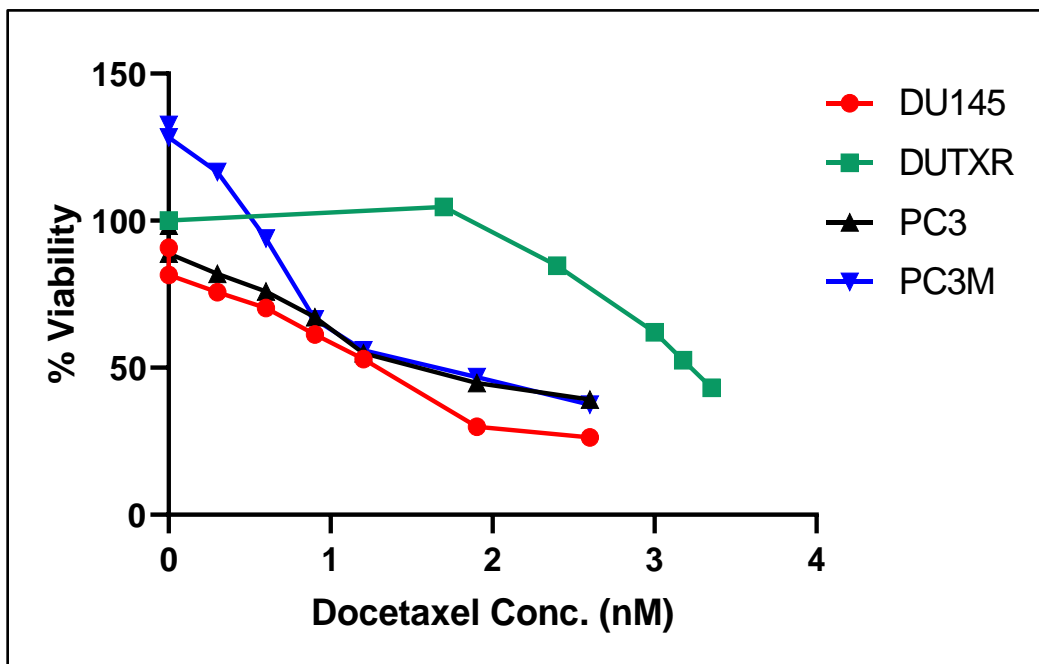
Figure 3E



### Top predicted secondary drugs effectively reduce cellular viability

We determined the cytotoxic effects of the top predicted secondary drug, TAK715, on a panel of the AR-ve mCRPC cell lines representing by DU145, PC3, the clonally-derived acquired taxane-resistant lines DUTXR and PC3-TXR (>50 fold) higher TX IC<sub>50</sub> compared to parental lines), (Figure 4A-B) and PC3M – the more aggressive and metastatic subline of PC3. Single-agent survival curves showed that TAK715 worked effectively against all the AR-ve -mCRPC cell lines and significantly diminished the viable cell numbers in a dose-dependent manner (Figure 4C). Furthermore, single-agent IC<sub>50</sub> values of Docetaxel and Cabazitaxel were negatively co-related with the IC<sub>50</sub> value of TAK715 in these cell lines (at p<0.05). The correlation co-efficient is -0.2 for Docetaxel and TAK715 and -0.4 for Cabazitaxel and TAK715.

Figure 4A



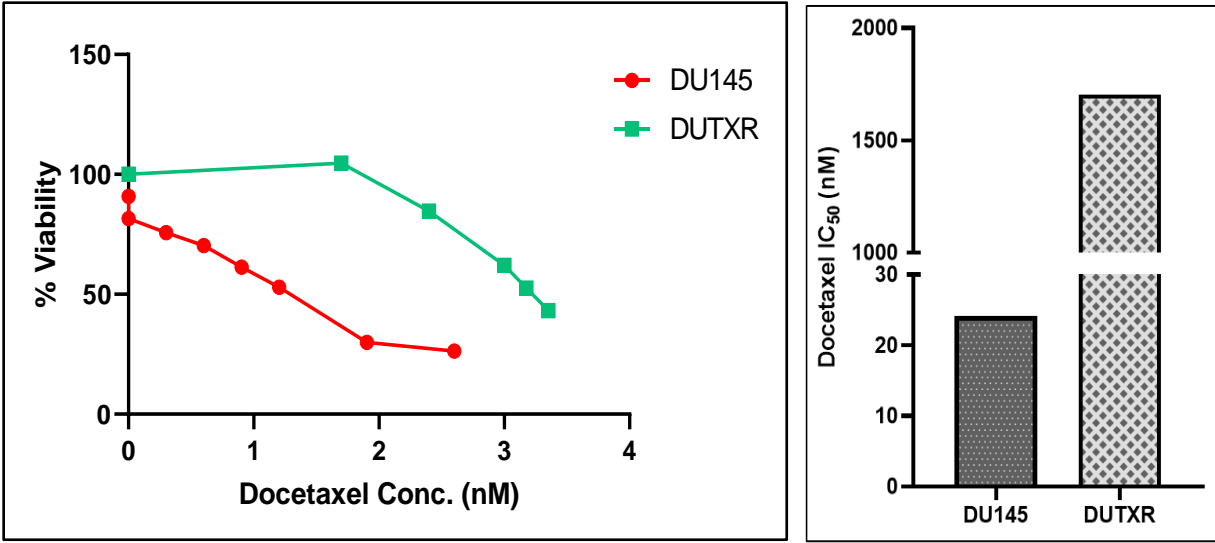
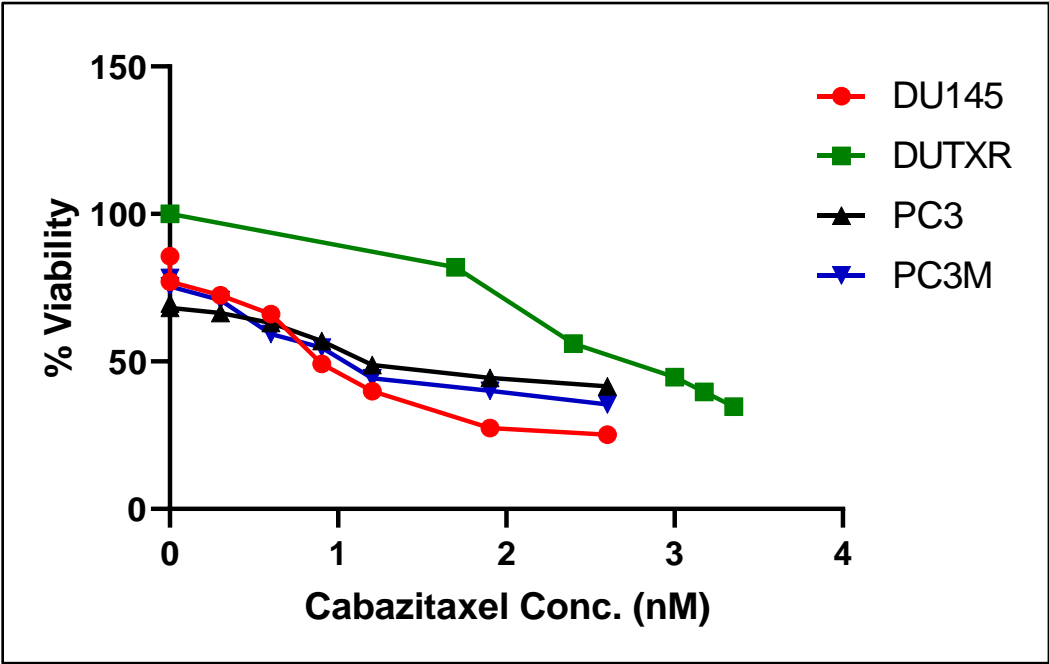
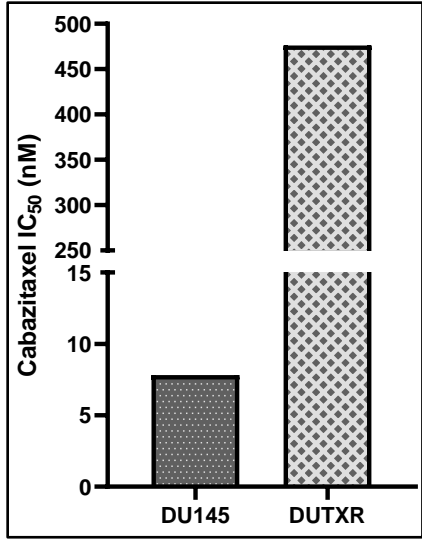
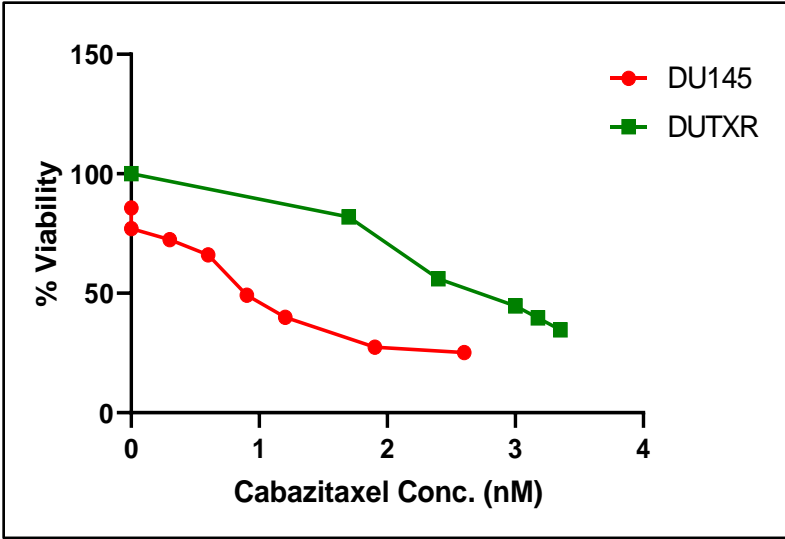


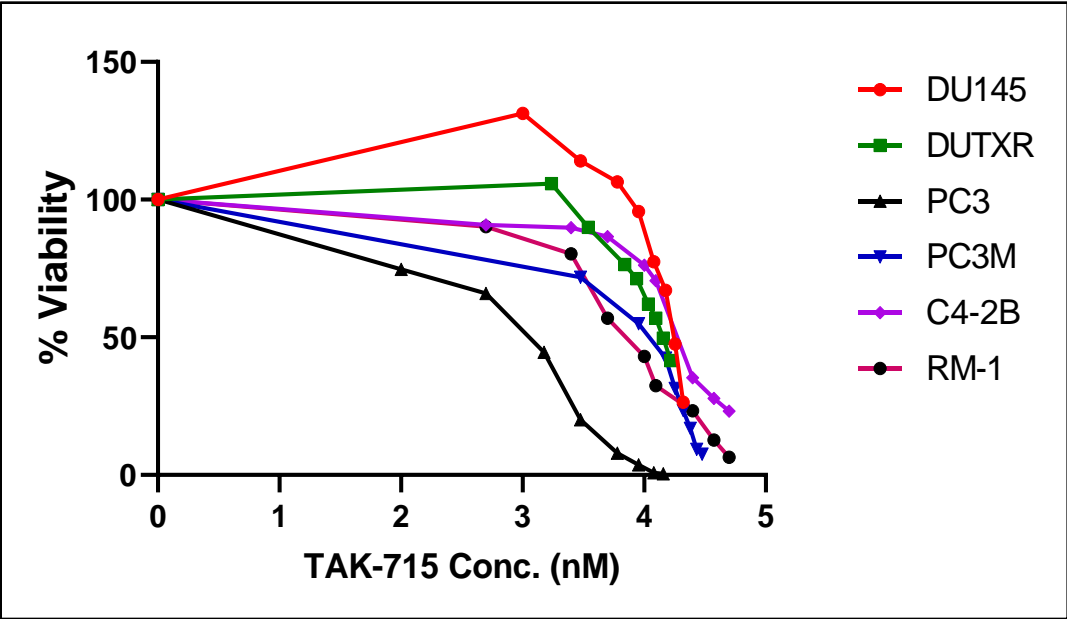
Figure 4B





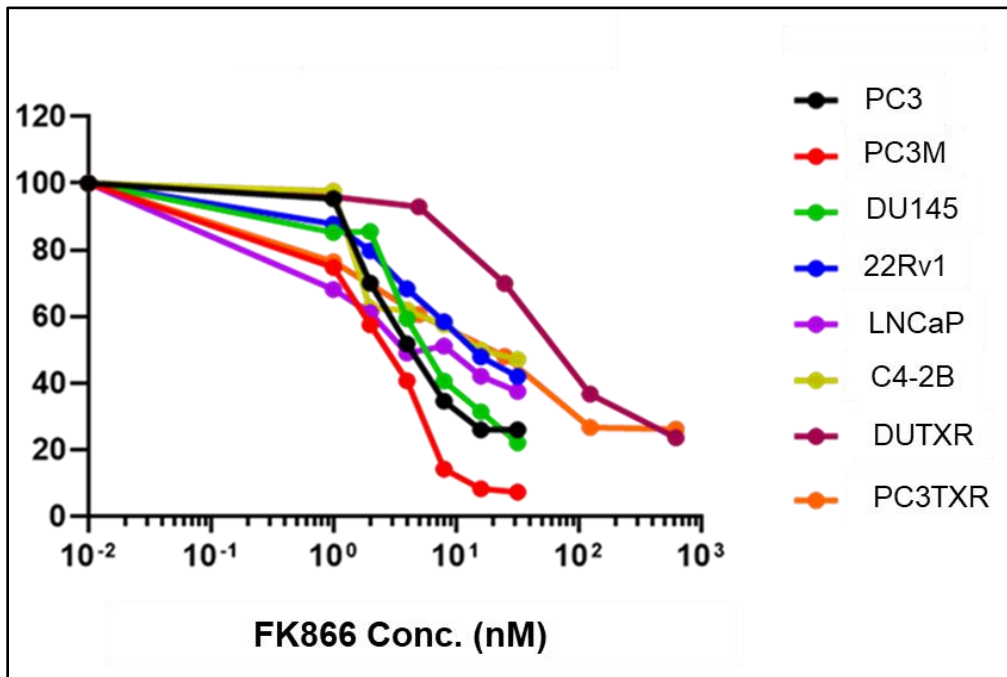
secDrug: TAK-715

Figure 4C



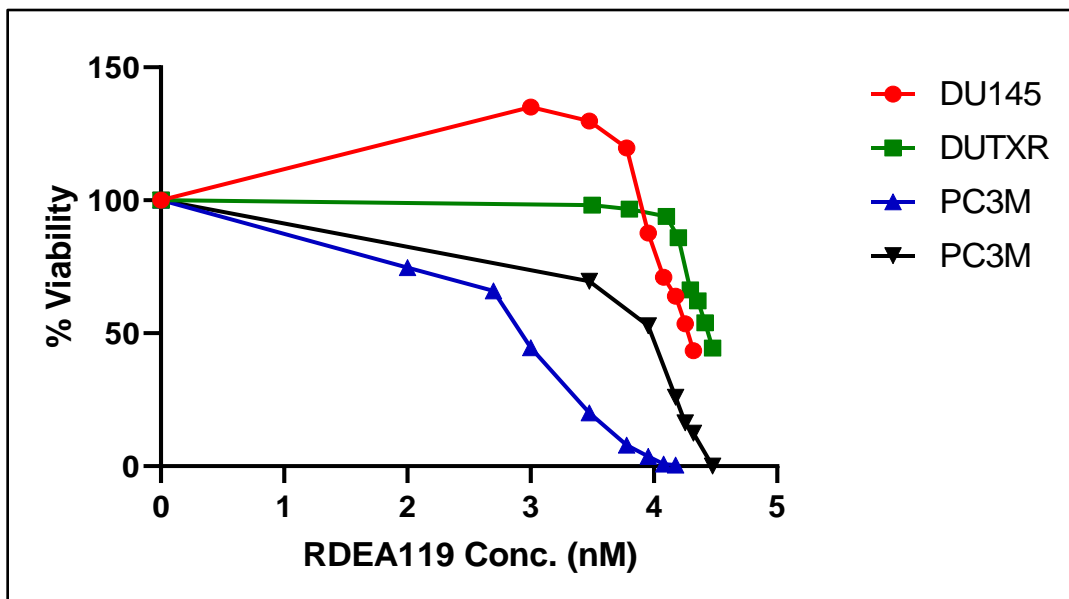
secDrug: FK-866

Figure 4D



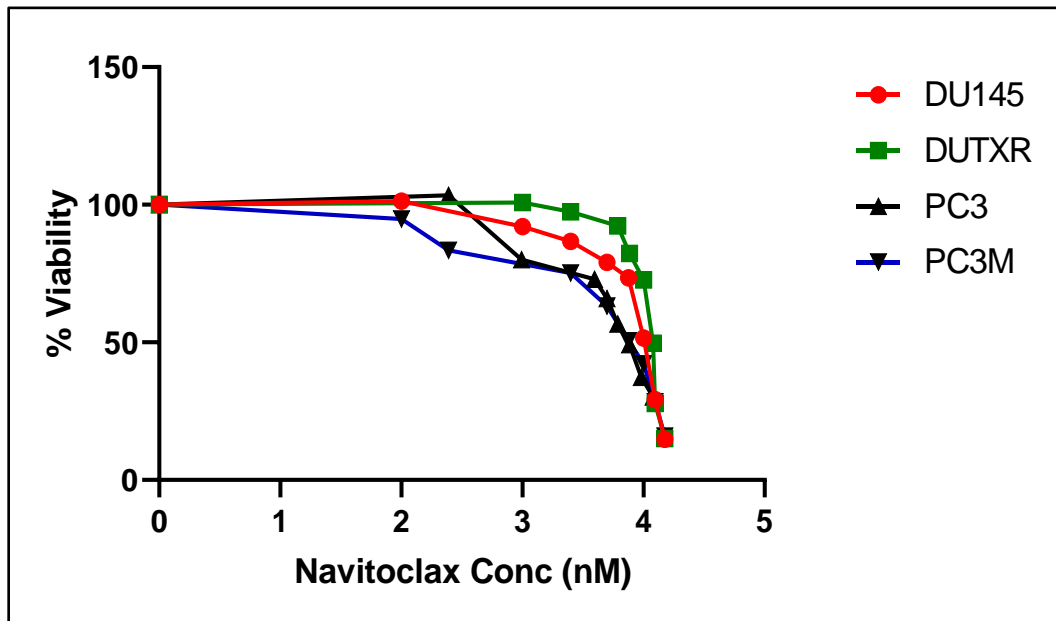
secDrug: RDEA-119

Figure 4E



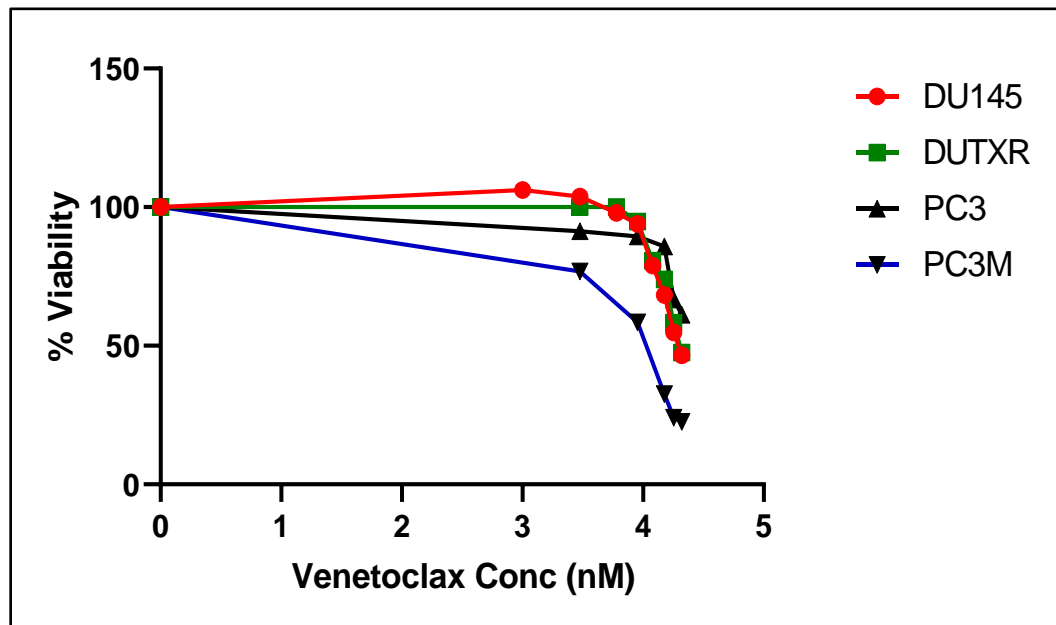
secDrug: Navitoclax

Figure 4F



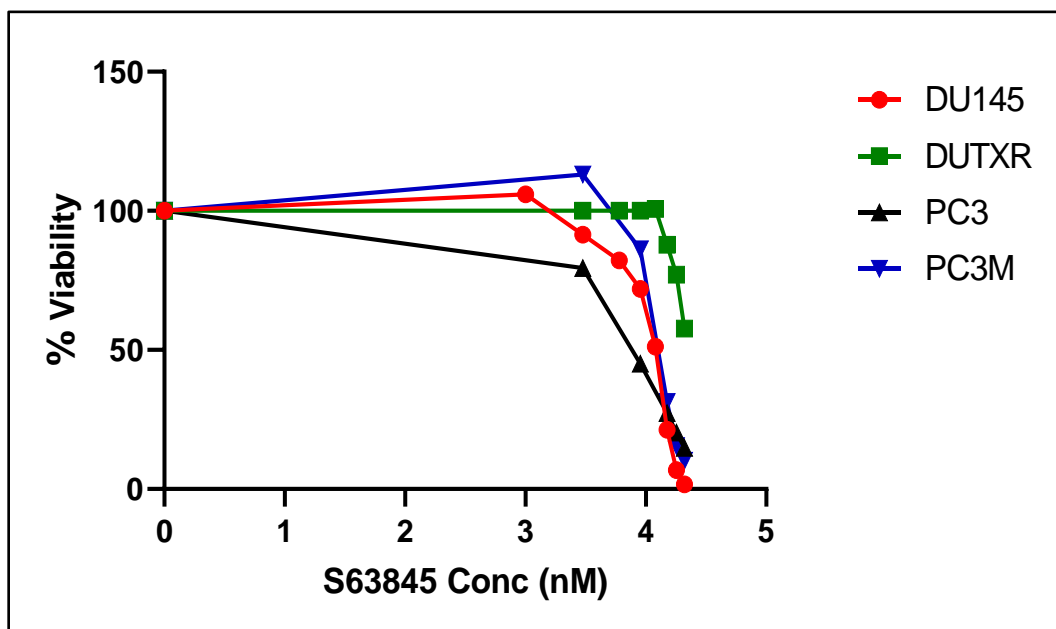
secDrug: Venetoclax

Figure 4G



secDrug: S63845

Figure 4H



**Figure 4.** Dose-response curves represent in vitro cytotoxicity of (A) Docetaxel, (B) Cabazitaxel, (C) TAK-715, (D) FK-866 (E) RDEA-119 (F) Navitoclax, (G) Venetoclax, (H) S63845 single agent treatment in mCRPC cell lines.

**Dose-response curves representing in vitro cytotoxicity of the FK866 drug combination in metastatic PCa cell lines.**

Next, we evaluated the cytotoxic effect of different secDrug in different treatment combinations with either Taxane drugs (Docetaxel/ Cabazitaxel) or Androgen receptor signaling inhibitor Enzalutamide. The dose-response curves for the drug combinations and CI values indicated high synergy, which was even more profound (CI between 0.2-0.37) in the TX-resistant lines (Figure 3E).

Docetaxel + secDrugs combination therapy exhibits synergy in mCRPC cells

Docetaxel+ secDrug TAK-715

Figure 5A

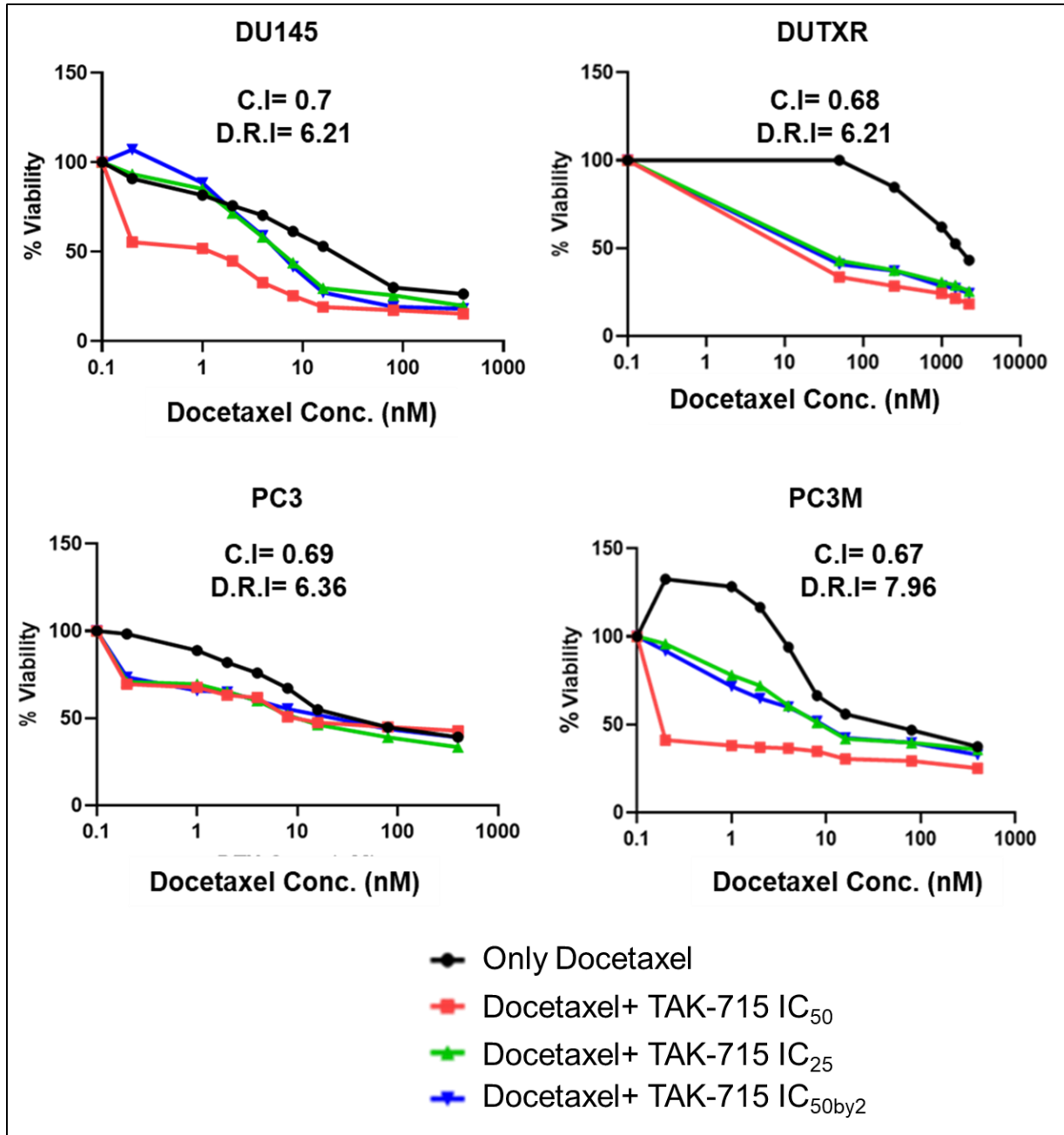
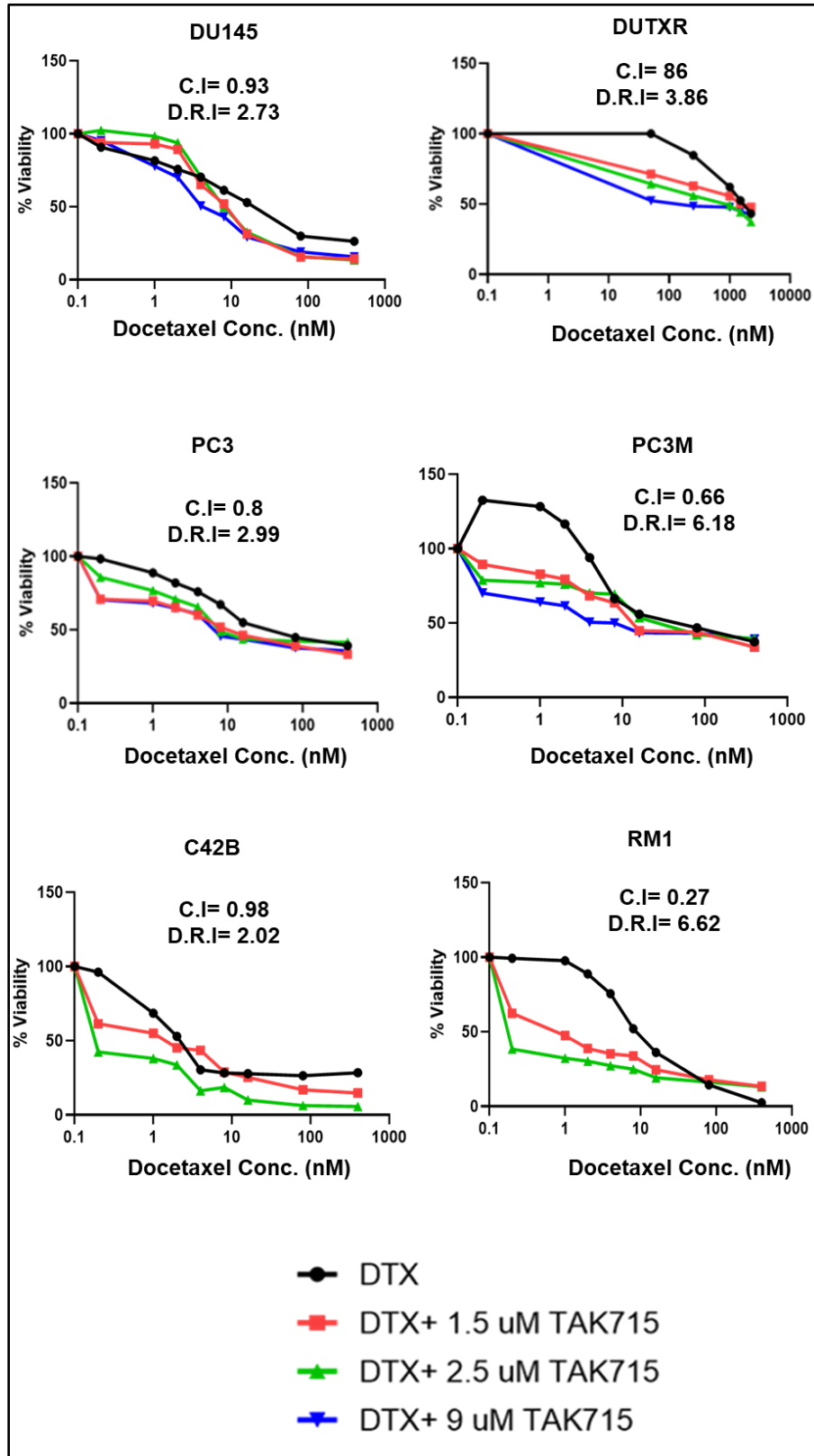
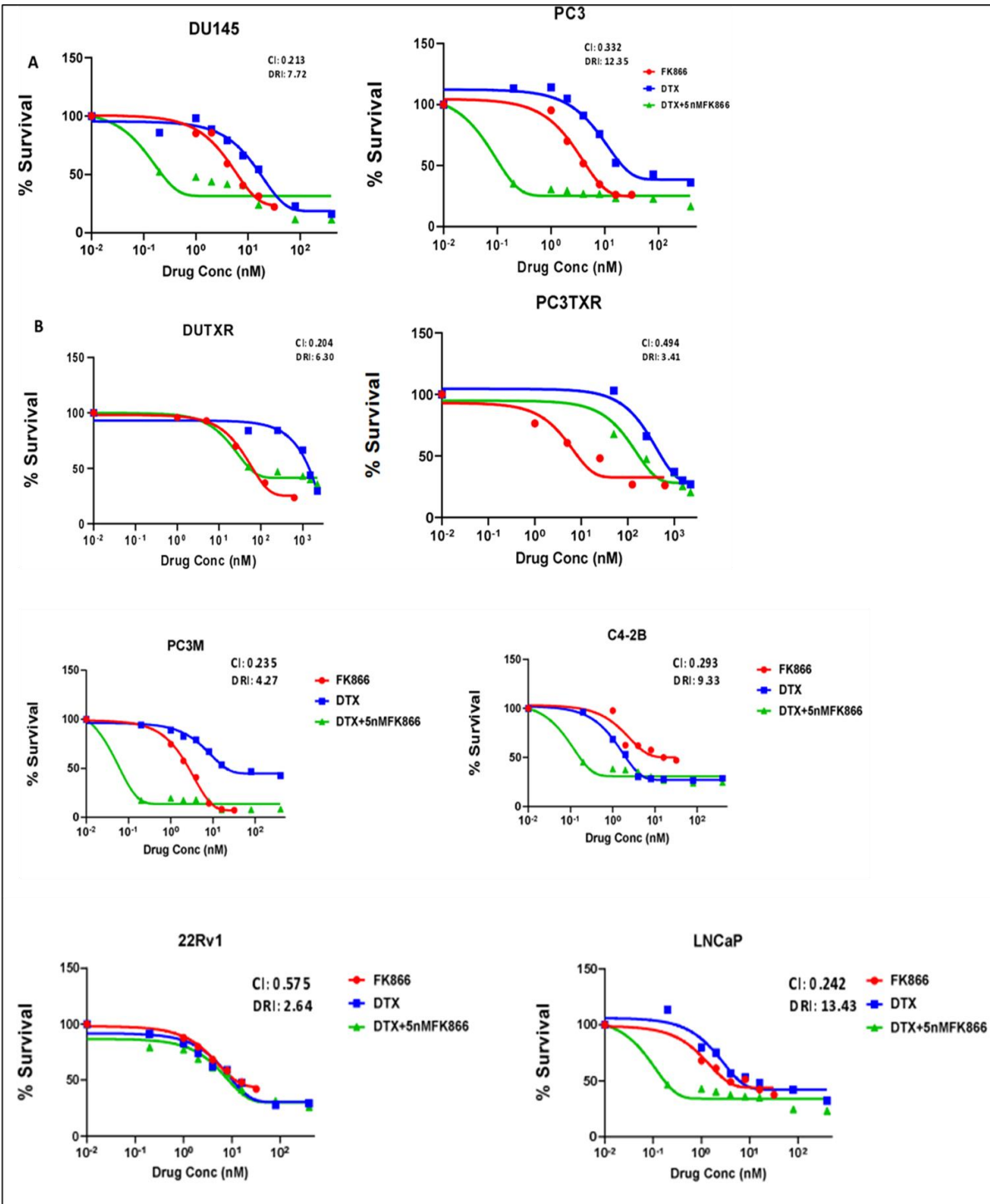


Figure 5B



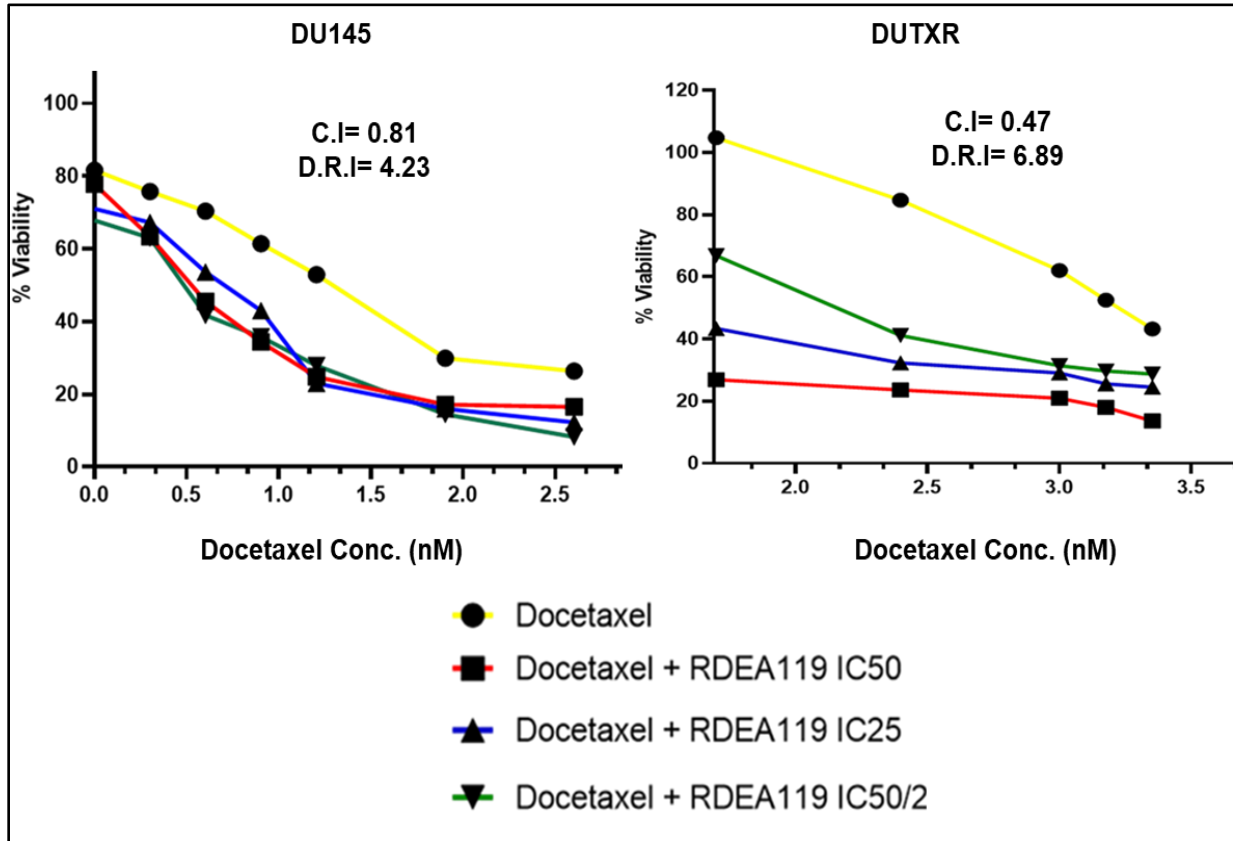
Docetaxel+ secDrug FK-866

Figure 5C



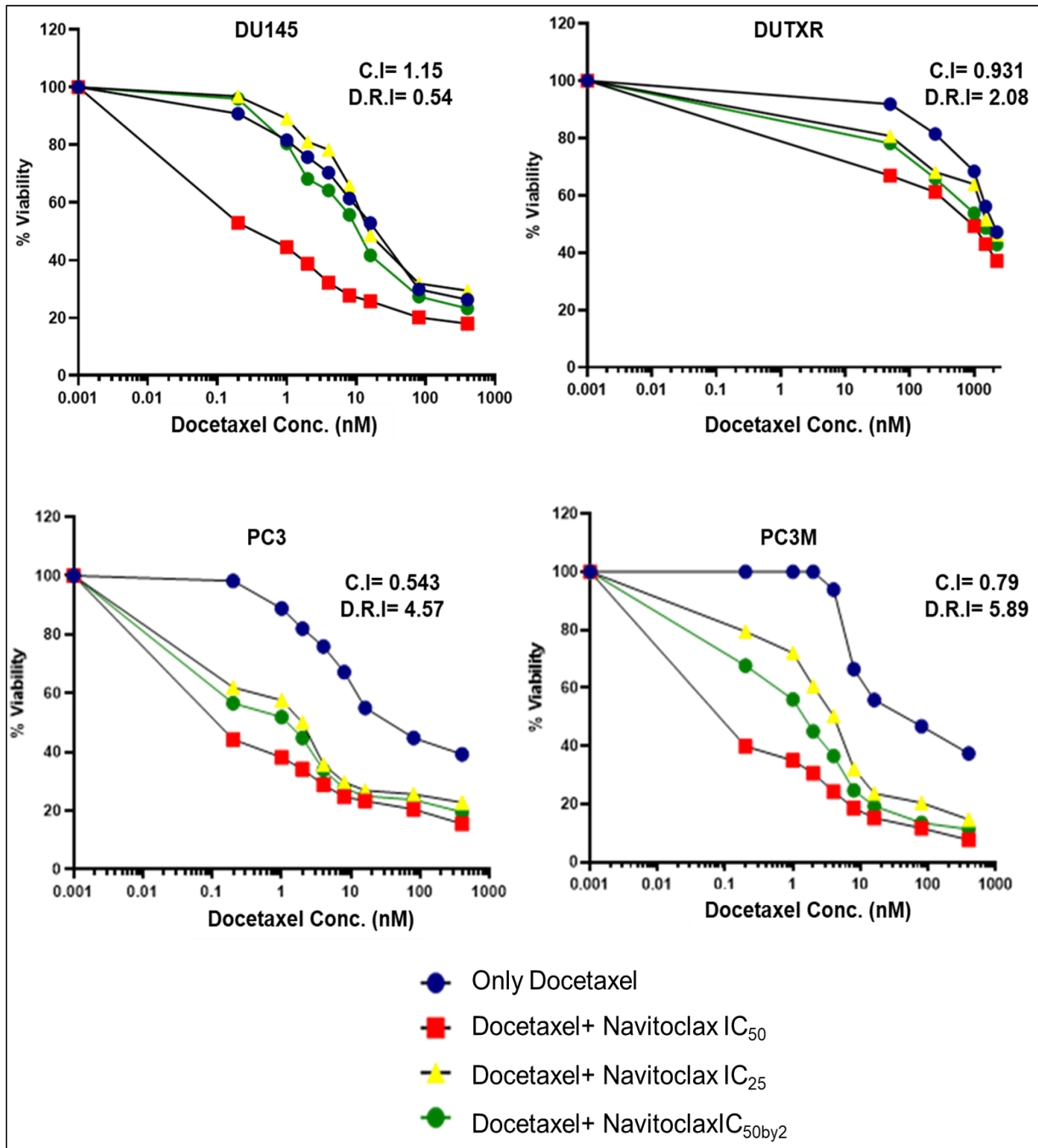
Docetaxel+ secDrug RDEA-119

Figure 5D



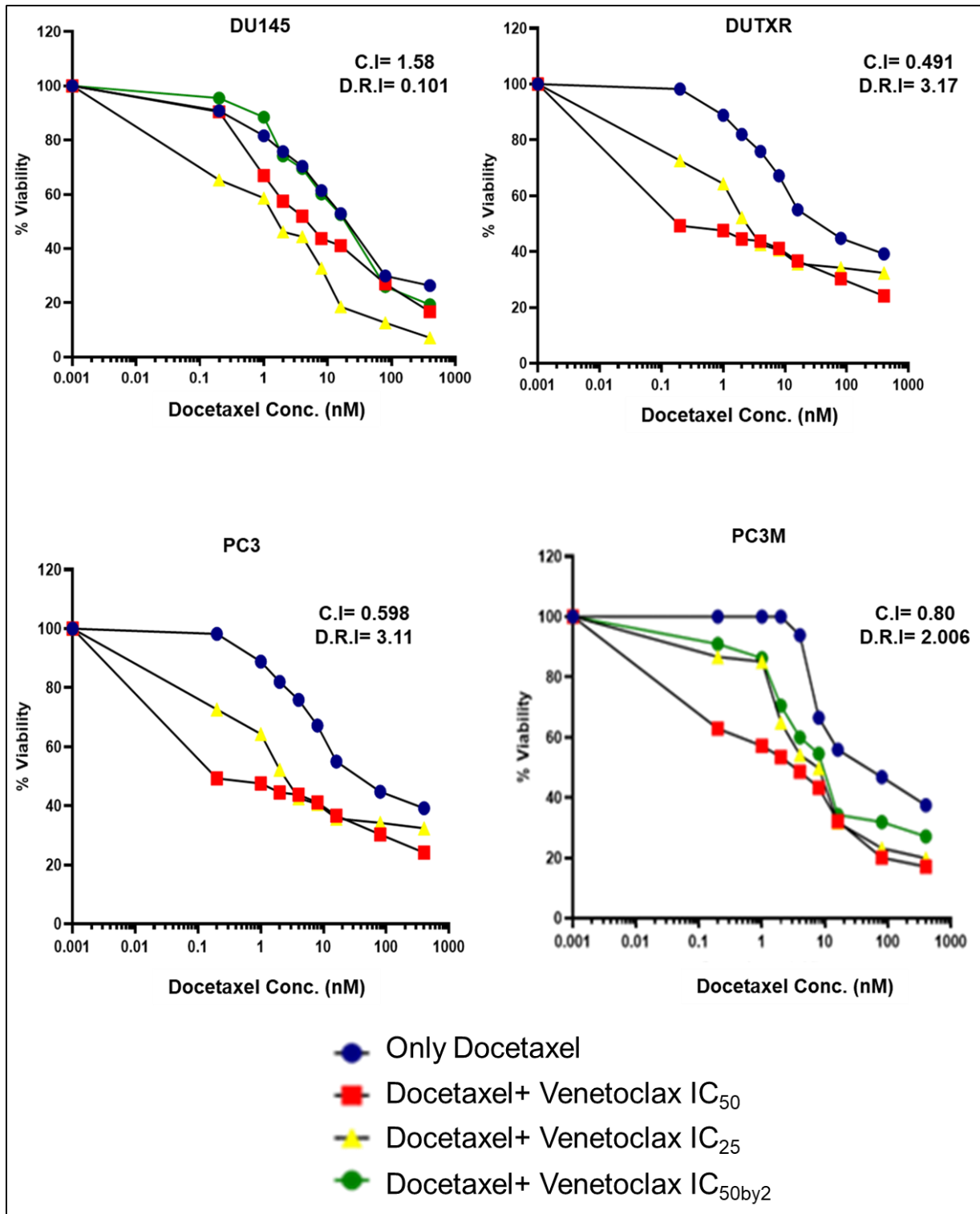
Docetaxel+ secDrug Navitoclax

Figure 5E



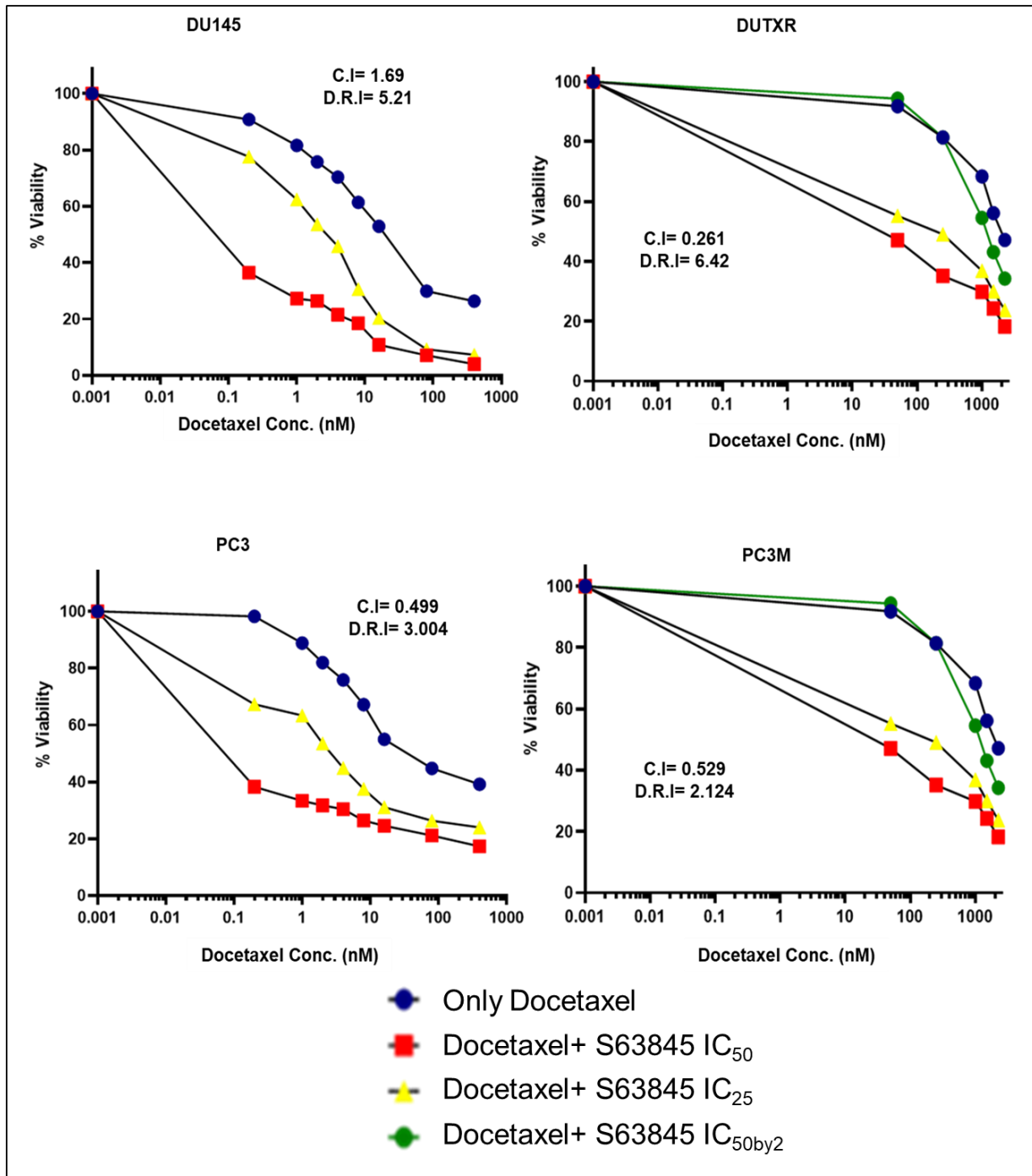
Docetaxel+ secDrug Venetoclax

Figure 5F



Docetaxel+ secDrug S63845

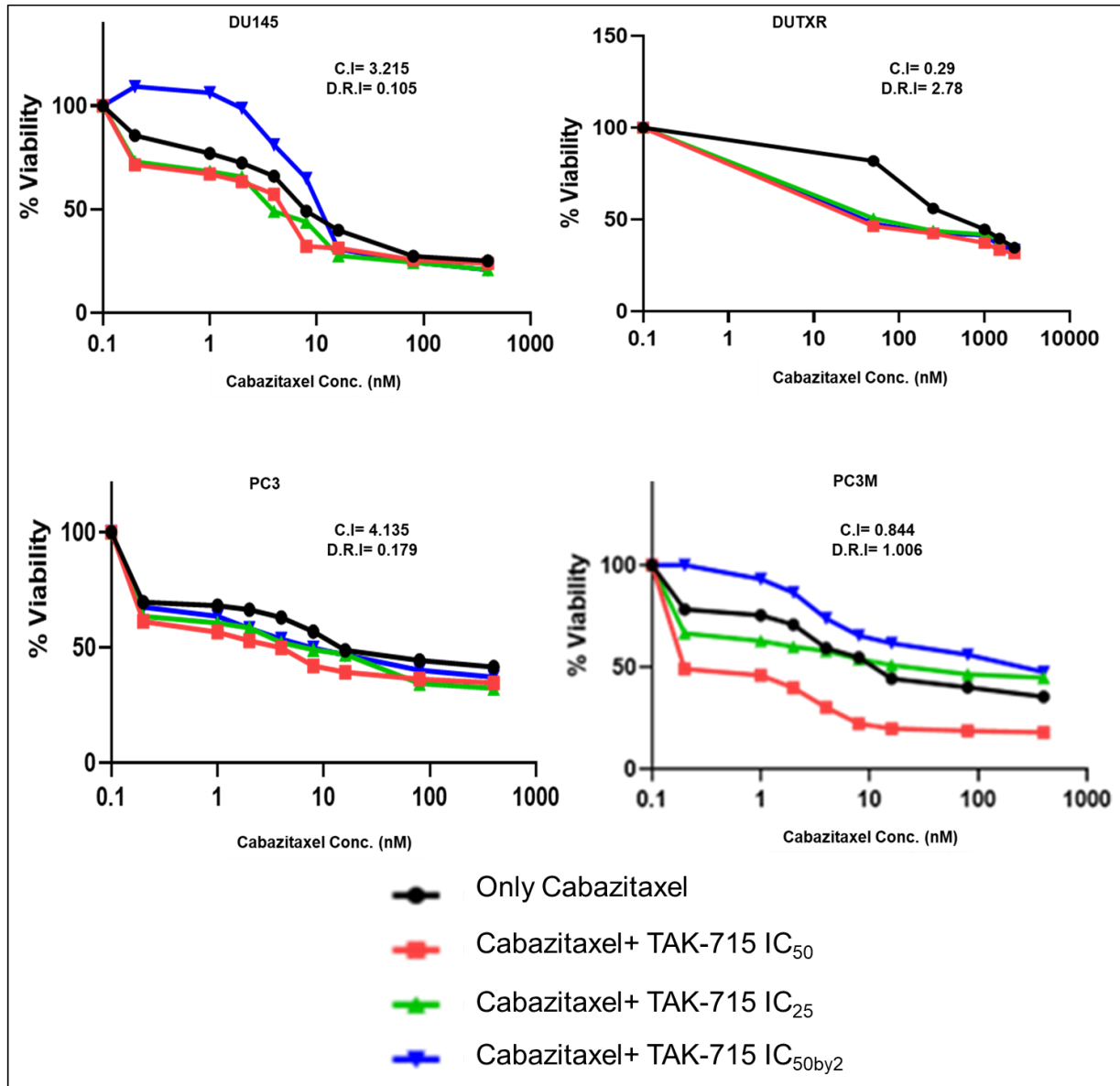
Figure 5G



Cabazitaxel + secDrugs combination therapy exhibits synergy in mCRPC cells

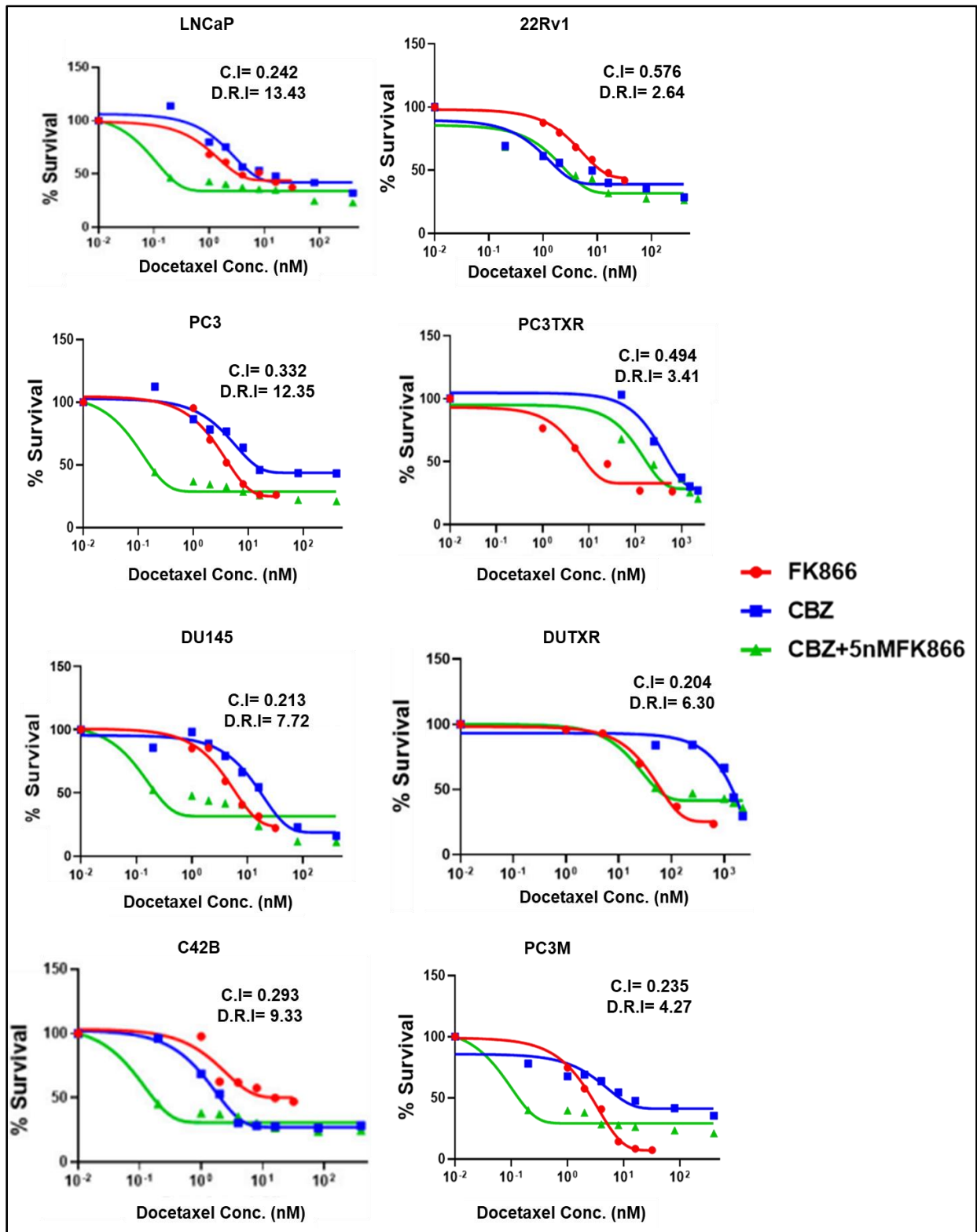
Cabazitaxel+ secDrug TAK-715

Figure 5H



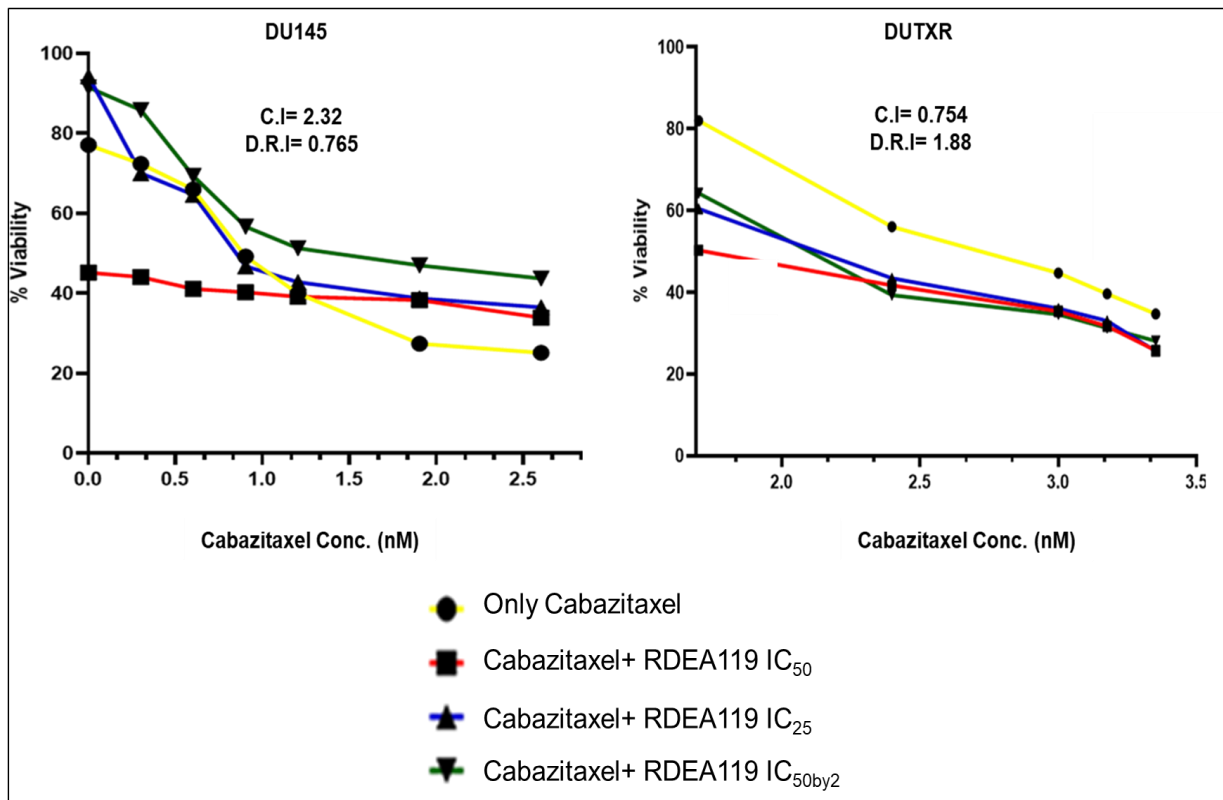
Cabazitaxel+ secDrug FK-866

Figure 5I



# Cabazitaxel+ secDrug RDEA-119

## Figure 5J



Enzalutamide + secDrugs combination therapy exhibits synergy in mCRPC cells

Enzalutamide+ secDrug FK-866

Figure 5K

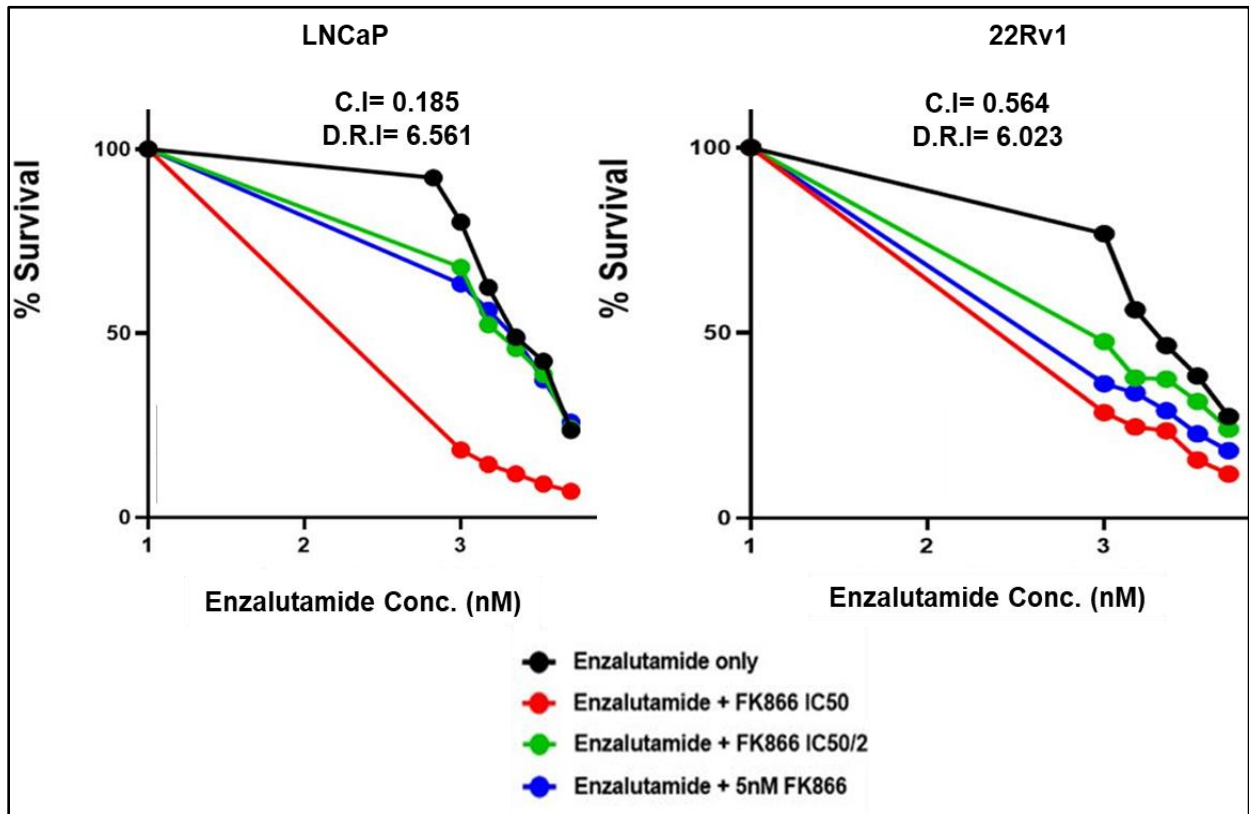


Figure 5L

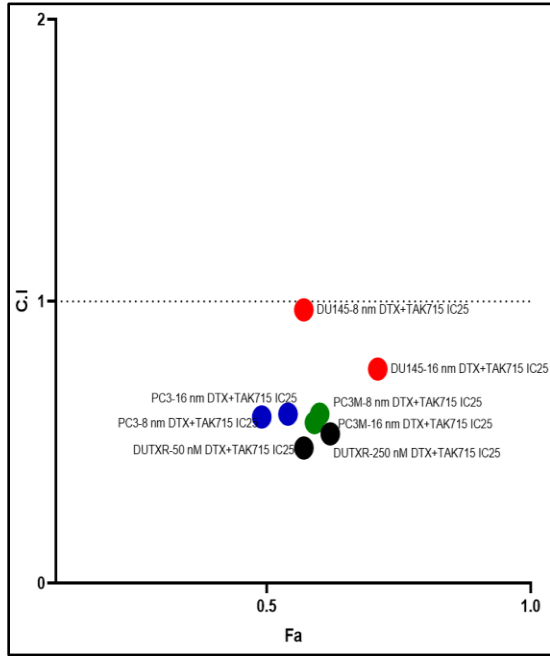


Figure 5M

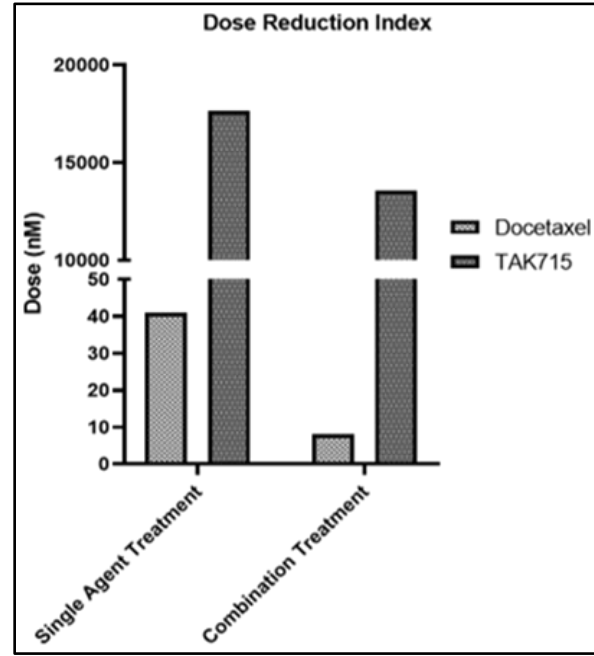


Figure 5N

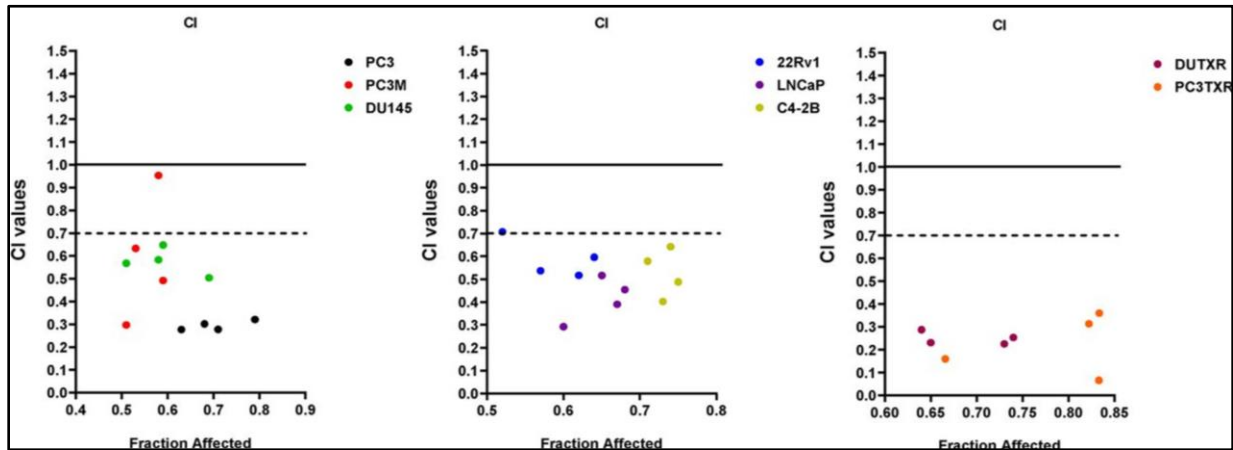
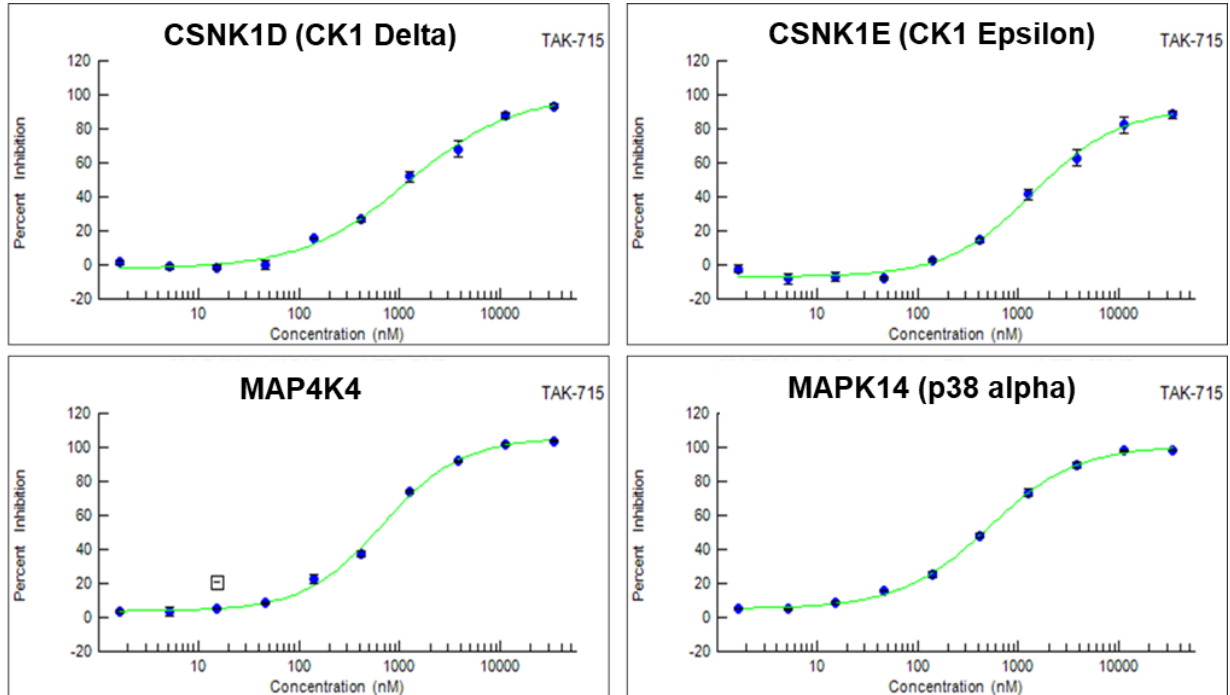


Figure 5. *in vitro* cell viability profile of mCRPC cell lines treated with (A-G) different combinations of Docetaxel+ secDrugs (H-J) different combinations of Cabazitaxel+ secDrugs (K) different combinations of Enzalutamide+ secDrug (L-N) Combination Index and Dose reduction index calculated using Chou-Talalay's combination index (CI) method and the isobologram algorithm (CompuSyn software; Biosoft, US)(Chou, 2011). CI values between 0.9-0.3 and 0.3-0.1 signify synergism and strong synergism, respectively, between the drugs treated in combination.

## TAK-715 inhibits multiple Kinases

Figure 6



Target	IC <sub>50</sub> (nM)
CSNK1D (CK1 Delta)	1190
CSNK1E (CK1 Epsilon)	1610
MAP4K4	677
MAPK14	606

**Figure 6.** Invitrogen (Madison, WI, USA) Z'LYTE Kinetic study of TAK-715 with varied concentrations to determine IC<sub>50</sub> against different target kinases. The data showed it has the most efficient inhibitory activity against MAPK14/ p38 $\alpha$

## Docetaxel/TAK715 combination enhances apoptosis in AR<sup>null</sup> mCRPC cell lines

The impact of TAK715 on cellular apoptosis as a single agent and in combination with Taxanes was assessed through Caspase 3/7 Glo Assay. We observed significantly elevated levels of Caspase 3/7 activity following treatment, indicating higher apoptosis, which was more profound when the drugs were used in combination compared to individual single-agent treatments (Figure 7A-D).

**Figure 7**

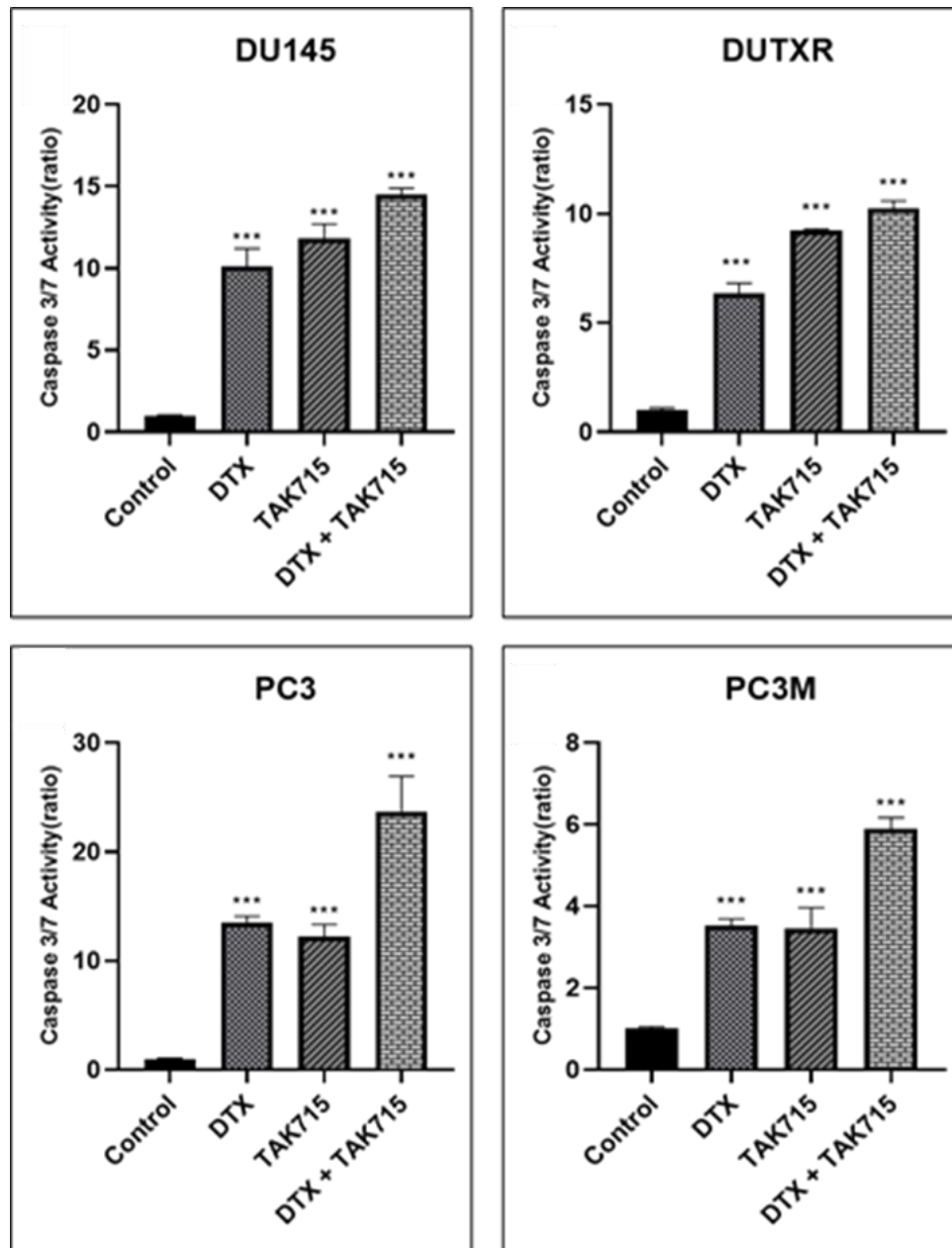


**Figure 7. Caspase-3/7 activity assay of Docetaxel and TAK715 single agent and combination-treated AR<sup>null</sup> mCRPC cell lines.** The data shows a higher level of induction of apoptotic pathway in combination treatment compared to single-agent treatment (Significance P-value \* =  $p \leq 0.05$ ). This was further confirmed by Annexin V-FITX/PI-based flow-cytometric apoptosis analysis (8A-B)

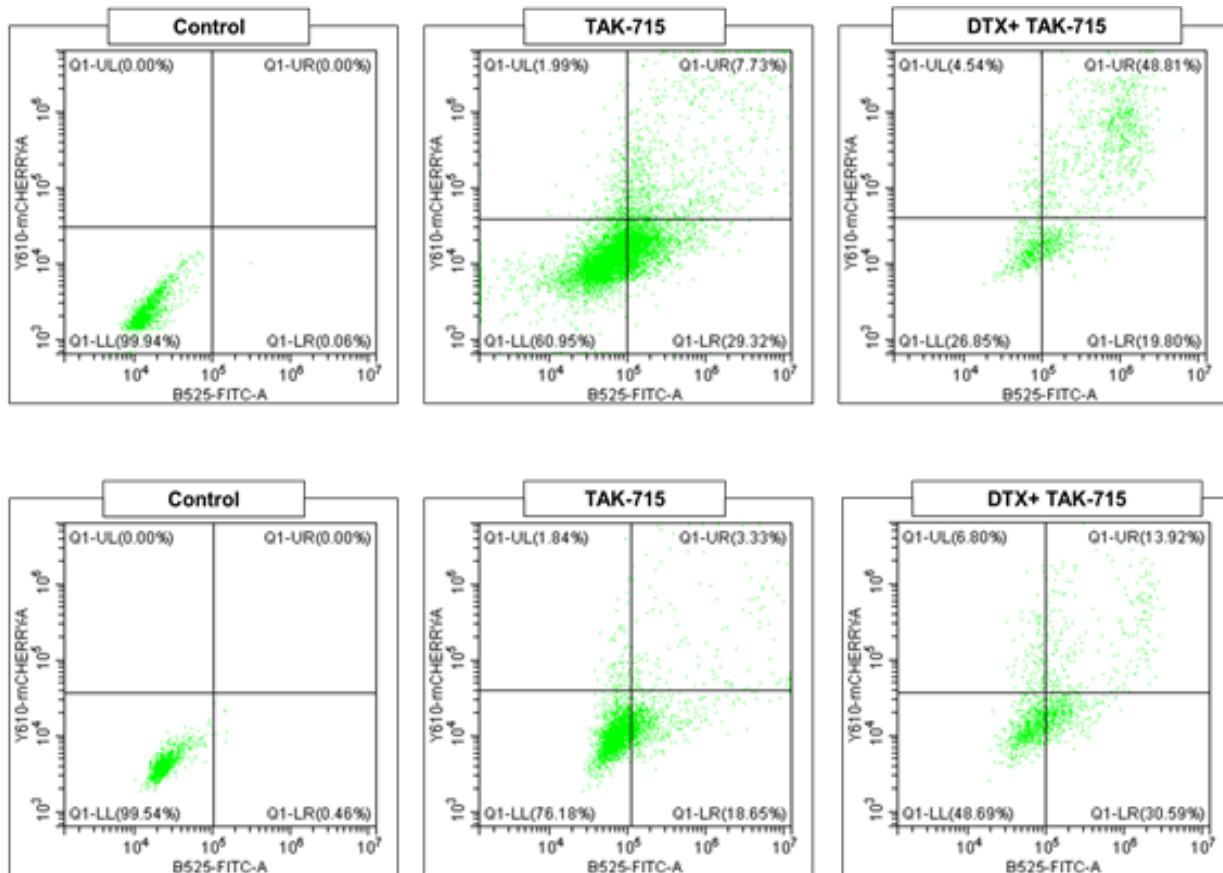


**Figure 8. Quantitative measurement of the % of the apoptotic AR<sup>null</sup> mCRPC cell lines (Annexin-V positively stained) exposed to TAK715 single agent and Docetaxel+TAK715 combination treatment.** The data shows higher apoptosis in combination treatment compared to single-agent treatment (Significance P-value \* =  $p \leq 0.05$ )

### **Co-treatment of Docetaxel & TAK715 significantly affects cellular and nuclear morphology**

To further validate the synergism of TAK715+Docetaxel, we performed live cell imaging to monitor the change in morphology and live cell count. Cells were treated with Docetaxel and

TAK715 alone or as a combination of the two drugs for 48 hours. We observed that the combination of IC<sub>25</sub> doses of both drugs reduced the average live cell count by 76±9% compared to the control and 52±17% as compared to docetaxel single agent treatment (Figure 9). Further, the average reduction in live cell count for the combination treatment with IC<sub>50</sub> doses of both drugs was 86±4% compared to the control and 73±8% compared to the IC<sub>50</sub> dose of Docetaxel as a single-agent treatment. Dose-dependent cell shrinkage or decrease in cell volume was also observed, which is a ubiquitous feature of programmed cell death.

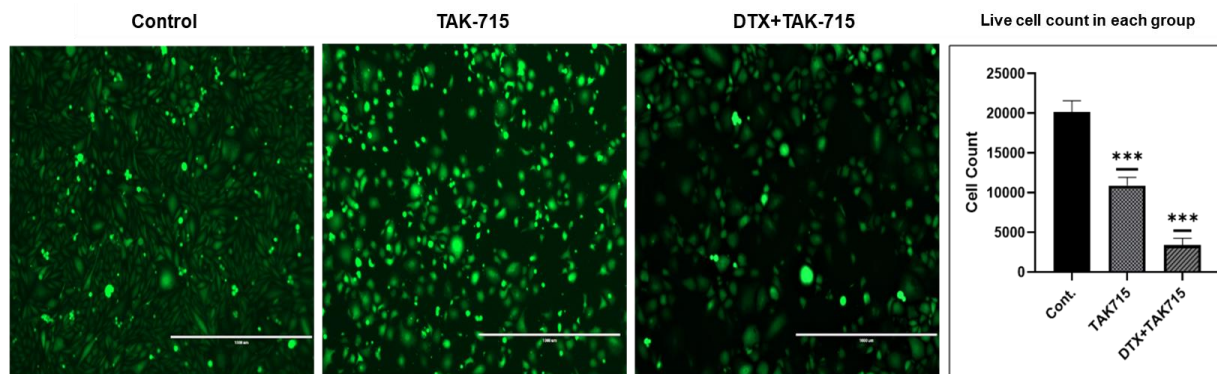


**Figure 9.** Assessment of cellular morphology: I-III. Representative figures show the effect of the primary (DTX) and secondary (TAK-715) drugs on cell count and cell morphology of mCRPC cells. The images were captured on the PC3-Luc cells before (0h) and after (48h) TAK-715 treatment either as a single agent or in combination. Microscopy results show significantly higher cell death in combination treatment compared to single-drug treatment for all cell lines; IV. ImageJ data analysis showed a significant difference in cell density for both TAK-715 single-agent and DTX+TAK-715 combination treatments. Results show significantly higher cell death in combination treatment at combination dose compared to single-drug treatment for PC3 cell lines (Significant value \* =  $p \leq 0.05$ ).

Further, an assessment of the nuclear morphology of attached cells using NucBlue staining, a reagent frequently used to distinguish condensed nuclei in apoptotic cells, suggested TAK-715-induced morphological changes like nuclear fragmentation and chromatin condensation, which are indicative of apoptosis (Figure 10). In addition, our results showed even higher cell death and more nuclear damage in the TAK-715+DTX combination treatment compared to the TAK-715 single drug treatment.

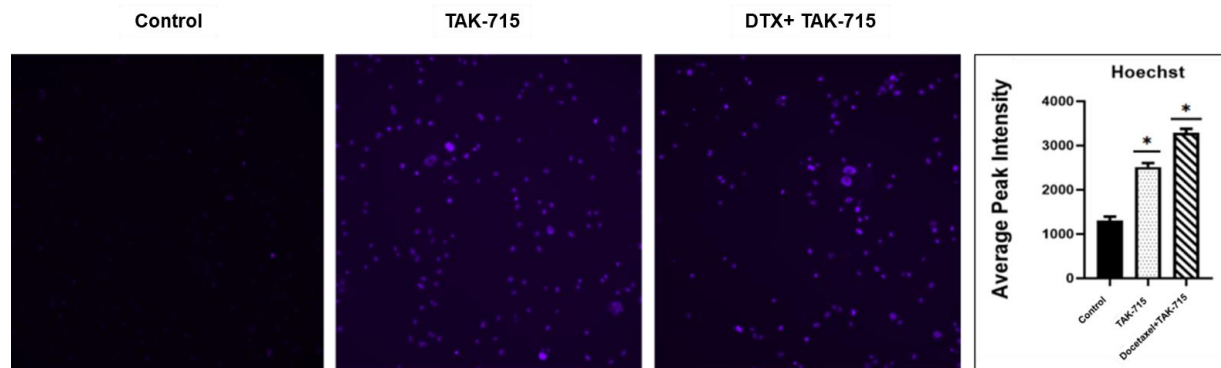


**Figure 10. Assessment of nuclear morphology.** Representative figures showing the TAK-715-based treatment (single-agent and combination with DTX) on cell nucleus morphology of mCRPC cells. NucBlue Live reagent is frequently used to distinguish condensed nuclei in apoptotic cells. The microscopy images were captured on the PC3-Luc cells before (0h) and after (48h) following treatment. Microscope images showing treatment effect on the cell lines PC3. Similar results were obtained for all mCRPC lines.

**A microfluidic screen showed TAK-715 is potentially effective against EMT trans differentiation and metastasis in treatment-refractory aggressive subclones**

A Polydimethylsiloxane-PDMS-based  $\mu$ -channel assay served as a physiologically relevant in vitro metastasis model for screening our top secDrugs. This allowed us to study the effect of our drug combination on tumor cell motility through  $\mu$ -channels of dimensions that mimic the size of channel-like tracks encountered by migrating cells in vivo (Paul et al., 2017; Weigelin et al., 2012). Briefly, we fabricated a PDMS-based  $\mu$ -channel assay using standard multilayer photolithography and replica molding as previously demonstrated (Mistriotis et al., 2019; Wisniewski et al., 2020; Wong et al., 2019). The device consisted of an array of parallel channels of variable width (3-50  $\mu$ m) and fixed length (200  $\mu$ m), and height (10  $\mu$ m). Perpendicular to the  $\mu$ -channels were two larger 2D-like channels that served as cell seeding and chemoattractant inlet lines. Prior to cell seeding, the  $\mu$ -fluidic devices were coated with 20  $\mu$ g/mL rat tail collagen type I (Corning) for 1 hour at 37  $^{\circ}$ C to facilitate cell adhesion.  $1-1.5 \times 10^5$  vehicle or TAK-715-treated mCRPC cells were introduced into the cell seeding inlet line via pressure-driven flow and allowed to adhere for 30 min at 37  $^{\circ}$ C, 5% CO<sub>2</sub>. Next, the cell suspension was removed and substituted with a serum-free medium. Medium supplemented with 10% FBS was added into the

chemoattractant inlet line to trigger cell entry into the channels. The devices were placed on an automated Nikon Ti2 Inverted Microscope equipped with a Tokai Stage-Top incubator unit, which maintains cells at 37 °C and 5% CO<sub>2</sub>. Cell motility was recorded via time-lapse microscopy. Images were taken every 20 min for 10 hours with a 10x /0.45 NA Ph1 objective. To assess the migration efficiency of drug-treated mCRPC cells compared to the control, we calculated the percentage of cell entry into the microfluidic channels defined as the total number of cells entering the channels divided by the total number of cells seeded within 50µm diameter from the µ-channel entrances. Because our prostate cancer cells did not frequently enter narrower microchannels ( $\leq 10 \mu\text{m}$ ), we focused our analysis on wider channels ( $\geq 20 \mu\text{m}$ ).

Our microfluidic-based cell migration assay revealed that our TAK-715 single-agent and DTX+TAK-715 combination treatment reduced cell entry into 50 and 20 µm wide channels, suggesting that these interventions may potentially suppress prostate cancer cell invasion and possibly metastasis (Figure 11A).

**Figure 11A**

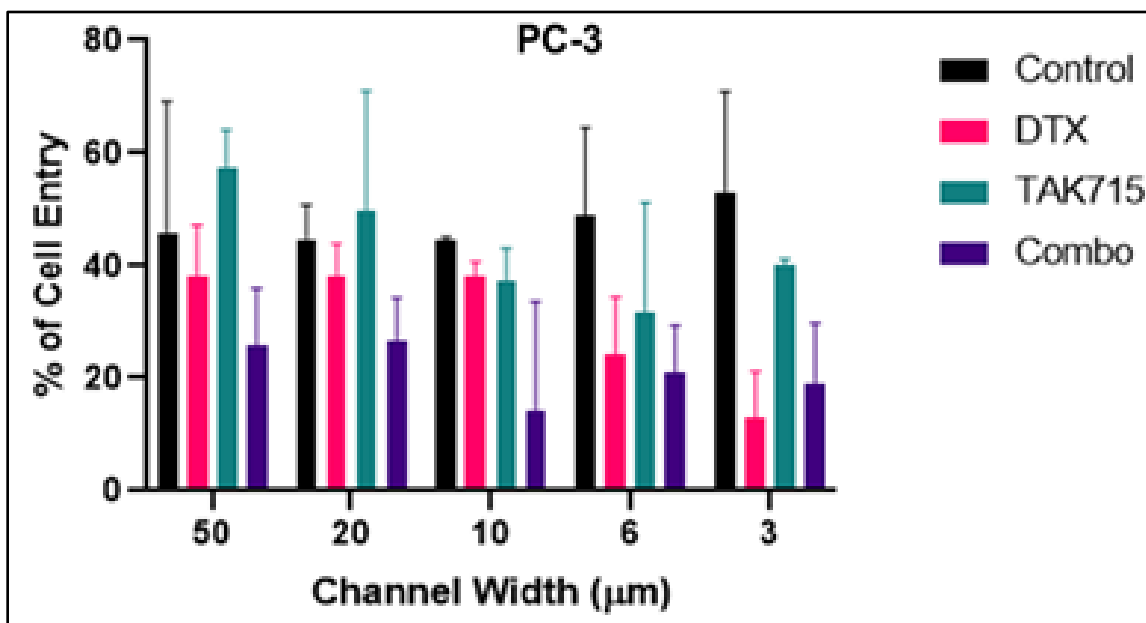


Figure 11B

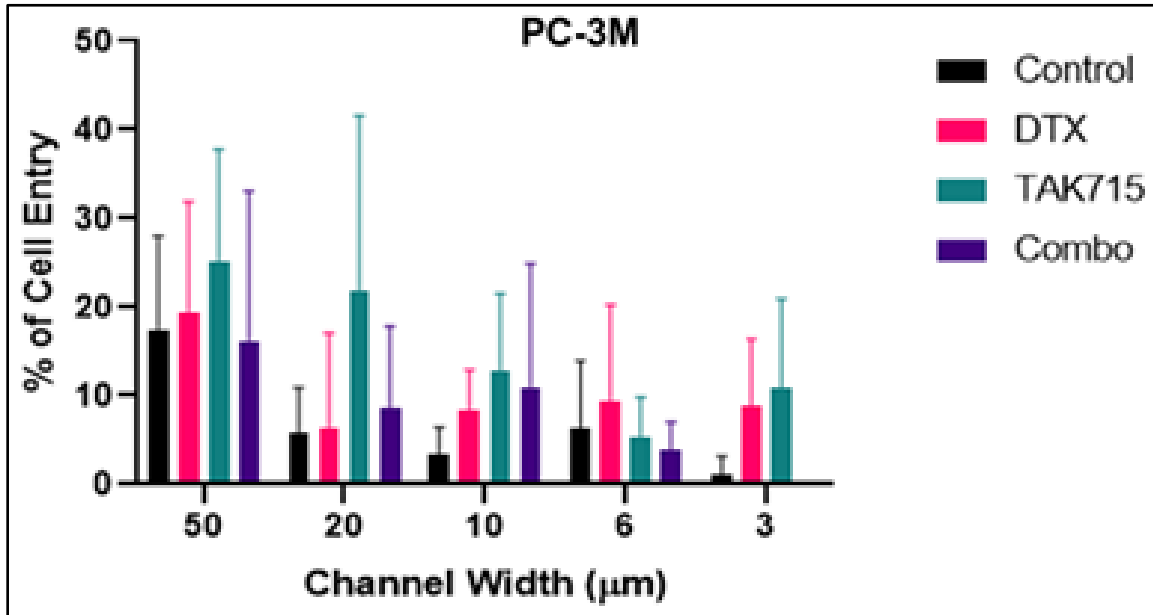


Figure 11C<sup>325</sup>

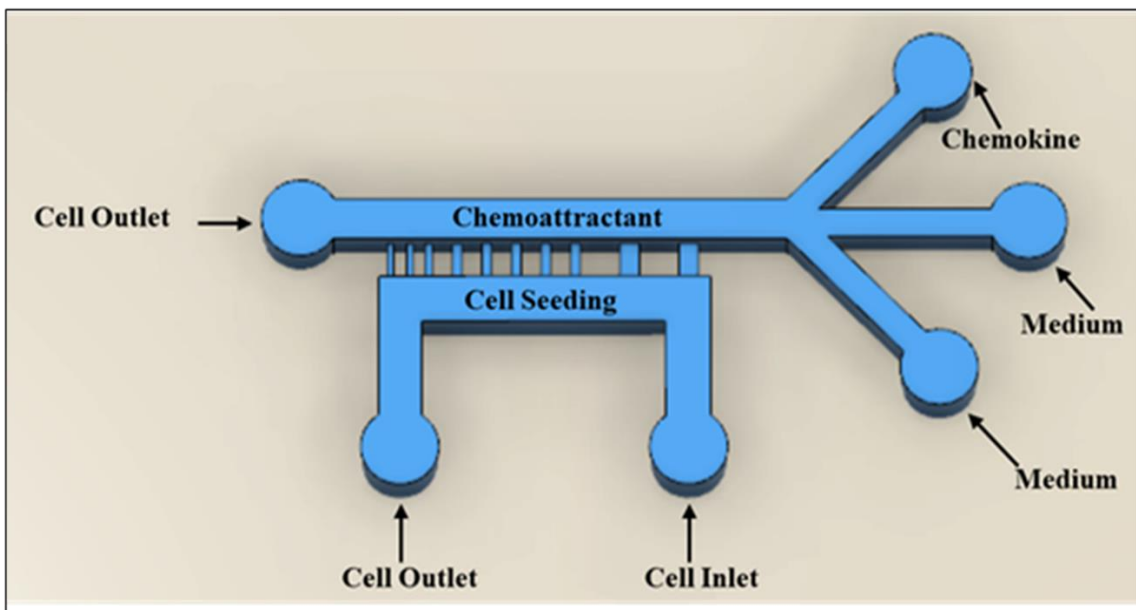


Figure 11. TAK-715 reduces cell migration and is potentially effective against metastasis and EMT trans differentiation in lethal PCa. TAK-715 single-agent and combination therapy with DTX reduces the entry of lethal PCa cells PC-3 and PC-3M into 50 and 20 μm wide μ-

channels, indicating a potential role of TAK-715 in abrogating the metastatic potential.  $n \geq 3$  experiments (Significance P-value \* =  $p \leq 0.05$  relative to control).

(C) Schematic representation of the Microfluidics-based cell Migration/Motility assay device

To confirm the effect of TAK715 on mCRPC cells' motility and migration, we performed a wound-healing assay. A scratch was made in the cell monolayer, and the cells were treated with TAK715 and Docetaxel single-agent and in combination. Images were captured at the beginning and at regular intervals (24 and 48 hours for all treatments). Image analysis of the scratches using the ImageJ software showed an average reduction of  $60 \pm 13\%$  in the wound area in the cells of the control well after 24 hours, whereas it was only an  $8.5 \pm 2.5\%$  reduction in the drug combination-treated cells. After 48 hours, it was  $81 \pm 2\%$  and  $18 \pm 8\%$ , respectively (Figure 12).

Thus, we can conclude that combination treatment (FK866+DTX) had a higher effect in reducing cell migration in PCa cell lines compared to treatment with FK866 alone ( $p < 0.05$ )

**Figure 12A**

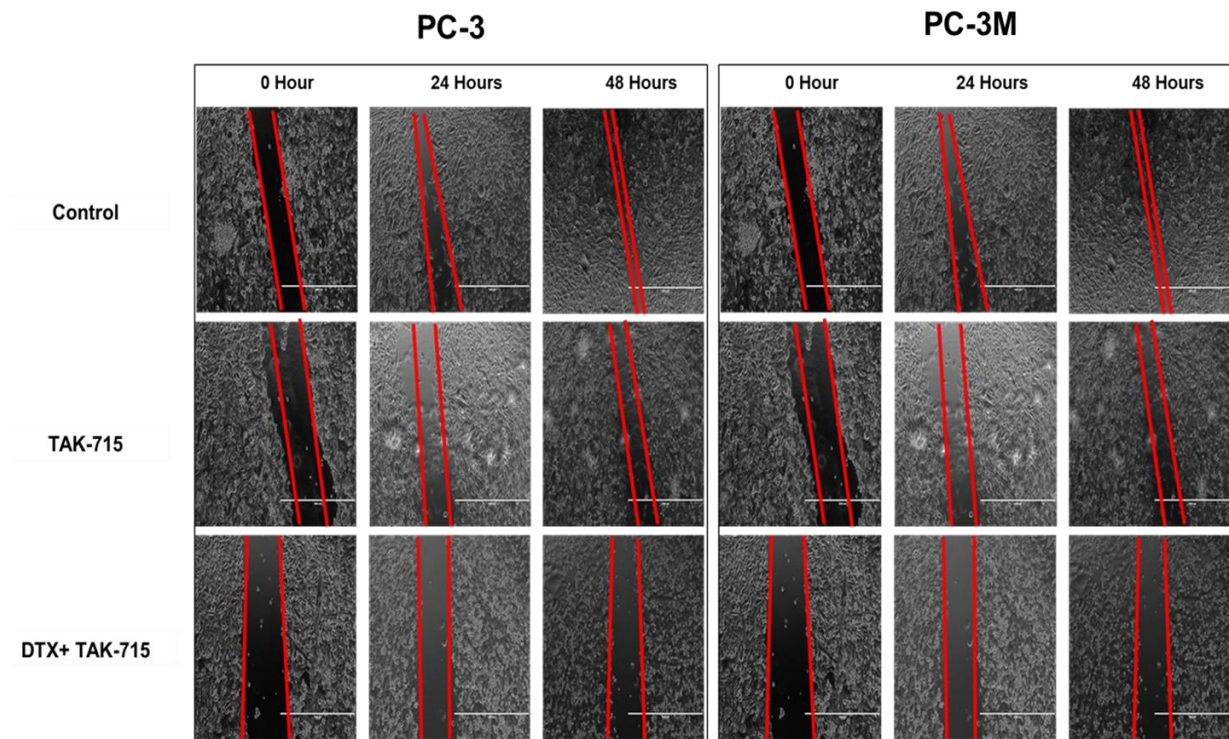


**Figure 12B**

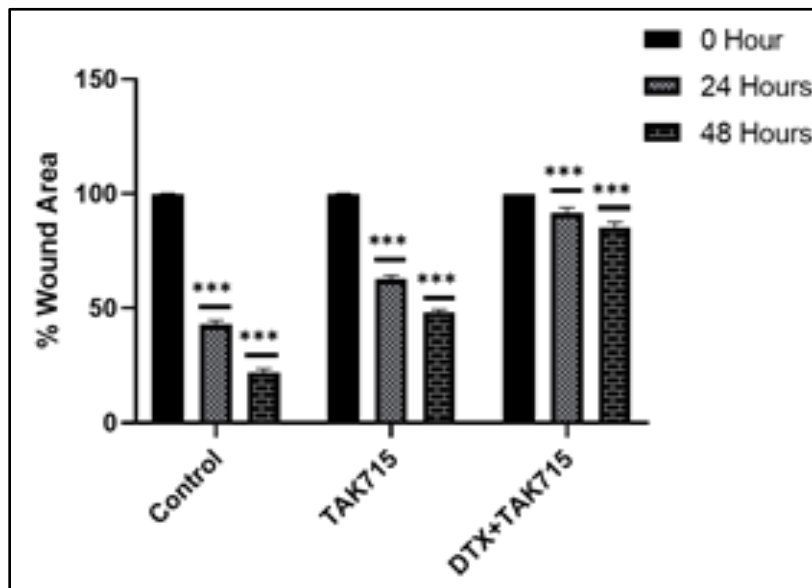


**Figure 12. Representative plots show results of wound healing (Scratch) assay using (A) PC-3 and PC-3M cells. Cell migration after 24 and 48h TAK-715 single-agent and TAK-715+DTX combination was assessed by measuring the scratch size. Images were captured before (0h) and after (24 hours and 48 hours) drug treatments (Significance P-value \* =  $p \leq 0.05$ ). (B)** Bar graphs showed a significant reduction in cell migration (wound healing) following TAK-715-based single agent and combination treatments.

**Docetaxel + TAK715 combination shows impaired Clonogenic properties of mCRPC cells.** Furthermore, we investigated the efficacy of our drug combination on the reproductive health of the cells by colony formation assay. Cells were treated with a single agent or combination for 24 hours and incubated for 2 weeks, followed by staining with crystal violet. We observed a significantly lower number of colonies in TAK715 single-agent and combination-treated wells compared to the no-treatment (Figure 16).

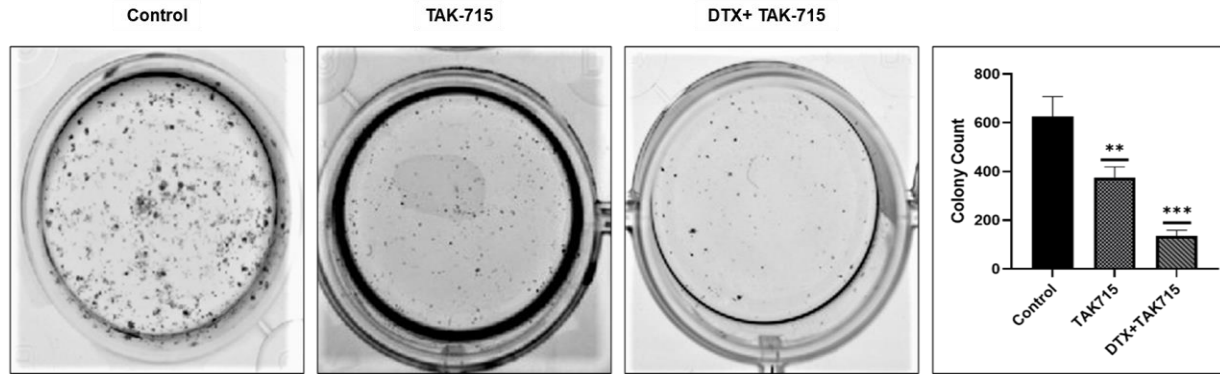


**Figure 13.** Effects of the Docetaxel+TAK715 combination on the Clonogenic formation of PC3 cells were evaluated by a colony formation assay.

**Gene expression profile reveals the mechanism of synergistic drug action of DTX+TAK715 combination.**

Next, we performed whole-transcriptome profiling by bulk tumor RNAseq to compare changes in gene expression induced by TAK-715 in AR<sup>null</sup> mCRPC cell lines in order to elucidate the mechanism of drug action. GEP data were normalized to baseline (no treatment). Heatmaps were generated following differential gene expression analysis (Figure 14A). Volcano plots in Figure 14B show differentially expressed genes (DEGs) following DTX, TAK-715 single-agent or combination treatment in AR<sup>null</sup> mCRPC cell lines.

**Figure 14A**

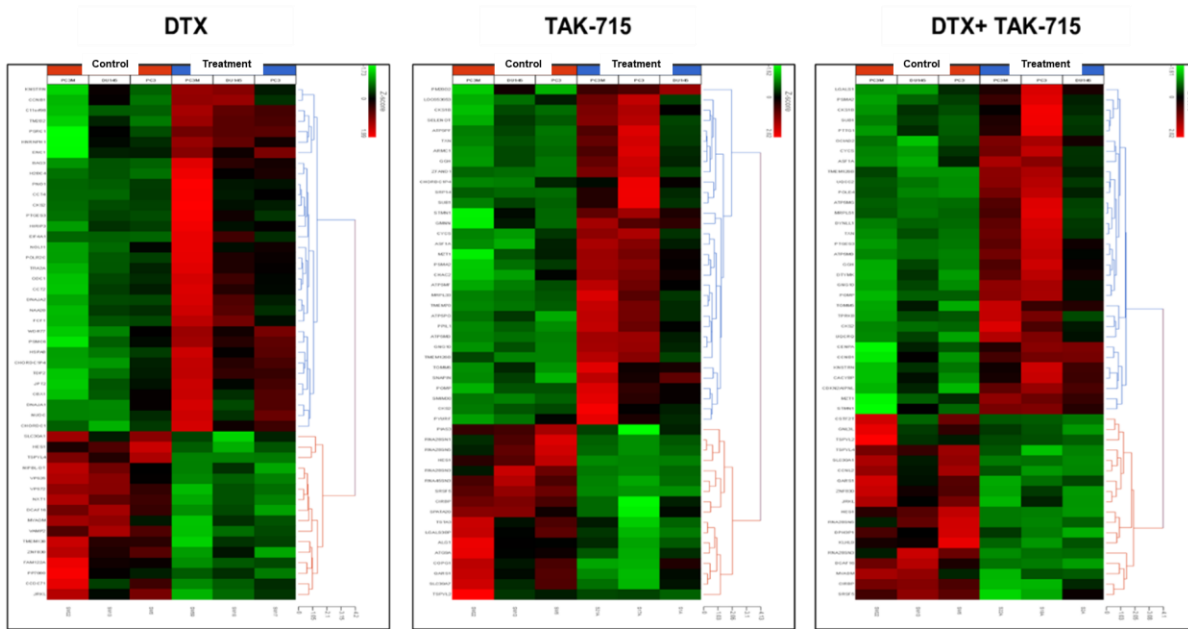
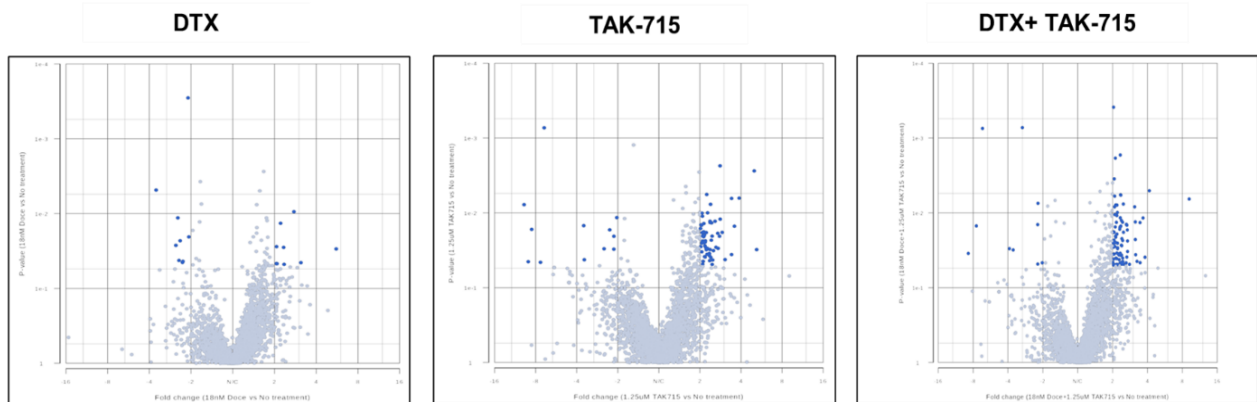


**Figure 14B**



A total of 35 genes were uniquely differentially expressed above the significance threshold ( $p < 0.05$ ) at 48hr post-TAK-715 single-agent treatment, while 21 and 49 genes were differentially expressed following DTX single-agent and DTX+ TAK-715 combination treatments, respectively (Figure 14C).

Combination-treated cells have 143 uniquely differentially expressed genes as compared to DTX single-agent treatment ( $p < 0.05$ ; fold-difference  $\geq 2$ ) (Figure 14D)

The top down-regulated genes are HES-1, SRSF5, TSPYL2, and TSPYL4. The top up-regulated genes are Cyclin B1, CHAC2, and SSBP1.

**Figure 14C**

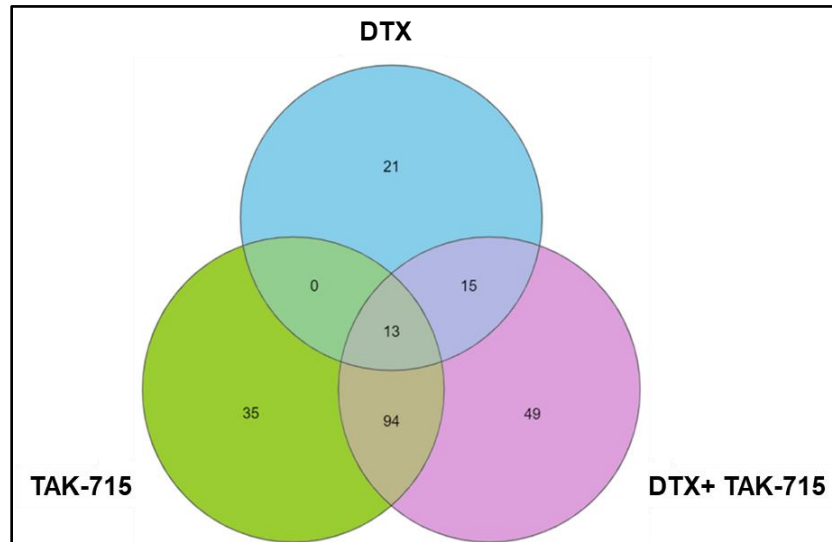


**Figure 14D**

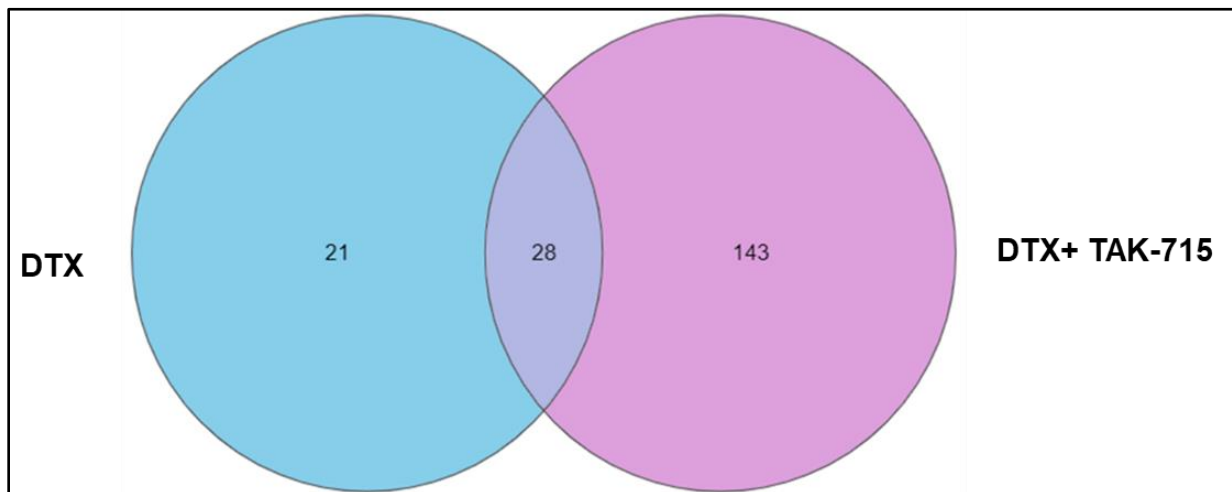


**Figure 14. Differential gene expression profiling analysis results**

(A) Heatmaps representing top differentially expressed genes (DEGs) following DTX, TAK-715 single-agent, or DTX+TAK-715 combination treatments in AR<sup>null</sup> mCRPC cell lines (n = 3), 24h following drug exposure. I) DTX single-agent treatment II) TAK-715 single-agent treatment. II) DTX+TAK-715 combination treatment. Log<sub>2</sub> ratios are depicted in a color scale

where red represents upregulation and green represents downregulation. Columns represent cell lines, and rows represent genes. Prior to hierarchical clustering, gene expression values were filtered (samples with max TPM < 1 were removed), and the z score was normalized.

**(B)** Volcano plots representing differentially expressed genes (DEGs) following DTX, TAK-715 single-agent or combination treatment in human mCRPC cell lines 24 h following drug exposure ( $|\text{fold-change}| > 2$ , and  $p < 0.05$ ). Log<sub>2</sub> ratios are depicted in a color scale where RED represents upregulation and BLUE represents downregulation. I) DEGs for DTX treatment for PCa cell lines. II) DEGs for TAK-715 treatments for PCa cell lines. III) DEGs for DTX+TAK-715 treatments for PCa cell lines.

**(C)** Venn diagrams representing unique and common DEGs ( $p < 0.05$ ) between DTX, TAK-715, and DTX+TAK-715 treatments in AR<sup>null</sup> mCRPC cell lines (n=3).

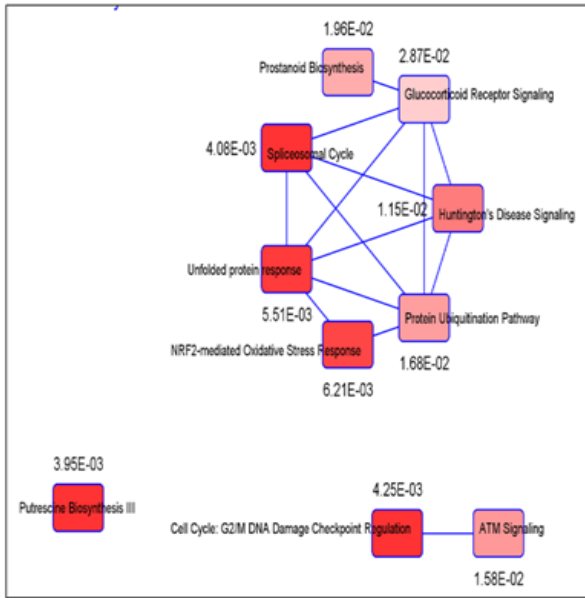
**(D)** Venn diagrams representing unique and common DEGs ( $p < 0.05$ ) between DTX and DTX+TAK-715 treatments in AR<sup>null</sup> mCRPC cell lines (n=3).

**Figure 15. Ingenuity Pathway Analysis (IPA) shows top pathways activated in response to different treatment**

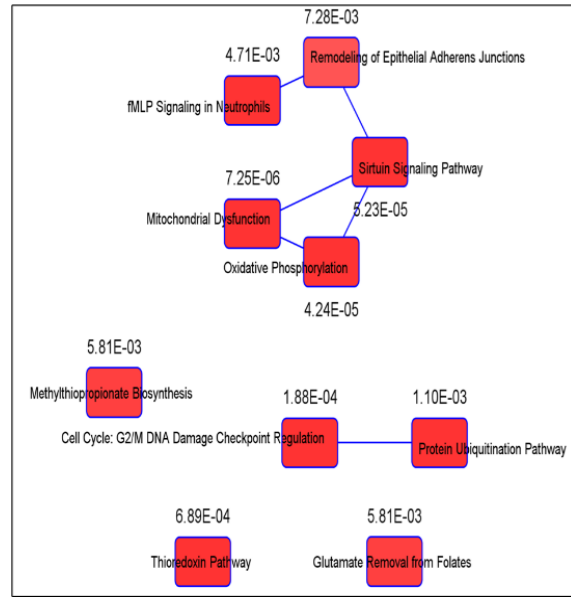
**(A)** IPA analysis based on the top DEGs associated with Docetaxel single-agent treatment, TAK-715 single-agent treatment, and DTX+TAK-715 combination treatment revealed mitochondrial dysfunction, oxidative phosphorylation, and cell cycle arrest at the G<sub>2</sub>/M phase as the top differentially regulated pathways.

**(B)** A detailed heatmap comparison among differentially regulated pathways in Docetaxel single-agent treatment, TAK-715 single-agent treatment, and DTX+TAK-715 combination treated cells. The data shows Cell cycle-G<sub>2</sub>/M damage, mitochondrial dysfunction, oxidative phosphorylation, and protein ubiquitination are the top differentially regulated pathways among the 3 treatment groups

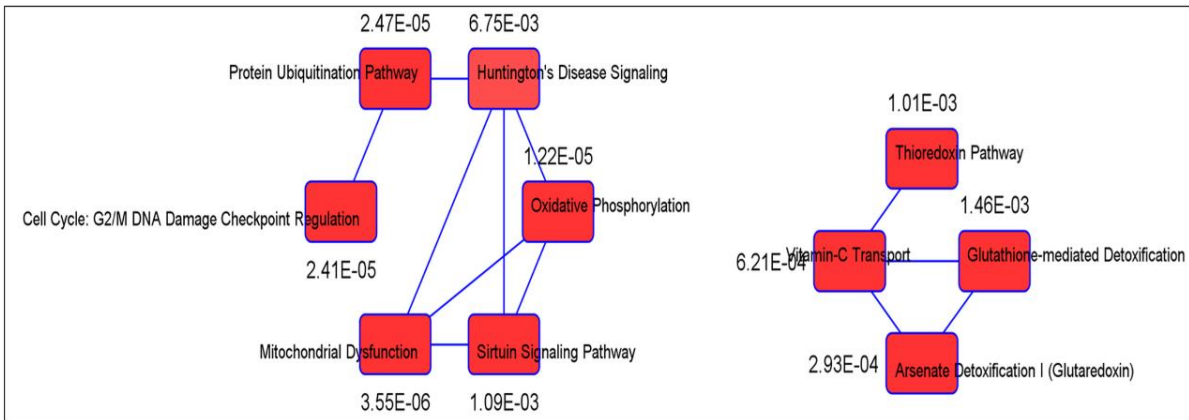
**DTX**

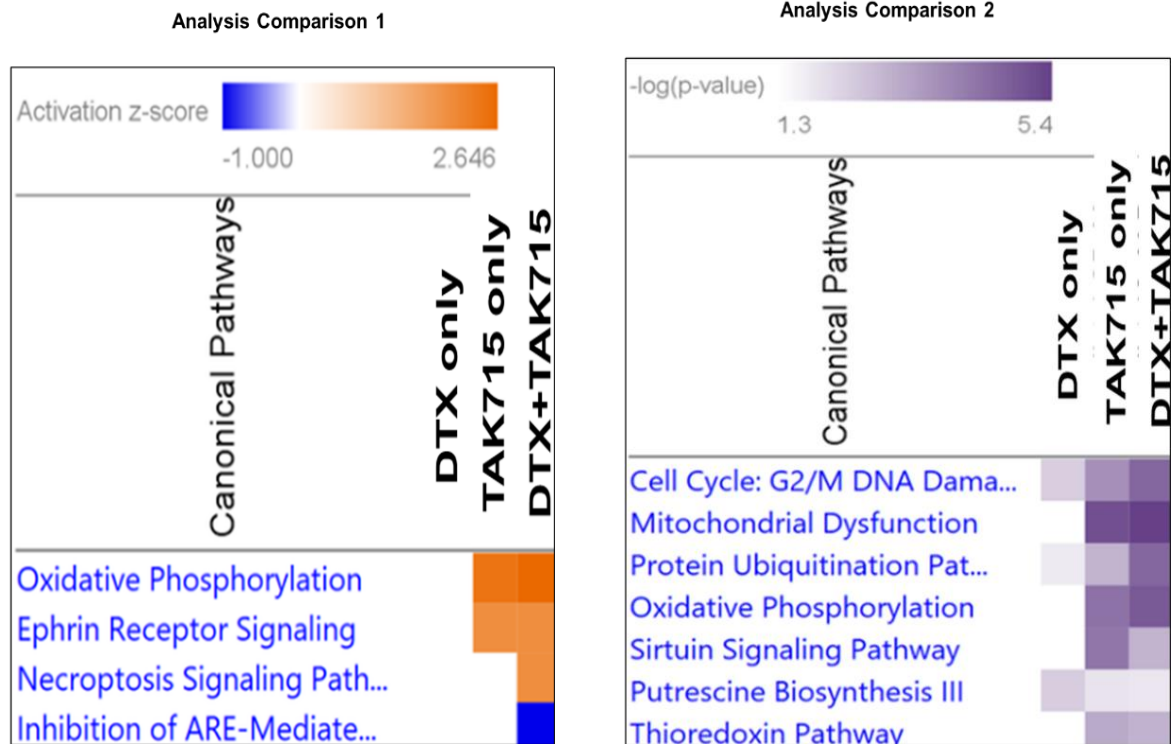


**TAK-715**



**DTX + TAK-715**





Furthermore, Causal Network Analysis, a component of IPA advanced analytics, predicted significant upregulation of microRNA-132 and downregulation of miR-21 in response to combination treatment.

In silico analysis on multiple GEO PCa datasets showed the low expression level of miR-132 was associated with poor clinical prognosis, the transition from androgen-dependent (AD) to independent (AI) stage, and metastasis.

miR-21 was significantly up-regulated in the GEO PCa datasets. miR-21 is an AR-regulated miRNA that plays a key role in nullifying the effect of castration, driving progression to AI stage, TX resistance, and cellular invasiveness through down-regulation of tumor suppressor PTEN.

Figure 16A

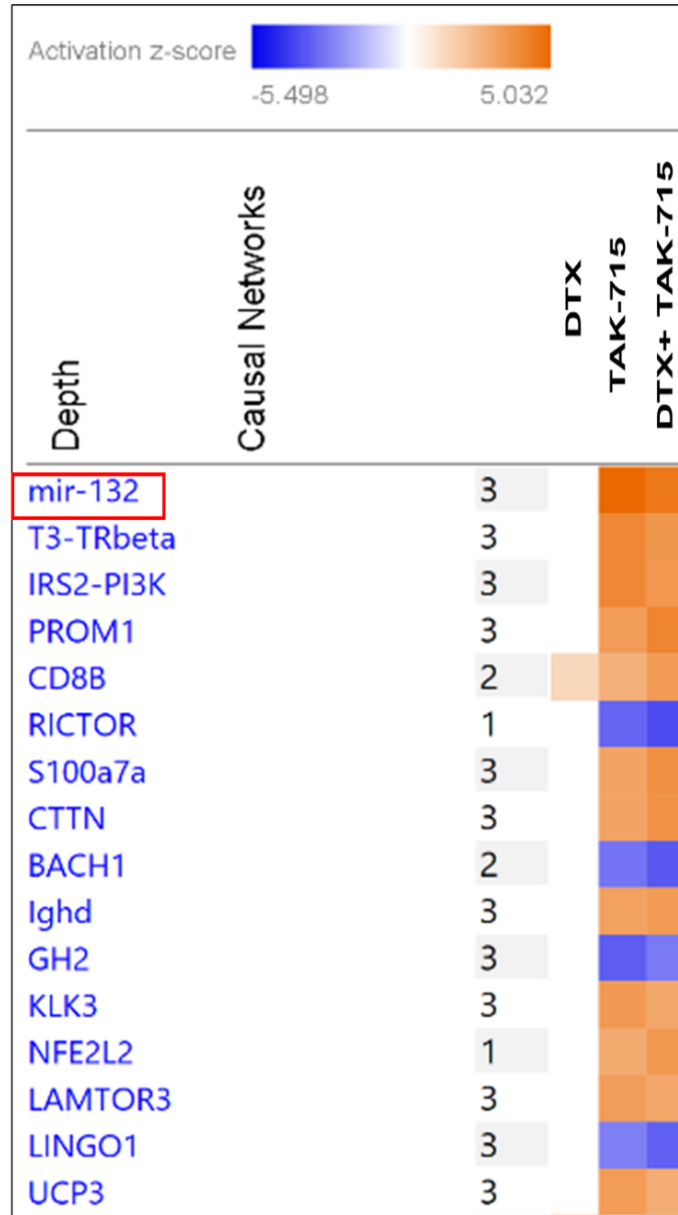


**Figure 16B**

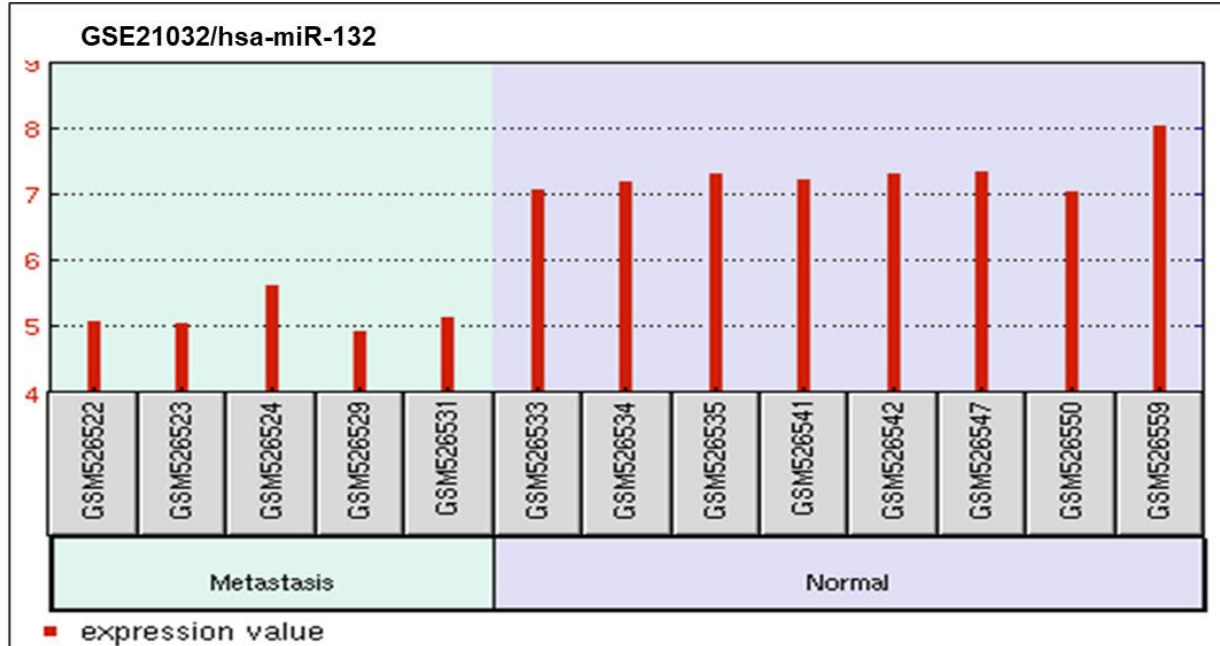


**Figure 16. Comparison of causal networks associated with each treatment group and its validation using in silico database analysis**

- (A) Causal network analysis based on the expression of the genes predicted the up-regulation of miR-132 and the down-regulation of the RICTOR pathway as the top upstream regulator.
- (B) GEO prostate cancer dataset (GSE21032) has shown that prostate cancer tissue has a low abundance of miR-132 compared to normal prostate tissue.

**Combination of Taxane and TAK715 significantly down-regulated HES1- a transcriptional repressor associated with cancer stemness and multi-drug resistance.**

Among the top DE genes in RNAseq data, HES1 was downregulated in all treatment groups, with the highest level of downregulation (~ 9-fold) following combination treatment

To investigate the clinical implications of HE1 in the context of prostate cancer, we performed in silico analysis using the prostate cancer adenocarcinoma database (PRAD) in the Oncomine database and TCGA portal. The Oncomine database suggests HES1 expression is elevated in Prostate cancer tissue as compared to normal prostate tissue (Figure 17A). TCGA database analysis shows that HES1 expression is associated with the Gleason score, which measures the

severity and risk of prostate cancer (Figure 17B). TCGA database analysis also shows that expression of HES1 gets significantly elevated as metastasis progresses. It gets upregulated substantially in nodal metastasis compared to no-nodal metastasis (Figure 17C). Next, we validated the dependency of cancer cells on HES-1 for proliferation and survival from the DepMap portal. DepMap portal is an ongoing project to uncover these gene dependencies in hundreds of cancer cell lines by Broad Institute. Distributions like the one shown for HES1 are an example of cell lines exhibiting strongly selective dependency on a gene. Here, we see many cell lines for which HES1 perturbation has little effect on survival (those centered around a gene effect score of 0 or more), as well as a number of cell lines that are strongly dependent on HES1, with negative scores. The Chronos score for HES1 perturbation in the DU145 cell line is -0.178. A negative score signifies that DU145 is dependent on HES1 for proliferation.

**Figure 17A**

**HES1 expression in Normal vs Prostate tumor tissue  
(Oncomine database)**

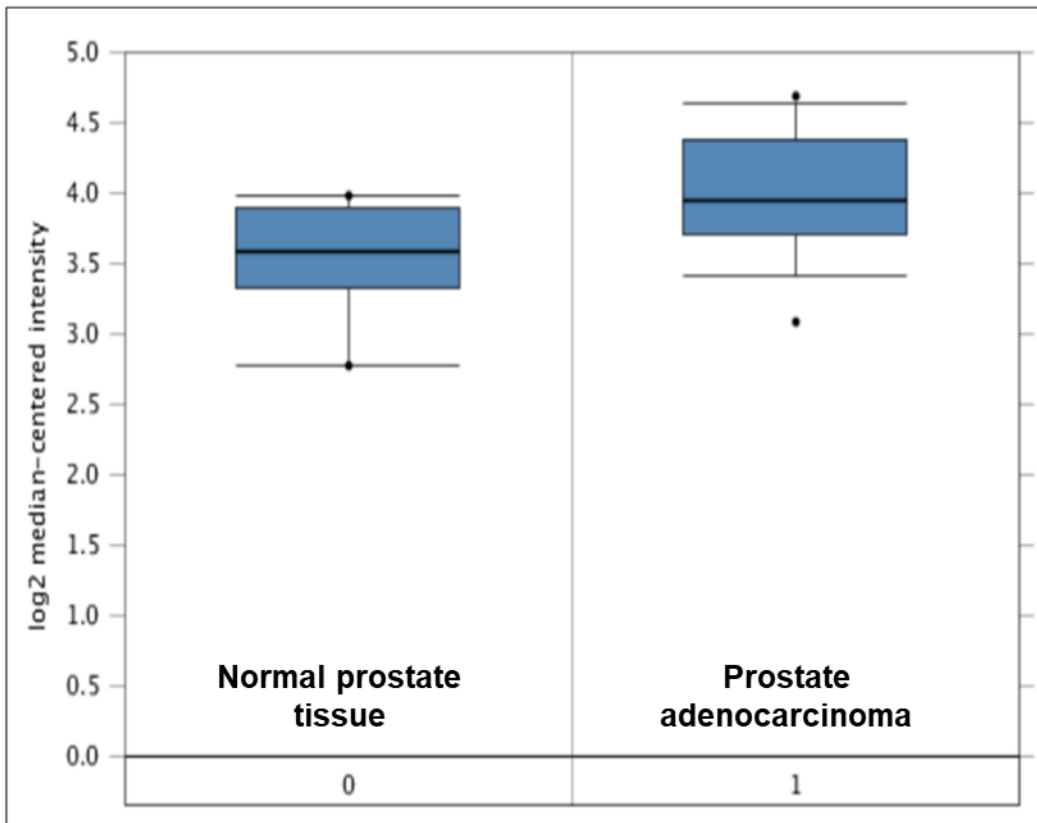


Figure 17B

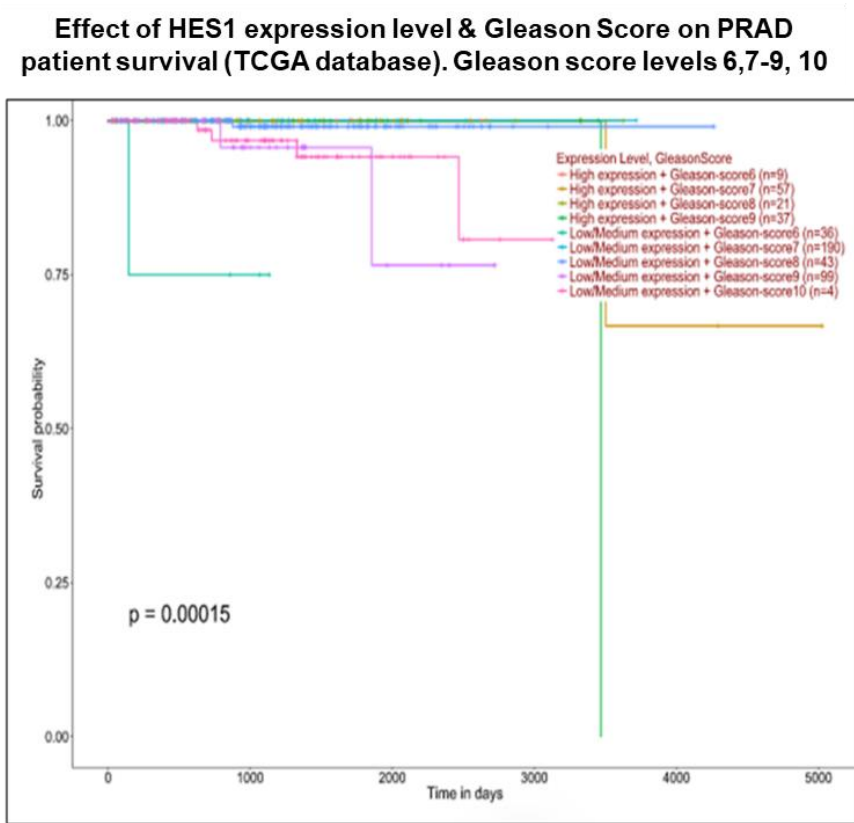
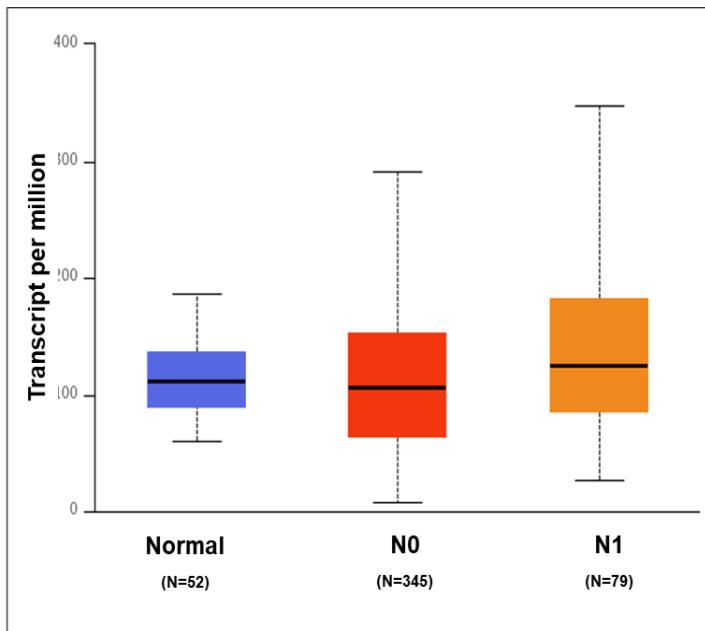


Figure 17C

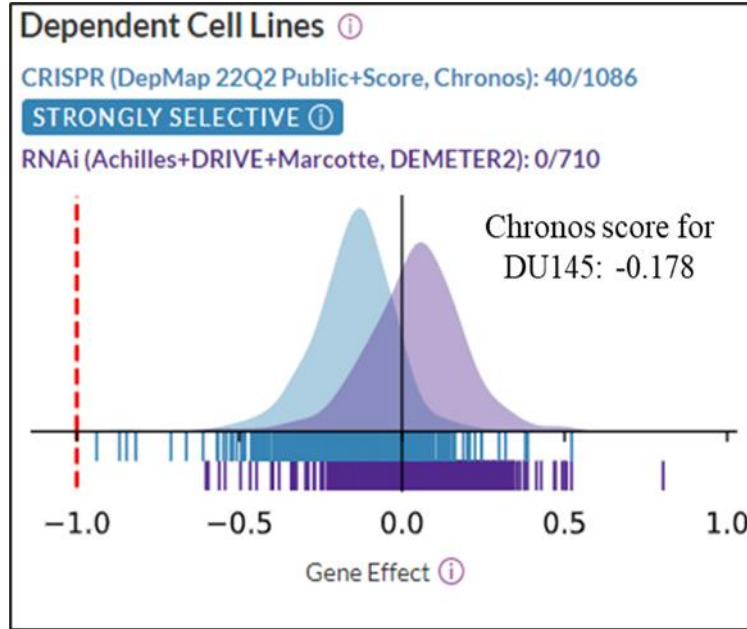


(TCGA database for patient samples)

Pathologic N descriptions			
<b>N0</b>	No regional lymph node metastasis	<b>N1</b>	Metastases in 1 to 3 axillary lymph nodes
<b>N2</b>	Metastases in 6 to 9 axillary lymph nodes	<b>N3</b>	Metastases in 10 or more axillary lymph nodes

Comparison	Statistical significance
Normal-vs-N0	3.332800E-01
Normal-vs-N1	3.678600E-01
N0-vs-N1	1.030610E-02

**Figure 17D**



We further validated the downregulation of the HES1 gene in response to our combination treatment by quantitative real-time PCR. The data shows, indeed, our drug combination is downregulating HES1 both in taxane-sensitive AR<sup>null</sup> mCRPC cell lines ( $\pm 80\%$ ) and taxane-resistant AR<sup>null</sup> mCRPC cell lines cells ( $\pm 40\%$ ). (**Figure 17D**) We also validated the downregulation of HES-1 at the protein level by western blot analysis. (**Figure 17F**)

**Figure 17E**

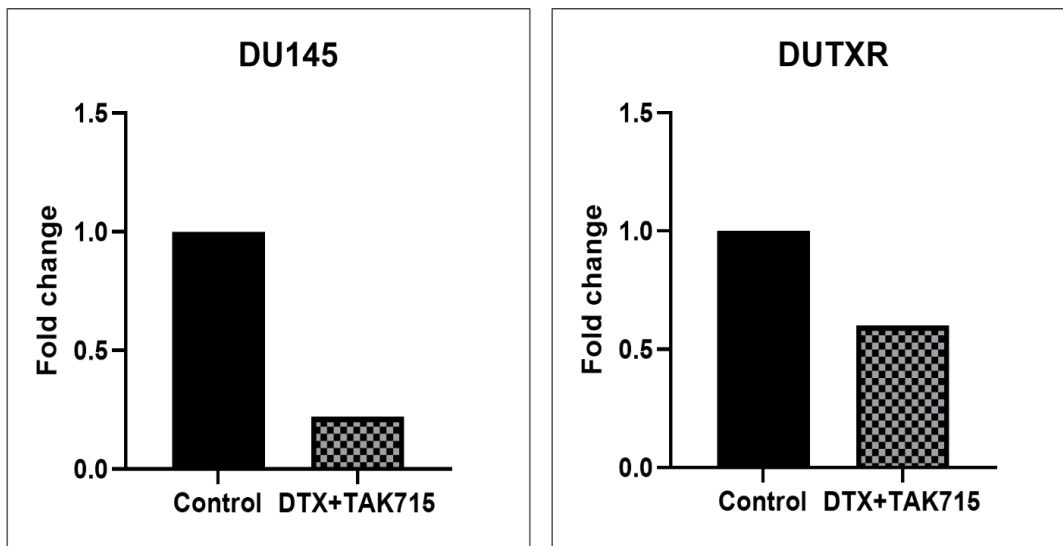


**Figure 17F**

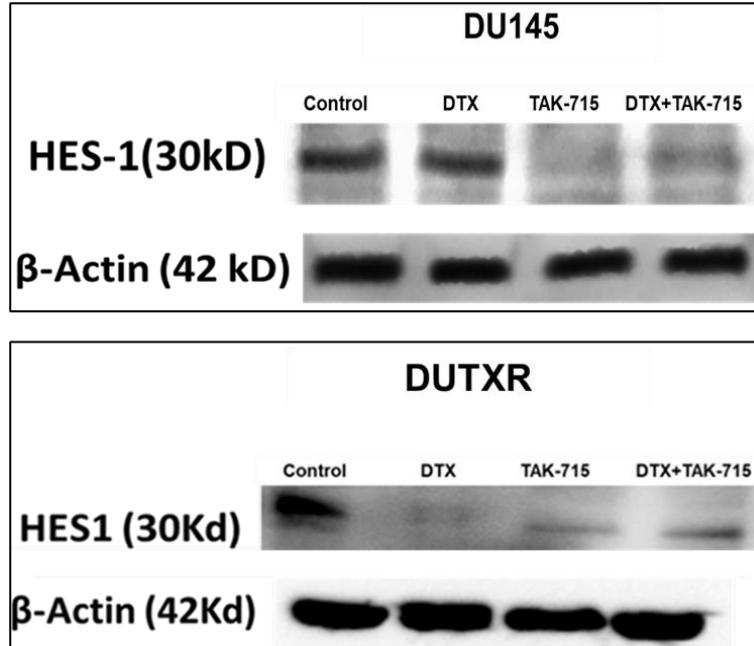


**Figure 17: In silico analysis of HES1 expression and its impact in prostate cancer followed by in vitro validation**

- (A) HES 1 expression in Normal vs. Prostate tumor tissue (Oncomine database)
- (B) Effect of HES1 expression level & Gleason Score on PRAD patient survival (TCGA database). Gleason score levels 6, 7-9, 10
- (C) The expression level of HES1 in PRAD in the different stages of nodal metastasis
- (D) DepMap dependency portal data of the effect of HES-1 expression in DU145 cell line.
- (E) Quantitative measurement of HES-1 expression in Control vs. DTX+TAK-715 combination treated AR<sup>null</sup> mCRPC cell lines.
- (F) Immunoblotting analysis of HES-1 expression in Control, single agent DTX, single agent TAK-715, and DTX+TAK-715 combination treated AR<sup>null</sup> mCRPC cell lines.

### **Docetaxel-TAK715 combination significantly upregulated cellular ROS generation**

To validate the mechanism of action of the drug combination, we quantified the intracellular ROS level in the pre- and post-treatment condition of TAK-715 as a single-agent vs. combination

with DTX using the fluorogenic probe 2,7- dichlorofluorescein diacetate (DCFDA), a cell-permeable non-fluorescent probe that shows fluorescence when it is oxidized. Cellular superoxide anions were measured by using the fluorescent dye DHE. Figure 18 depicts significant ROS generation following 2, 4, 8, and 24hr DTX or TAK-715 single agent and DTX+TAK-715 combination treatments. Further, combination treatment exhibited higher ROS generation than single-agent treatment and control in Acquired taxane-resistant AI-mCRPC (DUTXR) cell lines ( $p \leq 0.05$ ).

**Figure 18**

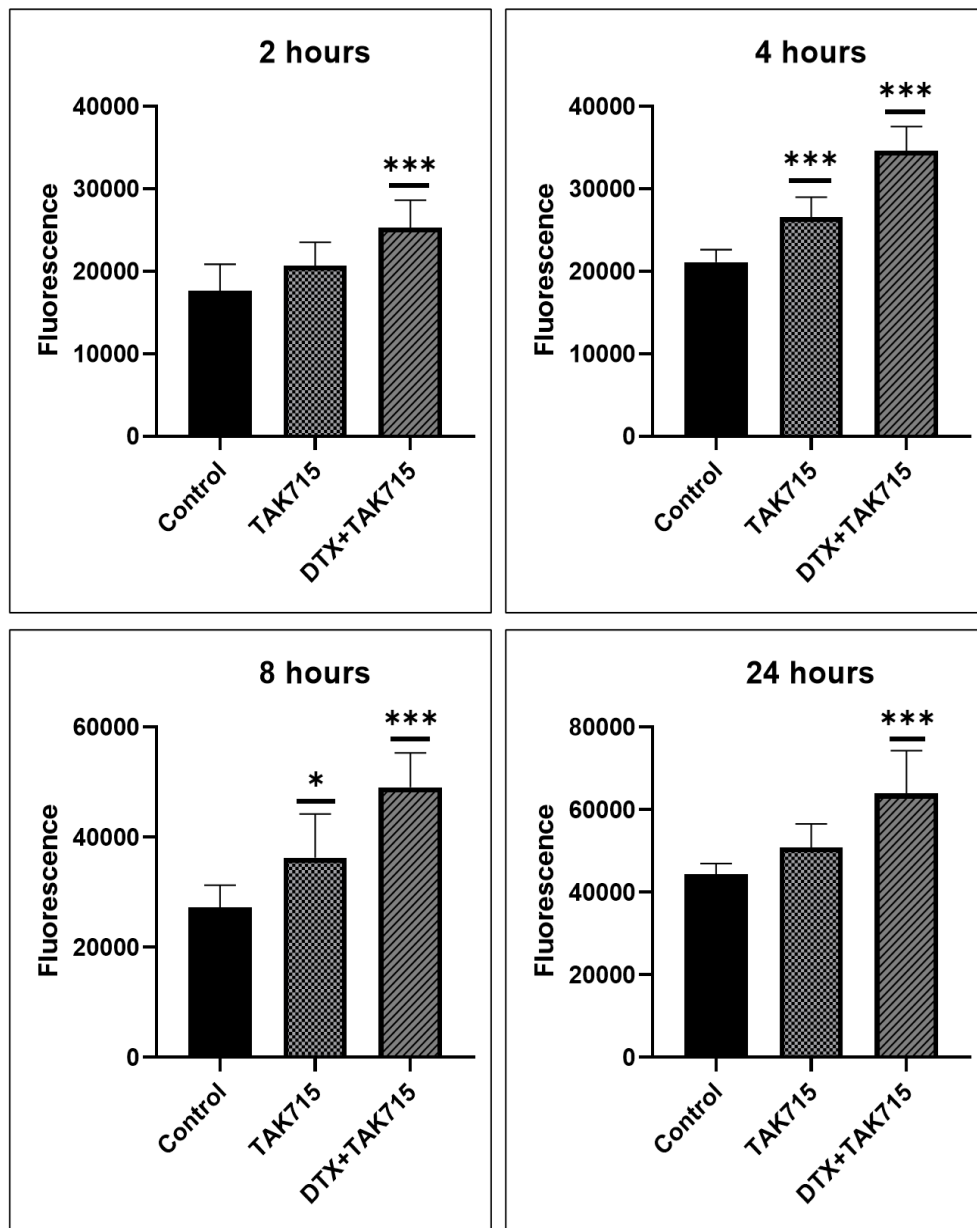


**Figure 18. DCFDA assay to measure cellular ROS level in Control (0.5% DMSO), TAK715 single agent, and DTX+TAK715 combination treated AR<sup>null</sup> mCRPC cell lines after 2 hours, 4 hours, 8 hours, and 24 hours**

Cellular superoxide anions were also measured by using the fluorescent dye DHE (Sigma)

**Figure 19**

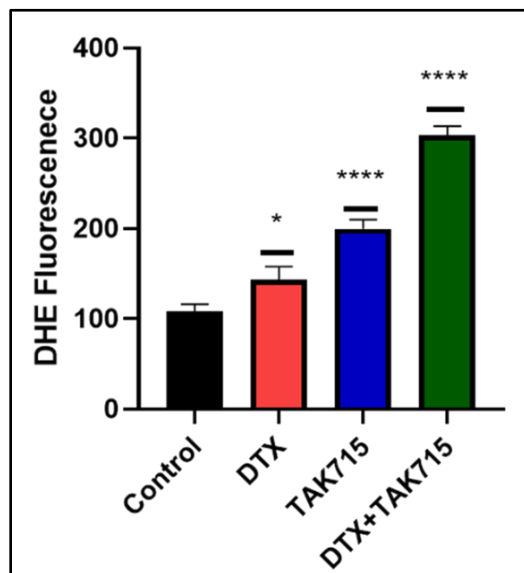


**Figure 19. DHE assay to measure cellular ROS level in Control (0.5% DMSO), TAK715 single agent, and DTX+TAK715 combination treated AR<sup>null</sup> mCRPC cell lines (DUTXR) after 24 hours**

**A combination of Docetaxel and TAK-715 reduced the mitochondrial membrane potential in AR<sup>null</sup> mCRPC cell lines**

To investigate if TAK715 induces its cytotoxic effects through the mitochondrial-mediated pathway, we measured the mitochondrial membrane potential using JC-1 dye (Abcam). JC-1 is a cationic carbocyanine dye that accumulates in mitochondria. The dye exists as a monomer (green fluorescence) at low concentrations and changes color from green to red in energized mitochondria. The cells were treated with either a single agent or in combination for 24 hours. We observed a significant shift from red fluorescence to green fluorescence (Figure 20). The

decrease in the red/green fluorescence indicated mitochondrial depolarization, which caused the JC-1 dye to become monomers from its aggregates form.

**Figure 20**

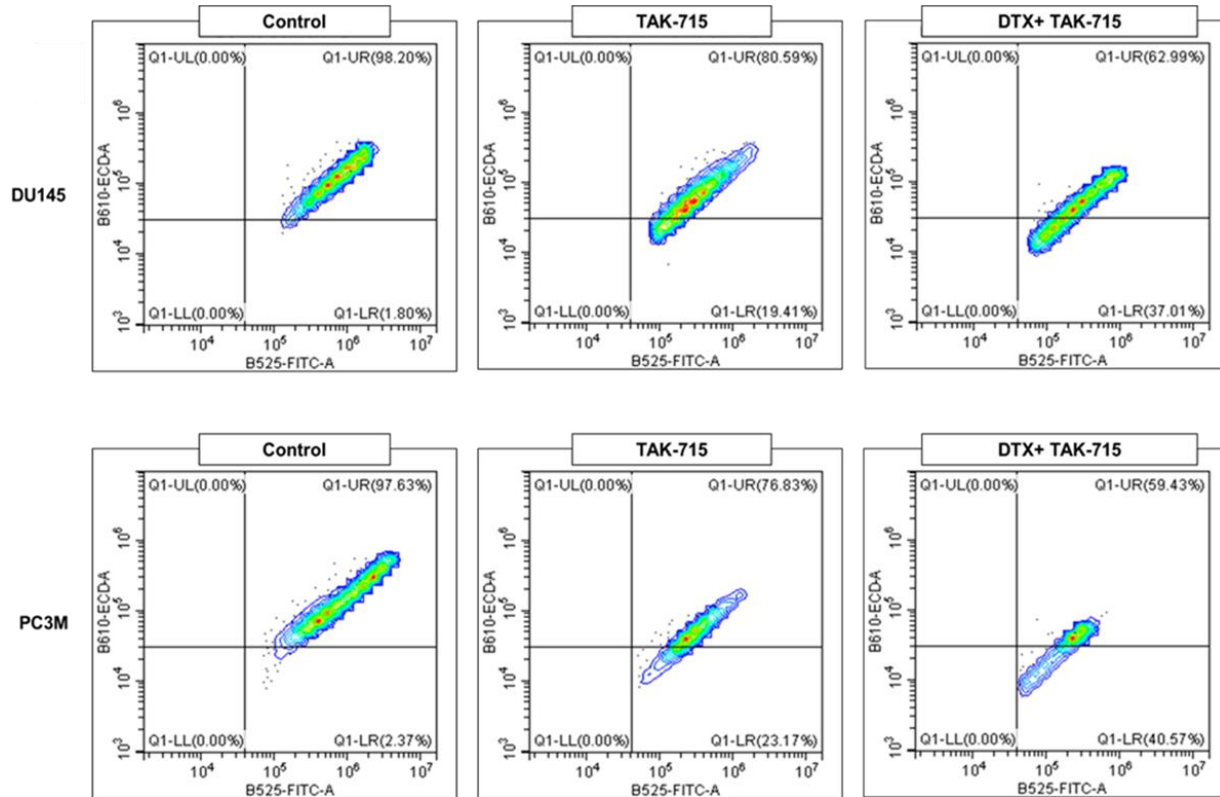


**Figure 20. TAK-715 treatment-induced mitochondrial dysfunction was measured by JC-1 Assay**

**Docetaxel and TAK715 combination exert synergistic drug action by arresting the cells in the G<sub>2</sub>/M phase**

To identify the mechanism of drug action of the Docetaxel-TAK715 combination, we measured the distribution of different phases of the cell cycle by Propidium Iodide (PI). The cells were treated with either a single agent or in combination for 48 hours, followed by staining with PI and flow cytometric analysis. We observed a significantly higher percentage of the cells are arrested at G<sub>2</sub>/M phases in response to the combination treatment as compared to the single agent treatment (Figure 21).

**Figure 21A**

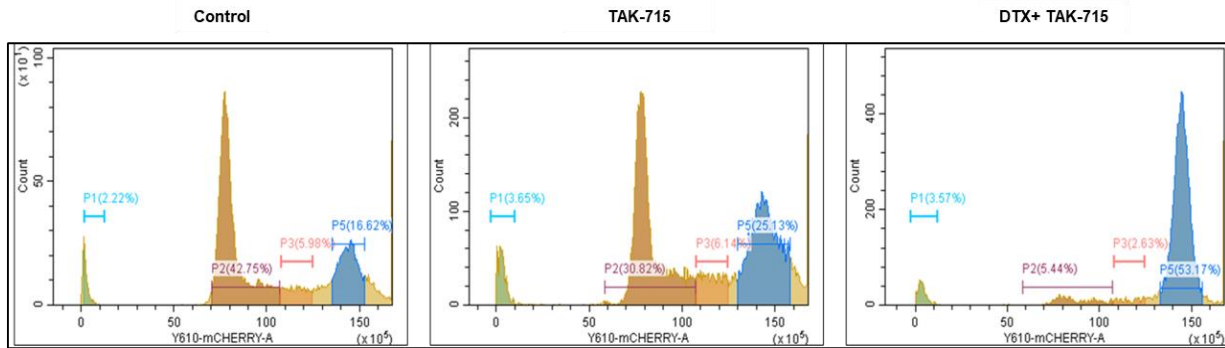


**Figure 21B**

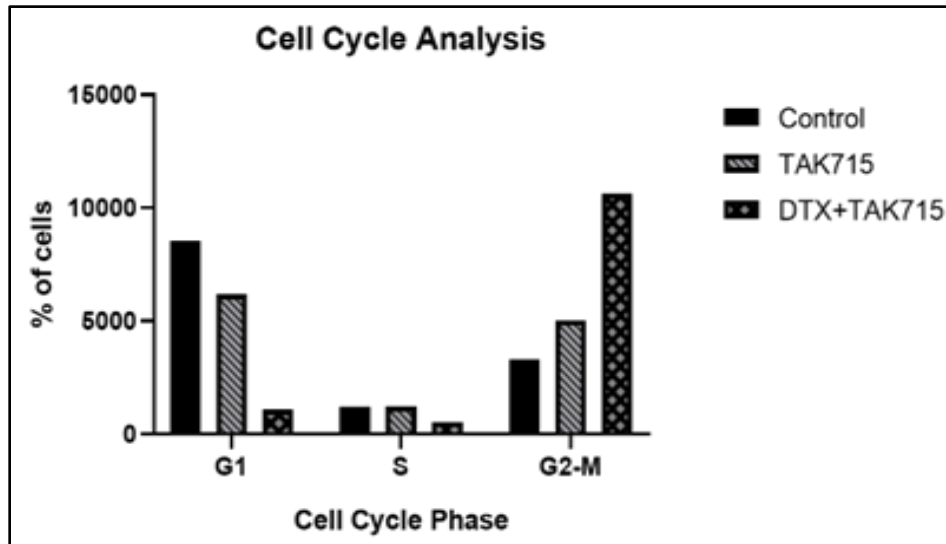


**Figure 21. TX+ TAK715 combination leads to the cell cycle arrest at the G<sub>2</sub>/M phase in AR<sup>null</sup> mCRPC cell lines**

(A-B) Propidium Iodide-based Analysis of the distribution of different phases of the cell cycle in Control (0.5% DMSO), TAK-715 single agent, and DTX+TAK-715 combination treated AR<sup>null</sup> mCRPC cell lines (DU145).

**TAK715, in combination with Docetaxel, elevated DNA damage in AR<sup>null</sup> mCRPC cell lines**

Next, to check the extent of DNA damage, we performed a Comet assay. Comet assay is a technique to measure DNA damage in cells. Undamaged DNA remains in the nucleus, and the damaged, fragmented DNA migrates through the cavity. The shape looks like a comet with a circular head corresponding to undamaged DNA, and the tail represents the damaged DNA. So,

the longer and brighter the tail, the higher the level of damage. The olive moment is tail length \* % of DNA in tail length. From the comet assay data, we observed in our combination treated cells both % of DNA in tail and tail length has increased considerably, indicating that our drug combination enhances DNA damage. (Figure 22).

**Figure 22**

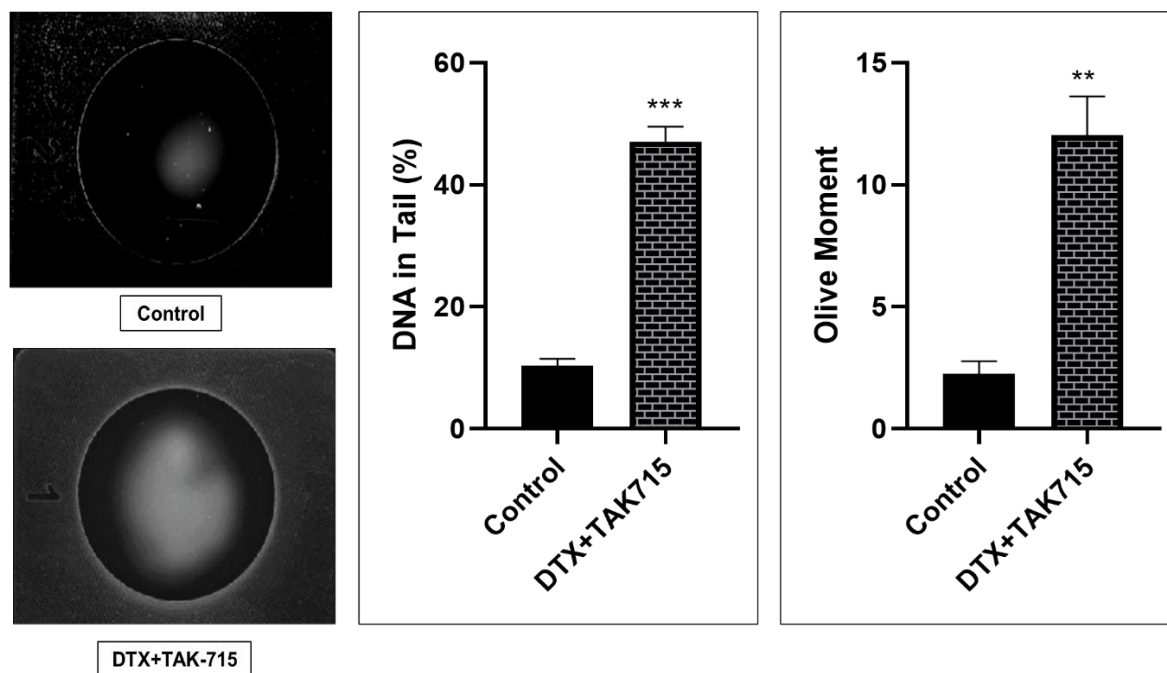


**Figure 22. Comet assay to measure the extent of DNA damage in AI-mCRPC cells (DU145) post-Docetaxel-TAK715 combination treatment.** We treated the cells with DTX+TAK715 combination for 48 hours and measured the extent of DNA damage induced by TAK715 treatment using Comet Assay. We observed a significant increase in DNA % in the tail and as well as in Olive moment (DNA % in tail x tail length), which indicates enhanced DNA damage in response to our drug combination

**TAK715 diminished the side population load in taxane-resistant AR<sup>null</sup> mCRPC cell lines.** We next gated and selected side population (SP) cells from main populations (MP) using DyeCycle violet, pre- and post- TAK-715 treatment. We found that baseline % SP is higher in resistant cells as compared to parental cells (data not shown here). Notably, TAK-715 alone or in combination (Docetaxel+ TAK-715) reduced SP in taxane-resistant AR<sup>null</sup> mCRPC cells

(Figures 23A-C). Our data showed that TAK715 has significantly reduced the side population load ( $\pm 30\%$ ) in taxane-resistant AR<sup>null</sup> mCRPC cells (DUTXR).

**Figure 23. DyeCycle Violet mediated measurement of side population in taxane resistant AR<sup>null</sup> mCRPC cell (DUTXR) post TAK715 combination treatment. (A) Control (B) TAK-715 treated (C) DTX+TAK-715 treated (D) Positive Control**

**Figure 23A**

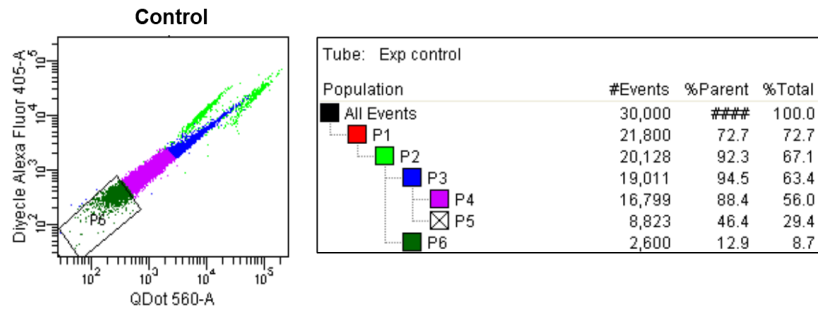


**Figure 23B**

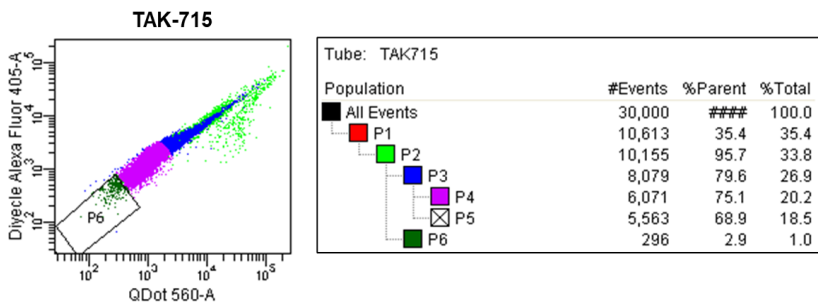


**Figure 23C**

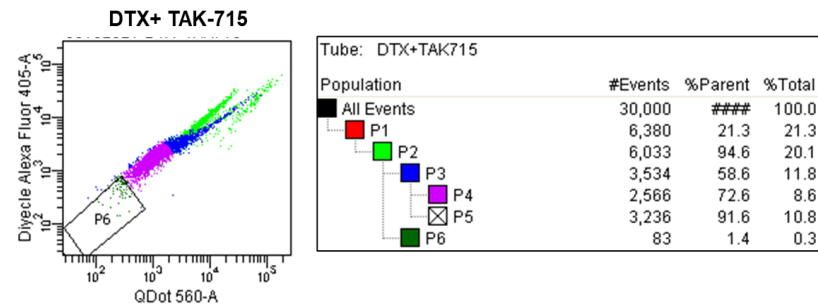
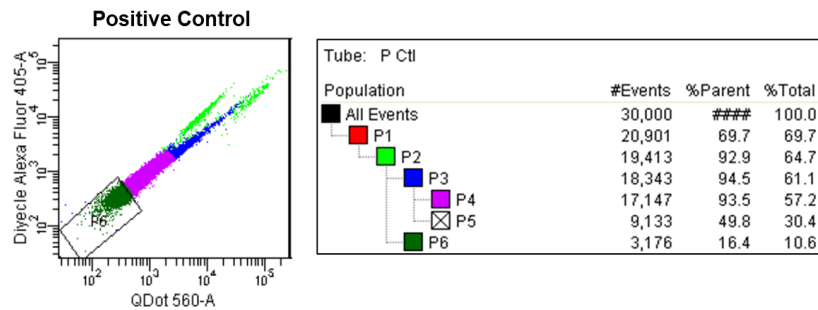


**Figure 23D**



## TAK-715 has a significant cytotoxic effect on the CD44<sup>+</sup> population in AR<sup>null</sup> mCRPC cells

Previous studies reported that in prostate cancer cells, the CD44<sup>+</sup> population represents stemness, i.e., they are a marker of cancer stem cells or cancer-initiating cells and promote ADT resistance as well as tumor recurrence. To study the effect of our secDrug TAK-715 on this cancer stem-cell population, we first sorted out the pool of CD44<sup>+</sup> population from DUTXR cell lines and treated it with two different doses of TAK-715.

Our data (Figure 24) shows TAK-715 was effective in depleting the population of CD44<sup>+</sup> in DUTXR cells. Next, we performed a Caspase 3/7 activity assay on sorted-out CD44<sup>+</sup> cells. The data showed dose-dependent induction of apoptosis by TAK-715 as compared to the untreated cells induced in this stem-like cell population. We further validated the effect of our secDrug on the isolated CD44<sup>+</sup> population cells by in-vitro cytotoxicity assay, which showed significant dose-dependent down-regulation in cell viability in response to TAK-715 treatment.

**Figure 24A**

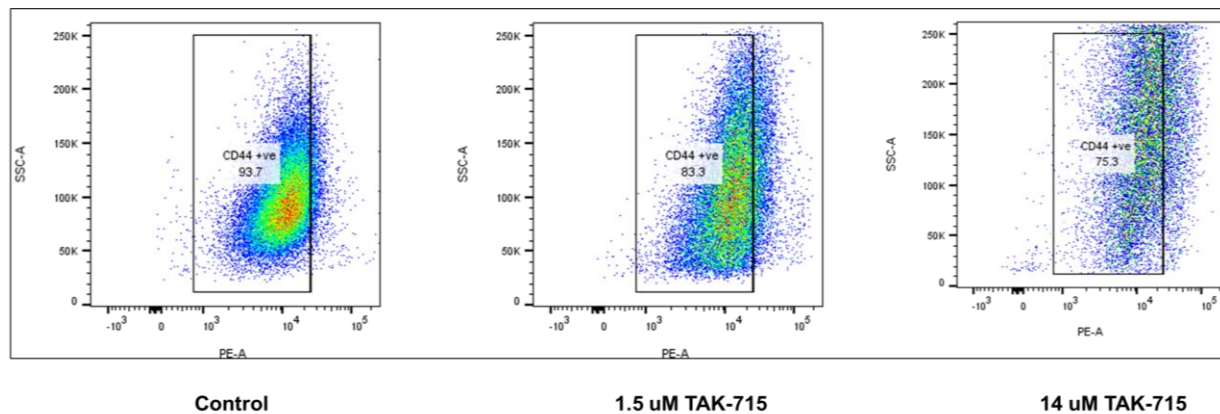


**Figure 24B**

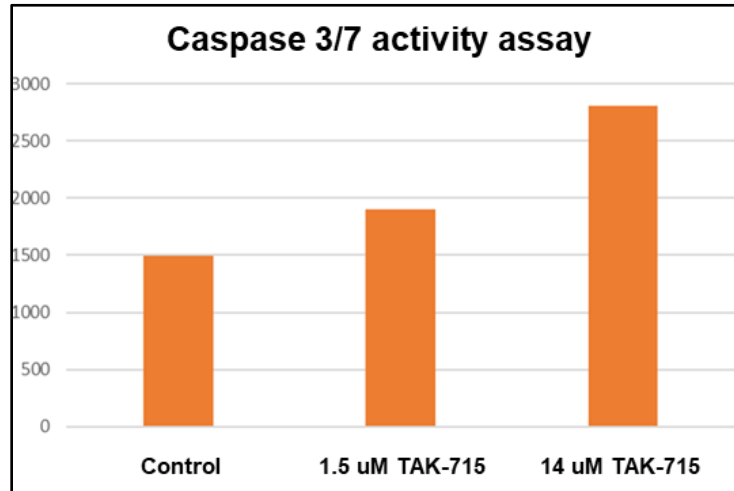


**Figure 24C**

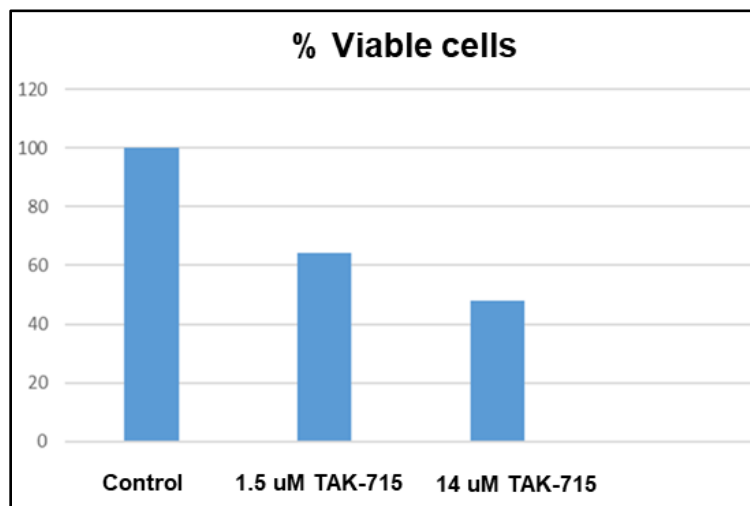


**Figure 24: Effect of TAK715 on the CD44 population**

(A) TAK-715 depletes CD44<sup>+</sup> population in ARnull mCRPC cells

(B) TAK-175 induces apoptosis in CD44<sup>+</sup> cells

(C) TAK-715 reduced the cell viability of CD44<sup>+</sup> cells

# TAK715 erodes sub-clones responsible for drug resistance and stemness

Figure 25A

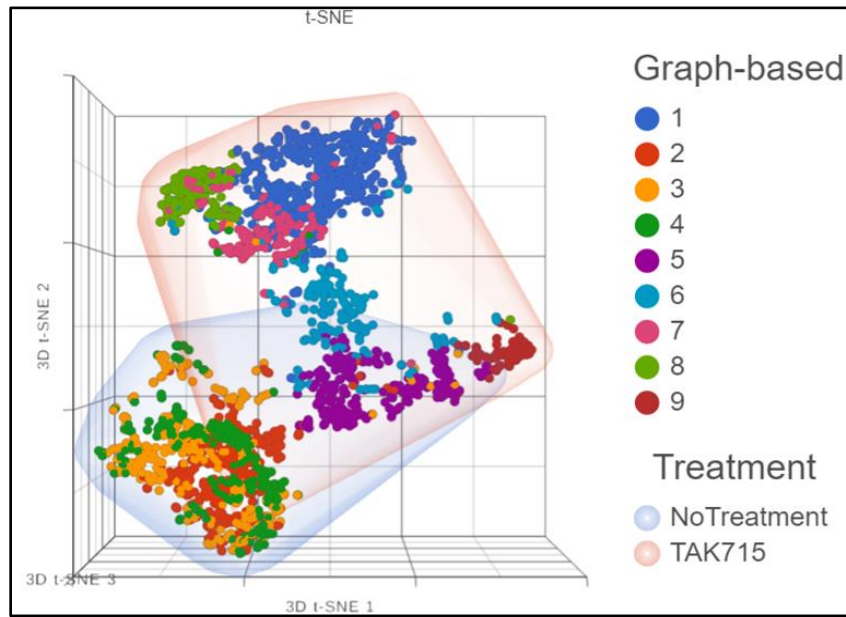
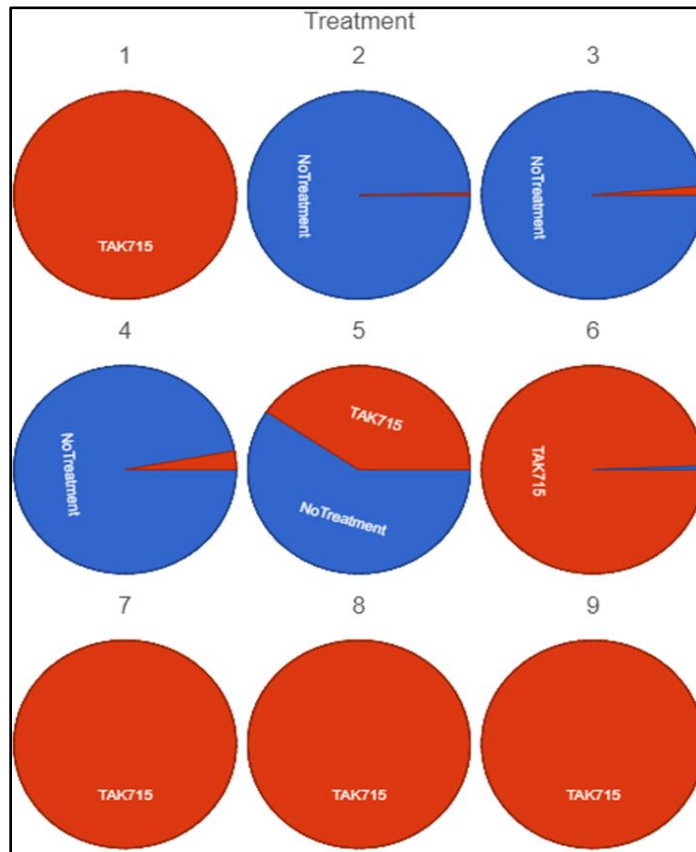


Figure 25B



**Figure 25: TAK-715 treatment leads to the depletion of clusters expressing oncogenes.**

TAK715 was effective in targeting the sub-clonal clusters with the enriched expression of oncogenic factors while inducing the expression of pro-apoptotic factors, thereby exerting its anti-tumorigenic activity.

TAK-715 targets the sub-clones involved in drug resistance and cancer stemness in taxane-resistant ARnull mCRPC cell line DUTXR. TAK-715 treated cells show erosion of Cluster 2, 3, 4, 5 and enrichment of cluster 6, while Cluster 1, 7, 8, and 9 are TAK-715 induced de novo. Gene expression analysis on these eroded clusters shows they are characterized by the expression of genes responsible for tumor aggressiveness and disease progression.

Cluster 2 has enriched expression for KRT8/ Cytokeratin 8, a cytoskeletal protein, and its expression is reported to be directly correlated with tumor metastasis, where it promotes tumor cell migration by up-regulating MMP2, MMP9, and TGF- $\beta$  signaling. It is also an independent risk factor for poor clinical prognosis, i.e., patients with high KRT8 expression tend to show unfavorable treatment outcomes. KRT8 is also involved in the development of chemoresistance through activating STAT3 signaling pathways.

CENPO (Centromere protein O) is another gene in Cluster 2 that is responsible for promoting cancer metastasis through modulating the expression of the genes responsible for EMT, such as N-cadherin, Vimentin, and Snail. It also induces oncogenic events by activating MAPK and PI3K/AKT signaling pathways.

The other significant genes expressed in the TAK-715-induced eroded clusters are NOP16 and Sorcin. NOP16 (Nucleolar Protein 16), is a c-Myc target gene that has been reported to play a role in cancer progression and adverse treatment outcomes. SRI/ Sorcin (Soluble Resistance-related Calcium-binding proteIN), an oncoprotein, is found to be frequently over-expressed in many cancers, including prostate cancer, and is associated with poor clinical outcomes. It is closely related to the MDR, where it shows co-amplification with the ATP-dependent efflux transporter ABCB1. Its expression confers resistance towards taxane drugs and platinum-based drugs, whereas its down-regulation restores the sensitivity. Sorcin also promotes EMT through activating the expression of matrix metalloproteinases 2 and 9 (MMP2, MMP9) and drives tumor progression by inducing oncogenic transcription factors such as STAT3 as well PI3K/

Akt/mTOR pathway. Targeting Sorcin restores the p53 function by preventing its MDM2-mediated ubiquitination and causes G<sub>2</sub>/M arrest and apoptosis in cancer cells.

Another TAK-715-driven eroded cluster, Cluster 4 has expression of PSAT1, RAD21, and CNBP1. Phosphoserine aminotransferase 1 (PSAT1) is involved in the emergence of chemoresistance in many cancers, including the colon and breast. Cellular nucleic acid-binding protein (CNBP), on the other hand, acts as a transcriptional factor to transcriptionally activate the genes involved in the proliferation, invasion, and migration of tumor cells, such as c-Myc, MMP-2, MMP-14, and E2F2. RAD21, a DNA double-strand-break repair protein and a member of the cohesion complex, is reported to be over-expressed in cancers like ovarian cancer, and its expression is associated with treatment relapse and chemotherapy resistance. Patients with high RAD21 expression develop resistance towards many classes of drugs, such as DNA-damaging agents and PAPRP inhibitors, and exhibit poor prognosis. It also promotes the expression of MMP-2 and MMP-9, the other two oncogenes involved in metastatic progression.

Caprin-1 also promotes cell growth by facilitating the cell cycle through c-Myc and Cyclin D1. IPO-7, TWF-1, MYOF, FGD6, and MAP4 are the other top significantly expressed genes present in the TAK-715 eroded clusters, which have reported oncogenic influences in the cancer cells.

### **TAK-715 reduces the oxygen consumption rate (OCR) in MCL cells**

Previous studies have shown that cancer cells have high levels of oxidative phosphorylation, which directly correlates with stemness. To characterize mitochondrial bioenergetics in taxane-resistant AR<sup>null</sup> mCRPC cells (DUTXR) and the effect of TAK-715 on it, we measured the oxygen consumption rate (OCR) directly proportional to the oxidative phosphorylation using Seahorse Extracellular Flux Technology.

Figure 25 showed that TAK-715 was significantly more effective in reducing the OCR in DUTXR cells than Docetaxel which may indirectly abrogate the hypoxia-mediated drug resistance.

Figure 26

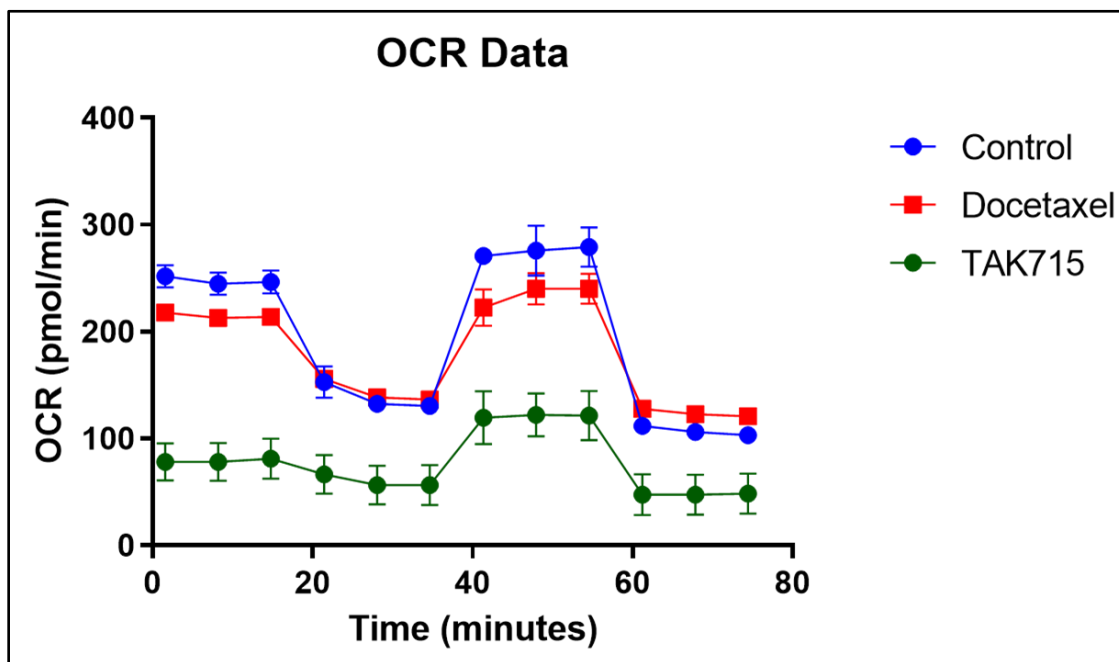


**Figure 26. TAK-715 reduces Mitochondrial respiration (measured by Oxygen Consumption rate) in DUTXR cells.** OCR measurement by Seahorse extra-cellular flux technology reveals that TAK-715 was effective in reducing mitochondrial respiration—a characteristic feature of cancer cells and chemoresistance.

### Validation of TAK-715 treatment-induced gene signatures using Patient datasets

We used reverse-matching using patient cohort datasets to show that TAK-715 treatment has the potential to reverse PCa lethality. RNAseq data on PCa patients were obtained from the Gene expression omnibus database. The dataset includes 100 PCa patients (49 with BCR, 51 with no BCR) from the Atlanta VA Medical Center, Moffitt Cancer Center, and Sunnybrook Health Science Center. First, we performed differential gene expression analysis between patients with or without biochemical recurrence (BCR). The left image shows the top pathways that were significantly different between BCR vs. no-BCR based on DEGs with  $p < 0.05$ . Next, as a reverse-matching approach, we compared the list of shared dysregulated (down or upregulated) genes with our list of top TAK-715-treatment-induced DEGs. The right image shows that several TAK-715 treatment-induced pathways were significantly downregulated in PCa patients with BCR. Pathway analysis was performed based on the top DEGs in A) PCa patient cohort; B) Top TAK-

715 treatment-induced downregulated pathways that were significantly upregulated in PCa patients with biochemical recurrence (BCR).

**Figure 27**

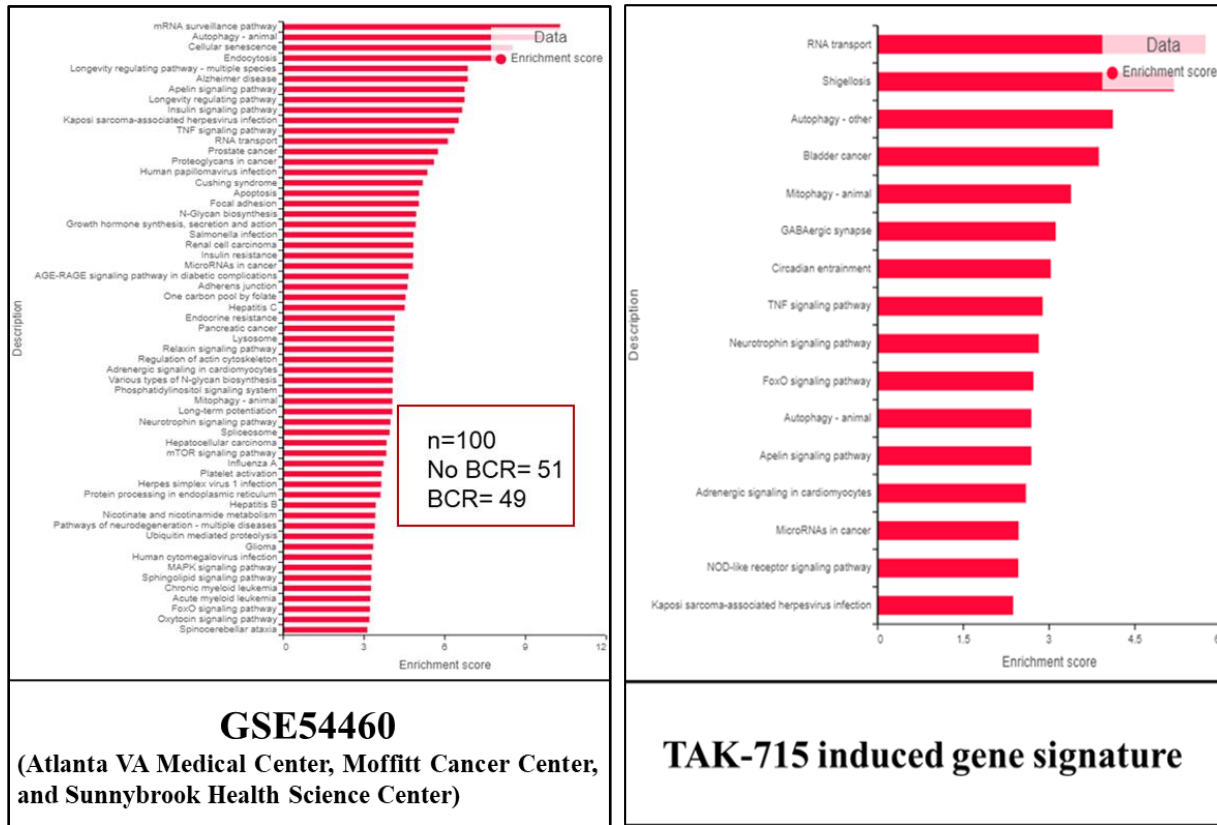


**Figure 27. KEGG pathway enrichment analysis provides mechanistic insights into TAK-715 drug action in MCL cells.** Comparison of Pathway enrichment analysis of the GSE54460 dataset that contains expression data from PCa patients with or without biochemical recurrence (BCR with TAK-715 gene signature shows a high degree of similarities indicating TAK-715 as a potent drug to curb resistance.

**Validation of TAK-715 treatment-induced gene signatures using Patient datasets with biochemical recurrence**

Next, we did validation using TCGA’s prostate adenocarcinoma (PRAD) GEP dataset: The top genes that were significantly upregulated in patients and showed significant downregulation

following TAK-715 treatment in PCa cell lines were LTB4R, MAN2C1, SPTBN2. Kaplan-Meier Curves showed that these genes were significantly associated with disease-free survival.

**Figure 28**

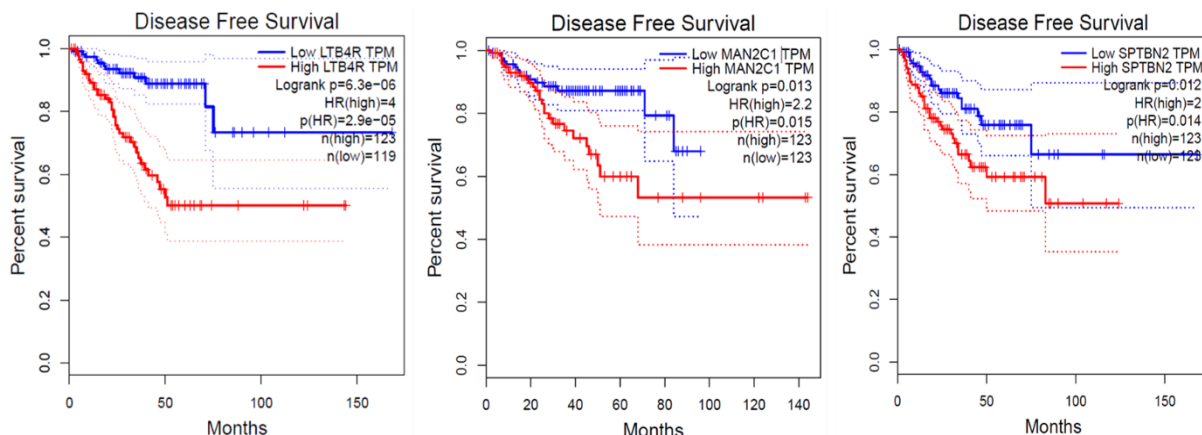


**Figure 28. TAK-715 treatment induced differential regulation of genes associated with disease free survival in PCa patients.** LTB4R, MAN2C1 & SPTBN2 were significantly over-expressed in PCa patients. Their high expressions are co-related with poor disease-free survival. TAK-715 treatment was effective in down-regulating these genes in PCa cells.

## Discussion

Drug development for aggressive and/or lethal treatment-resistant PCa poses a significant challenge with very few therapeutic successes. In this study, we introduced a pipeline that integrated a pharmacogenomics data-driven approach with a scRNAseq-based rapid drug screening method and identified TAK-715 as a proof-of-concept secondary drug ('secDrugs') against lethal PCa, including aggressive, acquired taxane resistant and stem-like cell types representing NEPC and stem-like (EMT) phenotypes. Notably, we used scRNA-seq as an innovative approach to demonstrate that a subset of AR<sup>low</sup> PCa cells in metastatic prostate cancer, including castration-sensitive and castration-resistant tumors, harbored signatures of Epithelial-mesenchymal transition (EMT) and cancer 'stemness' which we also showed as targets of TAK-715.

TAK-715 is a p38 MAPK inhibitor for p38 $\alpha$ . It has been observed that in PC, both upstream ( $\alpha$ -PAK, MEK-6) and downstream (Elk-1, ATF-2) components of the p38 are over-expressed,

resulting in enhanced cell proliferation and survival.<sup>326</sup> p38 is involved in IL-6 mediated androgen-independent prostate cancer cell proliferation and phosphorylated and activates key transcription factors (ATF2, Elk-1), which in turn up-regulate cell cycle regulators (CCND1) and other genes related to cellular proliferation.<sup>327,328</sup> p38 also inhibits apoptosis through NF- $\kappa$ B activation. It also stabilizes androgen receptors (AR), independent of androgens, by involving chaperons (HSP27).<sup>329,330</sup> Activation of p38MAPK may thus promote aggressive growth of prostate cancer cells and aberrant AR activity in the absence of androgens which may promote the onset of androgen independence. Hypoxia-associated p38-MAPK Mediated AR activation and increased Hif-1 $\alpha$  Levels contribute to the emergence of an aggressive phenotype in PC.<sup>331,332</sup> Inhibition of p38 decreases IL-1-induced cell proliferation and increases TNF- $\alpha$ -induced cell death.<sup>333</sup> It has also been found that Docetaxel (DTX) upregulates p53 and p21 in a p38-dependent manner to desensitize PC cells.<sup>334</sup> Increased p38MAPK activity is associated with DTX resistance in Docetaxel-resistant cell lines. Thus, p38MAPK appears to be a potential drug target for mCRPC treatment. Moreover, TAK715, by cross-reacting with CKI $\delta/\epsilon$ , also inhibits Wnt/ $\beta$ -catenin signaling, which is involved in cancer cell proliferation and drug resistance in metastatic castration-resistant prostate cancer. So, TAK715, in combination with Docetaxel, is an effective alternative approach to treating aggressive prostate cancer.

Since TAK-715 is a kinase inhibitor, we confirmed that TAK-715 inhibits multiple kinases, including MAPK14, MAP4K4, CSNK1D, and CSNK1E. Further, we combined a novel microfluidic-based cell migration assay, genome-wide bulk inter-tumor (RNAseq), and single-cell transcriptomics (scRNA-seq) analysis to elucidate in detail the treatment-induced genes and molecular pathways/networks underlying TAK-715 mechanism of action and its potential impact on tumor metastasis, migration, invasion, intracellular ROS activity, and most importantly, ‘cancer stemness,’ in AR<sup>null</sup> mCRPC cells.

We found HES1 (Hes Family BHLH Transcription Factor 1)– a transcriptional repressor that has a significant role in cancer stemness, metastasis, antagonizing drug-induced apoptosis, and multi-drug resistance to be significantly downregulated in our combination treatment group.<sup>335,336</sup> It is extremely relevant as cancer stem cells also contribute to the development of Taxane resistance in mCRPC.<sup>337</sup> So, to understand its biological implication in prostate cancer drug resistance, further investigation is required. CD133, CD44, ALDH, and  $\alpha$ 1 $\beta$ 2 integrin have

all been associated biomarkers for stemness in prostate cancer and new evidence suggests resistance to taxane therapy in prostate cancer is at least partially derived from the formation of cells with some or all of these markers. It is reported that the expression level of Hes1 in CD133+ cells is significantly elevated. Knockdown of Hes1 in CD133+ positive cells significantly decrease its colony-forming ability as well as depletion in number.<sup>335,336</sup>

RICTOR, or Rapamycin-Insensitive Companion Of mTOR, is an essential subunit of the mTORC2 complex that is inappropriately overexpressed across numerous cancer types, and this is associated with poor survival. RICTOR enhances angiogenesis in prostate cancer, and its downregulation impairs the proliferation of prostate cancer cells.<sup>338,339</sup> RICTOR gene amplification is associated with many types of cancers, and it drives its oncogenic effect by inducing Akt 473 phosphorylation.<sup>338</sup> DTX+TAK-715 combination significantly down-regulated the RICTOR pathway in AR<sup>null</sup> mCRPC cells.

BACH1 or BTB Domain And CNC Homolog 1 is a transcription factor that is highly expressed in mCRPC cell lines, and by up-regulating MMP, it promotes metastasis in prostate cancer. BACH1 promotes the progression of colorectal cancer and enhances the invasiveness and metastasis in pancreatic cancer and lung cancer.<sup>340,341</sup>

The expression of SRSF5 (Serine And Arginine Rich Splicing Factor 5), which is responsible for functional silencing of androgen inactivating enzyme HSD17B2 and TSPYL2 & TSPYL4 (Testis-Specific Y-Encoded-Like Protein 2 & 4), the transcriptional inducer of CYP17A1 which synthesizes DHEA, a major source of intra-tumor androgen, were inhibited by Docetaxel-TAK-715 combination treatment.<sup>342,343</sup>

In prostate cancer, the low miR-132 expression seems to signify a poorer clinical prognosis. miR-132 decreases cellular adhesion and consequently increases cell death. HB-EGF (heparin-binding epidermal growth factor), a pro-survival factor, has increased expression in androgen-independent PCa cell lines and contributes to the transition from an androgen-dependent to an androgen-independent state. It is a direct target of miR-132, which causes down-regulation of its expression. Reduction in miR-132 in prostate cancer cells enhances aerobic glycolysis by regulating Glut1 expression, thus promoting cell proliferation.<sup>344-346</sup>

NFE2L2/NRF2 or Nuclear Factor, Erythroid 2 Like 2 is a transcription factor that suppresses prostate cancer cells' growth and migration. NRF2 is negatively regulated by BACH1. NRF-2 suppresses the transactivation of AR. Loss of NRF-2 expression leads to a predisposition to tumorigenesis. TAK715, in combination with Docetaxel, was effective in suppressing the expression of BACH and up-regulated the expression of NRF-2.<sup>347</sup>

Cyclin B1 is reported that Increased expression of cyclin B1 sensitizes prostate cancer cells to apoptosis induced by chemotherapy by decreasing Bcl-2 and increasing p53.<sup>348</sup> CHAC2 (ChaC Cation Transport Regulator Homolog 2) acts as a tumor suppressor by inducing mitochondrial apoptosis and autophagy simultaneously through UPR. SSBP1 (Single-Stranded DNA Binding Protein 1) acts as a tumor suppressor.<sup>349</sup> All these genes were up-regulated by a TAK-715-based treatment regimen. Ephrin Receptor Signalling: Eph1, Eph5, and Eph7 are down-regulated in prostate cancer and co-related to higher Gleason scores and shorter survival time. TAK-715 stimulated this signaling pathway.<sup>350</sup>

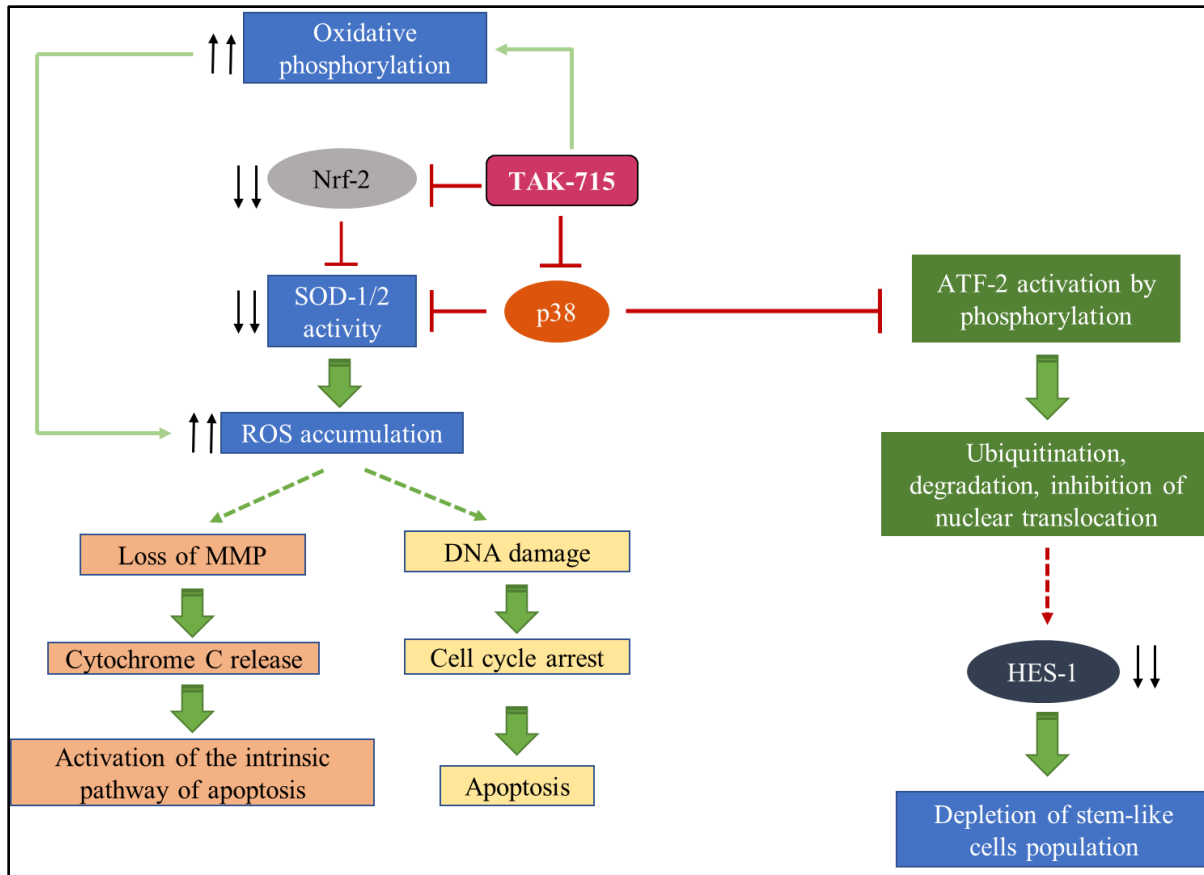
Defective Oxidative Phosphorylation is known to be one of the critical reasons for the attenuation of apoptosis in cancer cells. Anticancer agents enhance OXPHOS function causing elevation of mitochondrial ROS, which activates inflammatory response leading to mitochondria dysfunction and apoptosis.<sup>351,352</sup> ROS is a by-product in OxPhos and plays a role in the alteration of mitochondrial dynamics.<sup>353</sup> p38 $\alpha$  MAPK mediates Cell Survival in Response to Oxidative Stress via the induction of Antioxidant Genes like superoxide-dismutase 1 (SOD-1), SOD-2.<sup>354</sup> But, TAK715 is a p38 $\alpha$  MAPK inhibitor which prevents the expression of anti-oxidant genes. This leads to excessive oxidative stress, which can cause further dysfunction of mitochondrial proteins, leading to augmented production of ROS, creating a vicious cycle of mitochondrial damage and oxidative stress. This will eventually lead to the collapse of the mitochondrial membrane potential, permeabilization of the membrane, and induction of apoptosis.

TCGA's prostate adenocarcinoma (PRAD) GEP dataset analysis showed the top genes that were significantly upregulated in patients and showed significant downregulation following TAK-715 treatment in PCa cell lines were LTB4R, MAN2C1, SPTBN2. The previous study has suggested that LTB4R or leukotriene B4 receptor 2 is significantly over-expressed in androgen-independent samples as compared to androgen-dependent samples.<sup>355</sup> In Clear Cell Renal Cell Carcinoma, LTB4R Promotes the Occurrence and Progression by Regulating the AKT/mTOR

Signaling Pathway.<sup>356</sup>  $\alpha$ -mannosidase 2C1 or MAN2C1 inhibits PTEN function in prostate cancer (PC) cells and activates AKT.<sup>357</sup> Patients with elevated levels of MAN2C1 appear to be at greater risk for aggressive disease.<sup>357</sup> SPTBN2 is highly expressed in lung adenocarcinoma, positively correlated with poor prognosis, and can promote the proliferation, migration, and invasion of lung adenocarcinoma cells.<sup>358</sup> It also promotes endometrial cancer metastasis via PI3K/AKT pathway in Endometrial Cancer.<sup>359</sup>

Thus, our multi-pronged approach towards screening and pre-clinical validation for drug repurposing represents a new paradigm in the management of aggressive treatment-refractory subtypes of PCa. Together, we conclude that the TAK715+Taxane combination may be useful in curbing oncogenic progressions in AVPCa through simultaneous inhibition of multiple oncogenic factors/pathways.

## Proposed mechanism of action of TAK-715 in ARlow mCRPC cells



Defective Oxidative Phosphorylation is known to be one of the key reasons for the attenuation of apoptosis in cancer cells.<sup>360</sup> Anticancer agents enhance OXPHOS function causing elevation of mitochondrial ROS, which activates inflammatory response leading to mitochondria dysfunction and apoptosis.<sup>361–363</sup> IPA analysis showed TAK-715 upregulates Oxidative phosphorylation. ROS is a by-product of OxPhos. ROS scavenging enzymes such as Super-oxide dismutase 1/2 help in reducing oxidative stress and impart cytoprotective effects.<sup>364</sup> p38 $\alpha$  MAPK mediates cell survival in response to oxidative stress via the induction of antioxidant Genes like superoxide-dismutase 1 (SOD-1) and SOD-2.<sup>365</sup> But, TAK715 is a p38 $\alpha$  MAPK inhibitor, as a result, it inhibits p38 $\alpha$  MAPK-induced expression of the anti-oxidant genes. On the other hand, bulk RNAseq data shows TAK715 also down-regulates Nrf-2 expression. Nuclear factor-E2-related factor 2 (Nrf2) is a redox-sensing transcription factor, governing antioxidant response element (ARE), that drives an adaptive cellular defense in response to oxidative stress by driving the expression of numerous cytoprotective genes involved in antioxidant responses such as

superoxide dismutase.<sup>366,367</sup> Previous studies have suggested that p38MAPK signaling activates Nrf-2.<sup>368</sup> So, Nrf-2 downregulation leads to an enhanced accumulation of ROS that causes oxidative stress. This causes an alteration of mitochondrial dynamics that leads to the collapse of mitochondrial membrane potential due to oxidative stress and the release of cytochrome C from the mitochondria. This leads to the activation of the intrinsic pathway of apoptosis. Excessive oxidative stress also causes DNA damage that leads to cell cycle arrest and apoptosis.<sup>369</sup> On the other hand, TAK-715 inhibits the phosphorylation-mediated ATF-2 activation, which causes its ubiquitination-mediated degradation and prevents its nuclear translocation. HES-1 has an ATF-2 binding site on its promoter. So, the down-regulation of ATF-2 may lead to the transcriptional down-regulation of HES-1, which ultimately leads to the depletion of stem-like cells.

## **CHAPTER 4**

### **Validation of Secondary Therapies Against Mantle Cell Lymphoma**

**In silico Prediction Followed By In Vitro  
validation Identifies a Survivin Inhibitor and  
an MCL-1 Inhibitor As Potent Secondary  
Drug Against Refractory or Relapsed Mantle  
Cell Lymphoma**

## **Abstract**

Mantle cell lymphoma (MCL) is an aggressive lymphoid neoplasm that develops from malignant B-lymphocytes in the outer edge or mantle zone of a lymph node. This is a sub-type of B-cell non-Hodgkin lymphoma characterized by rapid clinical progression and poor response rate to conventional chemotherapeutic drugs with recurrent relapse resulting in a short estimated 5-year overall survival (OS) of 2-5 years depending on the clinical risk. Combination therapies such as R-CHOP, R-DHAP, Hyper-CVAD, and VcR-CAP constitute the front-line chemotherapeutic treatment landscape for MCL. Despite good initial responses to the combination regimens, all patients develop resistance over time. The Bruton's tyrosine kinase inhibitor (BTKi) Ibrutinib and the proteasome inhibitor (PI) Bortezomib are FDA-approved therapies for refractory or relapsed (R/R) MCL with demonstrated high initial response rates in clinical trials. However, highly variable treatment response along with dose-limiting toxicities has limited the efficacy in real-world settings with the median progression-free survival (PFS) of <15 months and Overall of 1-2 years.

Thus, the identification of novel drugs that function either alone or as a combination to curb the oncogenic progression as well as to reduce drug-associated toxicities is of high clinical significance.

We have designed a novel optimization-regularization-based computational prediction algorithm called “secDrug” that uses large-scale pharmacogenomics databases like the GDSC1000 to identify novel secondary drugs for the management of treatment-resistant B-cell malignancies. We hypothesize that a combination of our predicted secDrugs with BTKi/ PI will be useful in curbing oncogenic progressions of R/R MCL and abrogate drug resistance through simultaneous inhibition of multiple oncogenic factors/pathways. When applied to BTKi/PI-resistant R/R MCL, the top predicted secondary drugs (secDrugs) were YM155 (Survivin inhibitor) and S63845 (selective MCL-1 inhibitor). Interestingly, both Survivin and MCL-1 are reported to be over-expressed in MCL, and their expression is strongly correlated with the oncogenic progression and survivability of the patients.

To validate our in-silico predictions, we performed in vitro cytotoxicity assays with the top predicted secDrugs (YM155 and S63845) as single agents (IC<sub>50</sub> for YM155 4.87±0.66 nM, for

S63845  $0.9 \pm 1.1$   $\mu\text{M}$ ) as well as in combination with BTKi/PI against a panel of MCL cell lines representing PI/BTKi sensitive, innate resistant (representing refractory MCL) and clonally-derived acquired resistant (representing relapsed MCL). Our results showed that the YM155 and S63845 exhibited significant synergistic cell killing activities (Combination index/ CI value of  $0.31 \pm 0.49$  as calculated using Chou-Talalay's CI theorem,  $\text{C.I.} > 1$  depicts synergism) alone and in combination with Bortezomib (PI) and Ibrutinib (BTKi), especially in R/R MCL cell lines. Further, our results also showed that both YM155 and S63845, in combination with BTKi/PI were able to significantly lower the effective dose of both BTKi/PI required to achieve desired therapeutic response by  $>12$  times (Dose Reduction Index or DRI for YM155 in the combination is  $15.87 \pm 4.93$ ; DRI for S63845 in combination is  $12.34 \pm 2.67$ ), thereby making the cell lines relatively more BTKi/PI sensitive. Next, we performed next-generation RNA sequencing analysis to identify mechanisms of secDrug action and synergy. Our Gene expression profiling and Ingenuity pathway analysis of the RNAseq data among YM155-treated MCL cell lines revealed eIF4-p70S6K signaling and mTOR signaling as the top canonical pathways.

Our study thus identified YM155 and S63845 as potential novel candidates for repurposing as secondary drugs in combination with BTKi/PI for the treatment of R/R MCL.

## Introduction

Mantle cell lymphoma (MCL) is an aggressive lymphoid neoplasm that develops from malignant B-lymphocytes in the outer edge or mantle zone of a lymph node.<sup>178</sup> MCL is a sub-type of B-cell non-Hodgkin lymphoma characterized by rapid clinical progression & poor response rate to conventional chemotherapeutic drugs with recurrent relapse resulting in a short estimated 5-year overall survival (OS) of 2-5 years.<sup>176,193,195</sup> Combination therapies such as R-CHOP, R-DHAP, Hyper-CVAD, and VcR-CAP constitute the front-line chemotherapeutic treatment landscape for MCL. Despite good initial response to the combination regimens, all patients develop resistance over time.<sup>179,185</sup> The Bruton's tyrosine kinase inhibitor (BTKi) Ibrutinib and the proteasome inhibitor (PI) Bortezomib (BTZ) are FDA-approved therapies for refractory or relapsed (R/R) MCL with demonstrated high initial response rate in clinical trials.<sup>163,200</sup> Majority of the patients either have an innate resistance to ibrutinib therapy or eventually acquire resistance, thus progressing into a more aggressive disease state.<sup>192,195</sup> BTZ was the first PI approved by FDA in 2006 as a second-line treatment for MCL patients.<sup>163</sup> However, the majority of the patients eventually develop PI/ BTKi-resistance over the course of treatment. The presence of stem-like cells with inherent drug-resistant phenotypes plays a major role in this.<sup>213</sup> Thus, despite the recent advancement, currently approved chemotherapeutic drugs have limited efficacy in real-world settings, thus making MCL an incurable disease with a median progression-free survival (PFS) of <15 months.<sup>370,371</sup> In this context, the identification of novel drugs that function either alone or as a combination to curb the oncogenic progression as well as to reduce drug-associated toxicities is of high clinical significance. We have designed a novel optimization-regularization-based computational prediction algorithm called “secDrug” to identify novel secondary drugs for the management of treatment-resistant B-cell malignancies. We hypothesize that a combination of our predicted secDrugs with BTKi/ PI will be useful in curbing oncogenic progressions of R/R MCL and abrogate drug resistance through simultaneous inhibition of multiple oncogenic factors/pathways. When applied to BTKi/PI-resistant R/R MCL, the top predicted secondary drugs (secDrugs) were YM155 (Survivin inhibitor) & S63845 (selective MCL-1 inhibitor). Interestingly, both Survivin & MCL-1 are reported to be over-expressed in MCL & their expression is strongly correlated with oncogenic progression & survivability of the patients.

## Results

### Single Cell transcriptomics (scRNAseq)-based secDrug screening

We used scRNAseq as a novel biomarker-based drug screen to identify single-cell sub-clones (represented by t-SNE clusters) in the untreated drug-sensitive and BTKi-resistant MCL cell lines representing sensitive, relapse, and/or refractory MCL that harbor secDrug target genes.

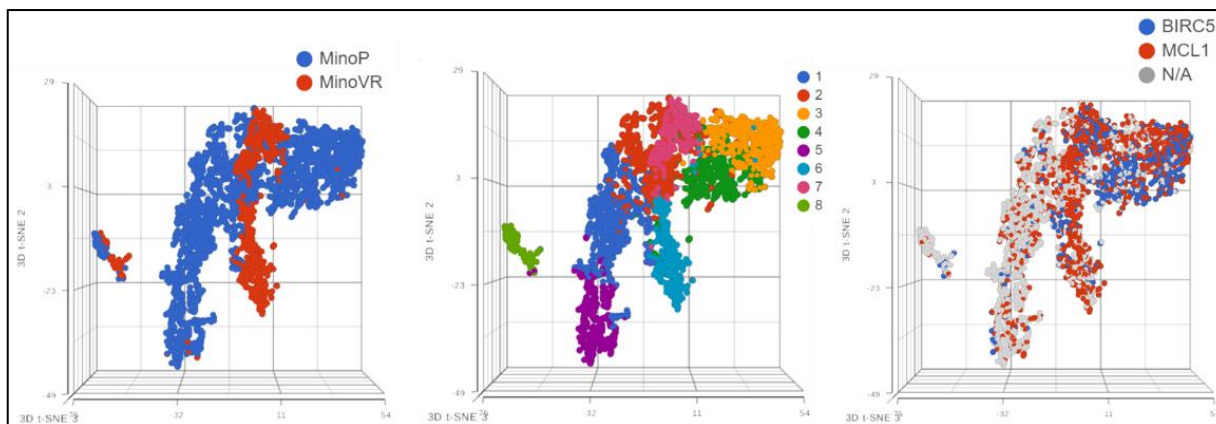


**Figure 1** shows a representative figure for the Mino sensitive/resistant pair where our scRNAseq data demonstrated that the majority of the single-cell clusters have high expression of YM155 target gene Survivin (BIRC5) and the S63845 target gene MCL1 indicating that the secDrugs YM155 and MCL1 may be effective against these subpopulation clusters.

### YM155 & S63845 inhibit human MCL cells proliferation

First, we evaluated the *in vitro* cytotoxic effect of YM155 & S63845 as single-agent against MCL cell lines representing drug-sensitive (JEKO1, MINO-P), PI-resistance (Mino-VR) and BTKi-resistance (Z-138) as *in vitro* model systems. We found that both YM155 & S63845 effectively reduced cell viability in all four MCL cell lines irrespective of PI/BTKi sensitivity/resistance. The median half-maximal inhibitory concentration ( $IC_{50}$ ) of single-agent YM155 & S63845 in human MCL cell lines were  $4.87 \pm 0.66$  nM, S63845  $0.9 \pm 1.1$  uM, respectively.

Figure 2A

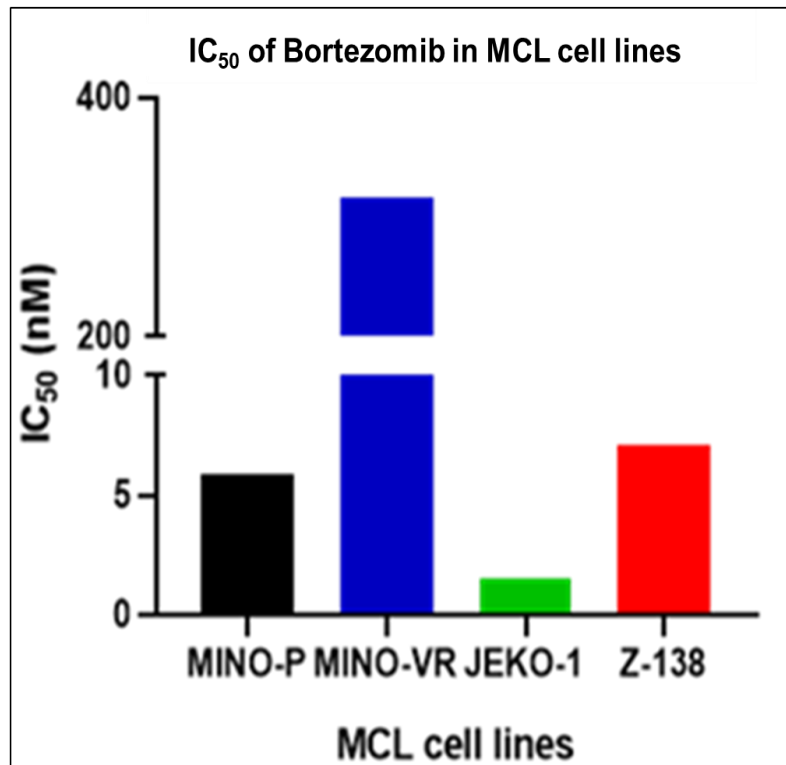
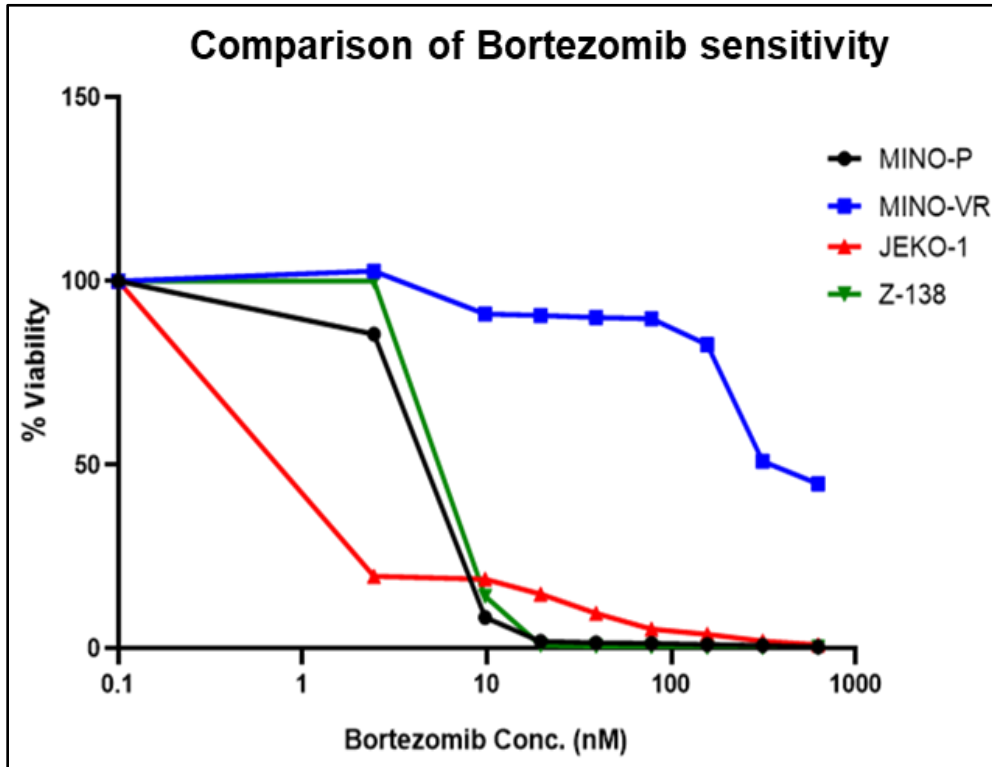


Figure 2B

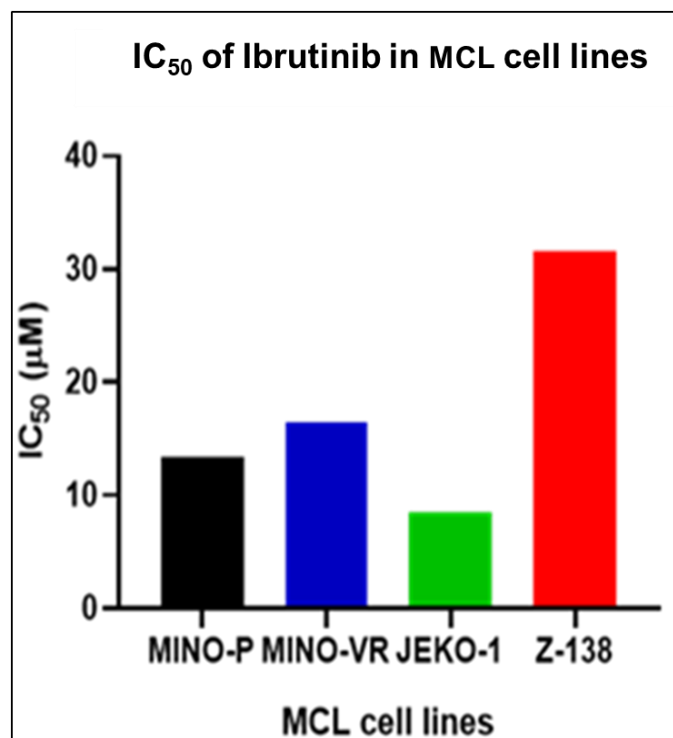
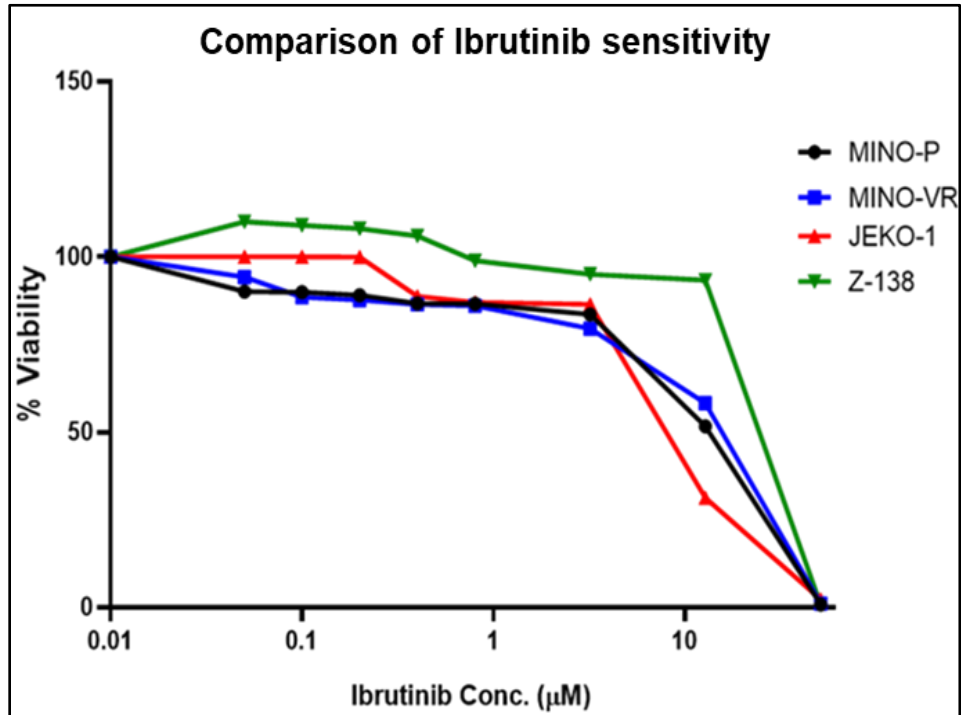


Figure 2C

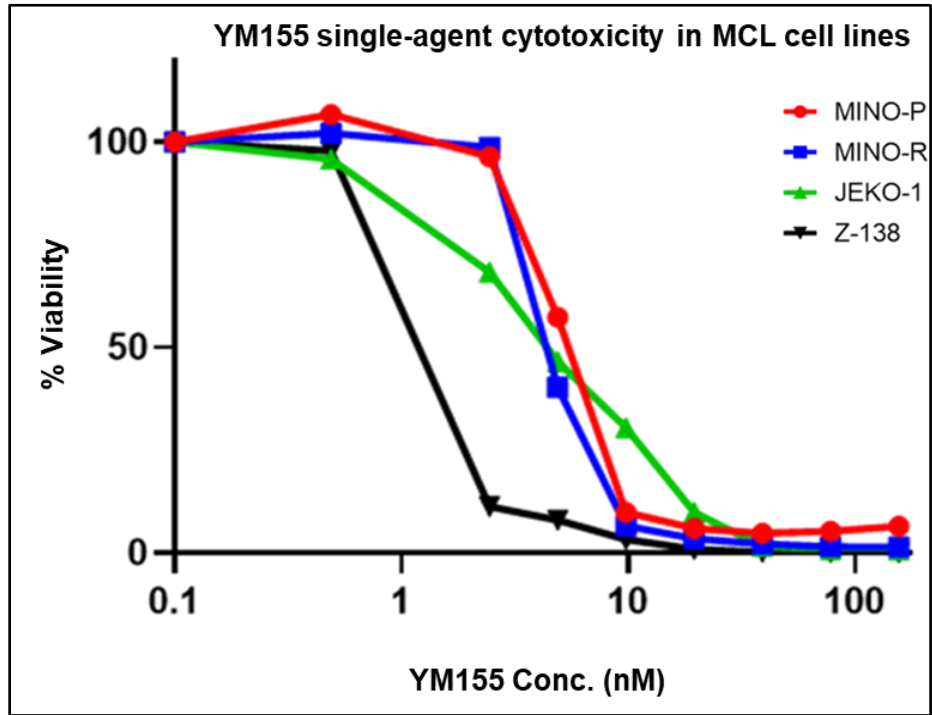
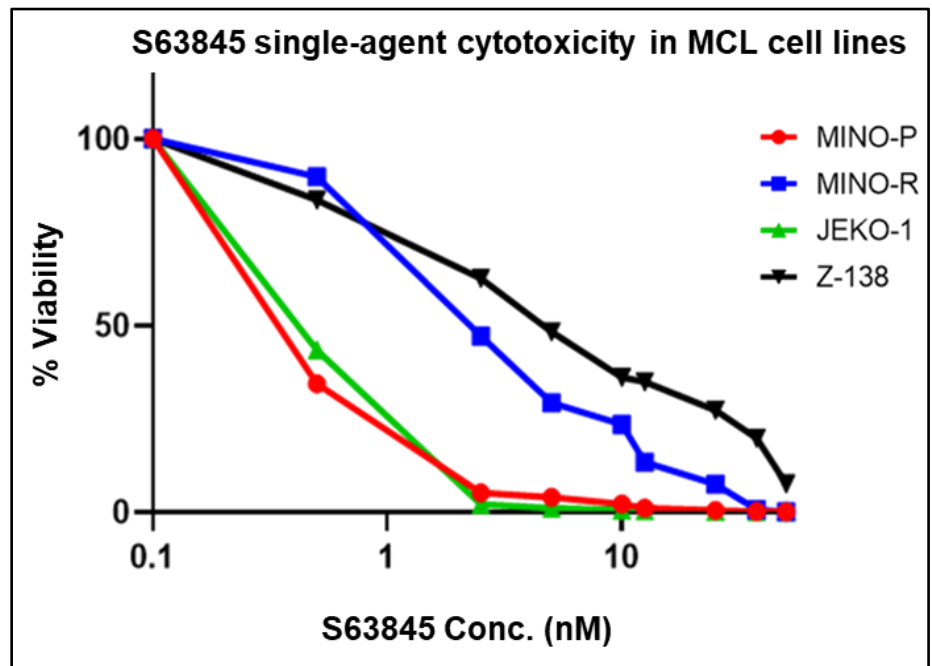


Figure 2D



**Figure 2. Single-agent cytotoxicity assay with PI & BTKi mirrors the extensive inter-individual variation in drug response in the MCL cell line panel.**

Dose-response curve reveals a wide range of drug sensitivity towards (Figure 2A) PI (Bortezomib/ BTZ) and (Figure 2B) BTKi (Ibrutinib/ IBR). MINO-VR has approx. 70 folds higher IC<sub>50</sub> value for Bortezomib than its parental cell line MINO-P. Z-138 has approx. 2.5 folds higher IC<sub>50</sub> value for Ibrutinib than MINO-P and JEKO-1. (Figure 2C) in vitro cell viability profile of YM155 single agent treatment in MCL cell lines. (Figure 2D) in vitro cell viability profile of S63845 single agent treatment in MCL cell lines. Both YM155 & S63845 showed high single-agent in vitro cytotoxicity in our MCL cell panel, including PI- resistant and BTKi-resistant MCL cell lines.

**YM155 & S63845 synergize with Proteasome inhibitors and BTK inhibitors**

Next, we investigated the impact of different concentrations of YM155 & S63845 in combination with an increasing range of Bortezomib (PI) or Ibrutinib (BTKi). We observed that all the combination treatment regimens showed higher cytotoxic effects compared to single-agent PI or BTKi treatment.

For drug synergy analysis, Combination Index (CI) values were calculated in CalcuSyn Software by using the Median Effect methods as described in Chou-Talalay's CI theorem combination index (C.I) theorem. The Combination Index (CI) value < 1 depicts synergism, CI value = 1 refers to additive effect, and CI value > 1 depicts antagonism for the drugs in combination.

Our results showed that the YM155 and S63845 exhibited significant synergistic cell killing activities (Combination index/ CI value of  $0.31 \pm 0.49$  as calculated using Chou-Talalay's CI theorem, C.I>1 depicts synergism) alone and in combination with Bortezomib (PI) and Ibrutinib (BTKi), especially in R/R MCL cell lines. Most of the combinations have shown synergy (i.e., C.I value<1.0). Synergistic effects were particularly profound in MINO-VR & Z-138. This observation is particularly relevant as they represent the acquired PI resistance and innate BTKi resistance. Similar data were obtained when we combined another BTKi (Acalabrutinib) with CLF.

Further, our results also showed that both YM155 and S63845 in combination with BTKi/ PI were able to significantly lower the effective dose of both BTKi/PI required to achieve desired

therapeutic response by >12 times (Dose Reduction Index or DRI for YM155 in the combination is  $15.87 \pm 4.93$ ; DRI for S63845 in combination is  $12.34 \pm 2.67$ ), thereby making the cell lines relatively more BTKi/PI sensitive.

**Figure 3A**

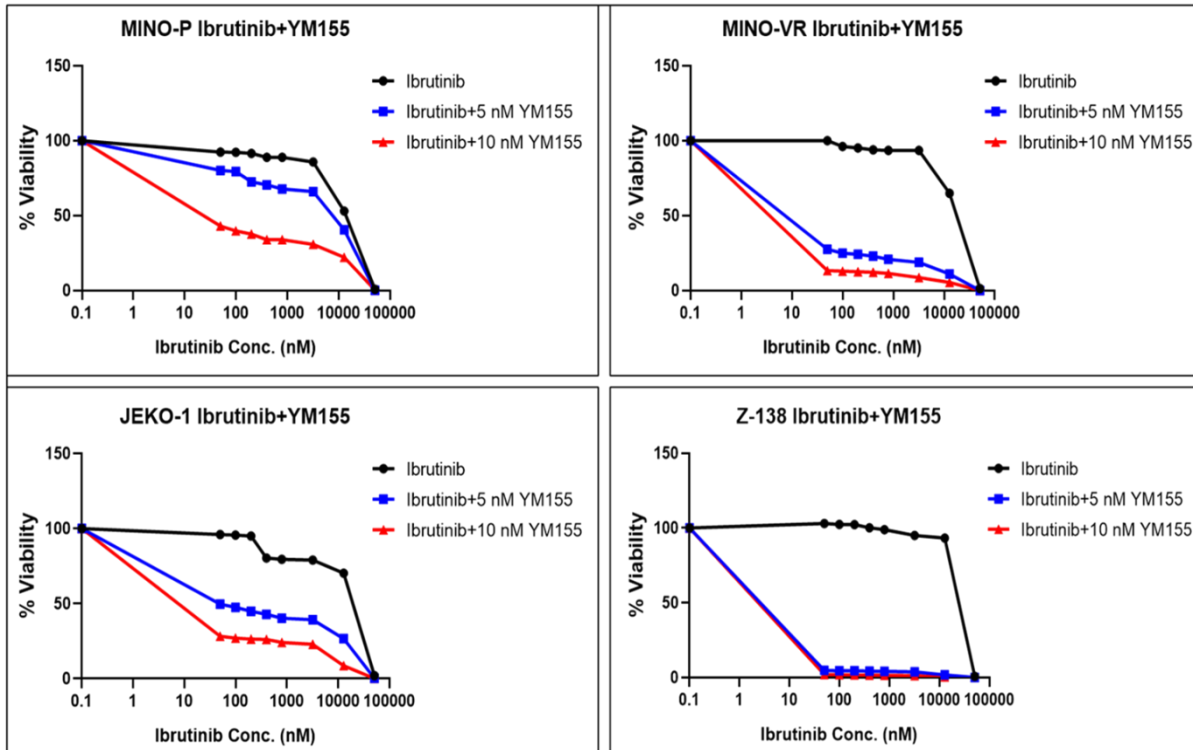


**Figure 3B**

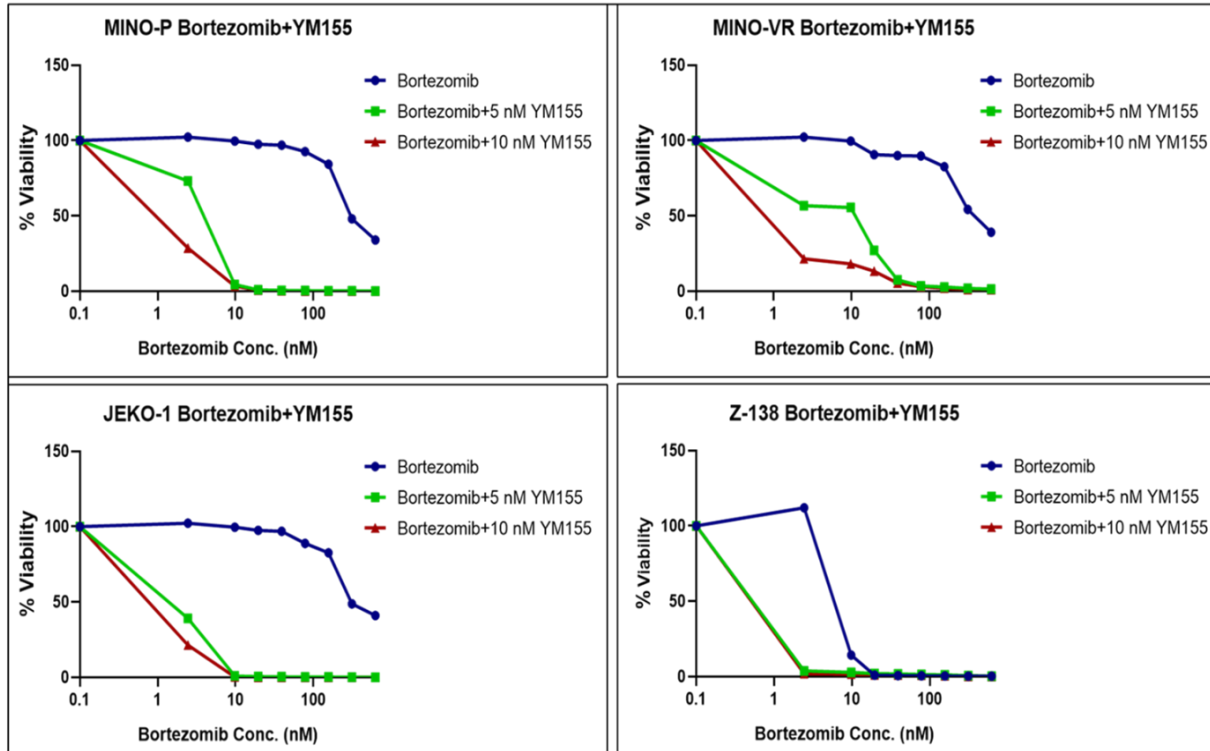


**Figure 3C**

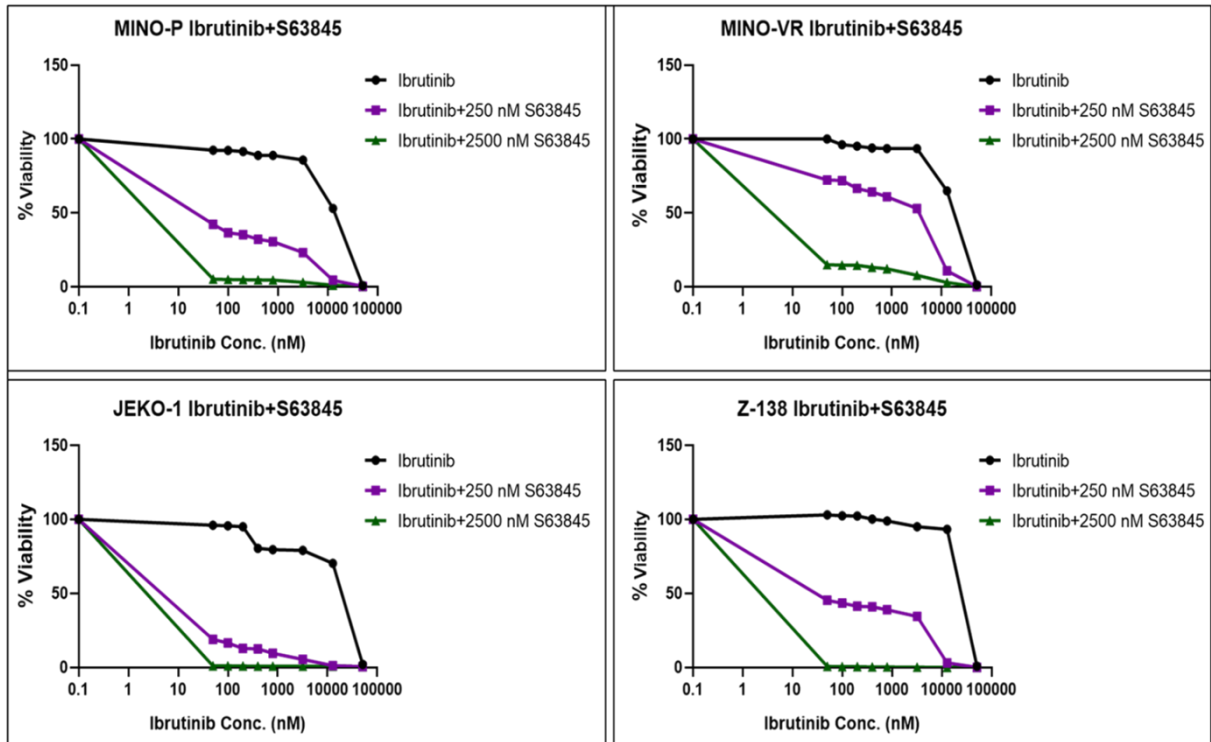


Figure 3D

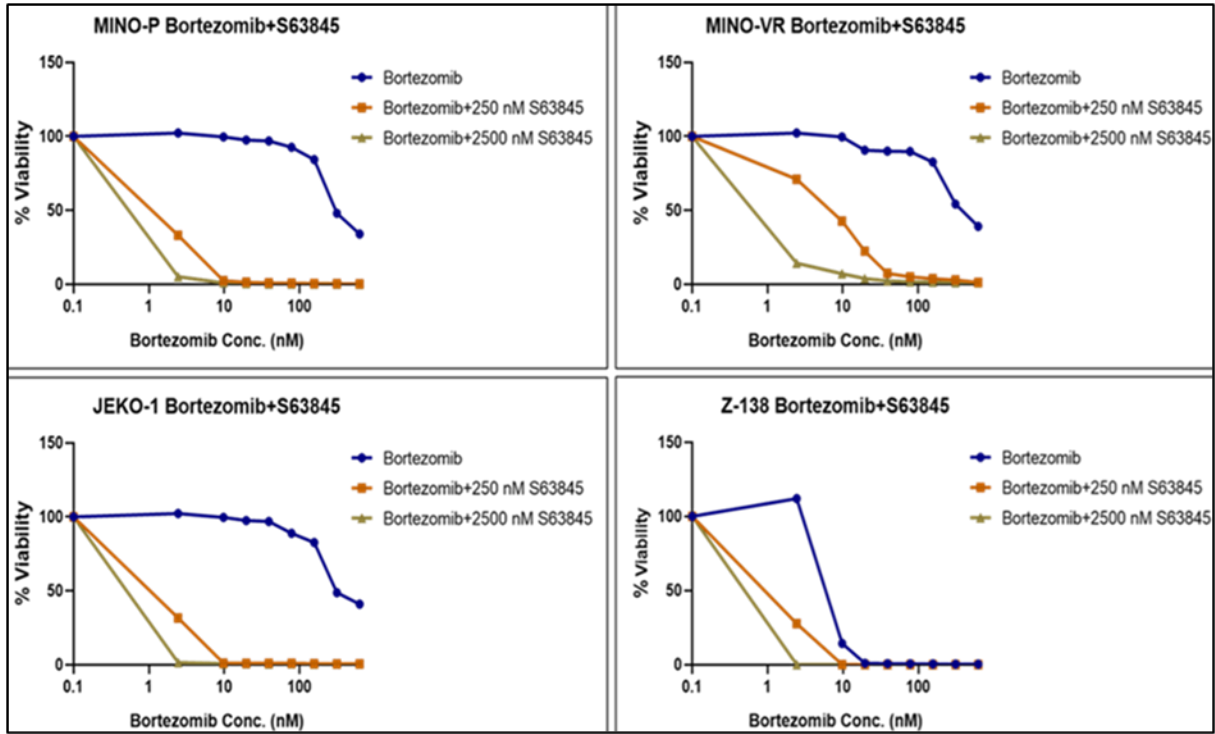
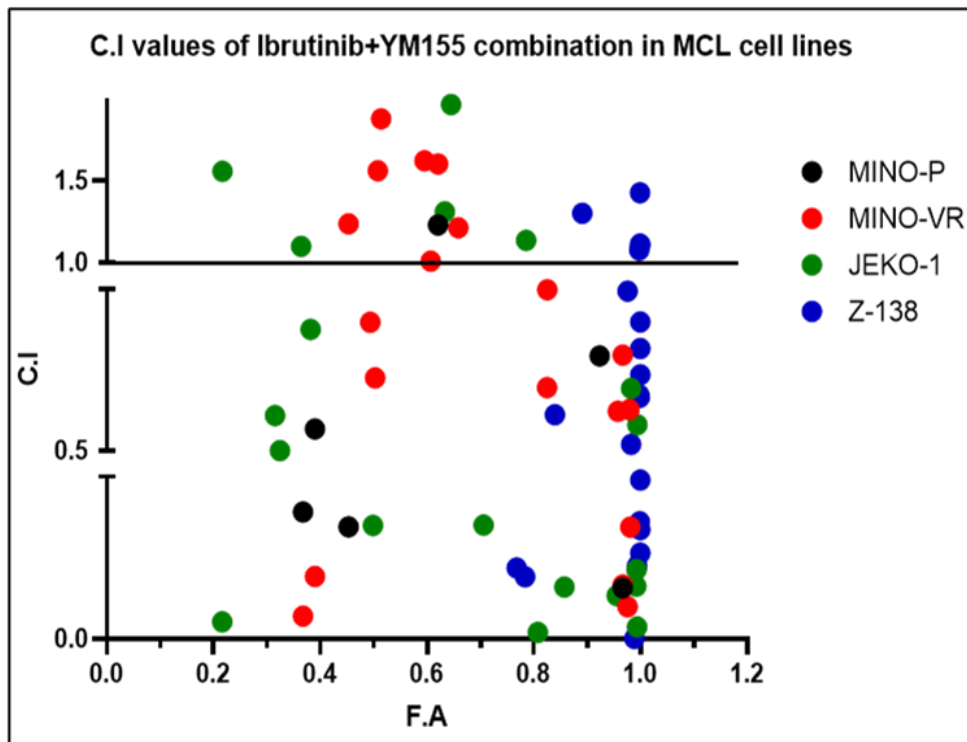
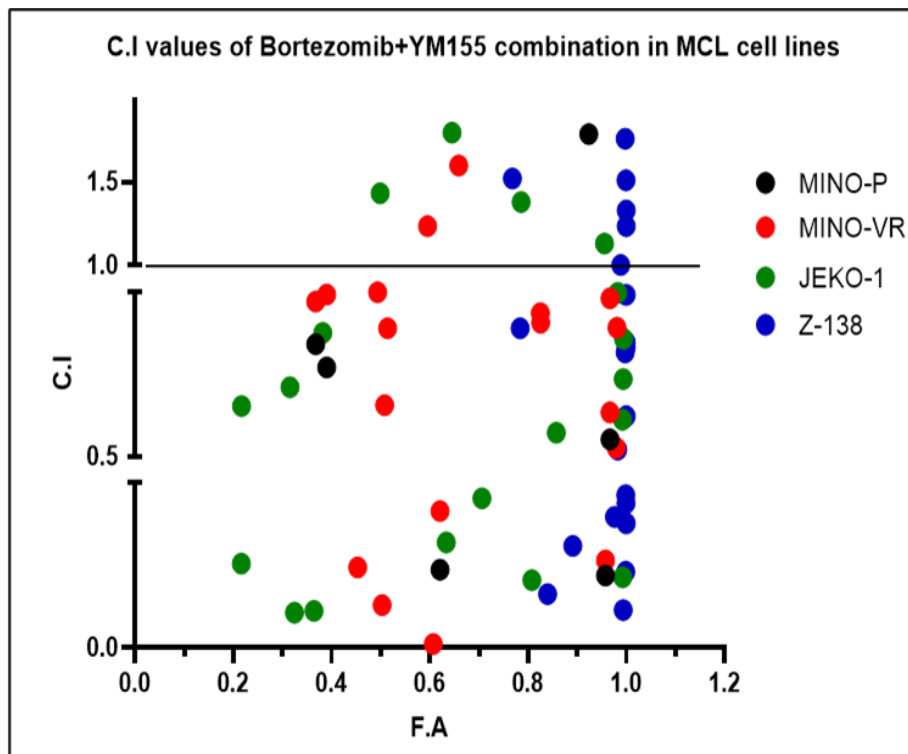


Figure 3E



**Figure 3F**



**Figure 3. YM155 & S63845 synergistic cell killing activity with PI & BTKi.** Figure 3A-D represents in vitro cell viability profile of MCL cell lines, including PI- resistant and BTKi-resistant MCL cell lines treated with different combinations of YM155 & S63845 with PI/ BTKi. All the combinations showed significant improvement in lowering cellular proliferation as compared to the effect of PI/ BTKi alone, which indicates drug synergy. We further quantitate the extent of synergistic action by CalcuSyn Software (BioSoft, USA) that calculates Combination Index (C.I) as a function of fraction affected based on Chou-Talalay's Combination Index (C.I) theorem. Most of the combinations have shown synergy (i.e., C.I value < 1.0). Synergistic effects were particularly profound in MINO-VR & Z-138. This observation is particularly relevant as they represent the acquired and innate resistance, respectively. (Figure 3E-F)

### **YM155 & S63845 down-regulate Survivin & Mcl-1 respectively in MCL cells**

Next, we validated the on-target effect of YM155 and S63845 in MCL cells by western blot. We observed that YM155, which is a known Survivin inhibitor, indeed down-regulates the

expression of Survivin in resistant MCL cell line Mino-VR. S63845 also suppresses the expression of its target, Mcl-1. This proves that these two drugs exert their anti-cancer effect by targeting their respective target in MCL cells.

**Figure 4A**

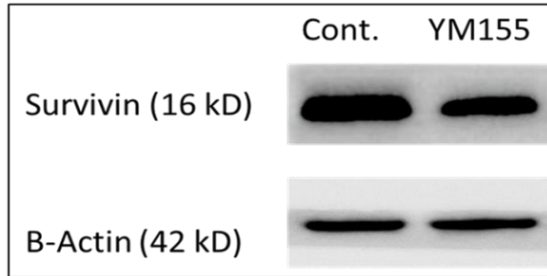


**Figure 4B**

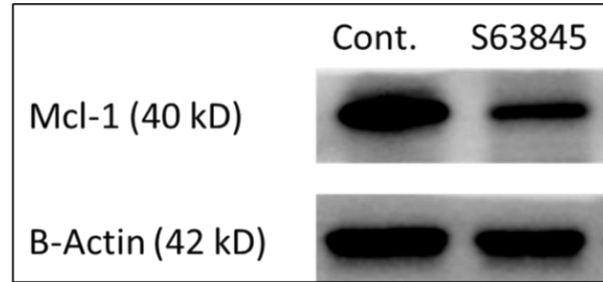


**Figure 4.** YM155 & S63845 drug target validation. YM155 & S63845 significantly down-regulate Survivin and Mcl-1 expression respectively, in MCL cells (Z-138)

**YM155 & S63845 combination has a synergistic effect in resistant MCL cell line**

Further, we explored whether these two secDrugs have any synergistic cell-killing action in MCL cells by in-vitro cytotoxicity assay and then calculated the synergy score using the Bliss independence model. We observed that in BTKi-resistant cell line Z-138, the constant ratio combination of YM155 and S63845 shows significant synergy (Bliss synergy score  $12.915 \pm 0.9$ ), which further validates Survivin and Mcl-1 targeting approach for the management of drug-resistant MCL.

**Figure 5**

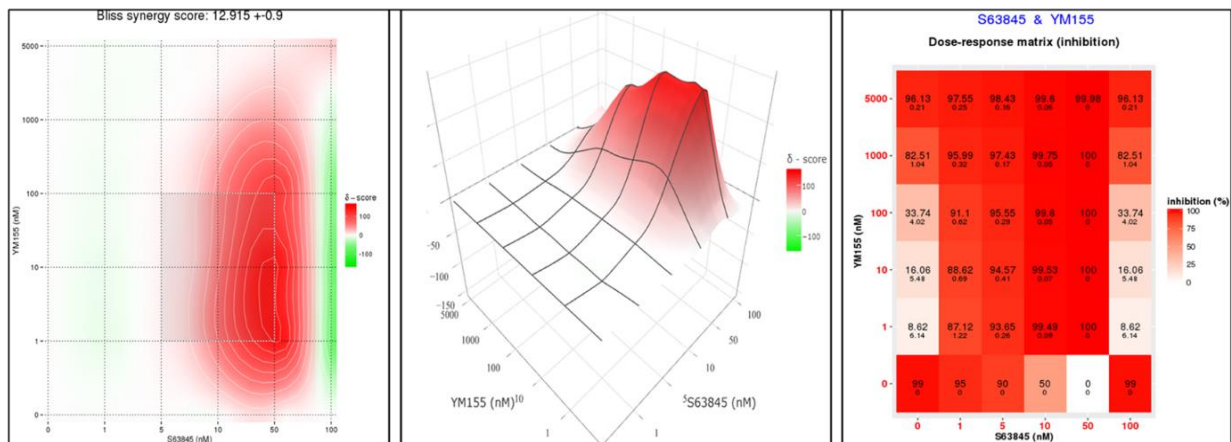


**Figure 5.** Visualization of the interactive analysis of multi-drug combination (YM155 & S63845) profiling data. The significance of the YM155 & S63845 drug combination was measured using the Bliss independence model. From our data, it is evident that the YM155-S63845 combination has synergistic activity (>10 Bliss synergy score signifies synergistic drug action) in resistant MCL cells Z-138 (representative Figures).

**Top predicted secDrugs augment apoptosis in sensitive as well as resistant MCL cells**

The quantitative analysis of the extent of apoptosis in Mantle Cell Lymphoma cells in response to CLF single agent-treatment and CLF+PI/BTKi treatment was done using Fluorescein isothiocyanate (FITC) conjugated Annexin-V staining followed by flow cytometry. The data shows a significantly higher population of cells are Annexin-V positive, which is an indicator of apoptosis in combination treatment as compared to single agent treatment in sensitive cell line Mino-P as well as in PI-resistant cell line Mino-VR (Figure 6A-B) and BTKi-resistant cell line Z138 (Figure 6B-C) indicating a significantly elevated level of induction of apoptosis in those cells. This further proves the synergistic activity of the drug combination.

**Figure 6A**

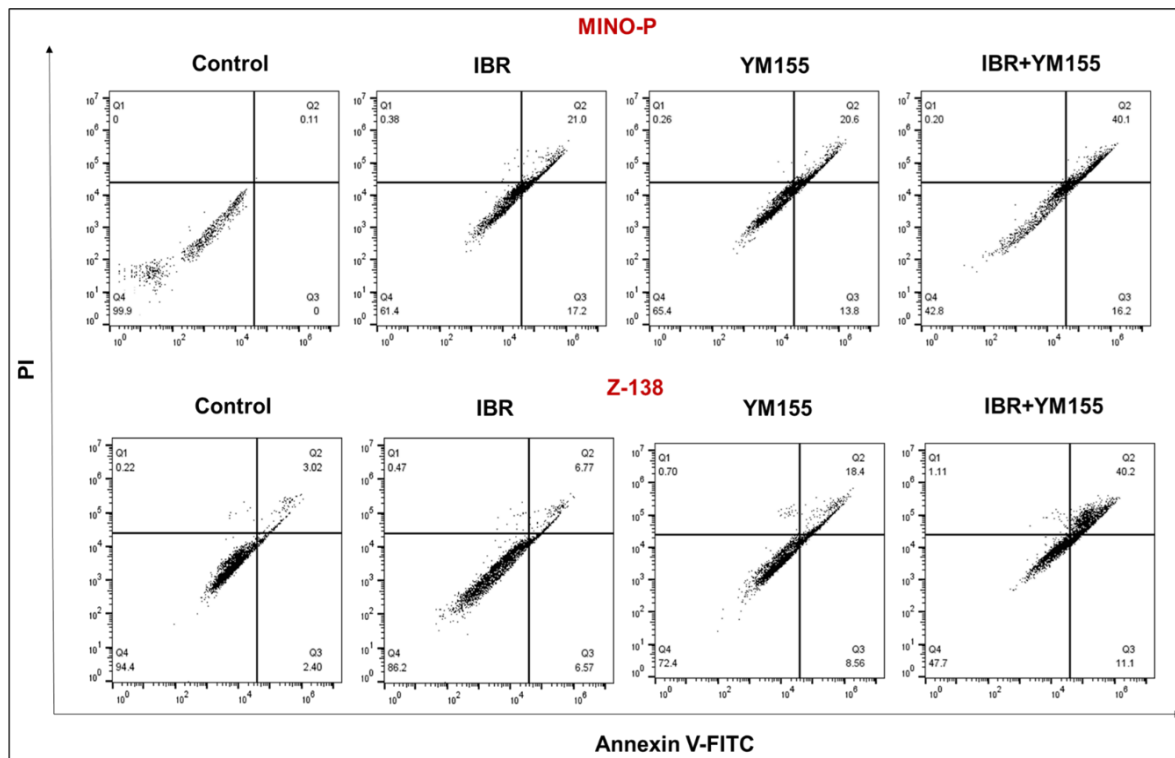


Figure 6B

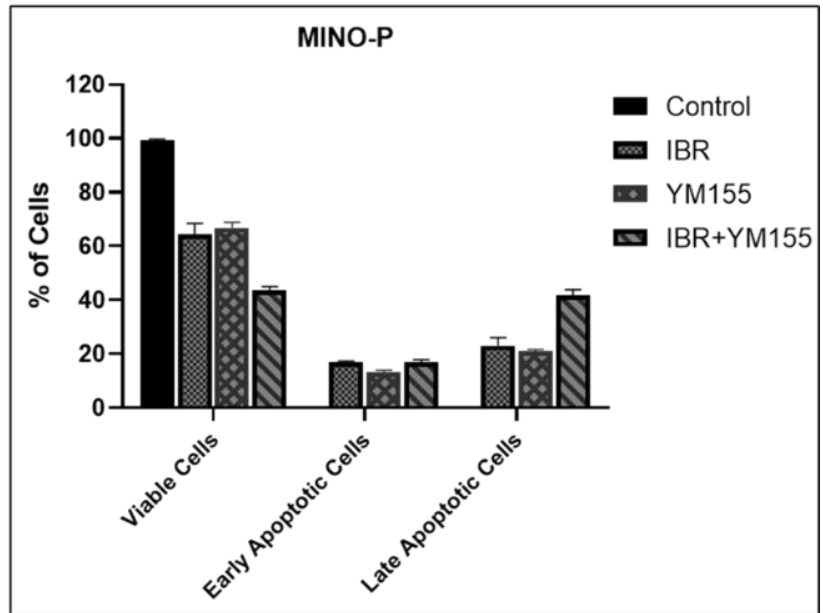
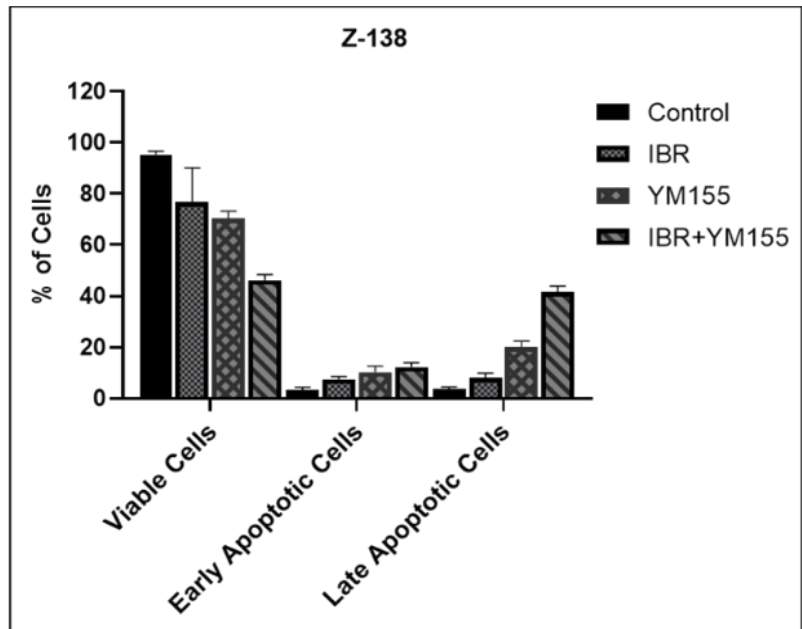
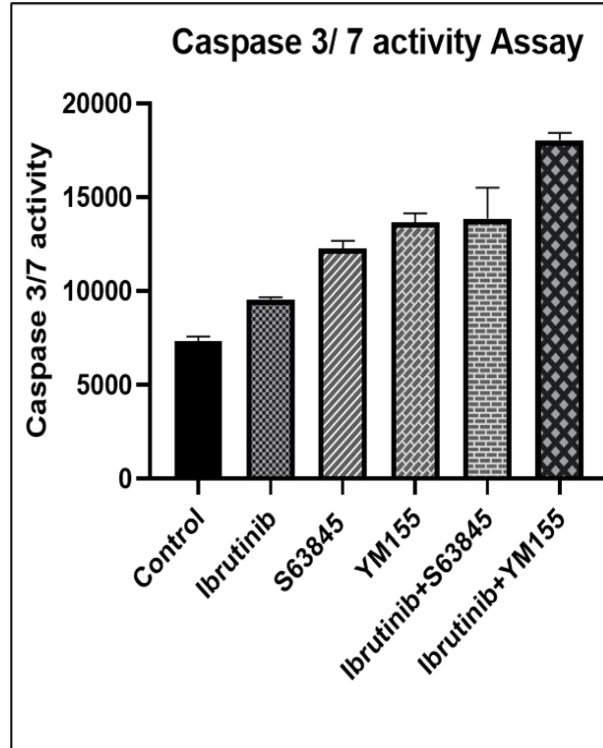


Figure 6C



**Figure 6D**



**Figure 6. Quantitative measurement of the % of the apoptotic MCL cells (Annexin-V positive) exposed to secDrug (YM155) single agent and secDrug+ BTKi combination treatment by flow cytometry. Figure 6A-C shows a significantly higher population of cells that are Annexin V positive in combination treatment as compared to single agent treatment indicating an elevated level of induction of apoptosis which was further confirmed by elevated cleaved caspase 3/7 activity (Figure 6D). This suggests that the drug combination worked in synergy to induce apoptosis.**

#### **YM155 reduces the adhesion of MCL cells to bone marrow stromal cells**

Previous studies have reported that bone-marrow stromal cells have a protective effect on the MCL cells against the chemotherapeutic agent. So, we check whether our top secDrugs are able to inhibit the adhesion of MCL cells to the bone marrow stromal cells. We did a co-culture of bone marrow stromal cells HS-5, and calcein AM stained MCL cells. MCL cells were pre-treated with YM155 for the indicated period of time before seeding on the top of HS-5 cells. Then, we washed out any loosely attached cells and took the reading of the bound cells. Data shows

YM155 was more effective than PI in inhibiting cellular adhesion of resistant MCL cells to HS-5 cells.

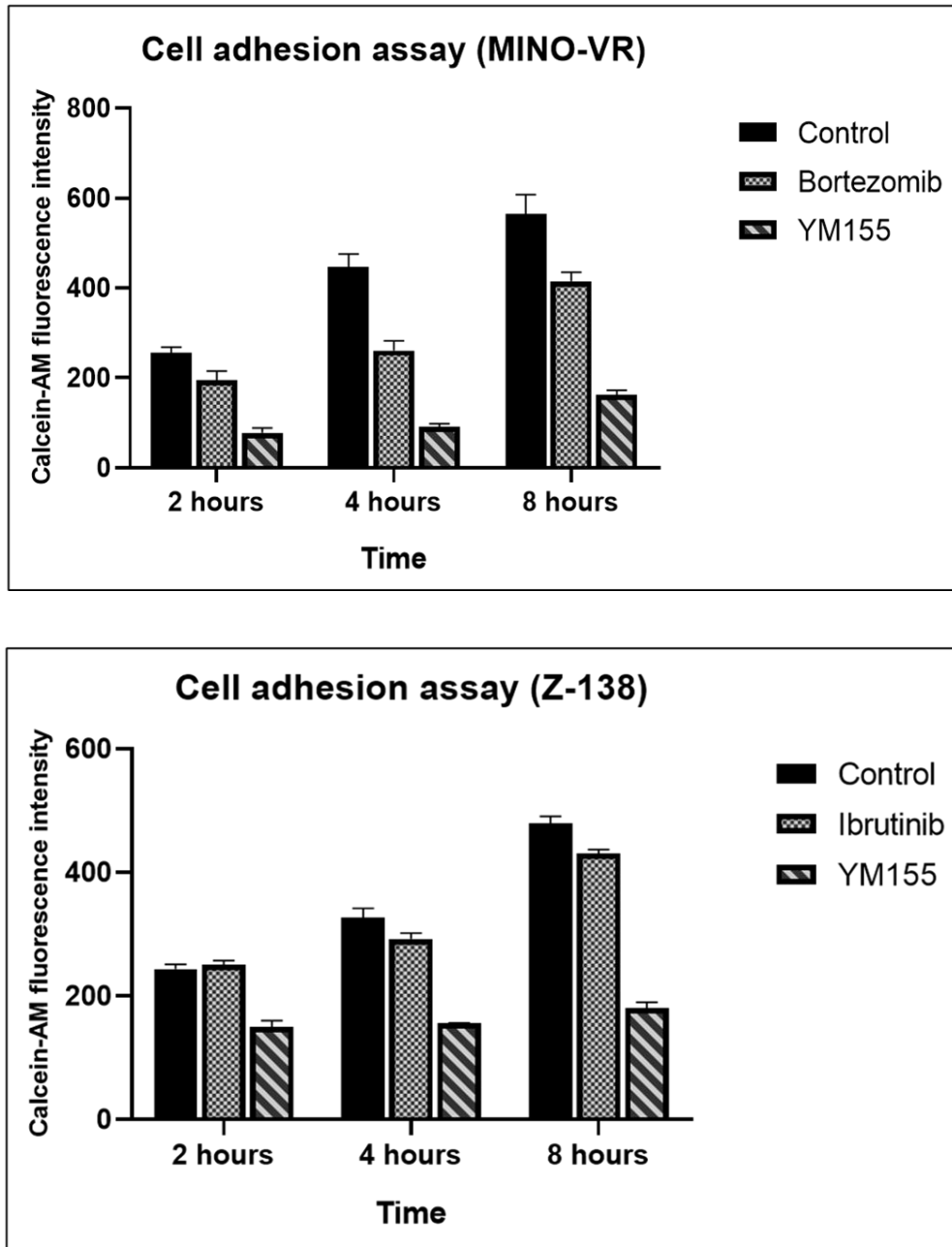


**Figure 7. YM155 inhibits cellular adhesion of MCL cells to the bone marrow stromal cells (HS-5).** We co-cultured bone-marrow stromal cells HS-5 and Calcein AM stained MCL cells. MCL cells were pre-treated with YM155 for an indicated period before seeding on the top of

HS-5 cells. Data shows YM155 was more effective than PI & BTKi in inhibiting cellular adhesion of resistant MCL cells to HS-5 cells.

### **YM155 targets cancer stem cells in MCL and reduces their ALDH activity**

As both YM155 and S63845 have reported activity against cancer stem-ness, we further investigated the effect of our novel drugs on the cancer stem-like cells (CSCs) in MCL, which have a potential role in treatment resistance. ALDH (aldehyde dehydrogenase) is an intra-cellular detoxification enzyme frequently over-expressed in CSCs and involved in drug resistance. We observed >4 times higher ALDH activity in the PI and BTKi-resistant MCL lines (MINO-VR – 11.7% ALDH activity, data not shown here and Z-138 – 10.4%, respectively) compared to the drug-sensitive MCL lines (Figure 8A, 8C). YM155 single-agent treatment led to a considerable decrease in ALDH activity in both MINO-VR (data not shown here) and Z-138 cells (Figure 8B-C) (approx. 68% and 91% reduction, respectively, as compared to the control).

**Figure 8A**

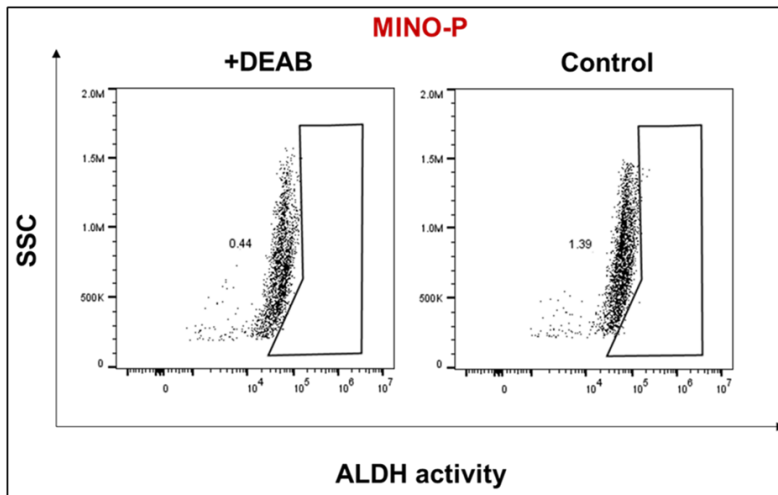


**Figure 8B**

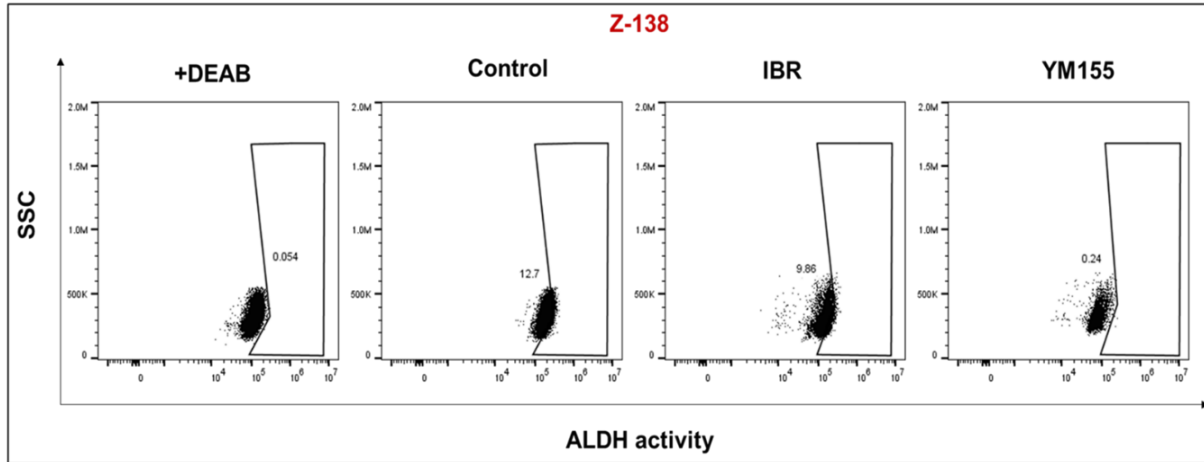


**Figure 8C**

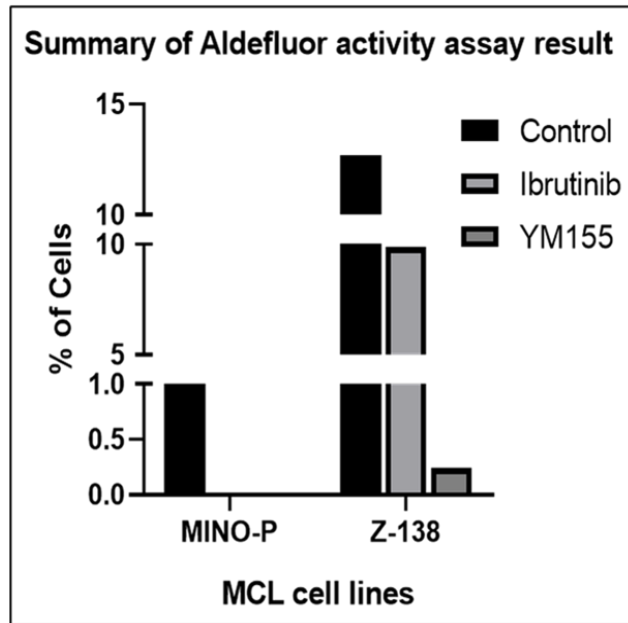


**Figure 8. Measurement of Aldehyde dehydrogenase (ALDH) activity in drug-resistant MCL cells.** Very low ALDH activity was observed in the PI/ BTKi sensitive cell line MINO-P (Figure 8A). It is found to be considerably higher in the innate BTKi-resistant Z-138 cell line (Figure 8B) & clonally derived PI-resistant MCL cell line MINO-VR (data not shown here), indicating the presence of a ‘stem-like phenotype.’ YM155 as a single agent led to a significant decrease in ALDH activity (>90%) in drug-resistant cells as compared to the Bortezomib single agent treatment (data not shown here) and Ibrutinib single agent treatment ( ~ 29%) (Figure 8B).

## Gene expression profile reveals the mechanism of action of YM155 in MCL cells

Differential gene expression analysis (ANOVA) of YM155 treatment-induced changes (baseline (untreated) vs. single-agent YM155 drug treatment) in PI-sensitive and PI-resistant MCLs showed a total of 143 genes were differentially expressed (DE) with ( $p < 0.05$ ; fold-difference  $\neq 1$ ). Among these, 38 genes had a  $|\text{fold-change}| \geq 2$ . 233 genes were common between the Treated vs. Untreated signatures at  $|\text{fold-change}| > 1$  ( $p < 0.05$ ). Figure 9A shows a heat map of the top DE genes. The Venn diagram (Figure 9B) shows the single-agent Bortezomib and YM155-induced kinetic changes separately for sensitive-resistant cell line pair Mino-P and Mino-VR. The Venn diagram (Figure 9C) shows the single-agent Ibrutinib and YM155-induced kinetic changes separately for sensitive-resistant cell line pair Mino-P and Mino-VR.

**Figure 9A**

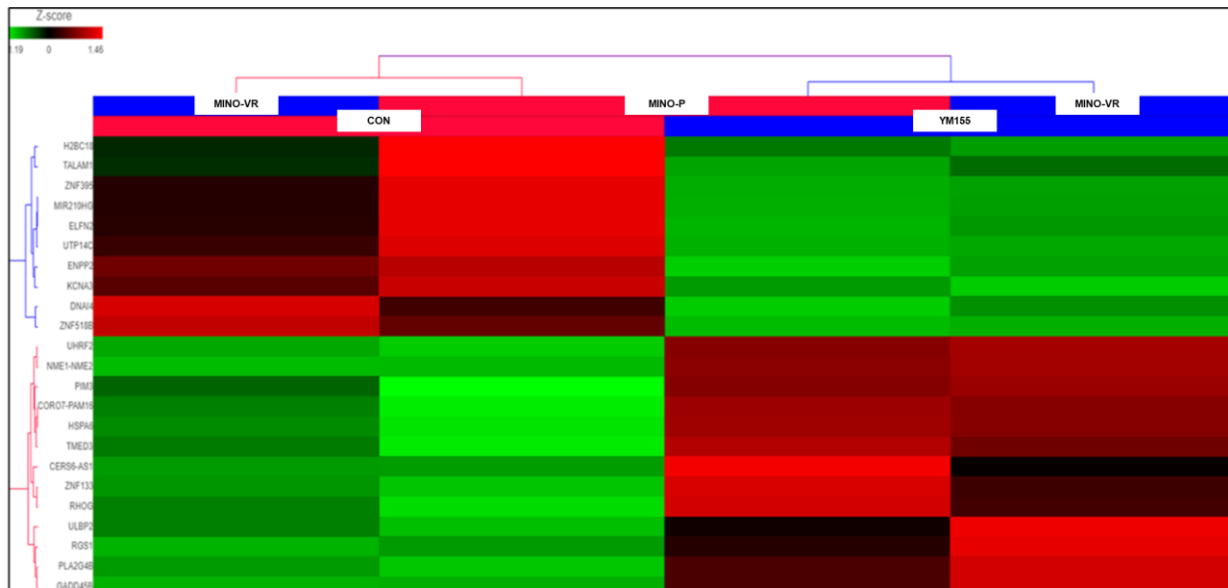


Figure 9B

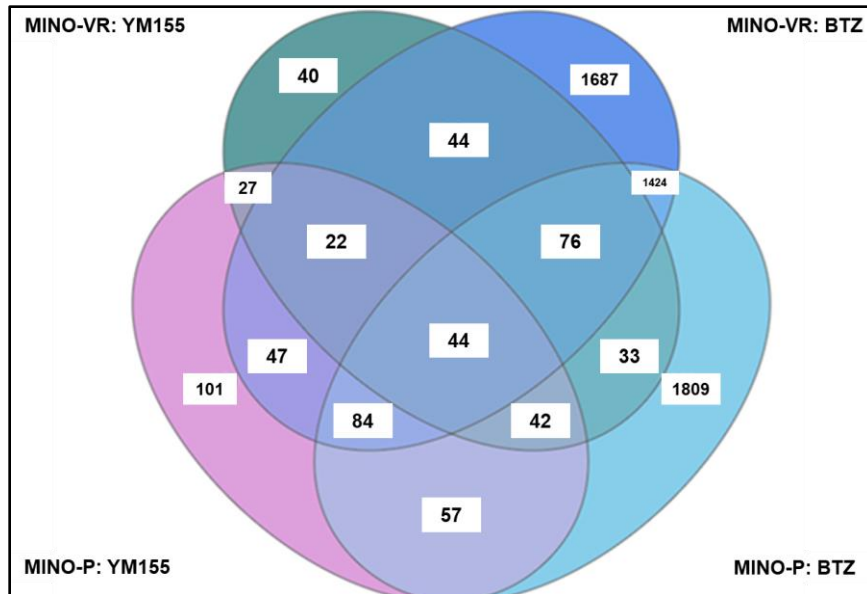


Figure 9C

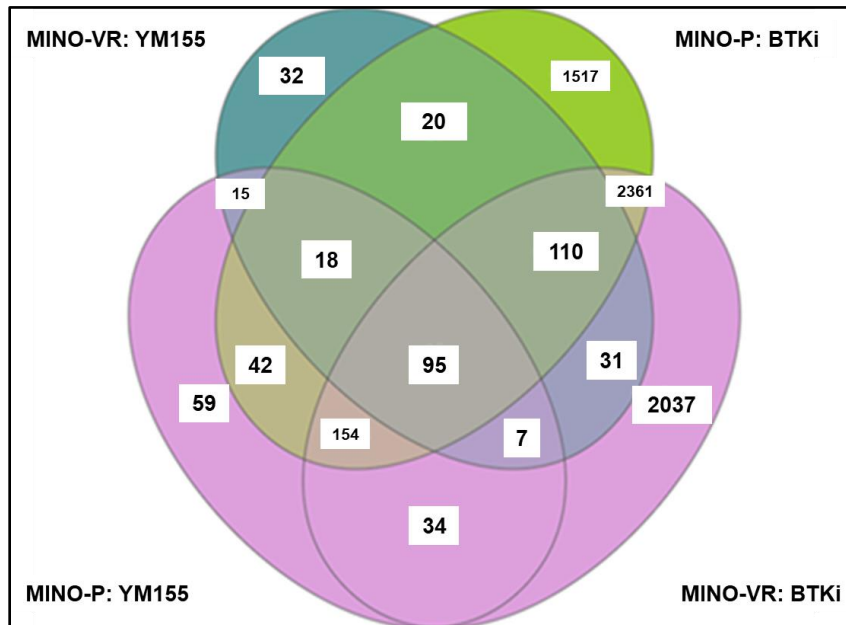
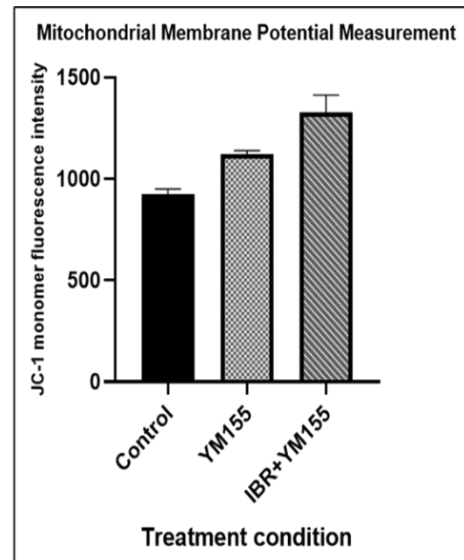


Figure 9. Heat map of the differential gene expression profile obtained from NGS-based RNA-seq analysis of the YM155 treated MCL cell lines to elucidate the underlying mechanism of drug action. YM155 treated cells have 143 uniquely differentially expressed genes ( $p < 0.05$ ; fold-difference  $\geq 2$ ) as compared to the untreated cells (baseline expression).

### IPA reveals top differentially regulated canonical pathways in YM155-treated MCL cells

Ingenuity pathway analysis revealed YM155-treated MCL cell lines revealed eIF4-p70S6K signaling and mTOR signaling as the top canonical pathways. The other top differentially regulated pathway was mitochondrial dysfunction which we have validated by measuring the mitochondrial membrane potential using JC-1 dye. JC-1 is a cationic carbocyanine dye that accumulates in mitochondria. The dye exists as aggregates at higher potential. A decrease in the red/green fluorescence indicates mitochondrial depolarization, which causes the JC-1 dye to become monomers from its aggregate form. We observed a significant shift from red to green fluorescence in response to YM155 single-agent treatment as well as in combination with Bortezomib indicating enhanced mitochondrial dysfunction or mitochondrial depolarization due to loss of mitochondrial membrane potential

Top Canonical Pathways	
Name	p-value
EIF2 Signaling	4.28E-07
Regulation of eIF4 and p70S6K Signaling	1.98E-05
mTOR Signaling	7.94E-05
Mitochondrial Dysfunction	4.64E-04
Dopamine Receptor Signaling	1.15E-02



**Figure 10. Ingenuity pathway analysis (IPA) of YM155-induced differentially expressed genes.** IPA reveals YM155-induced key canonical pathways such as mTOR signaling & Mitochondrial dysfunction (Figure 10A), which was further validated by measuring the mitochondrial membrane potential post-YM155 treatment (Figure 10B). The increase in JC-1 monomer intensity suggests mitochondrial depolarization that leads to mitochondrial dysfunction.

## Top differentially expressed genes have a significant association with Overall survival and Disease-Free Survival

Next, we validated the top DE genes expressed in YM155 treated vs untreated control cells using TCGA's Diffuse Large B-Cell Lymphoma (DLBC) GEP dataset Kaplan-Meier Curves showed that the top DE genes DNTT (Figure 11A) and AK8 (Figure 11B) were significantly associated with clinical outcome, i.e., overall survival and disease-free survival. YM155 up-regulates the expression of the DNTT gene and down-regulates the expression of the AK8 gene.

**Figure 11A**

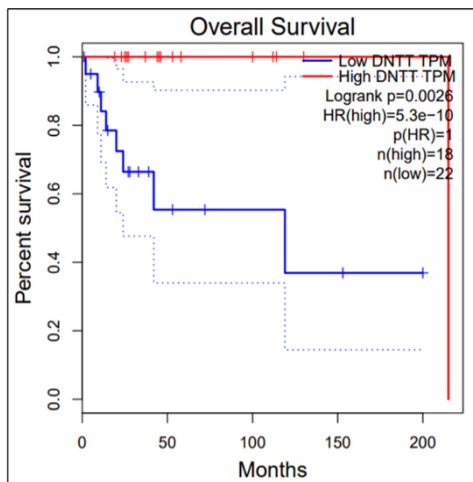


**Figure 11B**

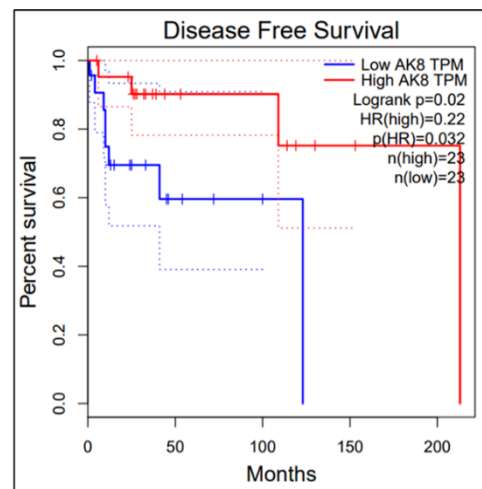


**Figure 11. YM155 treatment induced differential regulation of genes associated with patient survival. DNTT (DNA nucleotidylexotransferase) & AK8 (Adenylate Kinase 8) are up-regulated in response to YM155.** It is reported that all cases of mature B-cell malignancies are DNTT negative. On the other hand, AK8 is associated with metabolic signaling in cancer cells.

### Validation of YM155 treatment-related gene signatures using patient cohort datasets

Reverse-matching using patient cohort datasets show that YM155 treatment has the potential to reverse MCL lethality. Pathway analysis was performed based on the top DEGs in the Ibrutinib-sensitive and resistant MCL patient cohort (Figure 12A), and Top YM155 treatment-induced upregulated pathways (Figure 12B) that were significantly downregulated in Ibrutinib-resistant MCL patients.

Figure 12A

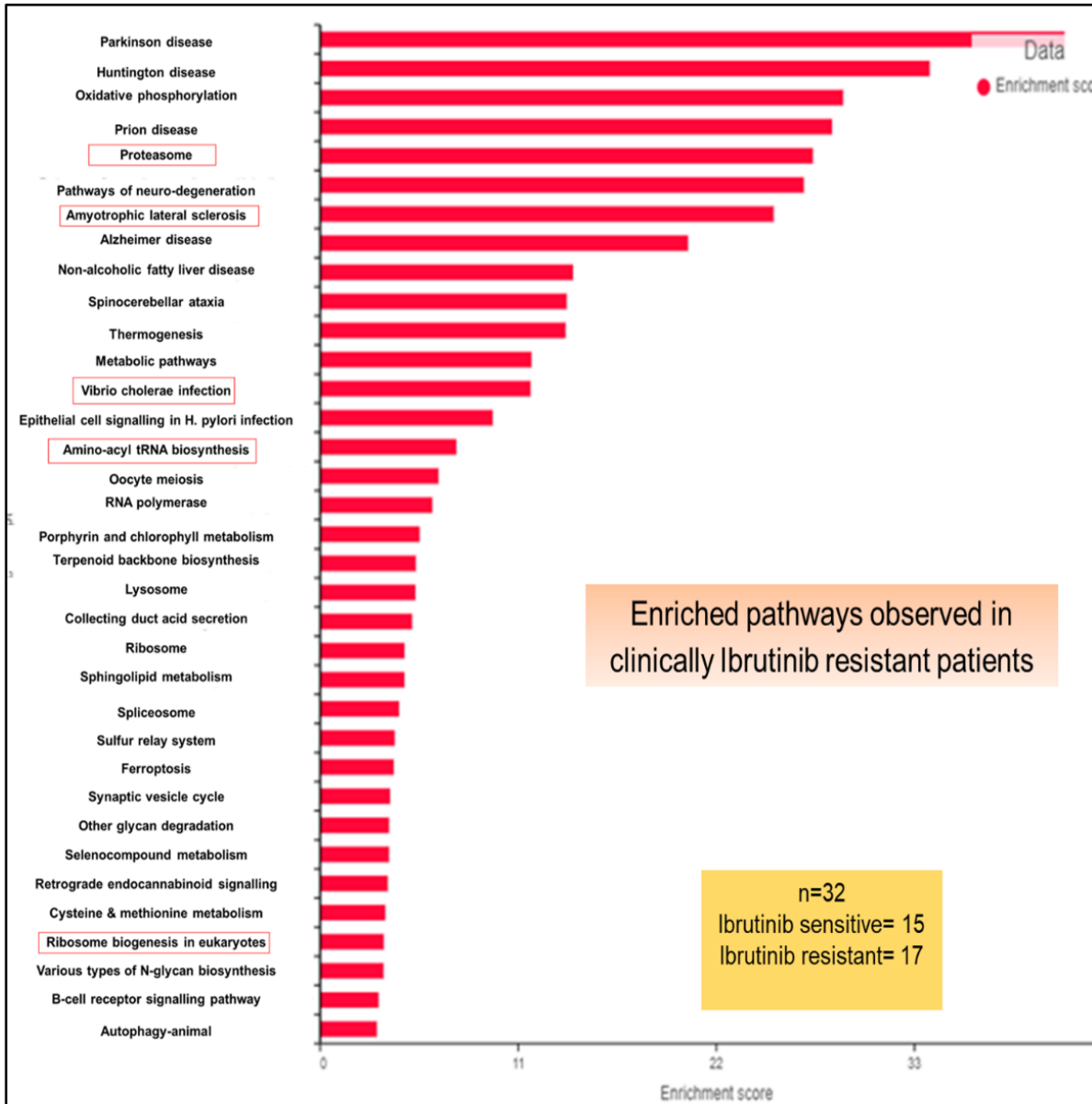


**Figure 12B**

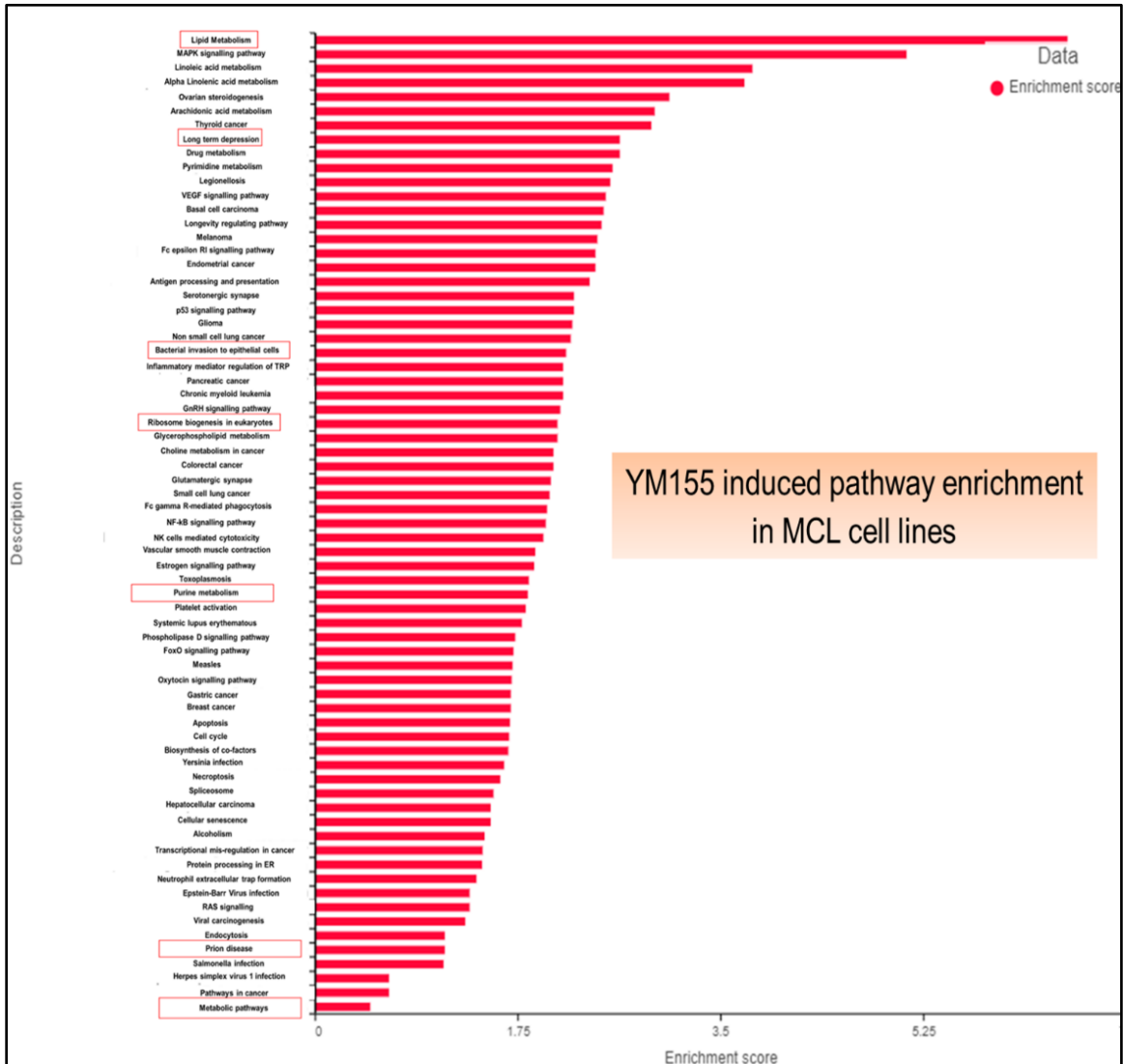


**Figure 12. KEGG pathway enrichment analysis provides mechanistic insights into YM155 drug action in MCL cells.** Comparison of Pathway enrichment analysis of GSE141335 dataset that contains expression data from clinically Ibrutinib responsive and unresponsive patients with YM155 gene signature shows a high degree of similarities indicating YM155 as a potent drug to curb resistance.

## Discussion

The target of one of our secDrugs, YM115, is Survivin which is a member of the inhibitor of apoptosis (IAP) protein family that inhibits caspases and blocks cell death.<sup>372</sup>

It is highly expressed in most cancers and fetal tissue but is entirely absent in terminally differentiated cells. Survivin expression is associated with a poor clinical outcome as it promotes angiogenesis and acts as a resistance factor in anticancer therapies. Survivin has been shown to inhibit apoptosis through caspase-dependent and independent pathways.<sup>373</sup> Survivin is also found in approximately 50% of high-grade non-Hodgkin's lymphomas.<sup>374</sup> This is an adverse prognostic factor for survival in diffuse large B-cell lymphoma patients as high Survivin expression correlated with shorter survival of the patients. So, Survivin is a promising therapeutic target in the management of R/R MCL.

Our study thus identified YM155 and S63845 as potential novel candidates for repurposing as secondary drugs in combination with BTKi/PI for the treatment of R/R MCL. Our results showed that YM155 & S63845 exhibited significant synergistic cell-killing activities alone & in combination with Bortezomib (PI) & Ibrutinib (BTKi), especially in R/R MCL cells. Further, our results also showed that both YM155 and S63845, in combination with BTKi/ PI, were able to significantly lower the effective dose of both BTKi/PI required to achieve desired therapeutic response, thereby making the cell lines relatively more BTKi/PI sensitive. We also found YM155 and S83845 combination has synergism in resistant MCL cell lines. As both YM155 & S63845 have reported activity against cancer stem-ness, we further investigated their effect on the cancer stem-like cells (CSCs) in MCL, which have a potential role in treatment resistance. YM155 was remarkably effective in reducing ALDH activity, a hallmark of CSCs, in resistant MCL cells.<sup>375</sup> Previous studies have reported that bone-marrow stromal cells have a protective effect on the MCL cells against the chemotherapeutic agent.<sup>376</sup> From our data, it is evident that YM155 inhibits the adhesion of MCL cells to the bone marrow stromal cells. Next, we performed next-generation RNA sequencing analysis to identify mechanisms of secDrug action & synergy. Gene expression profiling & IPA of the RNAseq data of YM155-treated MCL cell lines revealed down-regulation of the pro-survival pathway and genes, also up-regulation of pro-apoptotic markers.

Thus, the secDrug algorithm promises to serve as a universal prototype for the discovery of novel drug combination regimens for treatment outcomes in any cancer type by enhancing sensitivity or overcoming resistance to standard-of-care drugs.

# **CHAPTER 5**

## **Validation Of In Litero Predicted Secondary Therapies Against B-cell Malignancies**

## **CHAPTER 5.1**

### **The Anti-Leprosy Drug Clofazimine Synergizes with BTK Inhibitors and Proteasome Inhibitors in Drug-Resistant Mantle Cell Lymphoma**

## Abstract

Mantle Cell Lymphoma (MCL) is a difficult-to-cure, highly heterogeneous, and aggressive form of non-Hodgkin lymphoma comprising roughly 7% of all cases with a high recurrence rate and poor long-term prognosis. The reported progression-free survival is about 1-2 years, and the median overall survival/OS is < 3 years. Current first-line MCL therapies include combination regimens like R-CHOP, R-DHAP, Hyper-CVAD, VcR-CAP, etc. However, although patients respond well to initial treatment, most eventually progress to relapsed disease state. BTKi<sub>s</sub> (Bruton's tyrosine kinase inhibitors), such as Ibrutinib, are standard targeted therapeutic options for refractory or relapsed (R/R) MCL. The proteasome inhibitor (PI) drug Bortezomib/Velcade/Bz is another FDA-approved targeted drug for R/R MCL. However, despite these recent advances in the treatment landscape, R/R MCL still remains incurable with limited therapeutic options and a median OS<10-15 months. Therefore, there is an unmet need to discover novel drugs against R/R MCL.

Previously, we have demonstrated that Clofazimine (CLF), an anti-leprosy drug, could potentially be repurposed for the treatment of chronic myeloid leukemia and PI/IMiD-resistant multiple myeloma that also targets subclones representing putative stem-like-cells (CSCs). Notably, using single-cell analysis and high dimensional immunophenotyping or CyTOF (Cytometry Time of Flight), we have also identified molecular networks underpinning CLF+PI synergy. We hypothesize that CLF has strong potential to be repurposed as a novel anti-MCL drug, particularly in a relapsed/refractory setting.

For this purpose, we used MCL cell lines representing drug-sensitive (JEKO1, MINO), innate PI/BTKi-resistance (Z138; representing refractory patients), and clonally-derived acquired PI/BTKi-resistance (MINO-R; representing relapse patients) as in vitro model systems and showed i) the efficacy of CLF as a single agent ( $IC_{50}= 6.9\pm 3.6$  uM) and ii) in combination with PIs (Bz) and BTKis (Ibrutinib, Acalabrutinib) against innate and acquired resistant MCL (Figure 1), as well as iii) the unique targeting of putative CSCs by CLF. Remarkably, CLF+BTKi/PI combination lowered the effective BTKi, and PI doses required to achieve desired therapeutic response by >10-folds (estimated dose reduction index for BTKi and PI were 12.43 and 10.99, respectively). Further, mRNA-sequencing followed by differential gene expression analysis using DESeq2 and EdgeR revealed that the top significantly upregulated genes following

PI+CLF treatment were GSR, DAP3, and DOK1, which have reported anti-tumorigenic activity. The top significantly downregulated genes EHD1, CBX8, DDX17, SOX12, and COMMD3 have reported pro-survival function. Ingenuity pathway analysis revealed protein ubiquitination pathway and cell cycle arrest at the G2/M phase as the top canonical pathways. Causal network analysis showed synergistic drug action significantly elevated the levels of oxidative stress and unfolded protein response. Additionally, the PI+CLF combination potentiated AMPK-mediated down-regulation of the mTOR signaling pathway, which further led to a direct reduction of Cyclin D1 (aberrantly expressed in MCL) and the downregulation of eIF4-p70S6K signaling. The synergistic drug activity also led to the downregulation of oncogenic pathways like p38 MAPK and NF- $\kappa$ B signaling.

Recent studies have indicated that intra-tumor heterogeneity due to the presence of stem-like cells in MCL (MCL-CSCs), including CD45<sup>+</sup>CD19<sup>-</sup> MCL-initiating cells (MCL-ICs), relatively quiescent-highly clonogenic aldehyde dehydrogenase (ALDH)<sup>+</sup> cells and side populations (SP) may drive drug resistance and disease relapse. Notably, we found that several of the differentially regulated genes are critical for the maintenance and functioning of CSCs. For example, the PI+CLF combination downregulates Wnt/ $\beta$  catenin signaling, which is found to be frequently overexpressed in MCL-ICs. HIPPO, another signaling pathway involved in the maintenance of cancer stem-ness and emergence of drug resistance, was also down-regulated. Currently, we are validating the specific targeting of putative MCL-CSCs by CLF. Next, we plan to replicate our findings using PDX models of MCL.

CLF is an FDA-approved drug as well as on WHO's List of Essential Medicines. Thus, our study introduces CLF as a novel, safe, and inexpensive therapeutic option for the management of R/R MCL.

## Introduction

Mantle cell lymphoma (MCL) is rare cancer with an incidence rate of 1 per 200,000 each year. It is typically a difficult-to-cure, highly heterogeneous, and aggressive form of non-Hodgkin lymphoma, comprising roughly 5%-7% of all cases with a high recurrence rate and poor long-term prognosis.<sup>177,178,192</sup> The reported progression-free survival is about 1-2 years, and median overall survival (OS) is <3 years. MCL is predominant in an older population, and many affected individuals are diagnosed at approximately 60 to 70 years old (median age of diagnosis >60 years).<sup>179,192</sup> It has been seen that the incidence rate in men is nearly twice as high as that in females.<sup>177</sup> Reports suggest that most individuals with MCL have advanced (i.e., stage III or stage IV) disease at diagnosis. Further, potential exposure to Agent Orange increases susceptibility to MCL in U.S. veterans with a prevalence of ~10 cases and incidence of 0.6-2.6 cases per 100,000.<sup>177-179</sup>

Current first-line MCL therapies include combination regimens like R-CHOP (rituximab plus cyclophosphamide, doxorubicin, vincristine, and prednisone), BR (bendamustine and rituximab), rituximab, bendamustine and cytarabine (R-BAC), R-DHAP (Rituximab (Rituxan®), Dexamethasone (Decadron®), High-dose Ara-C (Cytarabine), CisPlatin), Hyper-CVAD (cyclophosphamide, vincristine sulfate, doxorubicin (Adriamycin), dexamethasone), VcR-CAP (bortezomib (Velcade), rituximab (Rituxan), cyclophosphamide, doxorubicin (Adriamycin), prednisone), etc.<sup>176,185,190</sup> Although patients respond well to initial treatment, most eventually progress to relapsed disease state. Immunomodulatory agents refer to drugs that alter the functioning of the immune system and include Revlimid (lenalidomide).<sup>166</sup> Targeted therapies are agents that target a specific protein and stop signals in cancer cells responsible for growth and survival.<sup>377</sup> Food and Drug Administration (FDA) approved targeted agents in refractory or relapsed (R/R) MCL include BTKi (Bruton's tyrosine kinase inhibitors) such as Imbruvica (ibrutinib), Calquence (Acalabrutinib), and Brukinsa (Zanubrutinib).<sup>206</sup> BTK is a non-receptor tyrosine kinase that serves as a critical component of the B-cell receptor signaling pathway responsible for cellular proliferation and is found to be frequently over-expressed in MCL.<sup>197,198</sup> The proteasome inhibitor<sup>163</sup> (PI) drug Bortezomib/Velcade/Bz is another FDA-approved targeted drug for R/R MCL.<sup>378</sup> However, despite these recent advances in the treatment landscape, R/R MCL remains incurable with limited therapeutic options owing to drug resistance, extensive inter-individual variation in response, and toxicity profile that limits

efficacy in clinical settings and a median OS < 10-15 months.<sup>370</sup> Therefore, there is an unmet need to discover novel drugs against R/R MCL.

Recent evidence indicates that intra-tumor heterogeneity due to the presence of treatment-refractory subpopulations or cancer stem-like cells (CSCs) drives drug resistance and disease relapse in various cancers.<sup>85,98,218</sup> These putative stem-like cells in MCL include CD45+CD19-cells/ MCL-initiating cells (MCL-ICs), relatively quiescent-highly clonogenic aldehyde dehydrogenase (ALDH)+ cells, and side populations (SP).<sup>213,214,216</sup> Once ibrutinib stops working, only one-third of patients respond to their following line of treatment; those who do respond experience only brief remissions and have poor outcomes, irrespective of stem cell transplantation. Ibrutinib is ineffective in targeting MCL-CSCs.<sup>370</sup>

Previously, we have demonstrated that Clofazimine (CLF), an anti-leprosy drug, could potentially be repurposed for the treatment of chronic myeloid leukemia (CML) and multiple myeloma (MM) that specifically targets subclones representing stemness in PI-resistant patients.<sup>379,380</sup> CLF, which is a peroxisome proliferator-activated receptor- $\gamma$  (PPAR $\gamma$ ) agonist binds to PPAR $\gamma$  that results in modulation of its transcriptional as well as E3 ubiquitin ligase activity.<sup>381</sup> This increased ubiquitin ligase activity of PPAR $\gamma$  induces proteasomal degradation of p65 (RelA), which in turn results in sequential transcriptional downregulation of MYC and PRDX1, resulting in the cellular effects of CLF, including regulation of cellular ROS levels.<sup>380</sup> CLF also leads to the transcriptional down-regulation of Signal Transducer and Activator of Transcription 3 (Stat3) and Hypoxia-inducible factor 1 (HIF-1 $\alpha$ )-the two reported oncogenes with reported involvement in cancer progression and stemness.<sup>380</sup> Furthermore, we compared the efficacy of CLF with that of other PPAR $\gamma$  agonists, such as-rosiglitazone and pioglitazone. Single-agent CLF was found to be the most potent among all the PPAR $\gamma$  ligands tested. (data not shown here).

Notably, using single-cell analysis and high dimensional immunophenotyping, we have also identified synergistic down-regulation of p65/NF-kB/IRF4/Myc signaling cascade-the molecular networks underpinning CLF+PI synergy.<sup>379</sup>

Therefore, we hypothesized that CLF has strong potential to be repurposed as a novel anti-MCL drug in combination with PIs and BTKi through the synergistic down-regulation of multiple key pathways critical for the maintenance and functioning of CSCs. We also investigated the intra-

tumor heterogeneity of the aggressive forms of MCL at the sub-clonal/single-cell level using single-cell transcriptomics. Furthermore, our study will also enable single-cell biomarker-based quantification of the contribution of MCL-CSC subclones toward drug resistance and tumor aggressiveness. This will serve as a prototype for future therapeutic applications to identify sub-clonal stemness and resistance in patient samples.

## **Material and Methods**

### **Drugs and Reagents**

Drugs, reagents, antibodies, and kits are listed in Table S1. All the drugs were dissolved in dimethyl sulfoxide/ DMSO (Sigma-Aldrich; St. Louis, MO, US) and stored at -20°C. Recombinant Human IL-6 was obtained from PeproTech, Inc. (Cranbury, NJ, US)

### **Cell culture**

Human MCL cell lines MINO, JEKO1, and Z-138 were obtained from ATCC (Manassas, VA, USA). All the cell lines were cultured in the media as recommended by the supplier and were maintained in an incubator at 37°C with 5% CO<sub>2</sub>. The cell lines were authenticated at source and at regular intervals and tested randomly at regular intervals for mycoplasma negativity.

### **Creation of clonally-related PI-resistant MCL cell line**

Bortezomib-resistant MINO (MINO-VR) was created from the clonally-related parental PI-sensitive MINO-P MCL cell line by dose escalation. Briefly, the Mino-P cell line was subjected to pulses of once-weekly Bortezomib treatment. Bortezomib concentrations were doubled after every three weeks of treatment. The process of dose escalation continued for 6 months. Cultures were removed from bortezomib for 14 days or 6 months before analysis and cultured in a manner consistent with the parental lines.

### **In vitro chemosensitivity assays and drug synergy analysis**

MCL cell lines were treated with increasing concentrations of CLF, PIs (represented by BTZ), and BTKis (represented by Ibrutinib and Acalabrutinib) as single agents or in combination for 48h, and cytotoxicity assays were performed using CellTiter-Glo® Luminescent cell viability assay (Promega Corporation, Madison, WI, USA). Luminescence was measured by Synergy 2 Microplate Reader (BioTek; Winooski, VT, US). Half-maximal inhibitory concentration (IC<sub>50</sub>)

values were determined by calculating the nonlinear regression using a sigmoidal dose-response equation (variable slope).

For combination therapy, cell lines were treated with an indicated concentration of PI and BTKi, and 2.5, 5, and 10  $\mu$ M CLF for 48 hours. The combination Index (CI) of each treatment was calculated in CalcuSyn Software (Biosoft, USA) using Chou-Talalay's Median Effect method. CI value < 1 depicts synergism, CI = 1 refers to additive effect, and CI > 1 depicts antagonism among the drugs in combination.

### **Apoptosis assays**

Human Mantle Cell Lymphoma cells treated with single-agent PI, BTKi, and CLF as well combination of drugs (PI+CLF, BTKi+CLF), then harvested and washed, followed by staining in the dark with Annexin V-FITC and Propidium Iodide according to manufacturer's protocol (BD; Franklin Lakes, NJ, USA). Data was acquired by BD LSR II flow cytometry (BD; Franklin Lakes, NJ, USA) and analyzed in FlowJo™ Software (Ashland, OR, USA).

Caspase-3/7 activity assay was performed on the MCL cell lines using Caspase-Glo 3/7 luminescent assay kit according to the manufacturer's instructions (Promega Corporation, Madison, WI, USA). Luminescence was measured using Synergy 2 Microplate Reader (BioTek; Winooski, VT, US). The caspase activity was normalized to the untreated controls, and the area under the relative caspase activity curve (AUC) was calculated by the trapezoidal method using the GraphPad Prism software (LaJolla, CA, USA).

### **Mitochondrial transmembrane potential measurement ( $\Delta\Psi_m$ )**

Mitochondrial membrane potential was measured using JC-1 - Mitochondrial Membrane Potential Assay Kit by following the manufacturer's protocol (Abcam, Cambridge, UK). Briefly, the cells were plated in a 96-well black plate and treated with 0.5% DMSO or the drugs (PI, BTKi, CLF- single agent and combination of drugs - PI+CLF, BTKi+CLF). Following incubation, the cells were stained with JC-1 dye, and fluorescence was recorded in a Synergy 2 Microplate Reader (BioTek; Winooski, VT, US).

### **Side population Assay**

Side population cells in PI/BTKi resistant MCL cell lines will be investigated using DyeCycle Violet/DCV (Thermo-Fisher Scientific; Waltham, MA, US) assay according to manufacturer's instructions using flow cytometry. Briefly, MCL cells were treated with either CLF alone and/or in combination with the PI/BTKi for the indicated time. Next, cells were stained with Vybrant DyeCycle Violet stain and with 7-AAD (Thermo-Fisher Scientific; Waltham, MA, US) for the recommended time. Following dye incubation, cells were washed with ice-cold PBS and were immediately analyzed by flow cytometry. The sample incubated with Verapamil (Sigma-Aldrich; St. Louis, MO, USA) for the recommended time was used as the positive control.

### **Aldefluor activity assay**

Aldehyde dehydrogenase (ALDH) activity was assessed using the Aldefluor assay kit according to the manufacturer's instructions (Stem Cell Technologies; Vancouver, Canada). Briefly, CLF single agent and CLF+ BTKi/PI treated MCL cells were harvested and resuspended in Aldefluor assay buffer containing the ALDH substrate, BODIPY-amino acetaldehyde (BAAA). Negative control samples were treated with diethylamino benzaldehyde (DEAB) - an inhibitor of ALDH1 enzymatic activity. Then, the MCL cells were suspended in ALDEFLUOR™ assay buffer, and the brightly fluorescent ALDH<sup>+</sup> cells were detected by BD LSR II flow cytometer (BD; Franklin Lakes, NJ, USA) and analyzed using FlowJo™ Software (Ashland, OR, USA).

### **Cellular viability measurement in the presence of tumor microenvironment**

MCL cell lines Mino-P and Mino-VR were plated in the normal cell culture media and also with 15% and 30% conditioned media derived from bone marrow stromal cells HS-5. The cells were then treated with increasing concentrations of PI (Bortezomib) and CLF as single agents for 48h, and a cytotoxicity assay was performed using the method mentioned above.

### **Measurement of Oxygen Consumption Rate (OCR)**

We measured the OCR using the Agilent Seahorse Extracellular Flux (XF) Technology. Briefly, we have coated the XFp plate with Poly-D-Lysine to make it compatible to use for the suspension cells. Then, Mino-VR cells were plated and treated with vehicle control (0.5% DMSO) and CLF (10 uM) for 24 hrs. On the next day, using the Agilent Seahorse XF Cell Mito Stress Test kit, the mitochondrial function was measured by the XFp seahorse analyzer. First, oligomycin and

Fluoro-carbonyl cyanide phenylhydrazine (FCCP) were injected sequentially, followed by a third injection of a mixture of Rotenone and Antimycin A. Oligomycin inhibits ATP synthase and reduces OCR, followed by FCCP that raises OCR to the maximal rate by collapsing the inner membrane gradient and increasing the electron transport chain activity. Lastly, rotenone and antimycin A, which are complex I and antimycin complex III inhibitors, respectively inhibit the electron transport chain and reduce the OCR to a minimal value.

Data were normalized to the protein concentration at the end of each experiment. Data was calculated, and graphs were plotted using Agilent Seahorse Wave Desktop software and report generator, MS Excel, and GraphPad Prism.

### **Whole-transcriptome gene expression analysis**

MCL cells were plated and incubated overnight at 37 °C in a 6-well plate, followed by treatment with CLF single agent and CLF+ BTKi/PI. After 24 hours, cells were harvested, and high-quality RNA was extracted using QIAshredder and RNeasy kit (Qiagen; Hilden, Germany) and stored at -80°C. RNA concentration was measured using a Nanodrop-8000 spectrophotometer (Thermo-Fisher Scientific; Waltham, MA, US), and RNA integrity was assessed using Agilent 2100 Bioanalyzer (Agilent Technologies; Santa Clara, CA, US). An RNA integrity number (RIN) threshold >8 was applied, and RNA-seq libraries were constructed using Illumina TruSeq RNA Sample Preparation kit v2 (Illumina; San Diego, CA). Libraries were then size-selected, and RNA sequencing was performed on Illumina's NovaSeq platform using a 150bp paired-end protocol with a depth of > 20 million reads per sample.

### **RNAseq data analysis**

RNA-seq data was pre-processed, genes with mean counts<10 were removed, and differential gene expression analysis was performed between two groups of RNAseq datasets (e.g., treated vs. untreated) using a combination of command-line based analysis pipeline (DEseq2 and edgeR) and Partek Flow software (Partek, Inc; St. Louis, MO, US). We used GSA to perform differential gene expression analysis between groups that applies limma, an empirical Bayesian method that increases statistical power, to detect the differentially expressed (DE) genes. Mean fold-change>|1| and p<0.05 was considered as the threshold for reporting significant differential gene expression. Further, Analysis of Variance (ANOVA) was used for continuous outcomes,

followed by post-hoc analysis using an unpaired two-tailed Student's t-test. Multiple testing was performed using Benjamini–Hochberg method. Genes with significant levels ( $p < 0.05$ ) were considered DEGs. Heatmaps were generated using unsupervised hierarchical clustering (HC) analysis based on the top DE genes (DEGs).

### **Ingenuity pathway analysis (IPA)**

The most significant differentially expressed genes (DEGs) were used to perform pathway analysis using the IPA (Qiagen; Hilden, Germany) software to identify the most significantly affected molecular pathways, upstream regulator molecules, downstream effects and causal networks predicted to be activated or inhibited in response to single-agent and combination treatment.

### **Cell Cycle Analysis**

Human Mantle Cell Lymphoma cells were treated with vehicle (0.5% DMSO), PI, BTKi, CLF-single agent, and a combination of drugs (PI+CLF, BTKi+CLF). Cells were harvested and washed with PBS, followed by fixation by adding ice-cold 70% ethanol for 30 minutes at 4 °C. Methanol was removed and washed twice with cold PBS. 0.5 ml of PI/RNase staining solution was added to each sample and incubated for 30 min at room temperature in the dark. Data was acquired by BD LSR II flow cytometry ((BD; Franklin Lakes, NJ, USA) at 488 nm wavelength and analyzed in FlowJo™ Software (Ashland, OR, USA).

### **Pre- vs. post-treatment single-cell gene expression analysis**

Untreated and CLF-treated MinoP and Mino-VR were subjected to automated single-cell capture and cDNA synthesis using 10X Genomics (Pleasanton, CA, US) Chromium platform. Single-cell RNA sequencing (scRNA-seq-based gene expression analysis) was performed on Illumina HiSeq 2500 Next-generation sequencing platform (Paired-end. 2\*125bp, 100 cycles. v3 chemistry) at ~5 million reads per sample.

scRNAseq datasets were obtained as matrices in the Hierarchical Data Format (HDF5 or H5). We used a combination of Seurat, Cell Ranger software, and Partek Flow software packages to pre-process scRNA-seq data and perform single-cell gene expression analysis for biomarker-based identification of PI/BTKi-resistant single-cell subpopulations subclones expressing cancer stem-like signature, as well as secDrug treatment-induced erosion of these subclones. Highly

variable genes will be selected for clustering analysis based on a graph-based clustering approach. t-distributed stochastic neighbor embedding (t-SNE), and UMAP (Uniform Manifold Approximation and Projection) plots were generated to visualize the cell subpopulation architecture based on markers of interest 39. Highly variable genes for clustering analysis were selected based on a graph-based clustering approach. Relative marker intensities and cluster abundances per sample were visualized by a heatmap.

### **Western Blotting**

Top differentially expressed genes (DEGs) genes were evaluated using Immunohistochemistry and densitometry analysis. Cells were treated with CLF, as a combination with PI or BTK, total protein was isolated, and immunoblotting assays were performed using the following antibodies from Cell Signaling Technology (Danvers, MA, US). Immuno-reactivity was detected by Chemiluminescent HRP Substrate (Bio-Rad Laboratories; Hercules, CA, US), and the exposed image was captured using a ChemiDoc™ MP Imaging System (Bio-Rad). Densitometry analysis was performed in triplicates using Image J software.

### **Patient data**

Further, a novel reverse-match approach was used to identify small molecule signatures that reverse the input signature (drug-induced gene expression profiles). Using this, we identified i) the most significantly affected molecular pathways; upstream regulator molecules; iii) downstream effects and biological processes; and iv) causal networks; predicted to be activated or inhibited in response to AKM1 & AKM2 treatment based on the most significant biomarkers. Thus, this biomarker-based method has also served as a novel tool to screen additional secondary Drugs against the aggressive single-cell subclones.

### 3.1.4 Results

#### CLF inhibits cell proliferation in human MCL cell lines

First, we evaluated the *in vitro* cytotoxic effect of CLF as a single agent against MCL cell lines representing drug-sensitive (JEKO1, MINO-P), PI-resistance (Mino-VR), and BTKi-resistance (Z138) as *in vitro* model systems. We found that CLF was effective in reducing cell viability in all four MCL cell lines irrespective of PI/BTKi sensitivity/resistance (**Figure 1**). The median half-maximal inhibitory concentration ( $IC_{50}$ ) of single-agent CLF in human MCL cell lines was  $6.9 \pm 3.6$   $\mu$ M.

**Figure 1. Single-agent cytotoxicity assay with PI & BTKi mirrors the extensive inter-individual variation in drug response in the MCL cell line panel.**

Dose-response curve reveals a wide range of drug sensitivity towards (**1A**) PI (Bortezomib/BTZ) and (**1B**) BTKi (Ibrutinib/IBR). MINO-VR has approx. 70 folds higher  $IC_{50}$  value for Bortezomib than its parental cell line MINO-P. Z-138 has approx. 2.5 folds higher  $IC_{50}$  value for Ibrutinib than MINO-P and JEKO-1. (**1C**) *in vitro* cell viability profile of Clofazimine (CLF) single agent treatment in MCL cell lines. CLF showed high single-agent *in vitro* cytotoxicity in our MCL cell panel, including PI- resistant and BTKi-resistant MCL cell lines.

**Figure 1A**

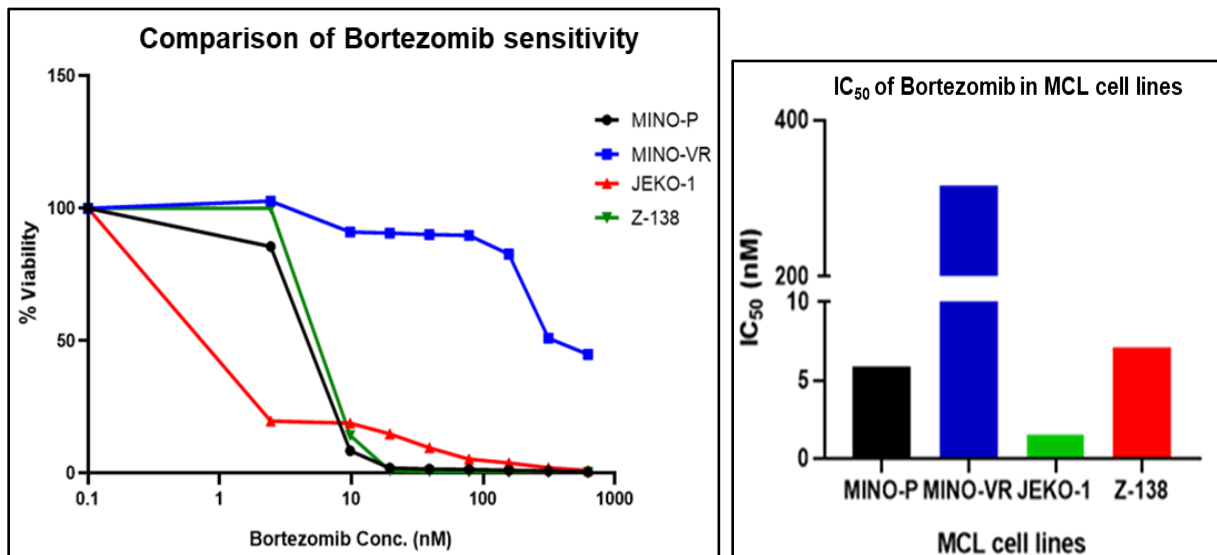


Figure 1B

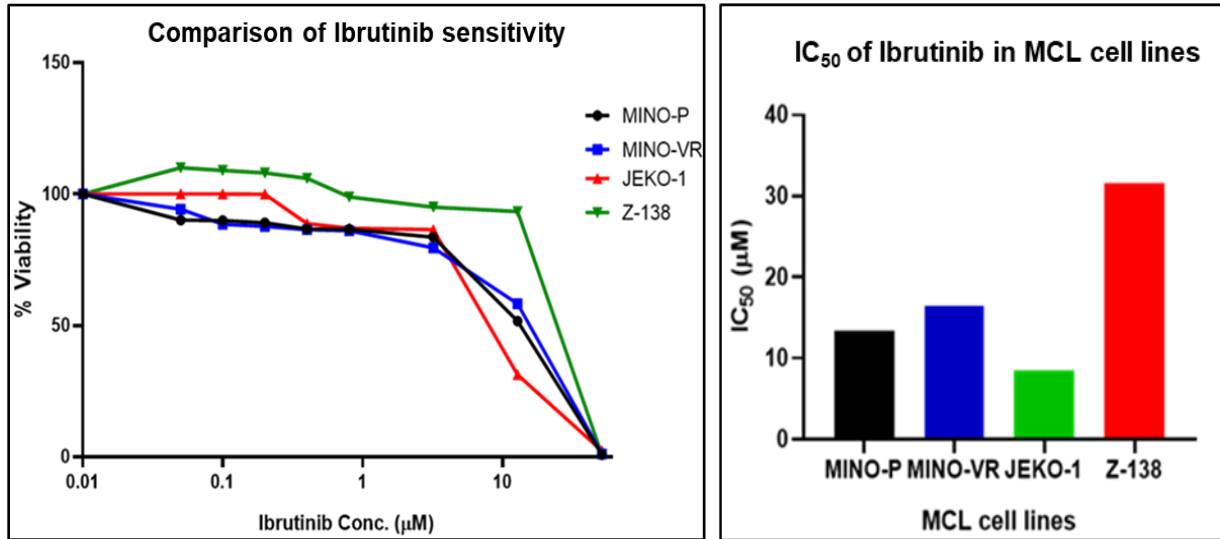
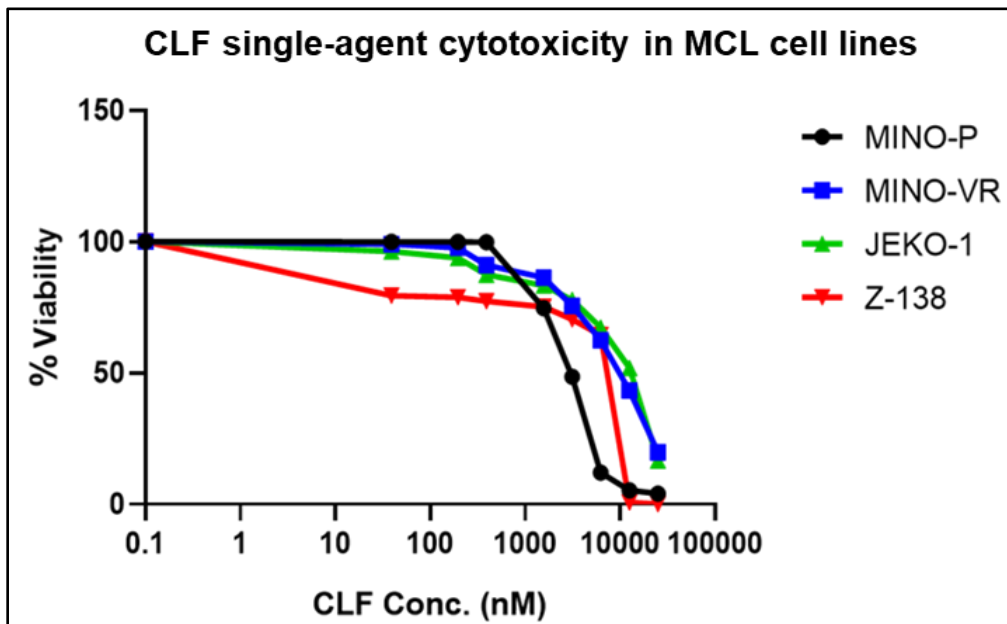


Figure 1C



### CLF synergizes with Proteasome inhibitors and BTK inhibitors

Next, we investigated the impact of three different concentrations of CLF (2.5, 5, and 10  $\mu\text{M}$ ) in combination with an increasing range of Bortezomib (PI) or Ibrutinib (BTKi). We observed that all the combination treatment regimens showed higher cytotoxic effects compared to single-agent PI (Figure 2A) or BTKi treatment (Figure 2B).

For drug synergy analysis, Combination Index (CI) values were calculated in CalcuSyn Software by using the Median Effect methods as described in Chou-Talalay's CI theorem combination index (C.I) theorem. The Combination Index (CI) value  $< 1$  depicts synergism, CI value = 1 refers to additive effect, and CI value  $> 1$  depicts antagonism for the drugs in combination.

Most of the combinations have shown synergy (i.e., C.I value  $< 1.0$ ). Synergistic effects were particularly profound in MINO-VR & Z-138. This observation is particularly relevant as they represent the acquired PI resistance and innate BTKi resistance. Similar data were obtained when we combined another BTKi (Acalabrutinib) with CLF.

**Figure 2. CLF shows synergistic cell-killing activity with PI & BTKi**

**(2A-B)** represents in vitro cell viability profile of MCL cell lines, including PI- resistant and BTKi-resistant MCL cell lines treated with different combinations of CLF & PI/ BTKi. All the combinations showed significant improvement in lowering cellular proliferation as compared to the effect of PI/ BTKi alone, which indicates drug synergy. We further quantitate the extent of synergistic action by CalcuSyn Software (BioSoft, USA) that calculates the Combination Index (C.I) as a function of fraction affected based on Chou-Talalay's Combination Index (C.I) theorem. Most of the combinations have shown synergy (i.e., C.I value  $< 1.0$ ) **(2C-D)**. Synergistic effects were particularly profound in MINO-VR & Z-138. This observation is particularly relevant as they represent the acquired and innate resistance, respectively.

Figure 2A

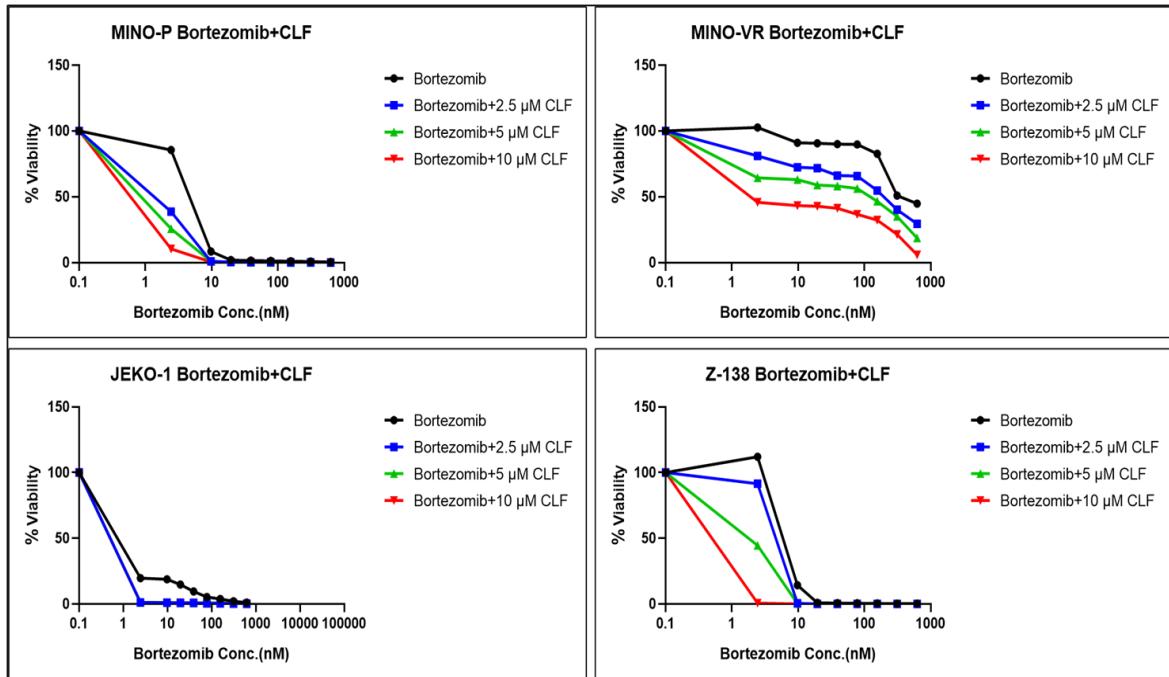
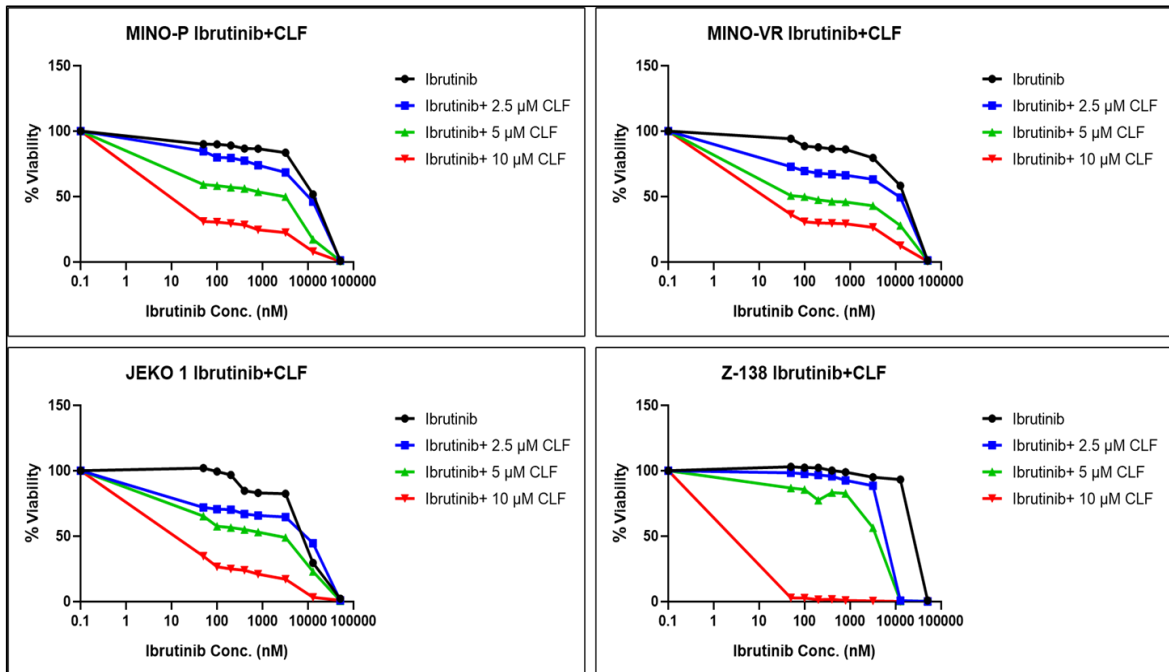
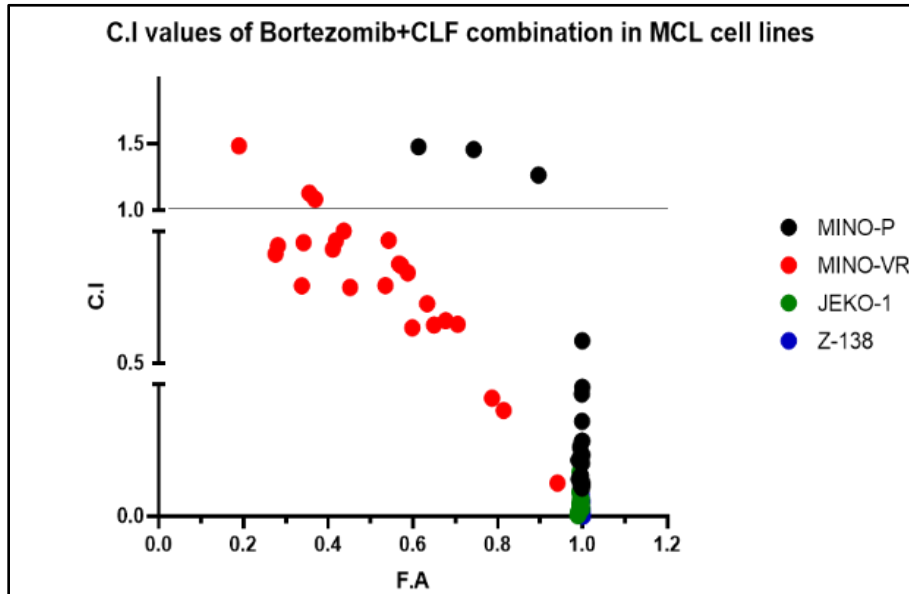


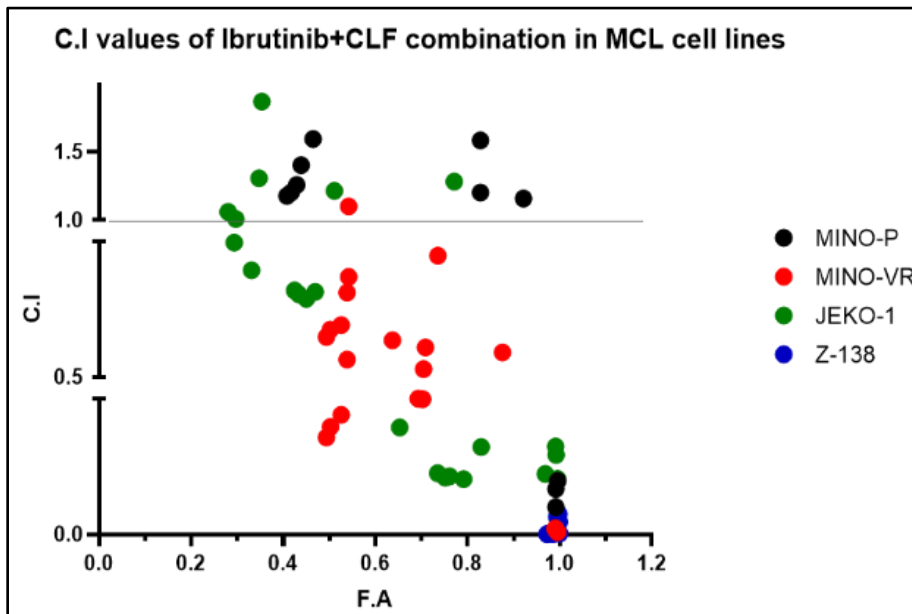
Figure 2B



**Figure 2C**



**Figure 2D**



**CLF, in combination with PI & BTKi, augments apoptosis in MCL cell lines**

The quantitative analysis of the extent of apoptosis in Mantle Cell Lymphoma cells in response to CLF single agent-treatment and CLF+PI/BTKi treatment was done using Fluorescein isothiocyanate (FITC) conjugated Annexin-V staining followed by flow cytometry. The data shows a significantly higher population of cells are Annexin-V positive, which is an indicator of

apoptosis in combination treatment as compared to single agent treatment in sensitive cell line Mino-P as well as in PI-resistant cell line Mino-VR (Figure 3B) and BTKi-resistant cell line Z138 (Figure 3C) indicating the significantly elevated level of induction of apoptosis in those cells. This further proves the synergistic activity of the drug combination.

**Figure 3. CLF+PI & CLF+BTKi enhance apoptosis in drug-resistant MCL cells**

Quantitative measurement of the % of the apoptotic MCL cells (Annexin-V positive) exposed to CLF single agent and CLF+ PI/ BTKi combination treatment by flow cytometry. The data shows a significantly higher population of cells are Annexin-V positive in combination treatment as compared to single agent treatment indicating an elevated level of apoptosis which further proves the synergistic activity of the drug combination.

**Figure 3A**

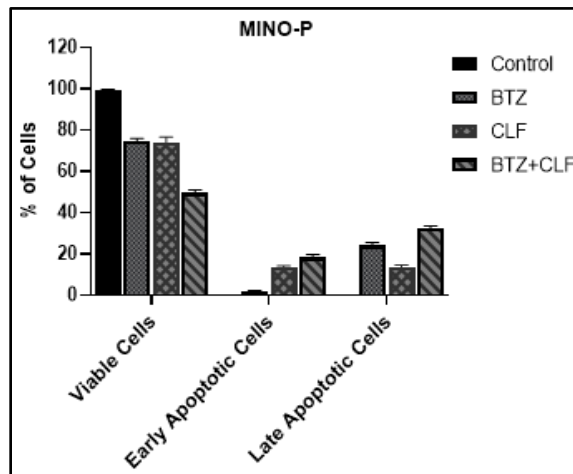
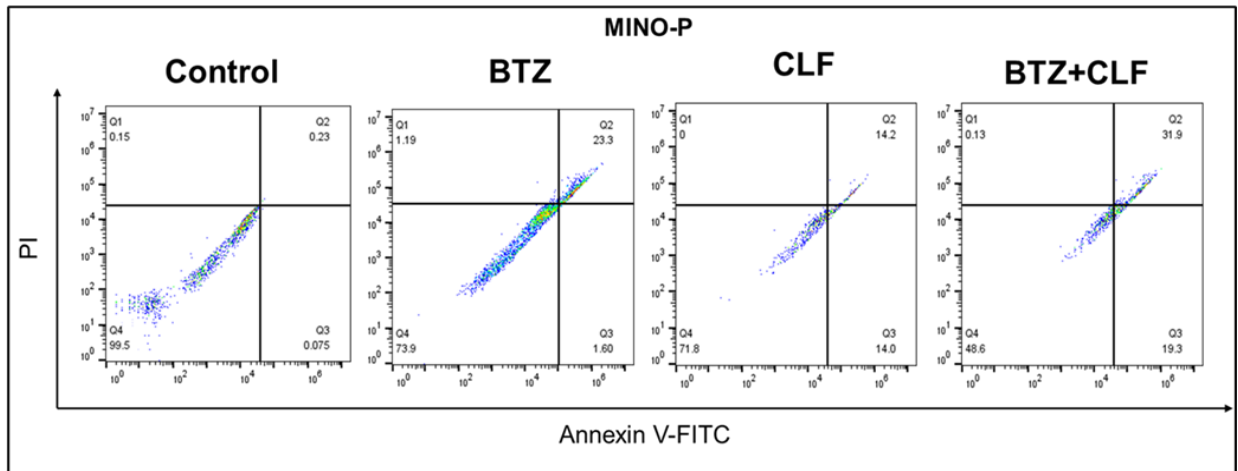


Figure 3B

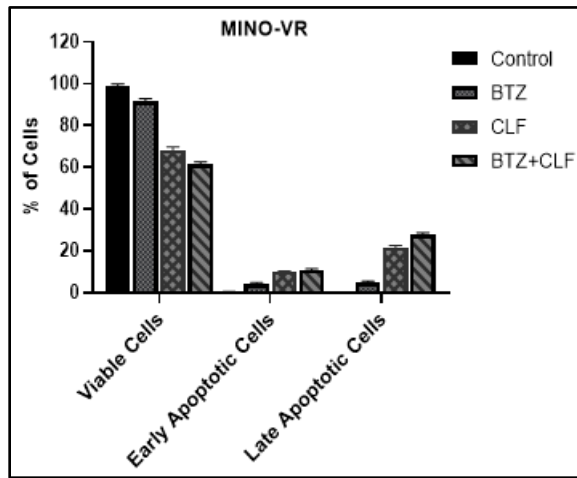
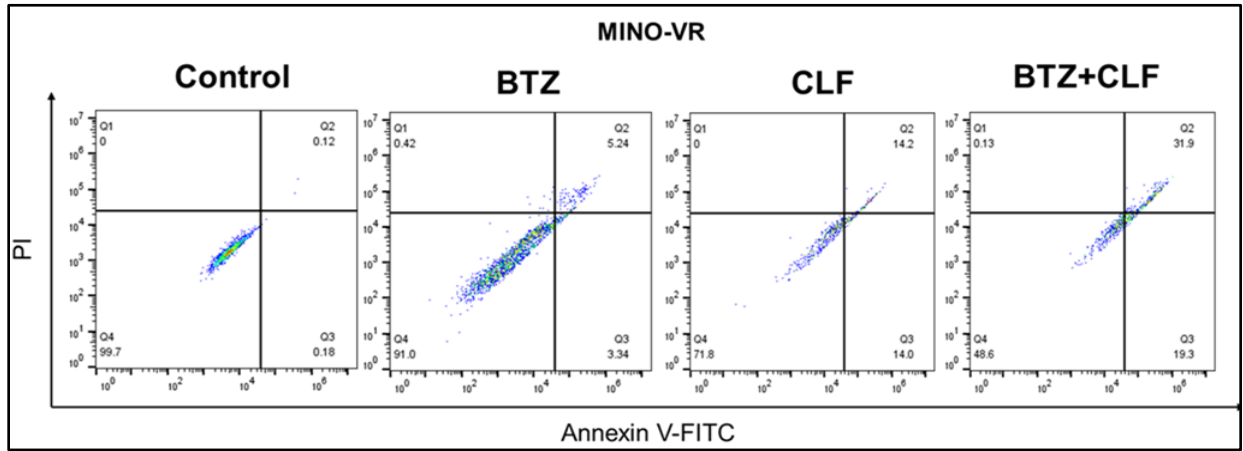
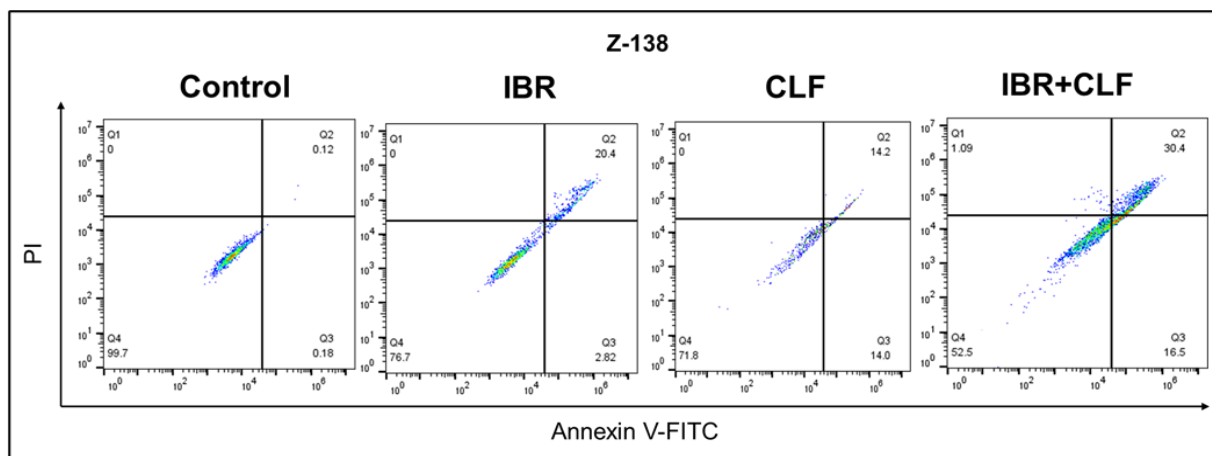
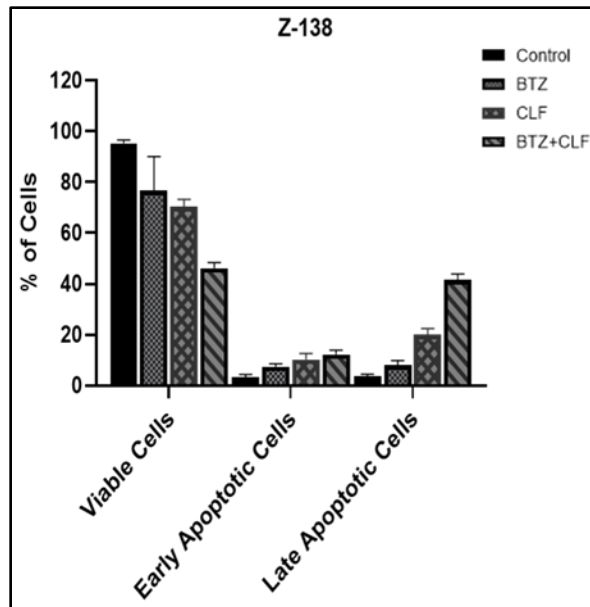


Figure 3C





### A combination of CLF and PI/BTKi induces a mitochondrial pathway of apoptosis

To evaluate the effect of the CLF -PI/BTKi combination on apoptosis, we performed a luminescence-based Caspase 3/7 Glo Assay. We observed elevated levels of Caspase 3/7 activity in combination-treated cells as compared to single-agent PI and BTKi treatment (Figure 4A).

The results were also confirmed by immunoblotting analysis that shows up-regulation of cleaved caspase 3 and 9 in response to CLF treatment (Figure 4B), indicating that CLF induced apoptosis through the mitochondria-mediated pathway.

Moreover, immunoblotting data also showed a decrease in the expression of anti-apoptotic proteins such as Bcl-2 and an increase in the expression of pro-apoptotic protein Bax (Figure 4B).

Previous studies have shown that CLF exerts its anti-bacterial activity by producing reactive oxygen species (ROS) that lead to mitochondrial depolarization. To investigate if CLF also generates ROS in the MCL cells, we measured cellular superoxide anions. An increase in DHE fluorescence indicates an increased accumulation of ROS in response to single-agent CLF treatment, which is further augmented when combined with Ibrutinib (Figure 4C)

Further, we measure the mitochondrial membrane potential using JC-1 dye. JC-1 is a cationic carbocyanine dye that accumulates in mitochondria. The dye exists as aggregates at higher potential. A decrease in the red/green fluorescence indicates mitochondrial depolarization, which

causes the JC-1 dye to become monomers from its aggregate form. We observed a significant shift from red to green fluorescence in response to CLF single-agent treatment as well as in combination with Bortezomib, indicating enhanced mitochondrial dysfunction or mitochondrial depolarization due to loss of mitochondrial membrane potential.

**Figure 4. CLF activates the mitochondrial-mediated pathway of apoptosis in MCL cells.**

**(4A)** CLF activates Caspase 3/7 in apoptotic MCL cells. The data shows significantly elevated Caspase 3/7 activity in combination-treated cells as compared to control, and single-agent treatment suggests that the drug combination worked in synergy to induce apoptosis. **(4B)** The data shows significant up-regulation of the Cleaved Caspase 3 and 9 expressions indicating that CLF-induced apoptosis was dependent on the mitochondria-mediated pathway. **(4C)** The data shows a significantly higher level of Dihydroethidium (DHE) fluorescence intensity in combination-treated cells as compared to single-agent treatment indicating enhanced cellular ROS production. **(4D)** The data shows the measurement of treatment-induced change in mitochondrial membrane potential. CLF alone and, in combination, a decrease in the red/green fluorescence indicates mitochondrial depolarization, which causes JC-1 dye to become monomers from its aggregates form.

**Figure 4A**

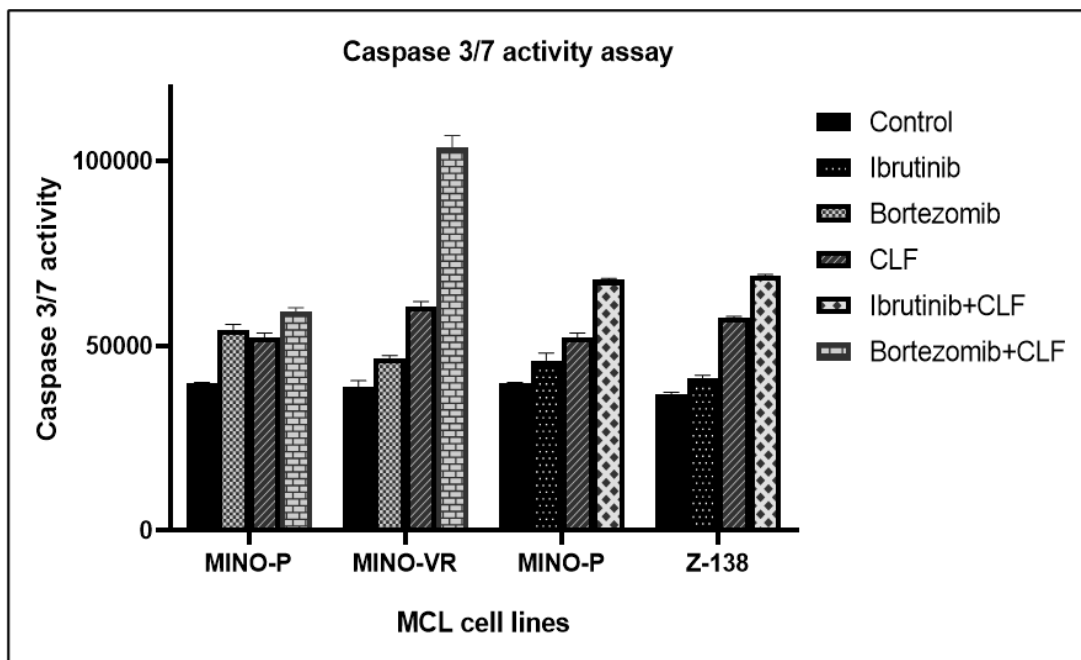


Figure 4B

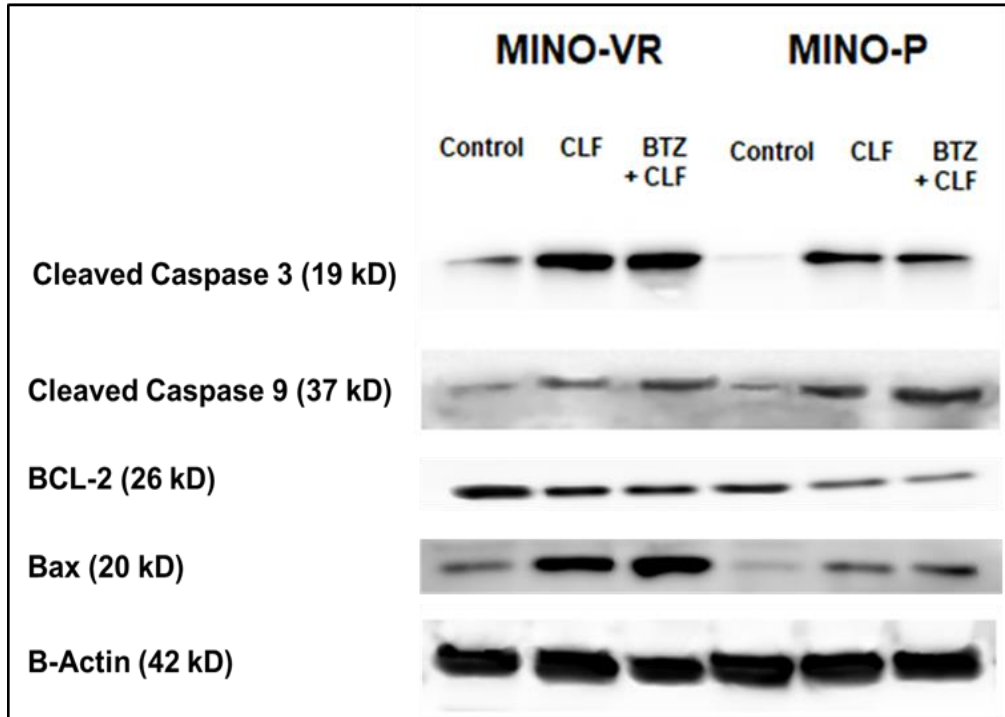
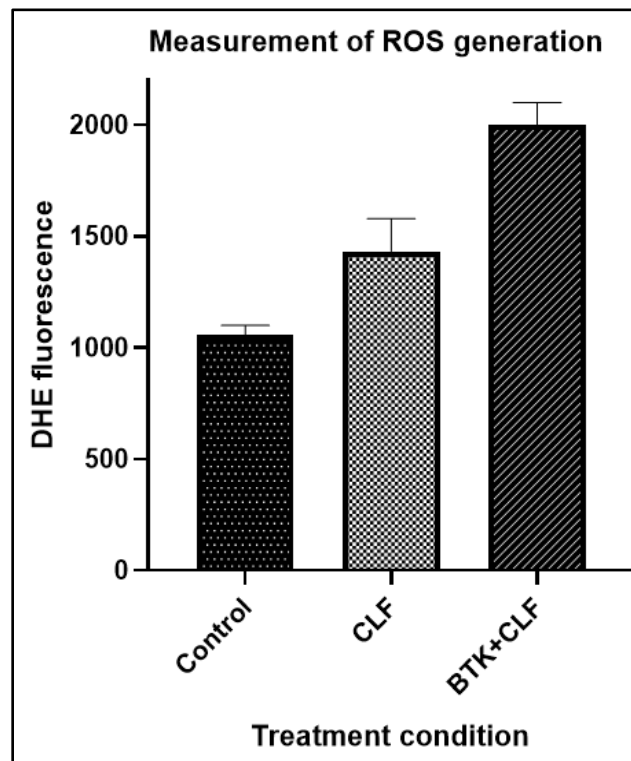
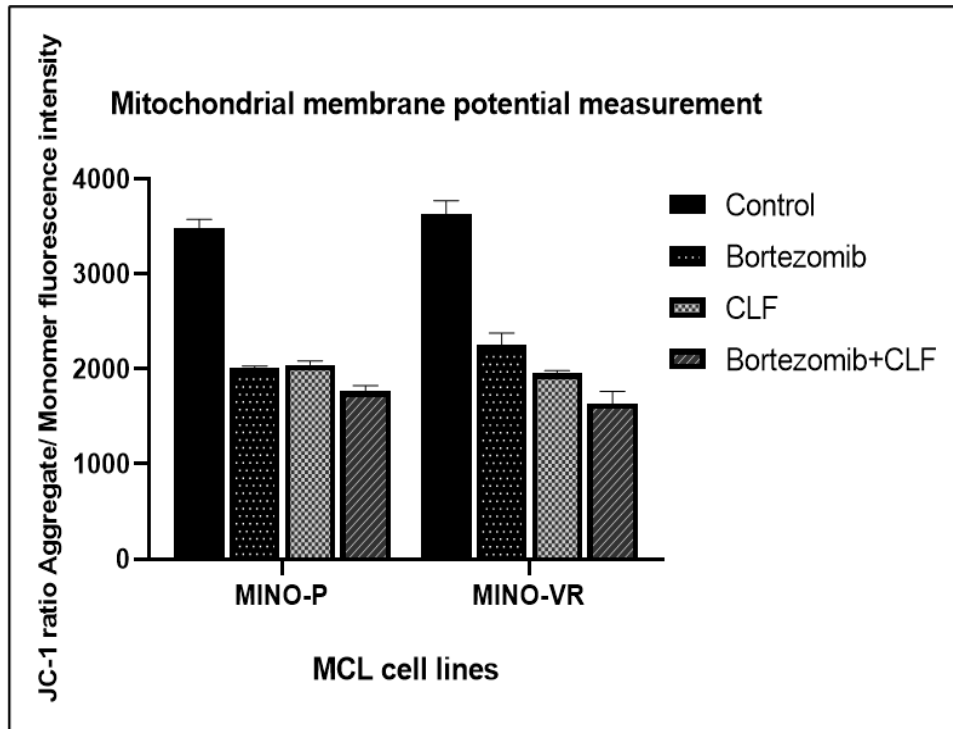


Figure 4C



**Figure 4D**



**CLF reduces the stem-cell load in MCL: CLF eroded side population cells and inhibited Aldefluor activity**

ALDH (aldehyde dehydrogenase) is an intra-cellular detoxification enzyme that is frequently over-expressed in CSCs and involved in drug resistance. We observed > 4 times higher ALDH activity in the PI and BTKi-resistant MCL lines (MINO-VR – 11.7% ALDH activity and Z-138 – 10.4%, respectively) compared to the drug-sensitive MCL lines (Figure 5A, 5D). CLF single-agent treatment led to a considerable decrease in ALDH activity in both MINO-VR (Figure 5B, 5D) and Z-138 cells (Figure 5C, 5D) (approx. 64% and 71% reduction, respectively, as compared to the control). When we combined CLF with PI and BTKi, we observed ALDH activity was further reduced to the level corresponding to that of the sensitive cell lines (Figure 5A).

**Figure 5. CLF erodes cancer stem cells in MCL**

CLF reduces side-population load in drug-resistant MCL cells. DyeCycle violet-based side population (SP) analysis following CLF single agent and combination treatment in sensitive and drug-resistant MCL cell lines reveals that resistant cells harbor a significantly higher % side

population as compared to sensitive cells (Figure 5A & 5D). Notably, CLF alone or a combination of CLF+ PI in PI-resistant MCL cell line (MINO-VR; Figure 5B) and a combination of CLF+ BTKi in BTKi-resistant MCL cell line (Z-138; Figure 5C) were able to reduce the load of the side population.

**Figure 5A**

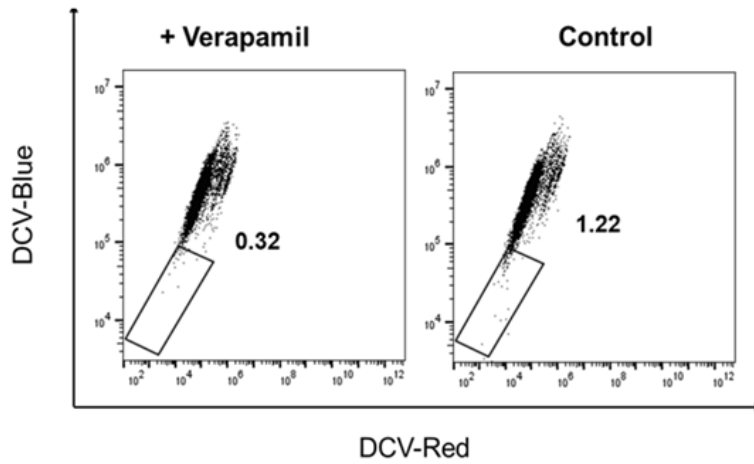


**Figure 5B**

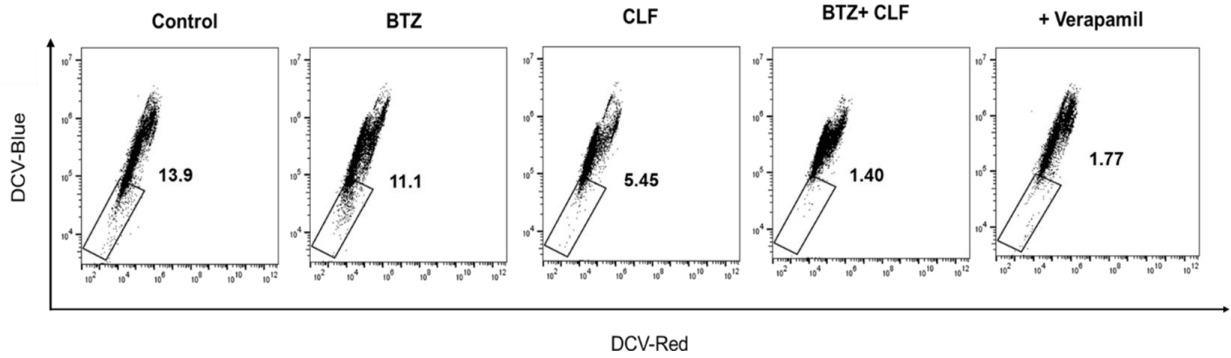


**Figure 5C**

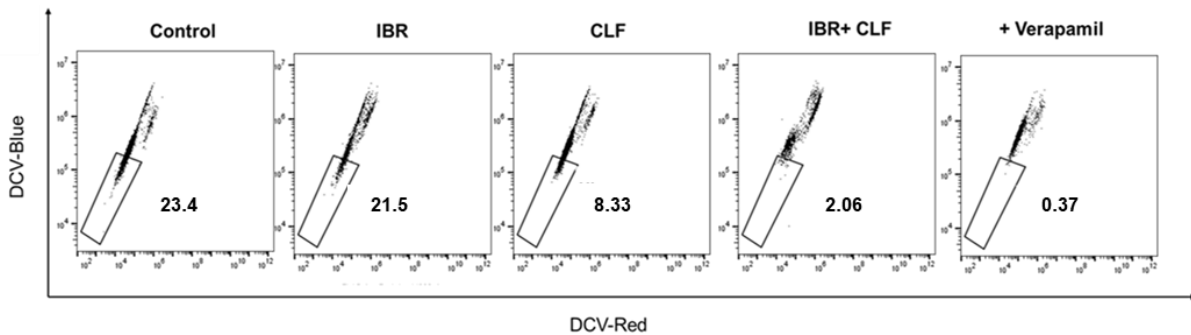
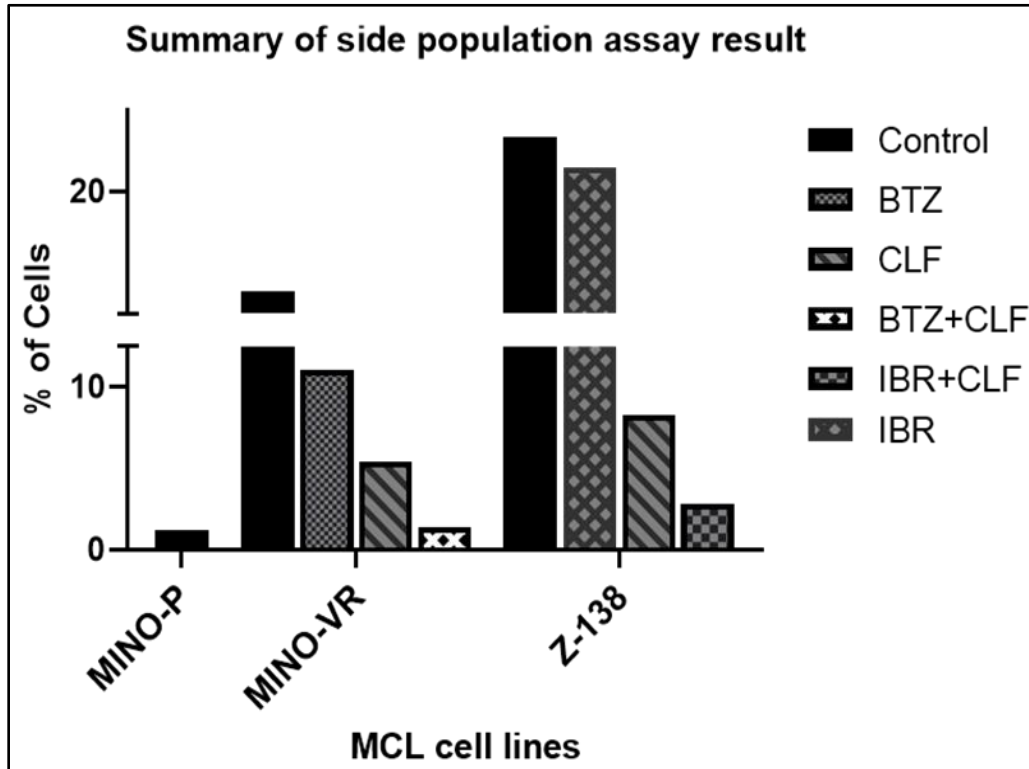


Figure 5D



Side populations (SP) cells are a subset of hematopoietic stem cells that possess several stem-cell-like features like high *in vivo* tumorigenicity and self-renewal capability. SPs are characterized by the ability to efflux DNA-binding dye via an ATP-binding cassette (ABC) transporter. We gated and selected side population/SP cells from main populations (MP) using DyeCycle violet, which is a cell-permeable DNA-binding dye, pre- and post- CLF treatment as single-agent and in combination with PI/ BTKi. Our results showed that at baseline (no treatment), both the resistant cells MINO-VR (Figure 6B, 6D) and Z-138 (Figure 6C-D) harbor considerably higher % SP compared to the sensitive cell lines Mino-P (Figure 6A, 6D) (>11 folds in MINO-VR and > 24 folds in Z-138 as compared to MINO-P). Further, CLF, as a single-agent treatment, eroded the SP by more than 52% in MINO-VR and 63% in Z-138 (Figure 6B-D). The combination of CLF with PI and BTKi resulted in a more profound effect, and ALDH activity was further reduced to the level corresponding to that of the sensitive cell lines.

### Figure 6. CLF erodes cancer stem cells in MCL

CLF reduces Aldefluor activity- a hallmark of cancer stem-ness implicated in drug resistance in MCL cells. Measurement of Aldehyde dehydrogenase (ALDH) activity in PI/ BTKi sensitive, PI-resistant & BTKi-resistant MCL cell lines showed very low-level ALDH activity in the PI/ BTKi sensitive cell line MINO-P. It is found to be considerably higher in clonally derived PI-resistant MCL cell line MINO-VR & in innate BTKi-resistant Z-138 cell line, indicating the presence of a ‘stem-like phenotype.’ CLF as a single agent and, in combination, caused a significant decrease in ALDH activity in drug-resistant cells.

Figure 6A

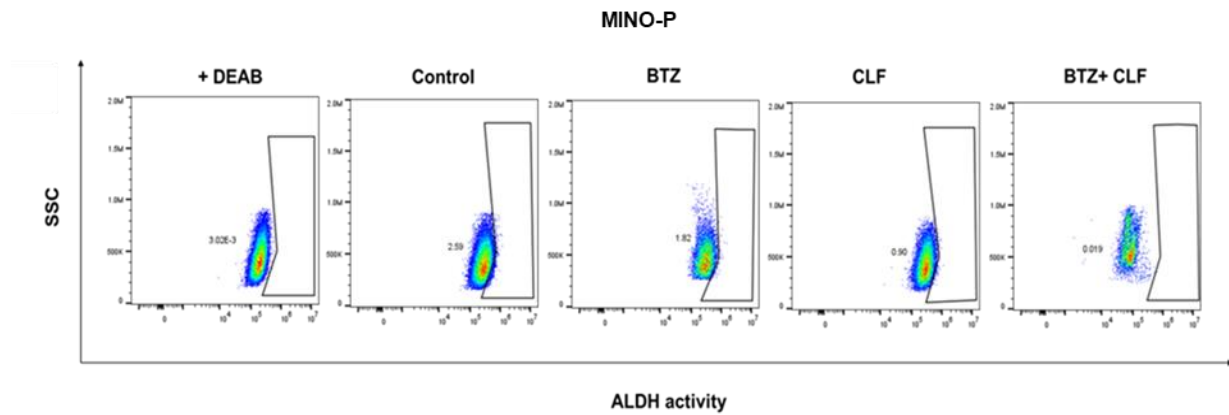
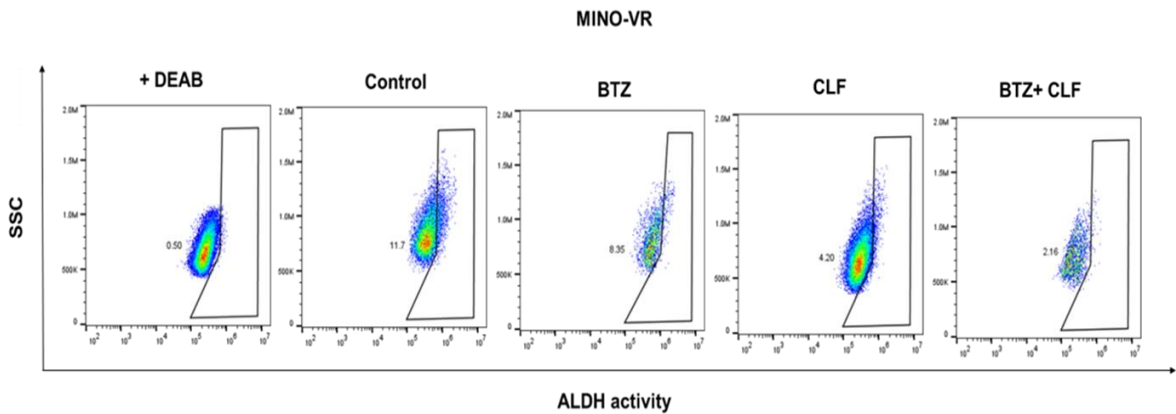
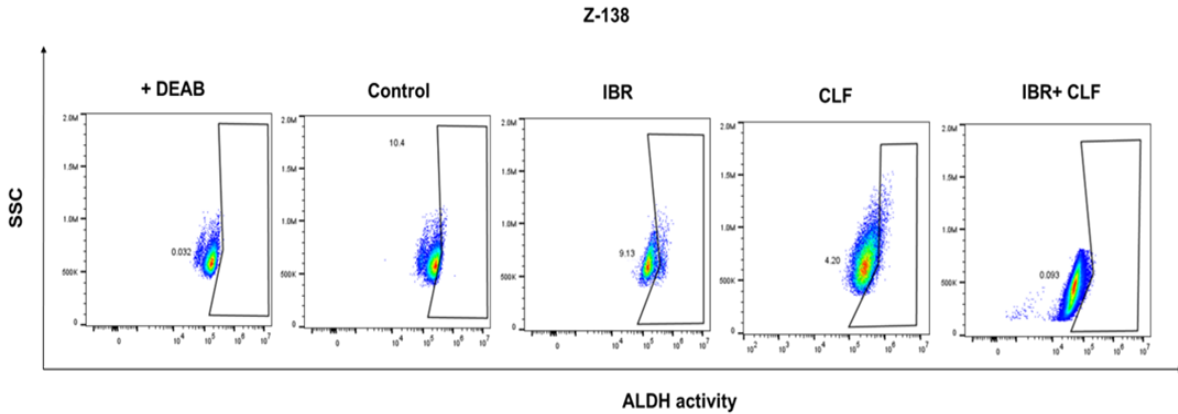


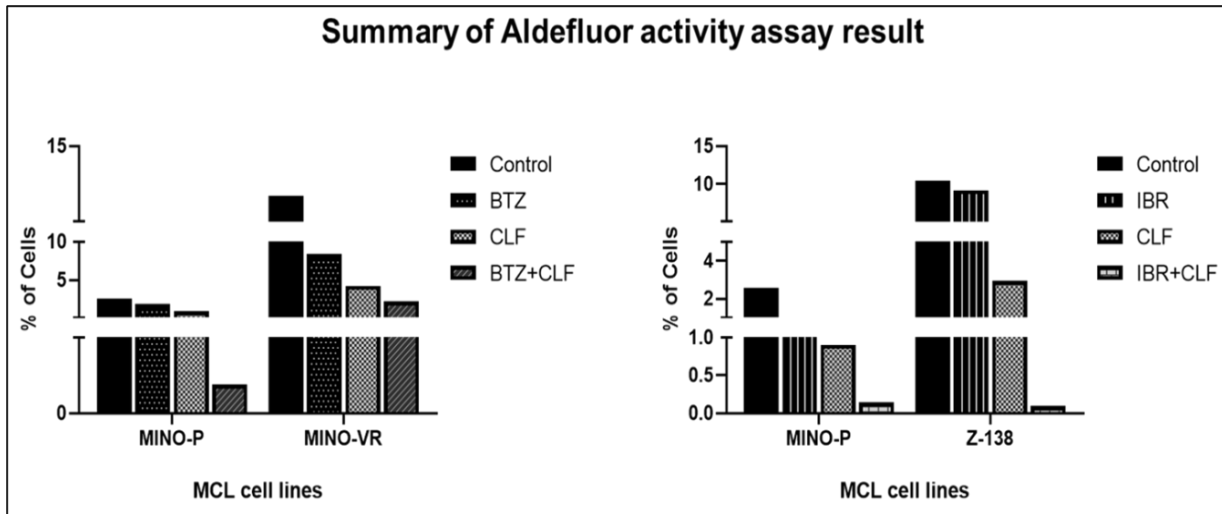
Figure 6B



**Figure 6C**



**Figure 6D**



**CLF alleviates the effect of the tumor microenvironment on the drug sensitivity of the MCL cells**

The tumor microenvironment (TME) provided by the bone marrow stromal cells (BMSCs) has a protective effect on the MCL cells. Interaction between BMSCs secreted factors and MCL cells help the latter to evade the cytotoxic effect of the chemotherapeutic drugs, which is one of the major reasons behind the treatment failure in R/R MCL. To check if CLF can negate this TME-induced drug resistance, we measured the IC<sub>50</sub> of Bortezomib and CLF in the presence of BMSC-conditioned media (CM). The data showed that in the presence of CM, the IC<sub>50</sub> of Bortezomib increased significantly (Figure 7A), indicating resistance, whereas, in the case of CLF, it didn't show significant change and remained more or less similar (Figure 7B) as compared to the

control media. This data suggests that CLF was more effective in nullifying the effect of TME than Bortezomib.

**Figure 7. in vitro cell viability profile of CLF single agent treatment in the presence of HS-5 (bone marrow stromal cell) conditioned media.**

CLF showed high single-agent in vitro cytotoxicity even in the presence of the resistance-inducing medium.

**Figure 7A**

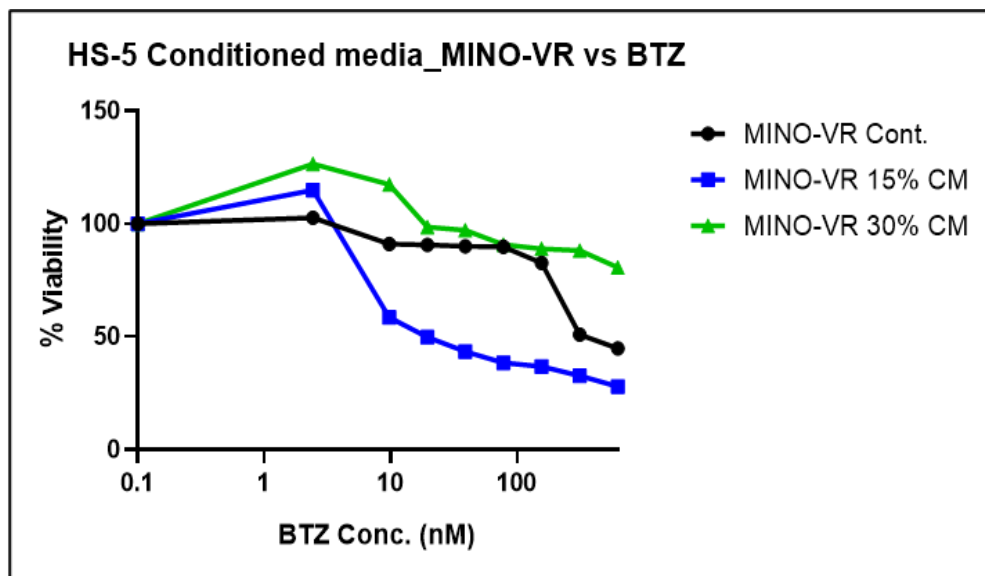
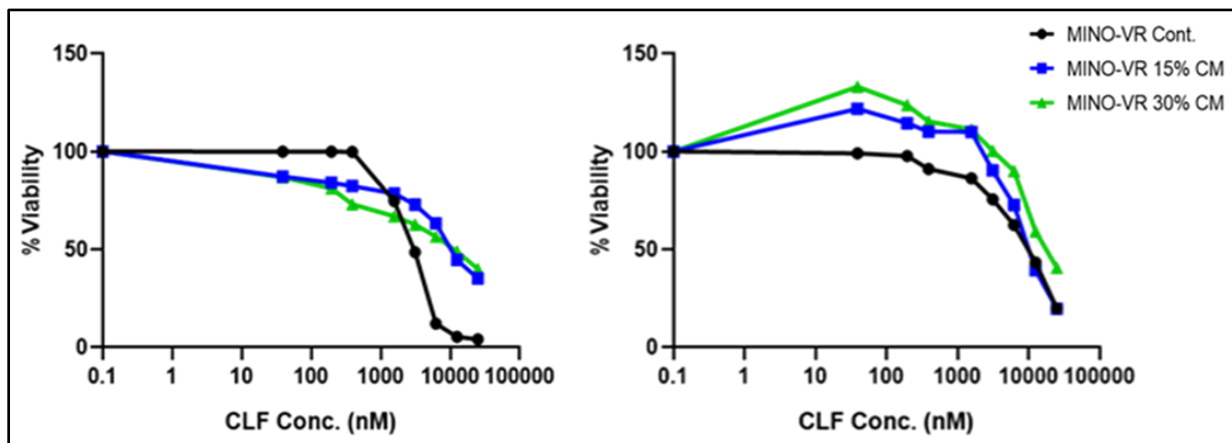


**Figure 7B**

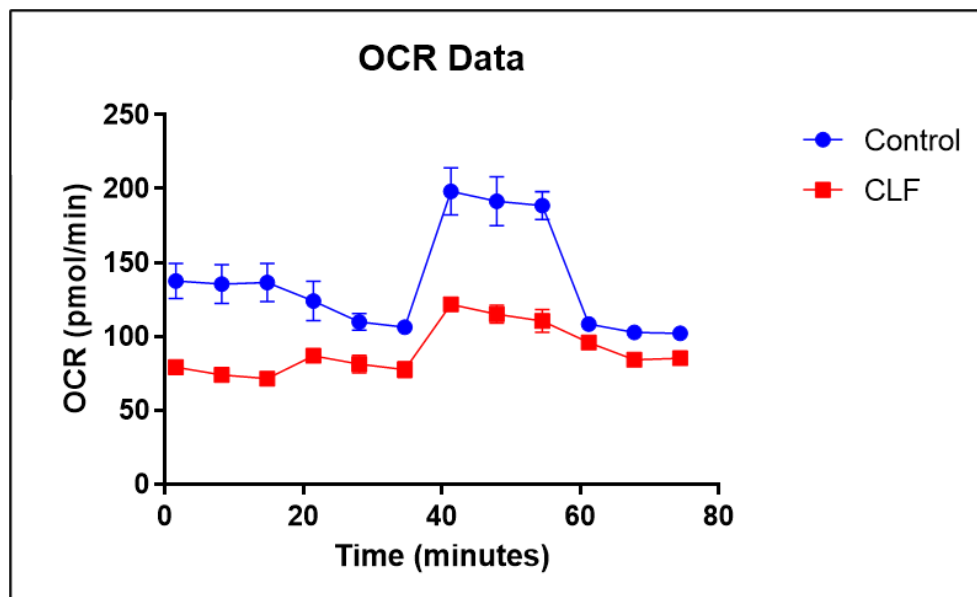


### CLF reduces the oxygen consumption rate (OCR) in MCL cells

Previous studies have shown that cancer cells have high levels of oxidative phosphorylation, which directly correlates with stemness. To characterize mitochondrial bioenergetics in resistant MCL cells and the effect of CLF on them, we measured the oxygen consumption rate (OCR), which is directly proportional to oxidative phosphorylation, using Seahorse Extracellular Flux Technology. The data showed that CLF was able to reduce the OCR in Mino-VR cells significantly, which may indirectly abrogate the hypoxia-mediated drug resistance.

**Figure 8. CLF reduces Mitochondrial respiration (measured by Oxygen Consumption rate) in MINO-VR cells.**

OCR measurement by Seahorse extra-cellular flux technology reveals that CLF was effective in reducing mitochondrial respiration—a characteristic feature of cancer cells and chemoresistance.



### Gene expression profiling revealed the potential mechanism of action and drug synergy in MCL cells

Differential gene expression analysis (ANOVA) of CLF-treated Mino-P, Mino-VR, and Z-138 vs. Control Mino-P, Mino-VR, and Z-138 showed a total of 9 genes that were commonly differentially expressed (DE) with ( $p < 0.05$ ; fold-difference  $\neq 1$ ) (**Figure 9B**). **Figure 9A** shows

the heatmap of single-agent CLF-induced kinetic changes separately for each MCL (Mino-P, Mino-VR, Z-138).

Differential gene expression analysis (ANOVA) of CLF treatment-induced changes (baseline (untreated) vs. single-agent CLF drug treatment) in PI-sensitive and PI-resistant MCLs showed a total of 267 genes were differentially expressed (DE) with ( $p < 0.05$ ; fold-difference  $\neq 1$ ). Among these, 38 genes had a  $|\text{fold-change}| \geq 2$ . 233 genes were shared between the treated vs. Untreated signatures at  $|\text{fold-change}| > 1$  ( $p < 0.05$ ). **Figure 9C** shows a heat map of the top DE genes.

Differential gene expression analysis (ANOVA) of CLF+BTZ combination-treated PI-sensitive and PI-resistant MCL cells vs. baseline (untreated) showed 4811 genes changed significantly ( $p < 0.05$ ; fold difference  $\neq 1$ ). Among these, 2350 genes showed  $|\text{fold-change}| \geq 2$  with a false discovery rate ( $\text{FDR} < 0.05$ ). **Figure 9D** depicts a heatmap of the top 50 genes associated with CLF+PI combination treatment. The top significantly upregulated genes following PI+CLF treatment were GSR, DAP3, and DOK1, which have reported anti-tumorigenic activity, whereas the top significantly downregulated genes were EHD1, CBX8, DDX17, SOX12, and COMMD3.

In Mino-VR cells, 1390 unique genes changed significantly ( $p < 0.05$ ; fold-difference  $\neq 1$ ) following CLF+BTZ treatment as compared to baseline (untreated), whereas single-agent BTZ-treated cells and single-agent CLF-treated cells showed 363 and 118 uniquely differentially expressed genes respectively. Among the 1390 genes, 454 genes showed  $|\text{fold-change}| \geq 2$  with a false discovery rate ( $\text{FDR} < 0.05$ ) (**Figure 9E**).

CLF+BTKi combination treatment ( $p < 0.05$ ; fold-difference  $\neq 1$ ) in Z-138 cells showed 143 uniquely differentially expressed genes as compared to the baseline (untreated) (**Figure 9F**).

Ingenuity pathway analysis revealed protein ubiquitination pathway and cell cycle arrest at the G2/M phase as the top canonical pathways (**Figure 9G**).

Causal network analysis (**Figure 9H**) showed synergistic drug action significantly elevated the levels of oxidative stress and unfolded protein response. Additionally, the PI+CLF combination potentiated AMPK-mediated down-regulation of the mTOR signaling pathway, which further led to the direct reduction of Cyclin D1 (aberrantly expressed in MCL) and the downregulation of eIF4-p70S6K signaling. The synergistic drug activity also led to the downregulation of oncogenic pathways like p38 MAPK and NF- $\kappa$ B signaling. PI+CLF combination downregulates

Wnt/ $\beta$  catenin signaling, which is found to be frequently overexpressed in MCL-ICs. HIPPO, another signaling pathway involved in the maintenance of cancer stem-ness and emergence of drug resistance, was also down-regulated.

**Figure 9A**

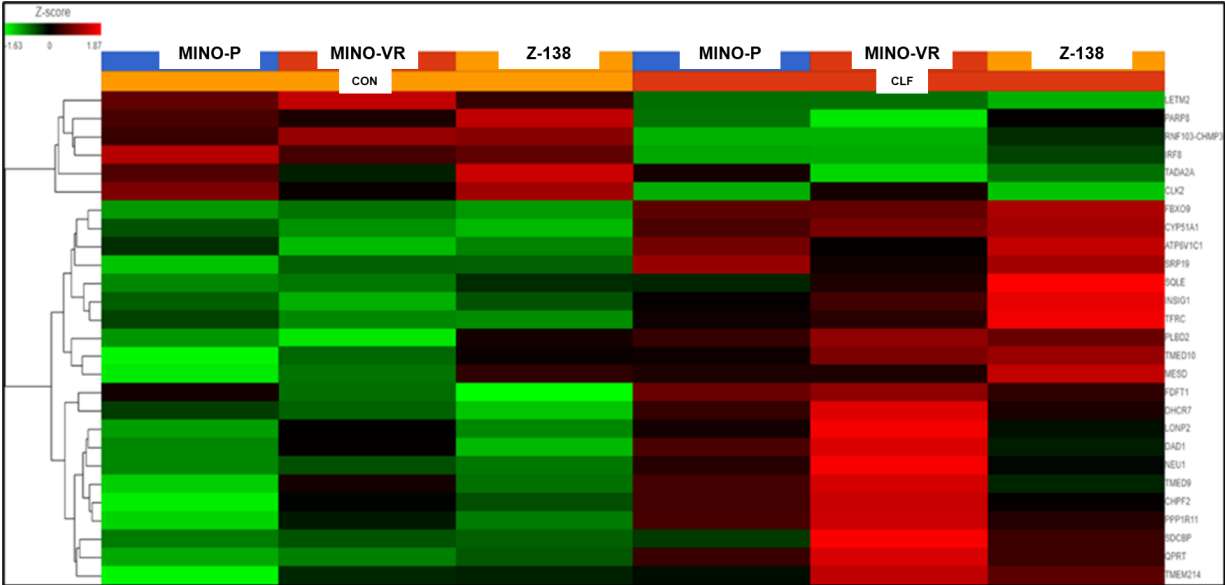


**Figure 9B**

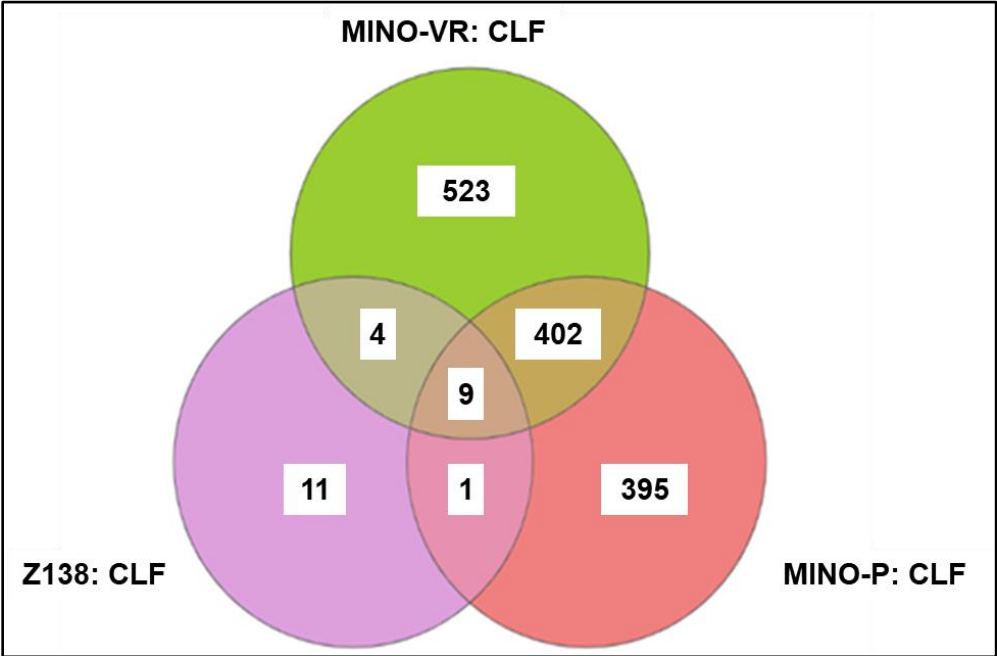


Figure 9C

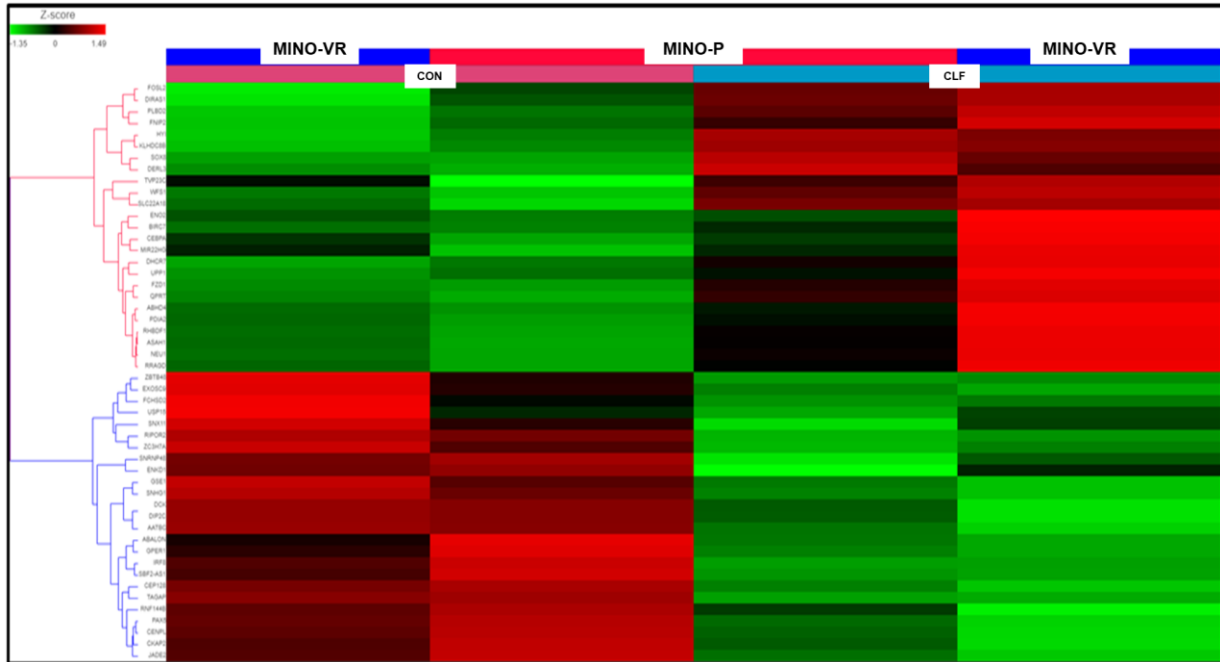
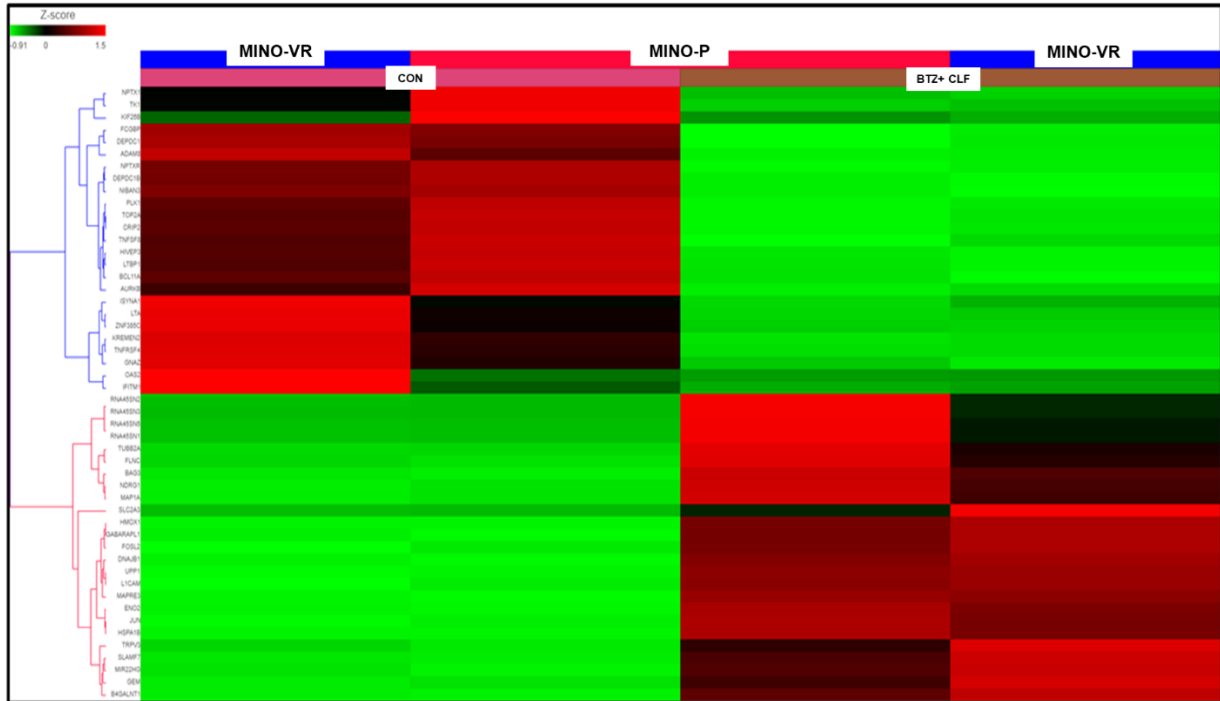
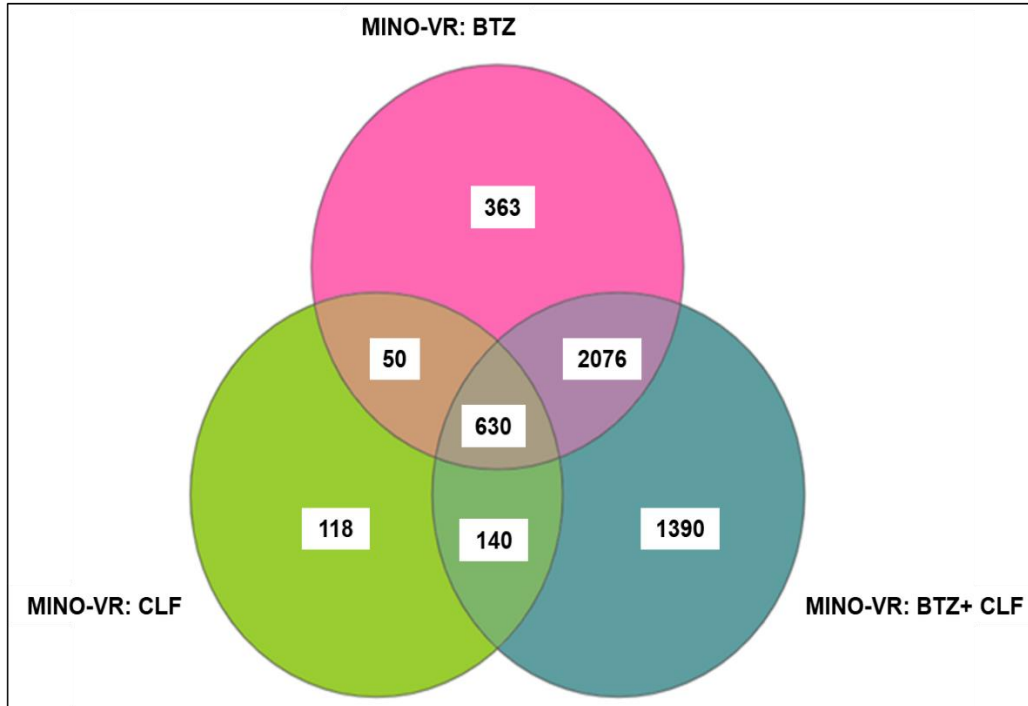


Figure 9D



**Figure 9E**



**Figure 9F**

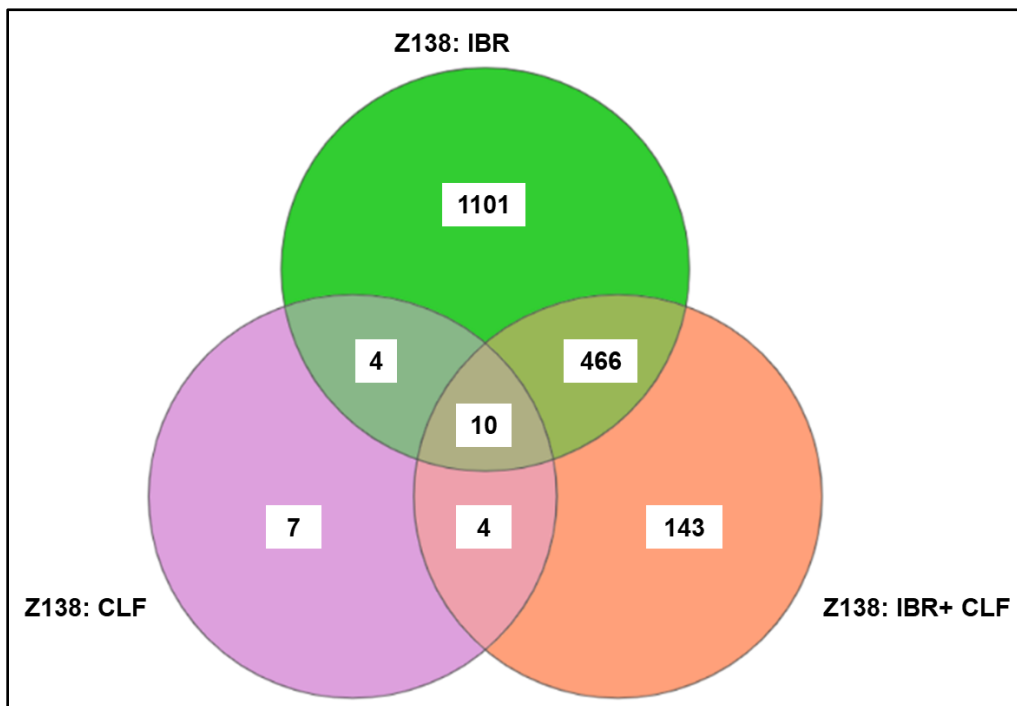


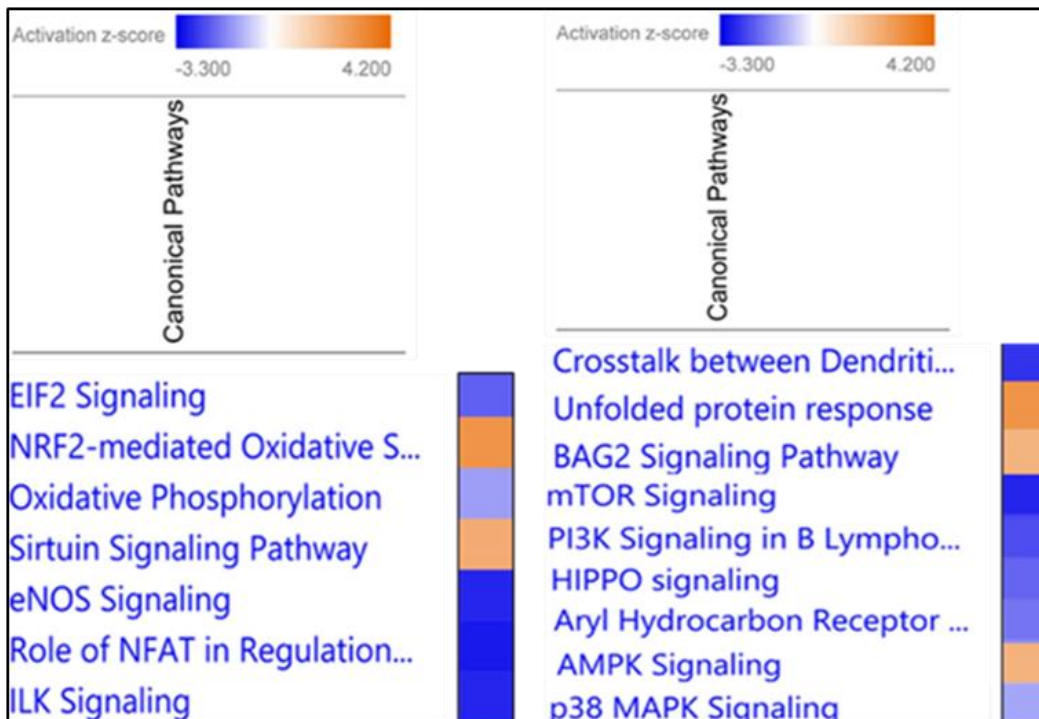
Figure 9G

Top Canonical Pathways	
CLF vs Cont.	
Name	p-value
Unfolded protein response	4.53E-06
EIF2 Signaling	5.66E-05
mTOR Signaling	3.17E-04
Regulation of IL-2 Expression in Activated and Anergic T Lymphocytes	6.22E-04
Regulation of eIF4 and p70S6K Signaling	6.25E-04

Top Canonical Pathways	
BTZ+CLF vs Cont.	
Name	p-value
Protein Ubiquitination Pathway	6.45E-23
Sirtuin Signaling Pathway	4.36E-13
Phagosome Maturation	5.71E-09
Antigen Presentation Pathway	1.13E-07
Cell Cycle: G2/M DNA Damage Checkpoint Regulation	3.24E-07

Figure 9H



### CLF down-regulates genes associated with poor disease-free survival

Next, we validated the top DE genes expressed in CLF treated vs. untreated control cells using TCGA's Diffuse Large B-Cell Lymphoma (DLBC) GEP dataset Kaplan-Meier Curves showed that the top DE genes SNHG1 (Figure 10A), EHD1 (Figure 10B) are significantly associated with the disease-free survival whereas another top DE gene GPER1 are significantly associated with the over-all survival (10C). CLF down-regulates the expression of the SNHG1 gene and EHD1 gene, whereas it up-regulates GPER1 expression.

Finally, immunoblotting results validated the down-regulation of Cyclin D1 in response to CLF treatment (Figure 10D).

### Figure 10. CLF down-regulates genes and pathways responsible for poor clinical outcome

#### Figure 10A

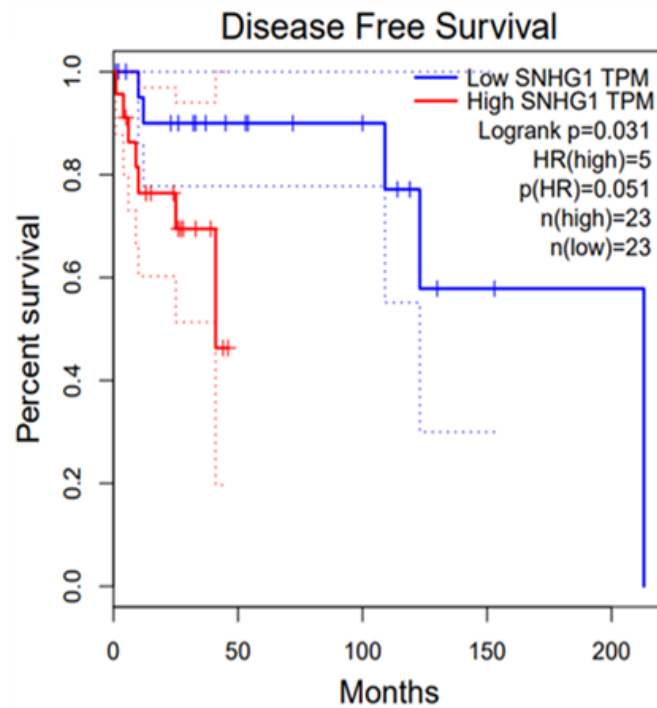


Figure 10B

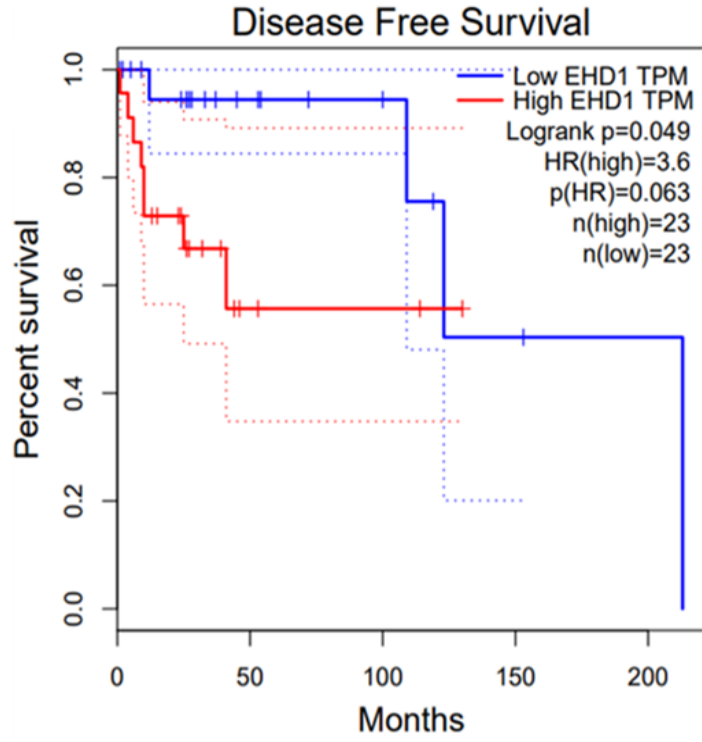
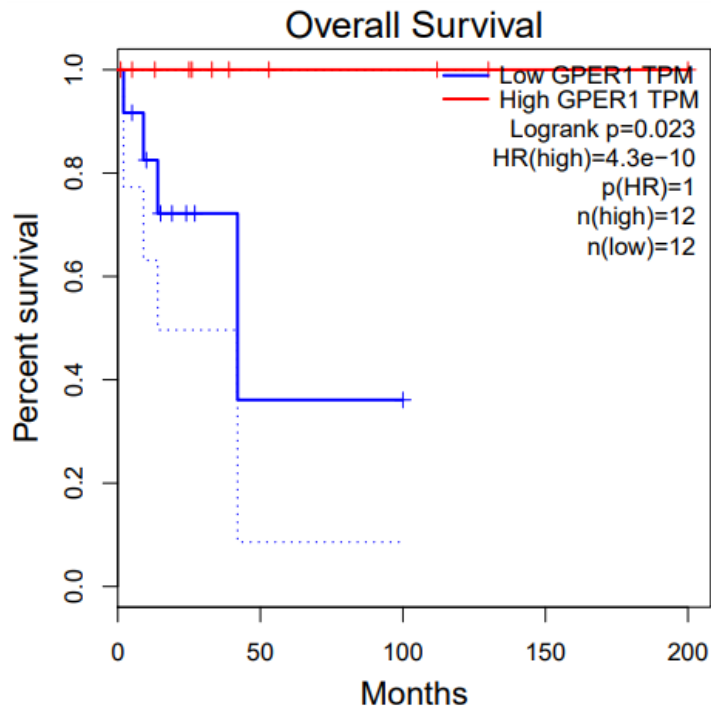
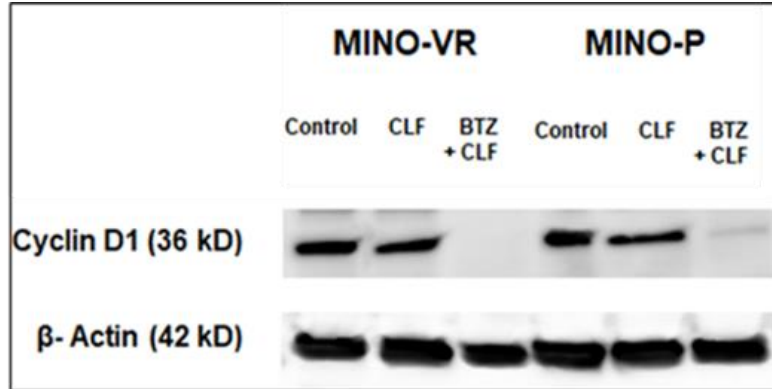


Figure 10C



**Figure 10D**

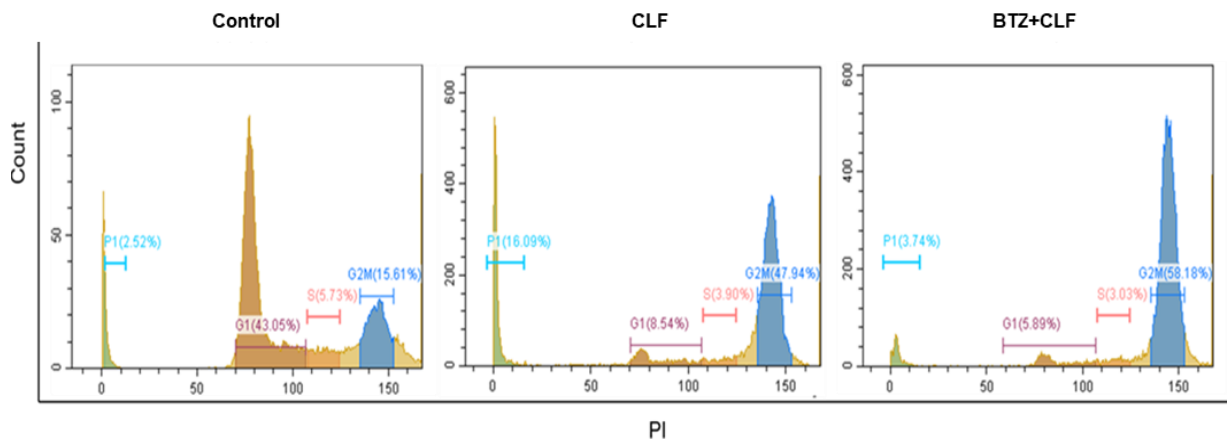


**CLF and PI/BTKi combination synergistically arrest MCL cells in the G<sub>2</sub>/M phase**

Since cell cycle arrest at the G<sub>2</sub>/M phase was predicted to be the top canonical pathway through IPA analysis, we investigated the distribution of different phases of the cell cycle by Propidium Iodide (PI). We observed a significantly higher % of the cells were arrested at G<sub>2</sub>/M phases in response to combination treatments compared to the single-agent treatments (Figure 11).

**Figure 11. CLF+ PI combination leads to the cell cycle arrest at the G<sub>2</sub>/M phase in MCL cells**

Propidium Iodide (PI) based analysis of the distribution of different phases of the cell cycle in Control CLF single agent and CLF+PI combination treated MCL cells (MINO-VR). The data shows a significantly higher percentage of cells in the G<sub>2</sub>/M phase in combination-treated cells as compared to the control cells.



### Single Cell transcriptomics (scRNA-seq) revealed single-cell sub-clusters killed by CLF

Finally, we used single-cell RNA sequencing (scRNA-seq) to identify CLF-induced changes in single-cell sub-clonal architecture (represented by t-SNE and UMAP clusters) in the drug-resistant Mino-VR cell lines. Our scRNA-seq data (Figure 12) showed erosion of the single-cell cluster #3 following CLF treatment. Cluster #3 is represented by the enrichment of expression of the following genes, indicative of CLF-induced death of MCL cells:

#### Figure 12. scRNA-seq data of Pre- & Post- CLF treated Mino-VR cells.

CLF-treated MINO-VR shows erosion of Cluster 1 & 2 and enrichment of cluster 3, whereas cluster 4 remains more or less the same.

Figure 12A

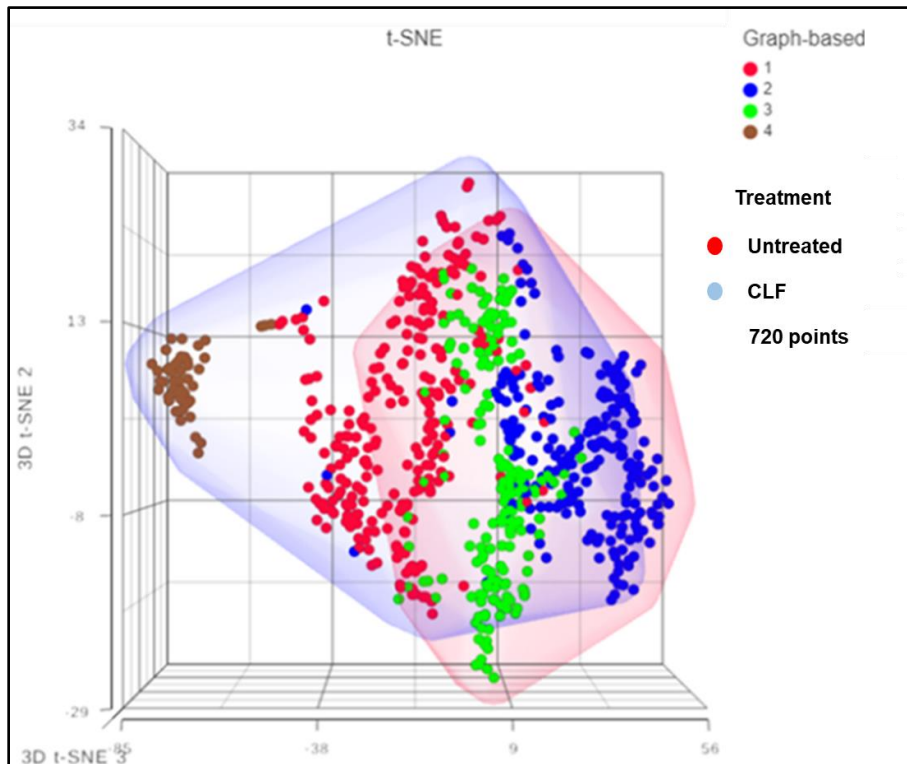


**Figure 12B**

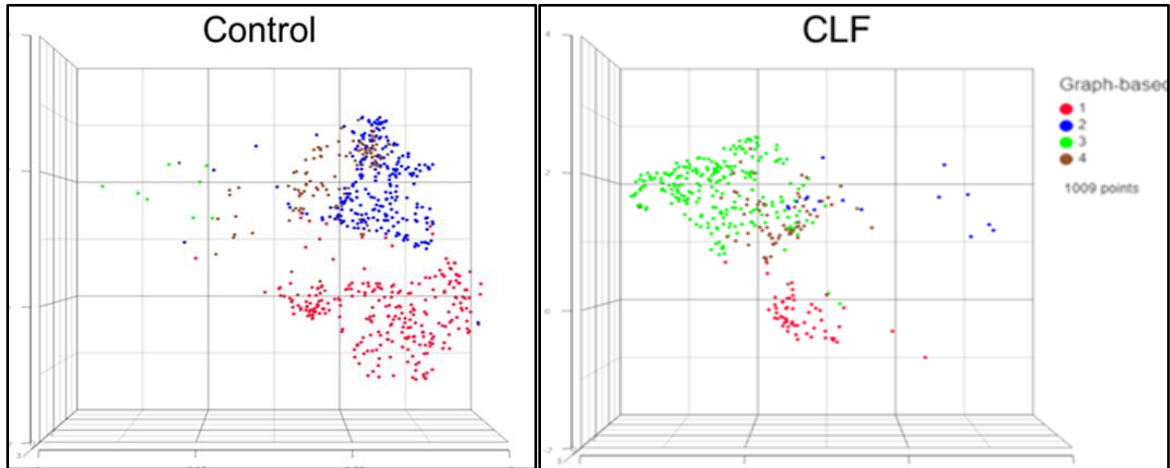
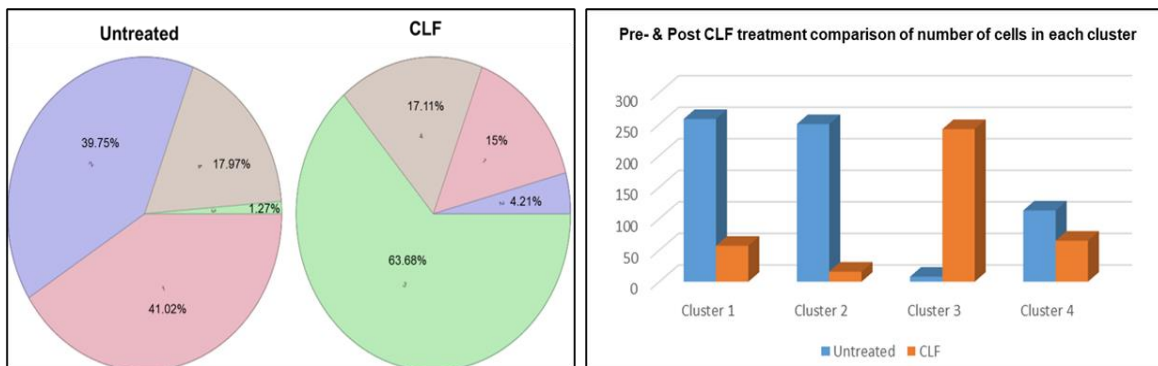


**Figure 12C**



**CLF reduces MYC and CCND1 expression in MCL-Initiating cells involved in relapse and chemo-resistance**

Interestingly, in CD45<sup>high</sup> CD19<sup>low</sup> cells, CLF induces the down-regulation of MYC (Figure 13A) and CCND1 (Figure 13B) expression. As these CD45<sup>high</sup> CD19<sup>low</sup> cells represent stem-ness in MCL and both MYC and CCND1 play a pivotal role in stem cell maintenance, their down-regulation indicates CLF's efficacy against CSCs.

**Figure 13A**

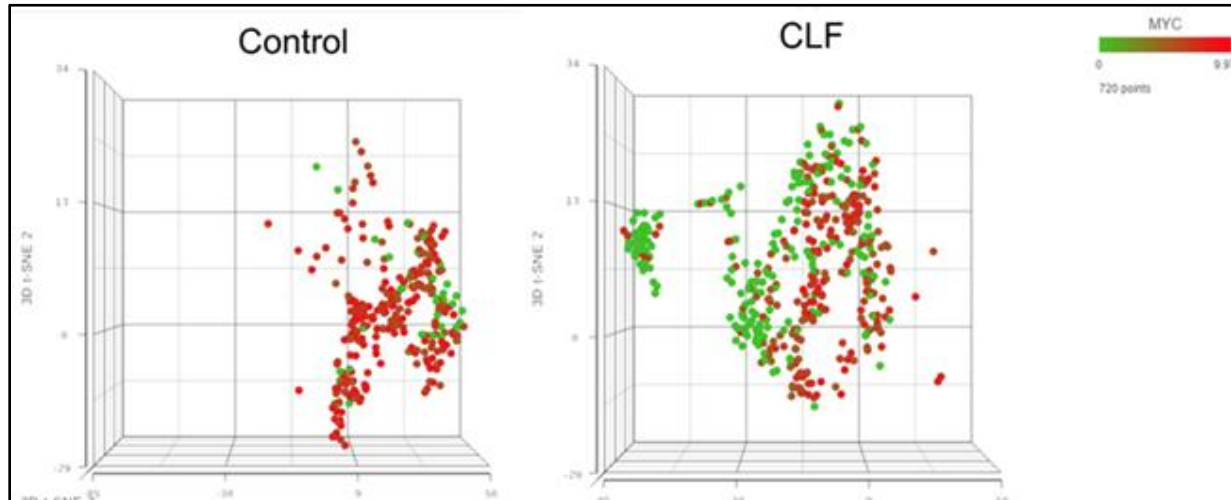
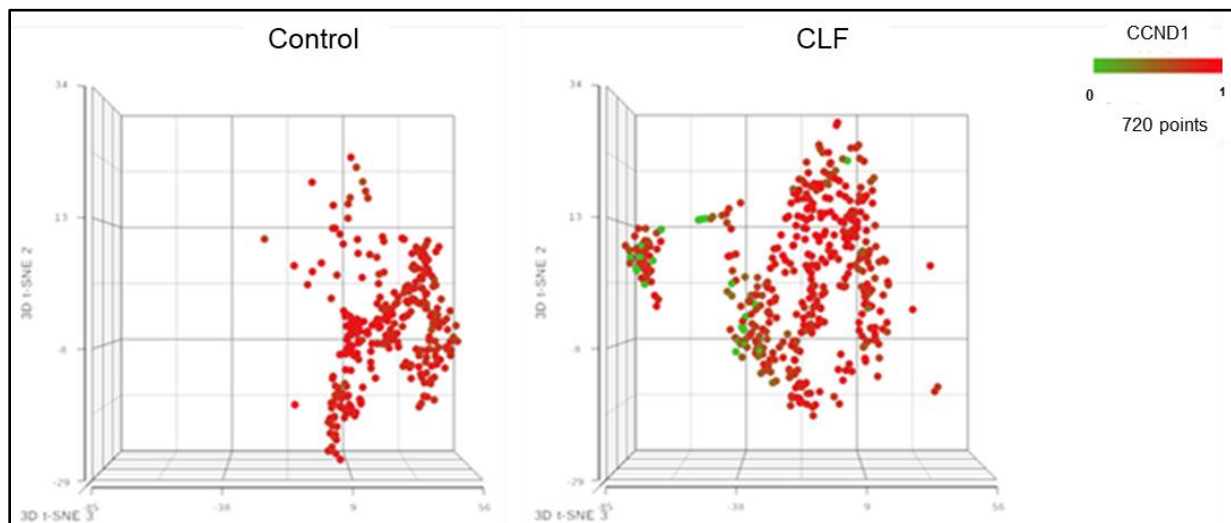


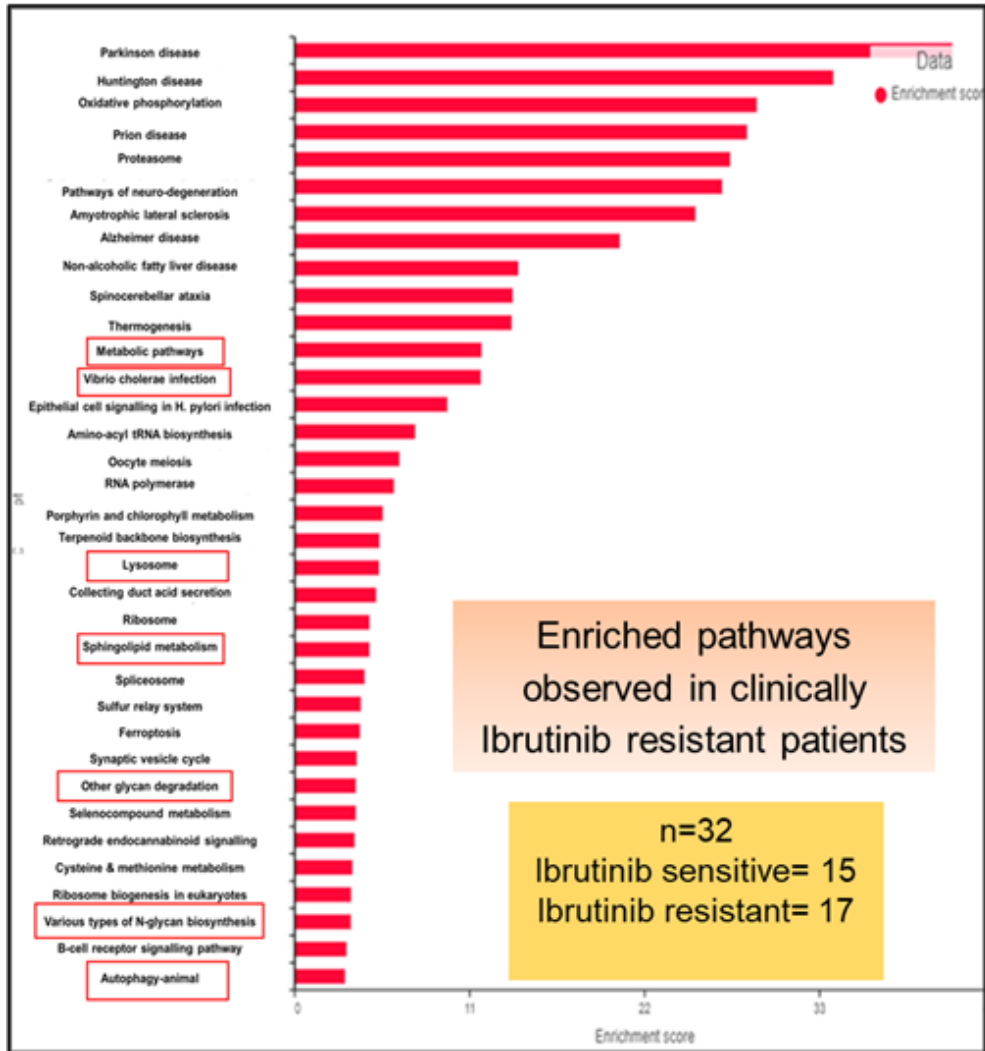
**Figure 13B**



### **Validation of CLF treatment-related gene signatures using patient cohort datasets**

Reverse-matching using patient cohort datasets shows that CLF treatment has the potential to reverse MCL lethality. Pathway analysis was performed based on the top DEGs in the Ibrutinib-sensitive and resistant MCL patient cohort (Figure 14A), and Top CLF treatment-induced upregulated pathways (Figure 14B) that were significantly downregulated in Ibrutinib-resistant MCL patients.

Figure 14A



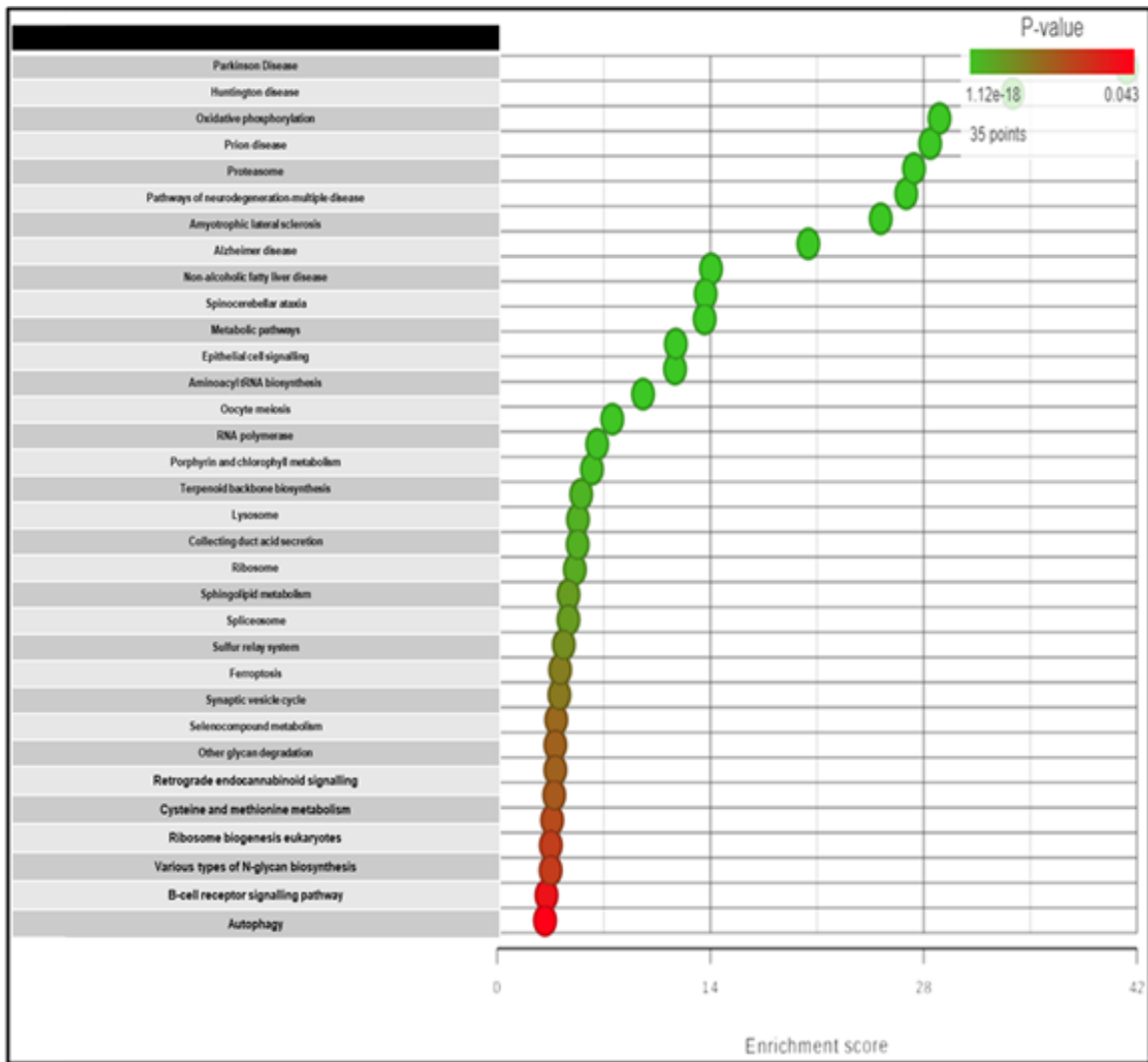
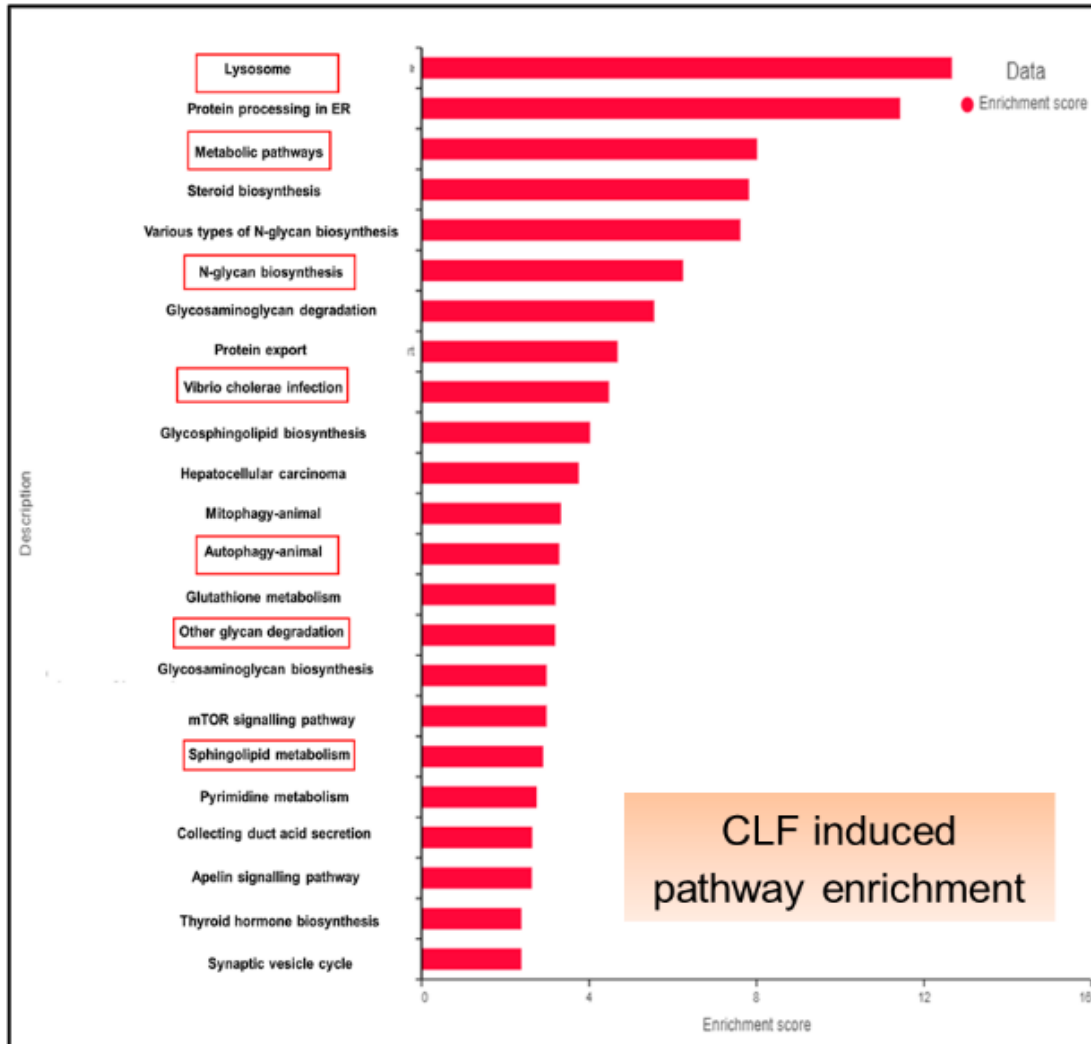
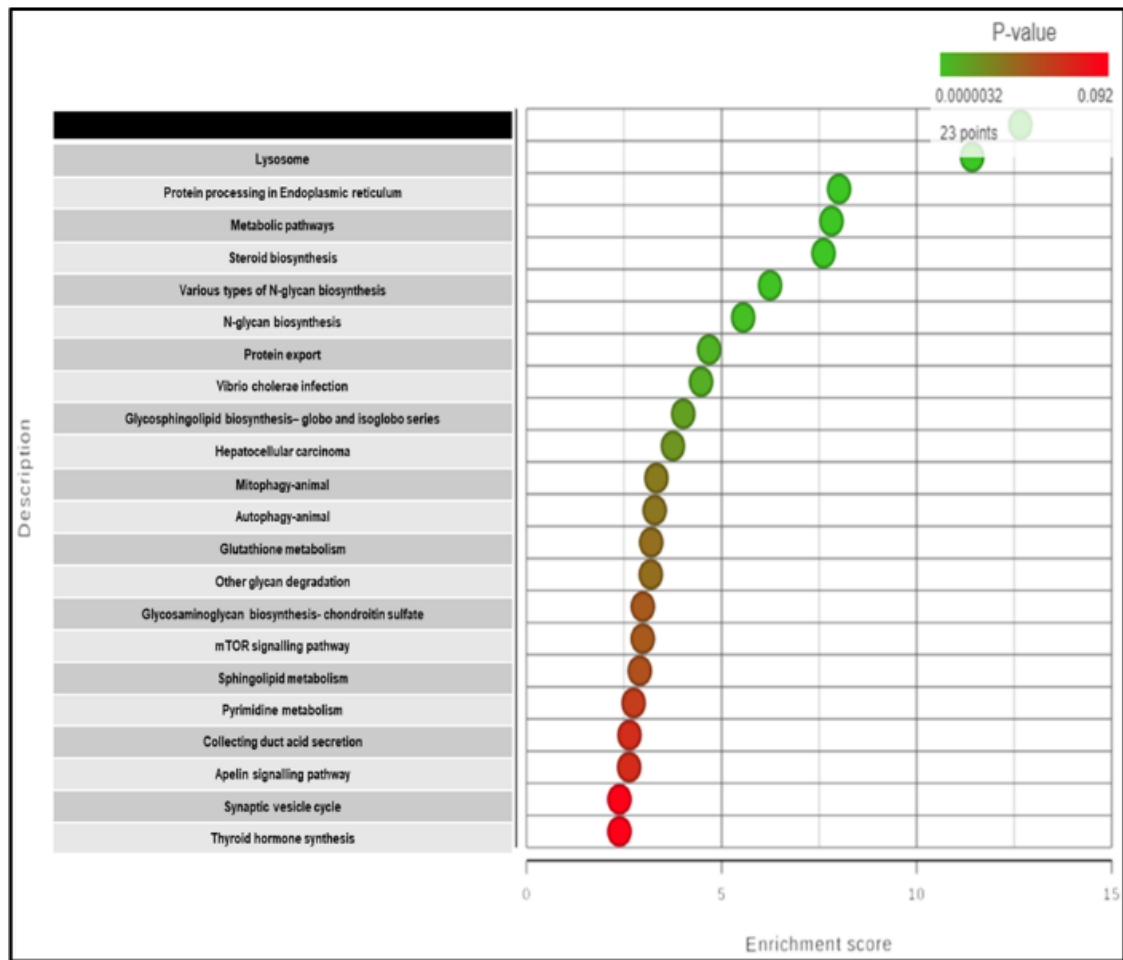


Figure 14B





**Figure 14.** KEGG pathway enrichment analysis provides mechanistic insights into CLF drug action in MCL cells. Comparison of Pathway enrichment analysis of GSE141335 dataset that contains expression data from clinically Ibrutinib responsive and unresponsive patients with CLF gene signature shows a high degree of similarities indicating CLF as a potent drug to curb resistance.

## Discussion

Mantle cell lymphoma (MCL) is an aggressive lymphoid neoplasm that develops from malignant B-lymphocytes in the outer edge or mantle zone of a lymph node.<sup>179</sup> This is a sub-type of B-cell non-Hodgkin lymphoma characterized by rapid clinical progression and poor response rate to conventional chemotherapeutic drugs with recurrent relapse resulting in a short estimated 5-year overall survival (OS) of 2-5 years depending on the clinical risk.<sup>192,195</sup> Combination therapies such as R-CHOP, R-DHAP, Hyper-CVAD, and VcR-CAP constitute the front-line chemotherapeutic treatment landscape for MCL.<sup>190</sup> Despite promising initial responses to the combination regimens, all patients develop resistance over time.<sup>371</sup> The Bruton's tyrosine kinase inhibitor (BTKi) Ibrutinib and the proteasome inhibitor (PI) Bortezomib are FDA-approved therapies for refractory or relapsed (R/R) MCL with demonstrated high initial response rates in clinical trials.<sup>194,195,370</sup> However, highly variable treatment response along with dose-limiting toxicities has limited the efficacy in real-world settings with the median progression-free survival (PFS) of <15 months and overall of 1-2 years.<sup>194,370</sup> Once ibrutinib stops working, only one-third of patients respond to their next line of treatment; those who do respond experience only brief remissions and have poor outcomes, irrespective of stem cell transplantation.<sup>195</sup>

To address this outstanding issue, we have designed a novel optimization-regularization-based computational prediction algorithm called “secDrug” that uses large-scale pharmacogenomics databases like the GDSC1000 to identify novel secondary drugs for the management of treatment-resistant B-cell malignancies. One of the top-predicted drugs was Clofazimine. Previously, we have demonstrated that Clofazimine (CLF), an anti-leprosy drug, could potentially be repurposed for the treatment of chronic myeloid leukemia and PI/IMiD-resistant multiple myeloma that also targets subclones representing putative stem-like-cells (CSCs).<sup>380</sup> CLF, which is a peroxisome proliferator-activated receptor- $\gamma$  (PPAR $\gamma$ ) agonist, binds to PPAR $\gamma$ , which results in modulation of its transcriptional as well as E3 ubiquitin ligase activity.<sup>380</sup> This increased ubiquitin ligase activity of PPAR $\gamma$  induces proteasomal degradation of p65 (RelA), which in turn results in sequential transcriptional downregulation of MYC and PRDX1, resulting in the cellular effects of CLF, including regulation of cellular ROS levels.<sup>379-381</sup> CLF also leads to the transcriptional down-regulation of Signal Transducer and Activator of Transcription 3 (Stat3) and Hypoxia-inducible factor 1 (HIF-1 $\alpha$ )-the two reported oncogenes with known involvement in cancer progression and stemness.<sup>380</sup> Notably, using single-cell analysis and high

dimensional immunophenotyping, we have also identified molecular networks underpinning CLF+PI synergy.

Recent evidence indicates that intra-tumor heterogeneity due to the presence of treatment-refractory subpopulations or cancer stem-like cells (CSCs) drive drug resistance and disease relapse in Mantle Cell Lymphoma.<sup>97,98</sup> These putative stem-like cells in MCL include CD45<sup>+</sup>CD1<sup>9-</sup> cells or MCL-initiating cells (MCL-ICs), relatively quiescent-highly clonogenic aldehyde dehydrogenase (ALDH)<sup>+</sup> cells, and side populations (SP).<sup>213,214,216,375</sup> Ibrutinib is ineffective in targeting MCL-CSCs.<sup>208,370</sup> Therefore, there is an unmet need to discover novel treatment strategies against refractory/relapsed (R/R) MCL.

For this purpose, using a panel of MCL cell lines as in vitro model systems, we have tested the efficacy of CLF as a single agent and in combination with the FDA-approved therapy for R/R MCL, i.e., PI (Bortezomib) and BTKi ((Ibrutinib, Acalabrutinib). We found that CLF effectively reduces the cell viability of innate and acquired resistant MCL cell lines where CLF+BTKi/PI combination lowered the effective BTKi, and PI doses required to achieve desired therapeutic response by >10-folds. We found that CLF+BTKi/PI combination induces apoptosis by arresting the cells in the G<sub>2</sub>/M phase. The drug combination also increases the intracellular ROS reactive oxygen species (ROS) production for, e.g., cellular superoxide anions followed by the collapse in mitochondrial membrane potential depolarization or depolarization that ultimately leads to the activation of the Caspase 3, 7- mediated intrinsic pathway of apoptosis.

Furthermore, Clofazimine also explicitly targets the putative CSCs. CLF as a single agent and in combination with the PI/ BTKi leads to the depletion of the side-population (SP) cells as well as reduces the ALDH activity, which is present at a high level in resistant MCL cells indicating the presence of stem-cell pools.

mRNA-sequencing followed by differential gene expression analysis gave us the mechanistic insights of the drug action where it showed simultaneous up-regulation of several anti-tumorigenic genes and down-regulation of pro-survival genes. Ingenuity pathway analysis followed by causal network analysis revealed the molecular network behind the synergistic drug actions. The drug combination led to the inhibition of critical oncogenic signaling pathways along with Cyclin D1, which is essential for the survival of MCL cells.

EHD1, a member of the EPS15 homology (EH) domain-containing proteins family, was found to be downregulated in response to PI+CLF treatment. EHD1 is involved in the endocytic recycling of the membrane and cell-surface receptor proteins, such as the Epidermal growth factor receptor (EGFR).<sup>382</sup> Previous studies have suggested that EHD1 has a positive correlation with disease progression and poor treatment outcomes in other cancers, such as cutaneous T-cell lymphoma and non-small cell lung carcinoma.<sup>382–384</sup> TCGA database analysis on the Diffuse Large B-cell lymphoma (DLBC) dataset, another sub-type of Non-Hodgkin Lymphoma) revealed that enhanced expression of EHD1 is significantly associated with low disease-free survival.

Long non-coding RNAs (lncRNA) are the transcripts that do not code for protein but instead act as an epigenetic modifier to control gene expression.<sup>385</sup> Due to their involvement in chromatin remodelling as well as regulating transcriptional and post-transcriptional processes, their role in oncogenesis is gaining importance.<sup>386</sup> Several cancers, like glioblastoma, colorectal carcinoma, etc., have reported dysregulation of lncRNA expression, leading to drug resistance and oncogenic progression.<sup>387,388</sup> In our study, we found that the PI+CLF combination down-regulated SNHG1 (Small Nucleolar RNA Host Gene 1), a lncRNA. In colorectal cancer cells, SNHG1 is found to be over-expressed, where it interacts with the Wnt- $\beta$  catenin signaling pathway to promote migration and invasion.<sup>389</sup> SNHG1 has also been implicated in the development of drug resistance and tumor progression in hepatocellular carcinoma and glioma, respectively.<sup>390,391</sup> TCGA database analysis of SNHG1 on the DLBC dataset showed that SNHG1 expression is negatively correlated with disease-free survival.

In the Z-138 cell line, the combination of Ibrutinib and CLF enhanced the downregulation of MYC as compared to single agent Ibrutinib treatment. MYC drives cancer stemness in various cancer and chemoresistance in various cancers.<sup>392</sup> It also promotes resistance towards Ibrutinib in MCL.<sup>393</sup>

SOX12, another known oncogene expression also found to be downregulated in response to BTKi+CLF treatment.<sup>394</sup> BTKi+CLF treatment also suppressed the expression of HK2, CCNF, NOTHC1, and DDX21. All of these genes are tumor progression, poor prognosis, and proliferation of the cancer cells.<sup>395–398</sup>

Finally, single-cell transcriptomic analysis (scRNA-seq) further elucidated the molecular mechanism of drug action at a single-cell resolution. We found that CLF eroded the drug-resistant sub-clones in clonally derived PI-resistant MCL cells. CLF-treated MINO-VR shows erosion of Cluster 1 & 2 and enrichment of cluster 3, whereas cluster 4 remains more or less the same.

Cluster 1 is characterized by the following genes which have reported activity in oncogenesis:

- i. **ESCO2 (Establishment of Sister Chromatid Cohesion N-Acetyltransferase 2)** is highly expressed in aggressive melanomas and breast cancer. In gastric cancer, ESCO2 promotes cell proliferation by modulating the p53 and mammalian target of rapamycin (mTOR) signaling pathways.<sup>399</sup>
- ii. **Topoisomerase II alpha (TOP2A)** is a proliferation marker with a positive association with tumor grade and Ki67 index.<sup>400</sup> DNA topoisomerase II $\alpha$  (TOP2A) encodes DNA topoisomerase, which during DNA replication and transcription, releases torsional stress.<sup>401</sup> TOP2A actively participates in cellular proliferation and acts as a critical gene in breast, endometrial, colon, and ovarian cancer.<sup>400</sup>
- iii. Previous studies have shown that enhanced **CDK1** expression is a key factor in the oncogenic progression of colorectal cancer, liver cancer, and lung cancer, where it causes reduced survival time.<sup>402</sup>
- iv. **KIF2C** is abnormally expressed in multiple types of cancer, such as lung cancer and glioma, and is associated with poor prognosis. KIF2C is critical for the regulation of microtubule dynamics and stabilization.<sup>403</sup>
- v. **Upregulated expression of NDC80 has been observed in human** pancreatic cancer tissues, and its down-regulation leads to the inhibition of cell cycle progression.<sup>404</sup>
- vi. **Abnormal spindle-like microcephaly-associated (ASPM), is a protein crucial for** the normal functioning of the mitotic spindle during cell replication. Enhanced expression of the ASPM gene is linked with aggressive cancer progression and poor treatment outcomes in bladder cancer & prostate cancer.<sup>405</sup>
- vii. **GTSE1** could promote breast cancer cell growth by activating the AKT pathway and enhance metastasis by regulating the Epithelial-Mesenchymal transition (EMT) pathway.

Furthermore, it could cause multidrug resistance in breast cancer cells. GTSE1 mRNA and protein levels are found to be upregulated in PCa, and the mRNA level is negatively associated with patient prognosis. GTSE1 can promote PCa cell proliferation via the SP1/FOXM1 signaling pathway, which facilitates tumorigenesis and progression.<sup>406</sup>

viii. Several cancers, like renal cell carcinoma & prostate cancer, display high **NCAPG** expression, which is responsible for poor patient disease-free and overall survival.<sup>407</sup>

**Cluster 2** is characterized by the following genes which have reported activity in oncogenesis:

- i. **CRIP1** activates the Wnt/ $\beta$ -catenin signaling pathway and induces cell migration and invasion through EMT in cervical cancer.<sup>408</sup>
- ii. Increased **T-cell leukemia/lymphoma 1A (TCL1)** expression has been identified in B-cell non-Hodgkin's lymphoma, where it plays a pivotal role in B-cell survival.<sup>408</sup>
- iii. **CD79b**, a component of the B-cell receptor (BCR), is expressed in over 90% of B-cell NHL malignancies.<sup>409</sup>

**OAS1** gene is expressed in **cluster 3**. It has tumor-suppressor activity in breast cancer.<sup>410</sup>

From the molecular signature of CLF action, we found that it has potential application in clinical settings. Pathway enrichment analysis of the GSE141335 dataset that contains expression data from clinically responsive and unresponsive patients showed strikingly similar to that of the CLF-induced pathway enrichment data indicating that CLF could be helpful in clinical settings. It is reported that enrichment of mTOR, NF- $\kappa$ B, and E2F signaling pathways, as well as MYC, are hallmarks of Ibrutinib resistance based on the patient samples data. Interestingly, the molecular signature of CLF action, as evident from the KEGG pathway enrichment analysis, shows enrichment of mTOR signaling, which we further investigated through causal network analysis in IPA and found to be downregulated to a much greater extent in BTZ+CLF combination treatment than treatment with BTZ alone. The causal network also predicts a similar trend for NF- $\kappa$ B signaling. Enrichment of metabolic pathways such as Oxidative phosphorylation was also observed in the Ibrutinib-resistant patients as well as in CLF-treated cells. The previous study has shown upregulation of the OXPHOS pathway is associated with ibrutinib resistance. In our study, causal network analysis shows a significantly higher level of

OXPLOS inhibition in combination treatment as compared to single-agent standard-of-care drug treatment.<sup>411</sup>

To summarize, we can conclude that CLF is effective as a single agent as well as in combination in R/R MCL cells, including the ones that are unresponsive to the standard-of-care drugs for R/R MCL, i.e., BTKi and PI. As it is FDA-approved and is on WHOS's list of essential medicine<sup>412</sup> with a well-tolerated safety profile, CLF has the strong potential to be repurposed as a novel, safe, broad spectrum therapeutic option for the management of advanced stage R/R MCL.

## **CHAPTER 5.2**

### **Repurposing Clofazimine As a Novel Drug For The Treatment of PI-Resistant Stem Cell-like Subclones in Multiple Myeloma**

## Abstract

Multiple myeloma (MM) is an incurable plasma cell malignancy with dose-limiting toxicities and inter-individual variation in response/resistance to the standard-of-care/primary drugs, proteasome inhibitors (PIs), and immunomodulatory derivatives (IMiDs). Although newer therapeutic options are potentially highly efficacious, their costs outweigh their effectiveness. Previously, we have established that clofazimine (CLF) activates peroxisome proliferator-activated receptor- $\gamma$ , synergizes with primary therapies, and targets cancer stem-like cells (CSCs) in drug-resistant chronic myeloid leukemia (CML) patients. In this study, we used a panel of human myeloma cell lines as *in vitro* model systems representing drug-sensitive, innate/refractory, and clonally-derived acquired/relapsed PI- and Cereblon (CRBN)-negative IMiD-resistant myeloma and bone marrow-derived CD138<sup>+</sup> primary myeloma cells obtained from patients as *ex vivo* models to demonstrate that CLF shows significant cytotoxicity against drug-resistant myeloma as single-agent and in combination with PIs and IMiDs. Next, using genome-wide transcriptome analysis (RNA-sequencing), single-cell proteomics (CyTOF; Cytometry by time-of-flight), and ingenuity pathway analysis (IPA), we identified novel pathways associated with CLF efficacy, including induction of ER stress, autophagy, mitochondrial dysfunction, oxidative phosphorylation, enhancement of downstream cascade of p65-NF $\kappa$ B-IRF4-Myc downregulation, and ROS-dependent apoptotic cell death in myeloma. Further, we also showed that CLF is effective in killing rare refractory subclones like side populations that have been referred to as myeloma stem-like cells. Since CLF is an FDA-approved drug and also on WHO's list of safe and effective essential medicines, it has strong potential to be rapidly re-purposed as a safe and cost-effective anti-myeloma drug.

## Introduction

Multiple myeloma (MM) is an incurable neoplasm characterized by clonal expansion of malignant antibody-producing post-germinal-center B-cell-derived plasma cells within the bone marrow.<sup>125,280</sup> Myeloma is the second-most common hematopoietic malignancy in the United States, with an estimated 34,920 new cases and 12,410 deaths in 2021. Proteasome inhibitors (PIs; bortezomib/Bz/Velcade, carfilzomib/Cz, and Ixazomib/MLN9708/Ix) are standard-of-care/primary chemotherapeutic agents for relapsed and refractory myeloma that impede tumor metastasis and angiogenesis by accelerating unfolded protein response (UPR) and by interfering with the NF- $\kappa$ B-enabled regulation of cell adhesion-mediated drug resistance.<sup>171,296158</sup> Combination therapy regimens incorporating PIs and immunomodulatory drugs (IMiDs; Lenalidomide/Revlimid, Pomalidomide) as backbone have significantly improved treatment responses, including progression-free survival (PFS) and overall survival (OS). However, despite these and other recent improvements in therapies, myeloma remains a difficult-to-cure disease with dose-limiting toxicities and drug resistance and a median survival rate of only around 7 years. Moreover, a recent study on the cost-effectiveness of anti-myeloma drugs suggested that although the current therapeutic regimens, including novel treatments (like monoclonal antibodies and Chimeric antigen receptor or CAR-T-cell therapy), are highly promising, the costs outweigh the effectiveness based on willingness-to-pay thresholds. Therefore, our goal was to search for new secondary therapeutic options with lower costs and higher cost-effectiveness to treat drug resistance in myeloma.

Previously, we have demonstrated that Clofazimine (CLF), an anti-leprosy drug, activates peroxisome proliferator-activated receptor- $\gamma$  and synergizes with the standard-of-care drug imatinib for the treatment of chronic myeloid leukemia (CML). Although two studies have shown the efficacy of CLF treatment in multiple myeloma, none of these have explored the synergistic effect of CLF in combination with PI or IMiD therapy or the impact of CLF-based therapy using model systems representing the wide inter- and intra- tumor heterogeneity in myeloma drug response. Further, the potential mechanisms underpinning CLF as an anti-myeloma drug have not been understood fully so far. Therefore, in this study, we used a diverse panel of human myeloma cell lines and patient-derived primary myeloma cells to investigate the potential of CLF as an anti-myeloma drug against inter-tumor and intra-tumor heterogeneity in PI and IMiD-resistant myeloma. Furthermore, using genome-wide transcriptomics (tumor

mRNA-sequencing) and single-cell proteomics (CyTOF or Cytometry by time-of-flight), we also identified several genes and potential molecular networks involved in the CLF mechanism of action and drug synergy with PIs and IMiDs.

Drug resistance is a manifestation of significant complexity and heterogeneity at the molecular level. In addition, the presence of rare subpopulations of tumor cells with stem cell-like properties, like greater clonogenicity, self-renewal, and differentiation capacities, are believed to significantly contribute towards treatment-refractory phenotypes in various cancers, including myeloma.<sup>55,57,98,217,218</sup> Since our previous study had shown that CLF erodes quiescent stem-cell populations (CD34<sup>+</sup>CD38<sup>-</sup>, CFSE<sup>bright</sup>) in drug-resistant CML patients, we also showed that CLF kills quiescent/dormant cells, ALDH<sup>+</sup> cells, and side populations (SPs), collectively referred to as putative stem-like cells in myeloma, with treatment-refractory phenotypes.<sup>380</sup> We propose clinical efficacy studies in relapsed/refractory myeloma using clofazimine-based drug combination regimens.

### **CLF Induces Loss of Viability in HMCLs and PMCs**

First, we evaluated the single-agent in vitro cytotoxicity of CLF for anti-myeloma activity in our HMCL panel, representing a wide variation in PI and IMiD responses (IC<sub>50</sub>) (Figure 1A). We found that CLF alone showed very potent inhibition of cell viability in HMCLs representing sensitive as well as innate and clonally-derived resistant HMCLs. The single-agent IC<sub>50</sub> (48h) values of CLF were between 0.2μM- 20.5μM. Next, we compared the link between CLF IC<sub>50</sub> of the myeloma cell lines and MM molecular/cytogenetic abnormalities. Our results showed no significant association of CLF response with cytogenetic abnormalities (data not shown).

**Figure 1.** CLF decreases the in vitro and ex vivo cell viability in multiple myeloma. **(A)** Response to single-agent CLF treatment in HMCLs (human myeloma cell lines). **(B)** Representative ex vivo CLF dose-response plots in patient bone marrow-derived primary myeloma cells.

Figure 1A

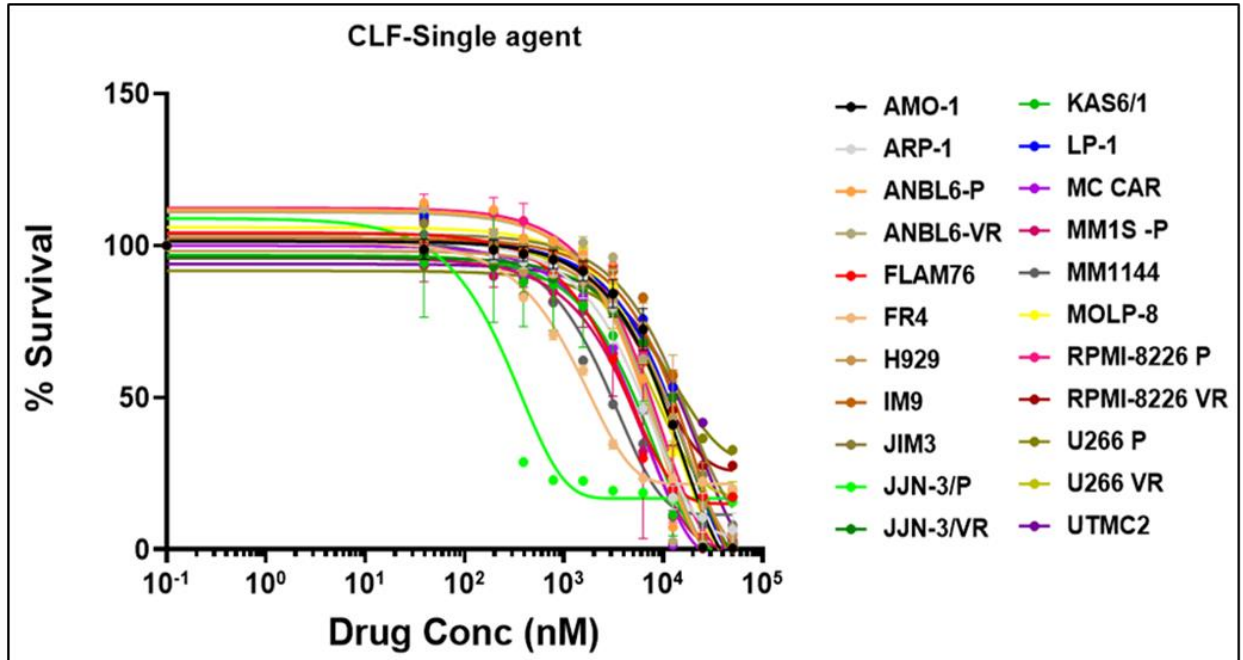
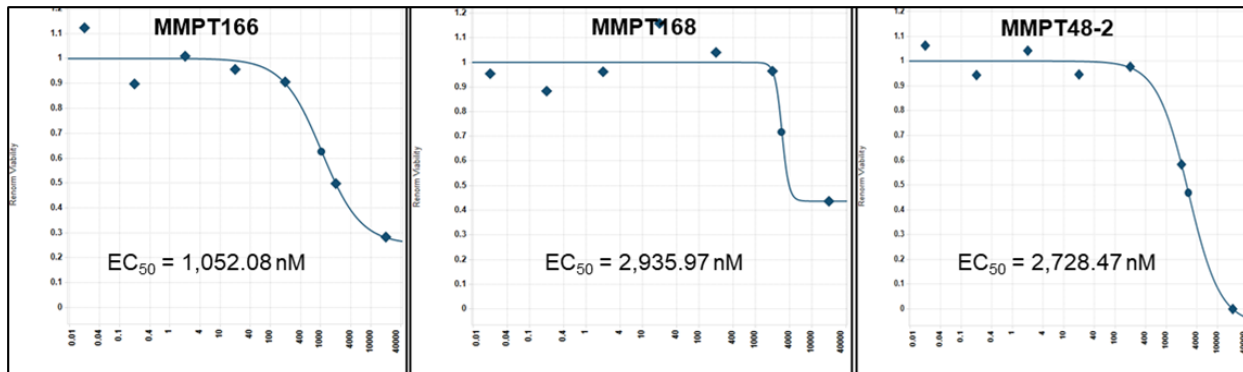


Figure 1B



Further, bone marrow-derived CD138<sup>+</sup> PMCs were obtained from patients (n=12) at Mayo Clinic and used as ex vivo model systems. Using our established direct-to-drug screening assay, we screened each patient's tumor in a Phase 0 assay for drug sensitivity to single-agent CLF. The ex vivo CLF EC<sub>50</sub> values (1-15  $\mu$ M; minimum EC<sub>50</sub> 1052.1nM, maximum EC<sub>50</sub> 15210nM, median EC<sub>50</sub> 2408.7nM) were within the in vitro IC<sub>50</sub> range. Figure 1B shows representative CLF single-agent ex vivo cytotoxicity plots in myeloma patients.

## CLF Shows Synergy with Proteasome Inhibitors and IMiDs

Next, we tested the cytotoxicity of CLF in combination with PIs (represented by Ixazomib; Figures 2A–C) or IMiDs (represented by Lenalidomide; Figures 2D, E) in HMCLs representing innate-sensitive (FLAM76, KAS6/1, MM1S), innate-resistance (JIM-3, LP-1), and acquired- PI or IMiD resistance (U266 P/VR, RPMI8226 P/VR, JJN-3 P/VR, and MM1S P/LenR). The CLF+PI and CLF+Len combination index (CI) values calculated using the Calcsyn program were consistently less than 0.9 (Figure 2D-E), indicating synergy (26). Further, CLF improved the therapeutic index of PI and IMiD administration to the cells and decreased the amount of PI/IMiD required to achieve effective responses, as indicated by dose reduction index (DRI) values and predicted decrease in  $IC_{50}$  (nM concentration).

**Figure 2.** Clofazimine synergizes with Proteasome inhibitors and Immunomodulatory drugs (IMiDs) in multiple myeloma. CLF + PI (represented by Ixazomib) treatment in (A) Innate-sensitive myeloma cell lines; (B) Innate-resistant myeloma cell lines. (C) Parental and clonally-derived acquired resistant myeloma cell lines. CLF + IMiD (represented by Lenalidomide) treatment in (D) Parental and clonally-derived acquired PI-resistant myeloma pairs; and (E) IMiD sensitive/resistant pair. (CI – Combination index calculated using Chou-Talalay’s CI theorem). (F-G) Demonstration of drug synergy using combination index (CI) values: (F) CLF+PI; (G) CLF+ IMiD

Cells were treated as a combination, and CI values were calculated for each fraction affected (FA; a fraction of cells affected/ killed)) using Calcsyn Software that applies a method proposed by Chou and Talalay. C.I value of less than 0.9 indicates synergism.

**Figure 2A**

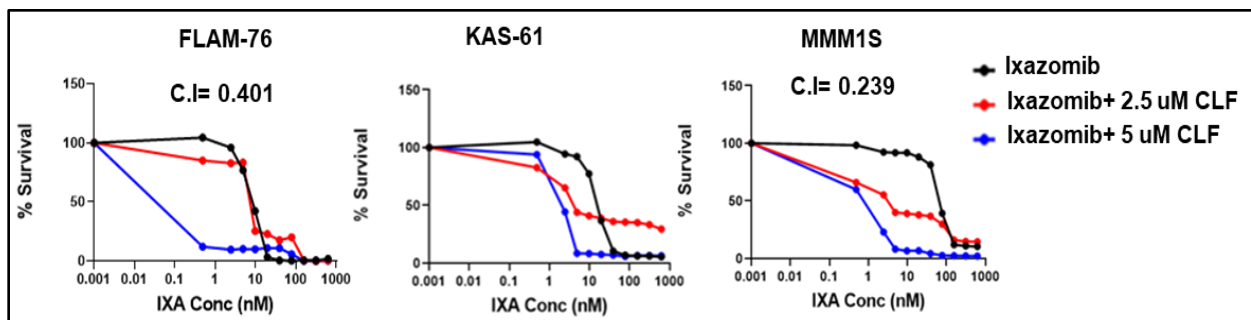


Figure 2B

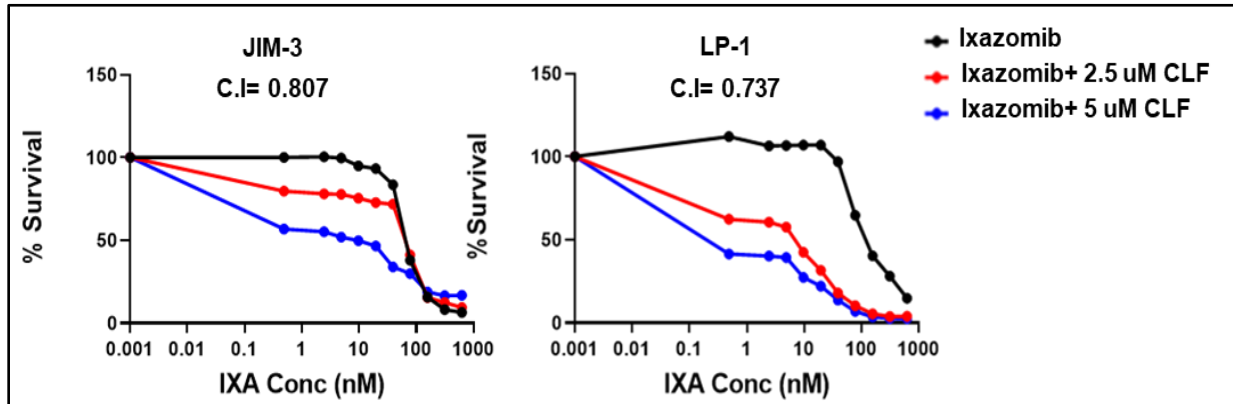
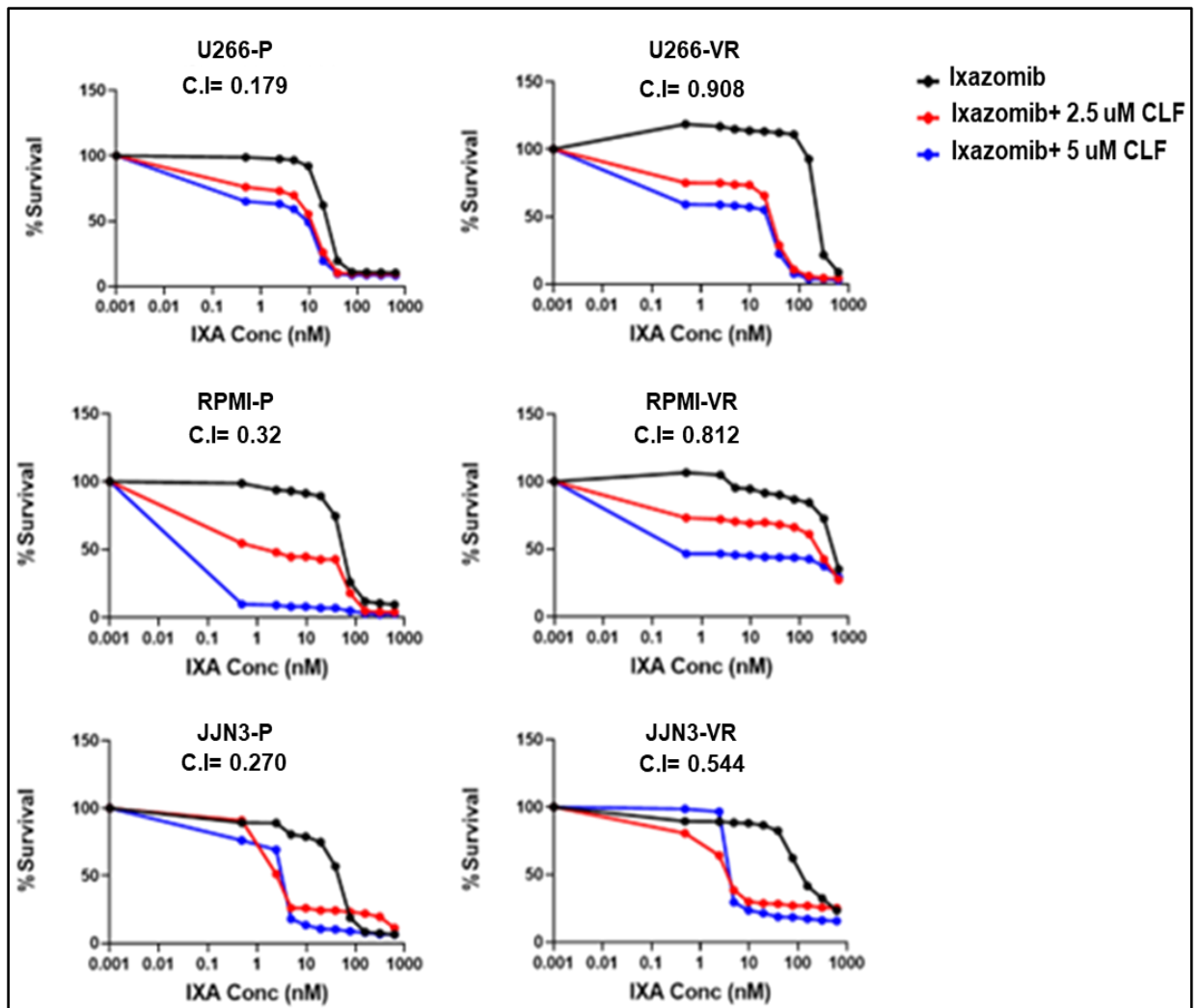
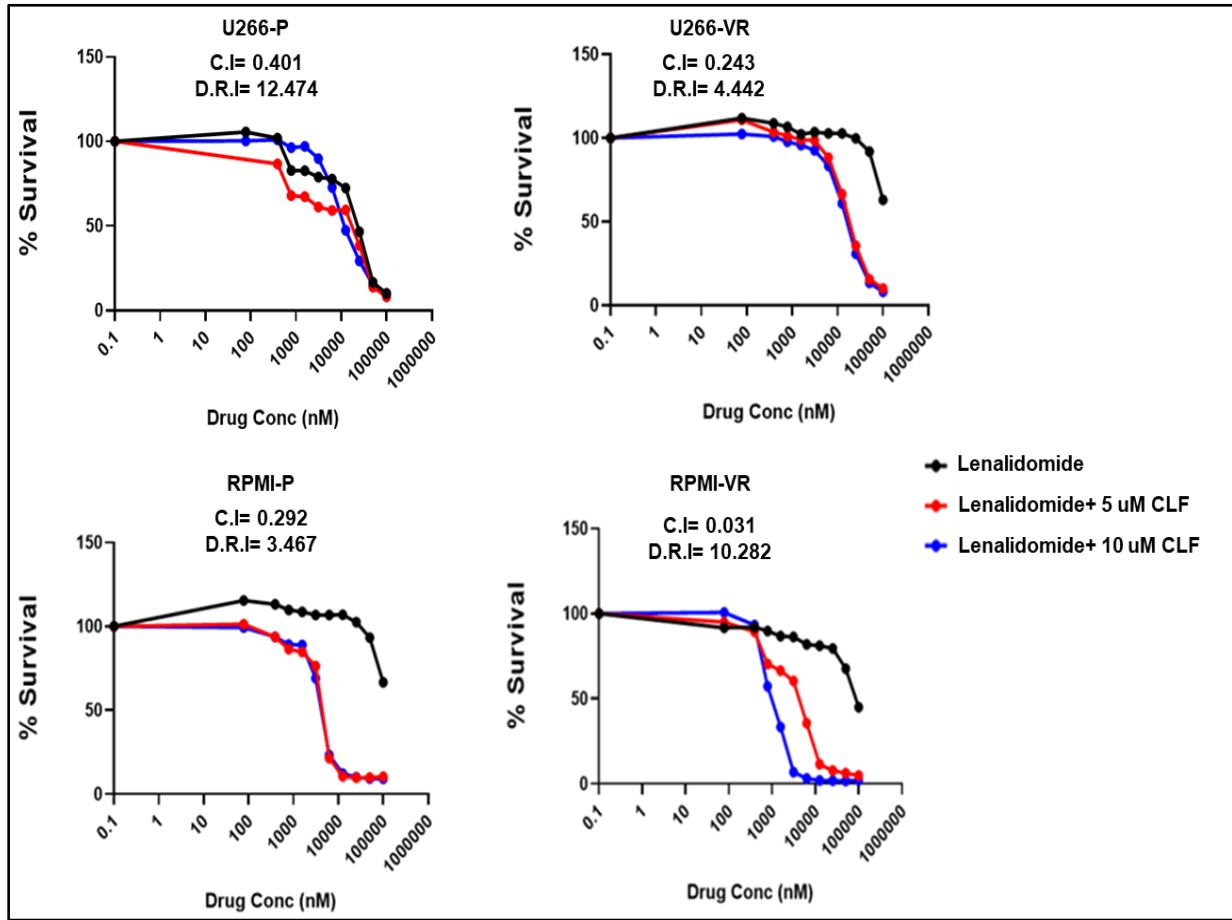


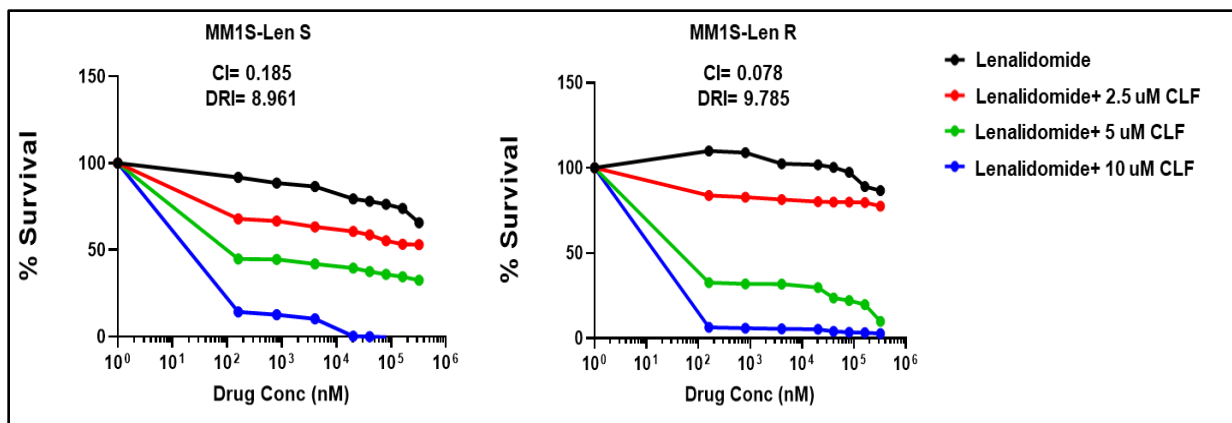
Figure 2C



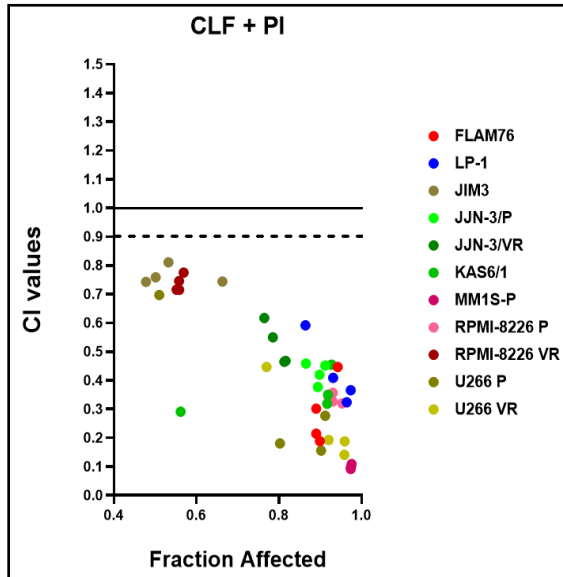
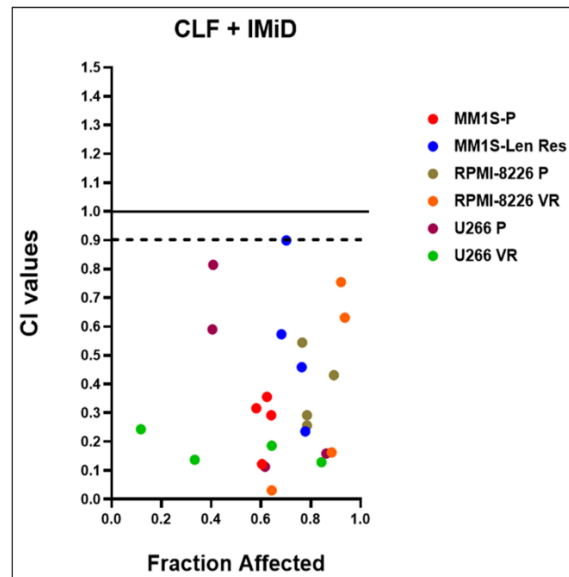
**Figure 2D**



**Figure 2E**



Although the CLF doses used in combination treatments were in the micromolar concentration range, this is within the safe dose range of 0.84-8.4 $\mu$ M, corresponding to human plasma C<sub>max</sub> of 0.4-4mg/L.

**Figure 2F****Figure 2G**

### CyTOF analysis reveals CLF-induced key proteomic changes at bulk and sub-clonal level

We performed Mass Cytometry (CyTOF) analysis to assess CLF-induced changes in phenotypic and functional markers in myeloma cells on a single-cell level and identify unique subgroups that change in relation to disease progression. CyTOF analysis was performed on 77 total samples across 7 Experiments/Batches. This included four isogenic sensitive/acquired PI and IMiD resistant pairs (U266, MM1S, RPMI8226, JJN3), eight innate-sensitive cell lines, and seven innate-resistant HMCLs. The batch correction was performed for combining samples. Similar clusters across all samples were grouped to compare sub-populations and to calculate the proportion of cells with increases or decreases in markers for each sample. CyTOF analysis revealed a distinct cluster of cells defined by elevated cleaved caspase levels in all cell lines and primary samples, which was enriched for cells exposed to high-dose CLF.

**Figure 3.** CyTOF analysis in multiple myeloma cell lines (representing sensitive, PI-resistance and IMiD-resistance) and primary patient cells. **(A)** CLF induces elevated cleaved caspase 3 levels. Samples were treated with CLF or DMSO and Gated on LIVE cells. Each ‘column’ represents a cell line pair (except for KP6, which is just the parental). The first three ‘rows’ are UMAP plots colored by cell line, CLF dose, and cc3 expression. For the final ‘row’, the FlowSOM meta-cluster results were condensed into cc3 positive and negative cell subsets based on cc3 expression UMAPs and plotted over CLF dose. cc3 is induced in all lines. **(B)** CLF

treatment results in the downregulation of genes associated with myeloma cell survival. A representative heatmap for CyTOF analysis is shown for sensitive and PI-resistant, IMiD-resistant, and primary patient cells showing expression of the complete panel. A heat plot was generated in Cytobank displaying the transformed ratio normalized to the first column (DMSO control) of the median of each marker. CyTOF analysis shows shifts in a number of myeloma cell survival markers following clofazimine treatment (10uM), including IRF4, IKZF1 (Ikaros), IKZF3 (Aiolos), CD229, CD27, pS6, pERK, and I $\kappa$ Ba. CLF acts as a PPAR-gamma agonist that synergizes with PIs to enhance the downstream cascade of p65/NF $\kappa$ B/IRF4/Myc downregulation followed by ROS-dependent apoptotic cell death. **(C)** Western blotting. Representative figure showing pre- vs. post-treatment (24hr) immunoblotting analysis of proteins involved in the p65/NF $\kappa$ B/IRF4/Myc axis and ROS-dependent apoptotic pathways. Beta-actin was used for the normalization of the Western blots. **(D)** Densitometry analysis showing relative band densities between untreated vs. treated cell lines. Band densities were compared to Beta-actin.

**Figure 3A**

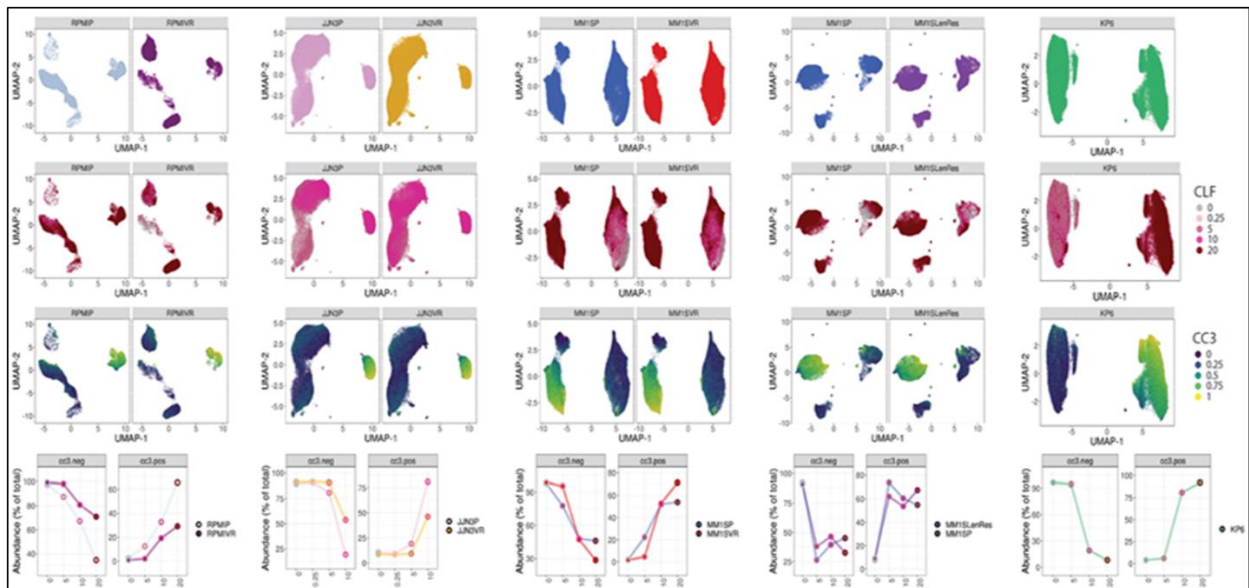


**Figure 3B**

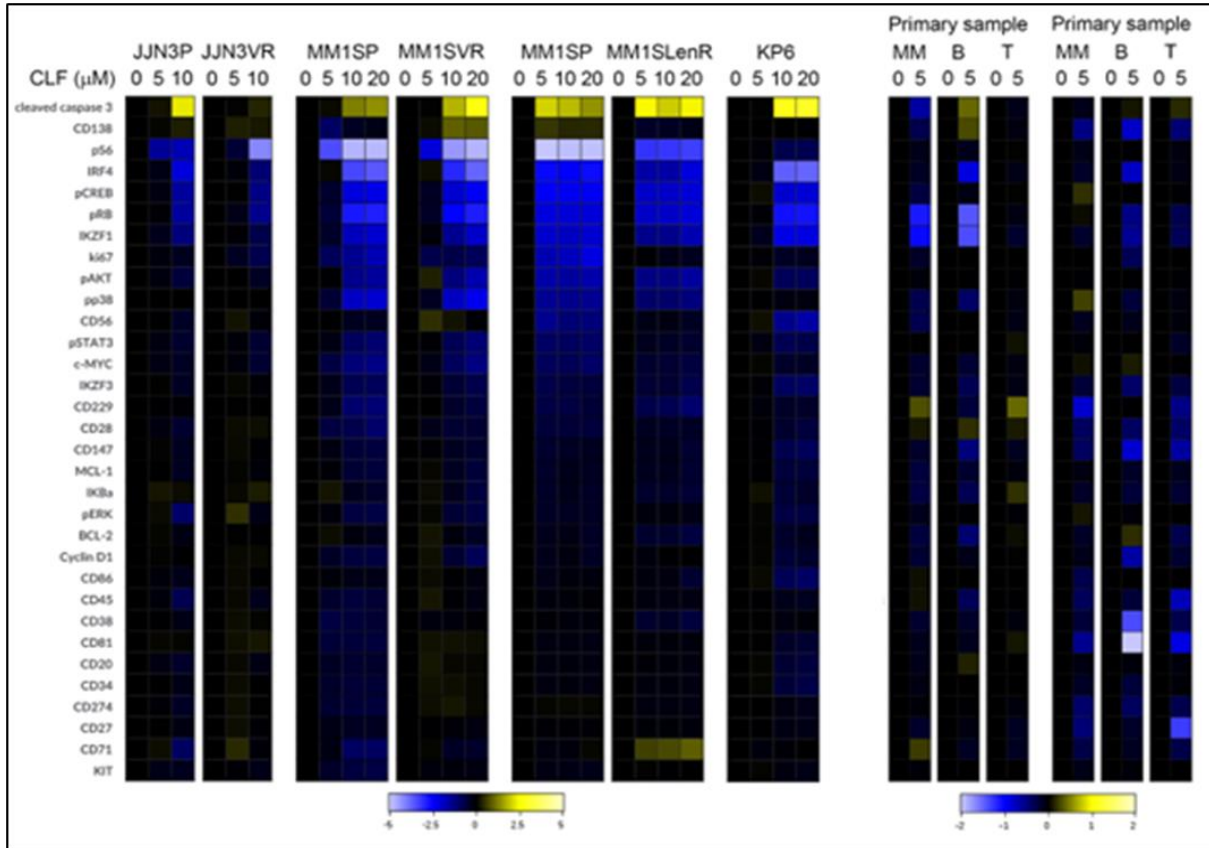


**Figure 3C**

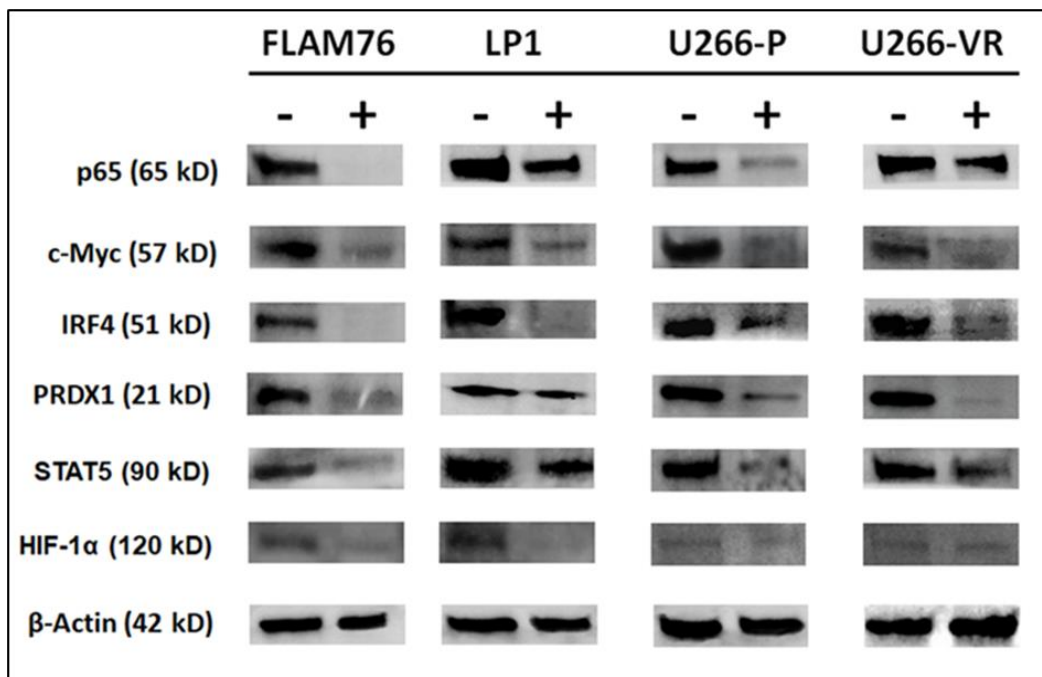
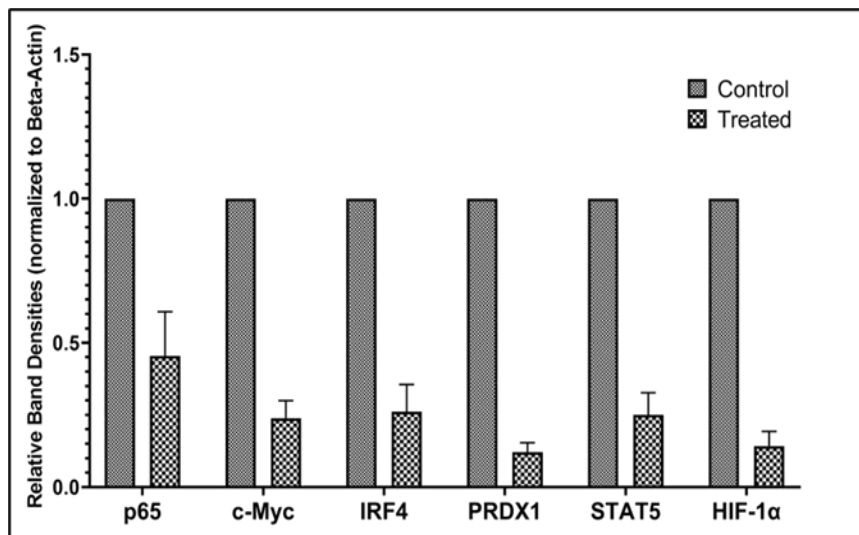


**Figure 3D**



Myeloma cells are addicted to several proteins like c-Myc, IRF4, and IKZF1. Our pre- vs. post-treatment differential expression analysis using CyTOF (Figure 3B) and immunoblotting (Figure 3C) revealed shifts in most of these markers following clofazimine treatment, including IRF4, IKZF1, IKZF3, CD229, CD27, pS6, pERK, and IκBa.

Furthermore, we had earlier found that CLF also suppresses STAT expression in CML and consequently downregulated stem cells maintenance factors like hypoxia-inducible factor-1α and -2α and Cbp/P300 interacting trans-activator with Glu/Asp-rich carboxy-terminal domain 2 (CITED2). Concurrently, we also showed the downregulation of STAT5 and HIF-1α in myeloma following CLF treatment (Figure 3D).

## **Discussion**

Drug resistance in multiple myeloma is attributed mainly to tumor heterogeneity and inter-individual variations in response to treatment, limiting therapeutic efficacy in myeloma patients. We have earlier demonstrated that wide inter-individual variation exists in response to PI treatment in a panel of HMCLs and PMCs representing the broad spectrum of biological and genetic heterogeneity of myeloma. Here, we show significant in vitro and ex vivo cytotoxicity of CLF against these PI- and IMiD-sensitive and resistant myeloma, both as a single agent and in combination with PIs and IMiDs. Further, we performed RNAseq-based next-generation tumor gene expression profiling, single-cell proteomics (CyTOF) analysis, and immunoblotting

analysis to identify genes and molecular networks involved in CLF mechanism of action and drug synergy in human myeloma.

Taken together, we conclude that CLF has potent single-agent cytotoxicity and the potential to increase the therapeutic efficacy of standard-of-care drugs (PI and IMiDs) in myeloma, including treatment-resistant and putative stem-like subclones.

Since CLF is FDA-approved, safe (FDA recommended dose is 100mg/day), well-tolerated in patients, and is on the WHO's List of Essential Medicines with low manufacturing cost, repurposing CLF as a novel clinical trial-ready anti-myeloma agent is an attractive approach for fast and cost-effective drug development.<sup>412</sup>

## **Summary**

To summarize, clinical success in anti-cancer treatment warrants a continuous search for novel secondary therapeutic options where new agents may be combined with standard-of-care drugs to achieve synergistic effects for treating drug resistance. However, assessing the survival endpoints in clinical applications requires the treatment of a large number of patients with these drugs that need to be measured in months to years. Thus, Our multi-faceted approach that includes in vitro, ex vivo, and in vivo model systems, cell-based assays, flow cytometry, mRNA sequencing, single-cell transcriptomics, and microfluidics chip-based assays will serve as an efficient pre-clinical model for cancer drug discovery with high predictive value to validate and characterize novel secondary therapies in chemotherapy-resistant cancers to circumvent resistance, by incorporating all the aspects of human-tumor biology and its inherent dynamic, deterministic, and stochastic nature and opens up a new paradigm in the management of advanced state human cancers.

## References

1. Hanahan, D. & Weinberg, R. A. Hallmarks of cancer: The next generation. *Cell* vol. 144 646–674 Preprint at <https://doi.org/10.1016/j.cell.2011.02.013> (2011).
2. Sarkar, S. *et al.* Cancer development, progression, and therapy: An epigenetic overview. *International Journal of Molecular Sciences* vol. 14 21087–21113 Preprint at <https://doi.org/10.3390/ijms141021087> (2013).
3. American Cancer Society: Cancer Stat and Facts.
4. CDC An update on cancer deaths in United States.
5. NCI Cancer Stat Facts: Common Cancer Sites.
6. World Health Organization: Cancer.
7. American Cancer Society: The Global Cancer Burden.
8. Sung, H. *et al.* Global Cancer Statistics 2020: GLOBOCAN Estimates of Incidence and Mortality Worldwide for 36 Cancers in 185 Countries. *CA Cancer J Clin* **71**, 209–249 (2021).
9. Wee, P. & Wang, Z. Epidermal growth factor receptor cell proliferation signaling pathways. *Cancers* vol. 9 Preprint at <https://doi.org/10.3390/cancers9050052> (2017).
10. Chen, J. *et al.* Expression and Function of the Epidermal Growth Factor Receptor in Physiology and Disease. *Physiol Rev* **96**, 1025–1069 (2016).
11. Cell Cycle Control by Oncogenes and Tumor Suppressors: Driving the Transformation of Normal Cells into Cancerous Cells.
12. Feitelson, M. A. *et al.* Sustained proliferation in cancer: Mechanisms and novel therapeutic targets. *Seminars in Cancer Biology* vol. 35 S25–S54 Preprint at <https://doi.org/10.1016/j.semcancer.2015.02.006> (2015).
13. Yuan, J., Dong, X., Yap, J. & Hu, J. The MAPK and AMPK signalings: Interplay and implication in targeted cancer therapy. *Journal of Hematology and Oncology* vol. 13 Preprint at <https://doi.org/10.1186/s13045-020-00949-4> (2020).
14. He, Y. *et al.* Targeting PI3K/Akt signal transduction for cancer therapy. *Signal Transduction and Targeted Therapy* vol. 6 Preprint at <https://doi.org/10.1038/s41392-021-00828-5> (2021).
15. Collins, K., Jacks, T. & Pavletich, N. P. *From the Academy The cell cycle and cancer.* vol. 94 [www.pnas.org](http://www.pnas.org). (1997).
16. Laiho, M. & Latonen, L. Cell cycle control, DNA damage checkpoints and cancer. *Annals of Medicine* vol. 35 391–397 Preprint at <https://doi.org/10.1080/07853890310014605> (2003).
17. Ding, L. *et al.* The roles of cyclin-dependent kinases in cell-cycle progression and therapeutic strategies in human breast cancer. *International Journal of Molecular Sciences* vol. 21 Preprint at <https://doi.org/10.3390/ijms21061960> (2020).
18. Abreu Velez, A. M. & Howard, M. S. Tumor-suppressor genes, cell cycle regulatory checkpoints, and the skin. *North American Journal of Medical Sciences* vol. 7 176–188 Preprint at <https://doi.org/10.4103/1947-2714.157476> (2015).
19. Shi, C. J., Xu, S. M., Han, Y., Zhou, R. & Zhang, Z. Y. Targeting cyclin-dependent kinase 4/6 as a therapeutic approach for mucosal melanoma. *Melanoma Research* vol. 31 495–503 Preprint at <https://doi.org/10.1097/CMR.0000000000000777> (2021).
20. Amin, A. R. M. R. *et al.* Evasion of anti-growth signaling: A key step in tumorigenesis and potential target for treatment and prophylaxis by natural compounds. *Seminars in*

- Cancer Biology* vol. 35 S55–S77 Preprint at <https://doi.org/10.1016/j.semcancer.2015.02.005> (2015).
21. Genetic Regulation of Cancer.
  22. Martin TA, Y. L. S. A. et al. Cancer Invasion and Metastasis: Molecular and Cellular Perspective.
  23. Chiang, S. P., Cabrera, R. M. & Segall, J. E. Tumor cell intravasation. *Am J Physiol Cell Physiol* **311**, 1–14 (2016).
  24. Shenoy, A. K. & Lu, J. Cancer cells remodel themselves and vasculature to overcome the endothelial barrier. *Cancer Letters* vol. 380 534–544 Preprint at <https://doi.org/10.1016/j.canlet.2014.10.031> (2016).
  25. Kai, F. B., Drain, A. P. & Weaver, V. M. The Extracellular Matrix Modulates the Metastatic Journey. *Developmental Cell* vol. 49 332–346 Preprint at <https://doi.org/10.1016/j.devcel.2019.03.026> (2019).
  26. Mariano N Carrizo et al. Loss of E-Cadherin Expression and Epithelial Mesenchymal Transition (EMT) as Key Steps in Tumor Progression.
  27. Serrano-Gomez, S. J., Maziveyi, M. & Alahari, S. K. Regulation of epithelial-mesenchymal transition through epigenetic and post-translational modifications. *Molecular Cancer* vol. 15 Preprint at <https://doi.org/10.1186/s12943-016-0502-x> (2016).
  28. Huang, Y., Hong, W. & Wei, X. The molecular mechanisms and therapeutic strategies of EMT in tumor progression and metastasis. *Journal of Hematology and Oncology* vol. 15 Preprint at <https://doi.org/10.1186/s13045-022-01347-8> (2022).
  29. Pei, D., Shu, X., Gassama-Diagne, A. & Thiery, J. P. Mesenchymal–epithelial transition in development and reprogramming. *Nature Cell Biology* vol. 21 44–53 Preprint at <https://doi.org/10.1038/s41556-018-0195-z> (2019).
  30. Pitsidianaki, I., Morgan, J., Adams, J. & Campbell, K. Mesenchymal-to-epithelial transitions require tissue-specific interactions with distinct laminins. *Journal of Cell Biology* **220**, (2021).
  31. Shay, J. W. & Wright, W. E. Role of telomeres and telomerase in cancer. *Seminars in Cancer Biology* vol. 21 349–353 Preprint at <https://doi.org/10.1016/j.semcancer.2011.10.001> (2011).
  32. Fernald, K. & Kurokawa, M. Evading apoptosis in cancer. *Trends in Cell Biology* vol. 23 620–633 Preprint at <https://doi.org/10.1016/j.tcb.2013.07.006> (2013).
  33. Zhang, Q. et al. Human telomerase reverse transcriptase is a novel target of Hippo-YAP pathway. *FASEB Journal* **34**, 4178–4188 (2020).
  34. Hoffmeyer, K. et al. *Wnt/b-Catenin Signaling Regulates Telomerase in Stem Cells and Cancer Cells*. [www.sciencemag.org](http://www.sciencemag.org).
  35. Reddel, R. R. *Send Orders for Reprints to reprints@benthamscience.net Telomere Maintenance Mechanisms in Cancer: Clinical Implications*. (2014).
  36. Karamysheva, A. F. Mechanisms of angiogenesis. *Biochemistry (Moscow)* vol. 73 751–762 Preprint at <https://doi.org/10.1134/S0006297908070031> (2008).
  37. Hashimoto, T. & Shibasaki, F. Hypoxia-Inducible Factor as an Angiogenic Master Switch. *Frontiers in Pediatrics* vol. 3 Preprint at <https://doi.org/10.3389/fped.2015.00033> (2015).
  38. Emami Nejad, A. et al. The role of hypoxia in the tumor microenvironment and development of cancer stem cell: a novel approach to developing treatment. *Cancer Cell International* vol. 21 Preprint at <https://doi.org/10.1186/s12935-020-01719-5> (2021).

39. Papetti, M. & Herman, I. M. invited review Mechanisms of normal and tumor-derived angiogenesis. (2002) doi:10.1152/ajpcell.00389.2001.-Often.
40. Papetti, M. & Herman, I. M. Mechanisms of normal and tumor-derived angiogenesis. (2002) doi:10.1152/ajpcell.00389.2001.-Often.
41. Gomis, R. R. & Gawrzak, S. Tumor cell dormancy. *Mol Oncol* **11**, 62–78 (2017).
42. Elmore, S. *Apoptosis: A Review of Programmed Cell Death*.
43. Brentnall, M., Rodriguez-Menocal, L., de Guevara, R. L., Cepero, E. & Boise, L. H. Caspase-9, caspase-3 and caspase-7 have distinct roles during intrinsic apoptosis. *BMC Cell Biol* **14**, (2013).
44. Cavalcante, G. C. *et al.* A cell's fate: An overview of the molecular biology and genetics of apoptosis. *International Journal of Molecular Sciences* vol. 20 Preprint at <https://doi.org/10.3390/ijms20174133> (2019).
45. Kale, J., Osterlund, E. J. & Andrews, D. W. BCL-2 family proteins: Changing partners in the dance towards death. *Cell Death and Differentiation* vol. 25 65–80 Preprint at <https://doi.org/10.1038/cdd.2017.186> (2018).
46. de Zio, D., Cianfanelli, V. & Cecconi, F. New insights into the link between DNA damage and apoptosis. *Antioxidants and Redox Signaling* vol. 19 559–571 Preprint at <https://doi.org/10.1089/ars.2012.4938> (2013).
47. Sen, T., Gay, C. M. & Byers, L. A. Targeting DNA damage repair in small cell lung cancer and the biomarker landscape. *Translational Lung Cancer Research* vol. 7 50–68 Preprint at <https://doi.org/10.21037/tlcr.2018.02.03> (2018).
48. Alhמוד, J. F., Woolley, J. F., al Moustafa, A. E. & Malki, M. I. DNA damage/repair management in cancers. *Cancers* vol. 12 Preprint at <https://doi.org/10.3390/cancers12041050> (2020).
49. Pfeffer, C. M. & Singh, A. T. K. Apoptosis: A target for anticancer therapy. *International Journal of Molecular Sciences* vol. 19 Preprint at <https://doi.org/10.3390/ijms19020448> (2018).
50. Chen, J. The cell-cycle arrest and apoptotic functions of p53 in tumor initiation and progression. *Cold Spring Harb Perspect Med* **6**, (2016).
51. Ozaki, T. & Nakagawara, A. Role of p53 in cell death and human cancers. *Cancers* vol. 3 994–1013 Preprint at <https://doi.org/10.3390/cancers3010994> (2011).
52. NCI Types of Cancer Treatment.
53. Mayo Clinic: Cancer Treatment.
54. American Cancer Society: Types of Cancer Treatment.
55. Housman, G. *et al.* Drug resistance in cancer: An overview. *Cancers* vol. 6 1769–1792 Preprint at <https://doi.org/10.3390/cancers6031769> (2014).
56. Mansoori, B., Mohammadi, A., Davudian, S., Shirjang, S. & Baradaran, B. The different mechanisms of cancer drug resistance: A brief review. *Advanced Pharmaceutical Bulletin* vol. 7 339–348 Preprint at <https://doi.org/10.15171/apb.2017.041> (2017).
57. Wang, X., Zhang, H. & Chen, X. Drug resistance and combating drug resistance in cancer. *Cancer Drug Resistance* vol. 2 141–160 Preprint at <https://doi.org/10.20517/cdr.2019.10> (2019).
58. Bukowski, K., Kciuk, M. & Kontek, R. Mechanisms of multidrug resistance in cancer chemotherapy. *International Journal of Molecular Sciences* vol. 21 Preprint at <https://doi.org/10.3390/ijms21093233> (2020).

59. Flaig, T. W. *et al.* Bladder Cancer, Version 3.2020, NCCN Clinical Practice Guidelines in Oncology. *Journal of the National Comprehensive Cancer Network* **18**, 329–354 (2020).
60. Colleoni, M. *et al.* Annual hazard rates of recurrence for breast cancer during 24 years of follow-up: Results from the international breast cancer study group trials I to V. *Journal of Clinical Oncology* **34**, 927–935 (2016).
61. Goss, P. E. *et al.* Extending Aromatase-Inhibitor Adjuvant Therapy to 10 Years. *New England Journal of Medicine* **375**, 209–219 (2016).
62. Pugh, S. A. *et al.* Site and stage of colorectal cancer influence the likelihood and distribution of disease recurrence and postrecurrence survival data from the FACS randomized controlled trial. *Ann Surg* **263**, 1143–1147 (2016).
63. Nabors, L. B. *et al.* Central nervous system cancers, version 3.2020. *JNCCN Journal of the National Comprehensive Cancer Network* vol. 18 1537–1570 Preprint at <https://doi.org/10.6004/JNCCN.2020.0052> (2020).
64. Brockstein, B. *et al.* Patterns of failure, prognostic factors and survival in locoregionally advanced head and neck cancer treated with concomitant chemoradiotherapy: A 9-year, 337-patient, multi-institutional experience. *Annals of Oncology* **15**, 1179–1186 (2004).
65. Townsend, W. & Linch, D. Hodgkin’s lymphoma in adults. *The Lancet* vol. 380 836–847 Preprint at [https://doi.org/10.1016/S0140-6736\(12\)60035-X](https://doi.org/10.1016/S0140-6736(12)60035-X) (2012).
66. Glimelius, I. & Diepstra, A. Novel treatment concepts in Hodgkin lymphoma. *Journal of Internal Medicine* vol. 281 247–260 Preprint at <https://doi.org/10.1111/joim.12582> (2017).
67. Li, S., Young, K. H. & Medeiros, L. J. Diffuse large B-cell lymphoma. *Pathology* vol. 50 74–87 Preprint at <https://doi.org/10.1016/j.pathol.2017.09.006> (2018).
68. Chihara, D. *et al.* The survival outcome of patients with relapsed/refractory peripheral T-cell lymphoma-not otherwise specified and angioimmunoblastic T-cell lymphoma. *Br J Haematol* **176**, 750–758 (2017).
69. Rockberg, J. *et al.* Epidemiology of cutaneous melanoma in Sweden—Stage-specific survival and rate of recurrence. *Int J Cancer* **139**, 2722–2729 (2016).
70. Maurizi, G. *et al.* Margin distance does not influence recurrence and survival after wedge resection for lung cancer. in *Annals of Thoracic Surgery* vol. 100 918–925 (Elsevier USA, 2015).
71. Ochiai, S. *et al.* The impact of epidermal growth factor receptor mutations on patterns of disease recurrence after chemoradiotherapy for locally advanced non-small cell lung cancer: A literature review and pooled analysis. *Journal of Radiation Research* vol. 57 449–459 Preprint at <https://doi.org/10.1093/jrr/rrw075> (2016).
72. Cipriano, C., Griffin, A. M., Ferguson, P. C. & Wunder, J. S. Developing an Evidence-based Followup Schedule for Bone Sarcomas Based on Local Recurrence and Metastatic Progression. *Clin Orthop Relat Res* **475**, 830–838 (2017).
73. Corrado, G. *et al.* Optimizing treatment in recurrent epithelial ovarian cancer. *Expert Review of Anticancer Therapy* vol. 17 1147–1158 Preprint at <https://doi.org/10.1080/14737140.2017.1398088> (2017).
74. Fischer, R. *et al.* Early recurrence of pancreatic cancer after resection and during adjuvant chemotherapy. *Saudi Journal of Gastroenterology* **18**, 118–121 (2012).
75. Nishio, K. *et al.* Preoperative predictors for early recurrence of resectable pancreatic cancer. *World J Surg Oncol* **15**, (2017).

76. Kurbegovic, S. *et al.* The risk of biochemical recurrence for intermediate-risk prostate cancer after radical prostatectomy. *Scand J Urol* **51**, 450–456 (2017).
77. Casali, P. G. *Adjuvant Chemotherapy for Soft Tissue Sarcoma*. (2015).
78. Wang, X., Zhang, H. & Chen, X. Drug resistance and combating drug resistance in cancer. *Cancer Drug Resistance* vol. 2 141–160 Preprint at <https://doi.org/10.20517/cdr.2019.10> (2019).
79. Bukowski, K., Kciuk, M. & Kontek, R. Mechanisms of multidrug resistance in cancer chemotherapy. *International Journal of Molecular Sciences* vol. 21 Preprint at <https://doi.org/10.3390/ijms21093233> (2020).
80. Sharma, P., Hu-Lieskovan, S., Wargo, J. A. & Ribas, A. Primary, Adaptive, and Acquired Resistance to Cancer Immunotherapy. *Cell* vol. 168 707–723 Preprint at <https://doi.org/10.1016/j.cell.2017.01.017> (2017).
81. Emran, T. bin *et al.* Multidrug Resistance in Cancer: Understanding Molecular Mechanisms, Immunoprevention and Therapeutic Approaches. *Frontiers in Oncology* vol. 12 Preprint at <https://doi.org/10.3389/fonc.2022.891652> (2022).
82. Tyner, J. W. *et al.* Understanding Drug Sensitivity and Tackling Resistance in Cancer. *Cancer Research* vol. 82 1448–1460 Preprint at <https://doi.org/10.1158/0008-5472.CAN-21-3695> (2022).
83. Crystal, A. S. *et al.* Patient-derived models of acquired resistance can identify effective drug combinations for cancer. *Science (1979)* **346**, 1480–1486 (2014).
84. Ria, R. & Vacca, A. Bone marrow stromal cells-induced drug resistance in multiple myeloma. *International Journal of Molecular Sciences* vol. 21 Preprint at <https://doi.org/10.3390/ijms21020613> (2020).
85. Prasetyanti, P. R. & Medema, J. P. Intra-tumor heterogeneity from a cancer stem cell perspective. *Molecular Cancer* vol. 16 Preprint at <https://doi.org/10.1186/s12943-017-0600-4> (2017).
86. Ramón y Cajal, S. *et al.* Clinical implications of intratumor heterogeneity: challenges and opportunities. *Journal of Molecular Medicine* vol. 98 161–177 Preprint at <https://doi.org/10.1007/s00109-020-01874-2> (2020).
87. Michor, F. & Polyak, K. The origins and implications of intratumor heterogeneity. *Cancer Prevention Research* vol. 3 1361–1364 Preprint at <https://doi.org/10.1158/1940-6207.CAPR-10-0234> (2010).
88. Zhu, L. *et al.* A narrative review of tumor heterogeneity and challenges to tumor drug therapy. *Ann Transl Med* **9**, 1351–1351 (2021).
89. Sun, X. X. & Yu, Q. Intra-tumor heterogeneity of cancer cells and its implications for cancer treatment. *Acta Pharmacologica Sinica* vol. 36 1219–1227 Preprint at <https://doi.org/10.1038/aps.2015.92> (2015).
90. Fu, F., Nowak, M. A. & Bonhoeffer, S. Spatial Heterogeneity in Drug Concentrations Can Facilitate the Emergence of Resistance to Cancer Therapy. *PLoS Comput Biol* **11**, (2015).
91. Baghban, R. *et al.* Tumor microenvironment complexity and therapeutic implications at a glance. *Cell Communication and Signaling* vol. 18 Preprint at <https://doi.org/10.1186/s12964-020-0530-4> (2020).
92. Wang, M. *et al.* Role of tumor microenvironment in tumorigenesis. *Journal of Cancer* vol. 8 761–773 Preprint at <https://doi.org/10.7150/jca.17648> (2017).

93. Ahmad, R. S., Eubank, T. D., Lukomski, S. & Boone, B. A. Immune cell modulation of the extracellular matrix contributes to the pathogenesis of pancreatic cancer. *Biomolecules* vol. 11 Preprint at <https://doi.org/10.3390/biom11060901> (2021).
94. Henke, E., Nandigama, R. & Ergün, S. Extracellular Matrix in the Tumor Microenvironment and Its Impact on Cancer Therapy. *Frontiers in Molecular Biosciences* vol. 6 Preprint at <https://doi.org/10.3389/fmolb.2019.00160> (2020).
95. Yuan, Y., Jiang, Y. C., Sun, C. K. & Chen, Q. M. Role of the tumor microenvironment in tumor progression and the clinical applications (Review). *Oncology Reports* vol. 35 2499–2515 Preprint at <https://doi.org/10.3892/or.2016.4660> (2016).
96. Labani-Motlagh, A., Ashja-Mahdavi, M. & Loskog, A. The Tumor Microenvironment: A Milieu Hindering and Obstructing Antitumor Immune Responses. *Frontiers in Immunology* vol. 11 Preprint at <https://doi.org/10.3389/fimmu.2020.00940> (2020).
97. Yu, Z., Pestell, T. G., Lisanti, M. P. & Pestell, R. G. Cancer stem cells. *International Journal of Biochemistry and Cell Biology* vol. 44 2144–2151 Preprint at <https://doi.org/10.1016/j.biocel.2012.08.022> (2012).
98. Ayob, A. Z. & Ramasamy, T. S. Cancer stem cells as key drivers of tumour progression. *Journal of Biomedical Science* vol. 25 Preprint at <https://doi.org/10.1186/s12929-018-0426-4> (2018).
99. Muriithi, W. *et al.* ABC transporters and the hallmarks of cancer: roles in cancer aggressiveness beyond multidrug resistance. *Cancer Biology and Medicine* vol. 17 253–269 Preprint at <https://doi.org/10.20892/j.issn.2095-3941.2019.0284> (2020).
100. MiKaela Olsen *et al.* Overview of Hematologic Malignancies.
101. The Leukemia and Lymphoma Society: Facts and Statistics Overview.
102. CDC. *Hematologic Cancer Incidence, Survival, and Prevalence*. [www.cdc.gov/uscs](http://www.cdc.gov/uscs).
103. Leukemias, Lymphomas, and Myelomas-University of Mississippi Medical Center.
104. Justin Taylor, W. X. O. A.-W. *et al.* Diagnosis and classification of hematologic malignancies on the basis of genetics.
105. Longjohn, M. N. *et al.* Deciphering the messages carried by extracellular vesicles in hematological malignancies. *Blood Reviews* vol. 46 Preprint at <https://doi.org/10.1016/j.blre.2020.100734> (2021).
106. Jagannathan-Bogdan, M. & Zon, L. I. Hematopoiesis. *Development (Cambridge)* **140**, 2463–2467 (2013).
107. Wu, Q., Zhang, J. & Lucas, D. Anatomy of Hematopoiesis and Local Microenvironments in the Bone Marrow. Where to? *Frontiers in Immunology* vol. 12 Preprint at <https://doi.org/10.3389/fimmu.2021.768439> (2021).
108. J. Hoggatt, L. M. P. *et al.* Hematopoiesis- an overview.
109. Orkin, S. H. & Zon, L. I. Hematopoiesis: An Evolving Paradigm for Stem Cell Biology. *Cell* vol. 132 631–644 Preprint at <https://doi.org/10.1016/j.cell.2008.01.025> (2008).
110. Seita, J. & Weissman, I. L. Hematopoietic stem cell: Self-renewal versus differentiation. *Wiley Interdisciplinary Reviews: Systems Biology and Medicine* vol. 2 640–653 Preprint at <https://doi.org/10.1002/wsbm.86> (2010).
111. Cuenca, M. & Peperzak, V. Advances and perspectives in the treatment of b-cell malignancies. *Cancers* vol. 13 Preprint at <https://doi.org/10.3390/cancers13092266> (2021).

112. He, M. Y. & Kridel, R. Treatment resistance in diffuse large B-cell lymphoma. *Leukemia* vol. 35 2151–2165 Preprint at <https://doi.org/10.1038/s41375-021-01285-3> (2021).
113. Shah, B., Zhao, X., Silva, A. S., Shain, K. H. & Tao, J. Resistance to Ibrutinib in B Cell Malignancies: One Size Does Not Fit All. *Trends in Cancer* vol. 4 197–206 Preprint at <https://doi.org/10.1016/j.trecan.2018.01.004> (2018).
114. Hardy, R. R. & Hayakawa, K. *B CELL DEVELOPMENT PATHWAYS*. [www.annualreviews.org](http://www.annualreviews.org) (2001).
115. Shahaf, G., Zisman-Rozen, S., Benhamou, D., Melamed, D. & Mehr, R. B cell development in the bone marrow is regulated by homeostatic feedback exerted by mature B cells. *Front Immunol* **7**, (2016).
116. Tucker W. LeBien, T. F. T. et al. B lymphocytes: how they develop and function.
117. The generation of diversity in immunoglobulins - Immunobiology - NCBI Bookshelf.
118. Li, L.-X., Goetz, C. A., Katerndahl, C. D. S., Sakaguchi, N. & Farrar, M. A. A Flt3- and Ras-Dependent Pathway Primes B Cell Development by Inducing a State of IL-7 Responsiveness. *The Journal of Immunology* **184**, 1728–1736 (2010).
119. Ramírez, J., Lukin, K. & Hagman, J. From hematopoietic progenitors to B cells: Mechanisms of lineage restriction and commitment. *Current Opinion in Immunology* vol. 22 177–184 Preprint at <https://doi.org/10.1016/j.coi.2010.02.003> (2010).
120. Geisberger, R. Models of signal transduction through the B-cell antigen receptor. doi:10.1046/j.1365-2567.2003.01770.x.
121. Kraus, M. et al. Interference with Immunoglobulin (Ig) Immunoreceptor Tyrosine-based Activation Motif (ITAM) Phosphorylation Modulates or Blocks B Cell Development, Depending on the Availability of an Ig Cytoplasmic Tail. *J. Exp. Med* vol. 194 <http://www.jem.org/cgi/content/full/194/4/455> (2001).
122. Noviski, M. et al. IgM and IgD B cell receptors differentially respond to endogenous antigens and control B cell fate. (2018) doi:10.7554/eLife.35074.001.
123. Guo, J., Mckenna, S. L., Odwyer, M. E., Cahill, M. R. & O’Driscoll, C. M. RNA interference for multiple myeloma therapy: Targeting signal transduction pathways. *Expert Opinion on Therapeutic Targets* vol. 20 107–121 Preprint at <https://doi.org/10.1517/14728222.2015.1071355> (2016).
124. Valentin Hansen, S. et al. Detailed characterization of the transcriptome of single B cells in mantle cell lymphoma suggesting a potential use for SOX4. *Sci Rep* **11**, (2021).
125. American Cancer Society: What is Multiple Myeloma.
126. Naymagon, L. & Abdul-Hay, M. Novel agents in the treatment of multiple myeloma: A review about the future. *Journal of Hematology and Oncology* vol. 9 Preprint at <https://doi.org/10.1186/s13045-016-0282-1> (2016).
127. Nakaya, A. et al. Impact of CRAB symptoms in survival of patients with symptomatic myeloma in novel agent era. *Hematol Rep* **9**, 16–18 (2017).
128. American Cancer Society: Myeloma Statistics.
129. American Cancer Society: Key Statistics About Multiple Myeloma.
130. Farkona, S., Diamandis, E. P. & Blasutig, I. M. Cancer immunotherapy: The beginning of the end of cancer? *BMC Medicine* vol. 14 Preprint at <https://doi.org/10.1186/s12916-016-0623-5> (2016).
131. Cho, S.-F., Yeh, T.-J., Anderson, K. C. & Tai, Y.-T. Bispecific antibodies in multiple myeloma treatment: A journey in progress. *Front Oncol* **12**, (2022).

132. van de Donk, N. W. C. J. & Usmani, S. Z. CD38 antibodies in multiple myeloma: Mechanisms of action and modes of resistance. *Frontiers in Immunology* vol. 9 Preprint at <https://doi.org/10.3389/fimmu.2018.02134> (2018).
133. Pazina, T. *et al.* The anti-SLAMF7 antibody elotuzumab mediates NK cell activation through both CD16-dependent and –independent mechanisms. *Oncoimmunology* **6**, (2017).
134. Palumbo, A. *et al.* International Myeloma Working Group consensus statement for the management, treatment, and supportive care of patients with myeloma not eligible for standard autologous stem-cell transplantation. *Journal of Clinical Oncology* **32**, 587–600 (2014).
135. Sonneveld, P. & Broijl, A. Treatment of relapsed and refractory multiple myeloma. *Haematologica* vol. 101 396–406 Preprint at <https://doi.org/10.3324/haematol.2015.129189> (2016).
136. Capp, J. P. & Bataille, R. Multiple myeloma as a bone disease? The tissue disruption-induced cell stochasticity (TiDiS) theory. *Cancers (Basel)* **12**, 1–12 (2020).
137. Mikulasova, A. *et al.* The spectrum of somatic mutations in monoclonal gammopathy of undetermined significance indicates a less complex genomic landscape than that in multiple myeloma. *Haematologica* **102**, 1617–1625 (2017).
138. Fairfield, H., Falank, C., Avery, L. & Reagan, M. R. Multiple myeloma in the marrow: Pathogenesis and treatments. *Annals of the New York Academy of Sciences* vol. 1364 32–51 Preprint at <https://doi.org/10.1111/nyas.13038> (2016).
139. Zhan, F. *et al.* The molecular classification of multiple myeloma. *Blood* **108**, 2020–2028 (2006).
140. Miller, A. *et al.* High somatic mutation and neoantigen burden are correlated with decreased progression-free survival in multiple myeloma. *Blood Cancer J* **7**, (2017).
141. Coffey, D. G. *et al.* Ultradeep, targeted sequencing reveals distinct mutations in blood compared to matched bone marrow among patients with multiple myeloma. *Blood Cancer Journal* vol. 9 Preprint at <https://doi.org/10.1038/s41408-019-0238-0> (2019).
142. Walker, B. A. *et al.* Mutational spectrum, copy number changes, and outcome: Results of a sequencing study of patients with newly diagnosed myeloma. *Journal of Clinical Oncology* **33**, 3911–3920 (2015).
143. Chng, W. J. *et al.* Clinical and biological significance of RAS mutations in multiple myeloma. *Leukemia* vol. 22 2280–2284 Preprint at <https://doi.org/10.1038/leu.2008.142> (2008).
144. Pasca, S. *et al.* Kras/nras/braf mutations as potential targets in multiple myeloma. *Front Oncol* **9**, (2019).
145. Zátopková, M. *et al.* Mutation landscape of multiple myeloma measurable residual disease: Identification of targets for precision medicine. *Blood Advances* vol. 6 368–372 Preprint at <https://doi.org/10.1182/bloodadvances.2020003876> (2022).
146. Rustad, E. H. *et al.* BRAF V600E mutation in early-stage multiple myeloma: Good response to broad acting drugs and no relation to prognosis. *Blood Cancer J* **5**, (2015).
147. Arozarena, I. & Wellbrock, C. Overcoming resistance to BRAF inhibitors. *Ann Transl Med* **5**, 1–12 (2017).
148. Lakshman, A. *et al.* Impact of acquired del(17p) in multiple myeloma. *Blood Adv* **3**, 1930–1938 (2019).

149. Bolli, N. *et al.* Analysis of the genomic landscape of multiple myeloma highlights novel prognostic markers and disease subgroups. *Leukemia* **32**, 2604–2616 (2018).
150. Grand, E. K., Chase, A. J., Heath, C., Rahemtulla, A. & Cross, N. C. P. Targeting FGFR3 in multiple myeloma: Inhibition of t(4;14)-positive cells by SU5402 and PD173074. *Leukemia* **18**, 962–966 (2004).
151. Kalf, A. & Spencer, A. The t(4;14) translocation and FGFR3 overexpression in multiple myeloma: Prognostic implications and current clinical strategies. *Blood Cancer Journal* vol. 2 Preprint at <https://doi.org/10.1038/bcj.2012.37> (2012).
152. Trudel, S. *et al.* The inhibitory anti-FGFR3 antibody, PRO-001, is cytotoxic to t(4;14) multiple myeloma cells. *Blood* **107**, 4039–4046 (2006).
153. Hu, Y., Chen, W. & Wang, J. Progress in the identification of gene mutations involved in multiple myeloma. *Onco Targets Ther* **12**, 4075–4080 (2019).
154. Cardona-benavides, I. J., de Ramón, C. & Gutiérrez, N. C. Genetic abnormalities in multiple myeloma: Prognostic and therapeutic implications. *Cells* vol. 10 1–28 Preprint at <https://doi.org/10.3390/cells10020336> (2021).
155. Kortüm, K. M. *et al.* Targeted sequencing using a 47 gene multiple myeloma mutation panel (M3P) in -17p high risk disease. *Br J Haematol* **168**, 507–510 (2015).
156. Kortuem, K. M. *et al.* Panel sequencing for clinically oriented variant screening and copy number detection in 142 untreated multiple myeloma patients. *Pak J Pharm Sci* **29**, 351–355 (2016).
157. Hofste op Bruinink, D. *et al.* M3P Sequencing Panel Identifies TP53 Mutational Status As a Prognostic Factor in Chemotherapy-Naive Multiple Myeloma. *Blood* **126**, 2984–2984 (2015).
158. Cook, G., Zweegman, S., Mateos, M. V., Suzan, F. & Moreau, P. A question of class: Treatment options for patients with relapsed and/or refractory multiple myeloma. *Critical Reviews in Oncology/Hematology* vol. 121 74–89 Preprint at <https://doi.org/10.1016/j.critrevonc.2017.11.016> (2018).
159. Ri, M. *Mechanism of action of bortezomib in multiple myeloma therapy.* *International Journal of Myeloma* vol. 6 (2016).
160. Hideshima, T., Richardson, P. G. & Anderson, K. C. Mechanism of action of proteasome inhibitors and deacetylase inhibitors and the biological basis of synergy in multiple myeloma. *Molecular Cancer Therapeutics* vol. 10 2034–2042 Preprint at <https://doi.org/10.1158/1535-7163.MCT-11-0433> (2011).
161. Chen, D. & Dou, Q. P. *The Ubiquitin-Proteasome System as a Prospective Molecular Target for Cancer Treatment and Prevention.* (2010).
162. Saavedra-García, P., Martini, F., Holger, X. & Auner, W. Proteasome inhibition in multiple myeloma: lessons for other cancers. *Am J Physiol Cell Physiol* **318**, 451–462 (2020).
163. Goy, A. *et al.* Bortezomib in patients with relapsed or refractory mantle cell lymphoma: Updated time-to-event analyses of the multicenter phase 2 PINNACLE study. *Annals of Oncology* **20**, 520–525 (2009).
164. Kale, A. J. & Moore, B. S. Molecular mechanisms of acquired proteasome inhibitor resistance. *Journal of Medicinal Chemistry* vol. 55 10317–10327 Preprint at <https://doi.org/10.1021/jm300434z> (2012).

165. Oerlemans, R. *et al.* Molecular basis of bortezomib resistance: Proteasome subunit 25 (PSMB5) gene mutation and overexpression of PSMB5 protein. *Blood* **112**, 2489–2499 (2008).
166. Bascones-Martinez, A., Mattila, R., Gomez-Font, R. & Meurman, J. H. Immunomodulatory drugs: Oral and systemic adverse effects. *Med Oral Patol Oral Cir Bucal* **19**, (2014).
167. Revlimid (Lenalidomide) Now FDA Approved as First-Line Therapy for Patients with Multiple Myeloma.
168. Fink, E. C. & Ebert, B. L. Blood Spotlight The novel mechanism of lenalidomide activity. (2015) doi:10.1182/blood-2015-07.
169. Kotla, V. *et al.* Mechanism of action of lenalidomide in hematological malignancies. *Journal of Hematology and Oncology* vol. 2 Preprint at <https://doi.org/10.1186/1756-8722-2-36> (2009).
170. Gribben, J. G., Fowler, N. & Morschhauser, F. Mechanisms of action of lenalidomide in B-cell non-hodgkin lymphoma. *Journal of Clinical Oncology* **33**, 2803–2811 (2015).
171. Zhu, Y. X. *et al.* Identification of lenalidomide resistance pathways in myeloma and targeted resensitization using cereblon replacement, inhibition of STAT3 or targeting of IRF4. *Blood Cancer J* **9**, (2019).
172. Martinez-Høyer, S. & Karsan, A. Mechanisms of lenalidomide sensitivity and resistance. *Experimental Hematology* vol. 91 22–31 Preprint at <https://doi.org/10.1016/j.exphem.2020.09.196> (2020).
173. Jones, J. R. *et al.* Mutations in CRBN and other cereblon pathway genes are infrequently associated with acquired resistance to immunomodulatory drugs. *Leukemia* **35**, 3017–3020 (2021).
174. Kortüm, K. M. *et al.* Targeted sequencing of refractory myeloma reveals a high incidence of mutations in CRBN and Ras pathway genes. *Blood* **128**, 1226–1233 (2016).
175. Bjorklund, C. C. *et al.* Evidence of a role for activation of Wnt/ $\beta$ -catenin signaling in the resistance of plasma cells to lenalidomide. *Journal of Biological Chemistry* **286**, 11009–11020 (2011).
176. *Mantle Cell Lymphoma rarediseases.org/rare-diseases/mantle-cell-lymphoma/ General Discussion.*
177. Wang, Y. & Ma, S. Risk factors for etiology and prognosis of mantle cell lymphoma. *Expert Review of Hematology* vol. 7 233–243 Preprint at <https://doi.org/10.1586/17474086.2014.889561> (2014).
178. Bertoni, F. & Ponzoni, M. The cellular origin of mantle cell lymphoma. *International Journal of Biochemistry and Cell Biology* vol. 39 1747–1753 Preprint at <https://doi.org/10.1016/j.biocel.2007.04.026> (2007).
179. Pé Rez-Galán, P., Dreyling, M. & Wiestner, A. Mantle cell lymphoma: biology, pathogenesis, and the molecular basis of treatment in the genomic era. doi:10.1182/blood-2010-04.
180. Üppers, A. K. *et al.* *Mechanisms of Disease CELLULAR ORIGINS OF HUMAN B-CELL LYMPHOMAS THE HUMAN PERIPHERAL B-CELL REPERTOIRE AND ITS GENERATION Antibody Specificity and Selection of B Cells. The New England Journal of Medicine* Downloaded from [nejm.org](http://nejm.org) at TEMPLE UNIVERSITY on (2013).

181. Paiva, A. S. *et al.* Importance of Flow Cytometry in the Immunophenotyping Characterization of Mantle Cell Lymphoma in State of Rio Grande Do Norte, Brazil. *Blood* **136**, 15–15 (2020).
182. Gao, J., Peterson, L. A., Nelson, B., Goolsby, C. & Chen, Y. H. Immunophenotypic variations in mantle cell lymphoma. *Am J Clin Pathol* **132**, 699–706 (2009).
183. Monabati, A. *et al.* Mantle cell lymphoma: pathologic and immunophenotyping study of 50 cases and correlation with survival-a single institute experience. doi:10.1007/s12308-020-00401-z/Published.
184. Navarro, A., Beà, S., Jares, P. & Campo, E. Molecular Pathogenesis of Mantle Cell Lymphoma. *Hematology/Oncology Clinics of North America* vol. 34 795–807 Preprint at <https://doi.org/10.1016/j.hoc.2020.05.002> (2020).
185. Sethi, S., Epstein-Peterson, Z., Kumar, A. & Ho, C. Current Knowledge in Genetics, Molecular Diagnostic Tools, and Treatments for Mantle Cell Lymphomas. *Frontiers in Oncology* vol. 11 Preprint at <https://doi.org/10.3389/fonc.2021.739441> (2021).
186. Beà, S. *et al.* Landscape of somatic mutations and clonal evolution in mantle cell lymphoma. *Proc Natl Acad Sci U S A* **110**, 18250–18255 (2013).
187. Jares, P., Colomer, D. & Campo, E. Genetic and molecular pathogenesis of mantle cell lymphoma: Perspectives for new targeted therapeutics. *Nature Reviews Cancer* vol. 7 750–762 Preprint at <https://doi.org/10.1038/nrc2230> (2007).
188. Narurkar, R., Alkayem, M. & Liu, D. SOX11 is a biomarker for cyclin D1-negative mantle cell lymphoma. *Biomarker Research* vol. 4 Preprint at <https://doi.org/10.1186/s40364-016-0060-9> (2016).
189. Meggendorfer, M., Kern, W., Haferlach, C., Haferlach, T. & Schnittger, S. SOX11 overexpression is a specific marker for mantle cell lymphoma and correlates with t(11;14) translocation, CCND1 expression and an adverse prognosis. *Leukemia* vol. 27 2388–2391 Preprint at <https://doi.org/10.1038/leu.2013.141> (2013).
190. Inwards, D. J. & Witzig, T. E. Initial therapy of mantle cell lymphoma. *Therapeutic Advances in Hematology* vol. 2 381–392 Preprint at <https://doi.org/10.1177/2040620711412418> (2011).
191. Payandeh, Z. *et al.* The applications of anti-CD20 antibodies to treat various B cells disorders. *Biomedicine and Pharmacotherapy* vol. 109 2415–2426 Preprint at <https://doi.org/10.1016/j.biopha.2018.11.121> (2019).
192. Bond, D. A., Martin, P. & Maddocks, K. J. Relapsed mantle cell lymphoma: Current management, recent progress, and future directions. *Journal of Clinical Medicine* vol. 10 1–14 Preprint at <https://doi.org/10.3390/jcm10061207> (2021).
193. Kirschey, S., Wagner, S. & Hess, G. Relapsed and/or refractory mantle cell lymphoma: What role for temsirolimus? *Clinical Medicine Insights: Oncology* vol. 6 153–164 Preprint at <https://doi.org/10.4137/CMO.S7327> (2012).
194. Wang, M. L. *et al.* Targeting BTK with Ibrutinib in Relapsed or Refractory Mantle-Cell Lymphoma. *New England Journal of Medicine* **369**, 507–516 (2013).
195. Al-Mansour, M. Treatment Landscape of Relapsed/Refractory Mantle Cell Lymphoma: An Updated Review. *Clinical Lymphoma, Myeloma and Leukemia* Preprint at <https://doi.org/10.1016/j.clml.2022.07.017> (2022).
196. Liang, A. J. M. *et al.* Bruton's tyrosine kinase (*Btk*): function, regulation, and transformation with special emphasis on the PH domain. *Blackwell Munksgaard • Immunological Reviews* vol. 228 <http://bioinf.uta.fi/BTKbase> (2009).

197. Hendriks, R. W., Yuvaraj, S. & Kil, L. P. Targeting Bruton's tyrosine kinase in B cell malignancies. *Nature Reviews Cancer* vol. 14 219–232 Preprint at <https://doi.org/10.1038/nrc3702> (2014).
198. Maas, A. & Hendriks, R. W. *Role of Bruton's Tyrosine Kinase in B Cell Development. Developmental Immunology* vol. 8 (2001).
199. Wiestner, A. Targeting B-cell receptor signaling for anticancer therapy: The Bruton's tyrosine kinase inhibitor ibrutinib induces impressive responses in B-cell malignancies. *Journal of Clinical Oncology* vol. 31 128–130 Preprint at <https://doi.org/10.1200/JCO.2012.44.4281> (2013).
200. de Claro, R. A. *et al.* FDA approval: Ibrutinib for patients with previously treated mantle cell lymphoma and previously treated chronic lymphocytic leukemia. *Clinical Cancer Research* **21**, 3586–3590 (2015).
201. Stephens, D. M. & Spurgeon, S. E. Ibrutinib in mantle cell lymphoma patients: Glass half full? Evidence and opinion. *Therapeutic Advances in Hematology* vol. 6 242–252 Preprint at <https://doi.org/10.1177/2040620715592569> (2015).
202. Davids, M. S. & Brown, J. R. Ibrutinib: A first in class covalent inhibitor of Bruton's tyrosine kinase. *Future Oncology* **10**, 957–967 (2014).
203. Wu, J., Zhang, M. & Liu, D. Acalabrutinib (ACP-196): A selective second-generation BTK inhibitor. *Journal of Hematology and Oncology* vol. 9 Preprint at <https://doi.org/10.1186/s13045-016-0250-9> (2016).
204. Abbas, H. A. & Wierda, W. G. Acalabrutinib: A Selective Bruton Tyrosine Kinase Inhibitor for the Treatment of B-Cell Malignancies. *Frontiers in Oncology* vol. 11 Preprint at <https://doi.org/10.3389/fonc.2021.668162> (2021).
205. Girard, J. *et al.* Evaluating acalabrutinib in the treatment of mantle cell lymphoma: Design, development, and place in therapy. *Onco Targets Ther* **12**, 8003–8014 (2019).
206. Estupiñán, H. Y., Berglöf, A., Zain, R. & Smith, C. I. E. Comparative Analysis of BTK Inhibitors and Mechanisms Underlying Adverse Effects. *Frontiers in Cell and Developmental Biology* vol. 9 Preprint at <https://doi.org/10.3389/fcell.2021.630942> (2021).
207. Woyach, J. A. *et al.* Resistance Mechanisms for the Bruton's Tyrosine Kinase Inhibitor Ibrutinib. *New England Journal of Medicine* **370**, 2286–2294 (2014).
208. George, B. *et al.* Ibrutinib resistance mechanisms and treatment strategies for B-cell lymphomas. *Cancers (Basel)* **12**, (2020).
209. Skanland, S. S. & Mato, A. R. Overcoming resistance to targeted therapies in chronic lymphocytic leukemia. *Blood Advances* vol. 5 334–343 Preprint at <https://doi.org/10.1182/BLOODADVANCES.2020003423> (2021).
210. Smith, C. I. E. & Burger, J. A. Resistance Mutations to BTK Inhibitors Originate From the NF- $\kappa$ B but Not From the PI3K-RAS-MAPK Arm of the B Cell Receptor Signaling Pathway. *Frontiers in Immunology* vol. 12 Preprint at <https://doi.org/10.3389/fimmu.2021.689472> (2021).
211. Wang, H., Zhang, W., Yang, J. & Zhou, K. The resistance mechanisms and treatment strategies of BTK inhibitors in B-cell lymphoma. *Hematological Oncology* vol. 39 605–615 Preprint at <https://doi.org/10.1002/hon.2933> (2021).
212. Ondrisova, L. & Mraz, M. Genetic and Non-Genetic Mechanisms of Resistance to BCR Signaling Inhibitors in B Cell Malignancies. *Frontiers in Oncology* vol. 10 Preprint at <https://doi.org/10.3389/fonc.2020.591577> (2020).

213. Chen, Z. *et al.* Prospective isolation of clonogenic mantle cell lymphoma-initiating cells. *Stem Cell Res* **5**, 212–225 (2010).
214. Mathur, R. *et al.* Targeting Wnt pathway in mantle cell lymphoma-initiating cells. *J Hematol Oncol* **8**, (2015).
215. Phi, L. T. H. *et al.* Cancer stem cells (CSCs) in drug resistance and their therapeutic implications in cancer treatment. *Stem Cells International* vol. 2018 Preprint at <https://doi.org/10.1155/2018/5416923> (2018).
216. Murase, M. *et al.* Side population cells have the characteristics of cancer stem-like cells/cancer-initiating cells in bone sarcomas. *Br J Cancer* **101**, 1425–1432 (2009).
217. Clark, D. W. & Palle, K. Aldehyde dehydrogenases in cancer stem cells: Potential as therapeutic targets. *Ann Transl Med* **4**, (2016).
218. Phi, L. T. H. *et al.* Cancer stem cells (CSCs) in drug resistance and their therapeutic implications in cancer treatment. *Stem Cells International* vol. 2018 Preprint at <https://doi.org/10.1155/2018/5416923> (2018).
219. Hirschmann-Jax, C. *et al.* A distinct “side population” of cells with high drug efflux capacity in human tumor cells. [www.pnas.org/cgi/doi/10.1073/pnas.0400067101](http://www.pnas.org/cgi/doi/10.1073/pnas.0400067101) (2004).
220. Eggener, S. Prostate cancer. *TheScientificWorldJournal* vol. 11 749–750 Preprint at <https://doi.org/10.1100/tsw.2011.79> (2011).
221. Rawla, P. Epidemiology of Prostate Cancer. *World J Oncol* **10**, 63–89 (2019).
222. Rebbeck, T. R. Prostate Cancer Genetics: Variation by Race, Ethnicity, and Geography. *Seminars in Radiation Oncology* vol. 27 3–10 Preprint at <https://doi.org/10.1016/j.semradonc.2016.08.002> (2017).
223. Leitzmann, M. F. & Rohrmann, S. Risk factors for the onset of prostatic cancer: Age, location, and behavioral correlates. *Clinical Epidemiology* vol. 4 1–11 Preprint at <https://doi.org/10.2147/CLEP.S16747> (2012).
224. Bostwick, D. G. *et al.* Human prostate cancer risk factors. *Cancer* vol. 101 2371–2490 Preprint at <https://doi.org/10.1002/cncr.20408> (2004).
225. *Risk Factors for Prostate Cancer.* (2002).
226. Grignon, D. J. Unusual subtypes of prostate cancer. *Modern Pathology* vol. 17 316–327 Preprint at <https://doi.org/10.1038/modpathol.3800052> (2004).
227. *Clinical features of prostate cancer before diagnosis: a population-based, case-control study.*
228. Grossman, D. C. *et al.* Screening for prostate cancer US Preventive servicetaskforcerecommendation statement. *JAMA - Journal of the American Medical Association* **319**, 1901–1913 (2018).
229. Ilic, D. *et al.* Prostate cancer screening with prostate-specific antigen (PSA) test: A systematic review and meta-analysis. *BMJ (Online)* **362**, (2018).
230. Descotes, J. L. Diagnosis of prostate cancer. *Asian Journal of Urology* vol. 6 129–136 Preprint at <https://doi.org/10.1016/j.ajur.2018.11.007> (2019).
231. Kweldam, C. F., van Leenders, G. J. & van der Kwast, T. Grading of prostate cancer: a work in progress. *Histopathology* vol. 74 146–160 Preprint at <https://doi.org/10.1111/his.13767> (2019).
232. Prostate Cancer Stages and Grades.
233. Pirtskhalaishvili, G., Hrebinko, R. L. & Nelson, J. B. *The Treatment of Prostate Cancer An Overview of Current Options.* (1065).
234. Initial Treatment of Prostate Cancer, by Stage and Risk Group.

235. Nevedomskaya, E., Baumgart, S. J. & Haendler, B. Recent advances in prostate cancer treatment and drug discovery. *International Journal of Molecular Sciences* vol. 19 Preprint at <https://doi.org/10.3390/ijms19051359> (2018).
236. Rao Gajula, S. N., Reddy, G. N., Reddy, D. S. & Sonti, R. Pharmacokinetic drug-drug interactions: An insight into recent US FDA-Approved drugs for prostate cancer. *Bioanalysis* vol. 12 1647–1664 Preprint at <https://doi.org/10.4155/bio-2020-0242> (2020).
237. Feng, Q. & He, B. Androgen Receptor Signaling in the Development of Castration-Resistant Prostate Cancer. *Frontiers in Oncology* vol. 9 Preprint at <https://doi.org/10.3389/fonc.2019.00858> (2019).
238. Aurilio, G. *et al.* Androgen Receptor Signaling Pathway in Prostate Cancer: From Genetics to Clinical Applications. *Cells* vol. 9 Preprint at <https://doi.org/10.3390/cells9122653> (2020).
239. Dai, C., Heemers, H. & Sharifi, N. Androgen signaling in prostate cancer. *Cold Spring Harb Perspect Med* **7**, (2017).
240. Zhou, Y., Bolton, E. C. & Jones, J. O. Androgens and androgen receptor signaling in prostate tumorigenesis. *Journal of Molecular Endocrinology* vol. 54 R15–R29 Preprint at <https://doi.org/10.1530/JME-14-0203> (2015).
241. Schrecengost, R. & Knudsen, K. E. Molecular pathogenesis and progression of prostate cancer. *Semin Oncol* **40**, 244–258 (2013).
242. TNM staging for prostate cancer.
243. Localized Prostate Cancer: Treatment Options.
244. Ng Shievon Smith Jonathan Shamash, K., Ng Á Smith Á J Shamash, K. S. & Ther, O. Metastatic Hormone-Sensitive Prostate Cancer (mHSPC): Advances and Treatment Strategies in the First-Line Setting. (2020) doi:10.6084/m9.figshare.12416507.
245. Bellmunt, J. & Oh, W. K. Review: Castration-resistant prostate cancer: New science and therapeutic prospects. *Therapeutic Advances in Medical Oncology* vol. 2 189–207 Preprint at <https://doi.org/10.1177/1758834009359769> (2010).
246. Hyuk Hong, J. & Kim, I. Y. Nonmetastatic Castration-Resistant Prostate Cancer. *Korean Journal of Urology ©The Korean Urological Association* **55**, 153–160 (2014).
247. Saad, F., Bögemann, M., Suzuki, K. & Shore, N. Treatment of nonmetastatic castration-resistant prostate cancer: focus on second-generation androgen receptor inhibitors. *Prostate Cancer and Prostatic Diseases* vol. 24 323–334 Preprint at <https://doi.org/10.1038/s41391-020-00310-3> (2021).
248. Henríquez, I. *et al.* Current and emerging therapies for metastatic castration-resistant prostate cancer (Mcrpc). *Biomedicines* vol. 9 Preprint at <https://doi.org/10.3390/biomedicines9091247> (2021).
249. Einstein, D. J. *et al.* Metastatic Castration-Resistant Prostate Cancer Remains Dependent on Oncogenic Drivers Found in Primary Tumors. (2021) doi:10.1200/PO.21.
250. He, L. *et al.* Metastatic castration-resistant prostate cancer: Academic insights and perspectives through bibliometric analysis. *Medicine (United States)* vol. 99 Preprint at <https://doi.org/10.1097/MD.0000000000019760> (2020).
251. Schweizer, M. & Antonarakis, E. S. Chemotherapy and its evolving role in the management of advanced prostate cancer. *Asian Journal of Andrology* vol. 16 334–340 Preprint at <https://doi.org/10.4103/1008-682X.122593> (2014).

252. Drake, C. G., Sharma, P. & Gerritsen, W. Metastatic castration-resistant prostate cancer: New therapies, novel combination strategies and implications for immunotherapy. *Oncogene* vol. 33 5053–5064 Preprint at <https://doi.org/10.1038/onc.2013.497> (2013).
253. Herbst, R. S. & Khuri, F. R. Mode of action of docetaxel - A basis for combination with novel anticancer agents. *Cancer Treat Rev* **29**, 407–415 (2003).
254. D. SCHALLIER, L. D. J. B. C. F. and J. D. et al. Docetaxel in the Treatment of Metastatic Castration-resistant Prostate Cancer (mCRPC): an Observational Study in a Single Institution.
255. Abidi, A. Cabazitaxel: A novel taxane for metastatic castration-resistant prostate cancer-current implications and future prospects. *Journal of Pharmacology and Pharmacotherapeutics* vol. 4 230–237 Preprint at <https://doi.org/10.4103/0976-500X.119704> (2013).
256. Paller, C. J. & Antonarakis, E. S. Cabazitaxel: A novel second-line treatment for metastatic castration-resistant prostate cancer. *Drug Design, Development and Therapy* 117–124 Preprint at <https://doi.org/10.2147/DDDT.S13029> (2011).
257. Herbst, R. S. & Khuri, F. R. Mode of action of docetaxel - A basis for combination with novel anticancer agents. *Cancer Treat Rev* **29**, 407–415 (2003).
258. Reed, E. & Li, Q. Q. *Molecular mechanism of antitumor activity of taxanes in lung cancer (Review)*. *INTERNATIONAL JOURNAL OF ONCOLOGY* vol. 27 (2005).
259. Greenberger, L. M. & Sampath, D. *Resistance To Taxanes INTRODUCTION RESISTANCE TO TAXANES ASSOCIATED WITH CHANGES IN MICROTUBULES RESISTANCE TO TAXANES ASSOCIATED WITH TRANSPORTERS CONTROL OF APOPTOSIS ACTIVATION OF TRANSCRIPTION FACTORS ROLE OF CYTOKINES AND CHEMOKINES IN PACLITAXEL DRUG RESISTANCE ROLE OF KINASES IN DRUG RESISTANCE CLINICAL CORRELATIONS WITH IN VITRO MECHANISMS ACKNOWLEDGMENTS REFERENCES*.
260. Sekino, Y. & Teishima, J. Molecular mechanisms of docetaxel resistance in prostate cancer. *Cancer Drug Resistance* vol. 3 676–685 Preprint at <https://doi.org/10.20517/cdr.2020.37> (2020).
261. Tan, J. L. *et al.* Androgen receptor targeted therapies in metastatic castration-resistant prostate cancer – The urologists’ perspective. *Urological Science* vol. 28 190–196 Preprint at <https://doi.org/10.1016/j.urols.2017.10.001> (2017).
262. Jacob, A., Raj, R., Allison, D. B. & Myint, Z. W. Androgen receptor signaling in prostate cancer and therapeutic strategies. *Cancers* vol. 13 Preprint at <https://doi.org/10.3390/cancers13215417> (2021).
263. Baciarello, G. & Sternberg, C. N. Treatment of metastatic castration-resistant prostate cancer (mCRPC) with enzalutamide. *Critical Reviews in Oncology/Hematology* vol. 106 14–24 Preprint at <https://doi.org/10.1016/j.critrevonc.2016.07.005> (2016).
264. Merseburger, A. S., Haas, G. P. & von Klot, C. A. An update on enzalutamide in the treatment of prostate cancer. *Therapeutic Advances in Urology* vol. 7 9–21 Preprint at <https://doi.org/10.1177/1756287214555336> (2015).
265. Zhang, Q. *et al.* Treatment-Emergent Neuroendocrine Prostate Cancer: A Clinicopathological and Immunohistochemical Analysis of 94 Cases. *Front Oncol* **10**, (2021).
266. Conteduca, V. *et al.* Clinical features of neuroendocrine prostate cancer. *Eur J Cancer* **121**, 7–18 (2019).

267. Beltran, H. & Demichelis, F. Therapy considerations in neuroendocrine prostate cancer: What next? *Endocrine-Related Cancer* vol. 28 T67–T78 Preprint at <https://doi.org/10.1530/ERC-21-0140> (2021).
268. Yamada, Y. & Beltran, H. Clinical and Biological Features of Neuroendocrine Prostate Cancer. *Current Oncology Reports* vol. 23 Preprint at <https://doi.org/10.1007/s11912-020-01003-9> (2021).
269. Wang, H. T. *et al.* Neuroendocrine Prostate Cancer (NEPC) Progressing from conventional prostatic adenocarcinoma: Factors associated with time to development of nepc and survival from NEPC Diagnosis-A systematic review and pooled analysis. *Journal of Clinical Oncology* **32**, 3383–3390 (2014).
270. Merkens, L. *et al.* Aggressive variants of prostate cancer: underlying mechanisms of neuroendocrine transdifferentiation. *Journal of Experimental and Clinical Cancer Research* vol. 41 Preprint at <https://doi.org/10.1186/s13046-022-02255-y> (2022).
271. Slovin, S. F. Neuroendocrine differentiation in prostate cancer: A sheep in wolf’s clothing? *Nature Clinical Practice Urology* vol. 3 138–144 Preprint at <https://doi.org/10.1038/ncpuro0435> (2006).
272. Hu, C. D., Choo, R. & Huang, J. Neuroendocrine differentiation in prostate cancer: A mechanism of radioresistance and treatment failure. *Frontiers in Oncology* vol. 5 Preprint at <https://doi.org/10.3389/fonc.2015.00090> (2015).
273. Hu, C. D., Choo, R. & Huang, J. Neuroendocrine differentiation in prostate cancer: A mechanism of radioresistance and treatment failure. *Frontiers in Oncology* vol. 5 Preprint at <https://doi.org/10.3389/fonc.2015.00090> (2015).
274. Epstein, J. I. *et al.* Proposed morphologic classification of prostate cancer with neuroendocrine differentiation. *American Journal of Surgical Pathology* **38**, 756–767 (2014).
275. Rosa, S. la & Uccella, S. Classification of neuroendocrine neoplasms: lights and shadows. doi:10.1007/s11154-020-09612-2/Published.
276. Spetsieris, N., Boukovala, M., Patsakis, G., Alafis, I. & Efstathiou, E. Neuroendocrine and aggressive-variant prostate cancer. *Cancers* vol. 12 1–20 Preprint at <https://doi.org/10.3390/cancers12123792> (2020).
277. Maeda, H. & Khatami, M. Analyses of repeated failures in cancer therapy for solid tumors: poor tumor-selective drug delivery, low therapeutic efficacy and unsustainable costs. *Clin Transl Med* **7**, (2018).
278. Wang, X., Zhang, H. & Chen, X. Drug resistance and combating drug resistance in cancer. *Cancer Drug Resistance* vol. 2 141–160 Preprint at <https://doi.org/10.20517/cdr.2019.10> (2019).
279. Vincent Rajkumar, S. Multiple myeloma: 2013 update on diagnosis, risk-stratification, and management. *Am J Hematol* **88**, 225–235 (2013).
280. Rajkumar, S. V. Myeloma today: Disease definitions and treatment advances. *Am J Hematol* **91**, 90–100 (2016).
281. Richardson, P. G. *et al.* Panobinostat plus bortezomib and dexamethasone in previously treated multiple myeloma: outcomes by prior treatment. (2016) doi:10.1182/blood.
282. Moreau, P. *et al.* Proteasome inhibitors in multiple myeloma: 10 Years later. *Blood* vol. 120 947–959 Preprint at <https://doi.org/10.1182/blood-2012-04-403733> (2012).

283. Munshi, N. C. & Anderson, K. C. New strategies in the treatment of multiple myeloma. *Clinical Cancer Research* vol. 19 3337–3344 Preprint at <https://doi.org/10.1158/1078-0432.CCR-12-1881> (2013).
284. Kortuem, K. M. & Stewart, A. K. Carfilzomib. *Blood* vol. 121 893–897 Preprint at <https://doi.org/10.1182/blood-2012-10-459883> (2013).
285. Kuehl, W. M. & Bergsagel, P. L. Molecular pathogenesis of multiple myeloma and its premalignant precursor. *Journal of Clinical Investigation* vol. 122 3456–3463 Preprint at <https://doi.org/10.1172/JCI61188> (2012).
286. Shaji Kumar, S. V. R. et al. Many facets of bortezomib resistance/susceptibility.
287. Mitra, A. K. et al. Single-cell analysis of targeted transcriptome predicts drug sensitivity of single cells within human myeloma tumors. *Leukemia* **30**, 1094–1102 (2016).
288. Rajkumar, S. V. & Kumar, S. Multiple Myeloma: Diagnosis and Treatment. *Mayo Clinic Proceedings* vol. 91 101–119 Preprint at <https://doi.org/10.1016/j.mayocp.2015.11.007> (2016).
289. Rowley, M. & Ness, B. van. Activation of N-ras and K-ras induced by interleukin-6 in a myeloma cell line: implications for disease progression and therapeutic response. *Oncogene* **21**, 8769–8775 (2002).
290. Mitra, A. K. et al. In vitro and ex vivo gene expression profiling reveals differential kinetic response of HSPs and UPR genes is associated with PI resistance in multiple myeloma. *Blood Cancer J* **10**, (2020).
291. Carlson-Stevermer, J. et al. CRISPRoff enables spatio-temporal control of CRISPR editing. *Nat Commun* **11**, (2020).
292. Yang, W. et al. Genomics of Drug Sensitivity in Cancer (GDSC): A resource for therapeutic biomarker discovery in cancer cells. *Nucleic Acids Res* **41**, (2013).
293. Garnett, M. J. et al. Systematic identification of genomic markers of drug sensitivity in cancer cells. *Nature* **483**, 570–575 (2012).
294. Keenan, A. B. et al. The Library of Integrated Network-Based Cellular Signatures NIH Program: System-Level Cataloging of Human Cells Response to Perturbations. *Cell Systems* vol. 6 13–24 Preprint at <https://doi.org/10.1016/j.cels.2017.11.001> (2018).
295. Chou, T. C. Drug combination studies and their synergy quantification using the chou-talalay method. *Cancer Research* vol. 70 440–446 Preprint at <https://doi.org/10.1158/0008-5472.CAN-09-1947> (2010).
296. Baughn, L. B. et al. Phenotypic and functional characterization of a bortezomib-resistant multiple myeloma cell line by flow and mass cytometry. *Leuk Lymphoma* **58**, 1931–1940 (2017).
297. Richardson, P. G. et al. Safety and efficacy of bortezomib in high-risk and elderly patients with relapsed multiple myeloma. *Br J Haematol* **137**, 429–435 (2007).
298. Vangsted, A., Klausen, T. W. & Vogel, U. Genetic variations in multiple myeloma II: Association with effect of treatment. *European Journal of Haematology* vol. 88 93–117 Preprint at <https://doi.org/10.1111/j.1600-0609.2011.01696.x> (2012).
299. Geeleher, P., Cox, N. & Stephanie Huang, R. PRRophetic: An r package for prediction of clinical chemotherapeutic response from tumor gene expression levels. *PLoS One* **9**, (2014).
300. Stessman, H. A. F. et al. Profiling bortezomib resistance identifies secondary therapies in a mouse myeloma model. *Mol Cancer Ther* **12**, 1140–1150 (2013).

301. Richardson, P. G. *et al.* Tanespimycin and bortezomib combination treatment in patients with relapsed or relapsed and refractory multiple myeloma: Results of a phase 1/2 study. *Br J Haematol* **153**, 729–740 (2011).
302. Richardson, P. G. *et al.* Tanespimycin with bortezomib: Activity in relapsed/refractory patients with multiple myeloma. *Br J Haematol* **150**, 428–437 (2010).
303. Richardson, P. G. *et al.* Inhibition of heat shock protein 90 (HSP90) as a therapeutic strategy for the treatment of myeloma and other cancers. *British Journal of Haematology* vol. 152 367–379 Preprint at <https://doi.org/10.1111/j.1365-2141.2010.08360.x> (2011).
304. Banerji, U., Affolter, A., Judson, I., Marais, R. & Workman, P. BRAF and NRAS mutations in melanoma: Potential relationships to clinical response to HSP90 inhibitors. *Mol Cancer Ther* **7**, 737–739 (2008).
305. Mulligan, G. *et al.* Mutation of NRAS but not KRAS significantly reduces myeloma sensitivity to single-agent bortezomib therapy. (2014) doi:10.1182/blood-2013-05.
306. Chiarugi, A., Dölle, C., Felici, R. & Ziegler, M. The NAD metabolome - A key determinant of cancer cell biology. *Nature Reviews Cancer* vol. 12 741–752 Preprint at <https://doi.org/10.1038/nrc3340> (2012).
307. Cagnetta, A. *et al.* Intracellular NAD<sup>+</sup> depletion enhances bortezomib-induced anti-myeloma activity. *Blood* **122**, 1243–1255 (2013).
308. Michele Cea, K. C. A. *et al.* Targeting NAD salvage pathway induces autophagy in multiple myeloma cells via mTORC1 and extracellular signal-regulated kinase (ERK1/2) inhibition.
309. Spaan, I. *et al.* Direct P70S6K1 inhibition to replace dexamethasone in synergistic combination with MCL-1 inhibition in multiple myeloma. *Blood Adv* **5**, 2593–2607 (2021).
310. El-Mesery, M. *et al.* The NEDD8-activating enzyme inhibitor MLN4924 sensitizes a TNFR1<sup>+</sup> subgroup of multiple myeloma cells for TNF-induced cell death. *Cell Death Dis* **10**, (2019).
311. Andrulis, M. *et al.* Targeting the BRAF V600E mutation in multiple myeloma. *Cancer Discov* **3**, 862–869 (2013).
312. Tse, C. *et al.* ABT-263: A potent and orally bioavailable Bcl-2 family inhibitor. *Cancer Res* **68**, 3421–3428 (2008).
313. Vogler, M., Dinsdale, D., Dyer, M. J. S. & Cohen, G. M. Bcl-2 inhibitors: Small molecules with a big impact on cancer therapy. *Cell Death and Differentiation* vol. 16 360–367 Preprint at <https://doi.org/10.1038/cdd.2008.137> (2009).
314. de Campos, C. B. *et al.* Identification of PIKfyve kinase as a target in multiple myeloma. *Haematologica* **105**, 1641–1649 (2020).
315. Bonolo de Campos, C. *et al.* “Direct to Drug” screening as a precision medicine tool in multiple myeloma. *Blood Cancer J* **10**, (2020).
316. prostate-cancer statistics.
317. Harada, K. *et al.* Treatment Strategies for Metastatic Castration-Sensitive Prostate Cancer: From “All-Comers” to “Personalized” Approach. *Onco Targets Ther* **Volume 14**, 2967–2974 (2021).
318. Docetaxel in the Treatment of Metastatic Castration-resistant Prostate Cancer (mCRPC): an Observational Study in a Single Institution.

319. Kumar, H. *et al.* secDrug: a pipeline to discover novel drug combinations to kill drug-resistant multiple myeloma cells using a greedy set cover algorithm and single-cell multi-omics. *Blood Cancer J* **12**, (2022).
320. Yang, W. *et al.* Genomics of Drug Sensitivity in Cancer (GDSC): a resource for therapeutic biomarker discovery in cancer cells. *Nucleic Acids Res* **41**, D955-61 (2013).
321. Chandrashekar, D. S. *et al.* UALCAN: A Portal for Facilitating Tumor Subgroup Gene Expression and Survival Analyses. *Neoplasia* **19**, 649–658 (2017).
322. Zheng, H. *et al.* Comprehensive Review of Web Servers and Bioinformatics Tools for Cancer Prognosis Analysis. *Front Oncol* **10**, 68 (2020).
323. Chou, T. C. The mass-action law based algorithm for cost-effective approach for cancer drug discovery and development. *Am J Cancer Res* **1**, 925–954 (2011).
324. Wilson, E., Rubel, C. & Schisler, J. Non-radiometric Cell-free Assay to Measure the Effect of Molecular Chaperones on AMP-Activated Kinase Activity. *Bio Protoc* **9**, (2019).
325. Mazumder, S. *et al.* Integrating Pharmacogenomics Data-Driven Computational Drug Prediction with Single-Cell RNAseq to Demonstrate the Efficacy of a NAMPT Inhibitor against Aggressive, Taxane-Resistant, and Stem-like Cells in Lethal Prostate Cancer. *Cancers (Basel)* **14**, 6009 (2022).
326. Cargnello, M. & Roux, P. P. Activation and Function of the MAPKs and Their Substrates, the MAPK-Activated Protein Kinases. *Microbiology and Molecular Biology Reviews* **75**, 50–83 (2011).
327. Maik-Rachline, G., Lifshits, L. & Seger, R. Nuclear p38: Roles in physiological and pathological processes and regulation of nuclear translocation. *International Journal of Molecular Sciences* vol. 21 1–23 Preprint at <https://doi.org/10.3390/ijms21176102> (2020).
328. Shida, Y., Igawa, T., Hakariya, T., Sakai, H. & Kanetake, H. p38MAPK activation is involved in androgen-independent proliferation of human prostate cancer cells by regulating IL-6 secretion. *Biochem Biophys Res Commun* **353**, 744–749 (2007).
329. Khandrika, L. *et al.* Hypoxia-associated p38 mitogen-activated protein kinase-mediated androgen receptor activation and increased HIF-1 $\alpha$  levels contribute to emergence of an aggressive phenotype in prostate cancer. *Oncogene* vol. 28 1248–1260 Preprint at <https://doi.org/10.1038/onc.2008.476> (2009).
330. Chandrasekar, T., Yang, J. C., Gao, A. C. & Evans, C. P. Mechanisms of resistance in castration-resistant prostate cancer (CRPC). *Transl Androl Urol* **4**, 365–380 (2015).
331. Cheung, S. *et al.* P38 mapk inhibition mitigates hypoxia-induced ar signaling in castration-resistant prostate cancer. *Cancers (Basel)* **13**, 1–13 (2021).
332. Qiu, G. Z. *et al.* Reprogramming of the Tumor in the Hypoxic Niche: The Emerging Concept and Associated Therapeutic Strategies. *Trends in Pharmacological Sciences* vol. 38 669–686 Preprint at <https://doi.org/10.1016/j.tips.2017.05.002> (2017).
333. Wang, Q. *et al.* RACK1 antagonizes TNF- $\alpha$ -induced cell death by promoting p38 activation. *Sci Rep* **5**, (2015).
334. Gan, L., Wang, J., Xu, H. & Yang, X. Resistance to docetaxel-induced apoptosis in prostate cancer cells by p38/p53/p21 signaling. *Prostate* **71**, 1158–1166 (2011).
335. Liu, Z. H., Dai, X. M. & Du, B. Hes1: A key role in stemness, metastasis and multidrug resistance. *Cancer Biology and Therapy* vol. 16 353–359 Preprint at <https://doi.org/10.1080/15384047.2015.1016662> (2015).

336. Gao, F. *et al.* Hes1 is involved in the self-renewal and tumorigenicity of stem-like cancer cells in colon cancer. *Sci Rep* **4**, (2014).
337. Bumbaca, B. & Li, W. Taxane resistance in castration-resistant prostate cancer: mechanisms and therapeutic strategies. *Acta Pharm Sin B* **8**, 518–529 (2018).
338. Jebali, A. & Dumaz, N. The role of RICTOR downstream of receptor tyrosine kinase in cancers. *Molecular Cancer* vol. 17 Preprint at <https://doi.org/10.1186/s12943-018-0794-0> (2018).
339. Guan, B. *et al.* *Oncotarget 1* [www.impactjournals.com/oncotarget](http://www.impactjournals.com/oncotarget) *Tumor-suppressive microRNA-218 inhibits tumor angiogenesis via targeting the mTOR component RICTOR in prostate cancer.* [www.impactjournals.com/oncotarget/](http://www.impactjournals.com/oncotarget/).
340. Padilla, J. & Lee, J. A novel therapeutic target, bach1, regulates cancer metabolism. *Cells* vol. 10 1–13 Preprint at <https://doi.org/10.3390/cells10030634> (2021).
341. Sato, M. *et al.* BACH1 promotes pancreatic cancer metastasis by repressing epithelial genes and enhancing epithelial-mesenchymal transition. *Cancer Res* **80**, 1279–1292 (2020).
342. Mostaghel, E. A. Alternative acts: Oncogenic splicing of steroidogenic enzymes in prostate cancer. *Clinical Cancer Research* **25**, 1139–1141 (2019).
343. Antonopoulou, E. & Ladomery, M. Targeting splicing in prostate cancer. *International Journal of Molecular Sciences* vol. 19 Preprint at <https://doi.org/10.3390/ijms19051287> (2018).
344. Qu, W. *et al.* miR-132 mediates a metabolic shift in prostate cancer cells by targeting Glut1. *FEBS Open Bio* **6**, 735–741 (2016).
345. Chen, L., Zhu, Q., Lu, L. & Liu, Y. MiR-132 inhibits migration and invasion and increases chemosensitivity of cisplatin-resistant oral squamous cell carcinoma cells via targeting TGF- $\beta$ 1. *Bioengineered* **11**, 91–102 (2020).
346. Moghbeli, M., Zangouei, A. S., Nasrpour Navaii, Z. & Taghehchian, N. Molecular mechanisms of the microRNA-132 during tumor progressions. *Cancer Cell International* vol. 21 Preprint at <https://doi.org/10.1186/s12935-021-02149-7> (2021).
347. Xue, D. *et al.* Nuclear transcription factor Nrf2 suppresses prostate cancer cells growth and migration through upregulating ferroportin. *Oncotarget* vol. 7 [www.impactjournals.com/oncotarget/](http://www.impactjournals.com/oncotarget/).
348. Gomez, L. A., de Las Pozas, A., Reiner, T., Burnstein, K. & Perez-Stable, C. Increased expression of cyclin B1 sensitizes prostate cancer cells to apoptosis induced by chemotherapy. *Mol Cancer Ther* **6**, 1534–1543 (2007).
349. Liu, S. *et al.* Chac2, downregulated in gastric and colorectal cancers, acted as a tumor suppressor inducing apoptosis and autophagy through unfolded protein response. *Cell Death Dis* **8**, (2017).
350. Xi, H. Q., Wu, X. S., Wei, B. & Chen, L. Eph receptors and ephrins as targets for cancer therapy. *J Cell Mol Med* **16**, 2894–2909 (2012).
351. Yadav, N. *et al.* Oxidative phosphorylation-dependent regulation of cancer cell apoptosis in response to anticancer agents. *Cell Death Dis* **6**, (2015).
352. Matsuura, K., Canfield, K., Feng, W. & Kurokawa, M. Metabolic Regulation of Apoptosis in Cancer. in *International Review of Cell and Molecular Biology* vol. 327 43–87 (Elsevier Inc., 2016).

353. Brillo, V., Chieragato, L., Leanza, L., Muccioli, S. & Costa, R. Mitochondrial dynamics, ROS, and cell signaling: A blended overview. *Life* vol. 11 Preprint at <https://doi.org/10.3390/life11040332> (2021).
354. Gutiérrez-Uzquiza, Á., Arechederra, M., Bragado, P., Aguirre-Ghiso, J. A. & Porras, A. p38 $\alpha$  mediates cell survival in response to oxidative stress via induction of antioxidant genes: Effect on the p70S6K pathway. *Journal of Biological Chemistry* **287**, 2632–2642 (2012).
355. Lee, J. W. & Kim, J. H. Activation of the leukotriene B4 receptor 2-reactive oxygen species (BLT2-ROS) cascade following detachment confers anoikis resistance in prostate cancer cells. *Journal of Biological Chemistry* **288**, 30054–30063 (2013).
356. Zhang, X., Wu, H., Yan, X., Ma, J. & Chen, Z. LTB4R Promotes the Occurrence and Progression of Clear Cell Renal Cell Carcinoma (ccRCC) by Regulating the AKT/mTOR Signaling Pathway. *Cells* **11**, (2022).
357. He, L. *et al.*  $\alpha$ -Mannosidase 2C1 attenuates PTEN function in prostate cancer cells. *Nat Commun* **2**, (2011).
358. Wu, C. *et al.* SPTBN2, a New Biomarker of Lung Adenocarcinoma. *Front Oncol* **11**, (2021).
359. Wang, P. *et al.* SPTBN2 regulated by miR-424-5p promotes endometrial cancer progression via CLDN4/PI3K/AKT axis. *Cell Death Discov* **7**, (2021).
360. Yadav, N. *et al.* Oxidative phosphorylation-dependent regulation of cancer cell apoptosis in response to anticancer agents. *Cell Death Dis* **6**, (2015).
361. Nakamura, H. & Takada, K. Reactive oxygen species in cancer: Current findings and future directions. *Cancer Science* vol. 112 3945–3952 Preprint at <https://doi.org/10.1111/cas.15068> (2021).
362. Yadav, N. *et al.* Oxidative phosphorylation-dependent regulation of cancer cell apoptosis in response to anticancer agents. *Cell Death Dis* **6**, (2015).
363. Kuo, C. L. *et al.* Mitochondrial oxidative stress in the tumor microenvironment and cancer immunoescape: foe or friend? *Journal of Biomedical Science* vol. 29 Preprint at <https://doi.org/10.1186/s12929-022-00859-2> (2022).
364. Fujii, J., Homma, T. & Osaki, T. Superoxide Radicals in the Execution of Cell Death. *Antioxidants* vol. 11 Preprint at <https://doi.org/10.3390/antiox11030501> (2022).
365. Gutiérrez-Uzquiza, Á., Arechederra, M., Bragado, P., Aguirre-Ghiso, J. A. & Porras, A. p38 $\alpha$  mediates cell survival in response to oxidative stress via induction of antioxidant genes: Effect on the p70S6K pathway. *Journal of Biological Chemistry* **287**, 2632–2642 (2012).
366. Wang, R. *et al.* Reactive Oxygen Species and NRF2 Signaling, Friends or Foes in Cancer? *Biomolecules* **13**, 353 (2023).
367. Shelton, P. & Jaiswal, A. K. The transcription factor NF-E2-related factor 2 (nrf2): A protooncogene? *FASEB Journal* vol. 27 414–423 Preprint at <https://doi.org/10.1096/fj.12-217257> (2013).
368. Ma, L. *et al.* p38 MAPK-dependent Nrf2 induction enhances the resistance of glioma cells against TMZ. *Medical Oncology* **32**, (2015).
369. Kuczler, M. D., Olseen, A. M., Pienta, K. J. & Amend, S. R. ROS-induced cell cycle arrest as a mechanism of resistance in polyan euploid cancer cells (PACCs). *Prog Biophys Mol Biol* **165**, 3–7 (2021).

370. Burkart, M. & Karmali, R. Relapsed/Refractory Mantle Cell Lymphoma: Beyond BTK Inhibitors. *Journal of Personalized Medicine* vol. 12 Preprint at <https://doi.org/10.3390/jpm12030376> (2022).
371. Roué, G. & Sola, B. Management of drug resistance in mantle cell lymphoma. *Cancers* vol. 12 1–26 Preprint at <https://doi.org/10.3390/cancers12061565> (2020).
372. Verhagen, A. M., Coulson, E. J. & Vaux, D. L. Protein family review Inhibitor of apoptosis proteins and their relatives: IAPs and other BIRPs Gene organization and evolutionary history. *Genome Biol* **2**, (2001).
373. Chen, X., Duan, N., Zhang, C. & Zhang, W. Survivin and tumorigenesis: Molecular mechanisms and therapeutic strategies. *Journal of Cancer* vol. 7 314–323 Preprint at <https://doi.org/10.7150/jca.13332> (2016).
374. Ambrosini, G., Adida, C. & Altieri, D. C. A novel anti-apoptosis gene, survivin, expressed in cancer and lymphoma. <http://www.nature.com/naturemedicine> (1997).
375. Marcato, P., Dean, C. A., Giacomantonio, C. A. & Lee, P. W. K. Aldehyde dehydrogenase its role as a cancer stem cell marker comes down to the specific isoform. *Cell Cycle* vol. 10 1378–1384 Preprint at <https://doi.org/10.4161/cc.10.9.15486> (2011).
376. Zhang, H., Chen, Z., Neelapu, S. S., Romaguera, J. & Mccarty, N. *Hedgehog inhibitors selectively target cell migration and adhesion of mantle cell lymphoma in bone marrow microenvironment.* vol. 7 [www.impactjournals.com/oncotarget](http://www.impactjournals.com/oncotarget) (2016).
377. Padma, V. V. An overview of targeted cancer therapy. *BioMedicine (Netherlands)* vol. 5 1–6 Preprint at <https://doi.org/10.7603/s40681-015-0019-4> (2015).
378. Hambley, B., Caimi, P. F. & William, B. M. Bortezomib for the treatment of mantle cell lymphoma: an update. *Ther Adv Hematol* **7**, 196–208 (2016).
379. Kumar, H. *et al.* Single-Cell Proteomics and Tumor RNAseq Identify Novel Pathways Associated With Clofazimine Sensitivity in PI- and IMiD- Resistant Myeloma, and Putative Stem-Like Cells. *Front Oncol* **12**, (2022).
380. Kumar, H. *et al.* Leprosy drug clofazimine activates peroxisome proliferator-activated with imatinib to inhibit receptor- chronicmyeloid and synergizes leukemia cells. *Haematologica* **105**, 971–986 (2020).
381. Hou, Y., Moreau, F. & Chadee, K. PPAR $\gamma$  is an E3 ligase that induces the degradation of NF $\kappa$ B/p65. *Nat Commun* **3**, (2012).
382. Tom, E. C. *et al.* *EHD1 and RUSC2 Control Basal Epidermal Growth Factor Receptor Cell Surface Expression and Recycling.* <https://doi.org/10> (2020).
383. Meng, Q. *et al.* Increased expression of Eps15 homology domain 1 is associated with poor prognosis in resected small cell lung cancer. *J Cancer* **6**, 990–995 (2015).
384. Lu, H. *et al.* Increased EHD1 in non-small cell lung cancer predicts poor survival. *Thorac Cancer* **4**, 422–432 (2013).
385. Statello, L., Guo, C. J., Chen, L. L. & Huarte, M. Gene regulation by long non-coding RNAs and its biological functions. *Nature Reviews Molecular Cell Biology* vol. 22 96–118 Preprint at <https://doi.org/10.1038/s41580-020-00315-9> (2021).
386. Begolli, R., Sideris, N. & Giakountis, A. Lncrnas as chromatin regulators in cancer: From molecular function to clinical potential. *Cancers* vol. 11 Preprint at <https://doi.org/10.3390/cancers11101524> (2019).
387. Peng, Z., Liu, C. & Wu, M. New insights into long noncoding RNAs and their roles in glioma. *Molecular Cancer* vol. 17 Preprint at <https://doi.org/10.1186/s12943-018-0812-2> (2018).

388. Cheng, Y. *et al.* Long Noncoding RNA Expression Signatures of Colon Cancer Based on the ceRNA Network and Their Prognostic Value. *Dis Markers* **2019**, (2019).
389. Chen, J. *et al.* Long Non-Coding RNA SNHG1 Regulates the Wnt/ $\beta$ -Catenin and PI3K/AKT/mTOR Signaling Pathways via EZH2 to Affect the Proliferation, Apoptosis, and Autophagy of Prostate Cancer Cell. *Front Oncol* **10**, (2020).
390. Chen, J. *et al.* Long Non-Coding RNA SNHG1 Regulates the Wnt/ $\beta$ -Catenin and PI3K/AKT/mTOR Signaling Pathways via EZH2 to Affect the Proliferation, Apoptosis, and Autophagy of Prostate Cancer Cell. *Front Oncol* **10**, (2020).
391. Min, J., Ma, J., Wang, Q. & Yu, D. Long non-coding RNA SNHG1 promotes bladder cancer progression by upregulating EZH2 and repressing KLF2 transcription. *Clinics* **77**, (2022).
392. Zhang, H. le, Wang, P., Lu, M. Z., Zhang, S. D. & Zheng, L. c-Myc maintains the self-renewal and chemoresistance properties of colon cancer stem cells. *Oncol Lett* **17**, 4487–4493 (2019).
393. Lee, J. *et al.* Activation of MYC, a bona fide client of HSP90, contributes to intrinsic ibrutinib resistance in mantle cell lymphoma. *Blood Adv* **2**, 2039–2051 (2018).
394. Wang, L. *et al.* Knockdown of *SOX12* expression inhibits the proliferation and metastasis of lung cancer cells. *Am J Transl Res* vol. 9 <http://rsb.info.nih.gov/ij/> (2017).
395. Cui, N. *et al.* Hexokinase 2 Promotes Cell Growth and Tumor Formation Through the Raf/MEK/ERK Signaling Pathway in Cervical Cancer. *Front Oncol* **10**, (2020).
396. Enrico, T. P. *et al.* Cyclin F drives proliferation through SCF-dependent degradation of the retinoblastoma-like tumor suppressor p130/RBL2. doi:10.7554/eLife.
397. Lu, P. *et al.* DDX21 Interacts with WDR5 to Promote Colorectal Cancer Cell Proliferation by Activating CDK1 Expression. *J Cancer* **13**, 1530–1539 (2022).
398. Gharaibeh, L., Elmadany, N., Alwosaibai, K. & Alshaer, W. Notch1 in cancer therapy: Possible clinical implications and challenges. *Molecular Pharmacology* vol. 98 559–576 Preprint at <https://doi.org/10.1124/MOLPHARM.120.000006> (2020).
399. Zhu, H. er *et al.* ESCO2 promotes lung adenocarcinoma progression by regulating hnRNPA1 acetylation. *Journal of Experimental and Clinical Cancer Research* **40**, (2021).
400. An, X. *et al.* The prognostic significance of topoisomerase II alpha protein in early stage luminal breast cancer. *BMC Cancer* **18**, (2018).
401. Pommier, Y., Nussenzweig, A., Takeda, S. & Austin, C. Human topoisomerases and their roles in genome stability and organization. *Nature Reviews Molecular Cell Biology* vol. 23 407–427 Preprint at <https://doi.org/10.1038/s41580-022-00452-3> (2022).
402. Yang, Y. *et al.* Systematic Pan-Cancer Analysis Identifies CDK1 as an Immunological and Prognostic Biomarker. *J Oncol* **2022**, (2022).
403. Gao, Z., Jia, H., Yu, F., Guo, H. & Li, B. KIF2C promotes the proliferation of hepatocellular carcinoma cells in vitro and in vivo . *Exp Ther Med* **22**, (2021).
404. Meng, Q.-C. *et al.* Overexpression of *NDC80* is correlated with prognosis of pancreatic cancer and regulates cell proliferation. *Am J Cancer Res* vol. 5 [www.ajcr.us/](http://www.ajcr.us/) (2015).
405. Xu, Z., Zhang, Q. I., Luh, F., Jin, B. & Liu, X. Overexpression of the ASPM gene is associated with aggressiveness and poor outcome in bladder cancer. *Oncol Lett* **17**, 1865–1876 (2019).
406. Lin, F. *et al.* GTSE1 is involved in breast cancer progression in p53 mutation-dependent manner. *Journal of Experimental and Clinical Cancer Research* **38**, (2019).

407. Sun, D. P. *et al.* Aberrant expression of NCAPG is associated with prognosis and progression of gastric cancer. *Cancer Manag Res* **12**, 7837–7846 (2020).
408. Aggarwal, M. *et al.* TCL1A expression delineates biological and clinical variability in B-cell lymphoma. *Modern Pathology* **22**, 206–215 (2009).
409. Myklebust, J. H. *et al.* Distinct patterns of B-cell receptor signaling in non-Hodgkin lymphomas identified by single-cell profiling. (2017) doi:10.1182/blood-2016-05.
410. Lu, D. *et al.* The long noncoding RNA TINCR promotes breast cancer cell proliferation and migration by regulating OAS1. *Cell Death Discov* **7**, (2021).
411. Liu, Y. *et al.* Targeting Oxphos Pathway Against Ibrutinib Resistance to Mantle Cell Lymphoma. *Blood* **128**, 290–290 (2016).
412. *World Health Organization Model List of Essential Medicines.*

